BRIAUD, JEAN-LOUIS CHARLES

THE PRESSUREMETER: APPLICATION TO PAVEMENT DESIGN

University of Ottawa (Canada) PH.D. 1979

THE PRESSUREMETER:

APPLICATION TO PAVEMENT DESIGN

by

Jean-Louis Briaud

Submitted in partial fulfillment

of the requirements for the degree of

Doctor of Philosophy

Department of Civil Engineering

School of Graduate Studies

University of Ottawa

Ottawa, Canada

February 1979

DEDICATED

to

JANET

RESUME

LE PRESSIOMETRE: APPLICATION AU CALCUL DES CHAUSSEES

J.-L. Briaud[1]

Pour des raisons de rentabilité, les compagnies d'aviation civile ont l'intention d'augmenter la capacité de transport de leurs avions de 450 passagers (Boeing 747) à 1 000 passagers; dans quelques années, les pistes d'aéroports seront donc soumises à des charges beaucoup plus élevées. Au Canada, le calcul des chaussées souples d'aéroports est basé sur l'essai de plaque Mc Leod; cet essai, qui nécessite un matériel lourd, est coûteux, encombrant et de plus, de longue durée. En outre, il ne donne pas une évaluation détaillée de la résistance de la chaussée et du sol en profondeur. Il semblait donc nécessaire d'améliorer et l'essai et la méthode de calcul qui s'y appliquait. C'est pourquoi un pressiomètre, le pressiomètre Briaud, a été conçu et construit spécialement pour résoudre ce problème des pistes et chaussées; en outre, une méthode opératoire standard de l'essai a été établie.

Ce pressiomètre spécial et la méthode employée pour réaliser l'essai permettent de proposer une nouvelle base de calcul pour le dimensionnement des chaussées souples d'aéroports. La sonde pressiomètrique est courte et monocellulaire et l'essai mesure un module cyclique. Cette sonde permet d'exécuter des essais tous les 0,3 m et à tous les niveaux jusqu'à 1,8 m de profondeur. Le pressiomètre Briaud, qui est portatif et

1. Assistant Professor, Geotechnical Division, Civil Engineering Department, Texas A&M University, College Station, Texas, U.S.A., 77843

relativement peu coûteux, permet des essais de courte durée et, par ses résultats, donne des renseignements précis de la résistance de la chaussée et du sol sous-jacent.

Pour étudier l'influence de la proximité de la surface sur les résultats, des essais, toujours au pressiomètre Briaud, ont été exécutés au voisinage de la surface d'un dépôt homogène de sable et d'un dépôt d'argile. Les résultats de ces essais et d'une simulation sur ordinateur montrent que quelle que soit la profondeur, la déformation autour de la sonde, tant qualitativement que quantitativement, est toujours pratiquement la même au cours de la phase de l'essai où le module cyclique est mesuré. Par contre, il faut noter qu'il n'en est pas de même au cours de la phase où la pression limite est mesurée.

Par ailleurs, 93 essais au pressiomètre Briaud et 11 essais de plaque Mc Leod ont été exécutés en parallèle sur deux aéroports: l'aéroport de Sarnia où le sous-sol est argileux et l'aéroport d'Ottawa où le sous-sol est sableux. Les résultats montrent qu'il existe une relation linéaire entre la force portante de la chaussée (mesurée à l'essai de plaque) et un module cyclique équivalent (à partir des essais au pressiomètre). C'est l'existence de cette relation précise qui prouve que l'essai au pressiomètre Briaud peut remplacer l'essai de plaque dans le calcul des chaussées souples d'aéroports. Une méthode empirique de calcul basée sur l'essai au pressiomètre est donc proposée; cette méthode est en tous points semblable à la méthode de calcul basée sur l'essai de plaque.

Les tassements de la surface de la chaussée, mesurés pendant les essais de plaque Mc Leod, ont été comparés avec les tassements calculés à partir de la théorie de l'élasticité et des modules cycliques pressiomètriques; les tassements théoriques sont très proches des

tassements mesurés, De plus, à partir des mêmes modules et de la théorie du multicouche élastique, on a calculé les déformations provoquées par la charge des avions de calcul, tant dans le revêtement de la chaussée que dans le sol sous-jacent; les valeurs des déformations trouvées sont semblables à celles données dans les publications. Les résultats de tassement et de déformation indiquent que l'essai au pressiomètre Briaud peut fournir les modules nécessaires au calcul des chaussées souples à partir de la théorie du multicouche élastique. La méthode basée sur le multicouche élastique convient mieux que la méthode empirique pour étudier les effets de l'augmentation du poids des avions et de la complication de leurs trains d'atterrissage, tant sur la chaussée que sur le sous-sol. Dans cette thése est décrite une méthode basée sur la théorie du multicouche. Cette méthode nous paraît préférable à la méthode empirique.

Les recherches à venir devraient désormais s'efforcer de développer l'automatisation du pressiomètre pour chaussée, d'étayer définitivement la relation que existe entre le paramètre de la plaque Mc Leod et le paramètre équivalent du pressiomètre Briaud et de mettre complétement au point la méthode de calcul basée sur la théorie du multicouche élastique et ce, à partir du pressiomètre.

Il paraît enfin souhaitable d'envisager et de rechercher les modes d'utilisation du pressiométre Briaud pour le calcul des chaussées autres que les pistes souples d'aéroports.

ABSTRACT

THE PRESSUREMETER: APPLICATION TO PAVEMENT DESIGN

J-L. Briaud[1]

For economic reasons, the civil aviation industry has plans to increase the maximum capacity of its planes from about 450 passengers (Boeing 747) to 1000 passengers; as a result, airport runways will have to carry much heavier loads in the future. In Canada, the design of flexible airport pavement is based on the McLeod plate test; this test is expensive, cumbersome, time consuming, and does not give a detailed assessment of the pavement strength over its full depth. There seems to be a need at this time to improve both the design method and the test on which the design is based.

A special pressuremeter, termed the Briaud pressuremeter, has been designed and built specifically for use in pavement engineering; also, a standard test procedure has been established. Both the special pressuremeter and test procedure are proposed as a basis for the traffic load design of flexible airport pavements. The pressuremeter probe is short and monocellular, and the test measures a cyclic modulus. The short probe allows tests to be performed every 0.3 m from the pavement or ground surface down to a depth of 1.8 m. The Briaud pressuremeter is portable and relatively inexpensive, the test is of short duration, and the results give a direct assessment of the condition of the pavement with depth.

---

1. Assistant Professor, Geotechnical Division, Civil Engineering Department, Texas A&M University, College Station, Texas, USA 77843

Briaud pressuremeter tests were carried out close to the surface of a uniform deposit of sand and a deposit of clay to check if the proximity of the surface had an influence on the measurement. The test results and a computer simulation have shown that the proximity of the surface boundary has no significant influence on the deformation process around the probe, during the phase of the test where the cyclic modulus is measured. This conclusion does not hold true, however, for the phase of the test where the limit pressure is measured.

Ninety three Briaud pressuremeter tests and 11 McLeod plate tests were carried out in parallel at two airport sites: Sarnia Airport with a clay subgrade and Ottawa Airport with a sand subgrade. It was found that a linear relationship exists between the pavement bearing strength (as measured by the McLeod plate test) and an equivalent cyclic modulus (from Briaud pressuremeter tests); the fact that a definite relationship exists shows that the Briaud pressuremeter test can replace the McLeod plate test in the design of flexible airport pavements. An empirical design method based on the pressuremeter is proposed; the method parallels the McLeod plate design procedure.

The settlements measured in the field under the McLeod plate were compared to the settlements calculated using the theory of elasticity and the Briaud pressuremeter cyclic moduli; close agreement was found. Also, using the same modulus and the multilayer elastic theory, asphalt and subgrade strains were calculated under the load of design planes; the magnitude of these strains compares well with values reported in the literature. Both settlement and strain results indicate that the Briaud pressuremeter test can provide the moduli which are required for

the multilayer, elastic, method of flexible pavement design. The effect of the increased weight of the planes and of the increased complication of their wheel configuration can be studied more easily with the multilayer elastic design procedure than with the empirical procedure. A multilayer elastic design procedure is presented in this thesis and is the one which is recommended.

Further research should be concerned with the mechanical development of the proposed pressuremeter (automation), with the confirmation of the relationship between the McLeod plate parameter and the Briaud pressuremeter equivalent parameter, and with the implementation of the multilayer elastic design of flexible pavement. The applicability of the proposed pressuremeter to pavements other than flexible airport pavements also should be investigated.

ACKNOWLEDGEMENTS

The following have contributed to the achievement of this research project; while listed in no particular order, they are all thanked very sincerely:

D. SHIELDS

and

his family

J. BRIAUD
D. SCOTT
G. BAUER
L. HUNTER
G. ARGUE
J. BERTOK
V. MAH
W. DOERING
C. LAVIGNE
G. DUCHESNE
G. FELIO
J. VEZINA

P. HARTMAN
W. BARKER
L. MENARD
F. BAGUELIN
J. F. JEZEQUEL
J. TAYLOR
W. STORTO
N. RENAUD
L. GOODRICH
P. SELVADURAI
W. BOWES
R. MOORE

K. KWAN
J. H. DESCHENES
G. HAILE
H. ABU SITTA
G. McENIRY
J. P. DEMARTINECOURT
H. BROWN
M. KELSALL
E. IRELAND
G. GOODWIN
L. DAL BELLO
L. BRIAUD

The following individuals and organizations have contributed financially to make this project possible:

TRANSPORT CANADA

D. SHIELDS

NATIONAL RESEARCH COUNCIL OF CANADA

CIVIL ENGINEERING DEPARTMENT
UNIVERSITY OF OTTAWA

TABLE OF CONTENTS

LIST OF FIGURES

LIST OF SYMBOLS

a_i	area under the strain influence factor curve within the i^{th} layer.
A	total area under the strain influence factor curve.
ALR	Aircraft Loading Rating.
B	diameter of a plate.
c_u	undrained shear strength.
CBR	California Bearing Ratio.
CPV	control unit for the pressuremeter.
D	diameter.
D_c	critical depth.
E	Briaud pressuremeter modulus (first loading).
E_a	asphalt modulus.
E_b	base course and subbase modulus.
E_c	Briaud pressuremeter cyclic modulus (second loading).
E_{cep}	pavement equivalent Briaud pressuremeter cyclic modulus.
E_{ces}	subgrade equivalent Briaud pressuremeter cyclic modulus.
E_{c33}	Briaud pressuremeter cyclic modulus at 90 cm^3 of injected volume.
E_{co}	modulus for sand (from the cone test).
E_e	equivalent modulus.
$E_{e\ell}$	modulus of elasticity.
E_{ep}	pavement equivalent Briaud pressuremeter modulus.
E_{es}	subgrade equivalent Briaud pressuremeter modulus.
E_i	pressuremeter, initial, modulus.

E_M	Menard pressuremeter (first loading) modulus.
E_n	modulus of the n^{th} layer.
$E_{p\ell}$	modulus of deformation obtained from plate test results.
E_s	subgrade modulus.
E_T	triaxial modulus (first loading).
E_{Tc}	triaxial cyclic modulus (fourth loading).
E_w	modulus measured in the wave propagation method.
E_z	modulus of the soil at the depth z.
ESWL	Equivalnet Single Wheel Load.
f	frequency.
FAA	Federal Aviation Administration.
F	factor of safety.
g	acceleration due to gravity.
h_b	thickness of the base layer.
h_o	difference in elevation between the pressure gauge of the control unit and the middle of the measuring cell.
I_D	density index.
I_z	strain influence factor at the depth z.
K	a constant.
K_b	ratio of $\frac{E_b}{E_s}$.
K_o	coefficient of earth pressure at rest.
ℓ_o	length of the measuring cell.
L	wave length.
M_R	resilient modulus.
N	number of blows per given length of penetration.

N_h	number of load repetitions characterizing the remaining life of the pavement (asphalt strain criterion).
N_v	number of load repetitions characterizing the remaining life of the pavement (subgrade strain criterion).
p	pressure applied to the wall of the cavity.
p	bearing pressure.
p_f	pressure at which the soil fails.
p_i	pressure due to membrane resistance.
p_ℓ	limit pressure.
p_ℓ^*	net limit pressure.
p_m	pressure read at the gauge of the control unit.
p_o	pressure applied to the wall of the cavity at the start of the straight line portion of the pressuremeter test curve.
p_{oh}	total stress, initial horizontal earth pressure.
p_r	pressure in the measuring cell.
Δp	increase in cavity pressure (first loading).
Δp_c	increase in cavity pressure (second loading).
Δp_r	difference between two consecutive gauge pressure reading.
q_c	cone bearing value.
Q	load.
Q_c	cone penetration resistance.
r	radial distance to a point in the soil.
r_o	initial radius of the borehole.
R	radius of a plate.
R_{equiv}	average radius of the inflated probe.
R_{max}	maximum radius of the inflated probe.

R_{min} average radius of the deflated probe.

s settlement.

S load applied to the McLeod plate.

S_p pavement bearing strength.

S_s subgrade bearing strength.

SPT Standard Penetration Test.

t equivalent granular thickness.

t_a thickness of the asphalt layer.

t_b thickness of the base course layer.

u_x vertical displacement.

u_y horizontal displacement.

v volume increase of the measuring cell.

v_d volume correction.

v_f volume injected in the measuring cell to reach the creep pressure (p_f).

v_m volumeter reading after setting the zero.

v_{max} maximum volume of water injected into the probe.

v_o difference between the volume of the cavity and the initial volume of the measuring cell.

v_v volumeter reading before setting the zero.

v_w wave velocity.

V volume of the measuring cell.

V_c initial volume of the measuring cell.

V_m volume of the cavity at midpoint of the straight line portion of the pressuremeter curve (first loading).

V_{mc}	volume of the cavity of midpoint of the straight line portion of the pressuremeter reloading curve (second loading).
V_o	initial volume of the cavity.
Δv	increase in volume injected in the measuring cell (first loading).
Δv_c	increase in volume injected in the measuring cell (second loading).
ΔV	increase in the volume of the cavity.
w	natural water content.
w_L	liquid limit.
w_p	plastic limit.
z	depth.
z_n	depth to the top of the n^{th} layer.
α	coefficient in the wave propagation formula.
γ	unit weight.
γ_{max}	maximum dry unit weight.
γ_{min}	minimum dry unit weight.
γ_w	unit weight of water.
ε_h	horizontal strain at the lower face of the asphalt layer.
ε_{ha}	allowable asphalt tensile strain.
ε_{hq}	lower quartile value of the asphalt tensile strains.
ε_v	vertical strain at the top of the subgrade.
ε_{va}	allowable subgrade compressive strain.
ε_{vq}	lower quartile value of the subgrade compressive strains.
ε_z	vertical strain.
μ	volumetric strain.

ν	Poisson's ratio.
ν_n	Poisson's ratio of the n^{th} layer.
σ_d	deviator stress.
σ_h	horizontal stress.
σ_{oct}	octrahedral stress.
σ_r	radial stress.
σ_v	vertical stress.
σ_1	major principal stress.
σ_3	minor principal stress.
ϕ_h	diameter of the hole.
ϕ_p	diameter of the probe.
ϕ_t	diameter of the calibration steel tube.

CHAPTER 1

INTRODUCTION

1.1 General

In this research, the possibility of using a pressuremeter for the design of flexible airport pavements is investigated.

A typical flexible airport pavement is made up of a thin asphalt layer (about 100 mm thick), a base course layer (about 300 mm) and if necessary a sub-base course layer (say 200 mm). The pavement rests on the natural soil subgrade (Fig. 1). It is proposed that a small pressuremeter probe be used to measure, in situ, subgrade, sub-base and base course characteristics which would be relevant for the design and evaluation of airport pavements.

To the author's knowledge this project marks the first time that an attempt has been made to employ the pressuremeter in this fashion.

1.2 Statement of the Problem

In the summer of 1954, Louis Ménard was employed to carry out compaction tests on a new airport runway which was then under construction near Paris. It was in connection with the evaluation of the base course for the runway that Ménard got the idea for the pressuremeter. Today (1979) the pressuremeter is used successfully in foundation engineering and to a minor degree in compaction control, but, suprisingly, nothing has been done to study the possible use of the pressuremeter for pavement design.

There are four categories of pavements: rigid highway pavements, flexible highway pavements, rigid airport pavements and flexible airport

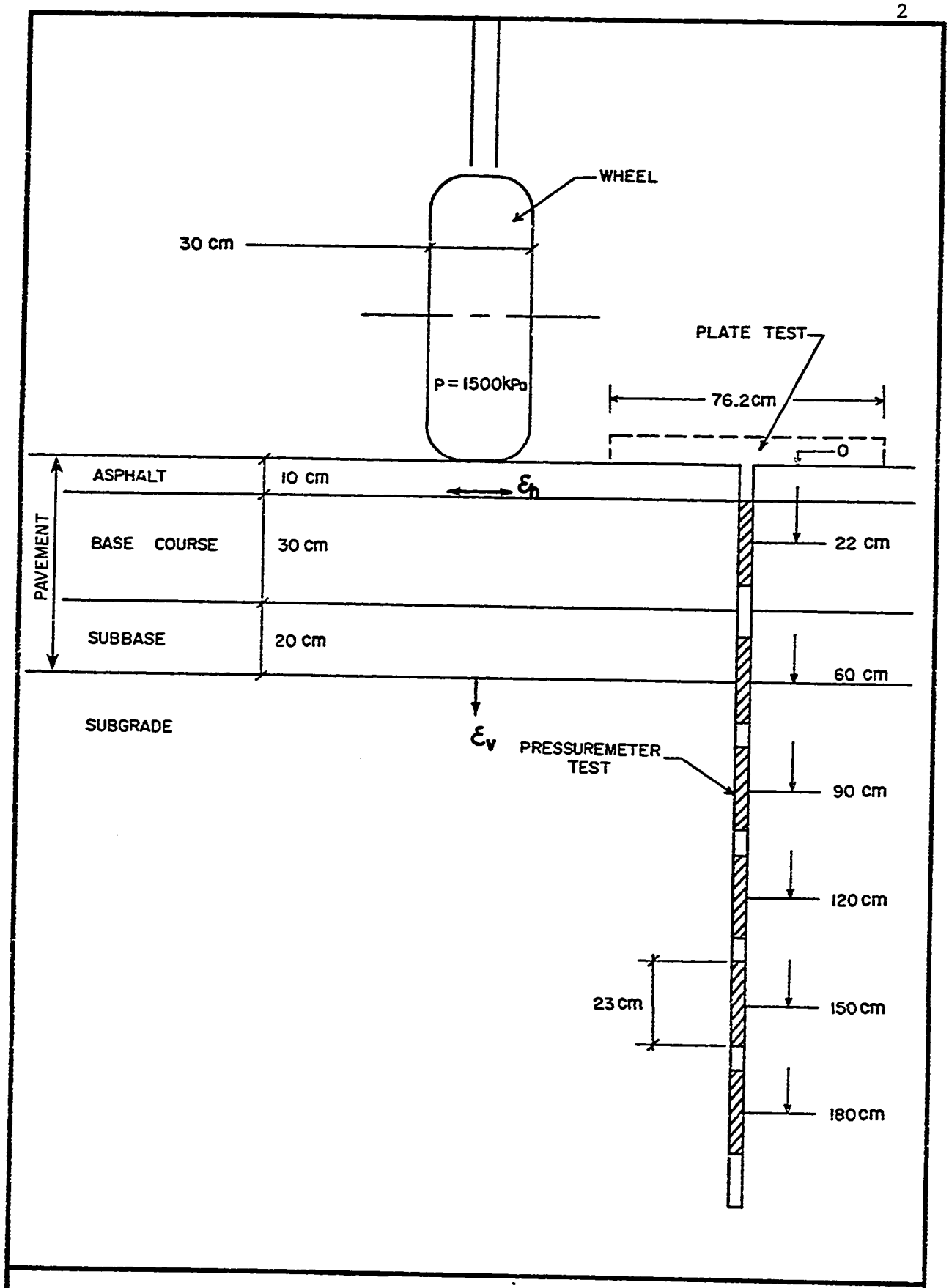

Fig. 1 – Typical Pavement Cross Section and Position of Tests.

pavements (p. 5 of (50)[2]). A properly designed pavement will behave satisfactorily under the anticipated traffic loads and environmental conditions for the duration of the required service life. This research deals only with the traffic load design of flexible airport pavements and not with the environmental aspects; there is need for improvement in traffic load design methods both in Canada and other countries as discussed in Section 2.4.1 of this thesis. This research attempts to answer the following question: can the pressuremeter be used as the basis for the traffic load design of flexible airport pavements?

1.3 Importance of the Problem

The traffic load design of flexible airport pavements includes the design of new pavements for new airports or for the extension of existing facilities, the evaluation of existing pavements approximately every two years, and the design of pavement-overlays approximately every 15 years (34). The traffic load design of flexible airport pavements requires the knowledge of three parameters: the type of loading (for example the type of plane which will use the runway), the traffic condition (for example the number of take offs and landings per day), and the subgrade strength. The design then consists of finding the pavement thickness which is required to accomodate a set of these three parameters during the pavement service life of approximately 15 years.

Subgrade strength is probably the most difficult parameter to evaluate. For the design of new pavements, the subgrade strength is

---

2. Numbers in parantheses refer to the corresponding reference in the List of References.

3. Strength is the word used in pavement engineering to refer to the deformability of a pavement.

usually estimated from the soil classification or by California Bearing Ratio (CBR) tests. For the evaluation of existing pavements, the McLeod plate test is the most commonly used method in Canada. To design an overlay, either soil classification, CBR values or plate test results are used together with the reverse design procedure; in the reverse design procedure the subgrade strength is evaluated, the required pavement thickness is calculated and this thickness is then compared with the actual pavement thickness.

A more general method of flexible pavement design considers the pavement as a multilayer elastic medium; strains are calculated at critical points in the pavement and the thickness of the pavement is chosen to limit the magnitude of these strains.

It is thought that the pressuremeter could replace both the CBR test and the plate test in many instances; the pressuremeter should also be able to provide the elastic moduli which are required for the multilayer method of pavement design. The pressuremeter method, if successful, would have the following major advantages over existing methods:

- it will be a general method; pressuremeter test results should be applicable for the design of new pavements as well as for the evaluation of existing pavements and the design of overlays.
- the pressuremeter test should be less expensive than the McLeod plate test since the pressuremeter equipment is less cumbersome and the pressuremeter test is less time consuming.
- the pressuremeter will evaluate the soil in situ and should give more reliable and relevant information than, say, the CBR test

and simple soil classification.

- since pressuremeter tests can be carried out at regular intervals of depth (a procedure which is not followed for the McLeod plate test), it should be possible to select the elastic moduli required in the multilayer elastic design method on a rational basis.

A more detailed list of advantages and drawbacks of the methods mentioned previously is included in Chapter 3.

1.4 Research Plan and Scope

The first phase of the research program includes:

Step 1. Design and build a suitable pressuremeter and establish an appropriate test procedure.

Step 2. Investigate the influence of the proximity of the ground surface on pressuremeter results since it is known that a critical depth exists for conventional pressuremeter tests and since the pressuremeter tests for pavements will be carried out close to the ground surface.

Step 3. Prove the reliability of the equipment and the practicality of the test.

The second phase investigates the possibility of using the first phase pressuremeter and test for airport runway design. The most appropriatesecond phase would be to run pressuremeter tests in an area; design and build or reconstruct a runway on the basis of the results; and test the runway to failure. The predicted and actual behavior could then be compared. For obvious reasons this is not feasible. Instead,

in the second phase, it has been decided to:

Step 1. Run in parallel, pressuremeter tests and plate tests and compare the results.

Step 2. Use the comparison of Step 1 and the Canadian design method to propose a pressuremeter based, semi-empirical pavement design procedure.

Step 3. Illustrate how the pressuremeter moduli can be used in a multilayer elastic design method.

The above six steps make up a relatively broad research subject; this wide scope of subject is to be expected from a new topic where little background information is available. The aim of the research, then, is not so much to give an irrefutable solution to each of the problems raised in the six steps, but the aim is to provide a definite indication of what the solution could be. This thesis will show that using the pressuremeter test as the basis for the traffic load design of flexible airport pavements is very promising; this thesis will also provide a starting point for the development of the pressuremeter method for runway pavement design.

CHAPTER 2

BACKGROUND

This chapter gives background information on 1) current methods of design for airport flexible pavements, 2) the Ménard pressuremeter and test and 3) the present state of the use of the pressuremeter for pavement design.

2.1 Airport Flexible Pavements: Current Design Methods

2.1.1 Canadian Design

In Canada, the traffic load design of flexible pavements makes use of a plate test to evaluate the pavement resistance to deformation. McLeod (28) developed the standard for this test which is called the McLeod plate test.

The McLeod plate test consists of loading a 762 mm diameter steel plate (Fig. 4) placed on the asphalt surface of the pavement. A trailor loaded with a huge rubber container filled with water is usually used as a reaction (Fig. 2); depending on the strength of the pavement, one or two truck-trailor combinations may be necessary. The test consists of applying to the plate a load S_p which, repeated 10 times, will cause a 12.5 mm deflection of the surface of the pavement. The deflection of the surface is measured with the aid of a reference beam (Fig. 3). This test is described in more detail in Section 5.1.

The traffic load design of new pavements is carried out in accordance with Transport Canada manual AK-68-12 (42) as follows:

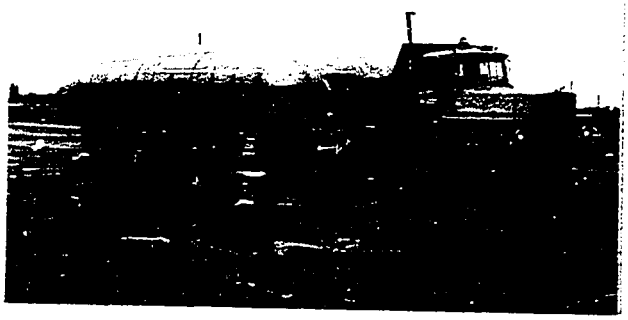

Fig.2 - McLeod Plate Test: Truck.

Fig.3 - McLeod Plate Test: Reference Beam.

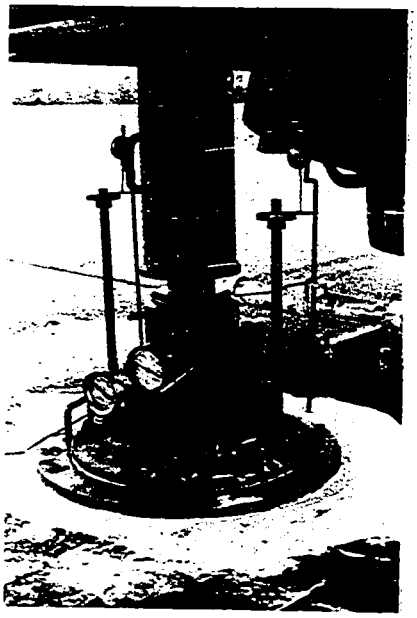

Fig.4 - McLeod Plate Test: Plate and Jack.

1) The subgrade of the airport site is classified according to the Unified Soil Classification System (p. 35 of (26)). The subgrade bearing strength (S_s) is estimated from the subgrade classification (Section 220 of (42)); S_s is the load in kN which, in theory, if applied to the surface of the subgrade, would create, at the 10th load repetition, a 12.5 mm deflection of a standard 762 mm diameter rigid plate. The S_s values range from 25 kN to 400 kN (it may be noted that in Transport Canada's experience, a 12.5 mm deflection after 10 repetitions corresponds roughly to an 8.5 mm deflection under the first application of a load).

2) The design plane which will be landing at the airport site is classified according to its Aircraft Loading Rating (ALR). The ALR is a number which ranges from 1 to 12; the ALR is 12 for a Boeing 747 or a Concorde and 1 for very small planes (Section 210 of (42)).

3) Once S_s and the ALR are known, the chart of Figure 5 is used to find the equivalent granular thickness (t) of the pavement; t takes into consideration the equivalency factors (Section 240 of (42)) for various components of the pavement. The equivalency factor is, for example, 1 for the base course (1 cm of base course = 1 cm of equivalent granular thickness) and 2 for asphalt concrete (1 cm of asphalt concrete = 2 cm of equivalent granular thickness).

4) The pavement is then designed to have the minimum required thickness of asphalt, the minimum required thickness of base course and the remaining portion of t in sub-base. These minimum requirements depend on the maximum tire pressure (Section 320 of (42)).

5) Once the pavement is built, a number of McLeod plate tests are carried out in accordance with Transport Canada manual AK-68-31 (43);

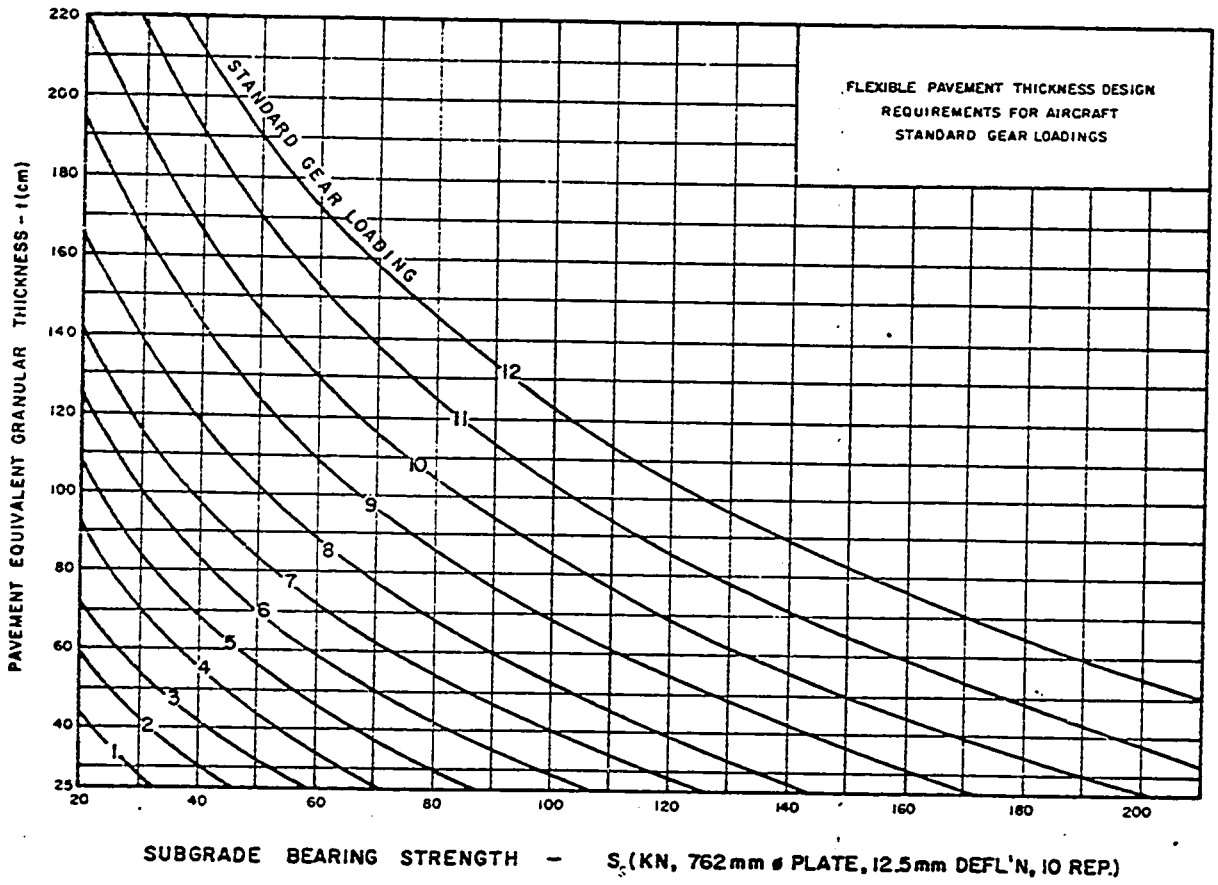

Fig. 5. Transport Canada Design Chart (from Transport Canada Manual AK-68-12).

the tests generate pavement bearing strength parameters (S_p) as discussed earlier. The S_p value can range from 50 kN to 2000 kN.

6) At any one plate test location, a new S_s value is deduced from the S_p value using the equation:

$$S_s = S_p \times 10^{-\frac{t}{165}} \quad \ldots\ldots\ldots\ldots\ldots\ldots\ldots\ldots \quad (1)$$

where S_s = subgrade bearing strength

S_p = pavement bearing strength

and t = equivalent granular thickness in centimeters

This equation is due to McLeod (28). The S_s values are multiplied by a reduction factor, if necessary, to account for springtime loss in strength (Section 2.07 of (43)); the lower quartile S_s value is determined (Section 2.05 of (43)) and is considered to be the in situ S_s value. Comparing the in situ S_s value and the design S_s value from Step 1 provides the engineer with a check on the design.

In Canada, the evaluation of existing pavements is carried out as follows:

1) A number of McLeod plate tests are performed on the pavement, giving rise to a number of S_p values; the corresponding S_s values are obtained by using Equation 1.

2) As is done during the design of new pavements, the S_s values are multiplied by a spring reduction factor, if necessary, the lower quartile S_s value is determined and is considered as the in situ S_s value.

3) The ALR of the design plane is obtained, and, using the thickness design chart of Figure 5, the required value of t is determined.

If the existing t is greater than the required t, the pavement is satisfactory. If the opposite is true, the pavement needs to be strengthened and the thickness of the necessary overlay is deduced from the difference between the required and existing t values.

2.1.2 American Design

In the United States of America, the design of new pavements is based on the same principles as the Canadian design. The subgrade strength is estimated from either its Federal Aviation Administration Classification (F.A.A.) or its California Bearing Ratio (CBR)(pp. 13-21 of (12)); the design plane is characterized by its gross weight. A design chart gives the equivalent granular thickness, as well as the asphalt and base course thicknesses as a function of the subgrade strength classification and the plane gross weight (p. 40 of (12)).

This chart, as does the Canadian design chart, considers an average traffic volume of 1200 departures per year of the design plane. In the U.S.A. design, higher traffic volume can be taken into consideration (p. 37 of (12)).

Existing pavements are evaluated and overlay thicknesses are calculated by the reverse design procedure.

It must be noted that the United States Navy has a design method based on a plate test which is similar to the McLeod plate test (49).

2.1.3 French Design

In France, the design of new pavements follows the same guidelines as in the U.S.A. and in Canada. The subgrade strength is quantified by

its CBR value and the design plane is characterized by its Equivalent Single Wheel Load (ESWL); the ESWL is the load on a fictitious single tire which would create the same maximum vertical subgrade stress as the loads on the tires of a multiple wheel gear.

A series of charts (one per type of plane) gives the equivalent granular thickness (t) as a function of the CBR and the ESWL (9).

Evaluation and overlay problems are also handled by the reverse design method. Recently, a plate test similar in principle to the McLeod plate test has been devised for the evaluation of existing airport pavements in France (22).

2.1.4 Multilayer Elastic Design

Another way of designing a pavement is to use multilayer elastic theory. A general outline of the method is as follows:

1) The pavement-subgrade system is considered to be a multilayer elastic continuum. Each layer is characterized by a modulus of elasticity (E_{el}) and a Poisson's ratio (ν); in most cases the hypothesis of perfect adherence between layers is made.

2) The strains generated in the multilayer elastic continuum by the design aircraft are calculated using a computer program[4]. Two strains are considered: the horizontal tensile strain (ε_h) at the lower face of the asphalt layer and the vertical compressive strain (ε_v) at the top of the subgrade (Fig. 1).

3) The design asphalt and pavement thicknesses are the thicknesses which are required to ensure that the magnitudes of ε_h and ε_v are within acceptable limits; these limits are called the limiting strains criteria.

---

4. Such a computer program is described on page 230.

This method of design has received considerable attention in the last few years; for instance, numerous articles related to the subject were published in the proceedings of the Third and Fourth International Conferences on the Structural Design of Asphalt Pavements ((41) and (13)).

BISAR (10) and CHEV5L (3) are two popular computer programs which handle the multilayer elastic problem. BISAR was developed by the Shell Oil Company and CHEV5L by the California Research Corporation. As input data, the two programs call for the load, the geometry of the gear of the design plane, and the elastic constants of the layers. The choice of both the elastic moduli and the limiting strain criterions are discussed below.

The asphalt is composed of bitumen, aggregates and voids. The modulus (E_a) of the asphalt can vary from about 10^3 to 5×10^7 kPa depending on bitumen content, percentage of voids and bitumen modulus (p. 47 of (10)). Also, temperature has a large influence on the bitumen modulus. Claessen et al (10) recommend the use of monographs (Fig. 6 and Fig. 7) for estimating the asphalt modulus. Barker et al. (3), on the other hand, prefer direct determination of the modulus by means of dynamic triaxial testing.

The base (base course and sub-base) modulus (E_b) is generally estimated from the subgrade modulus (E_s). Claessen et al. (10) suggest:

$$E_b = k_b E_s \quad \ldots\ldots\ldots\ldots\ldots\ldots\ldots\ldots \quad (2)$$

where $k_b = 0.2\, h_b^{0.45}$ with limits: $2 < k_b < 4$ $\ldots\ldots\ldots$ (3)

where h_b = thickness of the base layer in mm.

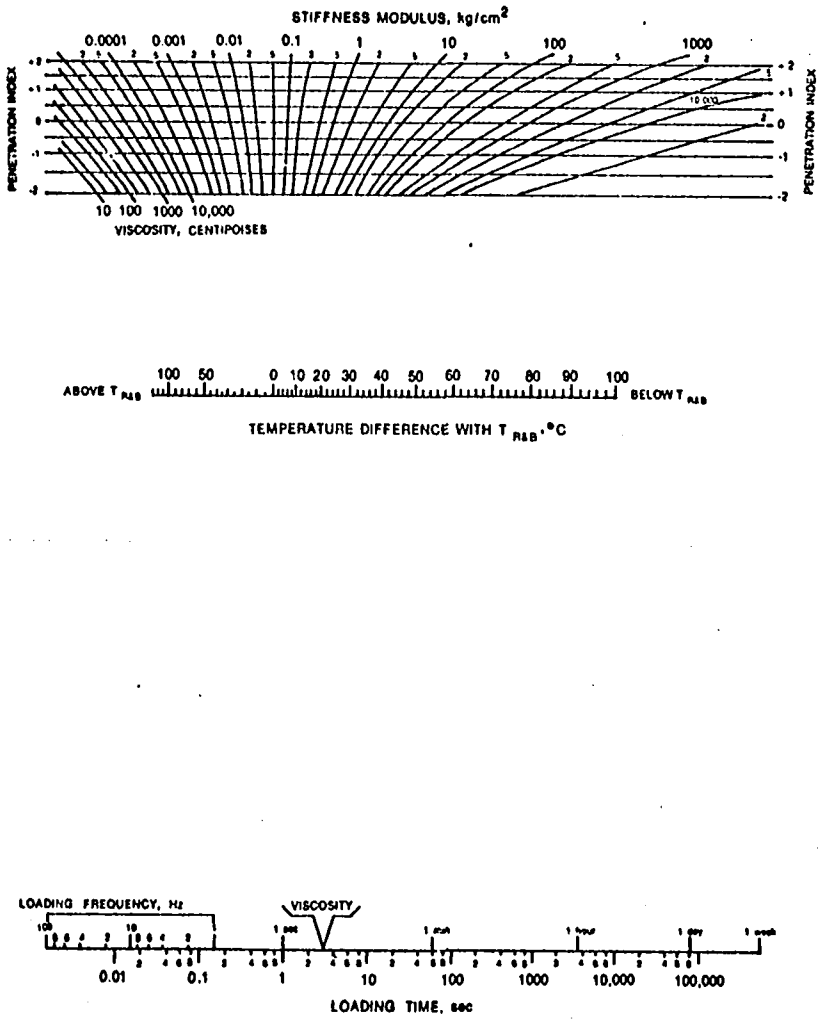

Fig. 6 - Nomograph for Determining the Modulus of Bitumen (from Barker et al, 1977).

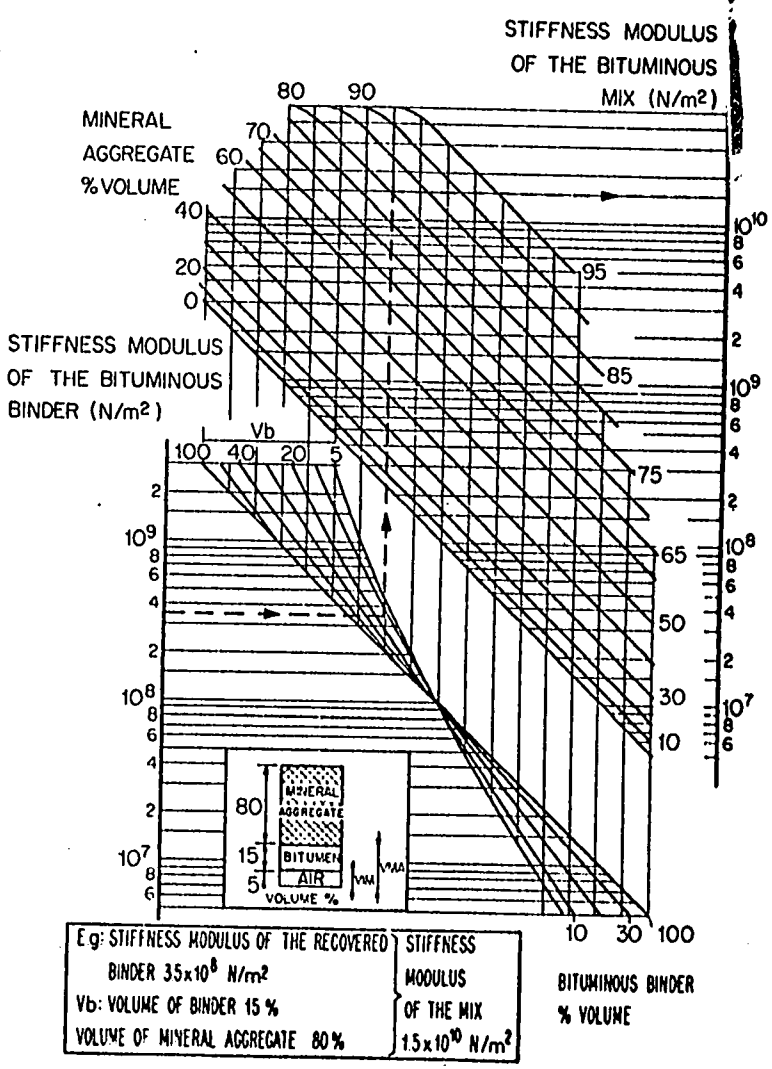

Fig. 7 - Nomograph for Determining the Modulus of Bituminous Mixes (from Claessen et al, 1977).

Barker et al. (3) present a more involved determination of E_b which is based on the same principle; they divide the base layer into n thin layers and, starting from the subgrade modulus (E_{n+1}), back calculate the modulus of the n^{th} base layer (E_n) using the chart of Figure 8. Knowing E_n, they determine E_{n-1} and so on.

The permissible horizontal tensile strain at the lower face of the asphalt (ε_h) depends on the type of asphalt, the asphalt modulus, and the number of strain load repetitions. As a result, setting an asphalt limiting strain criterion is not a simple matter. Claessen et al (10) present charts (Fig. 10) which purport to give permissible strain values for asphalt.

The permissible vertical compressive strain at the top of the subgrade (ε_v) seems to have been studied by more researchers than has ε_h. Barker et al. (3) present a graph (Fig. 11) which summarizes the work done in eight studies and gives recommendations for permissible subgrade strain.

It must be noted that both the asphalt and the subgrade limiting strain criterion seem to have been based more on calculated strain values than on actual measurements.

Bleyenberg et al (4) and others have found good agreement between the actual behavior of the pavement and the behavior which was predicted using the multilayer linear elastic theory.

2.1.5 Existing Methods of Modulus Determination for the Multilayer Theory

The subgrade modulus (E_s) is obtained in most cases from the subgrade

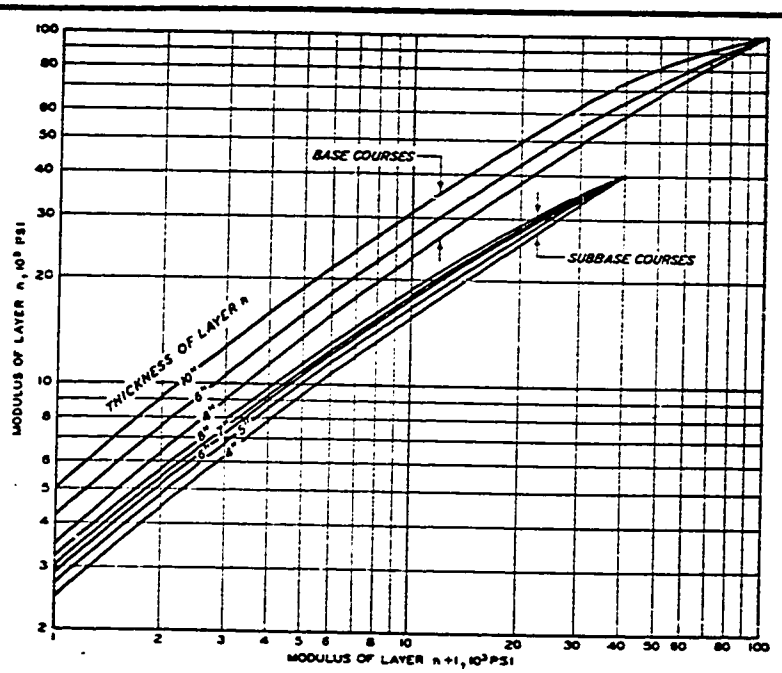

Fig. 8 - Chart for Determining the Base Moduli (from Barker et al, 1977)

Fig. 9 - Relationships between the Subgrade Modulus and the Subgrade CBR

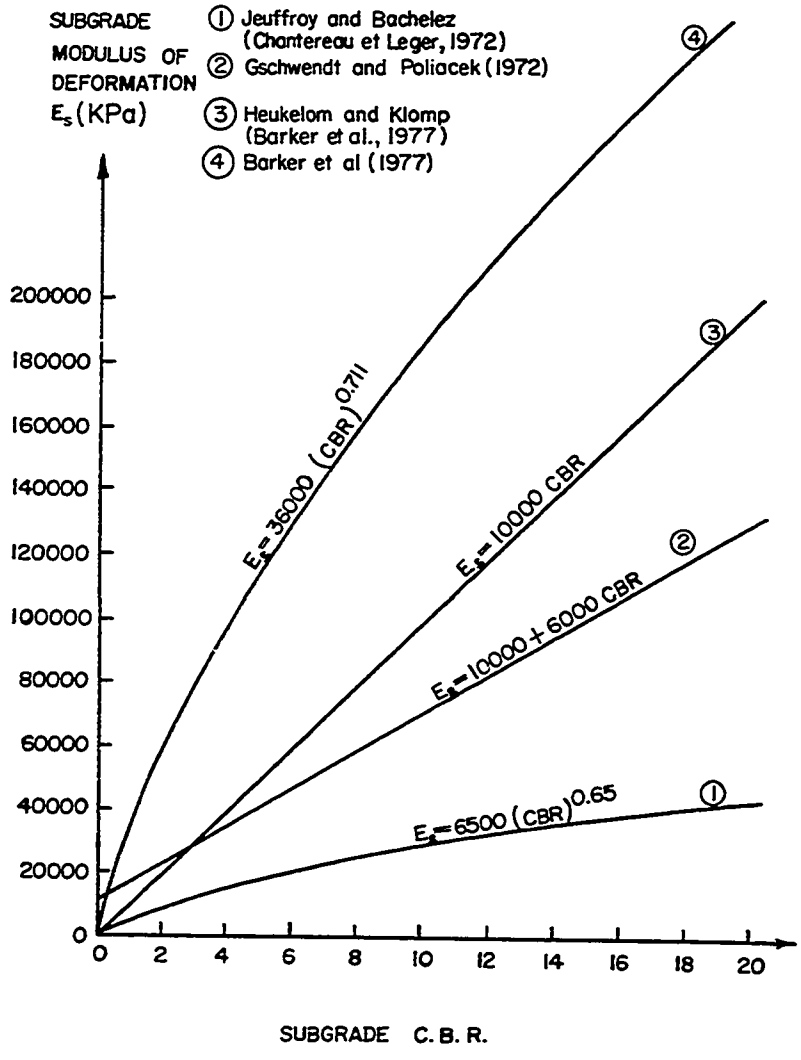

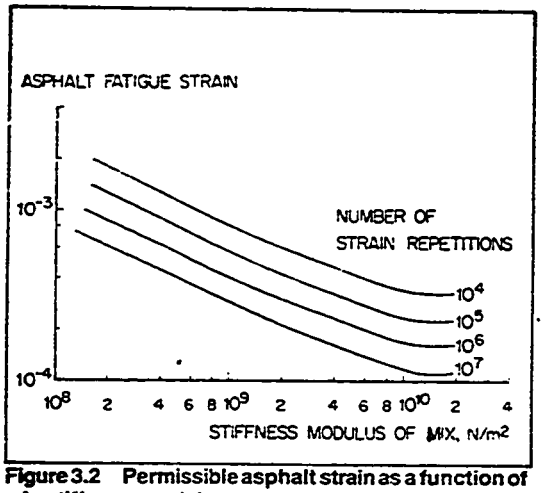

Figure 3.2 Permissible asphalt strain as a function of mix stiffness modulus
Dense bitumen macadam

A

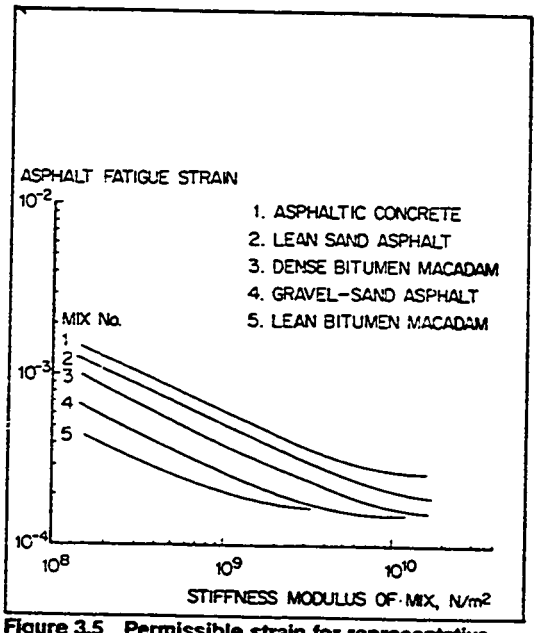

Figure 3.5 Permissible strain for representative asphalt mix types as a function of mix stiffness modulus

B

Fig. 10 - Asphalt Limiting Strain Criterion (from Claessen et al., 1977)

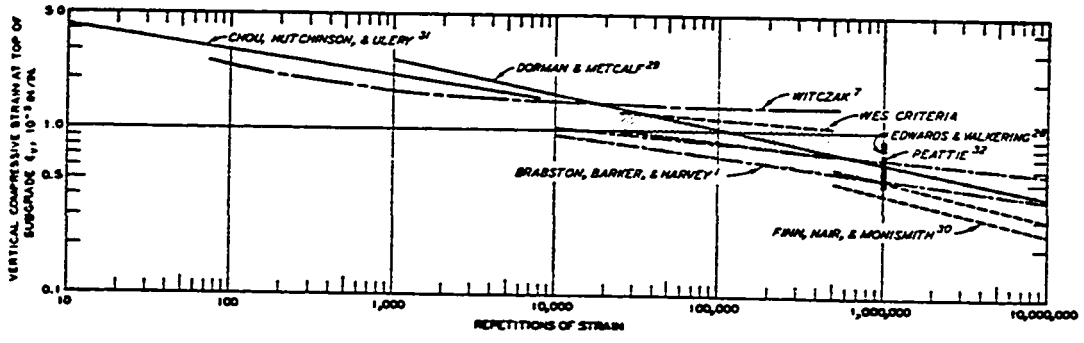

Fig. 11 - Subgrade Limiting Strain Criterion (from Barker et al, 1977).

CBR value. Many researchers have proposed relationships between E_s and CBR; these relationships are shown in Figure 9. The wide range of E_s values that may be obtained for the same CBR value brings into question the precision of this method of subgrade modulus determination; since the base modulus is said to depend on the subgrade modulus, the precision of the base modulus is also suspect if the subgrade modulus is determined from the CBR.

In addition to modulus-CBR relationships, other methods of modulus determination exist; the wave propagation method, the cone test and the triaxial test are three examples.

The wave propagation method (p. 272 of (50)) consists of placing a vibrator and a receiver on the pavement a few meters from one another. A vibration of given frequency (f) is applied to the pavement and the receiver records the wave velocity (v_w). The average modulus of deformation (E_w) of the material located between the pavement surface and a depth equal to the wave length (L) is given by:

$$E_w = \frac{2\,(1+\nu)\,v_w^2\gamma}{\alpha^2\, g} \quad \text{for Ralleigh waves} \quad \ldots\ldots\ldots\ldots \quad (4)$$

where ν = Poisson's ratio

g = acceleration due to gravity

γ = unit weight of the material within the zone of influence

α = 0.875 for ν = 0 and 0.955 for ν = 0.5

By varying f, a profile of moduli is obtained.

This method is nondestructive and gives detailed information on the

pavement layers. However, it is time consuming (about five hours per station) and the computations are complicated (45). In addition, the method gives moduli values which are much too high (35) and the high values do not corrolate well with those from the plate test (20). The very low strain levels developed by the vibrator lead to very high moduli (close to the origin of the stress-strain curve).

Cone tests have been used in the past in connection with pavement work. McLeod (28) describes a penetration test devised for pavements by W. S. Housel in 1933; this test could be referred to as a mini-standard penetration test which uses a weight of 91 N with a free fall of 860 mm. The sampler has a diameter of 35 mm. The parameter which is measured during the test is the number of blows per 150 mm of penetration (N).

McLeod (28) also described a cone bearing test devised for pavements by K. Boyd in 1942; this test consists in having a cone penetrate the soil under a constant load Q_c. The cone has a base diameter of 29 mm, a tip angle of 16^o and a length of 100 mm. A first load is applied (Q_c = 45 N); the cone settles under the load and the settlement (s) is recorded after one minute of load application. The cone bearing value (q_c) is calculated by:

$$q_c = \frac{Q_c}{\pi \frac{D^2}{4}} \quad \ldots\ldots\ldots\ldots\ldots\ldots\ldots\ldots\ldots\ldots \quad (5)$$

where Q_c = load applied,

D = diameter of the cone at the ground surface after one minute of load application.

This procedure is repeated for loads of 90, 180 and 360 Newtons and the overall cone bearing value is the average of the values calculated for the four different loads.

McLeod (28) compared N with the subgrade bearing strength (S_s) and found a reasonable correlation between them; the correlation between q_c and S_s was somewhat better than the one between N and S_s.

The Housel and Boyd penetration tests are performed through fairly large diameter holes which are cut through the pavement. A penetration test is carried out at a number of depths at each test location; at each depth the surface to be tested must be prepared.

Schmertmann (37) describes the use of the Dutch cone (base diameter: 36 mm, tip angle: 60°, length: 31 mm) to obtain the modulus of soil. The cone is driven into the ground at a standard rate of 20 mm/sec and the penetration resistance (Q_c) is recorded. The cone bearing value (q_c) is calculated using Equation 5 with D equal to the base diameter. A continuous q_c profile is obtained and this represents a definite advantage over the Housel and Boyd penetration tests, over the plate test and over the pressuremeter test. Schmertmann proposes that the modulus (E_{co}) of ordinary sand can be obtained using the empirical relationship:

$$E_{co} = 2\, q_c \quad \ldots\ldots\ldots\ldots\ldots\ldots\ldots\ldots\ldots\ldots \quad (6)$$

where q_c = cone bearing value

In all probability, similar relationships could be developed for the usual types of subgrade found at airports. If this was done, the Dutch

cone test might then be an in situ test on which to base the choice of layer moduli. Since it is recognized, however, that the pavement problem is a problem of small deformations and not of total failure, the cone test is probably not a good simulation of the pavement problem. From this it follows that an apparatus such as the pressuremeter, which is able to evaluate moduli for small deformations, is likely to predict pavement behavior better than the cone test.

The triaxial test is used to measure the moduli of the pavement layers (44). During one type of test the cell pressure σ_3 is kept constant and the deviator stress is cycled from 0 to σ_d at a rate of 20 cycles per minute with a load duration of 0.2 seconds per cycle. The value of σ_d can be varied from one test to another as can the value of σ_3 which is used. During a test the recoverable axial strain (ε_z) is measured and the resilient modulus (M_r) is computed where:

$$M_r = \frac{\sigma_d}{\varepsilon_z} \quad \ldots\ldots\ldots\ldots\ldots\ldots\ldots\ldots\ldots\ldots \quad (7)$$

where σ_d = deviator stress.

This test has the definite advantage of being able to illustrate the variation in modulus with the magnitude of σ_3 and with the number of stress cycles. A major problem with the triaxial method of testing is the effect of sample disturbance; also, the test is time consuming, taking about one day at the best of times.

Poisson's ratio is difficult to measure and depends on the stress level and ambient temperature. Fortunately, Claessen et al (10) have determined that changes in Poisson's ratio have little effect on the two

critical strains (ε_h, ε_v); they recommend the use of an average value of 0.35 for the Poisson's ratio of the three layers: asphalt, base and subgrade.

2.2 The Ménard Pressuremeter

2.2.1 Basic Principles

The pressuremeter (Fig. 12) is made up of an inflatable cylinder (the probe) which is connected by a flexible tubing to a control unit (CPV). A circular hole is bored in the soil; the diameter of the hole is slightly larger than the diameter of the deflated probe. The deflated probe is lowered to the desired depth in the ground and then the probe is inflated. The CPV unit provides the pressure which is necessary to inflate the probe and records this pressure as well as the volume of water which is injected into the probe. A pressure volume curve is obtained (Fig. 13).

While Kögler worked with the first pressuremeter as early as 1933, it was Ménard who from 1954 to 1978 devoted much of his life to its development. Today (1979) many different types of pressuremeters exist; they can be classified into two broad categories: the Ménard pressuremeters and the self boring pressuremeters.

In this chapter, a typical Ménard pressuremeter (Fig. 15) will be described. Unless otherwise specified the pressuremeter is the type GA which is similar to the widely used GC model.

2.2.2 The Apparatus

- Probe.

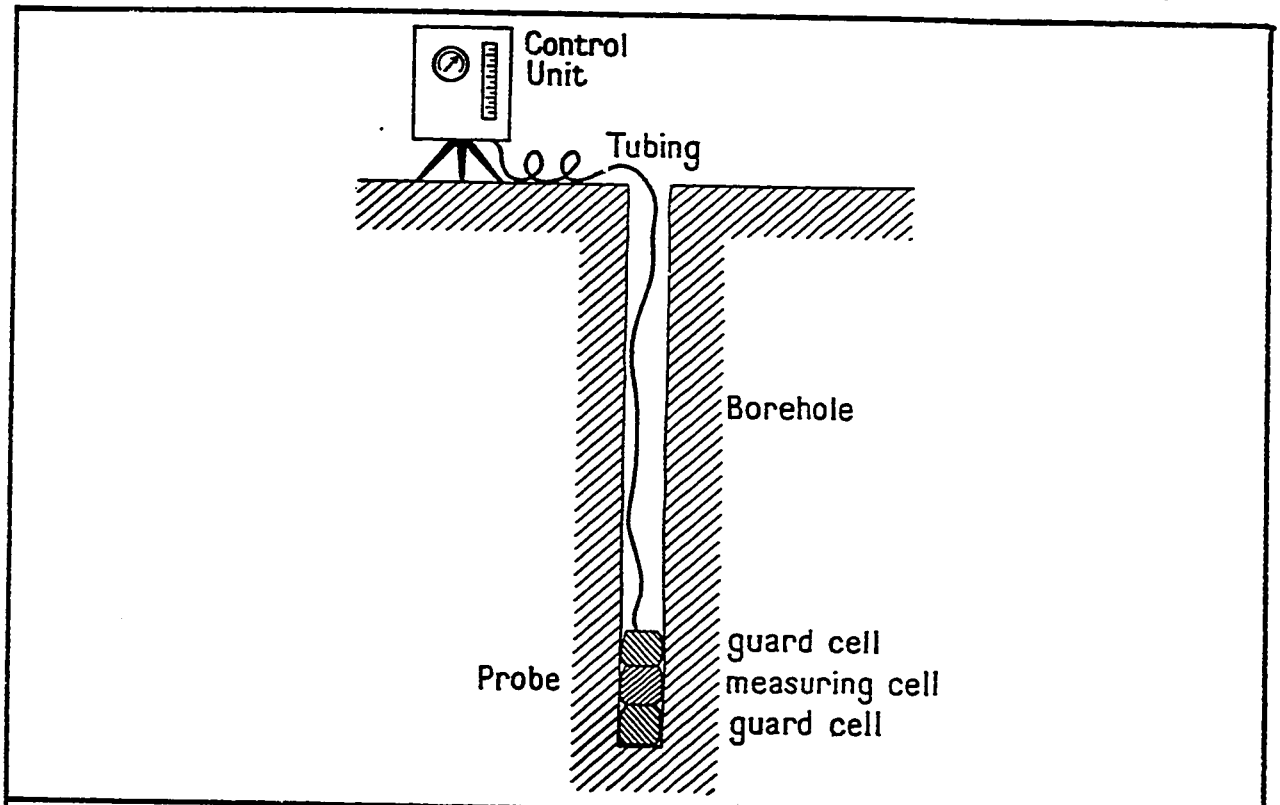

Fig. 12 – The Pressuremeter: Basic Diagram (from Baguelin et al, 1978).

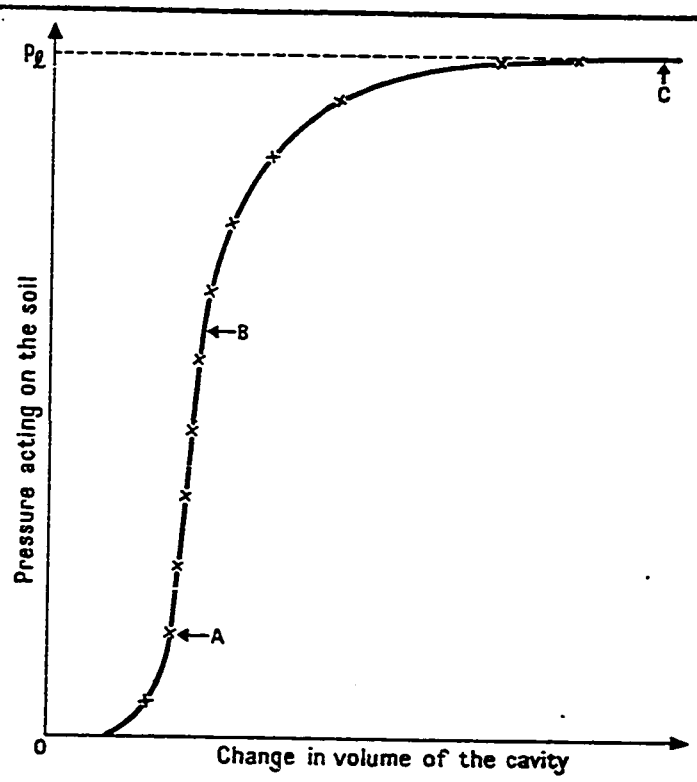

Fig. 13 – The Pressuremeter: Typical Result (from Baguelin et al, 1978).

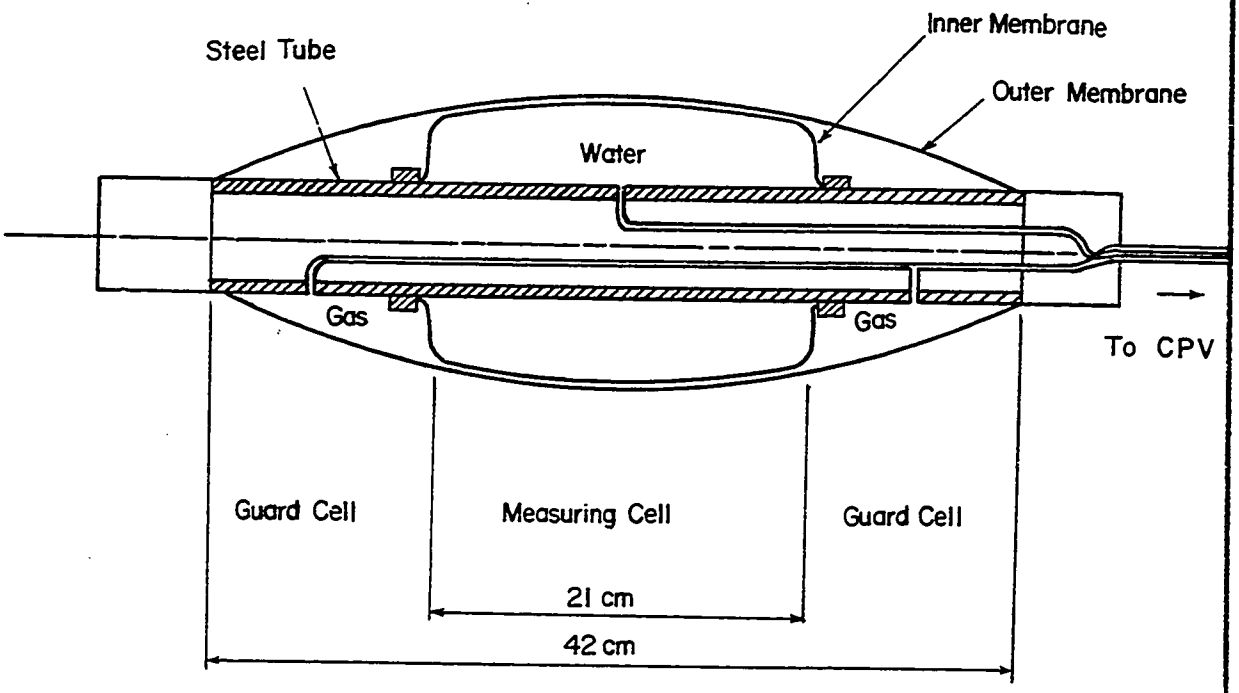

Fig. 14 -The GA Pressuremeter Probe: Basic Diagram.

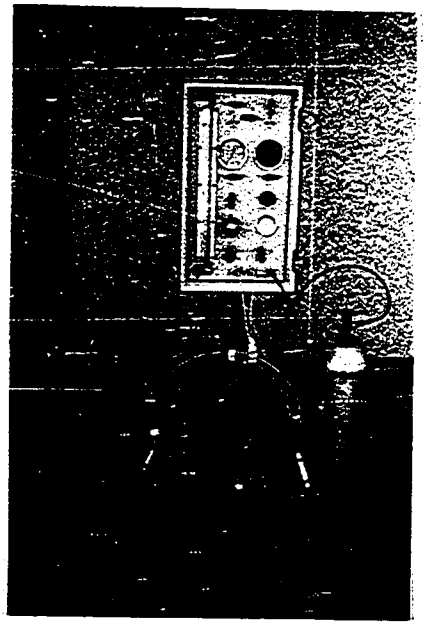

Fig. 15 -The Ménard GA Pressuremeter.

The backbone of the probe is a steel tube (Fig. 14); the middle half of the steel tube is covered by the inner rubber tube which is secured by the two steel rings. The chamber formed by this rubber membrane is the measuring cell. The entire length of the steel tube is covered by an outer rubber tube or sheath; the sheath is usually reinforced on the outside by metal strips and is secured at its ends by two steel rings. The BX probe has an active length of 42 cm and an outside diameter of 5.8 cm. Deflated, the measuring cell has a volume of 535 cm^3.

As the probe is inflated, the inner and outer membranes stay in contact (Section 2.2.4); this leaves an upper and a lower space between the steel tube and the outer membrane; these spaces are called the guard cells (Fig. 14).

The measuring cell is inflated with water and the guard cells with gas. Only the volume of water injected in the measuring cell is measured. The purpose of the guard cells is to take care of end effects and ensure that the expansion of the measuring cell is very close to cylindrical; the guard cells also prevent the inner rubber membrane from inflating up and down the hole rather than outward into the soil as desired.

- Tubing.

The nylon tubing is coaxial with the inner tubing carrying water to the measuring cell while the outer tubing brings gas to the guard cells. An advantage of coaxial tubing is that the pressures on both sides of the inner tubing are kept approximately the same; this means that the inner tubing will not dilate. If the tubing, carrying the water, were to dilate, part of the water coming from the control unit would not reach the probe and the volume change readings would be in error. The tubing inside diameters are approximately 4.5 mm for the inner tubing and 8 mm for the

outer tubing. Tubing lengths of 25 m are common.

- Control Unit.

A bottle of compressed gas provides pressure for the control unit. The water pressure is measured by a gauge and the volume of water injected into the probe is measured in a graduated cylinder. The capacity of the control unit is 2500 kPa of pressure and 800 cm^3 of water.

A detailed description of Ménard E, GB and GC pressuremeters can be found in Baguelin et al. (pp. 57-64 of (1)).

2.2.3 Making the Borehole

Getting the pressuremeter probe into the ground correctly is without doubt the most critical and difficult part of pressuremeter testing. Many different techniques are available; some techniques are practical and quick and some create little disturbance in the surrounding soil. Unfortunately, the more time saving methods generally cause the greatest amount of disturbance to the soil. The engineer must make a decision as to which method of insertion will give the optimum combination of the four basic parameters: time, cost, disturbance and precision. Of the four parameters, considerable weight must be given to minimizing disturbance if the results are to be meaningful.

As discussed in detail in Baguelin et al. (pp. 74-104 of (1)) the probe can be placed in the ground by:

1) inserting it in a predrilled hole. The hole can be made by rotary drilling (hand auger, continuous flight auger, blunt nosed drills, or core drills) or by percussion drilling (driving a sampler, percussion-rotation of a drill-bit, or

vibrating a sampler into place).

2) inserting it directly into the ground. In this case the probe is protected by a slotted steel tube and the whole assembly is either driven, jacked or vibrated down into the ground.

3) having the pressuremeter drill its own way into the ground (self boring pressuremeter).

Besides minimizing disturbance to the soil, the drilling technique which is employed to make a predrilled hole must make a hole which is well calibrated. The diameter of a well calibrated hole (ϕ_h) must be larger than the probe diameter (ϕ_p) by only a small amount. The following recommendations were made by Jezequel et al. (18):

- if $\frac{\phi_h}{\phi_p} < 1.17$, the test is to be discarded.
- ideally $\frac{\phi_h}{\phi_p} = 1.07$.

In an oversized hole, a large volume of water will have to be injected into the initially deflated probe just to bring the sheath into contact with the wall of the bore hole. This may mean that there will not be enough water remaining in the control unit to inflate the probe sufficiently to strain the soil laterally the required amount (Section 2.2.4); also, in an oversized hole, the lateral movement of the soil during a test will depart from right cylindrical expansion more than in a well calibrated hole. The major problem associated with a poorly calibrated hole, however, is that the membranes cannot be retained in place on the probe if the probe is made to expand the required amount to carry out a test properly; once the membrane clamping system fails, water escapes

and the test is terminated prematurely.

2.2.4 The Test Procedure

The correct procedure for a Ménard GA (or GC) pressuremeter test includes six steps which have to be executed in the following order:

Step 1. Saturating the circuits and the probe.

Step 2. Checking for leaks and saturation.

Step 3. Calibration of volume losses.

Step 4. Setting the initial volume.

Step 5. Calibration of membrane resistance.

Step 6. Testing.

These six steps are described in detail in Baguelin et al. (pp. 121-147 of (1)) and only a brief résumé will be made here.

Step 1. First the CPV, the tubing and the probe must be saturated. The probe is saturated by connecting it to the tubing and CPV, and then inflating it to 600 cm^3. When the probe-tubing connection is disconnected rapidly, water squirts out along with any entrapped air. Repeating this procedure three times generally ensures a satisfactory degree of saturation. The CPV and tubing are saturated initially by simply running the liquid through them until no air bubbles are apparent.

Step 2. To check for leaks and saturation, the probe is inserted in a thick walled steel tube (Fig. 15) and pressurized to 500 kPa. A volumeter reading is taken after one minute and three minutes. The procedure is repeated for 2000 kPa of pressure. If the volumeter reading changes noticeably between the one and three minute readings,

there is a leak. Satisfactory saturation of a GA or GC pressuremeter is reached when the change in volumeter reading between 500 kPa and 2000 kPa is less than 0.15 cm^3 per meter of tubing.

Step 3. Calibration for volume losses consists of the following: note the temperature, insert the probe in the steel tube, then raise the pressure by increments of 100 kPa to 500 kPa followed by increments of 300 kPa to 2500 kPa. Each pressure increment is held for one minute and a volumeter reading is taken at the end of each pressure increment. A pressure-volume curve is drawn (Fig. 16 (a)). At first the probe expands into contact with the steel tube; this means there is a large increase in volume for a small increase in pressure (first part of the curve on Fig. 16 (a)); judgement must be used to decide on the point of good contact (say, 360 kPa on Fig. 16 (a)). After the membrane is in contact, there is only a small increase in the volumeter reading with an increase in pressure; since the steel tube does not expand, the change in reading corresponds to the volume losses in the tubing, the control unit and the probe (second part of the curve on Fig. 16 (a)). It remains to evaluate the volume losses between zero pressure and the contact pressure (between 0 and 360 kPa in this case); to make this evaluation, a calibration test is run with the probe disconnected and the end of the tubing closed off (plugged)(Fig. 16 (b)). As is shown on Figure 16 (b), the volume loss A at 360 kPa is determined; this value is then transferred to Figure 16 (a) after the tangent to the point of full contact (360 kPa) is extended back to the volumeter reading axis (curve ii on Fig. 16 (a)). This last

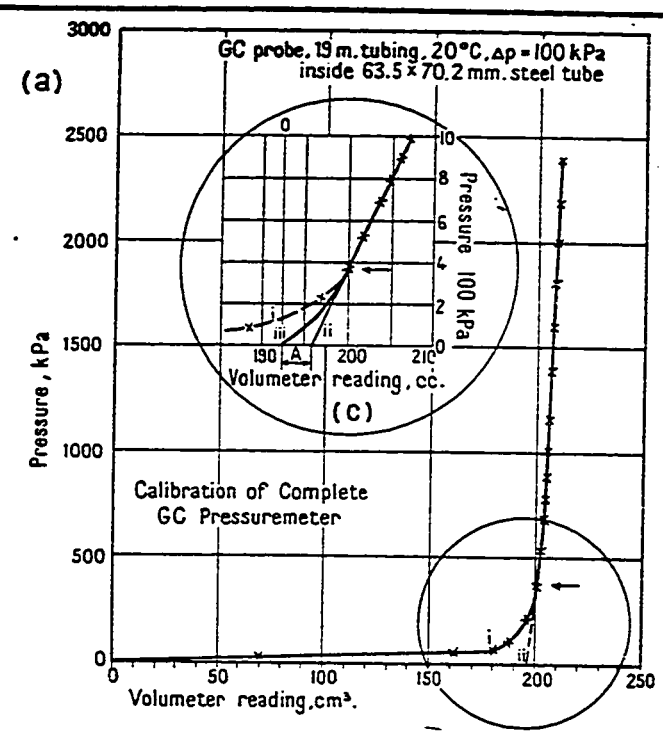

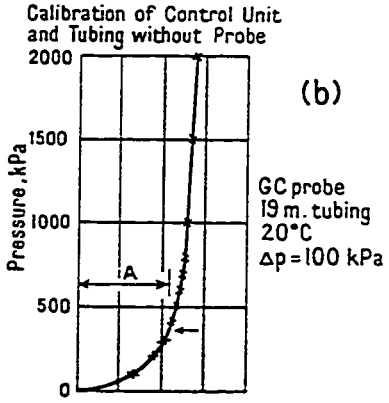

Fig. 16 - Volume Calibration for a GC Pressuremeter (from Baguelin et al, 1978).

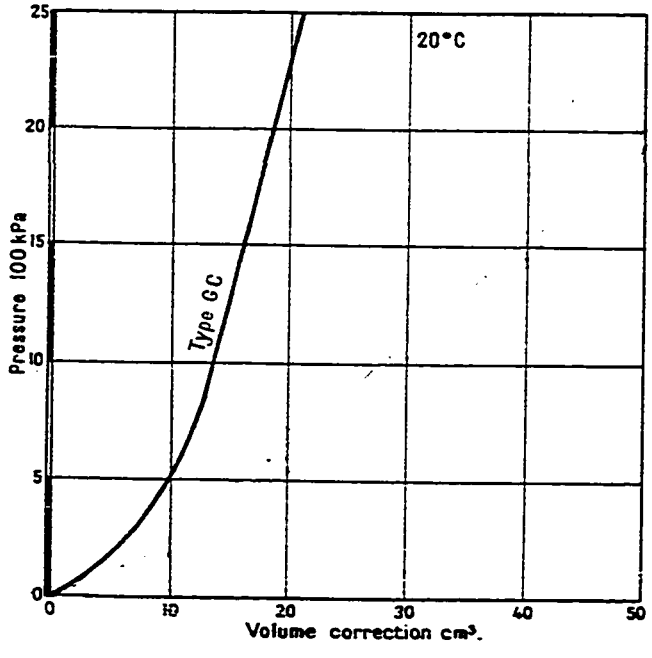

Fig. 17 Typical Volume Calibration for a GC Pressuremeter (from Baguelin et al, 1978).

operation is shown more clearly in the enlargement of Figure 16 (c). The calibration curve of volume losses is curve iii of Figure 16 (c) with the new origine '0' illustrated as a vertical line. A typical volume correction curve is shown in Figure 17.

It must be noted that in the GA (and GC) pressuremeter, the pressure in the guard cells must always be 100 kPa lower than the pressure in the measuring cell; this means, for example, that 500 kPa in the pressuremeter consists of putting 500 kPa in the measuring cell and 400 kPa in the guard cells. This requirement must be respected throughout the calibration of the pressuremeter as well as during an actual test.

Step 4. Setting the initial volume consists of the following: measure exactly the inside diameter of the steel tube (ϕ_t), set the volumeter and pressure gauge to zero, insert the probe in the steel tube, put 500 kPa pressure in the pressuremeter and take the volumeter reading (v_v) after one minute. The probe and the steel tube must be placed at the same horizontal level as the CPV unit so that the hydrostatic pressure in the probe is zero. Under the 500 kPa of pressure the membrane is now in good contact with the steel tube and the volume of the measuring cell is:

$$V = \frac{\pi}{4} \phi_t^2 \ell_o \quad \ldots\ldots\ldots\ldots\ldots\ldots\ldots\ldots\ldots\ldots \quad (8)$$

where ℓ_o is the length of the measuring cell.

The volumeter reading (v_m) that is required for the zero volumeter reading to correspond to a reference initial volume V_c of the measuring cell when the pressure reads zero is:

$$v_m = V + v_d - V_c \quad \ldots\ldots\ldots\ldots\ldots\ldots\ldots\ldots\ldots\ldots \quad (9)$$

where v_d is the volume correction at 500 kPa and V_c = 535 cm^3 as set by Menard for the GA pressuremeter. Generally, v_v is different from v_m; in order to have for a zero pressure reading, a zero volumeter reading that corresponds to the reference initial volume V_c it is necessary to:

- add $v_v - v_m$ of water to the volumeter if $v_v > v_m$
- drain $v_m - v_v$ of water from the volumeter if $v_m > v_v$.

Step 5. Various curves of membrane resistance calibrations are shown on Figure 18; the curves illustrate the fact that, although the probe is free to expand, a certain amount of pressure is required to overcome the resistance of the membrane. The procedure for calibration of the membrane is as follows: stand the probe upright on the ground; inflate and deflate the probe fully five times without taking any readings, in order to 'work' the rubber; then, inflate the probe in about 10 one minute pressure increments up to its maximum working volume while recording the pressure (p_m) and the volumeter reading (v_m) at the end of each pressure increment. The pressure in the measuring cell (p_r) is given by:

$$p_r = p_m + \gamma_w h_o \quad \ldots\ldots\ldots\ldots\ldots\ldots\ldots\ldots\ldots\ldots \quad (10)$$

where h_o is the difference in elevation between the gauge of the control unit and the middle of the probe during calibration and γ_w is the unit weight of water. The plot of p_r versus v_m is the curve of membrane resistance.

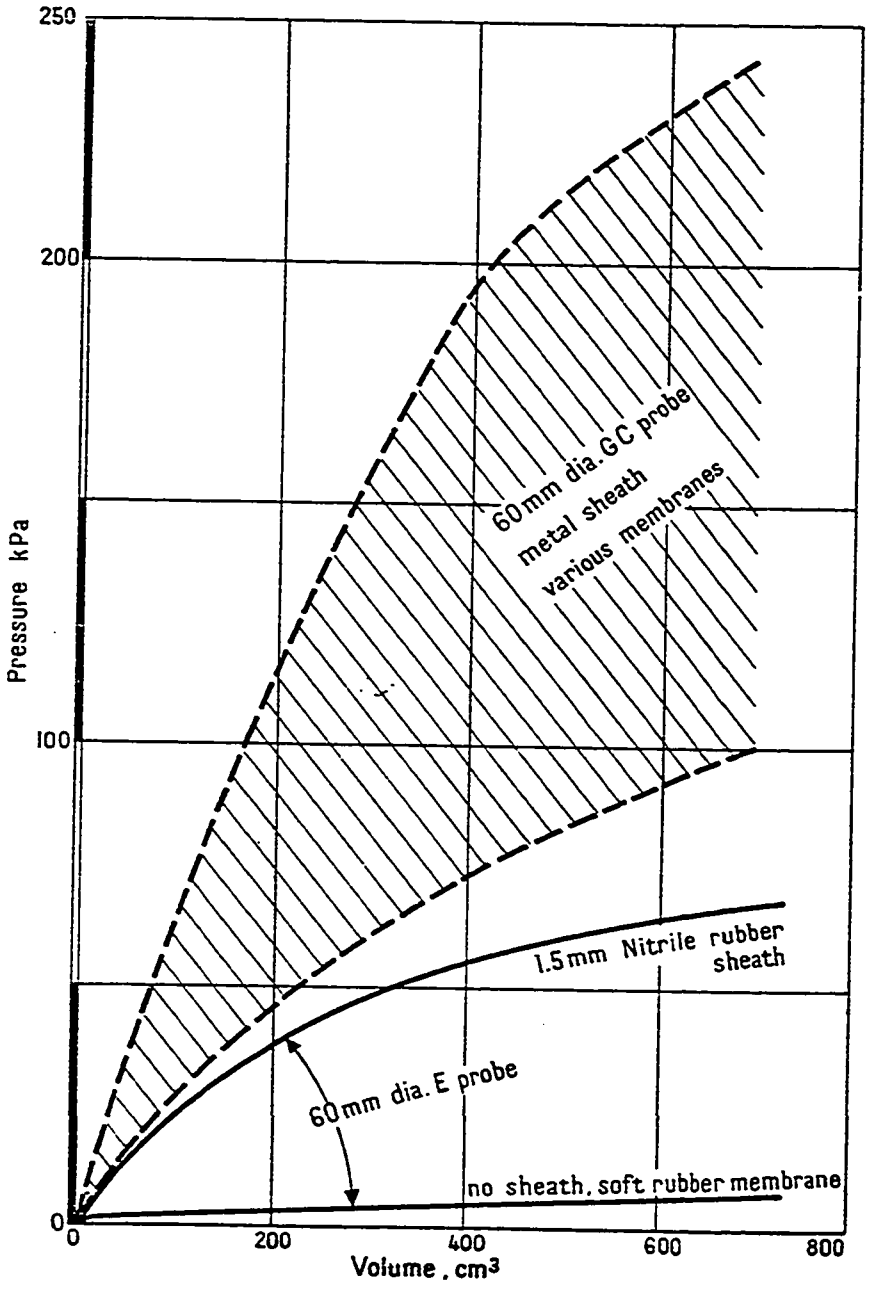

Fig. 18 - Typical Membrane Calibration for E and GC Probe (from Baguelin et al 1978).

Step 6. Only after the five previous steps have been performed can a test or series of tests be performed. Immediately after making the bore hole, the probe is positioned in the hole. The hydrostatic pressure acting in the measuring cell of the probe is:

$$\gamma_w (z + h_o)$$

where z is the depth from the ground surface to the center of the probe and γ_w and h_o were defined in Step. 5. The differential pressure gauge setting must be altered to take into consideration the fact that the hydrostatic pressure acting in the measuring cell is now making up part of the required 100 kPa difference between the pressure in the guard and measuring cell (p. 138 of (1)). The test is then carried out in 10, equal, one minute pressure increments. Ideally on the 10th increment, the limit pressure should be reached, that is to say, the size of the cavity should have doubled. In practice if the number of pressure increments required to read the limit pressure is from eight to 14 the test is acceptable. Volume readings are taken at 15, 30 and 60 seconds during the one minute when the pressure is held constant at p_m; the 60 second volumeter reading is v_m. The p_m versus v_m curve is called the raw pressuremeter curve. Figure 19 illustrates typical field notes and Figure 20 shows the corresponding raw pressuremeter curve.

2.2.5 Reduction of Data

Reducing pressuremeter data includes correcting the raw pressuremeter curve, calculating the pressuremeter modulus (E_M) and calculating the

PRESSUREMETER TEST

Job No: 122. Date: 23/2/76
Site: Strowtiff Tech: J.K.T

Hole No. 24 Tool dia. 60mm Type. Hand Auger / mud
Depth. 1m Gauge Ht 0.6m Water level. 1-5m Soil. Clay
Volumeter No. 424 Probe dia. BX Mem. Rubber Sheath. Nitrile
Rec.Press.Diff. 140kPa Water Press.10(Z+ho). 14kPa Diff.Req'd. 36

Pressure	Volume	Pressure	Volume
0		800	252
	8		258
			265
100	128	900	295
	143		309
	147		323
200	175	1000	376
	178		395
	181		416
300	186	1100	540
	188		590
	190		648
400	194	1140	750
	198		
	200		
500	205		
515	209		
	209		
600	214		
	217		
	220		
700	225		
	228		
	233		

Test Started at: 11:13 finished at: 11:29
Refer to membrane resistance: R 293-76

Fig.19 – Pressuremeter Form with Field Notes (from Baguelin et al, 1978).

Fig. 20 Raw Pressuremeter Curve (from Baguelin et al, 1978).

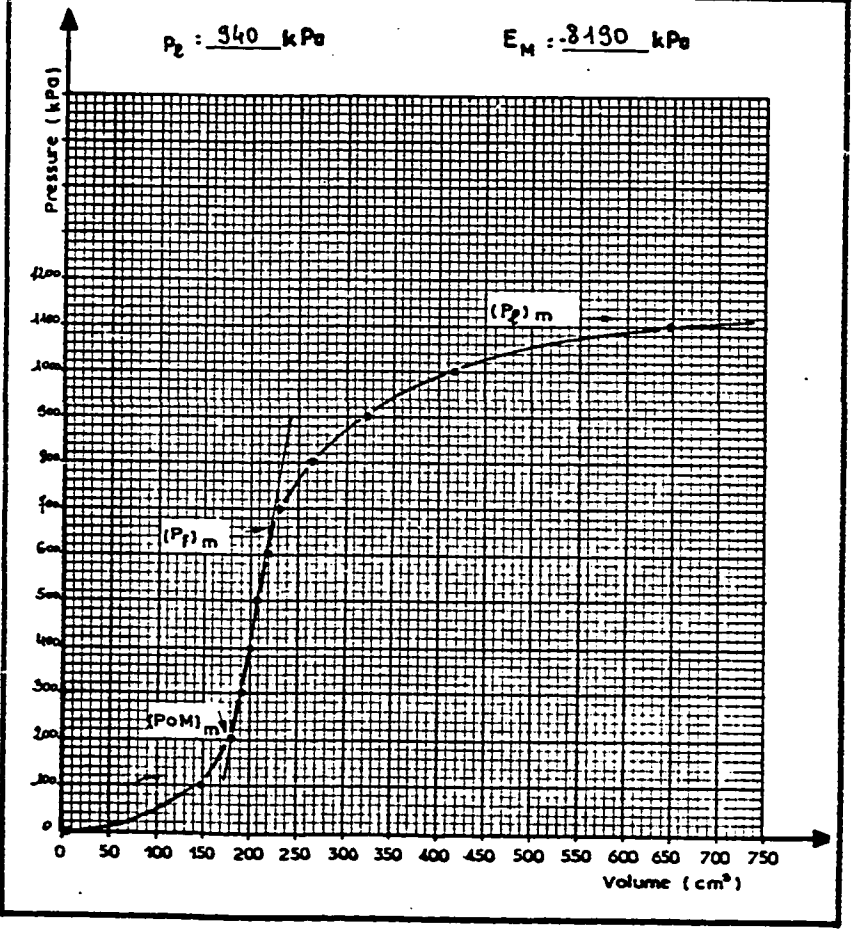

net limit pressure (p_ℓ^*).

The raw pressuremeter curve must be corrected for volume losses, membrane resistance and hydrostatic pressure. If the raw coordinates of a point are p_m, v_m, first the hydrostatic pressure $(h_o + z)\ \gamma_w$ is added to p_m (Fig. 21). Secondly, the volume correction (v_d) corresponding to $p_m + (h_o + z)\ \gamma_w$ is obtained from the calibration curve of volume losses (Fig. 16 (c) reproduced on Fig. 21) and is subtracted from v_m ($v_m - v_d$). Thirdly the membrane resistance (p_i) at the volume $v_m - v_d$ is obtained from the curve of membrane calibration (one curve of Fig. 18 reproduced on Fig. 21) and is subtracted from $p_m + (h_o + z)\ \gamma_w$ to give $p_m + (h_o + z)\ \gamma_w - p_i$. The corrected coordinates p, v are obtained from the raw coordinates p_m, v_m by:

$$p = p_m + (h_o + z)\ \gamma_w - p_i \quad \ldots\ldots\ldots\ldots\ldots\ldots \quad (11)$$

$$v = v_m - v_d \quad \ldots\ldots\ldots\ldots\ldots\ldots\ldots\ldots \quad (12)$$

The raw curve is corrected point by point to obtain the corrected curve.

The corrected curve represents the variation of the pressure against the wall of the cavity versus the increase in volume of the measuring cell. The increase in volume at zero pressure (0 to A on the curve of Figure 22) corresponds to the expansion of the measuring cell from the deflated position to the position where it comes into contact with the wall of the bore hole. From A to B, the probe is said to push the wall of the bore hole back to the original position it was in, before yielding of the wall occurred into the hole. The volume of the measuring cell at B corresponds to the original size of the cavity (V_o). From B to C,

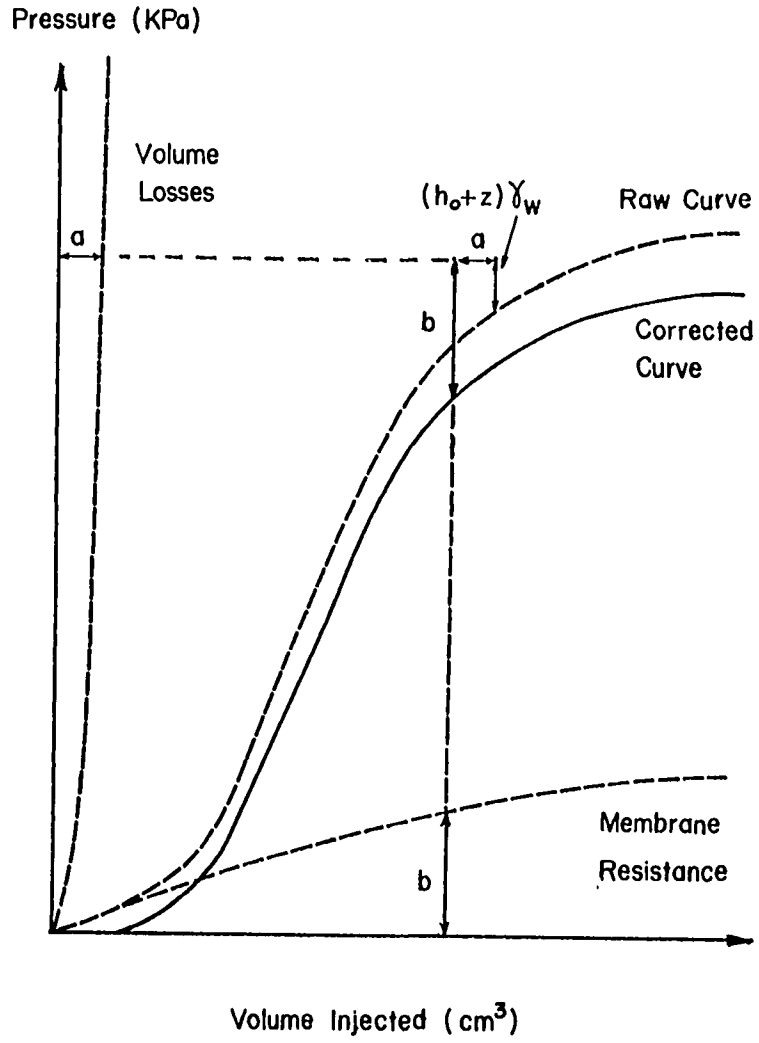

Fig. 21 - Correcting a Raw Pressuremeter Curve.

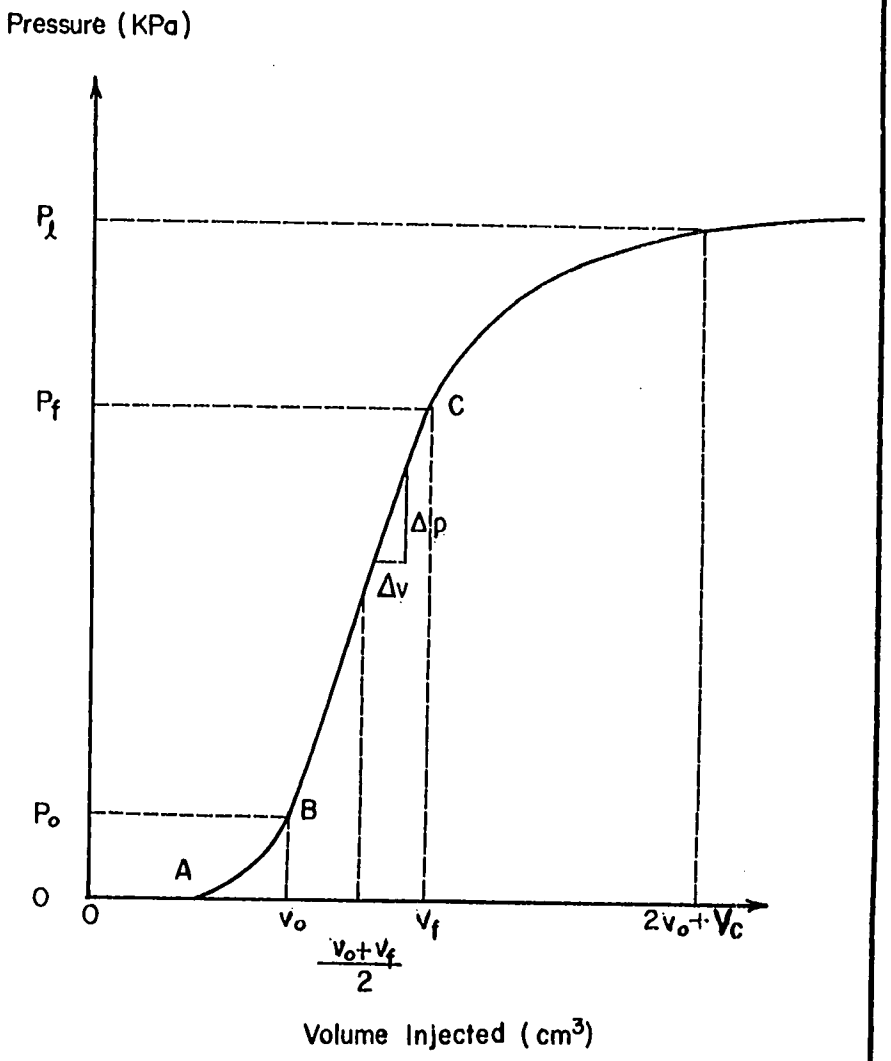

Fig. 22 - The Pressuremeter Parameters.

the soil deforms more or less linearly with increasing pressure and this phase is referred to as the elastic phase of the test. At C, the soil yields non linearly and the plastic phase commences.

The pressuremeter modulus is calculated in the elastic phase; the modulus is computed from the equation for the radial expansion of a cylindrical cavity in an infinite elastic medium developed by Lamé in 1852 (p. 153 of (1)):

$$E_{e\ell} = 2(1+\nu)\ V \frac{\Delta p}{\Delta V} \quad \ldots\ldots\ldots\ldots\ldots\ldots\ldots\ldots \quad (13)$$

where $E_{e\ell}$ = modulus of elasticity.

ν = Poisson's ratio.

V = volume of the cavity.

Δp = increase in pressure against the wall of the cavity.

ΔV = increase in volume of the cavity.

For the pressuremeter, the change in the volume of the cavity (ΔV) is equal to the change in the volume of the measuring cell (Δv) and $\frac{\Delta p}{\Delta V}$ is, therefore, the slope of the corrected pressuremeter curve.

The slope is constant but the volume V is not; as a result $E_{e\ell}$ will increase from A to B. Poisson's ratio also varies from soil to soil and depends on the drainage condition during the test. Ménard suggested the following simplifying rules in order to facilitate calculating the pressuremeter modulus (E_M).

1) Take V equal to V_m; V_m is the volume of the cavity corresponding to the midpoint of BC

2) Take 0.33 as the value of ν (this choice is discussed on page 197).

The following equation gives V_m (Fig. 22):

$$V_m = V_c + \frac{v_o + v_f}{2} \quad \ldots\ldots\ldots\ldots\ldots\ldots\ldots\ldots \quad (14)$$

where v_o = the volume injected at the beginning of the elastic phase,

v_f = the volume injected at the end of the elastic phase,

V_c = the initial volume of the measuring cell.

Then $$E_M = 2.66\ V_m \frac{\Delta p}{\Delta v} \quad \ldots\ldots\ldots\ldots\ldots\ldots\ldots\ldots \quad (15)$$

The limit pressure (p_ℓ) is by definition the pressure which is reached in order to double the original size of the cavity. Since,

$$V_o = V_c + v_o \quad \ldots\ldots\ldots\ldots\ldots\ldots\ldots\ldots \quad (16)$$

the limit pressure corresponds to an increase in measuring cell volume of $2\ v_o + V_c$ (Fig. 22). The net limit pressure (p_ℓ^*) is defined as:

$$p_\ell^* = p_\ell - p_{oh} \quad \ldots\ldots\ldots\ldots\ldots\ldots\ldots\ldots \quad (17)$$

where p_{oh} is the total stress, initial horizontal earth pressure at a depth in the ground corresponding to the center of the probe.

2.2.6 Present Use of the Pressuremeter Test

Today (1979) the pressuremeter test is used primarily in foundation engineering. Based on a semi-empirical approach, design rules (Chapter

3 of (1)) make use of p_ℓ^* for estimating ultimate bearing capacity, E_M for estimating settlement and the entire p - v curve for estimating the horizontal capacity of piles. In the case of self boring pressuremeters, theory is available to calculate the undrained shear strength (c_u) of clay and special field techniques allow the coefficient of earth pressure at rest (K_o) to be measured.

2.3 The Pressuremeter and Pavement Design

2.3.1 Literature Review

No previous publications were found dealing with the specific topic of the use of a pressuremeter to design pavements.

2.3.2 Related Topics in the Literature

During the literature search, a few publications were found that related indirectly to the subject. For example, the pressuremeter has been used for compaction control. Ménard (30) carried out, in parallel, minipressuremeter tests and CBR tests in a compacted embankment and found the following relationship:

$$CBR = 1.7 \times 10^{-2} \, p_\ell \quad \ldots\ldots\ldots\ldots\ldots\ldots \quad (18)$$

where p_ℓ is the limit pressure in kPa. Ménard claimed that this relationship is accurate to within 10%. In 1972, Tavenas and Blanchet[5] carried out about 30 minipressuremeter tests at depths ranging from 0 to 3 m in a compacted embankment and compared the results with density measurements.

5. Blanchet, G., Oral Communication, April 1978.

Lai (24) also performed shallow pressuremeter tests in sand deposits of different densities. Ménard (32) used the pressuremeter to check the efficiency of his huge dynamic consolidation machines at numerous sites around the world while Michel Poteur[6] used a pressuremeter to investigate the soil improvement which was obtained in the vibroflotation process.

All these researchers found that, in general, the relationship between the soil unit weight and the pressuremeter parameters E_M and p_ℓ is poor; this finding is understandable since both the modulus and the limit pressure depend on more than just the unit weight of the soil. The same researchers found, however, that the pressuremeter consistently will indicate a change in material behavior brought about by some physical process such as compaction.

The pressuremeter has been used to evaluate the properties of ice covers. As is the case with pavements, pressuremeter testing of ice covers involves testing relatively thin layers of material close to a free boundary. Ladanyi and Saint-Pierre (23) used a Ménard pressuremeter (type G, probe diameter: 62.2 mm, active probe length: 400 mm) to test a 1.5 m thick sea ice cover; they state that the equipment performed well and was quite convenient. They do not comment on the potential problem raised by the proximity of a free boundary.

---

6. Jezequel, J.-F., Oral Communication, April 1978.

CHAPTER 3

NEW IDEAS

This chapter explains 1) why the pressuremeter test has numerous potential advantages over, for example, the McLeod plate test and the CBR test for pavement design and 2) why a special pavement pressuremeter and test, different from the Ménard pressuremeter and test, are required. This explanation involves presenting 1) the advantages and disadvantages of the McLeod plate test and the CBR test, 2) the major differences between foundation engineering, where the Ménard pressuremeter is used, and pavement engineering, 3) the requirements for a pavement pressuremeter, 4) a brief description of the proposed pressuremeter and test for pavements and 5) the advantages and disadvantages of the Briaud pressuremeter test.

3.1 Advantages and Disadvantages of the McLeod Plate Test and the CBR Test

Some of the advantages and disadvantages of the wave propagation test, the triaxial test, the cone test are presented in Section 2.1.5. This section concentrates only on the McLeod plate test and the CBR test as they apply to the design of pavements.

3.1.1 Disadvantages

- McLeod plate test

The McLeod plate test is expensive: a truck and rubber water container (Fig. 2) cost about 100,000 dollars (1978) and must be replaced

regularly; running a test costs, on average, 1,000 dollars.

The McLeod plate test is time consuming, the standard test (10 repetitions of load) takes about eight hours and the nonrepetitive test takes about two hours.

The McLeod plate test requires heavy equipment that cannot be sent by air; only two trucks such as the one shown in Figure 2 are available in Canada and each summer they travel from coast to coast. Plate tests can be carried out only at airports which are accessible by highway.

In addition to the foregoing major disadvantages, the McLeod plate test is performed only after the pavement is built and the test is useless as a design tool for new pavements; the evacuation of the equipment from the runway is slow, and the test relates more to the load of a single wheel than of a multiple wheel gear. Of practical importance is the fact that only the deflection of the surface is measured; no direct assessment can be made of the pavement with depth. If there is a problem (there is too much deflection of the surface) it is impossible to tell which pavement component is at fault.

- CBR Test

The CBR test can be performed in the laboratory or in the field; if the test is carried out in the field a small pit must be opened up through the pavement in order to test each layer which makes up the pavement and the subgrade. The in situ CBR test is therefore a semi-destructive test. The laboratory CBR test has the specific drawback that it requires a sample. The samples are more or less disturbed and in the case of cohesionless soils, the samples have to be reconstructed by some method. As a result, it is difficult to assess the validity of the test results.

Both field and laboratory CBR tests are small scale plate tests

which raises the question of scale effects.

3.1.2 Advantages

- The McLeod plate test is a non destructive in situ test that simulates well the load of a single wheel.

- The CBR test is simple, portable and widely used.

3.2 Differences Between Pavement Engineering and Foundation Engineering

The Ménard pressuremeter is used in foundation engineering. It is now proposed to use some type of pressuremeter in pavement engineering. Some basic differences between pavement engineering and foundation engineering are presented here.

A first difference is that the contact pressure under an airplane tire can be twice that under a footing; for example, in the strongest soil categories the safe bearing capacity of a building foundation is about 700 kPa, whereas the contact pressure under the wheel of a large plane is about 1500 kPa.

A second difference concerns the range of dimensions involved in foundation and pavement engineering; the width of the contact area in foundation engineering varies from about 0.3 m for a pile tip to several hundred meters for a dam, whereas, the largest wheel width is about 0.45 m (Fig. 1). Therefore, in pavement engineering the depth of influence of the load is much shallower than in most foundation problems. Using a Boussinesq distribution, the vertical stress at 1.8 m depth from a wheel 0.45 m wide is less than 5% of the contact pressure.

A third difference between pavement and foundation engineering is that in pavement design the allowable bearing pressure must be only a

small fraction of the ultimate bearing capacity. Pavement design is a problem of limiting permanent deformation, particularly after a large number of load repetitions. The reason for limiting permanent deformation is to guarantee a smooth runway surface for take-off and landing. Given this fact, that deformation controls runway design, it is the modulus of deformation that is of interest in a pressuremeter test and not the limit pressure.

3.3 Requirements for a Pavement Pressuremeter

It must be emphasized that in setting the requirements for the pavement pressuremeter and the corresponding test procedure, the intent was to obtain a very practical in situ test, not a research tool; this means that consideration was given not only to the precision of the measurements but also to the practicality of the test.

To be practical, an in situ testing apparatus must be simple, robust and inexpensive; a monocellular probe would be preferable to a tricellular probe and single tubing would be preferable to coaxial tubing.

Since the test must be run in the base course and the intent is to make a reasonable number of measurements within the shallow depth of influence of a wheel, the pressuremeter probe has to be short.

The modulus of deformation of the soil must be measured accurately. This means that a strain controlled test will be preferable to a stress controlled test unless the load increments are made numerous. Strain control also facilitates cycling the expansion of the probe to obtain a cycled modulus.

In light of the above requirements, it was decided that the pavement

pressuremeter would have a short monocellular probe, single tubing, and a simple control unit which was designed specifically for the execution of strain controlled tests (Fig. 23). The Ménard pressuremeter has a long tricellular proble, a coaxial tubing and a control unit specifically designed for a stress controlled test. It was, therefore, necessary to build a pressuremeter specifically adapted for use in pavement design: the Briaud pressuremeter.

3.4 Proposed Pressuremeter and Pressuremeter Test for Pavements

The proposed apparatus and test procedure are largely inspired by the work of L. Ménard and J-F. Jézéquel. To prevent confusion with other pressuremeters and test techniques and for the purpose of referal, the apparatus and the procedure which are proposed for pavement design will be referred to as the Briaud pressuremeter and test procedure. The Briaud pressuremeter and test procedure are described in detail in Chapter 4; this section describes them only briefly.

The working principles of the new apparatus are as follows (Fig. 23): the wheel of the hand pump is rotated at a constant rate which, in turn, advances the piston at a constant rate; the volume of water which is injected into the tubing and probe is indicated by the movement of a columm of tinted kerosene; the pressure is measured by the pressure gauge.

The probe has a diameter of 32 mm and an active length of 230 mm. It is monocellular and is inflated with water. A 5 m long single nylon tubing connects the probe to the control unit. The control unit is made simply of a triaxial test hand pump, a pressure gauge and a triaxial test burette for volume measurements (Fig. 23).

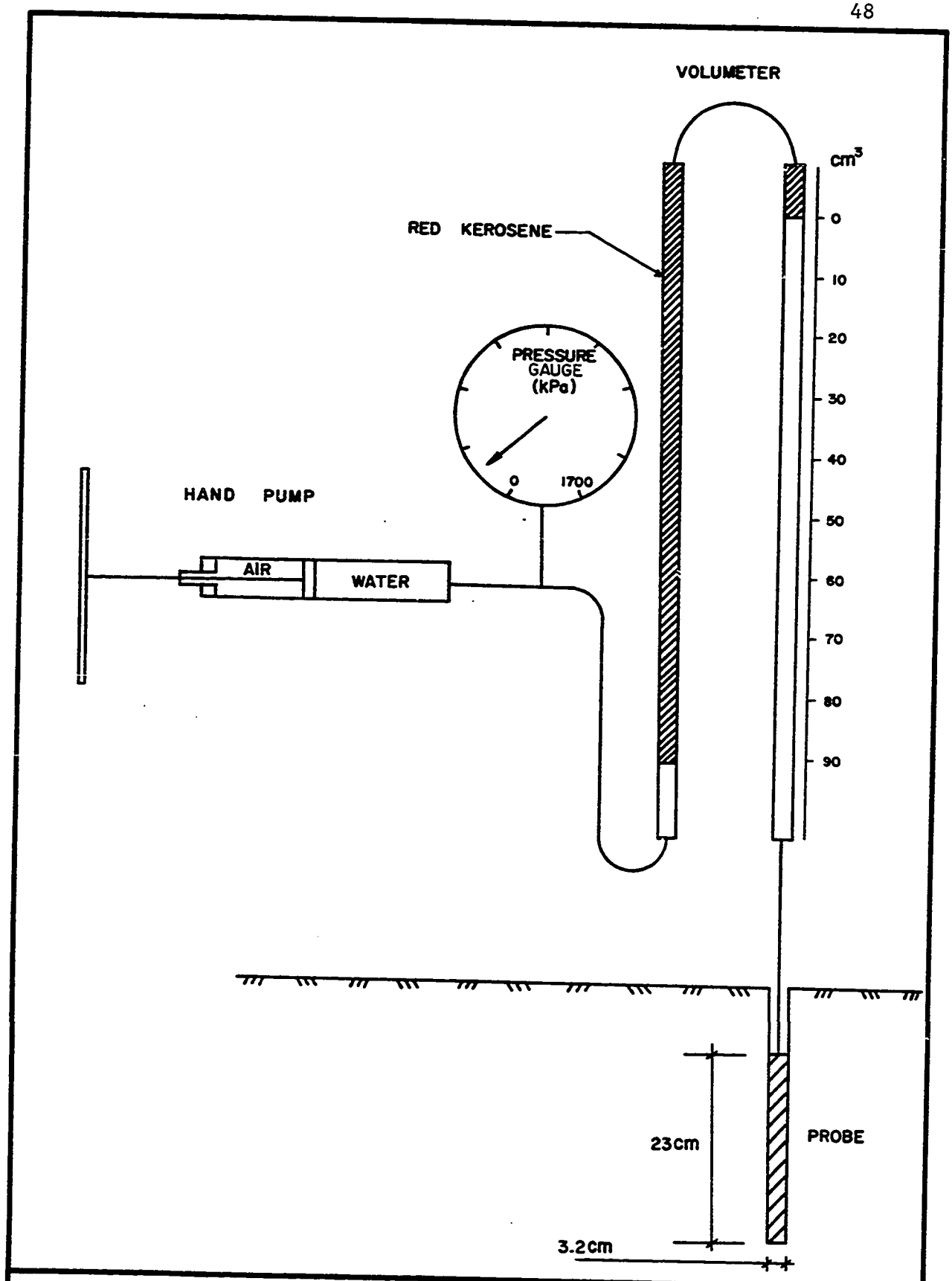

Fig. 23 - The Briaud Pressuremeter: Basic Principles.

The hole is made by driving a 34.9 mm diameter E rod through the pavement down to a depth of 2 m; the E rod is withdrawn and the probe is inserted into the hole at 1.8 m depth. A test is performed and then the probe is withdrawn up the hole to the 1.5 m depth where a second test is performed. The procedure is repeated at 0.3 m intervals up to the level of the pavement.

Driving the E rods takes from two to 10 minutes and one pressuremeter test takes on average 6.5 minutes. Therefore, a station (one hole, six tests) can be tested in an hour. Furthermore the pressuremeter equipment can be carried and handled by two persons. The equipment used for making the bore hole also could be portable.

3.5 Advantages and Disadvantages of the Briaud Pressuremeter and Test

3.5.1 Disadvantages

The Briaud pressuremeter test requires a 32 mm diameter hole through the pavement; this, according to Transport Canada practice is not a major drawback since a hole of this size can be backfilled and patched easily.

The pressuremeter loads the soil laterally, not vertically. This apparent criticism can be challenged by the following arguments. First, pressuremeter tests have been done in vertical and then horizontal bore holes (p. 594 of (1)) in a wide range of soils and the results show that the horizontal and vertical moduli are within 5% of each other. Also, Shields and Bauer (40) report similar results for horizontal and vertical plate test in a sensitive clay. Second, the wheel of a plane does not get soil support only from vertical soil reaction but also from

horizontal soil reaction. Third, as a comment more than an argument, if the characteristics of the pavement layers are to be found, the most logical way of doing this is to test the layers separately; separate tests can only be done by horizontal loading since vertical loading will involve more than one layer.

Although, as discussed above, pressuremeter and plate tests have not shown any influence of soil anisotropy in many cases, it is well accepted that soils exhibit varying degree of anisotropy. This anisotropy is attributable to geological processes (for example: sedimentation) and to the stress history of the soil. Both cause a difference between the horizontal and vertical soil structure and grain orientation which are responsible for anistropic properties. It seems that the ratio between horizontal and vertical moduli (E_h and E_v) generally varies between 0.5 and 2 (51). The influence of modulus anisotropy on the settlement of a rigid plate on an elastic half space can be evaluated (52); when $\frac{E_h}{E_v}$ varies between 0.5 and 2 and for different Poisson's ratio, the settlement of the plate will vary by 53%.

3.5.2 Advantages

The Briaud pressuremeter has a number of advantages. It is an inexpensive in situ test; for the price of the truck and rubber container required for the plate test, it is probable that all major airports in Canada could be equipped with a Briaud pressuremeter. Once equipped with the pressuremeter, it would then be only a matter of training local crews to make, say, a yearly evaluation of the pavement at this airport.

The pressuremeter is readily carried by two men and is easy to ship. Because of its portability, the equipment can be evacuated from the runway in only a few minutes.

The pressuremeter test is relatively quick, each test takes some 6.5 minutes and in an eight hour day a trained crew can perform, on average, some 48 tests (eight stations).

The pressuremeter tests give a profile of six moduli with depth at each station. The average magnitude of the six moduli allows an assessment of the overall pavement strength. The profile of the six moduli indicates the variation of pavement strength with depth and can be used, for example, to single out a weak layer. The location of a weak layer cannot be determined from the McLeod plate test. Therefore, the pressuremeter modulus profile allows the pavement engineer to better judge the cause of pavement weakness and therefore to better remedy the problem.

The Briaud pressuremeter test can be performed before, during or after the construction of the pavement; the test can, therefore, be used not only for the evaluation of existing pavements and the design of overlays but also for the design of new pavements.

The moduli measured during the pressuremeter tests can be considered as basic parameters that are more suited to the study of pavement performance under any wheel configuration (through the use of the elastic theory for example) than is the one plate parameter.

CHAPTER 4

THE BRIAUD PRESSUREMETER TEST

This chapter presents a detailed description of the Briaud pressuremeter with a discussion of the influence of its special features on the test results. The procedure used in this study to make the bore hole (in which to insert the pressuremeter probe) is given, and the soil disturbance generated by this procedure is discussed in light of related test results and a literature survey. The step by step procedure for running the test is explained as well as the way in which the collected data is reduced.

Version No. 1 of the Briaud pressuremeter was built in July 1977; this apparatus was used throughout the study and is described in detail in Briaud and Shields (6). Once the testing program was over, the experience gathered during four months of continuous use was employed to design and build Version No. 2. Version No. 2 incorporated a number of practical improvements but operated on the same principles as Version No. 1. Since Version No. 2 is the only version which will be proposed to the industry, it is the one which is described in detail in this chapter.

4.1 The Probe and the Tubing

4.1.1 Description

The Briaud pressuremeter probe is made of three parts: the body, the membrane and the sleeves (Fig. 24). The body is a metal tube 500 mm in length and 25 mm in diameter (Fig. 25); it is threaded at both ends

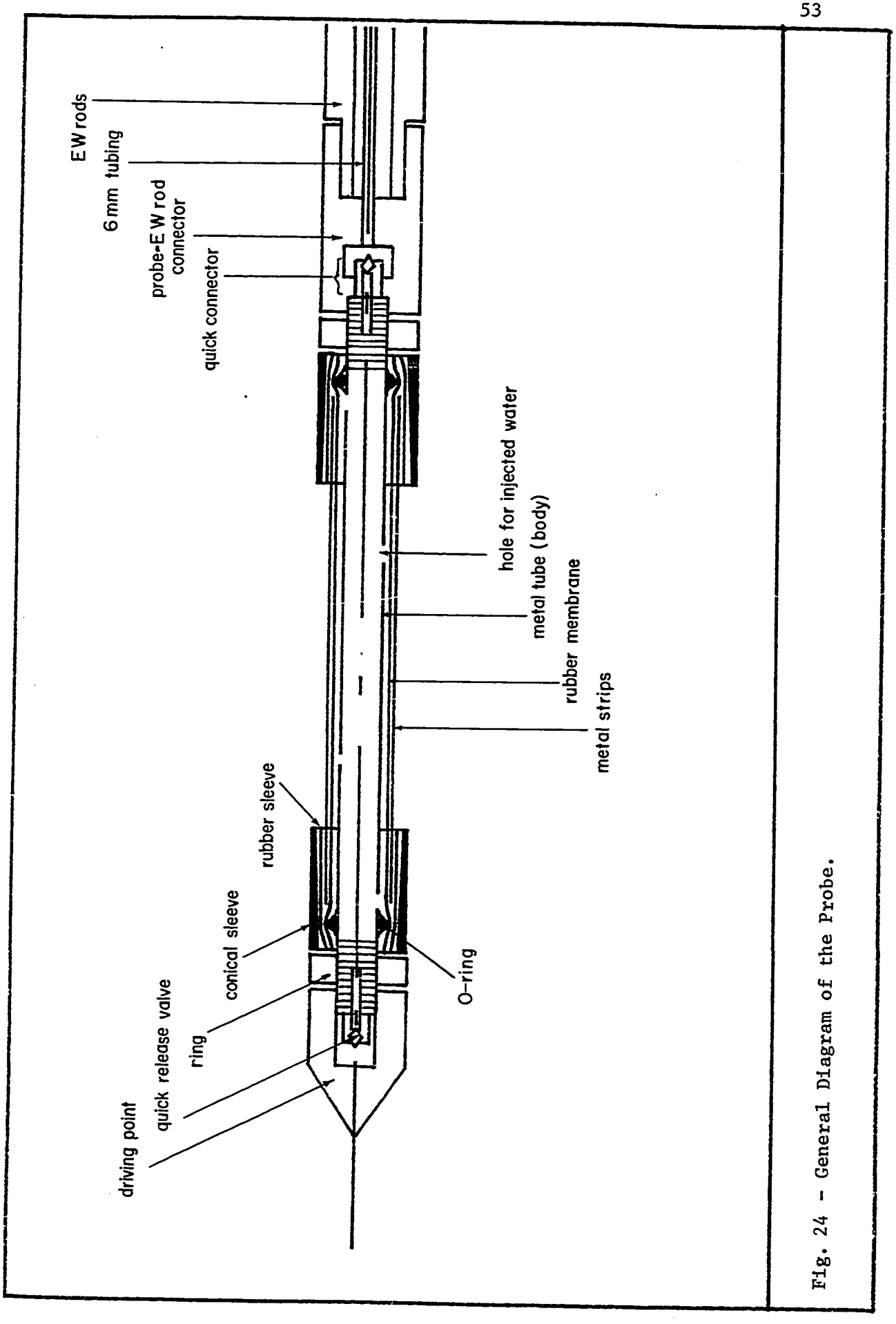

Fig. 24 - General Diagram of the Probe.

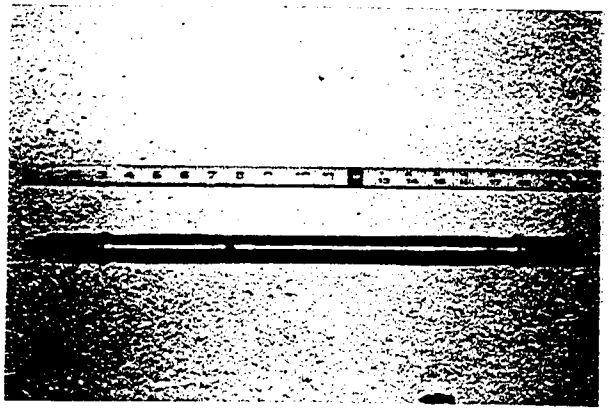

Fig. 25 - Body of the probe (Scale in inches).

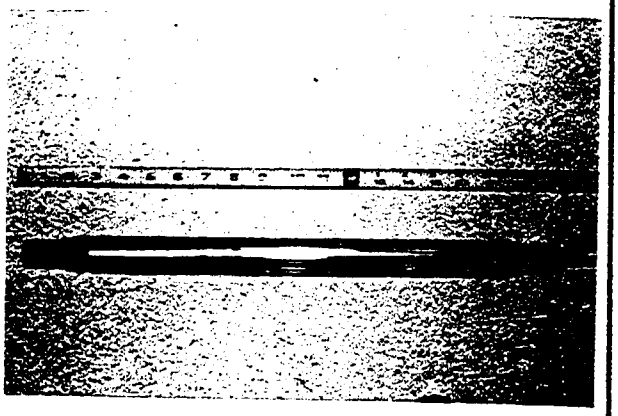

Fig. 26 - Body and Sheath (scale in inches)

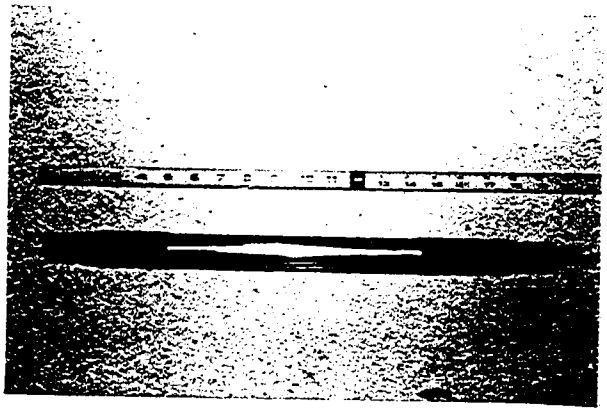

Fig. 27 - Body, Sheath and Rubber Sleeves (scale in inches).

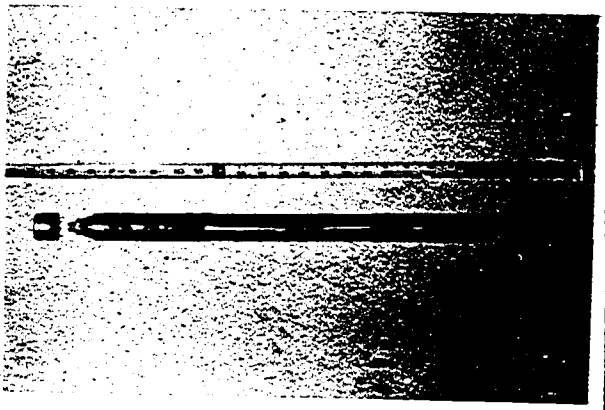

Fig. 28 - Body, Sheath, Sleeves and Rings (scale in inches).

and has two grooves for O-rings. The body is perforated by one or more holes to let water pass through from the inside to the outside to expand the membrane. When assembling the probe, the O-rings are installed first and then greased lightly to make mounting of the membrane easier; under no circumstances should the body of the probe be greased.

The combined membrane and sheath is a rubber tube, 430 mm long on which overlapping metal strips are glued (Fig. 26). The sheath has an outside diameter, once mounted, of about 31 mm.

To complete the assembly, first rubber sleeves and then conical metal sleeves are forced over the end of the sheath (Fig. 27); grease applied to the sliding surfaces will reduce the effort required for assembly. Finally two metal rings (Fig. 28) are screwed on to the ends of the body to force the metal sleeves closer together until the distance between the edges of the sleeves is 230 mm (Fig. 29). The sleeve-O-ring sealing system must be leakproof at pressures up to 2500 kPa.

There is a quick release valve at the lower (pointed) end of the probe (Fig. 24). In the normal position the valve is closed but if a nipple is depressed the valve opens. This valve is used during saturation of the probe and is protected by the drive point when the probe is driven.

The connection between the probe and the nylon tubing is made by a quick connector (Fig. 24). The nylon tubing is 5 m long and expands (volume loss) at the rate of approximately 3×10^{-4} $cm^3/m/kPa$. The outside diameter of this tubing is 6 mm and the inside diameter is 2 mm.

The tubing is threaded through the connection to the top of the

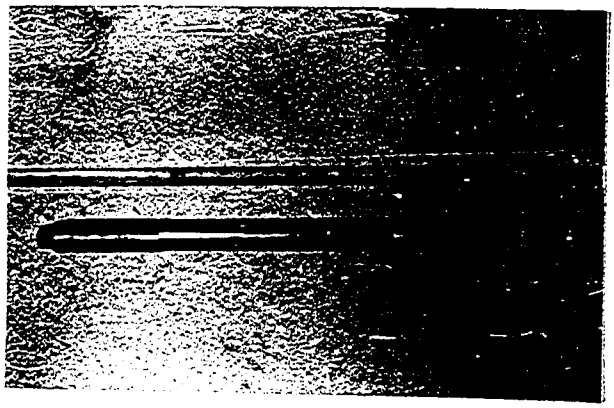

Fig. 29 - Probe Mounted (scale in inches.

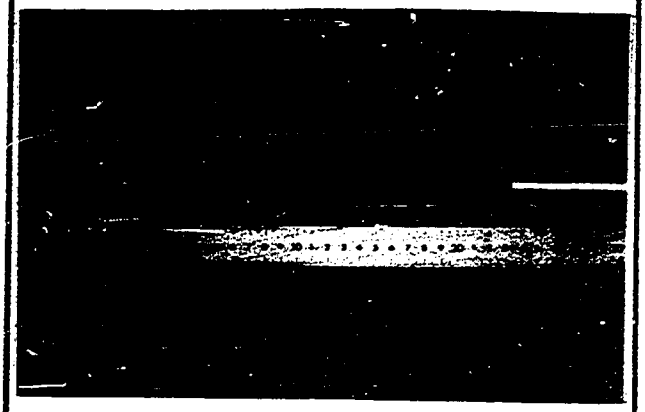

Fig. 30 - Probe Deflated (scale in centimeters).

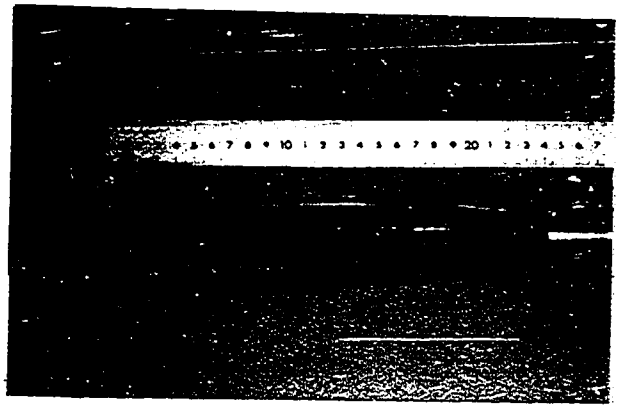

Fig. 31 - Probe Fully Inflated (scale in centimeters).

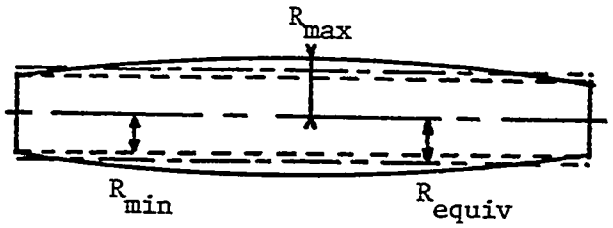

Fig. 32 - Probe Shapes.

probe and through four 0.6 m lengths of aluminum EW rods (Fig. 24). The EW rods have an outside diameter of 33.5 mm and the four lengths enable the probe to reach a depth of 2.4 m (Fig. 35).

The active length of the probe is defined as the distance between sleeves. The volume occupied by the active part of the probe is 180 cm^3 when deflated, V_c, (Fig. 30) and 270 cm^3 when fully inflated, $V_c + v_{max}$, (Fig. 31). As can be seen from the figure, the expansion in air is not cylindrical and the ratio R_{max} over R_{min} (Fig. 32) is 1.45; had the expansion been perfectly cylindrical the ratio R_{equiv}(Fig. 32) over R_{min} would have been 1.22.

4.1.2 Discussion

An active length of 230 mm was chosen because the probe must be able to fit entirely within the thin layers of base and subbase that make up the pavement; two hundred and thirty millimeters also corresponds to the minimum equivalent granular thickness. A reasonable estimate of the depth of influence of the large airplane tires which are used at present is about 1.8 m (Section 4.4.7); the 230 mm long probe can be used to give a reasonable number of test results within that depth of influence.

The probe is monocellular; therefore, its expansion departs somewhat from the true cylindrical expansion of the measuring cell in a three cell pressuremeter. The monocellular probe was chosen over a three cell probe for the following reasons:

- the probe is simple and simplicity is a must for routine field work, the small size of the probe makes it difficult to accomodate a complex structure in any event. Simplicity limits the chances of equipment breaking down.

Fig. 33 - Pulling the Briaud Pressuremeter.

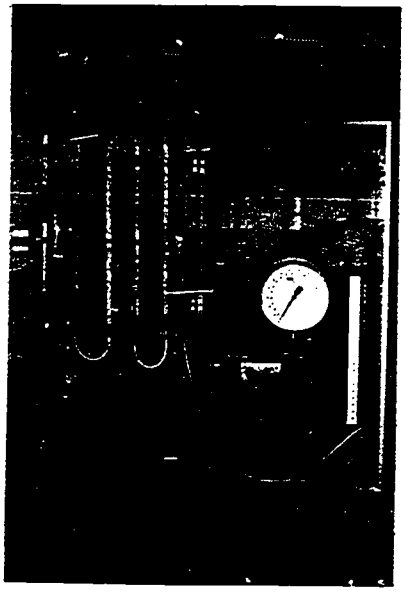

Fig. 34 - The Briaud Pressuremeter.

Fig. 35 - Probe, Rods and Driving Cap Assembled.

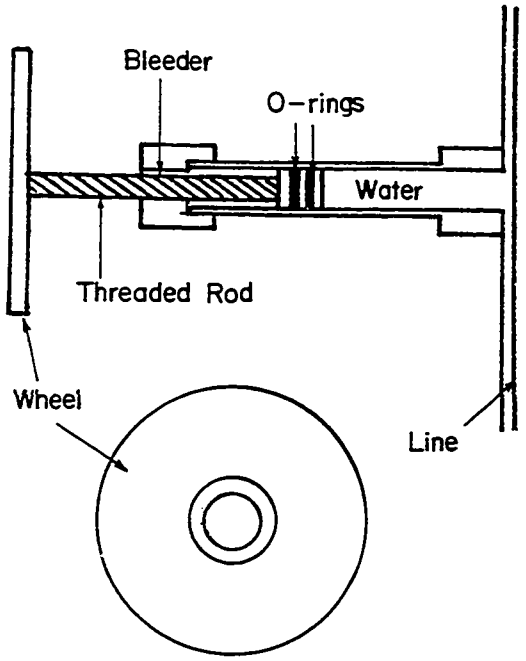

Fig. 36 - The Hand-Pump.

- cyclic tests are easier to perform and the probe can be deflated readily at the end of a test.

The fact that the probe is monocellular is not a drawback since:

- It can be shown that the maximum possible error in the measured modulus is limited. In the case of the radial expansion of a spherical cavity in an infinite elastic medium, Equation 13 becomes:

$$E_{e\ell} = 1.5\ (1 + \nu)\ V \frac{\Delta p}{\Delta V} \quad \ldots\ldots\ldots\ldots\ldots\ldots \quad (19)$$

If it is assumed that the expansion of a monocellular probe is not cylindrical but approaches spherical expansion, the calculated modulus will be higher than the cylindrical modulus by 33%. Since the expansion of the monocellular probe is much closer to being cylindrical than spherical, particularly with the probe surrounded by soil, this calculation shows that the induced error is small.

- the length to diameter ratio of the probe is $\frac{230}{32} = 7.19$; for this ratio Hartman (p. 25 of (17)), using the theory of elasticity maintains that the volume injected into a monocellular probe is only 5% less than the volume required for perfect cylindrical expansion. This error in volume corresponds to a 5% overestimation of the modulus.

- a number of other investigators have used a monocellular probe and have obtained useful results: examples are Jezequel with his self-boring pressuremeter (p. 482 of (1)) and Serota and Lowther (39) with their penetration pressuremeter.

- Since the test is standardized, any error due to the use of a monocellular probe is the same in all tests. The error will then be taken into consideration by the empirical relationship between the

proposed test results and the results of other tests or actual pavement performance.

Single tubing has been used rather than coaxial tubing. While coaxial tubing would give smaller volume losses, the short length of the single tubing (5 m) means that the volume losses are already small (Test No. 33, Appendix A). If required, coaxial tubing could be used from the probe to the control unit; the inner tubing carrying the water to the probe would go to the volumeter (Fig. 38) while the outer tubing would bypass the volumeter before reconnecting with the inner tubing. For this research, the complications arising from the use of a coaxial tubing were thought to be more trouble than the increase in accuracy was worth. Instead, the volume losses in the single tube were calibrated very carefully and the appropriate corrections were made when calculating the test results.

The complete probe alone, all equipped, costs 400 dollars to make (1977); one sheath costs 40 dollars (1977) but a sheath can be used for between 100 and 200 tests. During 178 pressuremeter tests, no sheath ever burst. If a sheath has to be replaced for any reason, two experienced technicians can change the sheath in less than an hour.

4.2 The Pressure Volume Control Unit

The purpose of the pressure volume control unit is to generate the pressure necessary to inflate the probe, to measure this pressure, and to indicate what volume of liquid is sent into the tubing. The control unit designed for this research had to carry out these functions but also had to be inexpensive, practical, portable, robust and simple.

4.2.1 Description of the Control Unit

The box in which the pressuremeter is transported is 1.2 m long, 0.6 m wide and 0.3 m deep; it is made of plywood 19 mm thick (Fig. 34). The box is able to carry the control unit, the probe, four lengths of 0.6 m aluminum EW rods and all the necessary accessories; full of equipment it weighs about 50 kg and can either be carried by two people or pulled along on the two back wheels by one person (Fig. 33). The front cover is removable and carries the following items which are held in place by pressure snaps (Fig. 34): the four aluminum EW rods, the probe, a sledge hammer, the metal calibration tube, the tubing exit coupling and the drive-cap.

The basic principles of the control unit, shown on Figure 23, were suggested by Baguelin et al. (p. 474 of (1)); the writer of this thesis is only responsible for implementing and finalizing the system. A detailed diagram of the control unit is shown in Figure 37; the unit is made of a hand pump, a pressure gauge, two plexiglass tubes, three plexiglass containers, 6 mm copper tubing, brass fittings and high pressure valves (Fig. 34). The hand pump is a regular pump which is used in triaxial testing (slightly altered) and has a capacity of 100 cm^3 (Fig. 36); the pressure gauge has a range of 0 to 3000 kPa and is a class 1 gauge; the two plexiglass tubes have an inside diameter of 16 mm, an outside diameter of 38 mm and a length of 550 mm.

Volume readings are taken from a scale which is graduated in cubic centimeters and which is mounted between the two plexiglass tubes. The upper part of the plexiglass tubes is filled with red kerosene, the rest of the circuits is filled with water; the kerosene water interface is

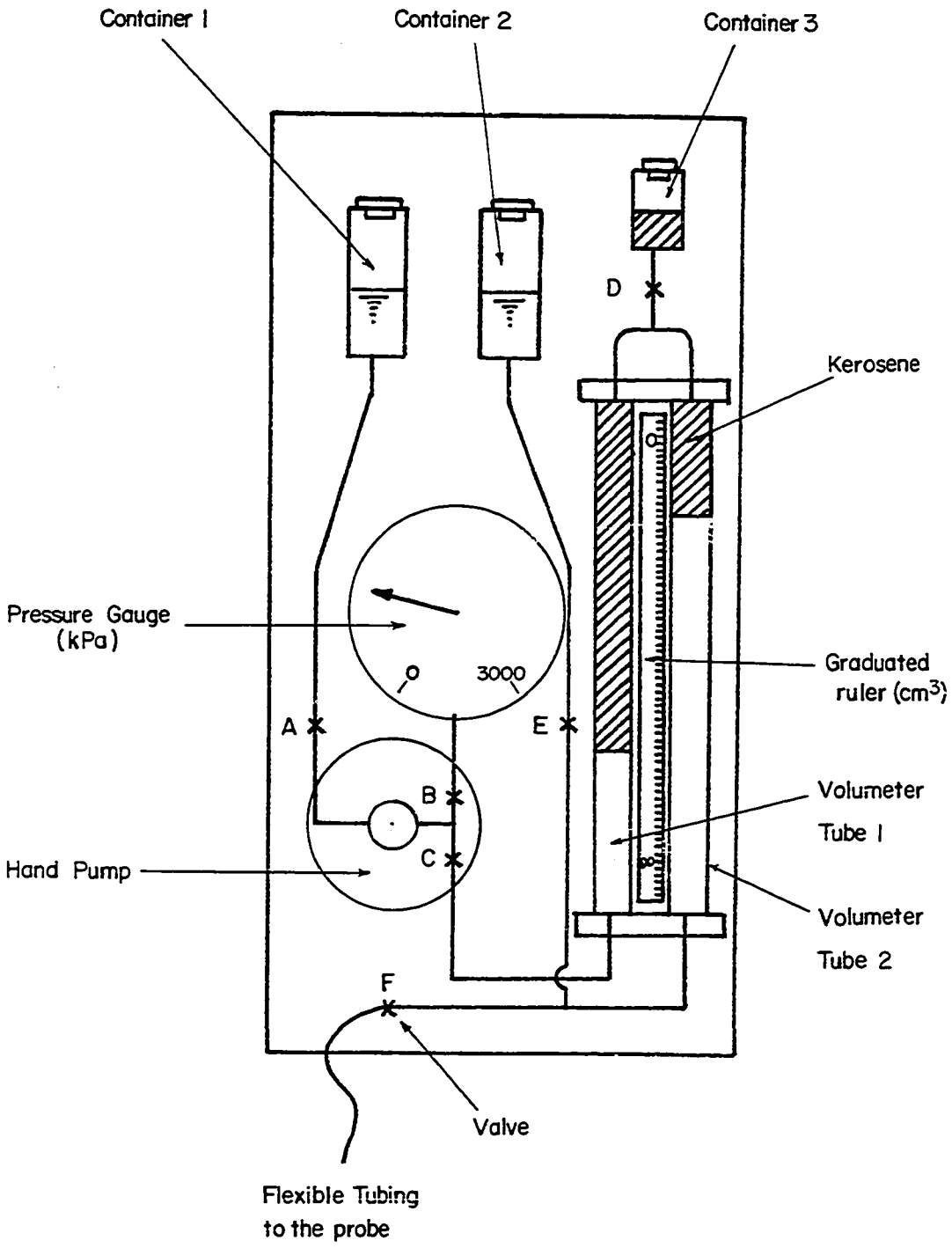

Fig. 37 - Detailed Diagram of the Briadd Pressuremeter Control Unit.

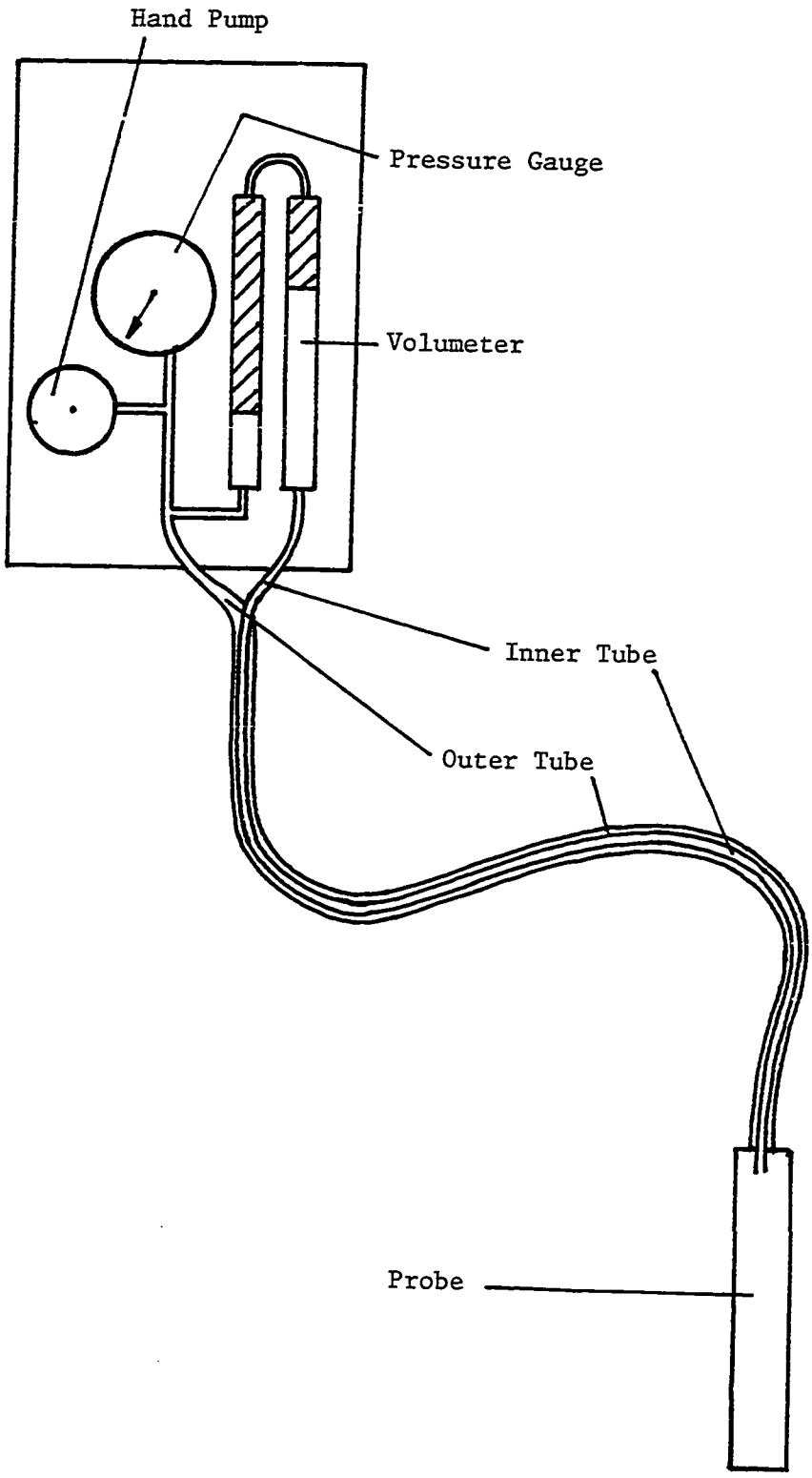

Fig. 38 - Use of a Coaxial Tubing for the Briaud Pressuremeter.

the indicator from which the volume of water injected into the probe is read. The scale is graduated from 0 to the maximum probe inflation of 90 cm^3.

The basic operation to be performed with the control unit is the test itself. With valves A, D and E closed and the others open, the wheel of the hand pump can be screwed in to advance the piston (Fig. 36). The piston forces water into the probe (installed in the ground); the water pressure increases as a result of the injection and of the resistance offered by the soil to the expansion of the probe. The pressure is read on the gauge and the volume of water which is injected is read on the graduated scale; the pressure and volume can be decreased easily (for, say, a cyclic test or to deflate the probe at the end of a test) by reversing the rotation of the wheel of the hand pump.

Other operations include: filling the pump-cylinder; adjusting the zero reading; saturating the control unit, tubing and probe, checking for leaks, calibrating for volume losses and calibrating for membrane resistance. All operations are described in detail in Section 4.4.

4.2.2 Discussion

The main reasons for building the new control unit were:

- a strain control was chosen to run the test as opposed to a stress control. In a strain control test, the volume of the probe increases at a constant rate, whereas in a stress control test, the pressure in the probe increases by increments of equal magnitude and equal duration.
- the problem had specific requirements such as the small volumeter capacity required for the small probe and the resulting need for

accurate volume change measurements.

- The off-the-shelf units were expensive. For example, the control unit for self boring pressuremeters is designed for strain controlled tests but costs in the neighborhood of 10,000 dollars (1977). The control unit shown on Figure 34 costs about 2000 dollars (1977).

Strain controlled tests are preferred over stress controlled tests because of numerous important advantages such as:

- the number of curve points in the elastic region can be unlimited (in theory at least); this wealth of data leads tc a better determination of the modulus.
- cyclic tests and probe deflation at the end of a test are much easier.
- an estimate of the limit pressure is not required before the test.
- the equipment is simple and flexible in operation.

4.3 Making the Hole and Installing the Probe

4.3.1 Preparing the Pressuremeter

The pressuremeter must be completely ready for use before drilling starts so that the probe-rod assembly can be inserted into the hole immediately after the hole is drilled. During assembly, the four 0.6 m lengths of EW rods, which are strung on the tubing, are slid along the tubing and coupled to one another and to the probe. In order to install the driving cap, a slotted coupling is used as shown on Figure 39. The pressuremeter is saturated and checked for leaks, the zero is set, the pressuremeter is calibrated if recent calibrations are not available

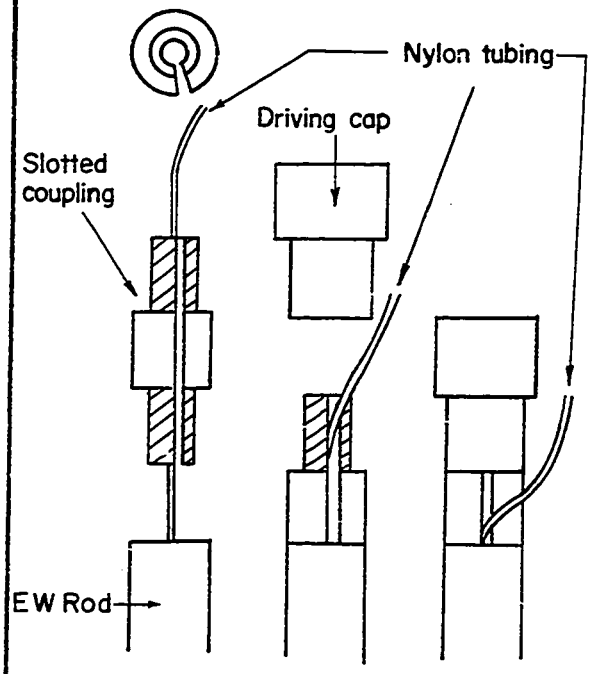

Fig. 39 - The Tubing Exit Coupling.

Fig. 40 - Continuous Auger Penetrating the Asphalt (diameter = 76 mm).

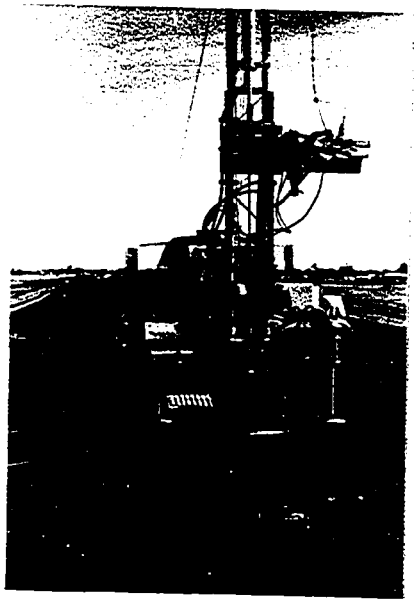

Fig. 41 - Driving the E Rod (O.D. = 34.9 mm).

Fig. 42 - Pressuremeter Probe in Place (O.D. of the EW Rods = 33.5 mm; O.D. of Probe=32 mm).

(Section 4.4) and valve F is closed (Fig. 37). The pressuremeter is ready.

4.3.2 Making the Hole

For this study, the hole was made in the following way. The continuous flight auger of an SPT drilling rig was used to make an 80 mm diameter hole through the asphalt without penetrating the base course (Fig. 40). Then the auger was removed, the hole cleaned out by hand, and the asphalt thickness measured accurately. Two 1.5 m long E rods (O.D. = 34.9 mm) with a driving point were placed under the SPT hammer and driven to 2 m (Fig. 41); the blow count per, say, 150 mm or 300 mm of penetration provides an indication of the resistance of the material.

Other types of machines or equipment can be used of course, to open a hole through the asphalt and drive E rods into the ground. Whatever equipment is used, the E rods should be guided while they are driven or withdrawn from the ground to prevent them from whipping back and forth, enlarging the top of the hole.

4.3.3 Installing the Probe

Immediately after the E rods are withdrawn from the ground, the probe-EW rod assembly is inserted down the hole to a depth such that the middle of the active part of the probe is 1.8 m lower than the surface of the asphalt (Fig. 42). Normally, the probe can be forced down the hole by the weight of one or two men; if this force is not sufficient, the probe can be driven with a sledge hammer. The probe-EW rod assembly cannot withstand an effort much greater than this and it is inadvisable to pry the probe down against the weight of the drilling machine or force it down using the hydraulic power from the machine. If sledge hammering does not suffice, the hole must be abandomed; in no instance should the

E rods equipped with a point be driven down in the same hole a second time and the probe reinserted. Instead a second hole is made at a distance of no less than 1 m from the first hole. Redriving the point must be avoided in order to have a standard hole making technique for all test.

4.3.4 Disturbance: Literature Survey

There is no doubt that the above method of bore hole preparation disturbs the soil. In order to evaluate the influence of this disturbance on the modulus value, the results of pressuremeter tests using the proposed insertion procedure should be compared to the results of pressuremeter tests using a 'non soil disturbing' insertion procedure. For both fine grained cohesionless soils and fine grained cohesive soils, self boring insertion of the probe is considered to be a 'low disturbance' insertion method but the equipment is not readily available. As an alternative in cohesive soils, the hand auger method is probably the next least disturbing method. In fact, for cohesive soils, the hand auger method is considered to be the bore hole preparation of reference for disturbance comparisons. For most granular soils, a 'non soil disturbing' insertion procedure does not exist and there is no well established bore hole preparation of reference.

This section and the following section attempt to evaluate the disturbance caused by the proposed insertion procedure by studying the difference between the modulus which is measured when using the proposed insertion procedure and the modulus which is measured when using a low disturbance method. In this section, this study is done by conducting a survey of related literature.

In the Briaud pressuremeter test, the hole is prepared by driving

rods into the ground, withdrawing them, and then inserting the pressuremeter probe; this method of insertion is called the rod driving method. Unfortunately, little research appears to have been done on disturbance to the soil caused by the rod driving method; the literature does contain, however, a number of articles and comments on the method of inserting the probe directly into the ground (direct insertion method) with or without the external protection of a slotted tube.

Jezequel et al. (18) say that direct insertion of the probe is unsuitable for the study of loose sands, soft to medium clays, and sensitive soils. They add that even in other more suitable soils, the method will result in a drop of modulus of about 20 to 30%.

Roy et al. (36) pushed a probe down into a very sensitive clay ($S_t > 16$) and found that the direct insertion method remolds these soils greatly and leads to much higher moduli (up to five times higher) than the moduli which are obtained with the hand auger method. However, they do not describe how they determined the various moduli; calculating the moduli from the curve they present in their paper and using the precise modulus determination method described in Section 4.5.2 gives moduli that are higher by, on average, only 30%.

Laier (25) performed pressuremeter tests in a sand container; he compared the direct insertion method with a low disturbance method. The low disturbance method consisted of placing a waxed paper cylinder in the container before filling the container with sand; the inside diameter of the paper cylinder was the same as the outside diameter of the probe so that the pressuremeter could be inserted without disturbing the sand. Laier made most of the comparisons in loose sand and generally found that the direct insertion method gives lower modulus values.

Baguelin et al. (p. 111 of (1)) discuss the influence of the insertion method in different soils; in almost all cases they found that the direct insertion method led to an underestimation of the modulus. In soft cohesive soils, the underestimation can reach 50%.

The influence of disturbance on modulus values has been studied theoretically; Hartman (p. 288 of (17)), using the finite element method and a non linear, stress dependent, soil model, shows that the presence of a remolded annulus of lower strength around the probe will lead to a pressuremeter modulus value which is smaller than the modulus of the intact soil; Baguelin et al. (p. 372 of (1)) illustrate the same effect by mathematical derivation. Hartman and Baguelin et al. both find, for example, that if the modulus of the remolded zone is equal to 0.5 times the modulus of the intact soil and if the remolded zone has a width which is equal to 0.6 times the radius of the hole, the pressuremeter modulus will be equal to 0.7 times the intact soil modulus. On the other hand, Hartman also found that if a bore hole is unloaded by withdrawing the drilling tool and then reloaded by the pressuremeter, the measured modulus will be greater than that of the intact soil by up to 50%. Hartman goes on to argue that the effects of remolding and unloading/reloading may cancel each other out.

Mittal and Morgenstern (33) show theoretically and experimentally that in sand the change of density introduced by driving a 41.2 mm diameter rod in the ground is about 1%. Thus density changes are not the reason for the changes in modulus.

4.3.5 Disturbance: Test Results

This section reports and analyzes the results of tests that have been

done to evaluate the influence of disturbance on the modulus value. In order to simplify the presentation, the modulus obtained from a test where the hole has been bored using a certain method will bear the name of that method (e.g.: the hand auger modulus). Tests were performed in three different soil deposits: a dry uniform sand (Section 6.3), a silty clay (Section 6.4) and a well graded sandy silty clay or till (Section 7.3).

In the dry uniform sand, the low disturbance method consisted of installing the probe in an empty container and then filling the container with sand. The Briaud probe connected to EW rods was positioned vertically and secured in position at the required depth in an empty 1.8 x 1.8 x 2.1 m steel and timber box (depth = 2.1 m). Sand was rained into the box at the required density until the box was filled. This method, called the buried probe method could not be compared with the rod driving method, since the hole in the sand collapses on withdrawal of the rods; instead, tests using the buried probe method were compared with a direct insertion method where the probe was tapped down to the required depth in a prepared bed of sand. This comparison was done in a dense sand (I_D = 95%) and in a compact sand (I_D = 65%). A summary of the results is presented on two modulus profiles (Fig. 82 and 83) and the individual test curves can be found in Appendix A.

In the dense sand, one test (Test No. 66) was run at 1.8 m depth using the buried probe method and measured a pressuremeter modulus of 6300 kPa. At the same depth and sand condition three tests were done using the direct insertion method (Tests Nos. 72, 74 and 80); the average moduli which was measured was 10,000 kPa. The latter modulus

corresponds to 1.59 times the buried probe modulus. While an increase in modulus due to the compaction effect of the direct insertion method might be expected, an increase of 59% seems high particularly for a soil that was at 95% of its maximum density. It is likely that the buried probe modulus is low for the following reason: as the sand is rained in place, a curtain of sand passes over the probe and drill rods, sand particles hit the probe and rods, and as a result the sand around the probe is probably looser than in the rest of the sand container. This reasoning also applies to the compact sand tests discussed below.

In the compact sand, two tests (Test No. 46 at 1.8 m depth and Test No. 82 at 1.2 m depth) were performed with the buried probe method and the results are compared with 10 tests (Tests Nos. 52, 58, 64, 88, and 96 at 1.8 m depth and Tests Nos. 50, 56, 62, 86, and 94 at 1.2 m depth) performed with the direct insertion method. At 1.8 m depth the average direct insertion modulus was equal to 1.71 times the buried probe modulus; at 1.2 m the same comparison gave a factor of 1.69. It must be noted that the curves of the three tests with the buried probe method do not have a straight line, elastic phase (refer to the result in Appendix A); this makes the determination of the modulus arbitrary. In all three tests, the modulus (E) was determined as outlined in Section 4.5.2 (best straight line fit over 20 cm^3 injected volume). For the same three tests an initial modulus (E_i) could be determined and E_i was found to be much closer to the direct insertion modulus. Considering the average of the three tests, the direct insertion modulus (E) was equal to 1.1 times the initial buried probe modulus. The test curves which were obtained by the direct insertion method present a clearly

defined elastic phase.

In the natural silty clay deposit of Fraser's farm (Section 6.4), 18 tests were performed for disturbance evaluation purposes. Two holes (Holes 6 and 7), one meter from each other, were tested down to 2.7 m depth (one Briaud pressuremeter test every 0.3 m). For Hole 7 the hand auger method was used as the low disturbance method (Tests Nos. 219 to 227 from bottom to top) and for Hole 6 the rod driving method was used (Tests Nos. 230 to 238 from bottom to top). The test results are presented on a modulus profile (Fig. 93) and in Appendix A (individual test curves).

Comparing the average pressuremeter modulus of Hole 6 with that of Hole 7 indicates that the rod driving modulus is equal to 1.1 times the hand auger modulus. The clay had a sensitivity (field vane) averaging five; it would seem reasonable to assume that the direct insertion method would weaken the sensitive structure of the clay and lead to lower moduli. Instead, slightly higher moduli were found, as in Roy et al. (36); this increased modulus may be due to increased pore pressures which are induced by the driving of the rod.

In the clay of Sarnia Airport (Section 7.3), 13 tests were performed for disturbance evaluation purposes; two holes (Holes 1 and 2), one meter from each other, were tested down to 1.5 m (one test every 0.3 m). For Hole 1 the hand auger method was used as the low disturbance method (Tests Nos. 99 to 103 from top to bottom) and for Hole 2 the rod driving method was used (Tests Nos. 105 to 109 from top to bottom). In addition, Hole 12 was prepared by the hand auger method and one test was performed at 1.2 m depth (Test No. 157); Holes 10 and 11 (close to Hole 12) were

prepared by the rod driving method and one test was done in each hole at 1.2 m depth (respectively Tests Nos. 143 and 144). The results are shown on a modulus profile (Fig. 103) and in Appendix A (individual test curves). On average, the rod driving moduli were equal to 1.16 times the hand auger moduli.

Also, in Sarnia, two holes were prepared using the rod driving method. Hole 15 (Tests Nos. 151 to 156, top to bottom) were prepared in the usual way by driving the E rods once. Hole 14 (Tests Nos. 145 to 150, top to bottom) was 1 m away from Hole 15 and was prepared by driving the E rods three times in the same location. The results are shown on a modulus profile (Fig. 108) and in Appendix A (individual test curves). On average, the modulus obtained from the hole where the E rods were driven once was equal to 1.94 times the modulus obtained from the hole where the E rods were driven three times. This shows that repeated driving of the rods to prepare the hole can greatly reduce the measured modulus. Redriving should never be permitted.

The tests performed in this study show that the rod driving modulus is always higher than the low disturbance method modulus; the difference is less than 20% except in the case of the uniform dry sand where the low disturbance method gave questionable results.

When the test results in the literature are also considered, it seems that, on average, the disturbance induced by the rod driving or the direct insertion method results in modulus changes of the order of 30%; disturbance is particularly important in soft and loose soils.

4.3.6 Discussion

The rod driving method was chosen to make the hole in all types of soil for the following reasons:

- having one method for all soils avoids errors that can be generated by letting the field crew choose the "best" method for the subgrade which is encountered.

- the base course has particles up to 35 mm in size and the diameter of the hole must be 32 mm; the use of a 32 mm diameter hand auger or a 32 mm sampler to make the hole in the base course is simply not feasible.

- the rod driving method is simple, fast and leaves a hole with relatively smooth sidewalls since the rod is driven and withdrawn only once (unlike the multiple insertion of the hand auger for example).

- the rod driving method probably compacts the walls of the hole; this helps them to stand up (holes made with the rod caved in only once in twenty-one attempts).

- airports are rarely built on soft and loose soils where disturbance due to rod driving has the most pronounced effect.

- if disturbance has an influence on the modulus and no influence on the limit pressure, disturbance should have reduced influence on the cyclic modulus which is measured at an intermediate strain level between the first modulus and the limit pressure.

- the method is standardized and any deviation from the 'ideal' is lost in the empirical correlations with actual pavement behavior.

- other researchers (Serota and Lowther (39) and Saint John[7]) have used the direct insertion technique with success.

---

7. Saint John, H.D., Written Communication, March 1978.

4.4 The Test Procedure

The following steps must be followed in the order which is given.

4.4.1 Saturating the Circuits and the Probe

To empty or fill the hand pump, close valves B and C, open valve A and expell or draw in water by turning the hand wheel in the appropriate direction. Now, the control unit must be filled with water and kerosene; to do this, empty the hand pump completely, close valve F (Fig. 37), open the other valves and the three containers; then, pour water into containers 1 and 2 and keep them full until the water rises in container 3 and comes to equilibrium. Once equilibrium is obtained, close valve D and fill container 3 with red colored kerosene; close valves A, E and F, open the other valves, and now draw water in the hand pump. Kerosene will fill the volumeter tube 1 from the top down; when the water kerosene interface is at division 100 on the graduated scale pumping should be stopped. Then, close valves D, A and F, open the other valves and push water up into tube 1 with the hand pump. Kerosene will appear in tube 2; stop pumping when the two water kerosene interfaces are at the same level.

The control unit still has to be deaired; to deair the unit, close valves A, D, E and F and open the other valves, pump 1000 kPa of pressure into the control unit and then open valve A until the pressure drops back to zero; to continue deairing the unit, close valve A, pressurize the system to 1000 kPa pressure, then open valve E until the pressure drops back to zero; to end deairing the control unit, close valve E, pressurize the system to 1000 kPa, then open valve D until the pressure drops back to

zero. The control unit shoud now be deaired.

To saturate the flexible tubing, connect it to valve F and close valves A, E and D. Open the other valves and push water through the tubing by means of the water pump; the water-kerosene interface will drop in tube 2. Do not let the kerosene level drop below the bottom of tube 2. If the kerosene level gets too low, the level can be raised back to the top of tube 2 as follows: close valves A, D and F and open the other valves, then, using the hand pump, draw water from container 2 until the kerosene level has receded to the top of tube 2. There should now be sufficient water available to fill the tubing and to deair it completely.

To saturate the probe, plunge it entirely into a pail of water with the open end of the probe up; then squeeze and release (work) the sheath by hand until no more air bubbles escape even when the sheath is squeezed hard. The probe should be kept under water while the connection is made with the tubing. Now, inflate the probe to 90 cm^3 and, with the driving end of the probe pointed upward, depress the quick release valve (Fig. 24) until the probe is deflated; repeat this procedure three times. As a final check to ensure that the pressuremeter is saturated, insert the probe in the calibration tube so that only the quick release valve is exposed; pump up 1000 kPa of pressure, and, with the driving end of the probe pointed upward, depress the quick release valve until the pressure drops back to zero. This check should be repeated at least three times to ensure that the whole system is saturated.

It should be noted that only that portion of the circuit from the kerosene–water interface of tube 2 to and including the probe need be fully saturated since the injected volume is recorded at the interface. Also, unless absolutely necessary, the flexible nylon tubing should not

be disconnected from either the control unit or the probe to avoid having to resaturate the circuits and reset the zero readings (Section 4.4.4).

In order to transport the pressuremeter, the kerosene should be pumped back into container 3. This can be done by closing valves D, A and F and opening the other valves. Draw water with the pump until all the kerosene is in tube 1; close valves A, E and F and open the other valves to allow the pump to push all the kerosene back into container 3.

4.4.2 Checking for Leaks and Saturation

The procedure to check for leaks and saturation is identical to the one for the Ménard GA pressuremeter described in Section 2.2.4, Step 2. Make certain that the control unit is in position "test" with valves A, E and D closed and the other valves open. Complete saturation is reached when the change in volumeter reading between 500 kPa and 2000 kPa is less than 0.8 cm^3 per meter of tubing; this tolerance is higher than for the Ménard GA pressuremeter because a single tubing is used with the Briaud pressuremeter.

4.4.3 Calibration of Volume Losses

The calibration procedure is similar to the one for the Ménard GA pressuremeter described in Section 2.2.4, Step 3. The probe is inserted in the steel calibration tube. Close valves A, E and D and open the other valves. Now, inflate the probe at the rate of 0.33 cm^3/sec (Section 4.4.6). Take readings of pressure and volume every 5 cm^3 from 0 to 500 kPa and every 1 cm^3 after 500 kPa. A form such as the one of Figure 43 is used to record the data and a curve like the one shown in Figure 44 can be plotted. Then, disconnect the tubing at the probe, screw a plug on to

Volume losses

Project : Site :
Date : Temp :
Calib. no: Probe :
Length of tubing: Unit :

C.P.V.+Tubing + Probe		C.P.V. + Tubing	
V	P	V	P

Fig. 43 - Form for a Calibration of Volume Losses.

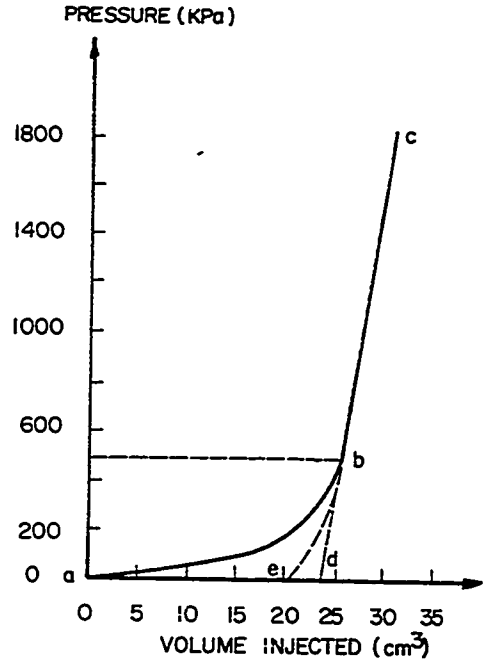

Fig. 44 - Calibration of Volume Losses of the Control Unit, Tubing and Probe.

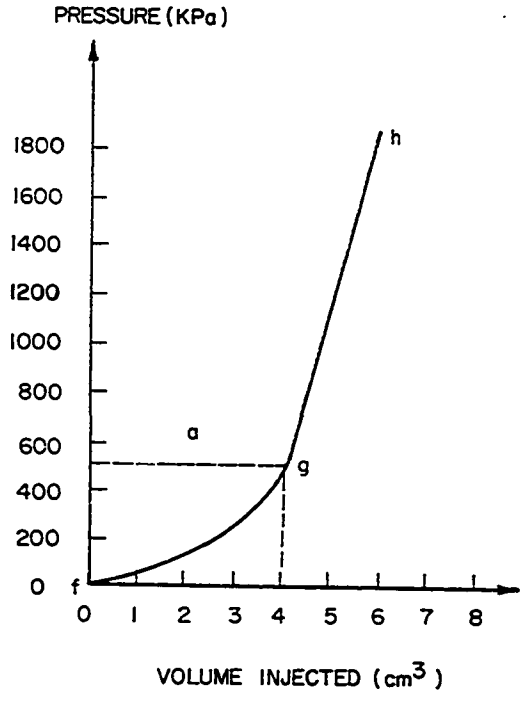

Fig. 45 - Calibration of Volume Losses of the Control Unit and Tubing.

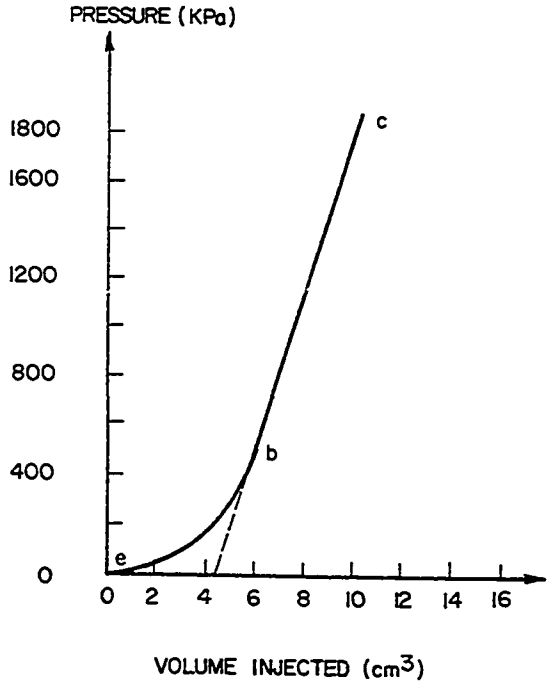

Fig. 46 - Volume Losses: Typical Correction Curve.

the end of the tubing and repeat the calibration, taking readings every 1 cm^3 right from the start. A curve such as the one in Figure 45 is obtained. The volume loss plot of Figure 46 is derived from the curves of Figure 44 and 45 as explained in Section 2.2.4, Step 3.

4.4.4 Setting the Zero

The procedure for setting the zero is identical to the one for the Ménard GA pressuremeter described in Section 2.2.4, Step 4. For the probe described here, the initial reference volume (V_c) is 180 cm^3. To set the zero, the control unit is placed in position "test" with valves A, E and D closed and the other valves open. If the volumeter reading (v_v) is different from what it is required to be (v_m as explained in Section 2.2.4, Step 4), proceed as follows: close valve F, open valve E and set the required volumeter reading by either drawing in or expelling water with the pump. Once v_m is set, close valve E, open valve F and reduce the pressure back to zero.

4.4.5 Calibration of Membrane Resistance

The procedure for the membrane resistance calibration is similar to the one for the Ménard GA pressuremeter which is described in Section 2.2.4, Step 5. Before starting the calibration, the probe must be inflated to 90 cm^3 and deflated to 0 cm^3 at least five times in order to 'work' the rubber. Once this is done, the probe is set vertically on the ground and the difference in height (h_o) between the center of the probe and the gauge of the control unit is recorded on a form such as the one in Figure 47. Close valve A, E and D and open the other valves and then inflate the probe at the rate of 0.33 cm^3/sec. Take pressure readings every 5 cm^3 of expansion. Figure 48 shows a typical result.

Membrane Resistance

Project : Site :
Date : Temp :
Calib. no. : Probe :
h_o : Unit :

Morning		Evening	
V	P	V	P
0		0	
5		5	
10		10	
15		15	
⋮		⋮	
80		80	
85		85	
90		90	

Fig. 47 – Form for a Calibration of Membrane Resistance.

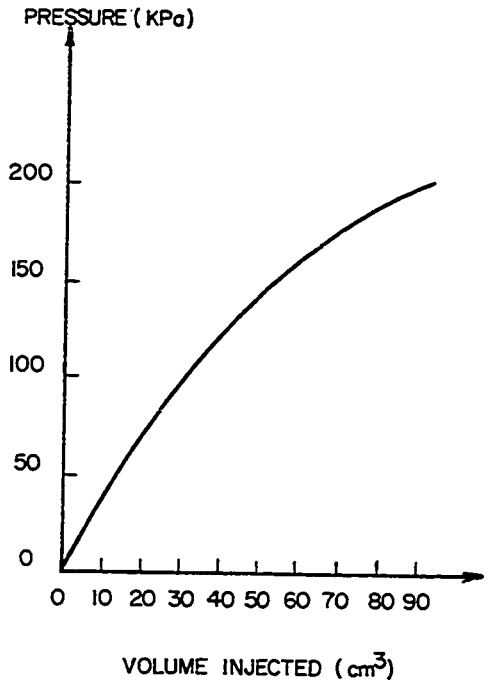

Fig. 48 – Membrane Resistance: Typical Results.

Pressuremeter Cyclic Test

Project : Hole prep. :
Date : Water level :
Site : $h_o + Z$: 2.2 m
Soil : Memb. Cal. :
Hole no. : Vol. loss. Cal. :
Test no. : Unit no. :
Temp. :

V	P	ΔP	V	P	ΔP
0	0	/	55	560	50
5	20	20	35	70	/
10	45	25	40	150	80
15	80	35	45	260	110
20	120	40	50	380	120
25	190	70	55	500	120
30	250	60	60	600	100
35	320	70	65	660	60
40	400	80	⋮	⋮	⋮
45	460	60	90	810	/
50	510	50			

Fig. 49 – Form for a Briaud Pressuremeter Tests.

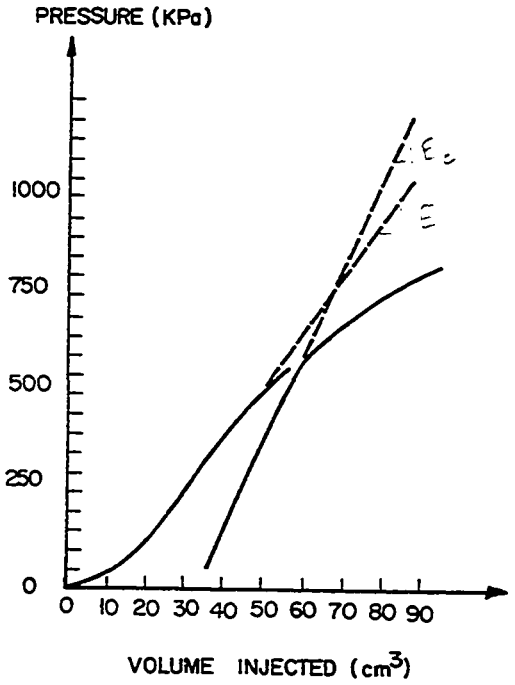

Fig. 50 – Briaud Pressuremeter Test: Typical Raw Results.

4.4.6 The Cyclic Strain Controlled Test Procedure

The first test in a hole is performed at 1.8 m depth. Once the volumeter has been set at 'zero', the pressure gauge reads zero, the hand pump is full, valves A, E, D and F are closed and the other valves are open, the test can be started. One person turns the pump at a rate of 0.33 cm^3/sec and reads the volumeter every 5 cm^3; a second person reads the pressure gauge and records the data.

The rate of expansion of 0.33 cm^3/sec has been chosen so that the test duration corresponds to the time required for the Ménard stress controlled pressuremeter test. During a standard Ménard test, the probe doubles in volume in 10 minutes. Therefore, the Briaud probe, which has a deflated volume of 180 cm^3, should be inflated by 180 cm^3 in 10 minutes to meet Ménard's requirements. The equivalent rate is:

$\frac{180^3}{10 \times 60 \text{ sec}} = 0.3$ cm^3/sec. The rate of 0.33 cm^3/sec is chosen for convenience since it is easy to control this rate by noting whether or not 1 cm^3 of water is pumped every three seconds.

There is little doubt that the rate at which the probe is inflated has an influence on the pressuremeter modulus. Fast rates induce undrained behavior while slow rate induce drained behavior of the soil; also it may be that for the same rate a clay would have an undrained response and a sand would have a drained response. Therefore the strain rate is important. In the future, it may be found that different rates are more appropriate but presently, a single value of 0.33 cm^3/sec is proposed for sake of standardization.

It should be noted that, since only the modulus is required from the Briaud pressuremeter test, the probe need be inflated to only 90 cm^3; the test lasts on the order of five minutes. The rate of 0.33 cm^3/sec

can be obtained by rotating the pump wheel by hand; at first the operator must time himself carefully but after a few dozen tests a rythm develops and a rate of between 0.3 and 0.35 cm^3/sec can be obtained without timing. Alternatively, a flow meter could be built into the system and a battery operated constant speed electric motor could be incorporated into the control unit with the required gear reduction mechanism to give the required flow rate; both a flow meter and a constant speed motor are found in the French CPV-1000 (Baguelin et al., p. 477 of (1)).

The form to be used to record the data during the test is shown on Figure 49. To start the test, open valve F; the pressure and volume readings should not change very much but if they do, it is advisableto wait for a few minutes for conditions to stabilize. Once the readings are stable, pumping can start; the gauge pressure should be recorded every 5 cm^3. As the test progresses, the column 'Δp_r' should be filled in; Δp_r is the difference between the last two pressure gauge readings. During the test Δp_r will increase at first, reach a peak and then decrease. When Δp_r is smaller than the maximum Δp_r three times in a row, it is time to start the cycled part of the test. If this Δp_r criterion has not occurred before 90 cm^3, cycled testing should start anyway at 90 cm^3. An example of Δp_r calculations is shown on Figure 49.

The probe should be deflated at the same rate of 0.33 cm^3/sec until the volumeter reading is decreased by 20 cm^3 or the pressure has decreased to zero, whichever occurs first. Then the probe should be reinflated while readings are taken every 5 cm^3; the reloading cycle should be continued until 90 cm^3 is reached, deflate the probe and bring the pressure gauge back to zero; close valve F. This marks the end of the test and the form should be completed before proceeding to the next test. Figure 50 presents a typical plot of the raw results. Tests are performed every 0.3 m, starting at 1.8 m depth and working up to the ground surface.

4.4.7 Discussion

Because the resistance to expansion of the plastic tubing is temperature dependent, the temperature must be recorded during the calibration for volume losses; in addition, the temperature of the tubing during calibration must be the same as it will be during the test. During the test, it is necessary to shade the tubing from the sum or other heat source which could change the calibration and also change the volume of the fluid in the tubing.

The probe must be fully inflated and deflated at least five times before the membrane resistance calibration is made. A new sheath or a sheath that has not been used for, say, 24 hours or more will be stiff at first and have a higher resistance; during the first few inflations the membrane resistance will decrease and will stabilize itself after some five inflations. In order to decrease the errors due to temperature and membrane stiffness, daily volume and membrane calibrations are recommended.

During the test, a cycle is performed at the end of the elastic phase. Very little has been published on the cyclic pressuremeter test procedure and on the use of the results. Baguelin et al. (p. 146 of (1)) give a procedure for the cyclic test where the cycle is performed at the end of the sixth pressure increment. This method, which applies to stress controlled tests, does not determine the unloading point precisely since the choice of pressure increment is operator dependent.

In the Netherlands, a laboratory at Delft (31) has performed dynamic pressuremeter tests. In these tests the cycles are more rapid (one cycle in 10 seconds) than in the Briaud pressuremeter test (one cycle in two minutes). The Delft procedure was used to check the liquefaction

potential of the soil and to determine if the soil could be compacted efficiently.

Using the results of a finite element parametric study, Hartman (p. 339 of 17) shows that the cyclic pressuremeter modulus is less influenced by the soil disturbance created during the bore hole preparation than the first loading pressuremeter modulus.

Jezequel (19) compared the self-boring pressuremeter modulus at 2% strain with the moduli obtained with a Ménard pressuremeter. Jezequel found that the self-boring modulus was close to the first loading modulus of a driven Ménard probe and close to the third cycle modulus of a Ménard probe inserted with the hand auger technique. This finding seems to indicate that cycling reduces the effects of bore hole unloading. Jezequel also found that the third cycle modulus was about 15% greater than the first cycle modulus; all the tests were done in a loose sand.

The test procedure recommended here determines the pressuremeter cyclic modulus (E_c) at a well defined point during the inflation of the pressuremeter, namely the end of the elastic or straight part of the curve. It is necessary to define this point precisely because the value of E_c was found to be dependent on the point along the curve at which the cycle was performed. On the other hand, Windle and Wroth (46) found, using a self-boring pressuremeter in clay, that E_c was independent of the point at which first loading is stopped; Windle and Wroth's experience is supported by Hartman (p. 303 of (17)) who found analytically that E_c does not depend on the stopping point when bore hole unloading is not allowed by the insertion method. Hartman did show, however, that E_c does depend on the stopping point when bore hole unloading is allowed, that is to say, when

the hole is drilled first and yields inwards before the probe is inserted.

In all, eight tests were run to check if the Briaud pressuremeter cyclic modulus (E_c) depended on the strain at which first loading was stopped; these eight tests were Tests Nos. 230 to 233 and 219 to 221 in Fraxer's clay and Test No. 198 in the sand of Ottawa Airport. In these tests, E_c was measured as described in Section 4.4.6; as well, another cyclic modulus E_{c33} was measured by carrying out a cycle at 90 cm^3 inflation. The results are presented in two moduli profiles (Fig. 93 and 114) and in Appendix A in the case of the individual test curves. The results show that E_{c33} was equal, on average, to 1.25 times E_c in the clay and 1.28 times E_c in the sand.

It seems that two important phenomena take place during the inflation process: there is radial compression which makes the soil stiffer and there is a mobilization of shearing resistance making the soil less stiff. According to the results of Fraser's farm and Ottawa Airport, the soil becomes stiffer as expansion progresses since E_{c33} is larger than E_c. This tends to indicate that compression has a dominant influence on the cyclic modulus.

The maximum testing depth of 1.8 m was chosen because at that depth below a large tire (imprint diameter of 480 mm) the maximum vertical stress has become a very small percentage of the tire pressure. According to Barker (2) this percentage is:

- 5% by the Boussinesq theory.
- 2.6% by the Finite Element Method considering a certain pavement configuration.
- 1.1% by multilayered elastic theory considering the same pavement.

According to the Boussinesq theory, which is thought to be conservative, three additional tires of the same size located around the first tire at a distance of two tire diameters (dual tandum wheel gear) will increase this percentage to 10%. This calculation is extreme in the sense that very few planes have tire imprint diameters as large as 480 mm.

The distance between two consecutive tests has been chosen to be 0.3 m or 1.3 times the active length of the probe. Baguelin et al. (p. 133 of (1)) say that the minimum distance between tests, so that the zones of influence do not overlap significantly, is 1.19 times the active length of the probe. Therefore, the minimum distance for the small probe would be 0.27 m.

A particular problem exists when the probe straddles two layers with different stiffness properties. If the two layers have moduli that differ greatly (for example the probe is half in the base course and half in the subgrade), the elastic part of the pressuremeter curve will be a broken line presenting two distinct slopes (Test No. 115). The chances of this occurring can be reduced by determining the pavement cross section before testing (from construction records, for example) or by keeping track of the driving resistance when making the test hole .

It takes about eight hours to get the Briaud pressuremeter ready for testing (saturating the circuits, checking and stopping leaks, setting the zero and calibration); it then takes 6.5 minutes to perform one test once the probe is in place. In an eight hour day, 48 tests (eight holes) can be run.

4.5 Reduction of Data

4.5.1 Correcting the Raw Pressuremeter Curve

The volumeter and gauge readings of Figure 50 are the raw results; these results have to be corrected for hydrostatic pressure, volume losses and membrane resistance. The correction process is identical to the one for the GA pressuremeter described in Section 2.2.5. Test No. 216 (Appendix A) is a typical corrected curve for the Briaud pressuremeter test.

4.5.2 Moduli Determination

Once a stress-strain curve is obtained, the value of the modulus of deformation depends on the method used to determine the "straight line" part of the curve; this part may be more or less well defined but often leaves the engineer with a range of possible slope values. In order to avoid this variable in the standard procedure, an effort is made in this section to give a precise procedure for determining the pressuremeter modulus.

Equation 15 is used to calculate the soil modulus in the Briaud pressuremeter test. The volumes V_m and V_{mc} are determined as shown on Figure 51. In this test, the slope $\frac{\Delta p}{\Delta v}$ of the first loading elastic phase (AB on Fig. 51) and the slope $\frac{\Delta p_c}{\Delta v_c}$ of the cyclic phase (CD on Fig. 51) are evident.

In the case of Test No. 46 (Appendix A), however, a linear part does not exist and it is recommended that a linear regression analysis be used over a volumetric strain interval, μ, of 10% where:

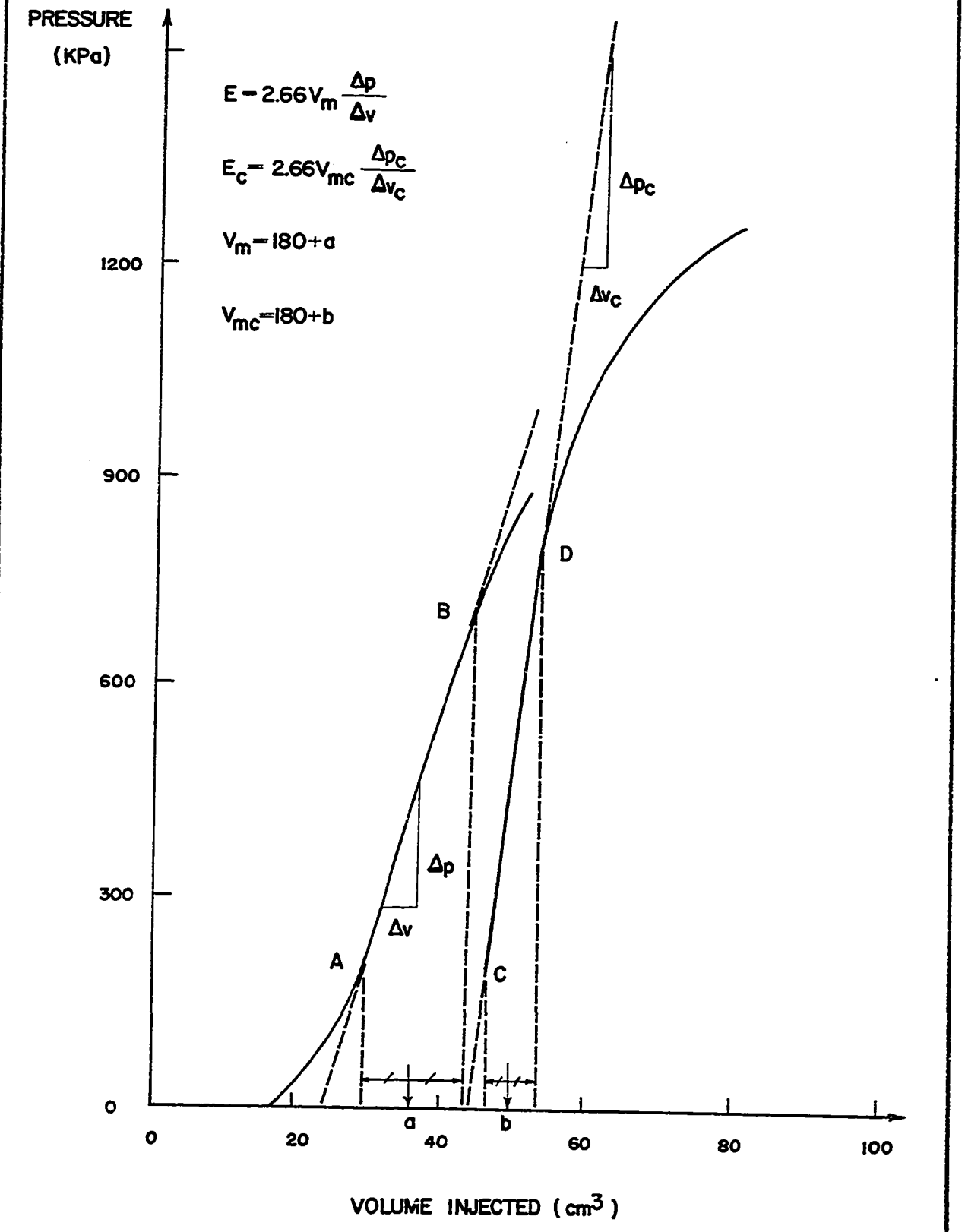

Fig. 51 - Briaud Pressuremeter Tests: Typical Corrected Curve.

$$\mu = \frac{v - v_o}{V_c + v} \quad \ldots\ldots\ldots\ldots\ldots\ldots\ldots\ldots\ldots\ldots \quad (20)$$

and v = the volume injected into the probe

v_o = the difference between the original volume of the cavity V_o and V_c

V_c = the initial volume of the measuring cell; here 180 cm^3.

Ten percent volumetric strain corresponds to a value of $v - v_o$ of about 20 cm^3. The slope $\frac{\Delta p}{\Delta v}$ is obtained by drawing the straight line which is judged to be the linear regression line over 20 cm^3 of injected volume as shown for Test No. 46. Also, as is done for Test No. 46 the initial pressuremeter modulus, E_i, is determined from the test curve; E_i corresponds to the slope of the tangent at the origin.

Determining the slope $\frac{\Delta p_c}{\Delta v_c}$ of the cyclic phase of a test has never presented a problem for any of the tests reported here because this portion of the curve is always a clearly defined straight line; this fact alone is a great incentive for using the cyclic pressuremeter modulus (E_c) rather than the first loading (or standard) pressuremeter modulus (E).

The relative errors $\frac{dp}{p}$ and $\frac{dv}{v}$ on the coordinates (p, v) of a point on the corrected curve are due to possible errors in the calibration corrections. The values $\frac{dp}{p}$ and $\frac{dv}{v}$ can be evaluated in the following manner. The volume loss correction, in an average test, represents about 15% of the volume of water injected during the elastic phase (Fig. 52). If the precision on the volume correction is 10%, then the maximum error induced by the volume correction on the volume coordinate (v) of a curve point is: $\frac{dv}{v} = 0.015$.

Similarly, the membrane resistance correction represents, in an average test, 20% of the test pressure (p)(Fig. 52). The precision on the membrane correction appears to be greater than on the volume losses; a reasonable estimate would be 5% giving a precision on the pressure coordinate (p) of a point, $\frac{dp}{p}$, of 0.01.

Since the hydrostatic pressure is small and known precisely it does not induce any error; the overall precision on the coordinates of a point is therefore a few percent.

The precision on the modulus E or E_c can be evaluated from Equation 15 by a calculation of error as follows:

$$E = 2.66\ V_m \frac{\Delta p}{\Delta v} \quad \ldots\ldots\ldots\ldots\ldots\ldots\ldots \quad (15)$$

or

$$E = 2.66\ (180 + \frac{v_o + v_f}{2})\ \frac{p_f - p_o}{v_f - v_o} \quad \ldots\ldots\ldots\ldots \quad (21)$$

where v_f, v_o, p_f, p_o are given on Figure 22. Then the relative precision on E is given by:

$$\frac{dE}{E} = \frac{1}{2}\ \frac{dv_o + dv_f}{180 + \frac{v_o + v_f}{2}} + \frac{dv_o + dv_f}{v_f - v_o} + \frac{dp_o + dp_f}{p_f - p_o} \quad \ldots\ldots \quad (22)$$

If the following seemingly reasonable assumptions are made (Fig. 52):

$$dv_o = dv_f = 1\ cm^3;\quad v_o = 15\ cm^3;\quad v_f = 45\ cm^3$$

$$dp_o = dp_f = 10\ kPa;\quad p_o = 100\ kPa;\quad p_f = 800\ kPa$$

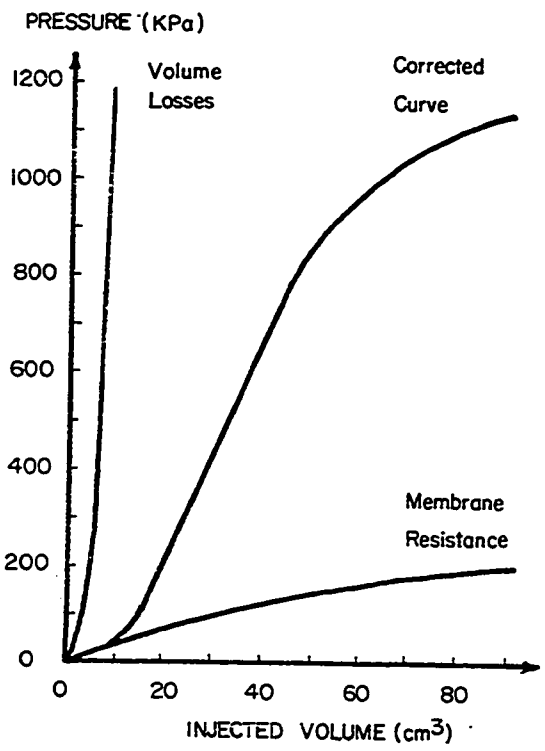

Fig. 52 - Relative Magnitude of Corrections and Test Curve.

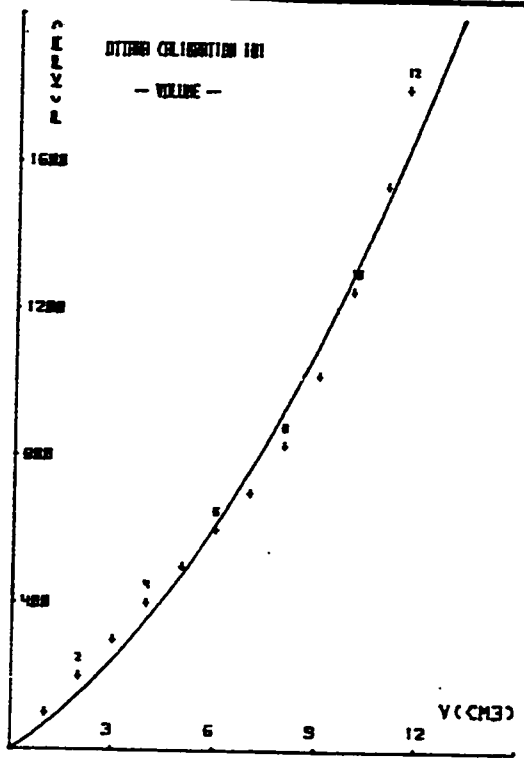

Fig. 53 - Computer Regression for Volume Losses Curve

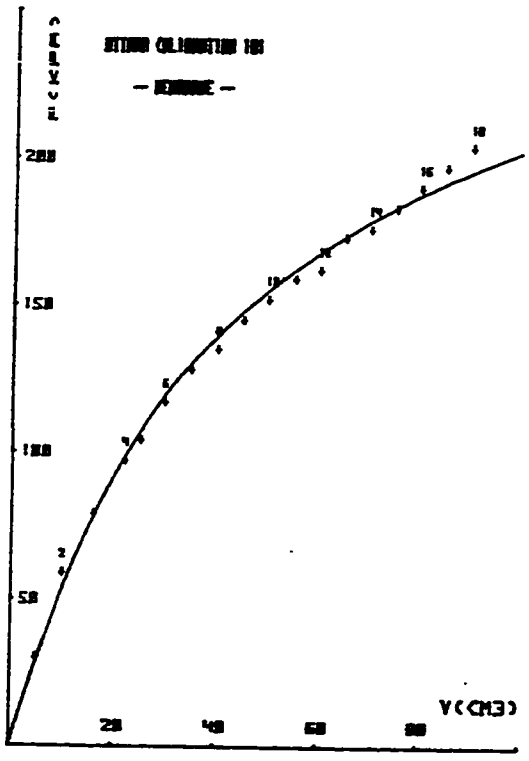

Fig. 54 - Computer Regression for Membrane Resistance Curve

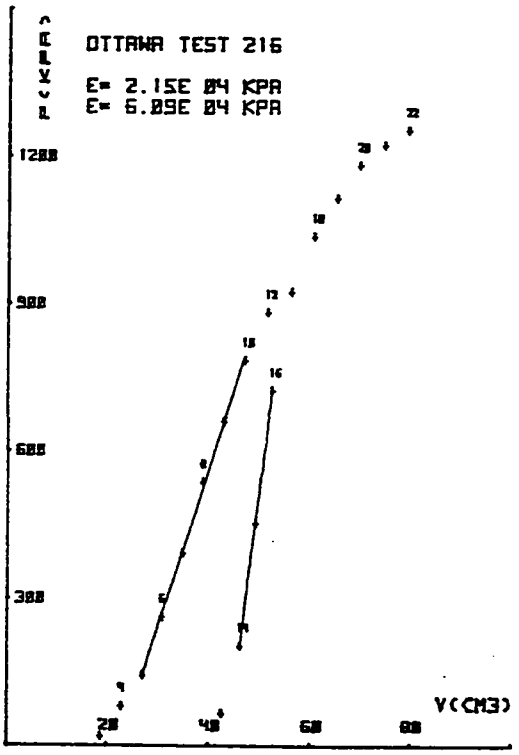

Fig. 55 - Computer Plot of a Briaud Pressuremeter Test Curve

then: $\frac{dE}{E} = \frac{1}{2} \times \frac{2}{210} + \frac{2}{30} + \frac{20}{700} = 0.10$

In this case, the modulus would be 13,000 kPa and the precision would be 10%; therefore, moduli need only be quoted with two significant figures. In a similar case, Kunio Suyama and Tsuneo Imai (21) report a precision on $\frac{dE}{E}$ of 17%.

It must be said that, statistically, errors may have opposite influences on the dimension being measured; a simple addition of all the errors involved, as was done above, is a very conservative estimate of the possible error involved in any particular calculation.

As discussed in Baguelin et al. (p. 107 of (1)), the shape of the curve gives an indication of the quality of the test. For example, in Test No. 179 (Appendix A) the hole was too large and the probe did not start to pressurize the cavity walls until late on the volume injected scale. In Test No. 219 (Appendix A) the hole was too small, the probe had to be forced into the ground; the soil exerted a pressure on the probe before any injection of water and as a result, the curve starts on the pressure axis. Test No. 111 (Appendix A) is a case of great disturbance to the soil. The shape of the curve for Test No. 115 is probably due to the presence of two layers with different moduli within the active length of the probe; in this case the modulus was obtained from an average slope.

4.5.3 Reduction of Data by Computer

Each Briaud pressuremeter test generates about 22 points. It takes an experienced engineer about one hour to correct the curve and calculate the modulus using a desk calculator. An airport evaluation program might

include 10 to 20 holes, therefore, 60 to 120 tests. In order to cut down the time required and avoid human error, a computer program has been developed that will correct the field curve and plot the result. This program makes use of a Hewlett Packard 9125A calculator and 9862A plotter.

Lemée and Saintilan (27) and, later Carlo (7) wrote computer programs to reduce Ménard pressuremeter test results; the computer program presented here specifically for the Briaud pressuremeter test was inspired by Lemée's and Carlo's work.

The program represents the volume losses curve by drawing a parabola through the volume loss calibration data points;

$$p = Av + Bv^2 \quad \ldots\ldots\ldots\ldots\ldots\ldots\ldots\ldots \quad (23)$$

The regression method is used and a parabolic equation was chosen by trial and error from actual volume loss calibration curves. Figure 53 shows a typical computer representation of a volume losses curve. As recommended by Lemée and Saintilan (27) the program draws a curve through the data points of the membrane resistance calibration, using the following equation:

$$v = pe^{ap^2+b} \quad \ldots\ldots\ldots\ldots\ldots\ldots\ldots\ldots \quad (24)$$

The regression method is used. Figure 54 shows a typical computer representation of a membrane resistance curve.

For the test curve, the program corrects the test data points, one by one, applying the hydrostatic, volume loss and membrane resistance

correction; the correction for membrane resistance is obtained from Equation 24 by the Newton-Raphson method. The corrected points are plotted and numbered on a graph (Fig. 55). The engineer can then tell the computer the points between which he wants to make a linear regression to obtain a modulus value. In the case of the test shown in Figure 55, the regression was made between points 5 to 10 for E and 14 to 16 for E_c.

The listing of the program is in Appendix D.

CHAPTER 5

OTHER TESTS AND THE TEST PROGRAM

Besides pressuremeter tests, the following other tests were performed: McLeod plate tests, triaxial tests, vane tests, Standard Penetration Tests and soil classification tests. The procedure and data reduction for these tests are discussed in this chapter along with a general outline of the testing program.

5.1 The McLeod Plate Test

5.1.1 The Test

The McLeod plate test is described briefly in Section 2.1.1 and is shown in Figures 2, 3 and 4. This section (Section 5.1.1) gives a detailed presentation of the test procedure and the test results. The aim of the McLeod plate test is to evaluate the subgrade bearing strength (S_s); S_s is the basic design parameter (Section 2.1.1) for airport pavements in Canada at the present time. S_s is the load which, when applied to the subgrade surface through a standard 762 mm diameter plate, will create a 12.5 mm deflection at the 10th load application. Generally S_s is not measured directly but is deduced from the measurement of the pavement bearing strength (S_p); S_p is the load which, when applied to the pavement surface through a standard 762 mm diameter plate, will create a 12.5 mm deflection at the 10th repetition of load.

The test to measure S_p takes about eight hours and is called the repetitive test; since the repetitive test takes so long, Transport

Canada now performs a large number of non repetitive tests instead that last only two hours. An S_p value can be deduced from the non repetitive test. Also, although the standard plate is 762 mm in diameter, a smaller plate is sometimes used so that the load can be kept within the limits of the load reaction that one or two trucks can provide; the S_p value can be estimated from the test performed with a smaller plate.

The test procedure and data reduction for the repetitive and non repetitive tests are given in detail in Transport Canada manual AK-68-31 and are based on McLeod's work (28).

The non repetitive plate test consists of the application of six load increments to the plate (Fig. 56). The magnitude of the load increments is chosen so that each load will create an additional deflection of about 1.25 mm; the i^{th} load increment is applied when the deflection rate under the $(i-1)^{th}$ load increment has been 0.25 mm/min or less for three consecutive minutes. The load-deflection curve is obtained by plotting, for each load increment, the load versus the deflection at the end of the application of that load (Fig. 57). The pavement bearing strength S_p is obtained from the load-deflection curve and the table of Figure 58. The load-deflection curve allows the load S corresponding to one of the deflections of Figure 58 (preferably close to 8.5 mm) to be determined. Then, using the same figure, the ratio $(\frac{S_p}{S})$ for the given plate diameter and the chosen deflection is noted. S_p can now be calculated.

The repetitive plate test consists of the application of three load increments with each increment being cycled six times (Fig. 59). The load increments are chosen so that they create approximately 1 mm, 5 mm

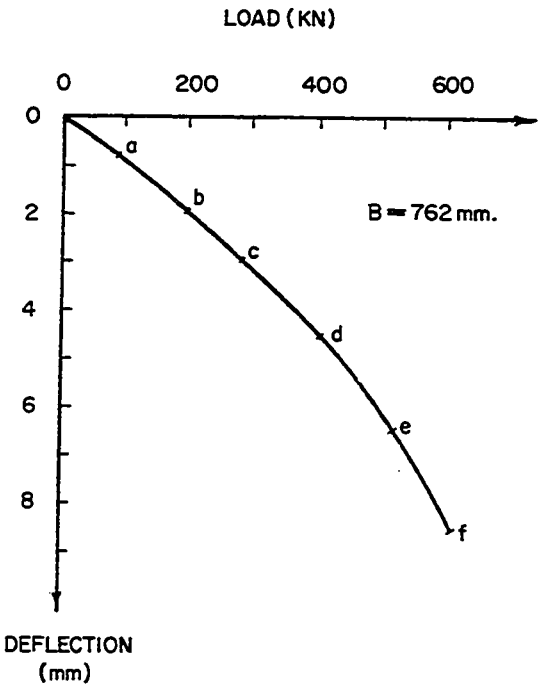

Fig. 57 - Non Repetitive Plate Test - Typical Load-Deflection Curve

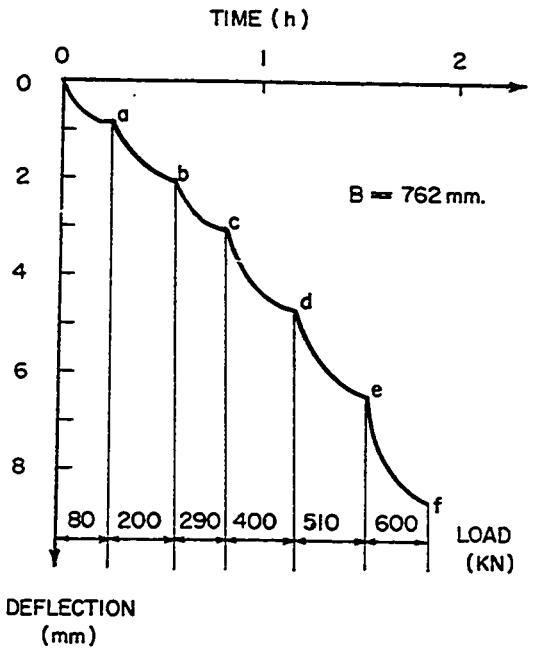

Fig. 56 - Non Repetitive Plate Test - Typical Time - Deflection Curve.

Ratio $\frac{\text{Load on 762 mm diameter plate, 12.5 mm deflection, 10 rep.}}{\text{Load on plate of diameter } \Phi\text{, deflection } \Delta\text{, 0 rep.}}$

Test Plate Diameter	Load Ratios						
	Test Deflection (mm)						
mm	2.50	3.75	5.00	6.25	7.50	8.75	10.00
305	5.780	4.255	3.448	2.941	2.667	2.451	2.299
457	4.000	2.899	2.326	2.000	1.802	1.653	1.550
610	2.941	2.151	1.724	1.493	1.351	1.242	1.168
762	2.358	1.724	1.377	1.208	1.081	0.985	0.922

(load ratios for test on surface of asphalt pavements)

Fig. 58 - Non Repetitive Plate Test. Bearing Strength Ratio for Plates of Different Diameters (from Transport Canada Manual AK-68-31).

and 10 mm deflection of the plate at the first application. Cycling means removing the load completely. The criterion for determining when to end a loading or unloading increment in a cycle is the same as for the non repetitive test. Three graphs are drawn for each repetitive plate test: two load-deflection graphs and one deflection-load repetitions graph. The first graph is the plot of the deflection at the end of the first cycle versus the load cycled during that step (Fig. 60). The second graph is a plot of the deflection versus the number of load repetitions on a log scale (Fig. 61); for each load step, the deflection at the end of a cycle is plotted versus the cycle number. Six points are plotted (e.g.: b_1, b_2, b_3, b_4, b_5, b_6 of Fig. 59 on Fig. 61); a straight line is drawn through these points and the line is extended to 1000 cycles (b_{1000}). Three such lines are obtained, one for each load step. The third graph is a plot of the deflection at the end of a standard number of cycles within a load increment versus the load cycled during that increment (Fig. 62). The standard numbers of cycles are 1, 10, 100, 1000 and the coordinates of the points to be plotted are read on Figure 61. Then, as shown in Figure 62, S is read at 12.5 mm deflection on the 10^{th} repetition curve. If the diameter of the plate which is used is 762 mm, S is equal to S_p; if not the S_p value for a 762 mm diameter plate must be deduced from the S value for the actual plate using the table of Figure 63.

Once the S_p value is obtained from either test, the S_s value is deduced by using Equation 1 as explained in Section 2.1.1:

$$S_s = S_p \, 10^{-\frac{t}{165}} \quad \ldots\ldots\ldots\ldots\ldots\ldots\ldots\ldots \quad (1)$$

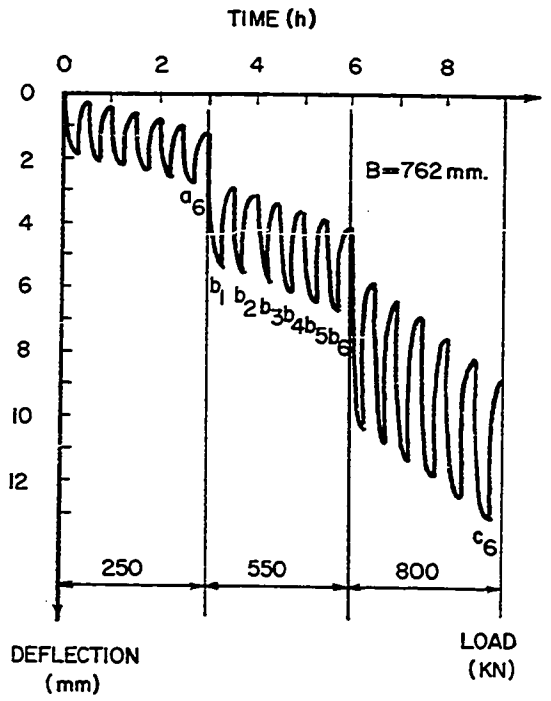

Fig. 59 - Repetitive Plate Test - Typical Time - Deflection Curve.

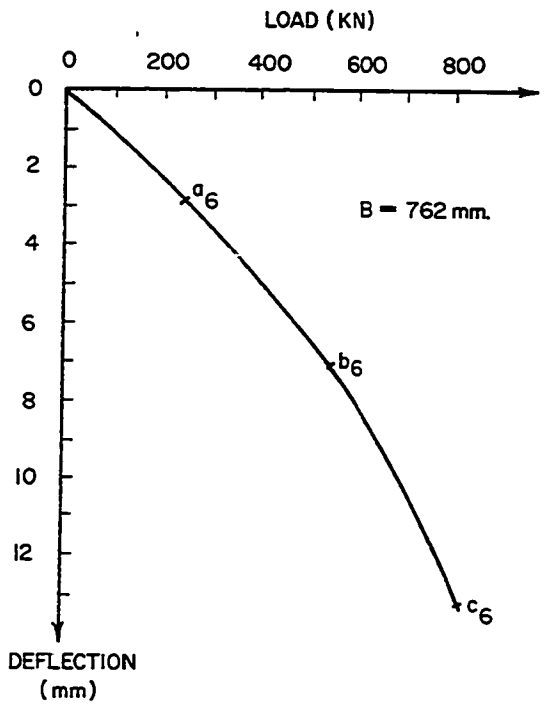

Fig. 60 - Repetitive Plate Test - Typical Load-Deflection Curve.

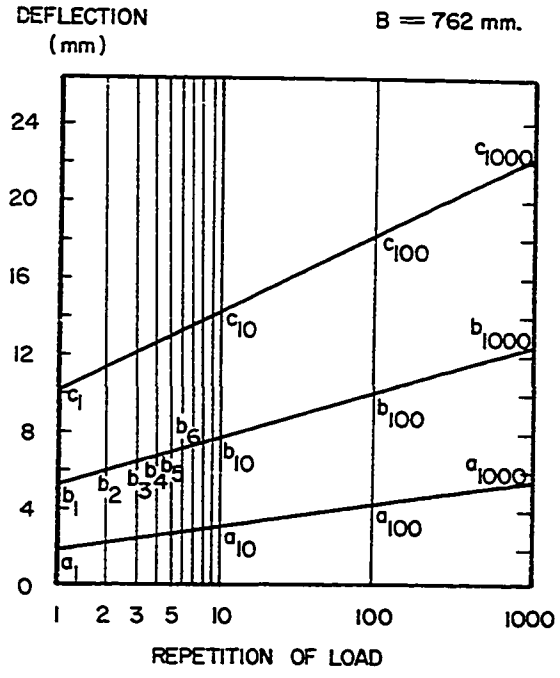

Fig. 61 - Repetitive Plate Test - Typical Deflection - Load Repetition Graph.

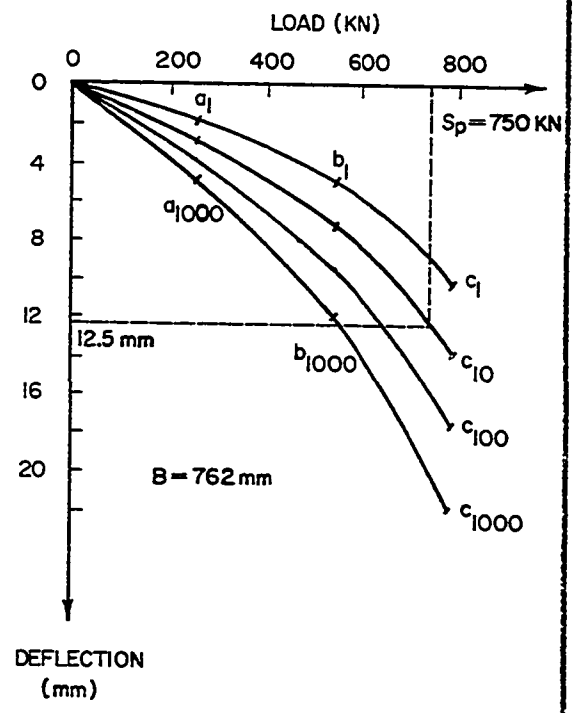

Fig. 62 - Repetitive Plate Test - Typical Extrapolated Load - Deflection Curve.

5.1.2 Precision

The basic parameter S_s calls for: a test on the subgrade surface, a repetitive test, a 762 mm diameter plate and 12.5 mm of deflection at the 10^{th} load repetition; in practice, the above requirements are never all satisfied at one time. Often enough, none of these requirements are satisfied. In order to obtain S_s from the measurement actually made during the test (S), extensive use is made of conversion procedures such as Equation 1, Figure 58 and Figure 63. Although these conversion procedures are based on extensive testing experience, they induce error. To these conversion errors must be added the measurement errors (for example, calibration of the loading jack, precision of the deflection measurement, etc.).

A 10 to 20% measurement error seems to be a reasonable range. The procedural errors are difficult to evaluate but they certainly are not negligeable; for example, for the conversion procedure used to get S_p from a non repetitive test (Fig. 58), Transport Canada quotes the standard duration of percentage error which is introduced by using the procedure (Fig. 64). The standard deviation of percentage error ranges from 10 to 30%. It seems then, that taking into account measurement and procedure error, S_p is accurate to within about 35%.

S_s then is obtained from S_p by using Equation 1; this equation is due to McLeod (28) and is based on many plate tests at many airport sites. In Equation 1 the only parameter that characterizes the pavement is its equivalent granular thickness t; in otherwords, as was pointed out by McLeod (p. 49 of (28)) Equation 1 is based on the assumption that all airport base courses have the same carrying capacity and that they

Ratio $\frac{\text{Load on 762 mm diameter plate, 12.5 mm deflection, 10 rep.}}{\text{Load on plate of diameter } \phi\text{, deflection } \Delta\text{, 10 rep.}}$

Test Layer	Test Plate Diameter	Land Ratios					
		Test Deflection Δ (mm)					
	mm	1.25	2.5	5.0	7.5	10.0	12.5
Surface	305	10.904	6.362	4.054	3.259	2.834	2.559
Subgrade	305	12.743	7.482	4.748	3.797	3.291	2.984
Surface	457	7.252	4.280	2.725	2.182	1.890	1.692
Subgrade	457	7.979	4.700	3.022	2.410	2.082	1.887
Surface	610	5.323	3.215	2.050	1.636	1.409	1.250
Subgrade	610	5.521	3.334	2.150	1.714	1.476	1.318
Surface	762	4.287	2.589	1.655	1.315	1.129	1.000
Subgrade	762	4.188	2.536	1.646	1.312	1.125	1.000
Surface	914	3.475	2.174	1.391	1.100	0.935	0.827
Subgrade	914	3.296	2.013	1.313	1.047	0.894	0.791
Surface	1067	2.940	1.871	1.199	0.945	0.799	0.703
Subgrade	1067	2.708	1.675	1.083	0.861	0.730	0.658

Fig. 63 - Repetitive Plate Test. Bearing Strength Ratio for Plates of Different Diameters (from Transport Canada Manual AK-68-31).

Plate Diameter (mm)	Test Deflection						
	1.25	2.50	3.75	5.00	6.25	7.5	8.75
610	32.8	23.2	16.9	13.0	10.8	10.8	10.6
762	28.1	19.3	15.1	13.5	11.1	10.2	9.5

Fig. 64 - Non Repetitive Plate Test. Standard Deviation of Percentage Errors (from Transport Canada Manual AK 68-31).

have this capacity at all times. This assumption induces error; based on Figures 98, 99, 100 in McLeod (28), this error is about 50%. If S_p is known with a precision of 35% and t is known with a precision of 10%, the possible error on the basic design parameter S_s approaches 100%.

5.2 The Triaxial Tests

In this study, nine multistage cyclic triaxial tests and four one-stage cycled triaxial tests were performed (Appendix C). For all tests, the sample and the apparatus were prepared as for an isotropically consolidated, undrained triaxial test. The sample was then consolidated under its estimated in situ lateral stress. During the test, drainage was allowed for sand samples and prevented for clay samples; the rate of strains for loading and unloading was 0.38 mm/minute throughout each test.

The procedure for the one-stage cycled triaxial test was as follows: the cell pressure σ_3 was increased to the chosen value; the sample was loaded to one-third of the estimated failure deviator stress and from that point, three full load cycles were performed, then the sample was taken to failure.

The procedure for the multistage cyclic triaxial test was as follows: the cell pressure σ_3 was increased to the first testing value (~ 14 kPa); the sample was loaded to one-third of the estimated failure deviator stress and from that point three full cycles were performed; the cell pressure was increased to the second testing value (~ 35 kPa); the sample was loaded once again to one-third of the estimated failure deviator stress under the increased cell pressure; three cycles were performed; this procedure was repeated for σ_3 = 105 kPa and σ_3 = 210 kPa; then, the

sample was finally brought to failure.

For both tests, volume changes were measured by the air displacement method for dry and moist samples and by the water displacement method for saturated samples. The samples were cylindrical with a height to diameter ratio of two; the height of the samples varied from 8 cm to 20 cm. One cycle lasted anywhere from one to five minutes.

Area and volume change corrections were applied to the raw data and the deviator stress ($\sigma_1 - \sigma_3$) versus vertical strain (ε_z) curve was plotted (e.g.: Test No. 255 Appendix C); each test curve contained about 100 points. The modulus determination for the triaxial test simply consisted of fitting the best straight line through the points of the curve. The triaxial modulus (E_T) was given by the slope of the initial part of the curve (see, for example, Test No. 255) and the triaxial cyclic modulus (E_{Tc}) by the slope of the third cycle (again, refer to Test No. 255).

For each multistage cyclic triaxial test, one E_T value (at the first σ_3) and four E_{Tc} values (one E_{Tc} for each cell pressure σ_3) were obtained. In addition, three other E_T values could be obtained by assuming that the ratio E_{Tc}/E_T of the first σ_3 was applicable to the other σ_3 values; these E_T are called 'extrapolated' E_T (Test No. 255).

5.3 Other Tests

The other tests of this study include Standard Penetration Tests (SPT), classification tests and vane tests.

Standard Penetration Tests were performed at Sarnia Airport on the centerline of the runway; the asphalt was removed with a 100 mm diameter

continuous flight auger, then SPT tests were run according to A.S.T.M. D1586-67 every 0.3 m of depth down to 2.1 m.

The classification tests included grain size analyses (A.S.T.M. D422-63), Atterberg limits (A.S.T.M. D423-66, A.S.T.M. D424-59), and moisture content determinations.

Vane tests were performed in the clay of Fraser's farm. The vane was 67 mm wide, 149 mm high (vertical edge) and had 45° tapered ends. The test procedure followed the one which is described in A.S.T.M. D2574-72. The accuracy of the vane results as evaluated from the precision of the readings is 5 to 10%.

5.4 The Test Program

The test program involved 344 tests which are listed with details in Figures 65 and 66; there were 235 pressuremeter tests (37 with the standard Ménard GA pressuremeter and 199 with the Briaud pressuremeter), 11 standard McLeod plate tests, 14 multistage cyclic triaxial tests, 33 classification tests, 20 vane tests and 30 SPT tests.

The tests were performed at four different sites: a sand site (simulated by the large sand box of the University of Ottawa), a clay site (Fraser's farm near Ottawa), an airport on sand (Ottawa International Airport) and an airport on clay (Sarnia Airport).

The pressuremeter tests which were performed at the sand site and the clay site were devoted primarily to the study of the critical depth problem (Chapter 6) and to evaluating the disturbance generated by the chosen method of borehole preparation (Section 4.3). The sand box was chosen as the sand site because the unit weight of the sand could be

Symbol	Type of Test
Cl	Classification tests: water content + Atterberg limits + grain size analysis.
I_D	Density index.
DR	Driven rod (hole preparation).
GA	Ménard GA pressuremeter.
HA	Hand auger (hole preparation).
P	Pressuremeter test (Briaud type except when specified otherwise.
PCy	Pressuremeter test (Briaud) with cycle.
PCMR	Pressuremeter calibration: membrane resistance.
PCVL	Pressuremeter calibration: volume losses.
PS	Pressuremeter test (GA) with surface movement measurement.
PLNRp	Plate test: non repetitive.
$PLNR_p$	Plate test: repetitive.
SPT	Standard penetration test.
T	Triaxial tests, undrained - cyclic - 1 cell pressure.
T_m	Triaxial tests, undrained - multistage cyclic - 3 or 4 cell pressures.
V	Vane tests.

Fig. 65 - List of Symbols for Fig. 66.

Test No.	Type of Test	Site	Hole No.	Depth (m)	Observations
1,2,4,5	P	Sand box			GA - Pilot tests. Not plotted
3	PCVL	Sand box			GA
5,7,8	PCMR	Sand box			GA
9	P	Sand box		1.49	GA - I_D = 63.5
10	P	Sand box		1.45	GA - I_D = 64
11	P	Sand box		0.65	GA - I_D = 46
12 to 15	PCVL, PCMR	Sand box			GA
16	P	Sand box		1.22	GA - I_D = 59.4
17	P	Sand box		0.92	GA - I_D = 53.3
18	P	Sand box		1.89	GA - I_D = 65.9
19	P	Sand box		0.32	GA - I_D = 50.3
20	P	Sand box		1.53	GA - I_D = 93.3
21	P	Sand box		0.61	GA - I_D = 94.5
22	P	Sand box		0.94	GA - I_D = 94.8
23	P	Sand box		1.83	GA - I_D = 93.4
24	P	Sand box		1.22	GA - I_D = 94.9
25	P	Sand box		1.22	GA - I_D = 94.9
26	PS	Sand box		0.31	GA - I_D = 92.5
27	PS	Sand box		0.31	GA - I_D = 92.5
28	PS	Sand box		0.91	GA - I_D = 94.7
29	PS	Sand box		1.27	GA - I_D = 64.5
30	PS	Sand box		0.94	GA - I_D = 62.8
31	PS	Sand box		0.61	GA - I_D = 74.5
32	PS	Sand box		0.30	GA - I_D = 68.9
33 to 37	PCVL, PCMR	Sand box			
38 to 45	P	Sand box			Pilot tests: test proc., Rate determin. Not plotted.
46	P	Sand box		1.83	Buried probe. I_D = 70
47 to 52	P	Sand box		0.3 to 1.8	Driven probe. I_D = 70 Test every 0.3 m
53 to 58	P	Sand box		0.3 to 1.8	Driven probe. I_D = 70 Test every 0.3 m
59 to 64	P	Sand box		0.3 to 1.8	Driven probe. I_D = 70 Test every 0.3 m
65	PCMR, PCVL	Sand box			
66	P	Sand box		1.8	Buried probe. I_D = 95
67 to 72	P	Sand box		0.3 to 1.8	Driven probe. I_D = 95 Test every 0.3 m
73	PCMR	Sand box			
74	P	Sand box		1.8	Driven probe. I_D = 95
75 to 80	P	Sand box		0.3 to 1.8	Driven probe. I_D = 95 Test every 0.3 m
81	PCMR	Sand box			
82	P	Sand box		1.25	Buried probe. I_D = 65

Fig. 66 - List of Tests (for legend see Fig. 65).

Test No.	Type of Test	Site	Hole No.	Depth	Observations
83 to 88	P	Sand box		0.3 to 1.8	Driven probe. I_D = 65 Test every 0.3 m
89,90	PCMR	Sand box			
91 to 96	P	Sand box		0.3 to 1.8	Driven probe. I_D - 65 Test every 0.3 m
97	P	542 King Edward		1.46	Pilot test - HA. Not plotted.
98	P	Sarnia Airport	1A	0.3	HA - Hole too large
99 to 104	P	Sarnia Airport	1	0.3 to 1.8	HA
105 to 109	P	Sarnia Airport	2	0.3 to 1.5	DR - probe damaged at 1.2 and 1.5 m
110 to 115	P	Sarnia Airport	3	0.3 to 1.8	DR - test every 0.3 m
116 to 121	P	Sarnia Airport	6	0.3 to 1.8	DR - test every 0.3 m
122	PCMR	Sarnia Airport			
123 to 128	P	Sarnia Airport	5	0.3 to	DR - test every 0.3 m
129 to 134	P	Sarnia Airport	4	0.3 to 1.8	DR - 7.5 m off centerline Test every 0.3 m
135 to 140	P	Sarnia Airport	7	0.3 to 1.8	DR - twice. Test every 0.3 m
141	P	Sarnia Airport	8	0.3	DR - twice
142	P	Sarnia Airport	8A	0.3	DR
143	P	Sarnia Airport	10	1.2	DR
144	PCy	Sarnia Airport	11	1.2	DR - 10 cycles
145 to 150	P	Sarnia Airport	14	0.3 to 1.8	DR - 3 times. Tests every 0.3 m
151 to 156	P	Sarnia Airport	15	0.3 to 1.8	DR - Tests every 0.3 m
157	P	Sarnia Airport	12	1.2	HA
158	PCMR	Sarnia Airport			
159 to 168	P	Fraser's clay	1	0.3 to 3	HA. Test every 0.3 m Before slab
169	PCMR	Fraser's clay			
170 to 179	P	Fraser's clay	2	0.3 to 3	HA. Test every 0.3 m Before slab
180	PCMR	Fraser's clay			
181,182	PCMR, PCVL	Ottawa Airport			
183 to 187	PCy	Ottawa Airport	1	0.3 to 1.5	DR. Tests every 0.3 m
188 to 192	PCy	Ottawa Airport	2	0.3 to 1.5	DR. Tests every 0.3 m
193 to 198	PCy	Ottawa Airport	3	1.8 to 0.3	DR. Tests every 0.3 m
199 to 204	PCy	Ottawa Airport	4	1.8 to 0.3	DR. Tests every 0.3 m

Fig. 66 (cont'd). List of Tests (for legend see Fig. 65).

Test No.	Type of Test	Site	Hole No.	Depth	Observations
205 to 210	PCy	Ottawa Airport	5	1.8 to 0.3	DR. Tests every 0.3 m
211 to 216	PCy	Ottawa Airport	6	1.8 to 0.3	DR. Tests every 0.3 m
217	T	Sand box			Vibrated $I_D = 65$. Not plotted.
218	T	Sand box			Vibrated $I_D = 93$
219 to 227	PCy	Fraser's clay	7	2.7 to 0.3	DR. Tests every 0.3 m After slab
228,229	PCMR, PCVL	Fraser's clay			
230 to 238	PCy	Fraser's clay	6	2.7 to 0.3	HA. Tests every 0.3 m After slab
239 to 246	V	Fraser's clay	3	0.3 to 2.4	Test every 0.3 m Before slab
247,248	T_m,T	Sand box			I_D = 95 - rained
249,250	T_m,T	Sand box			I_D = 65 - rained
251	T_m	Ottawa Airport	5	0.3	Vibrated
252	T_m	Ottawa Airport	6	0.3	Vibrated
253	T_m	Ottawa Airport	1	0.3	Vibrated
254	T_m	Ottawa Airport	3	0.3	Not performed
255	T_m	Fraser's clay	5	1.0	
256	T_m	Fraser's clay	5	1.8	
257,258	T_m	Sarnia Airport	10 to 12	1.2	
259 to 260	V	Fraser's clay	3	2.7 to 3.0	Test every 0.3 m Before slab
261 to 270	V	Fraser's clay	4	0.3 to 3.0	Test every 0.3 m After slab
271	Cl	Ottawa Airport	1	0.3	
272	Cl	Ottawa Airport	5	0.3	
273	Cl	Ottawa Airport	6	0.3	
274 to 279	SPT	Sarnia Airport	3	0.3 to 1.8	
280 to 285	SPT	Sarnia Airport	5	0.3 to 1.8	
286 to 291	SPT	Sarnia Airport	6	0.3 to 1.8	
292 to 297	SPT	Sarnia Airport	15	0.3 to 1.8	
298 to 303	SPT	Sarnia Airport	7	0.3 to 1.8	
304 to 309	Cl	Sarnia Airport	3	0.3 to 1.8	
310 to 315	Cl	Sarnia Airport	5	0.3 to 1.8	
316 to 321	Cl	Sarnia Airport	6	0.3 to 1.8	

Fig. 66 (cont'd). List of Tests (for legend see Fig. 65).

Test No.	Type of Test	Site	Hole No.	Depth	Observations
322 to 327	C1	Sarnia Airport	15	0.3 to 1.8	
328 to 333	C1	Sarnia Airport	7	0.3 to 1.8	
334	P1Rp	Sarnia Airport	7	0	Station 124+90. B=0.762 m
335	P1Rp	Sarnia Airport	6	0	Station 105+00. B=0.762 m
336	P1NRp	Sarnia Airport	15	0	Station 122+50. B=0.762 m
337	P1NRp	Sarnia Airport	3	0	Station 95+00. B=0.762 m
338	P1NRp	Sarnia Airport	5	0	Station 97+50. B=0.762 m
339	P1Rp	Ottawa Airport	1	0	B = 0.45 m
340	P1Rp	Ottawa Airport	4	0	B = 0.762 m
341	P1NRp	Ottawa Airport	2	0	B = 0.61 m
342	P1NRp	Ottawa Airport	3	0	B = 0.61 m
343	P1NRp	Ottawa Airport	5	0	B = 0.61 m
344	P1NRp	Ottawa Airport	6	0	B = 0.762 m

Fig. 66 (cont'd). List of Tests (for legend see Fig. 65).

controlled at will; the clay site was chosen because the geotechnical properties of the clay were well known.

The Briaud pressuremeter tests and McLeod plate tests at the two airport sites were performed in order to compare the two types of test under actual field conditions, to establish and refine the Briaud pressuremeter testing procedure, and to check how practical and robust was the Briaud pressuremeter.

The triaxial tests, SPT tests and vane tests were performed to provide additional information such as an independent appraisal of the modulus of elasticity of the soil.

Because no soil classification test results were available at the Sarnia and Ottawa International Airports, classification tests were performed on disturbed samples which were obtained at each of these two sites.

The testing sequence went as follows:

1. Testing in the sand box - May to August 1977.
2. Testing at Sarnia Airport - September 1 to 15, 1977.
3. Testing at Fraser's farm before silo - September 20 to 27, 1977.
4. Testing at Ottawa Airport - October 6 to 13, 1977.
5. Testing at Fraser's farm after silo - October 15 to 20, 1977.

The Menard and Briaud pressuremeter test curves are given in Appendix A, the McLeod plate test curves in Appendix B and the multistage cyclic triaxial test curves in Appendix C.

CHAPTER 6

THE CRITICAL DEPTH PROBLEM

6.1 General

In a deep pressuremeter test, the soil around the probe moves laterally only and plane strain conditions ($\varepsilon_z = 0$) are closely approximated. In a shallow test it may be that the soil around the probe moves both laterally and upward due to the close proximity of the free boundary; in this case, the plane strain assumption would not be warranted. For the same pressure level, the probe at shallow depth would be expected to deform more than a probe at a deeper position. This would lead to lower $\frac{\Delta p}{\Delta v}$ values at shallow depth and according to Equation 15 to lower E values. Since the Briaud pressuremeter is used close to the surface, this chapter studies the influence of the proximity of the ground surface in detail and tries to answer the following question: is there a critical depth for the Briaud pressuremeter modulus?

The critical depth concept usually refers to a failure phenomenon such as the tip capacity of a pile. In the case of pile tip capacity, the following definition applies: the critical depth is the depth beyond which the failure pattern does not involve the ground surface. In the case of the elastic modulus, there is no failure pattern and, therefore, a more general definition of critical depth must be found. The following definition is proposed and will be used in this study: the critical depth is the depth beyond which the surface has no significant influence on the deformation process. This means that the deformation of the ground surface during the loading process is very small.

Theoretically, the ground surface has an influence on the modulus which is measured at any depth. At a depth z the vertical and horizontal stresses in the ground are γz and $k_o \gamma z$ and at a depth 2z these stresses are doubled. Since the horizontal stress has an influence on the moduli of deformation, especially in sands (47), the modulus will increase with depth. A clear distinction, then, must be made between the variation of modulus with depth due to increasing horizontal stress and the variation due to a critical depth effect.

The critical depth study included tests in sand, tests in clay, and computer simulations. The tests in sand were carried out in the large sand box of the University of Ottawa; both Ménard (GA) and Briaud pressuremeter tests were performed every 0.3 m of depth in a 2.1 m deep deposit of dry uniform sand. Tests were run with the sand in two states of density. The intent was to check if there was a break in the profiles of moduli values which would indicate a critical depth. In addition, triaxial tests were performed to evaluate the variation of the modulus of the sand with confining pressure and to compare the triaxial and pressuremeter moduli.

The clay site was a natural site near Ottawa; Briaud pressuremeter tests were carried out every 0.3 m down to 3 m depth. Subsequently, a 1 m thick concrete slab was built on the ground surface for a silo; Briaud pressuremeter tests were carried out through the slab close to the location of the previous tests. The slab had the effect of increasing the effective depth of testing. If there were a critical depth indicated on the test profile before the slab was poured, it seems reasonable to expect that the break in the profile would move upward once the slab was

in place. Vane tests were performed before and after construction of the slab for comparison purposes. Triaxial tests were also performed.

The computer study consisted of simulating a shallow pressuremeter test and a deep pressuremeter test in an isotropic, homogeneous, linear elastic soil using the finite element method. The results of the computer study were analysed to give an idea of what the deformation could be around the probe both during a test close to the ground surface and a test at considerable depth.

6.2 Literature Survey

Very little has been published on the precise topic of critical depth and pressuremeter modulus profile. A number of articles have been published however on critical depth and limit pressure profile. Both Ménard (29) and Jezequel (18) acknowledge the existence of a critical depth in the limit pressure profile; Jezequel goes on to say that the pressuremeter modulus is less influenced by the critical depth phenomenon than is the limit pressure.

Wong and Duncan (47) proposed a model in which the modulus depends on the minor principal stress (σ_3). Hartman (p. 91 of (17)) used this model to show that there would be an increase in in situ modulus with depth due to the increase in at rest horizontal pressure.

Beguelin et al. (p. 185 of (1)) state that as a rule of thumb the pressuremeter seems to be below the critical depth if it is at least one meter deep in clay and two meters deep in sand. From the context of their remarks, these authors seem to be referring to the limit pressure when talking about critical depth.

6.3 The Sand Site

6.3.1 The Sand Box

The sand box of the University of Ottawa is a steel box 14.5 m long, 1.85 m wide, 1.85 m deep (inside dimensions) which holds some 40 tonnes of sand. One end of the box is used to store the sand, the other end is reserved for tests. At the storage end, a bucket elevator brings the sand into the hopper of a spreader (Fig. 67); the spreader rides on two rails parallel to the box (Fig. 68). Immediately under the hopper is a cylinder or drum; when this cylinder rotates, sand rains into the box over its full width. The hopper unit can be raised or lowered, the speed of rotation of the cylinder can be varied within a certain range, and the speed of travel of the spreader, back and forth along the box, is adjustable. A particular choice of these three parameters allows the sand to be spread layer by layer at the required density. This large piece of equipment is described in detail in Deschênes (11).

6.3.2 The Sand

The sand used in this part of the study can be described as a dry, uniform (medium to coarse) angular silica sand (Fig. 69). Its minimum and maximum dry unit weights were determined according to A.S.T.M. standard procedure (A.S.T.M. D2049-69):

$$I_D = 100\% \quad \rightarrow \quad \gamma_{min} = 13.02 \text{ kN/m}^3$$

$$I_D = 0\% \quad \rightarrow \quad \gamma_{max} = 16.28 \text{ kN/m}^3$$

Then, for any unit weight γ in kN/m^3:

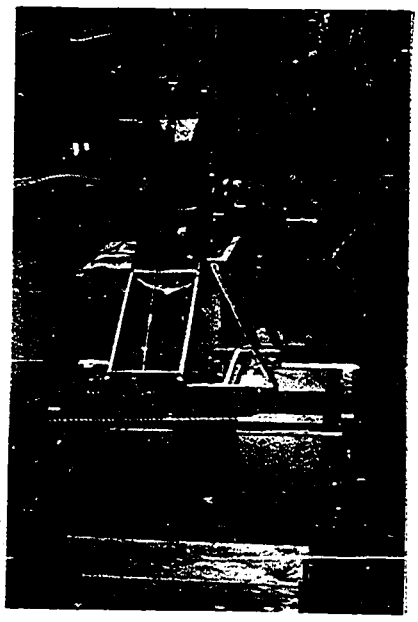

Fig. 67 - Sand Box: The Bucket Elevator.

Fig. 68 - Sand Box: The Spreader Spreading the Sand.

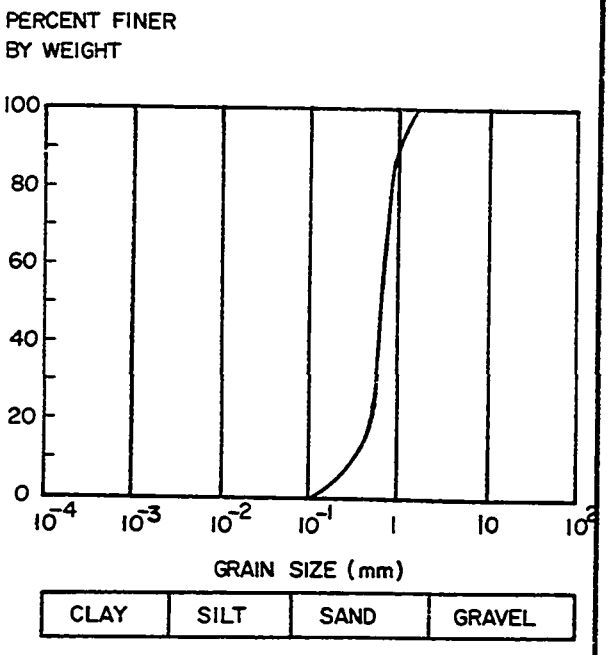

Fig. 69 - Sand: Grain Size Curve.

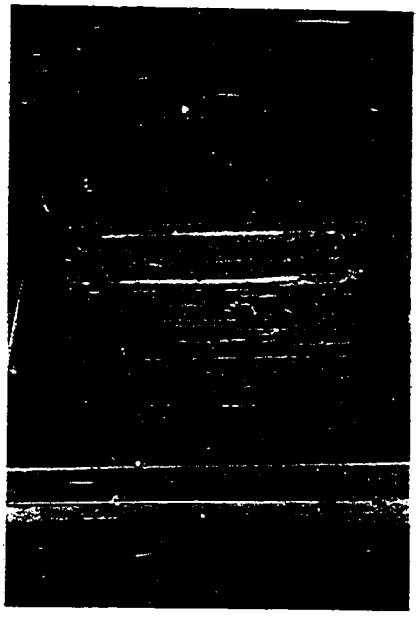

Fig. 70 - The Two Test Containers.

$$I_D = 499.4 \frac{\gamma - 13.02}{\gamma} \quad \ldots\ldots\ldots\ldots\ldots\ldots \quad (25)$$

where I_D = density index.

It should be noted that due to the uniformity of the sand, the dry unit weights are low and vary within a narrow range. In the sand box, the unit weight measurements were made by placing plexiglass cylinders of known volume on the sand surface, spreading sand over the containers until they were full, and then weighing the full containers. Tests were run with the sand at two density indexes, namely I_D = 65 to 70% and I_D = 90 to 95%; these two indexes will be referred to respectively as compact and dense sand. In the compact state, the sand had an effective stress internal friction angle ϕ' of 37^o as measured in the triaxial test; in the dense state, ϕ' was 41^o. The properties of this sand are detailed in Deschênes (11).

6.3.3 The Ménard (GA) Pressuremeter Tests

In order to run pressuremeter tests, the box was partitioned and extended in height to make two containers 1.83 m by 1.83 m and 2.14 m deep (Fig. 70). When a test was to be performed at a depth z (z = depth to the middle of the probe), the sand was spread up to a depth of z + 0.21 m (0.21 m is half the active length of the GA probe); at that point, density pots were installed and the probe was gently pushed about 70 mm into the sand (up to the beginning of the active part, Fig. 71). This amount of insertion was enough to make the probe stable when the sand was spread over it, up to the final height. It was thought that this procedure would simulate an ideal non disturbed hole. For each filling of the box, two probes were set into each of the two

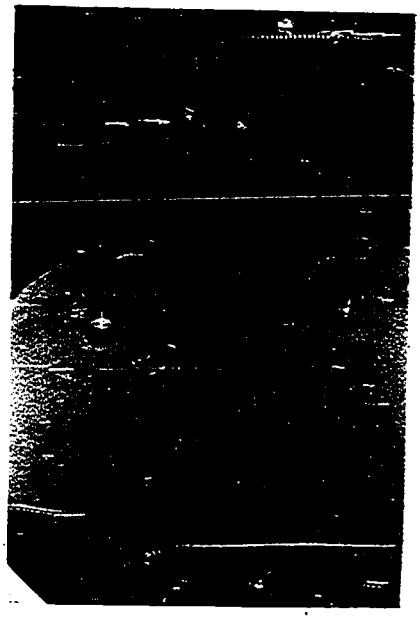

Fig. 71 - Placing the Ménard GA Probe.

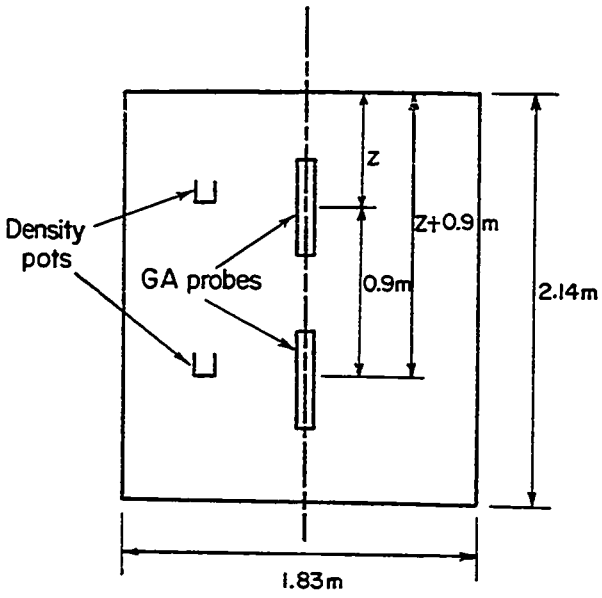

Fig. 72 - Position of the GA Probes in the Test Container.

Fig. 73 - Measurement of the Surface Movements.

containers, one probe at depth z and one at depth z + 0.9 m (Fig. 72). At each test depth, the density was measured.

The standard procedure (Section 2.2.4) was followed for all tests. Tests Nos. 1, 2, 4 and 5 were pilot tests to allow the operators to familiarize themselves with the apparatus; the results are not plotted. Tests Nos. 3, 6, 7 and 8 and 12 to 15 were calibration tests; the results are shown in Appendix A. Tests Nos. 9, 10 11 and 16 to 32 are the 20 GA pressuremeter tests: nine of these tests are in dense sand and eleven in compact sand; the test curves are given in Appendix A. The modulus E and the net limit pressure p_ℓ^* were calculated as described in Sections 2.2.5 and 4.5.2. The 20 Ménard GA pressuremeter tests generated one modulus and one limit pressure profile for each state of density (Fig. 74, 75, 76 and 77).

Whenever two tests are performed in one container, the inflation of the probe during the first test may influence the results of the second test. To check this point, the following steps were taken: the two containers were filled with compact sand; the first container had two probes at 0.6 m and 1.5 m depth while the second container had one probe at 1.5 m depth. The 0.6 m test (Test No. 11) was performed before carrying out the two 1.5 m tests (Tests Nos. 9 and 10); since the curves of the two 1.5 m tests were almost identical (Appendix A) it was concluded that the 0.6 m test had a negligible influence on the 1.5 m test in the same container and that the distance of 0.9 m between the two probes (Fig. 72) was acceptable.

For Tests Nos. 29 to 32 in the compact sand, surface movements were measured. Square aluminum plates (3 cm x 3 cm) were laid at 15 cm

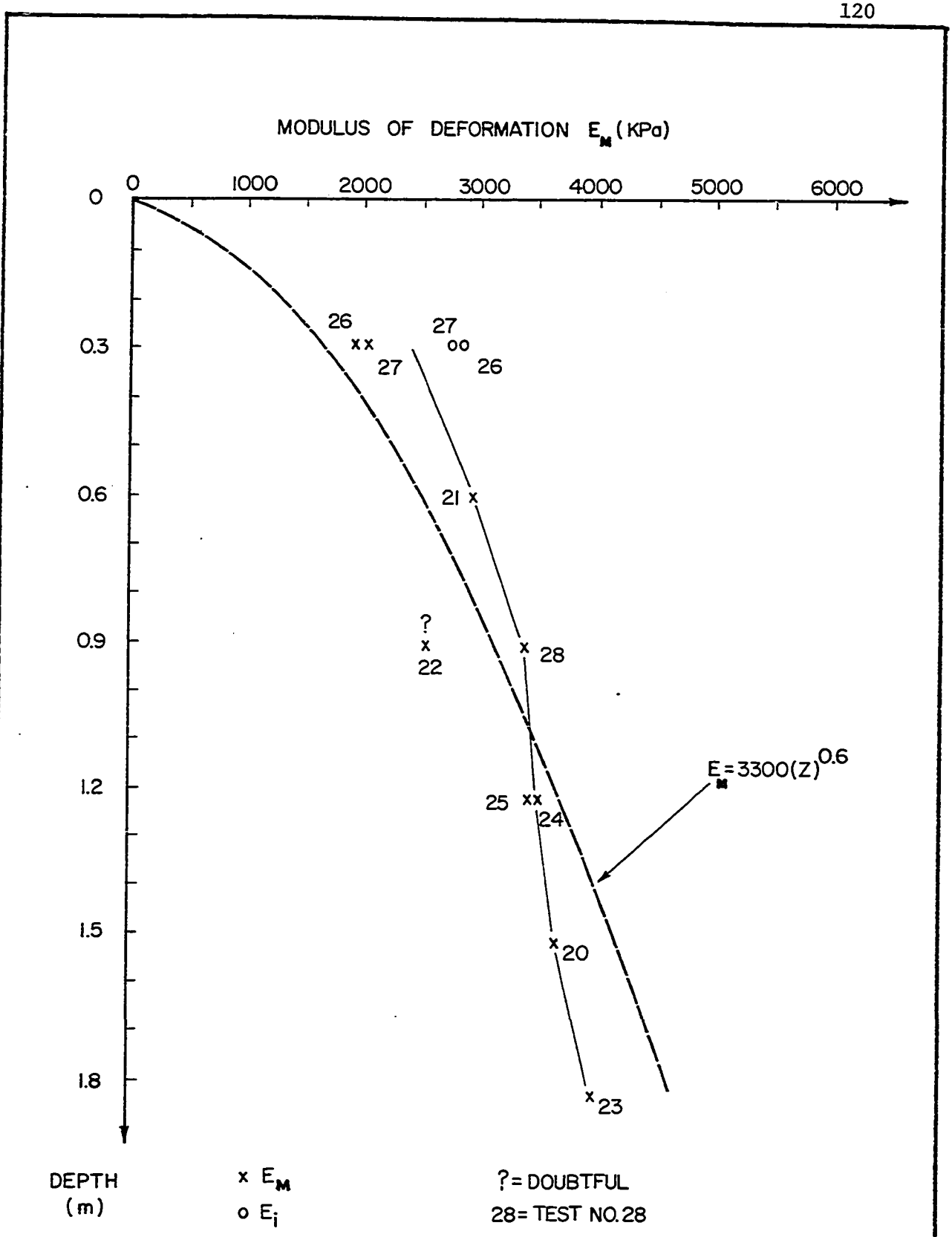

Fig. 74 - Sand Box. Dense Sand. Ménard GA Pressuremeter. Modulus vs. Depth.

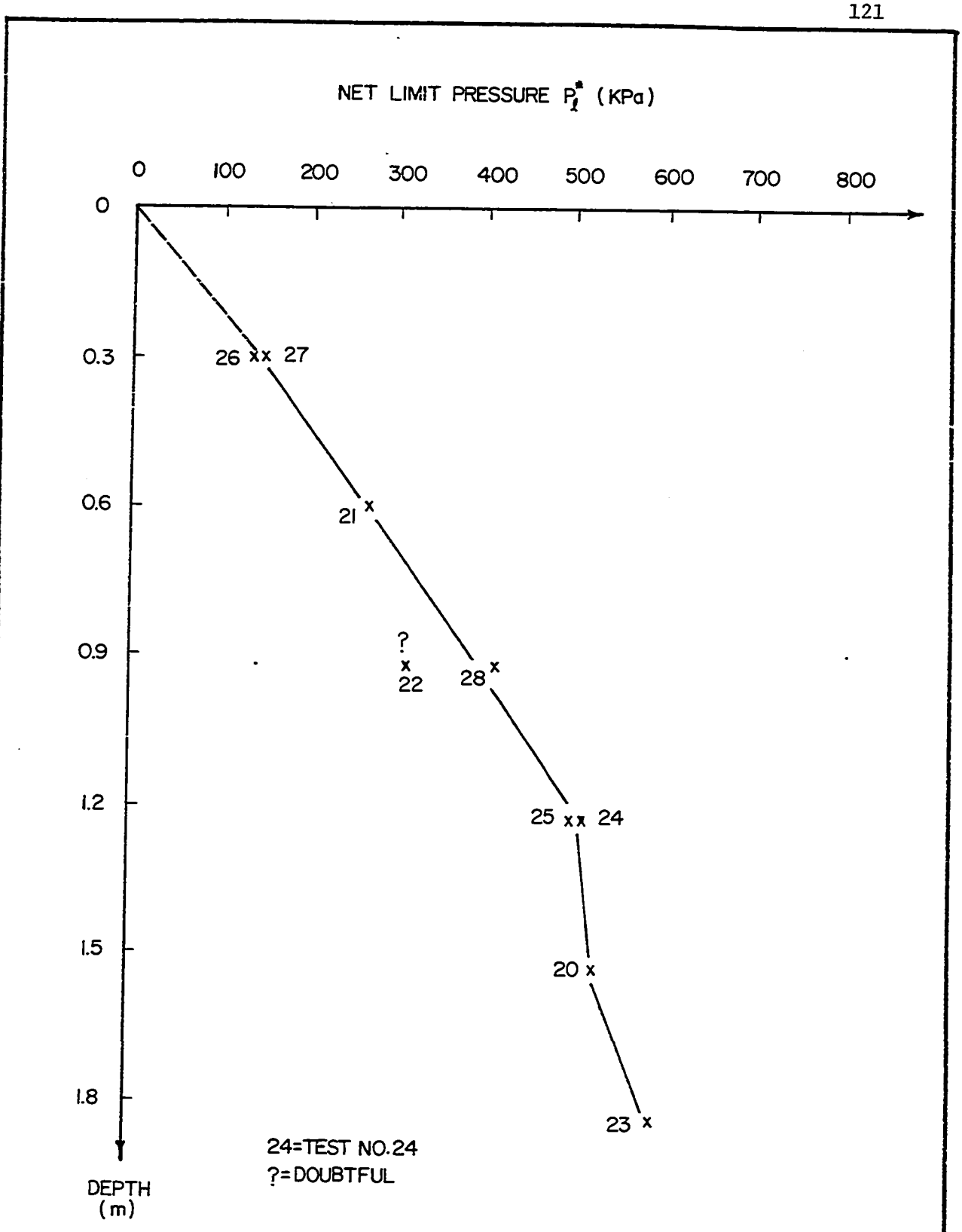

Fig. 75 – Sand Box. Dense Sand. Ménard GA Pressuremeter. Limit Pressure vs Depth.

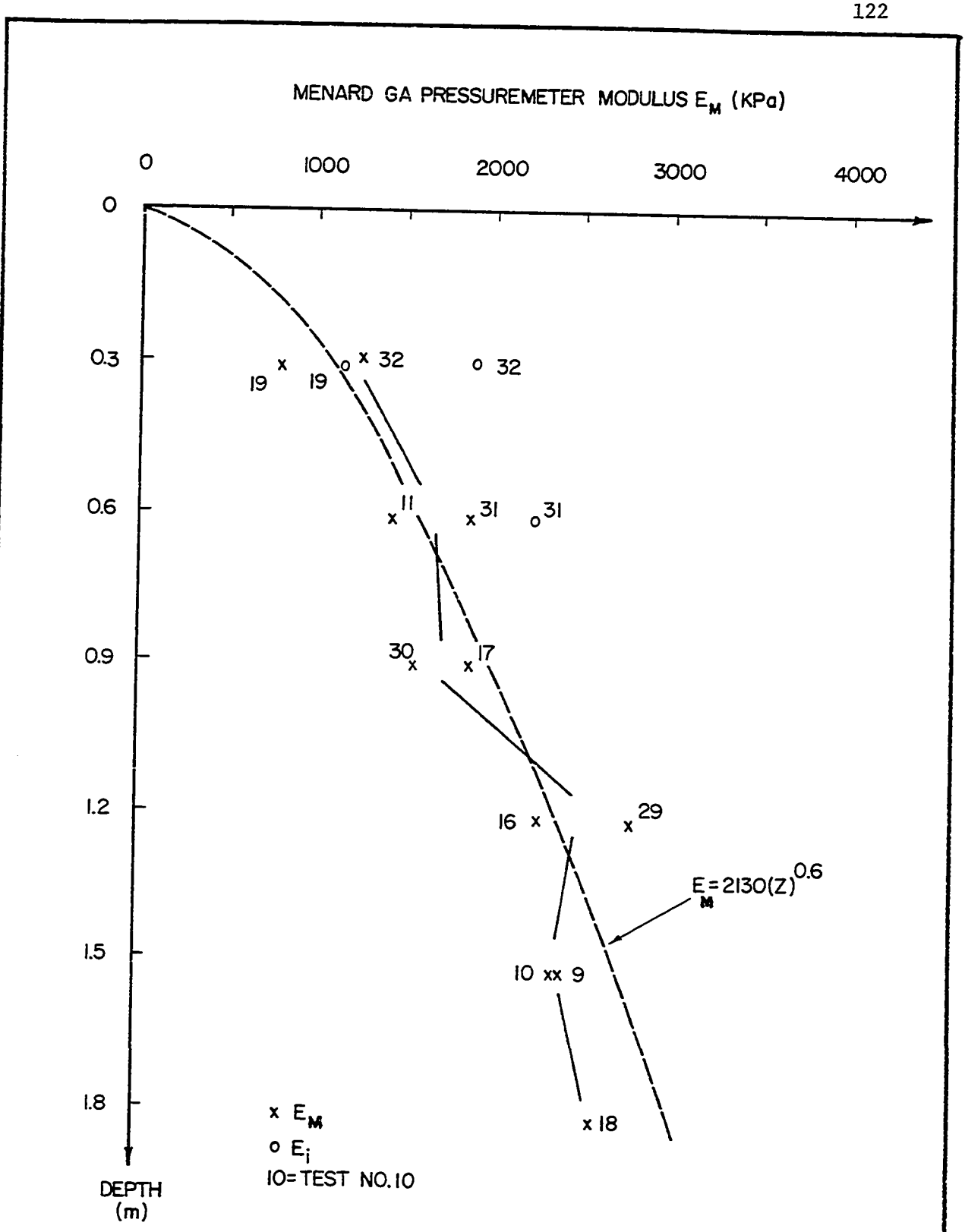

Fig. 76 – Sand Box. Compact Sand. Ménard GA Pressuremeter. Modulus vs Depth.

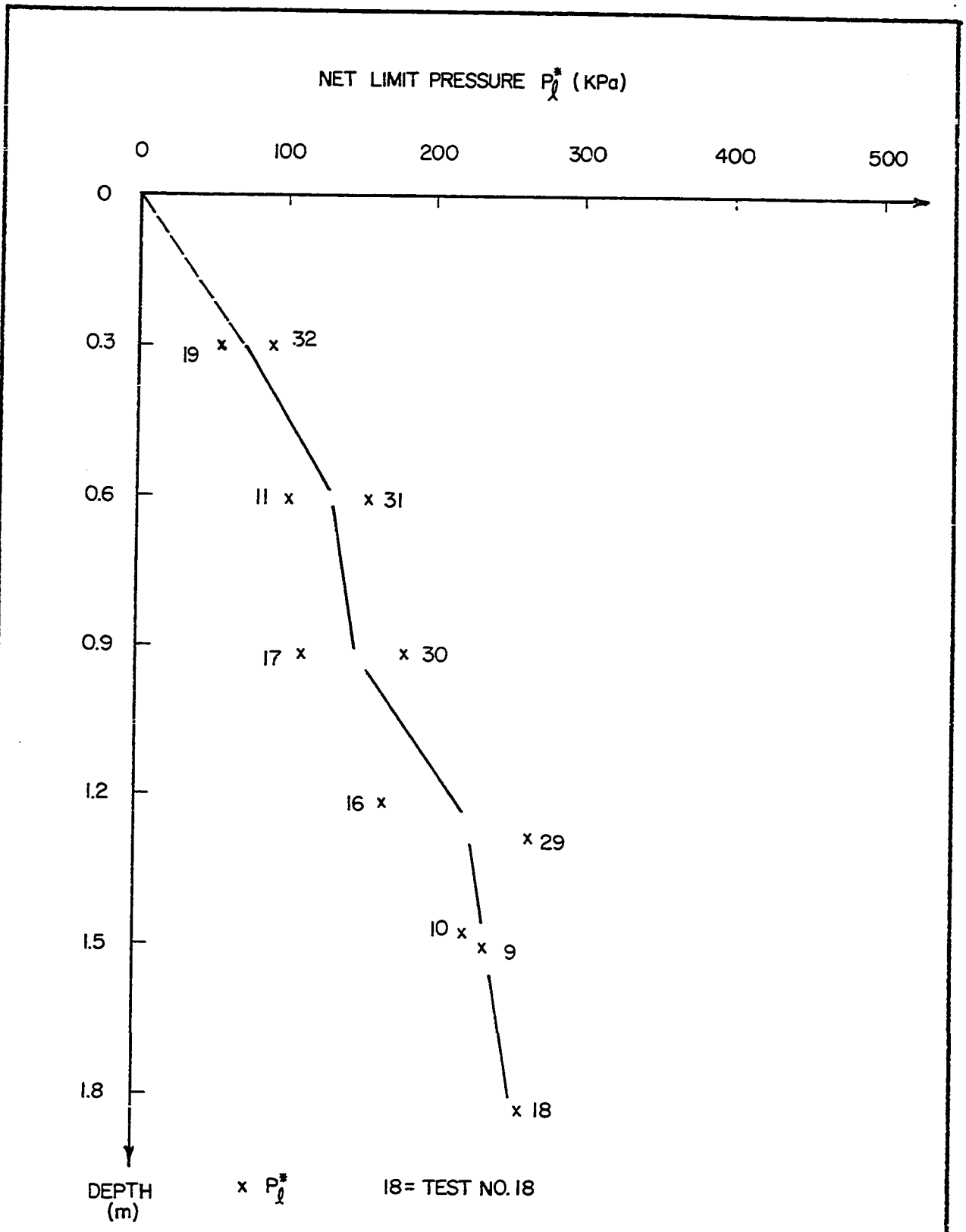

Fig. 77 - Sand Box. Compact Sand. Ménard GA Pressuremeter. Limit Pressure vs. Depth.

intervals across the box on the sand surface. A graduated pointer, riding across the box on a graduated rail, was lowered into contact with a mark made on each aluminum plate (Fig. 73). Measurements were taken on each plate before inflation and at maximum inflation of the probe; the absolute error on the measurement is about 0.5 mm. The surface contours at full inflation are shown on Figures 78, 79, 80 and 81.

6.3.4 The Briaud Pressuremeter Tests

The probe was inserted directly into the sand for most tests, that is to say, the probe-rod assembly was tapped down into the sand and tests were performed every 0.3 m of penetration. For a few tests, the probe was placed by the buried probe method (Section 4.3.5). Tests Nos. 38 to 45 were pilot tests used for familiarization with the equipment and procedure; the results of these eight tests are not plotted. Tests Nos. 65, 73, 81, 89 and 90 were calibration tests and the results are reported in Appendix A. Tests Nos. 46 to 64, 66 to 72, 74 to 80, 82 to 88 and 91 to 96 are the 46 Briaud pressuremeter tests performed in the sand of the sand box; 32 of these tests were in the compact sand (30 direct insertions, 2 buried probes) and 14 in the dense sand (13 direct insertions, 1 buried probe). The results are shown as curves in Appendix A. The modulus E was calculated as described in Section 4.5.2. Two modulus profiles were obtained: one for the compact sand (Fig. 82) and one for the dense sand (Fig. 83). No p_ℓ^* profiles were obtained since the Briaud pressuremeter does not measure this parameter, (the probe can be expanded only 1.5 time its original volume.

During these tests, a first attempt was made at measuring the cyclic

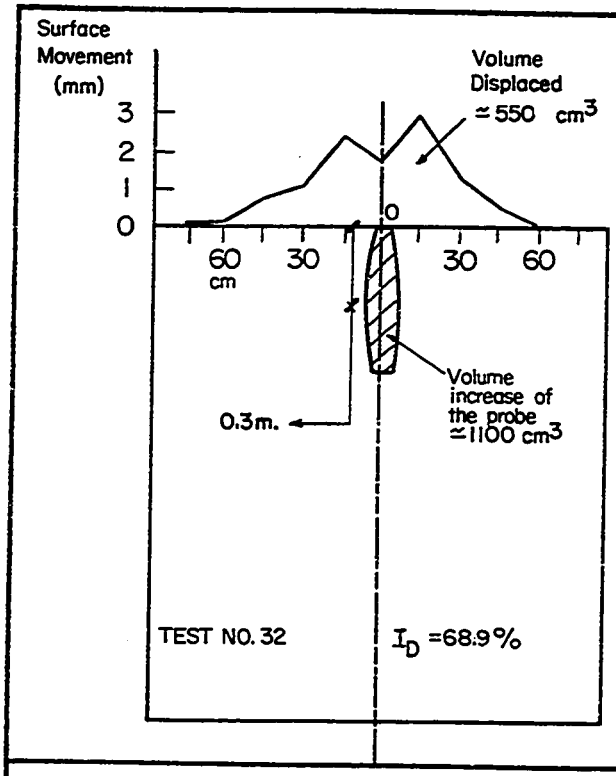

Fig. 78 - Sand Box. Compact Sand. Ménard GA Pressuremeter. Surface Movements, z = 0.3 m.

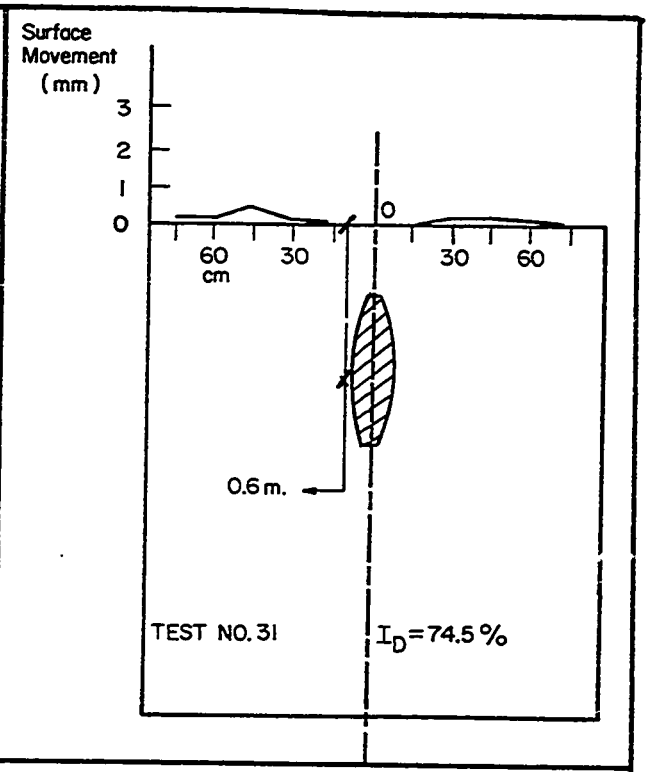

Fig. 79 - Sand Box. Compact Sand. Ménard GA Pressuremeter. Surface Movements. z = 0.6 m.

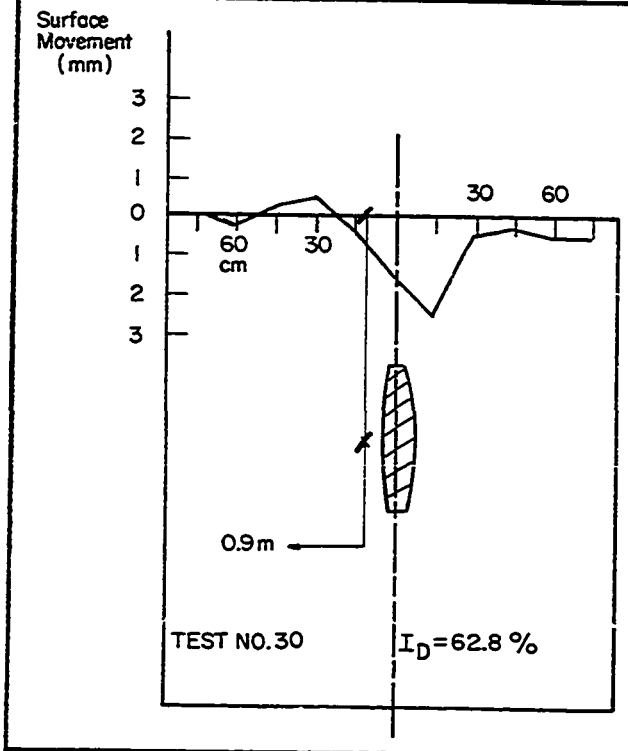

Fig. 80 - Sand Box. Compact Sand. Ménard GA Pressuremeter. Surface Movements. z = 0.9 m.

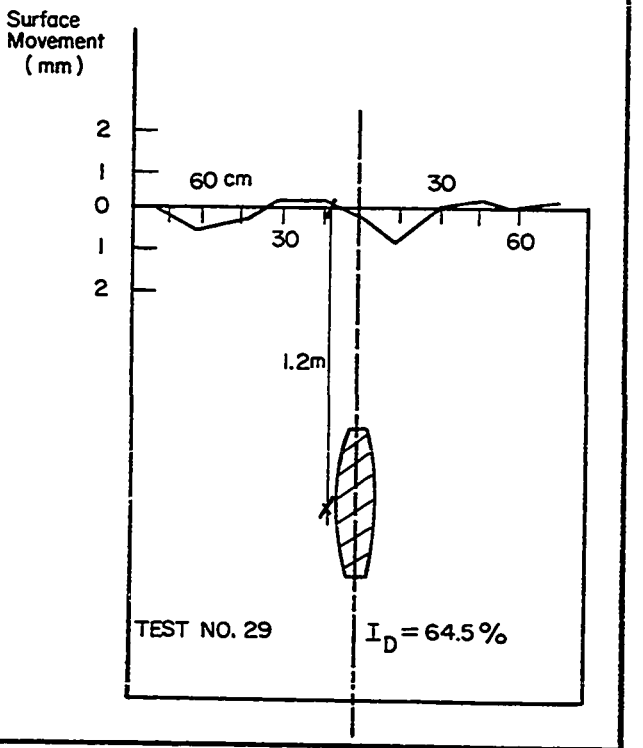

Fig. 81 - Sand Box. Compact Sand. Ménard GA Pressuremeter. Surface Movements. z = 1.2 m.

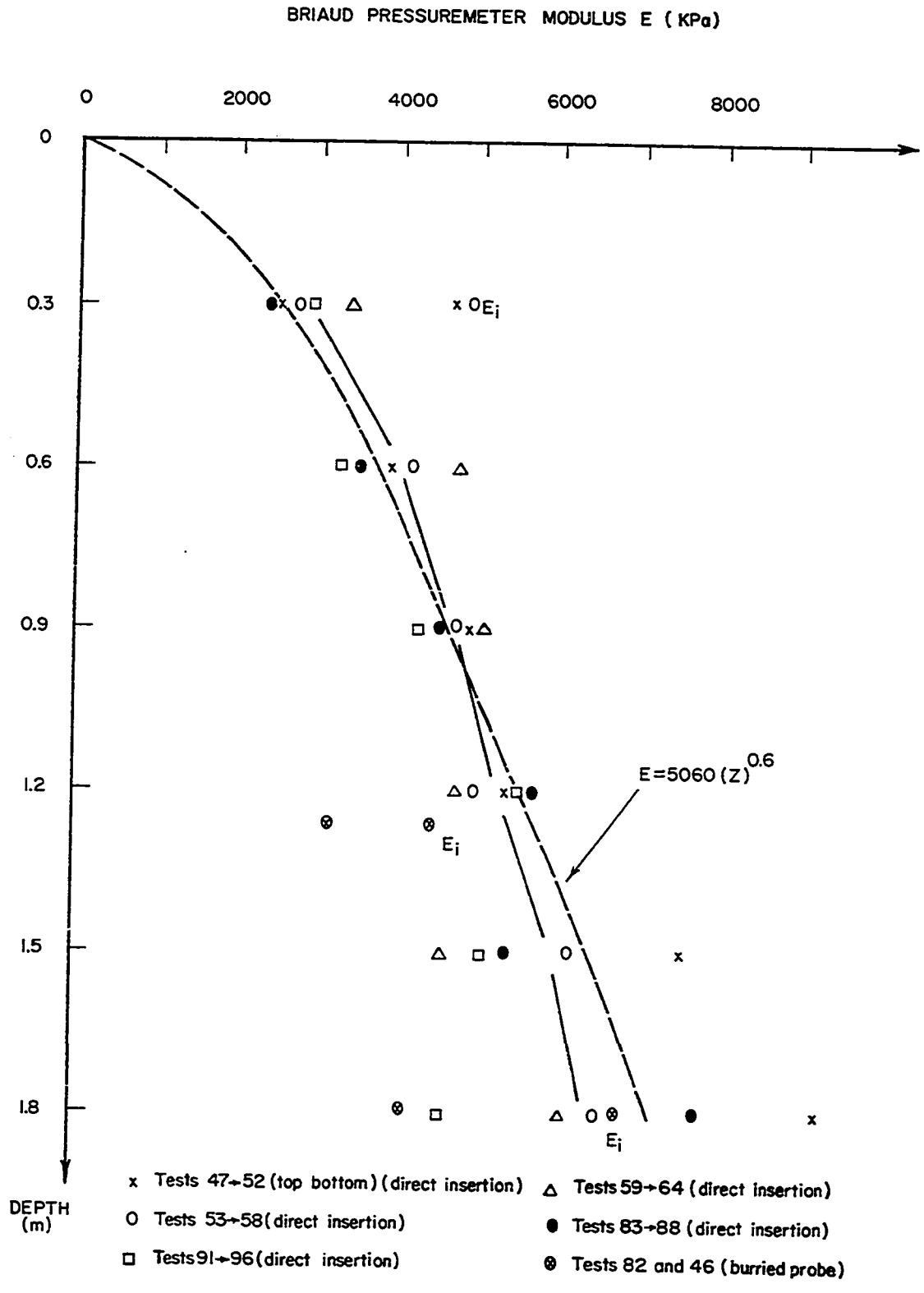

Fig. 82 - Sand Box. Compact Sand. Briaud Pressuremeter. Modulus vs. Depth.

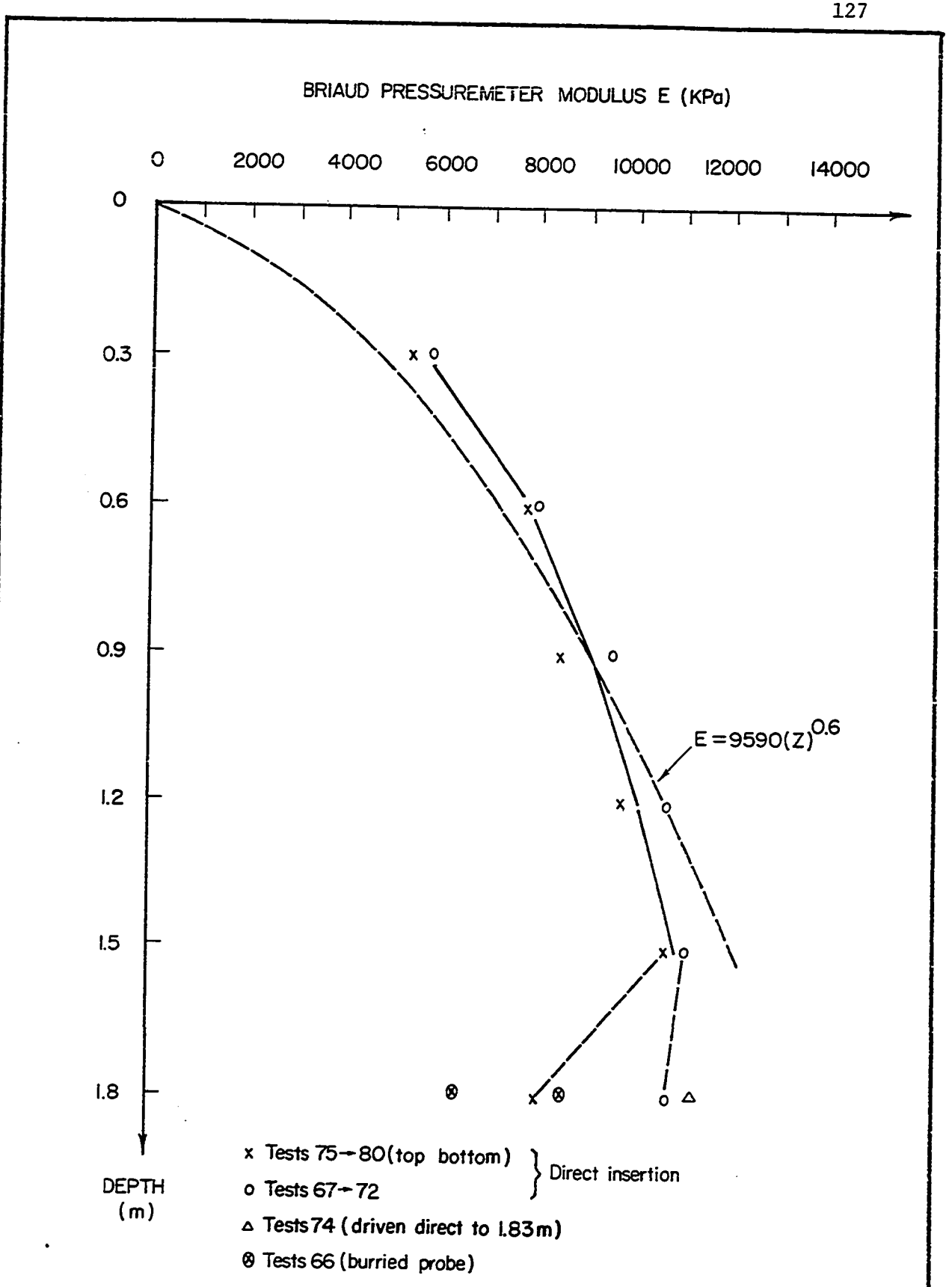

Fig. 83 - Sand Box. Dense Sand. Briaud Pressuremeter. Modulus vs. Depth.

pressuremeter modulus; the problem was to determine the point at which to stop inflating the probe and start the cycled part of the test. For the sand box tests, this point was set arbitrarily at 10 cm^3 of injected volume. As it turned out, this criterion was not suitable because the cycles are crowded close to the origin and the moduli do not differ significantly from the first loading modulus (Test No. 60). Also, as was discovered in Sarnia in a predrilled hole, 10 cm^3 inflation generally means that the probe has not touched the walls of the cavity. For these reasons, the cyclic part of the tests in the sand box has not been plotted on the test curves in Appendix A (except for Tests Nos. 53, 54, 60).

6.3.5 The Triaxial Tests

Five triaxial tests were performed on samples of sand 100 mm in diameter and 200 mm high. The test procedure is described in Section 5.2. All the test curves are plotted in Appendix C.

Four samples of the dry sand were prepared by raining the sand into the membrane which was secured within the vacuum mold. For this, a miniature spreader (Fig. 85) was used in order to simulate the same sand deposition process and obtain the same sand density as in the sand box pressuremeter tests. These four samples were used for Tests Nos. 247 to 250. Tests Nos. 250 and 248 were cyclic tests with σ_3 = 207 kPa and were performed with compact and dense sand respectively. The first loading triaxial modulus (E_T) and the cycled triaxial modulus (E_{Tc}) were determined (Section 5.2) and are presented on the modulus vs cell pressure plot of Figure 84. Tests Nos. 249 and 247 were multistage cycled tests with σ_3 = 34, 104 and 207 kPa; the tests were on compact and dense sand. The values E_T, E_{TC} and extrapolated E_T (Section 5.2) which were generated by

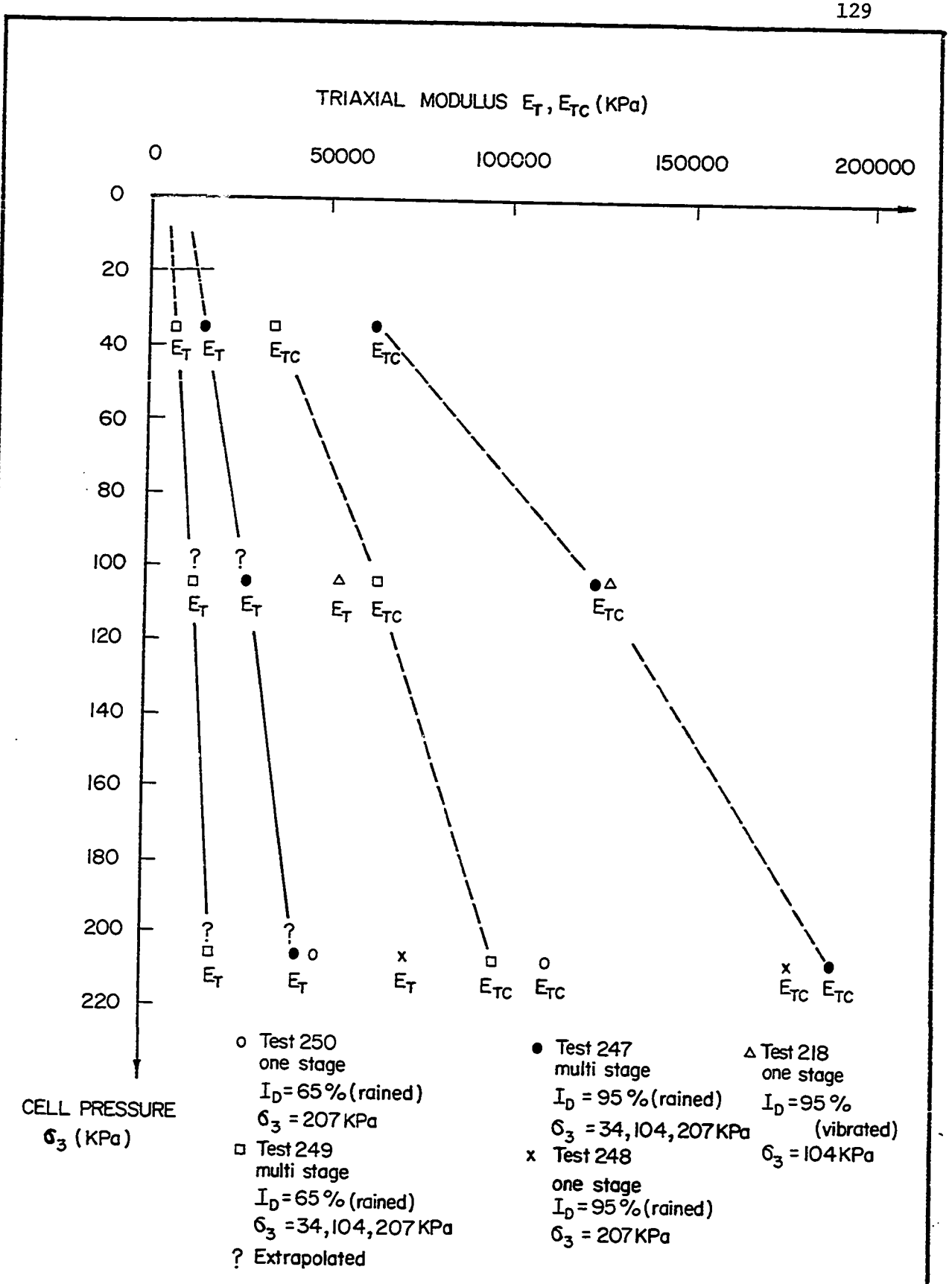

Fig. 84 – Sand Box. Compact and Dense Sand. Triaxial Modulus vs. Cell Pressure

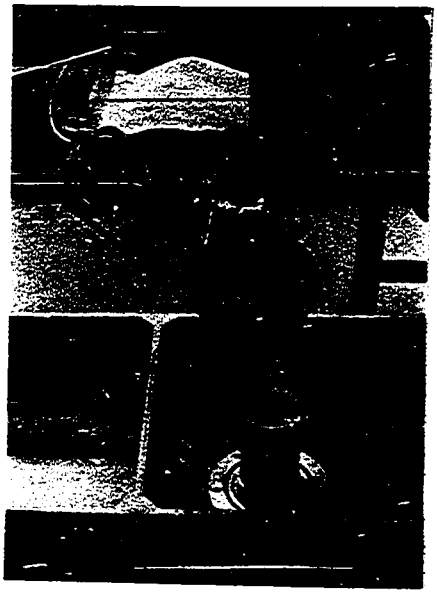

Fig. 85 - Sand Box. Triaxial Test. The Miniature Sand Spreader.

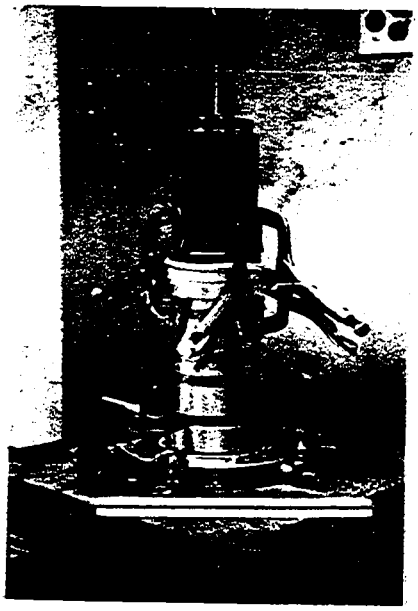

Fig. 86 - Sand Box. Triaxial Test. Vibrating the Sample.

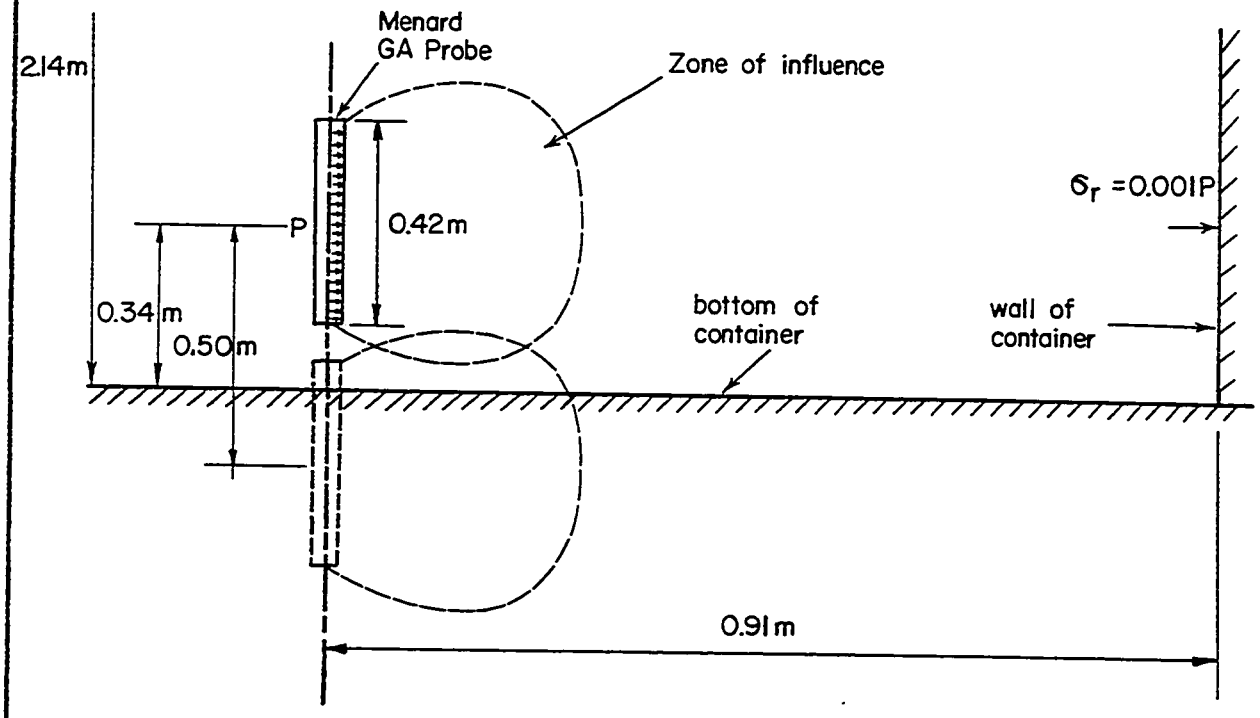

Fig. 87 - Sand Box. Relative Position of the Rigid Boundary of the Container for the Deepest GA Pressuremeter Test.

these tests are presented in Figure 83.

The fifth sample was prepared on a vibrating table (Fig. 86); this sample of sand was used for Test No. 218 which is a cyclic test in dense sand at σ_3 = 104 kPa. The E_T and E_{Tc} values for this test are shown on Figure 84. Test No. 217 was not carried out properly and is not presented in Appendix C.

6.3.6 Discussion

In this section the shape of the profiles of modulus values and the factors which may have influenced the results are discussed.

Among the factors which may have influenced the results are: the proximity of the walls and the bottom of the container and the uniformity of the deposit. In the sand box container, the smallest distance between the wall and the probe is 0.9 m; this distance represents 31 times the Ménard GA probe radius and 58 times the Briaud probe radius. For a linear elastic soil, the radial stress created by cylindrical expansion (p. 354 of (1)) at a distance of 31 cylinder radii from the cylinder is 0.1% of the pressure in the cylinder (Fig. 87); at 58 cylinder radii it is 0.03% of the pressure in the cylinder. Based on these calculations, the walls of the container were considered to have a negligible influence on the results.

The smallest distance between the middle of the probe and the plywood bottom of the container was 0.34 m for the tests at 1.8 m depth (Fig. 87). Baguelin et al. (p. 133 of (1)) state that when two tests are performed at 1.19 probe lengths from one another (Fig. 87) the zones of influence do not overlap significantly. According to Figure 87, this

statement means that the bottom of the container has no significant influence on the results.

The uniformity of the deposit is questionable in the case of a small number of tests. It was found easier to reproduce the high density of the dense sand than the density of the compact sand; this is due to better control over the deposition process being possible in the case of the dense sand. Within the depth of the box, the relative density was found to vary by 5% for the dense sand and by as much as 20% for the compact sand. This explains the scatter in the compact sand results (Fig. 75, 77, 82). Also for the Briaud pressuremeter tests, mechanical difficulties were experienced when spreading the sand between 1.5 and 2.14 m depth; these difficulties explain the appreciable scatter of the profiles of the moduli values between these depth (Fig. 82 and 83).

The p_ℓ^* profiles from the Ménard pressuremeter tests have two important characteristics; one is a break in the profile and the second is the fact that a straight line extension of the profile goes through the origin (Fig. 75, 77). These two characteristics are more obvious for the tests in the dense sand than in the compact sand. The break in the profile occurs around 1.2 m. After the break however, the p_ℓ^* values still increase with depth.

The surface movements (Fig. 78 to 81) seem to indicate that below 0.9 m depth at full inflation of the probe, the surface is not involved significantly in the deformation process. These observations lead to the conclusion that there is a critical depth (D_C) in the limit pressure profile and that, for this probe and this compact to dense sand D_C is about 1.2 m. In this case, the ratio of the critical depth (D_C) to the probe

diameter (ϕ_p) is:

$$\frac{D_c}{\phi_p} = \frac{120}{5.8} \approx 20 \quad \ldots\ldots\ldots\ldots\ldots\ldots\ldots\ldots \quad (26)$$

Interestingly, this ratio of 20 is also the ratio of depth over pile diameter which is said to be the critical depth ratio for pile design in dense sand (38).

The modulus profiles from the Menard pressuremeter tests (Fig. 74 and 76) and the Briaud pressuremeter tests (Figs. 82 and 83) do not present a clear break the way the limit pressure profile does; the modulus profiles show a simple increase in modulus with depth. The shape of the pressuremeter modulus profiles is very similar to the shape of the triaxial moduli vs cell pressure curve (Fig. 84); in the case of the triaxial tests no critical depth phenomenon can be involved. According to Janbu (as cited by Wong and Duncan, p. 5 of (47)) the deformation modulus of granular soils varies as a power of the minor principal stress; applying this law of behavior to the E_{Tc} vs σ_3 profile (Fig. 84) means that:

$$E_{Tc} = K\,(\sigma_3)^n \quad \ldots\ldots\ldots\ldots\ldots\ldots\ldots\ldots \quad (27)$$

or that:

$$\log E_{Tc} = \log K + n \log \sigma_3 \quad \ldots\ldots\ldots\ldots\ldots\ldots \quad (28)$$

Indeed Equation 27 holds true for the triaxial test results of Figure 84; this is shown in Figure 88 where the results can be plotted as two

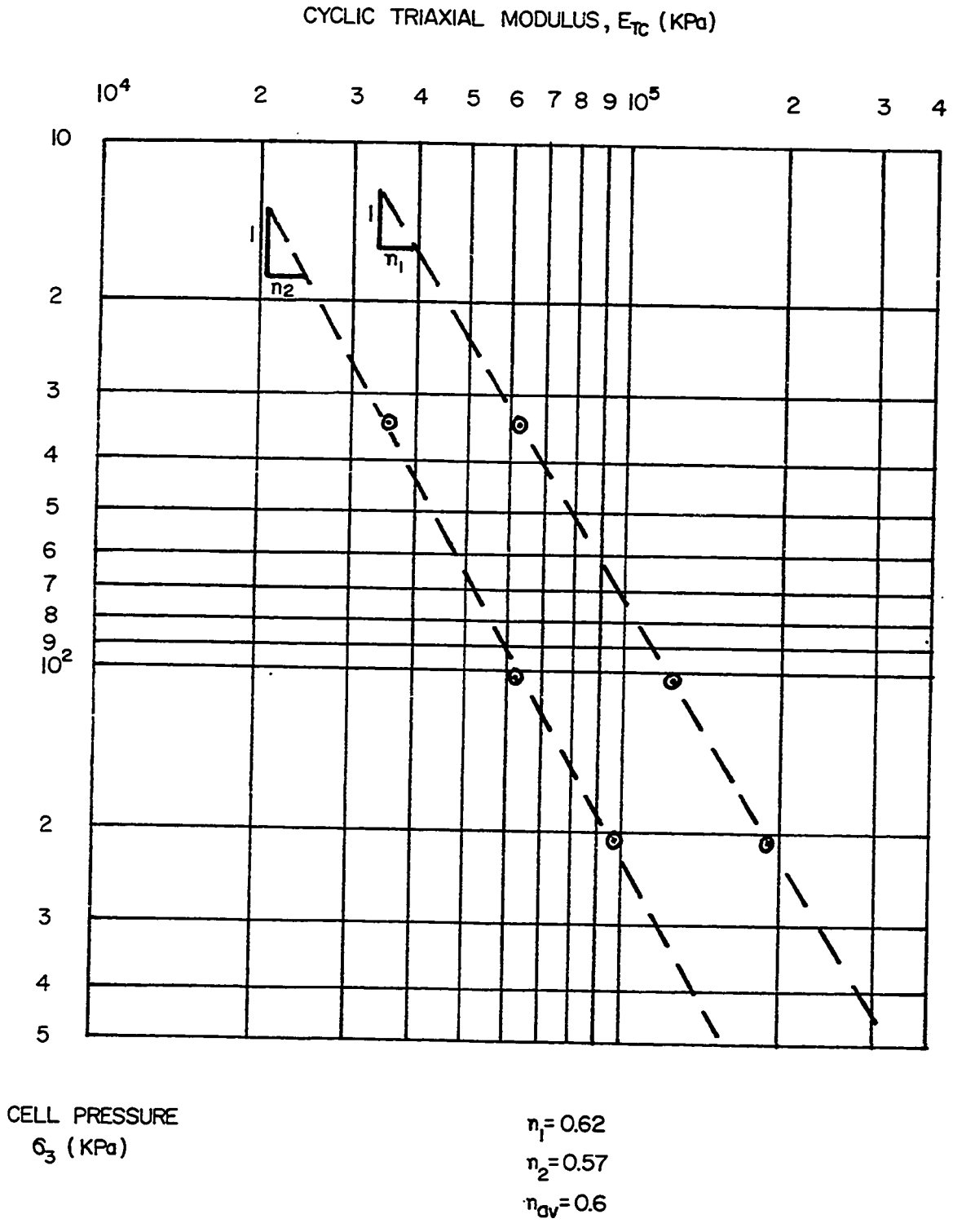

Fig. 88 - Sand Box. Compact and Dense Sand. Triaxial Modulus vs. Cell Pressure (Log-Log scale).

straight lines with a slope of 0.6. The dense and compact sands are therefore characterized by an exponent n of 0.6.

As the pressuremeter testing depth increases the σ_3 stress level around the pressuremeter also increases. One problem is that it is difficult to know which stress around the probe is the σ_3 equivalent to the triaxial cell pressure. However the at rest vertical stress (σ_v), horizontal stress (σ_h), octohedral stress (σ_{oct}) are linearly proportional to the depth (z) and it seems reasonable to conclude that the pressuremeter modulus vs depth profiles of Figures 74, 76, 82, 83 can be characterized by:

$$E = K\ (z)^{0.6} \quad \ldots\ldots\ldots\ldots\ldots\ldots\ldots\ldots \quad (29)$$

In each figure the constant K has been determined for z = 0.9 m and for the corresponding E value on the profile; the resulting theoretical curves are plotted in dotted lines in the four figures. It is found that the theoretical E values match the measured E values very well.

Surface movements could not be measured with the required degree of accuracy at the end of the elastic phase of a pressuremeter test, because the movements were too small for the method of measurement which was used (Section 6.3.3). However, from the above observations (no clear break in the curve and similarity between the $E_T - \sigma_3$ profiles and the E - z profiles) it can be concluded that there is no evidence of a critical depth in the pressuremeter modulus profiles in this compact and dense sand; there is, however definite influence by the initial state of stress on the pressuremeter modulus.

The following additional comments can be made concerning the moduli results; both in the Menard tests and in the Briaud tests, it was found that the ratio of the pressuremeter modulus of the dense sand (I_D = 95%) over the pressuremeter modulus of the compact sand (I_D = 65%) was approximately two (compare, for example, Fig. 74 with 76 and 82 with 83). Interestingly, the ratio of the square of the density indexes is also approximately two: $\frac{95^2}{65^2} \simeq 2$.

The Menard moduli are much smaller than the Briaud moduli; this is mainly attributed to the difference in the method used to place the probe (Section 4.3.5).

The triaxial modulus versus cell pressure (σ_3) graph (Fig. 84) shows the large influence σ_3 has on E_T: when σ_3 was increased by a factor of six, the modulus E_{Tc} was increased by about three in both the dense and compact sand. Also the average ratio of E_{Tc} over E_T was three (from Tests Nos. 218 and 247 to 250: Fig. 84).

The triaxial modulus is the same whether the sample is prepared by raining or by vibrating the sand to the correct density; this statement is based on a comparison between Tests Nos. 218 and 248 as illustrated in Figure 84.

In the multistage triaxial test, it was thought possible that, after testing the sample under the first cell pressure, the sample would be either compacted or loosened by the cycling of the load; this change in material properties would invalidate the measurements of the modulus during the following cell pressure increment. This concern appears to be unwarranted since the moduli E_{Tc} measured during the last cell pressure increment (σ_3 = 207 kPa) of the multistage tests were within 10% of the moduli E_{Tc} at the same σ_3 in the one stage test (Fig. 84).

The Briaud pressuremeter modulus (E) and the triaxial modulus (E_T) can be compared, provided that equivalent σ_3 conditions are considered. For this purpose, the σ_3 of the triaxial test will be considered to be equivalent to the estimated at rest vertical stress σ_v at the depth of the pressuremeter test. A value of 20 kPa was selected as a common value for σ_3 and σ_v; a σ_v of 20 kPa is encountered at 1.33 m depth in the compact sand and at 1.24 m depth in the dense sand. The Briaud pressuremeter modulus is 5500 kPa at 1.33 m in the compact sand and 10,300 kPa at 1.24 m in the dense sand. By linear extension of the profiles to a σ_3 of 20 kPa (Fig. 84), the modulus E_T is 6000 kPa for the compact sand and 13,000 kPa for the dense sand. The Briaud pressuremeter and triaxial modulus are therefore close to one another.

6.4 The Clay Site

6.4.1 The Site and the Clay

Fraser's farm is about 20 miles southwest of Ottawa. In 1976, a silo overturned due to a bearing capacity failure of the soil; since then, two new silos have been built. The tests reported here are at the site of the second new silo. The clay soil found at the site is described in detail in Haile (16).

The soil down to 0.3 m depth (the zone within which all tests were performed) is a brown silty clay containing angular stones, a few root fibres and some sand. The natural water content is 35%, the liquid limit is 34%, and the plastic limit is 17%. The natural unit weight is about 18 kN/m^3. Figure 89 gives a grain size curve for the clay (39% clay, 50% silt, 11% sand).

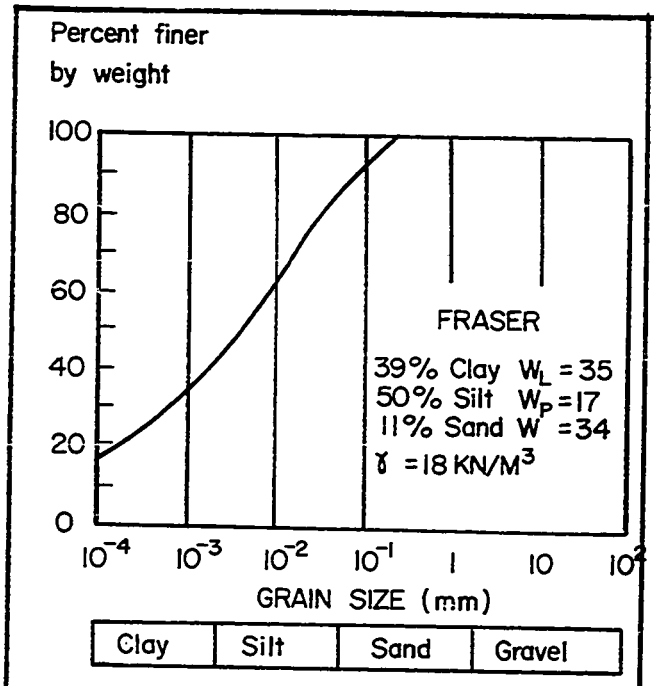

Fig. 89 - Fraser's Clay: Grain Size Curve.

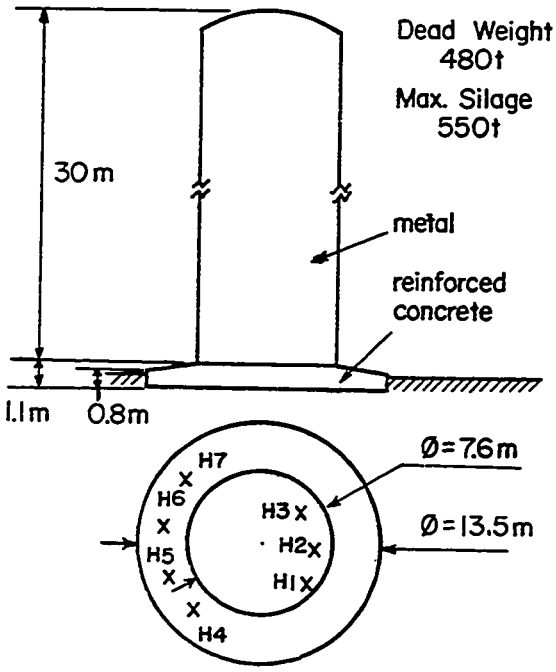

Fig. 90 - Silo Diagram and Location of Test Holes.

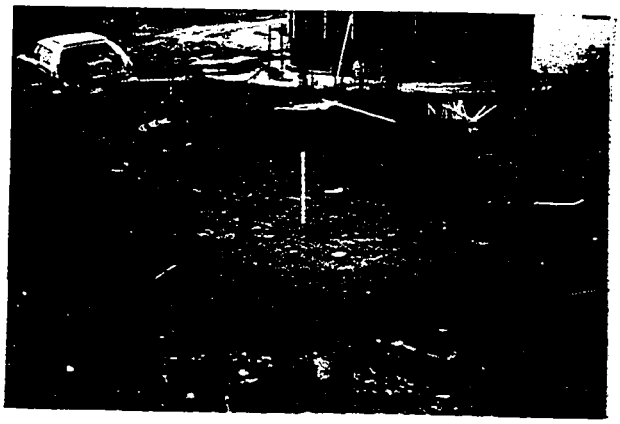

Fig. 91 - Before Construction. Silo Foundation Bed.

Fig. 92 - After Construction. Test Through the Raft.

The ground water level before construction was 0.34 m below excavation level (24 hr observation); three weeks after construction the water level was 0.3 m above excavation level (4 hr observation).

The second silo and its circular raft foundation are shown in Figures 90, 91 and 92. Empty, the structure exerted an average bearing pressure of 34 kPa (full, the pressure would be 73 kPa).

6.4.2 The Briaud Pressuremeter Tests

Tests were performed just before and just after the silo was built. Before construction, two pressuremeter holes (H1 and H2 on Fig. 90) were tested; the holes were bored with a 32 mm hand auger down to 2.1 m and the pressuremeter was inserted to 2.1 m and then pushed to 3 m. Tests were done from the bottom of the hole up. Sleeves were installed during the construction of the concrete raft to allow tests to be carried out through the raft.

After construction of the raft and while the silo was still empty, two holes were tested with the Briaud pressuremeter (H6 and H7 on Fig. 90). In the case of H6, the hole was prepared with a 32 mm hand auger down to 2.1 m; for H7, EW rods (ϕ = 33.5 mm) were driven to 2.1 m and withdrawn. In both holes, the pressuremeter was inserted to 2.1 m and pushed to 3m. All depths refer to the excavation level which is 0.6 m below the original ground surface.

The pressuremeter results are presented in Appendix A in the case of the individual test curves and in Figure 93 for the modulus vs depth profile. The cyclic pressuremeter moduli were measured only during the tests which were carried out after construction of the raft and the silo;

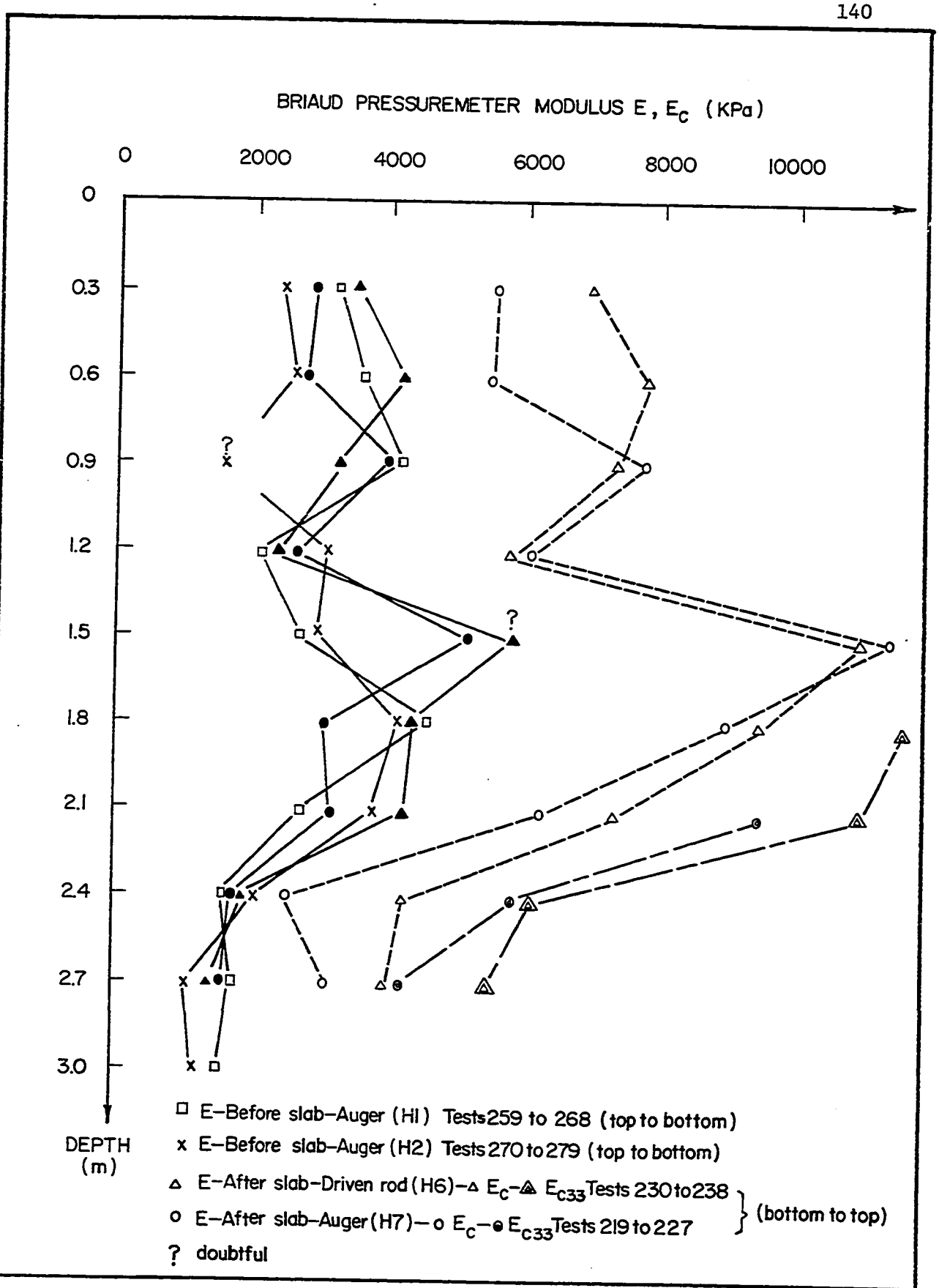

Fig. 93 - Fraser's Clay. Briadd Pressuremeter. Cyclic Pressuremeter and Pressuremeter Modulus vs. Depth.

by that time an appropriate cyclic test procedure had been established. The E and E_c values have been calculated according to Section 4.5.2. The modulus E_{c33} is the cyclic pressuremeter modulus at:

$$v_m = 90 \text{ cm}^3 \text{ or } \frac{v_m}{V_c+v_m} = \frac{90}{180+90} = 33\%$$

The measurements and the calculations which are involved to determine E_{c33} are similar to those for E_c.

6.4.3 The Vane Tests

The vane and the test are described in Section 5.3. Two holes were tested with the vane down to 3 m depth (H3 and H4 on Fig. 90); H3 and H4 were tested respectively before and after the construction of the silo. The vane shear strength (c_u) versus depth profiles are given on Figure 94. The sensitivity of the soil, as determined by the vane, averaged 4 between 0 and 2 m and 8 between 2 and 3 m depth.

6.4.4 The Triaxial Tests

In hole H5 (Fig. 90), undisturbed samples were taken with 63 mm diameter Shelby tubes at 1 m and 1.8 m depth; the Shelby tube samples were taken after the construction of the silo. The triaxial specimens were 38 mm in diameter and 76 mm high.

Two multistage tests were performed (Test No. 255 and Test No. 256) and the results are in Appendix C. The values of E_T, E_{Tc} and extrapolated E_T are presented in Figure 95 as a profile of modulus vs cell pressure (σ_3).

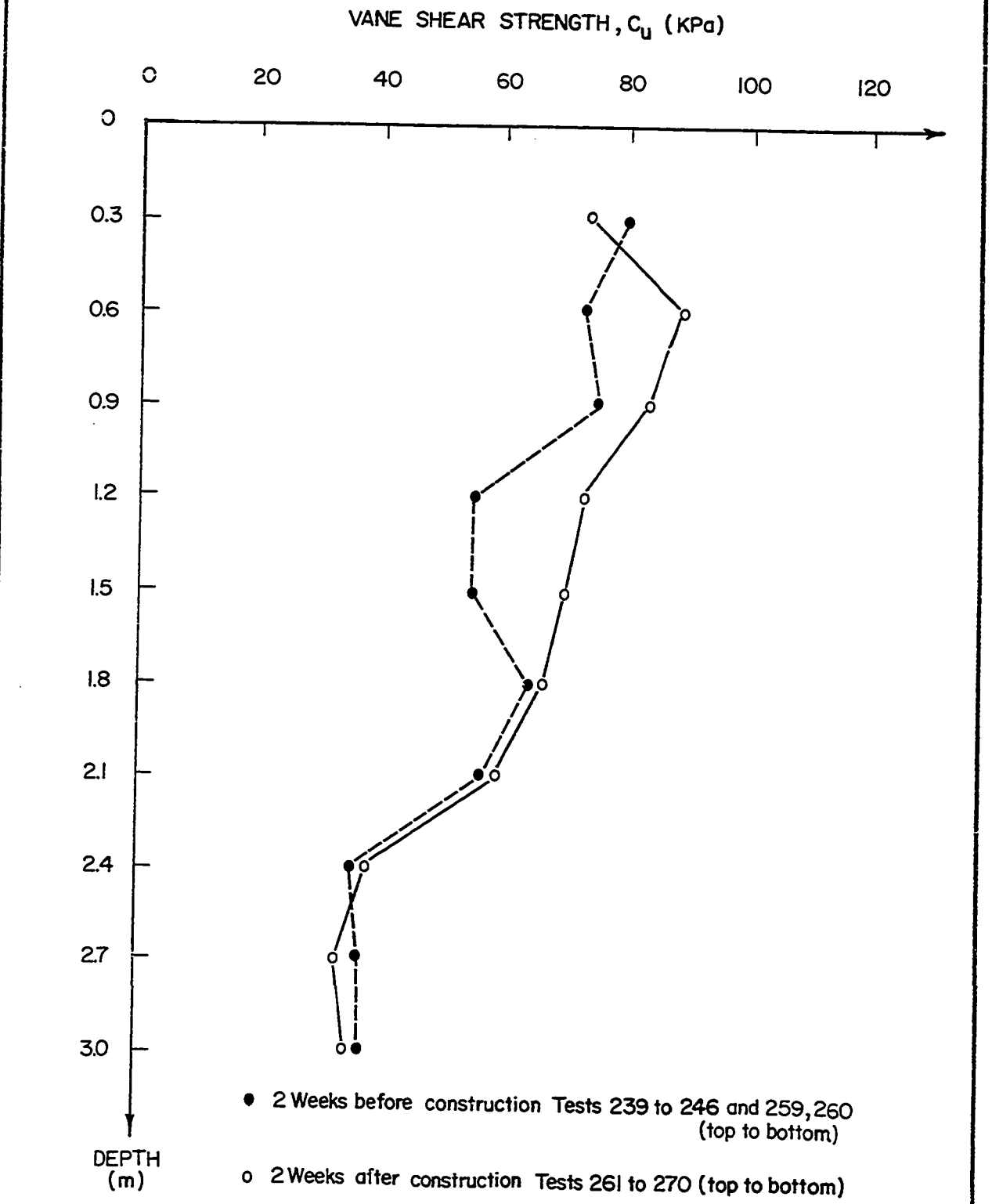

Fig. 94 – Fraser's Clay. Vane Shear Strength vs. Depth.

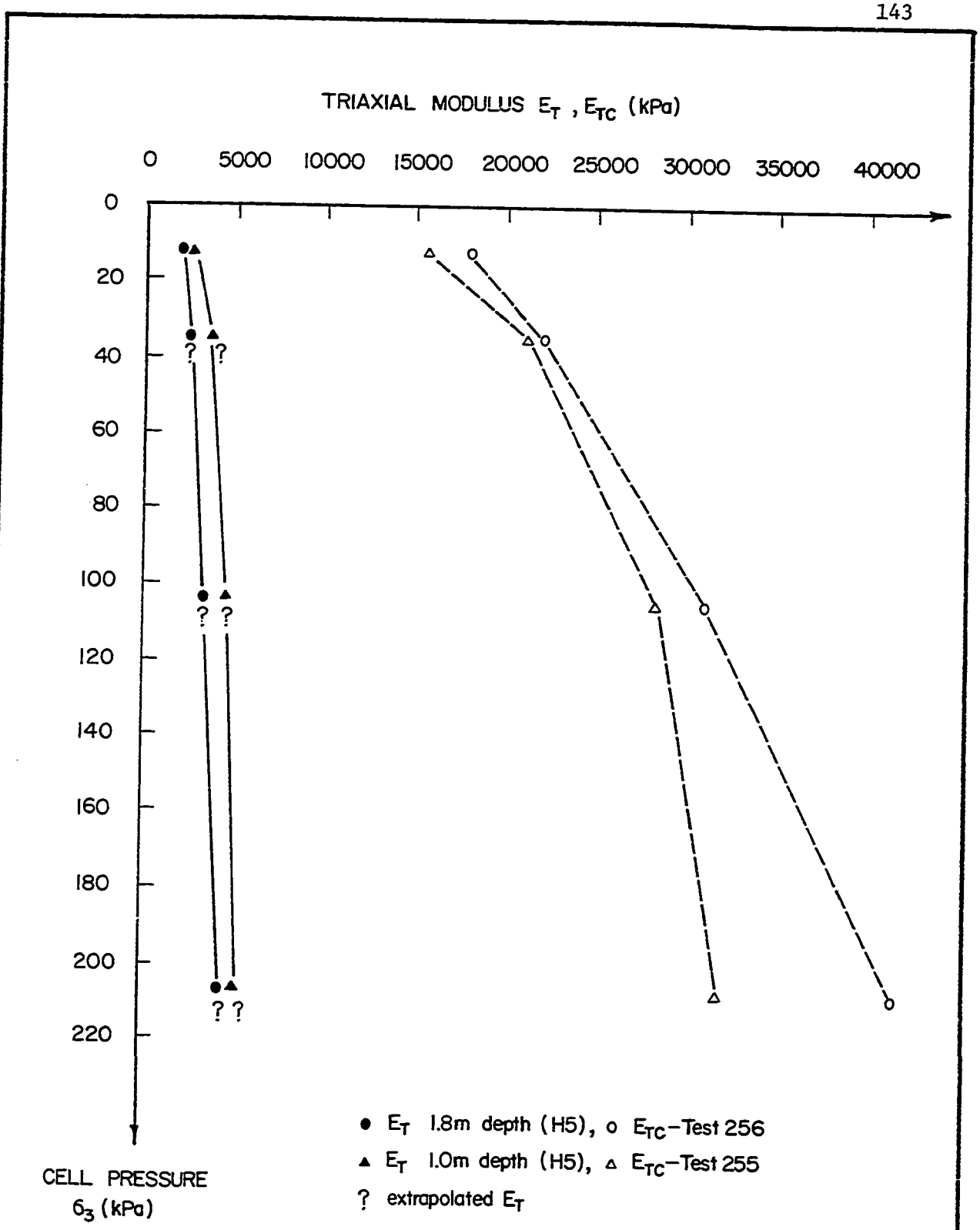

Fig. 95 - Fraser's Clay - Triaxial Modulus vs Cell Pressure

6.4.5 Discussion

As can be seen from the vane profile (Fig. 94), the deposit is stronger from 0 to 2 m depth than it is from 2 m to 3 m depth. From 0 to 2 m, the vane shear strength averages 70 kPa and the undrained shear strength as measured in the two multistage triaxial tests (Test No. 255 and 256), averaged 100 kPa. The Briaud pressuremeter modulus profile (Fig. 93) shows the same overall strong-soft variation with depth.

The pressuremeter modulus profiles, before the concrete slab was poured (Holes H1 and H2, Fig. 93), show a slight increase in modulus with an increase in depth from 0 to 2 m but there is no clear break in either profile. Once built, the slab and the silc applied a pressure of 34 kPa to the ground surface; this pressure is equivalent to about 2 m of clay. Pressuremeter tests through the raft foundation of the silo were carried out in Holes H6 and H7 at the same levels as the tests in H1 and H2. If there were a critical depth, it should have appeared at a different depth before and after the slab was built. Comparison of the profiles of H1 and H2 with the profiles of H6 and H7 (Fig. 93) yields no obvious difference. It can be concluded, therefore, that there is no evidence of a critical depth in the Briaud pressuremeter modulus profiles.

The slight increase in modulus values with depth may be due to the increase in confining stress around the pressuremeter with depth. It is known that the influence of σ_3 on the modulus of deformation is less pronounced in clays than in sand; the triaxial test profile (Fig. 95) shows the variation of E_{Tc} with σ_3 and when σ_3 was multiplied by a factor of six, the modulus E_{Tc} of Fraser's clay was increased by a factor of 1.65. For the same increase in σ_3, the sand modulus increased by a factor of three.

Using Equation 27 and a log-log plot of Figure 95, the exponent n for the influence of σ_3 on the E values of Fraser's clay was found to be 0.3. It must be remembered that in addition to σ_3 other factors such as strength and preconsolidation pressure have a strong influence on the way the modulus varies with depth; these other factors may in fact overshadow the influence of σ_3.

The triaxial modulus E_T and the Briaud pressuremeter modulus E can be compared at the same confining stress of 20 kPa (Section 6.3.6). The average E_T at σ_3 = 20 kPa for the two triaxial samples was 2600 kPa; the Briaud pressuremeter modulus between 1 m and 2 m averaged 3400 kPa. As was found in the tests in the sand of the sand box, both the pressuremeter and triaxial modulus are reasonably close to one another.

The ratio of the cyclic Briaud pressuremeter modulus to the Briaud pressuremeter modulus ($\frac{E_c}{E}$) and the ratio of the cyclic triaxial modulus to the triaxial modulus ($\frac{E_{Tc}}{E_T}$) can be evaluated for Fraser's clay; the average value of $\frac{E_c}{E}$ was 2.1 and the average value of $\frac{E_{Tc}}{E_T}$ was 7.2. Since E and E_T are reasonably similar, this finding means that in the clay of Fraser's farm, the E_{Tc} values are about 3.4 times higher than the E_c values.

6.5 Computer Simulation

6.5.1 The Program

The intent was to use the finite element method to calculate the deformation around the Briaud pressuremeter and at the free boundaries (if any) for a shallow test (z = 0.2 m) and a deep test (z = ∞). If the deformation field of the shallow test was significantly different from

that of the deep test, it would indicate that the surface boundary had a significant influence on the deformation process (in other words, there was a critical depth).

The soil was simulated by a linear elastic homogeneous, isotropic continuum. The assumption of elasticity was made because this assumption is used in flexible pavement design (Section 2.1.4) and because the Briaud pressuremeter is used only to give soil parameters in the "elastic phase" of the test. The soil was assumed to be weightless to simplify the comparison between the shallow and the deep test.

The finite element mesh is shown in Figure 96. The probe is 200 mm long and has a radius of 12.5 mm. The vertical rigid boundary (BC) is assumed to be supported on rollers at a distance of 50 probe radii from the probe; this distance was found to be acceptable by Hartman (p. 230 of (17)). For the deep test the two horizontal boundaries (AB, DC) were assumed to be rigid and supported by rollers; by preventing vertical movement at these boundaries, the deformation of the continuum was made horizontal and complied with the requirements of plane strain. For the shallow test, the lower horizontal boundary (DC) was made rigid and supported on rollers; the upper horizontal boundary (AB) was free. The vertical boundaries AF and DE were always kept free. The shallow calculation simulated a pressuremeter test at 0.2 m depth.

The total number of elements which were used is 128; this is the limit that the program could handle. The mesh is finer where there is rapid variation of the stress field such as close to the probe and in particular close to the probe ends. The program was written by Bowes and Russell (5); it applies to axisymetric solids and uses quadrilateral ring elements.

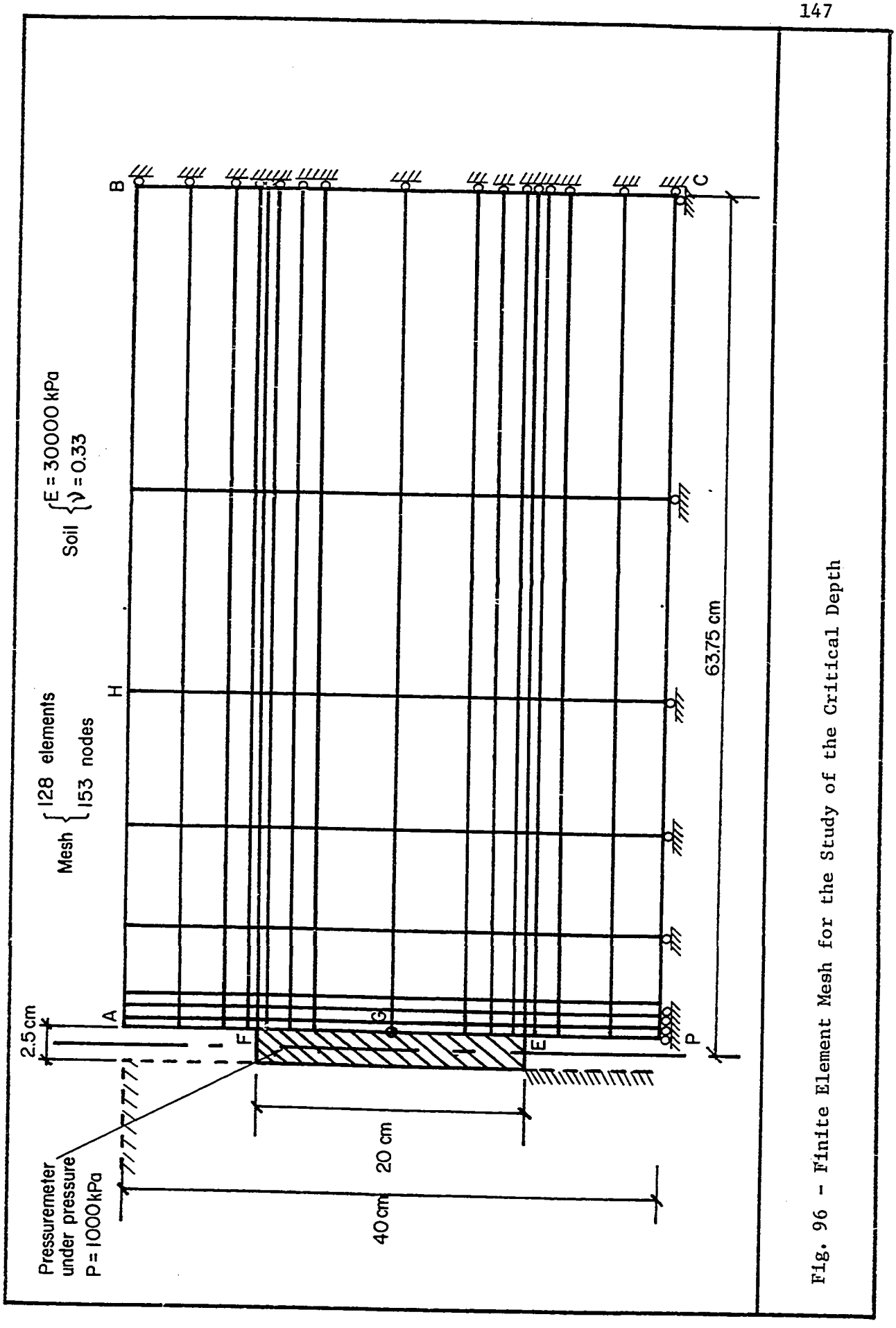

Fig. 96 - Finite Element Mesh for the Study of the Critical Depth

A check was run on the program by working out the problem of the stress field under a flexible circular plate loaded vertically and resting on a linear elastic homogeneous, isotropic half space; the results were compared with the closed form Boussinesq solution. The finite element results were extremely close to the Boussinesq results.

6.5.2 The Tests

The detailed results of the computer work are presented in Appendix E. The soil has a modulus of elasticity of 30,000 kPa and a Poisson's ratio of 0.33; the pressure in the pressuremeter is 1000 kPa.

For the deep test the horizontal displacement (u_y) of point G (Fig. 95) is 0.5518 mm; for the shallow test the displacement at G was 0.5523 mm. The difference between the two values is 0.09% (Fig. 97). Comparing the horizontal displacement of other nodes in contact with the probe leads to similar, extremely small differences (Fig. 97).

In the case of the shallow test, the free horizontal boundary (ground surface) moved upward slightly. The maximum vertical displacement (u_x) occurred at point H (Fig. 96) where it was 0.00495 mm. A movement of 0.00495 mm represents 0.9% of the horizontal displacement at G.

6.5.3 Discussion

It is possible and even probable that a greater number of elements would have given a more accurate representation of the displacement of the soil during a pressuremeter test. The following points indicate that the results are reliable:

- the comparison with the Boussinesq solution was excellent.

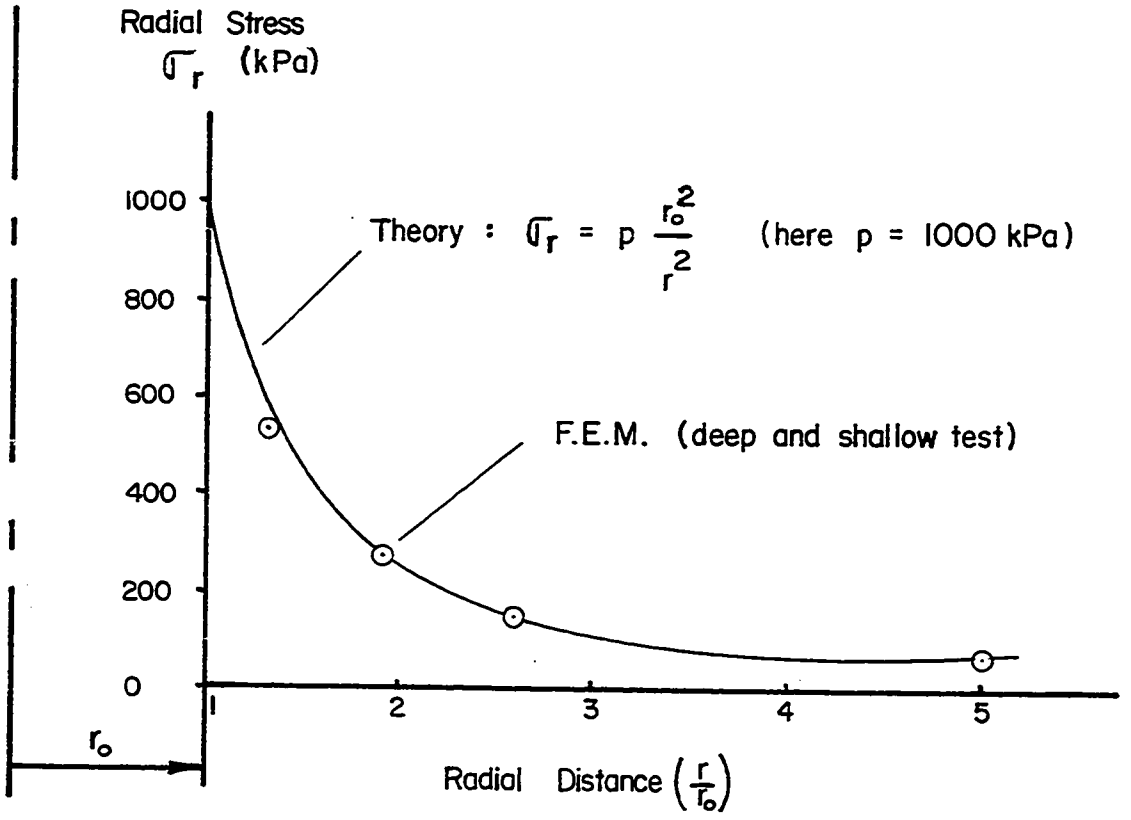

Fig. 98 - Pressuremeter Test - Radial Stress Versus Radial Distance - Comparison Between Theory and FEM Results

Node No. (Appendix E)	U_y for the Deep Test (mm)	U_y for the Shallow Test (mm)	Percent Difference
37 (F)	0.2559	0.2570	0.43 %
46	0.4570	0.4580	0.22 %
55	0.5006	0.5015	0.18 %
64	0.4157	0.4165	0.19 %
73 (G)	0.5518	0.5523	0.09 %
82	0.4157	0.4161	0.10 %
91	0.5006	0.5009	0.06 %
100	0.4570	0.4573	0.07 %
109 (E)	0.2559	0.2563	0.16 %

Fig. 97 - Radial Displacement of the Wall of the Hole in the Pressuremeter Test. Comparison Between a Shallow and a Deep Test.

- the comparison between the shallow and the deep test makes use of the relative magnitude of the results and not of the absolute values.
- Figure 98 is a plot of the radial stress (σ_r) versus the radial distance from the probe axis (r) in terms of probe radii (r_o). Figure 98 compares the curve given by the expansion of an infinitely long cylinder in an infinite linear elastic homogeneous isotropic continnuum (p. 349 of (1)) with the points given by the finite element method; the agreement is excellent.

From the above computer work which shows an extremely small difference between a deep and shallow pressuremeter test; it is concluded that for the cases which are studied in this thesis, the proximity of the surface has no significant influence on the deformation process around the probe; therefore, for these cases, there is no critical depth.

6.6 Conclusions

The results of the 66 pressuremeter tests in the sand of the sand box, the results of the 38 pressuremeter tests in the clay of Fraser's farm and the results of the computer simulation all indicate that the surface boundary has no significant influence on the elastic deformation of the soil around the pressuremeter probe. On the basis of this evidence, it is concluded that critical depth is not of importance in pressuremeter tests to measure the modulus of the soil.

In the field, when the Briaud pressuremeter is used for evaluation purposes, the asphalt layer is present; the layer has a beneficial effect on the tests carried out below the asphalt. When the pressuremeter is at

its shallowest position (in the base course, Fig. 1) it tries, to some extent at least, to lift up the asphalt cover. Although the overburden pressure due to the asphalt is small (2 to 3 kPa), the shear and tensile strengths of the asphalt membrane are high; this means that the pressuremeter has to exert a considerable effort to attempt to lift the pavement, this phenomenon, in effect, increases the equivalent depth of testing.

The abscence of a critical depth in the pressuremeter modulus profile leads to the following corollaries:

- the deformation process around the probe in a deep test is similar to the process in a shallow test in the case of E only.
- Equation 15 is as applicable to a shallow test as it is to a deep test.

The results of the 20 Menard GA pressuremeter tests indicate that there is a critical depth as far as limit pressure is concerned; a critical depth shows up in the test profiles for the sand of the sand box. In compact and dense sand this critical depth is about 1.2 m.

CHAPTER 7

COMPARISON BETWEEN THE BRIAUD PRESSUREMETER TEST AND THE McLEOD PLATE TEST

7.1 General

This chapter reports and discusses the results of 11 McLeod plate tests and 93 Briaud pressuremeter tests performed in parallel on the flexible pavements of two airports, namely Sarnia Airport and Ottawa International Airport. Testing at any one location on the runways consisted of one plate test on the surface of the pavement and a profile of pressuremeter tests in a nearby hole. Tests were performed at Sarnia Airport first and then at Ottawa Airport. As more and more pressuremeter tests were carried out, the drilling crew and the pressuremeter operator gained experience; as a result, the quality of the pressuremeter tests went from very poor (Tests Nos. 110, 111, Appendix A) to very good (Test No. 216, Appendix A).

During the Briaud pressuremeter test, a cyclic modulus is measured. The appropriate procedure to measure a cyclic modulus was not discovered until half the testing program at Ottawa Airport was completed. As explained in Section 6.3.4, a pressuremeter test procedure was first established while testing in the sand box; this procedure was applied to the first tests in Sarnia and it was soon realized that this method was not acceptable. As a result, no Briaud pressuremeter cyclic moduli are available for the tests at Sarnia Airport except for the special study involving Tests Nos. 143 and 144 (Appendix A).

Ottawa International and Sarnia Airports are two very different airports. The type of subgrade is different; for example there is sand in Ottawa and clay in Sarnia. The type and intensity of traffic is different: the design plane is the DC8-63 for Ottawa and the Convair 440 for Sarnia. The runway condition is different; the Sarnia runway had an overlay whereas the Ottawa pavement had not.

7.2 Literature Survey

Only two articles reporting the results of comparison studies between a plate test and pressuremeter tests were found.

Greenland, as reported by Baguelin et al. (p. 589 of (1)), compared the plate modulus ($E_{p\ell}$) with the Ménard pressuremeter modulus (E_M) in a stiff varved clay. Greenland found that $E_{p\ell}$ was about 1.25 E_M.

Shields and Bauer (40) also compared the two tests and found, in a sensitive clay, that $E_{p\ell}$ was about 2 E_M. It must be emphasized that in the case of a plate test, the initial secant modulus is very sensitive to which point of intersection with the curve is chosen. Using the load-settlement curve of Shields and Bauer's footing test (p. 416 of (40)) one can calculate a modulus of deformation of between 29,000 and 79,000 kPa, depending on which point of intersection is chosen. The ratio of $E_{p\ell}$ over E_M would then vary from 2 to 5.5.

7.3 Sarnia Airport

7.3.1 The Site and the Soil

Sarnia is on the U.S.A.-Canada border between Lake Huron and Lake Erie. The airport has two runways (Fig. 100) and the testing program was

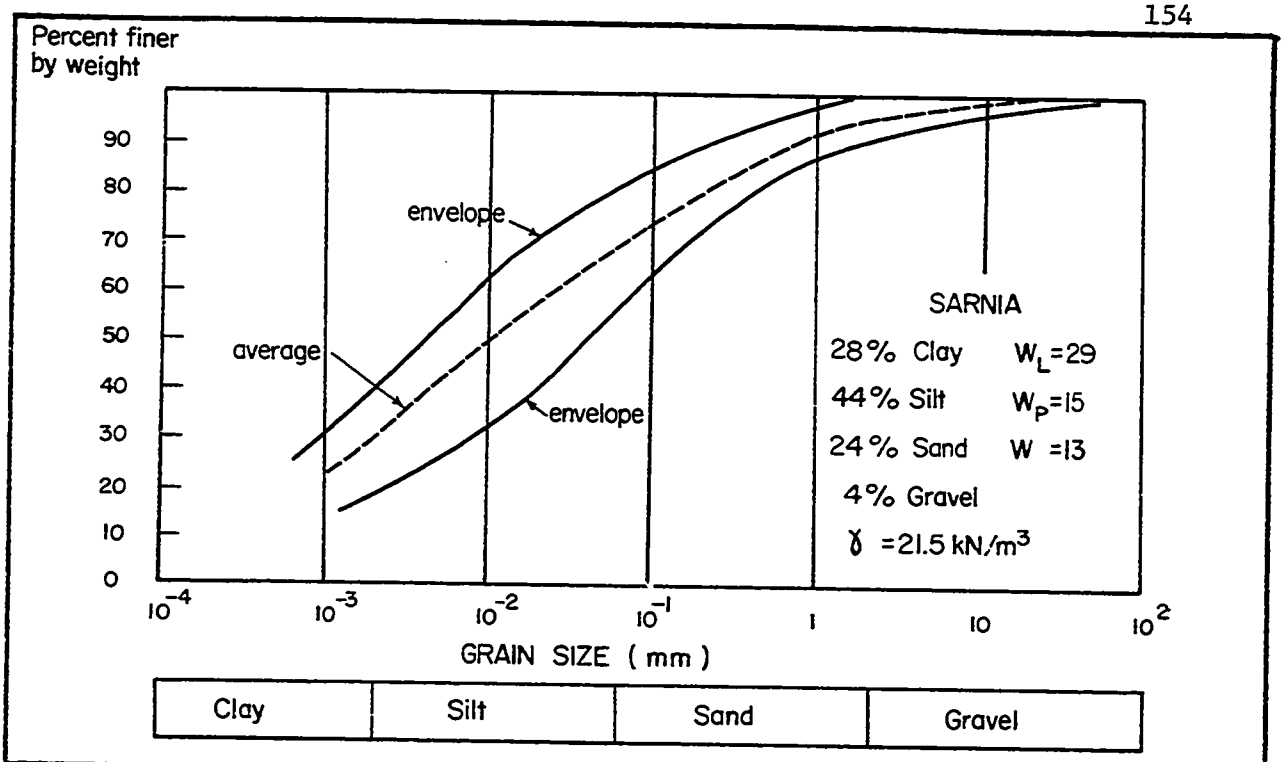

Fig. 99 - Sarnia Airport. Grain Size Curve.

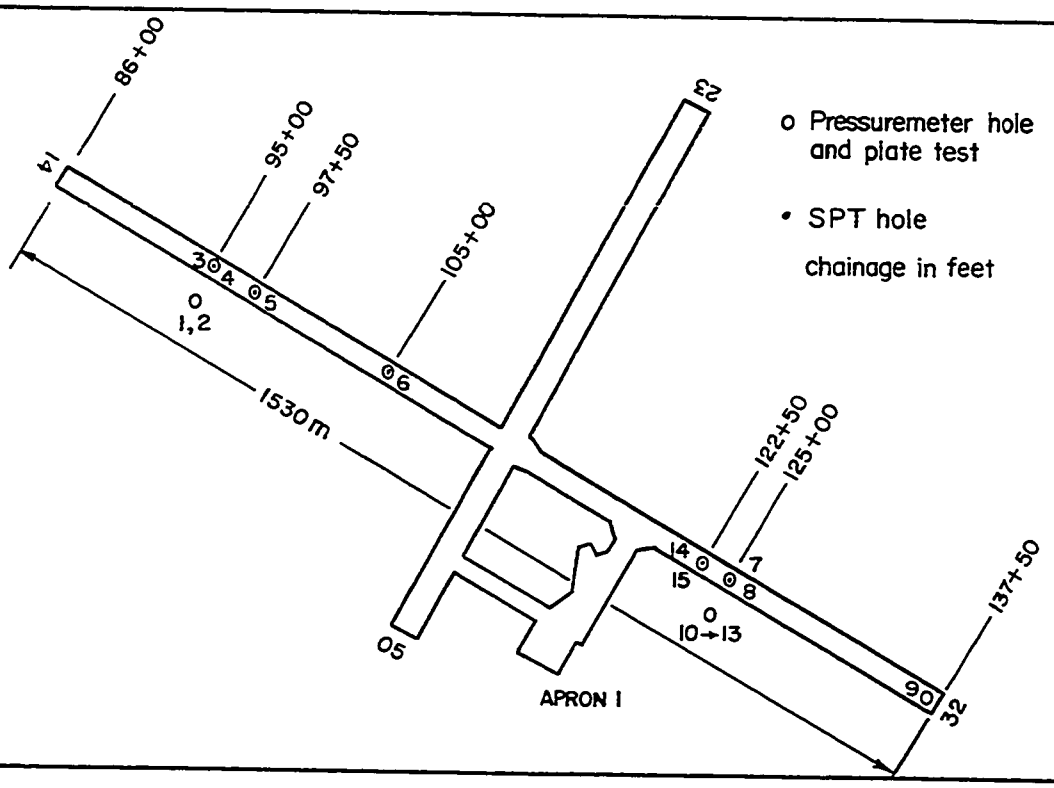

Fig. 100 - Sarnia Airport. Plan View.

carried out on the main runway 14-32. The pavement of this runway is made up, on average, of 6.5 cm of original asphalt and 28 cm of moist, medium sized sandy gravel (particles up to 2 cm in size). After the overlay, the asphalt thickness was increased to about 14 cm on average.

Forty-eight Atterberg limits, 30 sieve and hydrometer analyses, and 30 natural water content determinations were performed in order to identify the subgrade. It is a silty clay with the grain size distribution presented in Figure 99. The liquid limit varies from 21 to 35 and averages 29; the plastic limit varies from 10 to 21 and averages 15; the natural water content varies from 11 to 21 and averages 13.

The grain size curve indicates that the material is well graded and the soil could be called a clayey till. Its average unit weight is 21.5 kN/m^3. The water table beside the runway was lower than 2 m below the ground surface whereas under the runway, the pressuremeter holes filled to the top with water fairly rapidly on removal of the pressuremeter. The high water level under the runway is probably not a true water table but simply a perched water table since the base course layer can act as a water reservoir over the impervious subgrade layer.

7.3.2 The Testing Program

The testing program at Sarnia involved 59 Briaud pressuremeter tests in 15 different holes, five McLeod plate tests, Standard Penetration tests at the five plate location and two triaxial tests on samples of the subgrade.

The pressuremeter holes are numbered from 1 to 15; their exact location is given in Figure 101. Hole 1 was made with a 31.75 mm diameter hand auger; augering was difficult and the tests were done from top to

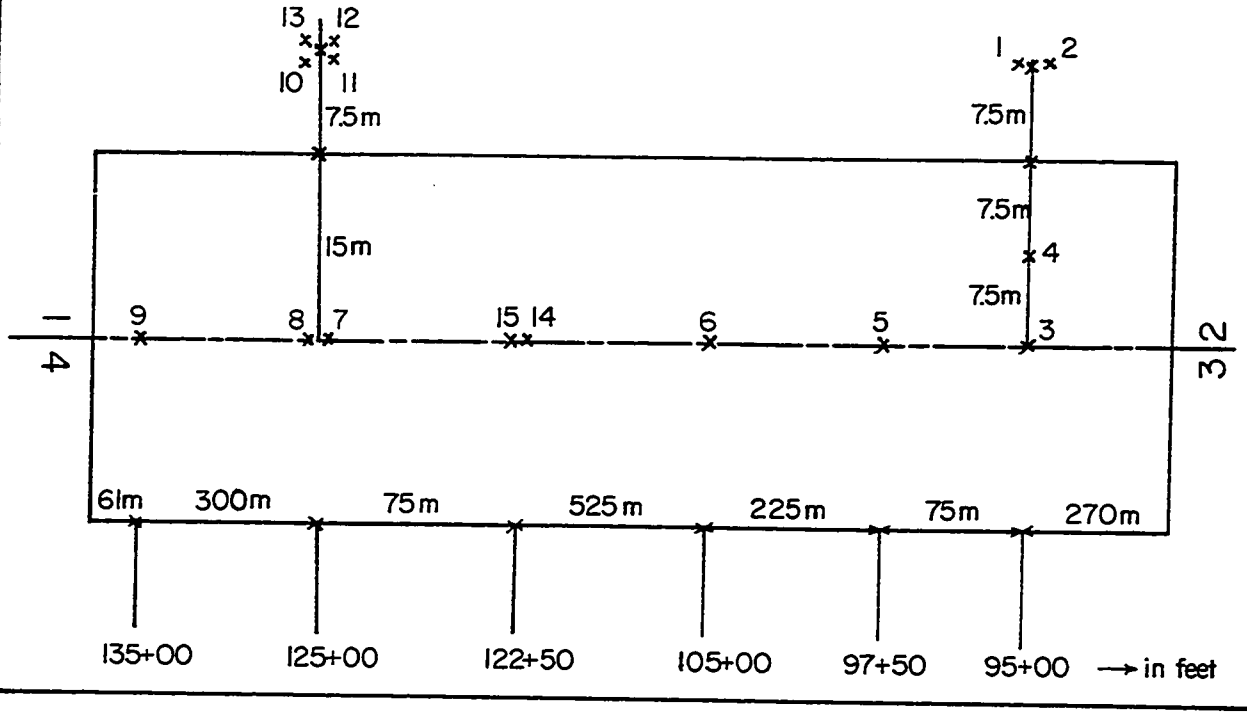

Fig. 101 - Sarnia Airport. Detailed Position of the Test Holes.

Hole	Pavement Bearing Strength S_p (kN)	Thickness Base Course t_b (cm)	Thickness Asphalt t_a (cm)	Equivalent Pavement Thickness t (cm)	Subgrade Bearing Strength S_s (kN)
3	196	20	5	30	129
5	186	23	7	37	111
6	243	24	6	36	147
7	265	29	14.5	58	118
15	208	24	14.5	53	100

Fig. 102 - Sarnia Airport. Summary of the McLeod Plate Test Results.

bottom.

Hole 2 was made by driving a 28.57 mm diameter rod into the ground close to Hole 1; the tests were done from top to bottom. From 0.9 m depth on, penetration of the pressuremeter probe was impossible by hand or by using the sledge hammer. The drill rig was used to force the probe in and the probe was damaged. Below 0.9 m depth, the test results are of doubtful value.

Hole 3 was made by driving and redriving rods several times down to 2 m depth; the tests were done from top to bottom.

Holes 4 and 5 were made by driving 34.92 mm diameter E rods once; the tests were done from top to bottom.

Hole 6 is similar to Holes 4 and 5 except that when the 1.5 m deep test was to be performed, the probe could not be pushed to 1.5 m. The probe was removed and the 34.92 mm diameter E rods were driven a second time to 2 m; then the 1.5 m and 1.8 m deep tests were carried out.

Hole 7 was made by first driving 28.57 mm diameter rods to 0.5 m depth; then, since the probe could not be inserted in this small diameter hole, the 34.92 mm diameter E rods were driven to the full depth of 2m. The tests were done from top to bottom.

Hole 8 was made by driving 34.92 mm diameter E rods to 0.5 m once; only the 0.3 m test was performed. Hole 7, 8 and 8A are about 1 m from each other.

Hole 9 is similar to Hole 4 except that the probe could not be inserted; the hole was abandoned.

Hole 10 was made by driving the 34.92 mm diameter E rods to 1.5 m; the test was done at 1.2 m.

Hole 11 is similar to Hole 10. The test done at 1.2 m depth is the only cyclic test which was performed in Sarnia; 10 cycles were made.

Hole 12 was made with the 31.75 mm diameter hand auger down to 1.5 m depth; the test was done at 1.2 m. Holes 10, 11 and 12 are about 1 m from each other. Hole 13 was not tested.

Hole 14 was made by driving the 34.92 mm diameter E rods to 0.5 m and withdrawing them; the 0.3 m test was performed. After the probe was withdrawn, the E rods were driven to 2m, withdrawn, and redriven three times before inserting the pressuremeter probe for testing; the tests were done from bottom to top.

Hole 15 is similar to Hole 14 except that the E rods were driven only once.

Plate tests were carried out close to Holes 3, 5, 6, 7 and 15. Repetitive plate tests were done close to Holes 6 and 7; the other plate tests were non repetitive. The thicknesses of the base course (t_b) and the asphalt (t_a) layer under the plate at the time of the plate test are given in Figure 102; the values of t_a vary significantly from one hole to another because testing took place during the construction of the overlay.

SPT tests were performed close to Holes 3, 5, 6, 7 and 15. Also, samples were taken with two 75 mm diameter Shelby tubes at 1.2 m depth close to Holes 10 to 13; the samples were used for two multistage, cycled triaxial tests.

7.3.3 The Test Results

The results of the Briaud pressuremeter tests are shown in Appendix A as individual curves and on Figures 103 to 108 as profiles of modulus

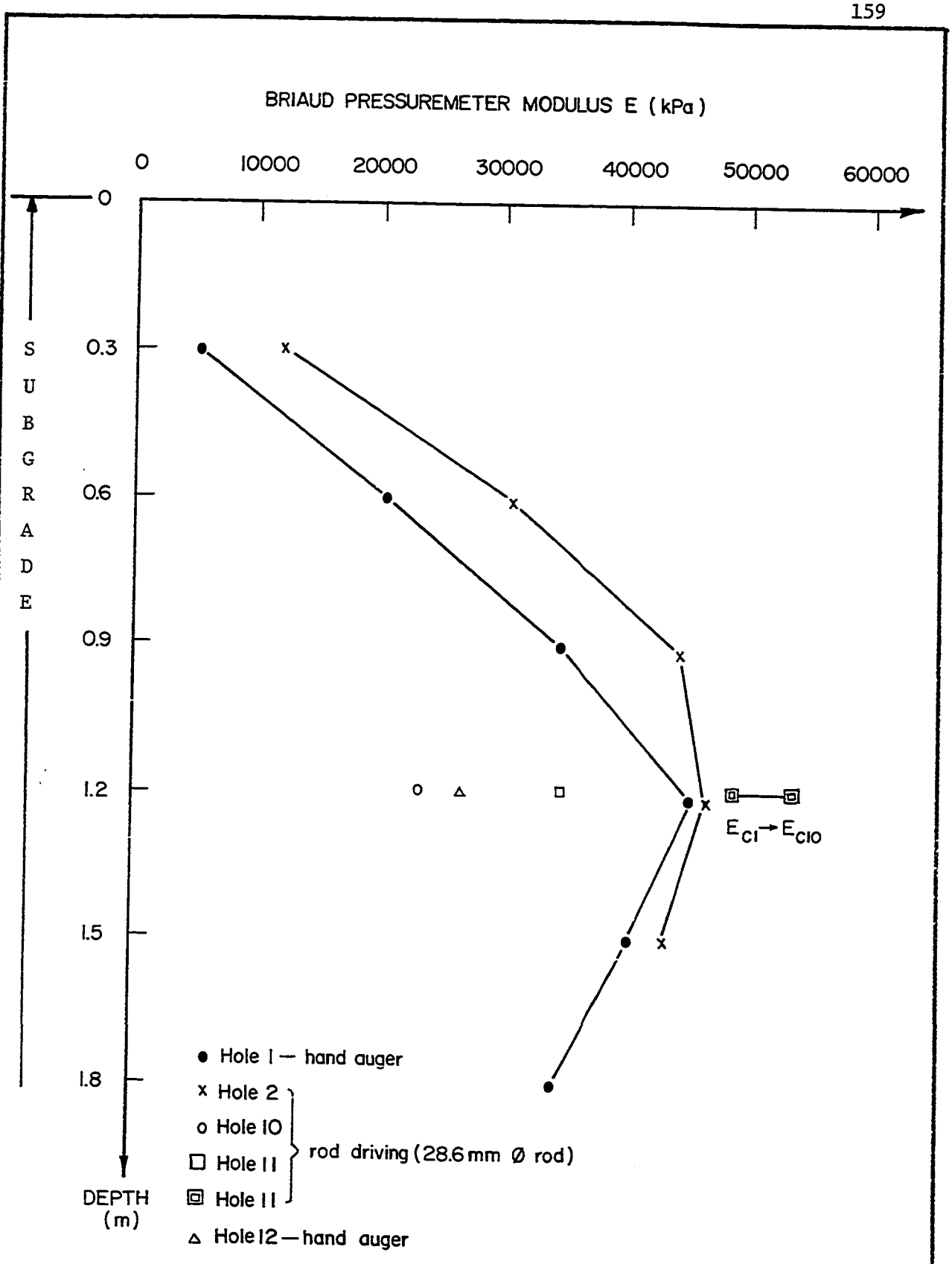

Fig. 103 - Sarnia Airport. Briaud Pressuremeter. Modulus vs. Depth. Hole 1, 2, 10, 11, 12.

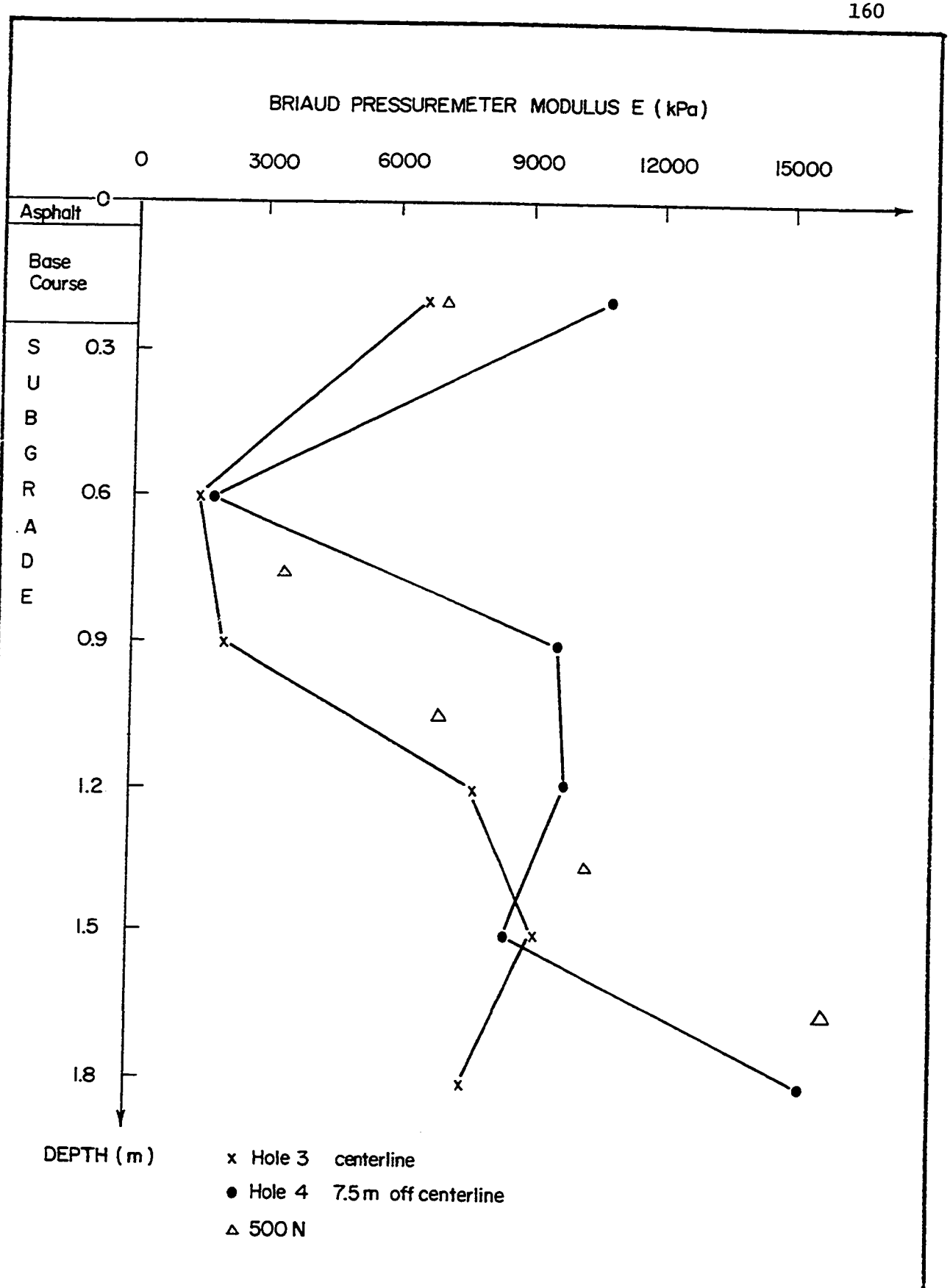

Fig. 104 - Sarnia Airport. Briaud Pressuremeter. Modulus vs. Depth. Hole 3, 4.

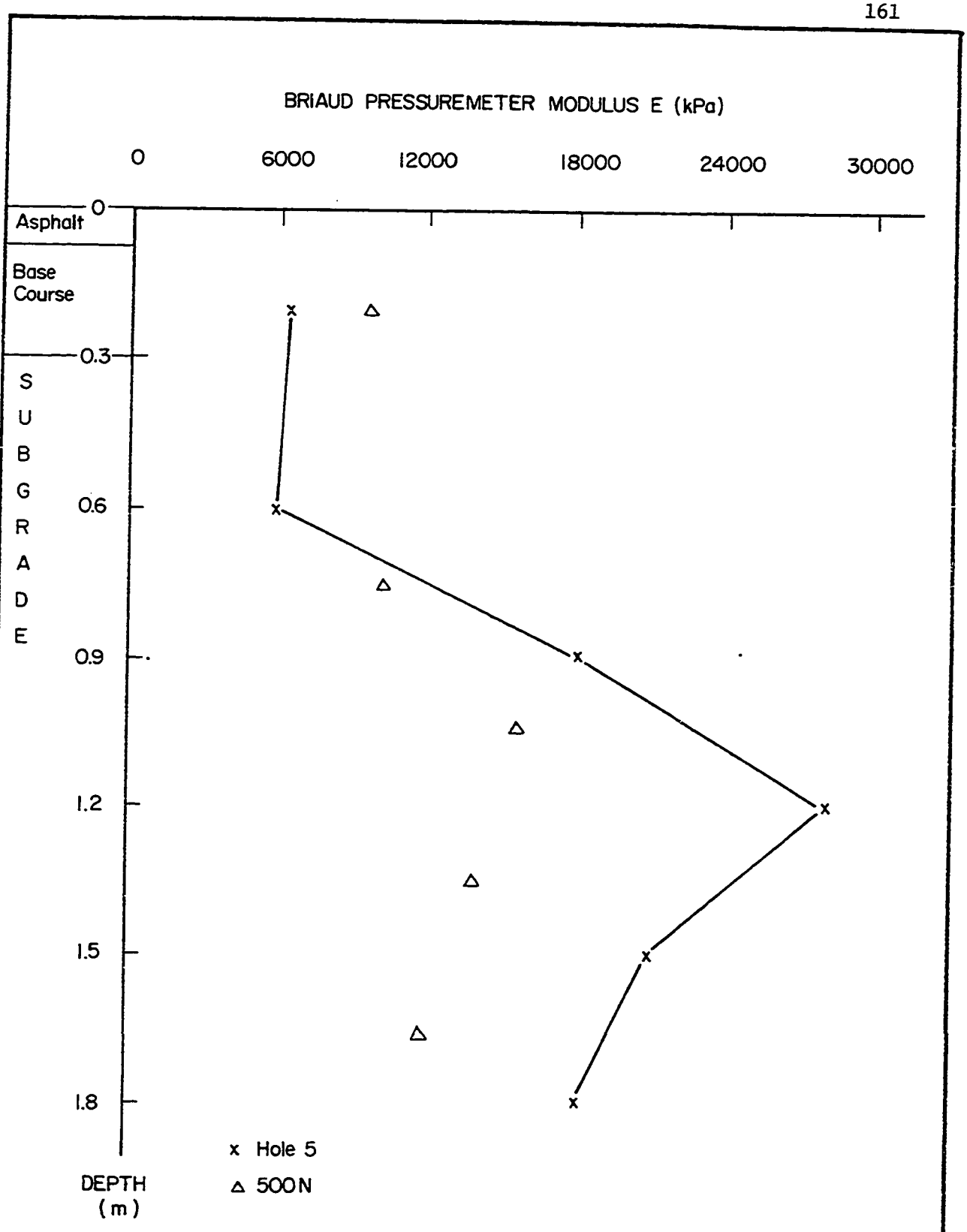

Fig. 105 - Sarnia Airport. Briaud Pressuremeter. Modulus vs. Depth. Hole 5.

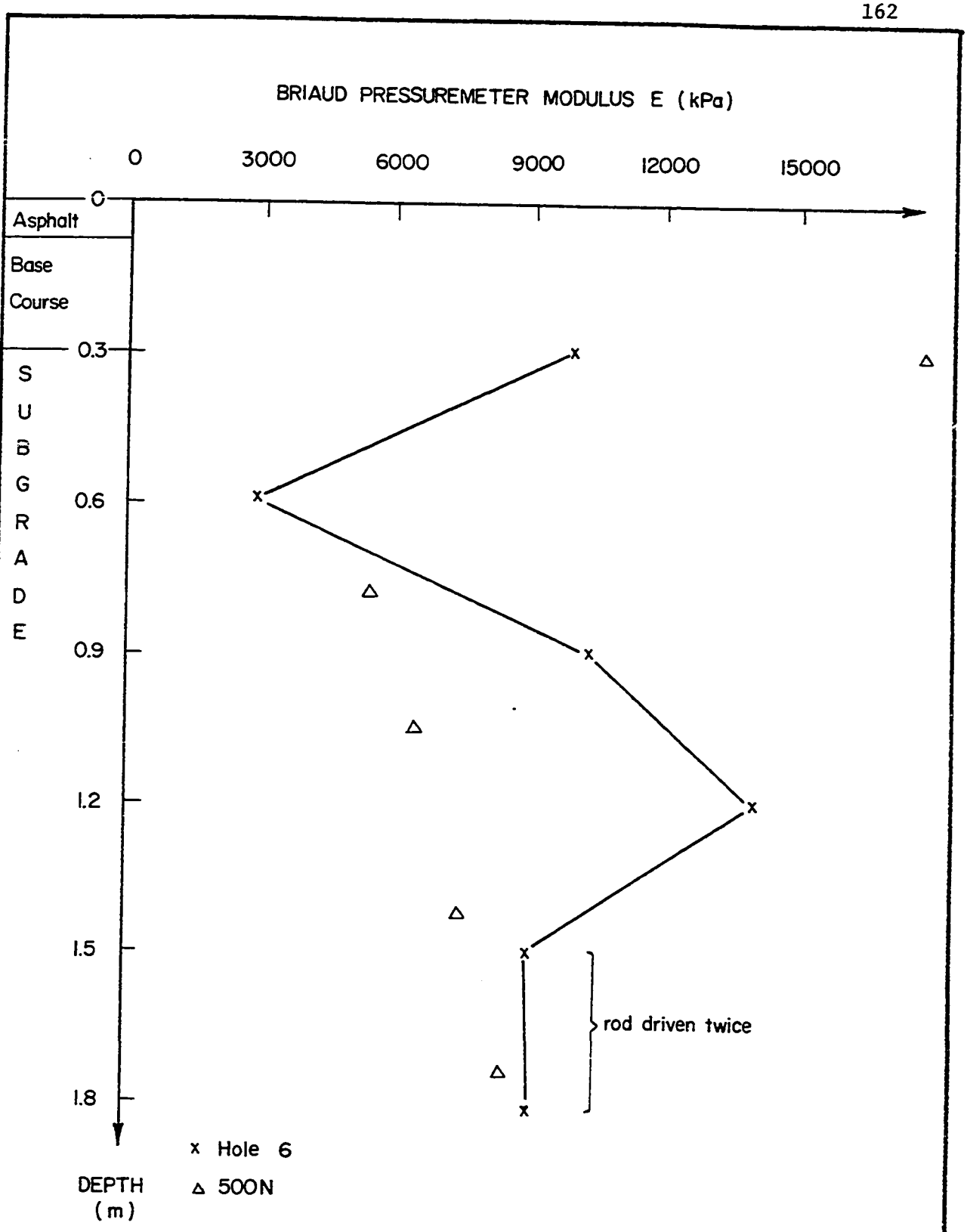

Fig. 106 – Sarnia Airport. Briaud Pressuremeter. Modulus vs. Depth. Hole 6.

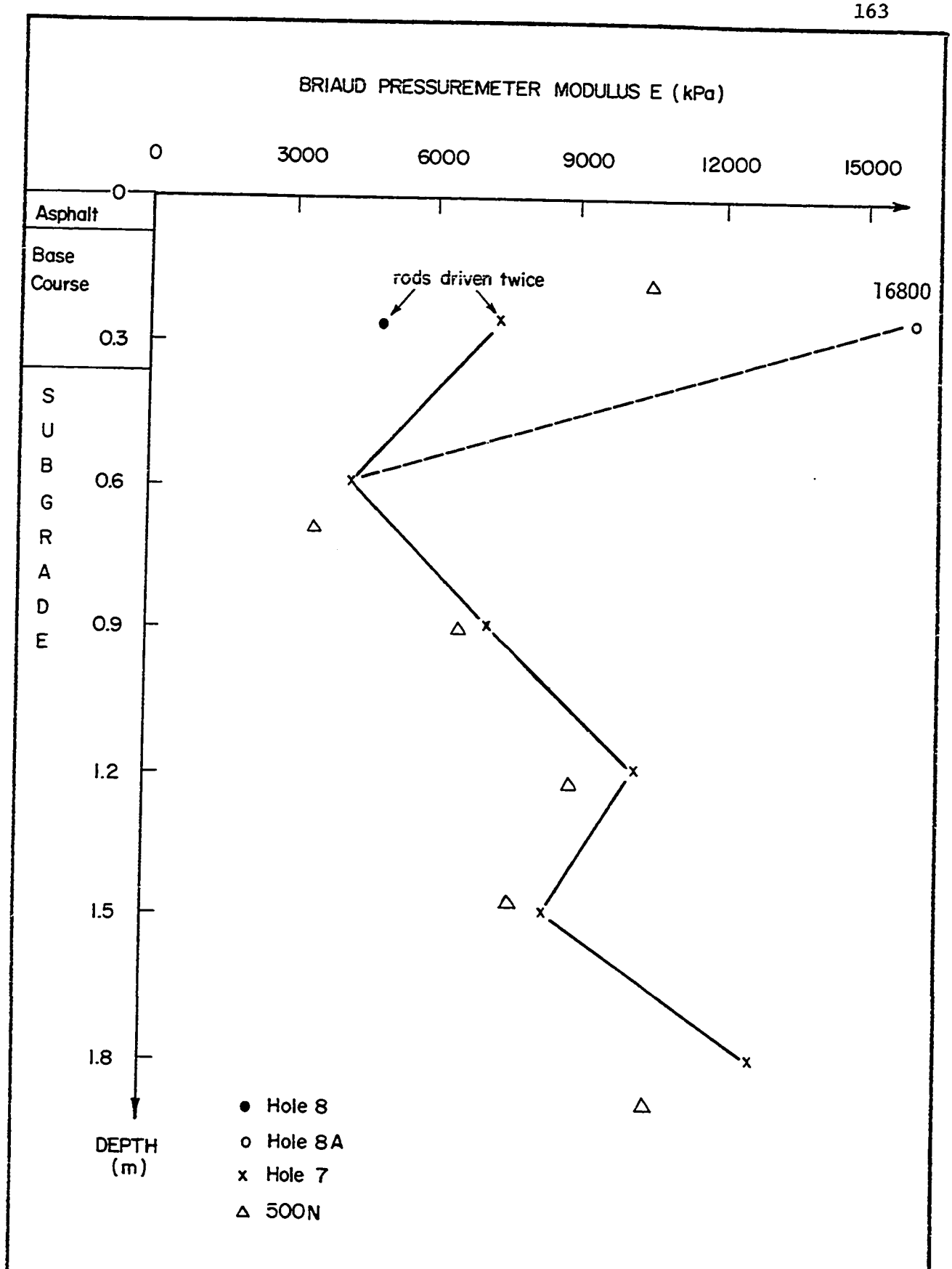

Fig. 107 – Sarnia Airport. Briaud Pressuremeter. Modulus vs. Depth. Hole 7, 8, 8A.

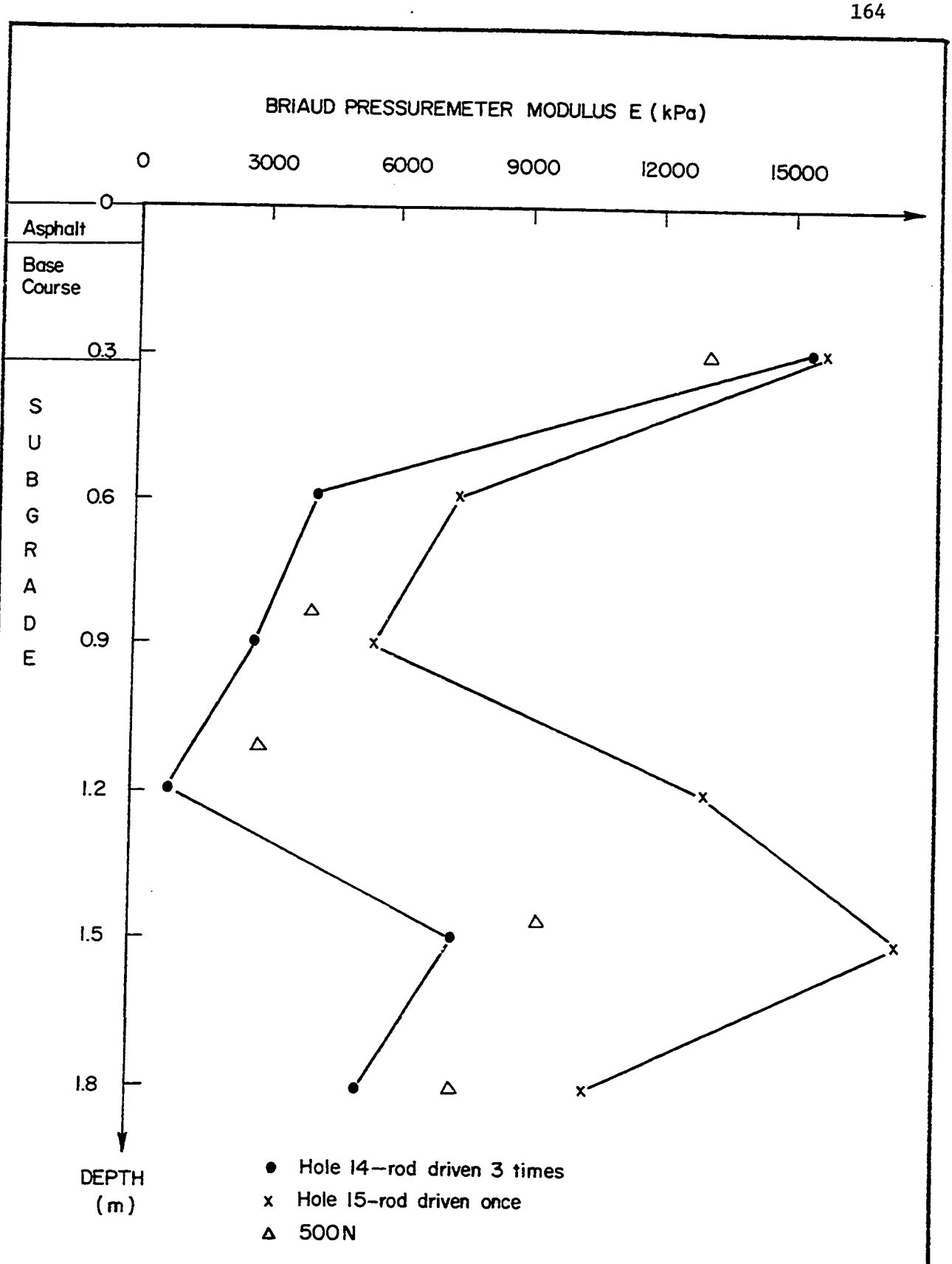

Fig. 108 - Sarnia Airport. Briaud Pressuremeter. Modulus vs. Depth. Hole 14, 15.

versus depth. Figure 103 shows the results of the tests which were performed off the runway for special studies (disturbance and cyclic test). The results of the pressuremeter tests at five different chainages on the runway are presented on Figures 104 to 108; these figures also give the results of the SPT tests since the quantity 500 N is plotted as a modulus (in kPa).

The results of the five McLeod plate tests are given in Appendix B as individual tests curves and on Figure 102 as both pavement bearing strengths (S_p) and subgrade bearing strengths (S_s). The diameter of the plate, (B), was 0.762 m for all five tests. The parameters S_p and S_s have been calculated according to the procedure described in Section 5.1.1. The thicknesses of base course and asphalt layers listed in Figure 102 were obtained from inspection of the SPT samples and were used for calculating the equivalent granular thickness with an equivalence factor of one for the base course and two for the asphalt.

The results of the two multistage cyclic triaxial tests are shown in Appendix C as individual test curves and on Figure 109 as a profile of the modulus versus the cell pressure σ_3. The samples were taken with Shelby tubes and the test specimens were 75 mm in diameter and approximately 140 mm high. The specimens were extremely difficult, if not impossible, to trim because they were hard, brittle and contained gravel up to 3 cm in size. One of the samples had to be capped like a concrete cylinder.

7.3.4 Discussion

The quality of a pressuremeter test can be judged by the shape of the test curve; in Test No. 98 (Appendix A) the hole was too big, and in Test

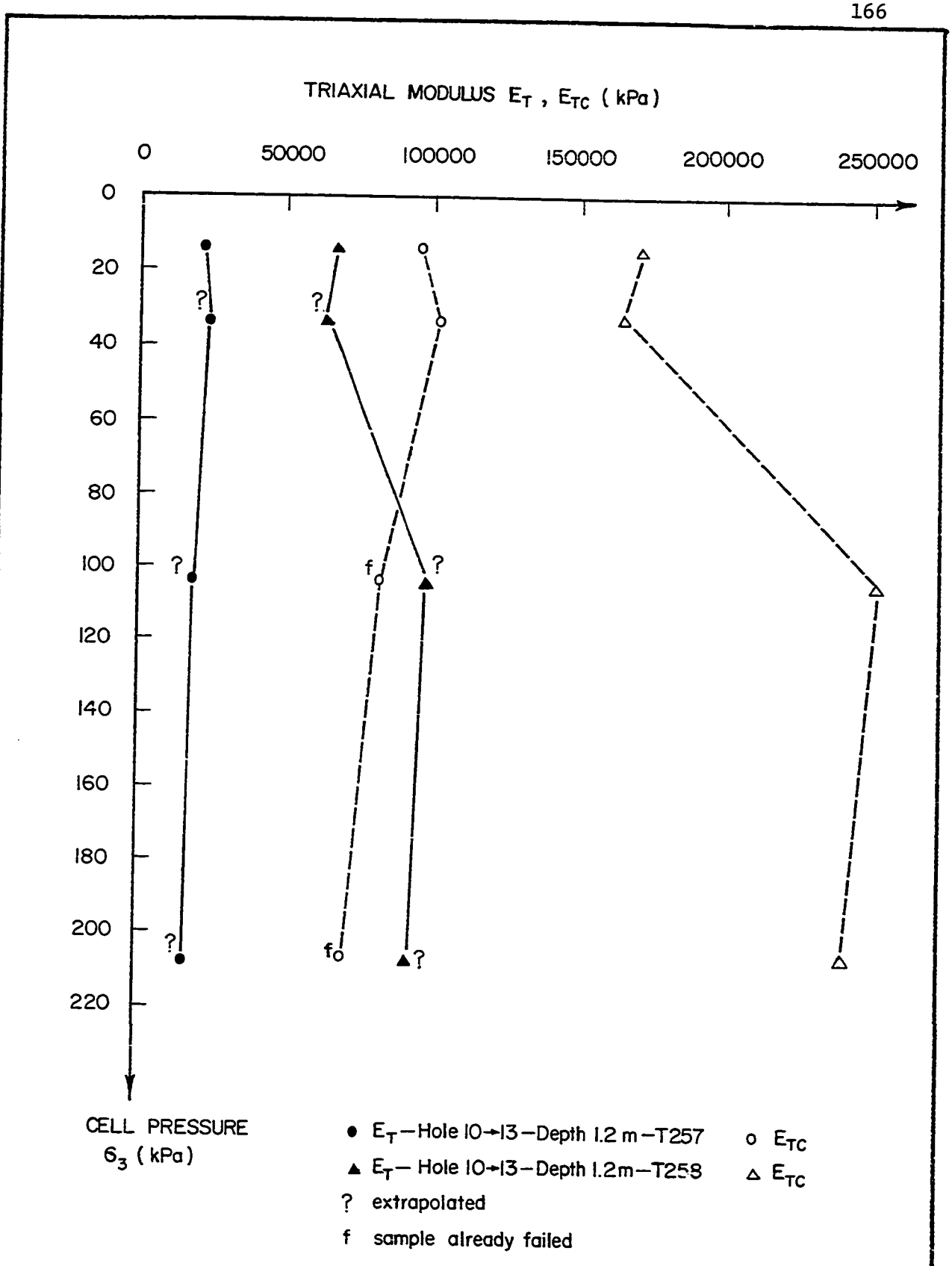

Fig. 109 - Sarnia Airport. Triaxial Modulus vs. Cell Pressure. Hole 10 to 12.

No. 112 (Appendix A) a large amount of disturbance was probable. After the first few tests, the shape of the test curve improved and the results are thought to be acceptable (Tests Nos. 126 or 156, Appendix A). From an examination of the test curves, it is concluded that the results of Hole 3, 8 and 14 cannot be used because of excessive disturbance to the wall of the borehole. In the case of Hole 6, the tests at 1.5 m and 1.8 m depth (Tests Nos. 120 and 121, Appendix A) may have given moduli which are too low since the pressuremeter tests were performed after the E rods had been driven twice; however, the test curves for these two tests do not show any anomaly. For Hole 7, the test at 0.3 m was performed after driving the rods twice (Test No. 135); the test at 0.3 m depth in Hole 8A was done properly, in that the rods were only driven once (Test No. 142) and the results should be perferred to those of Test No. 135.

The quality of a McLeod plate test can also be judged from the shape of the test curves; the usual shape of a load-deflection curve of a McLeod plate test (repetitive or not) looks like the one shown for Test No. 337 (Appendix B). The usual curve bends gradually and it is for this reason that the shape of the load-deflection curve for first loading of Test No. 334 (Appendix B) is somewhat surprising. The jack which was installed between the plate and the truck (Fig. 4) was found difficult to calibrate since a powerful press is required to carry out the calibration. At Sarnia Airport the pavement bearing strength (S_p) varied from 186 kN to 265 kN and the subgrade bearing strength (S_s) varied from 100 kN to 147 kN.

The results of the two triaxial tests are erratic due to the

difficulty which was encountered in trimming the samples and due to the presence of fissures within the samples themselves. In the first test (Test No. 257, Appendix C), a fissure existed at an angle of 45° with the horizontal and the sample failed before the cycles could be performed. In the second test (Test No. 258, Appendix C), a fissure existed in almost a horizontal direction and the sample was much stronger. Although both samples came from the same location, the first loading modulus measured in Test No. 258 was 3.2 times the first loading modulus measured in Test No. 257. Also, in Test No. 257, the sample passed its peak strength at the end of the second stage thereby invalidating the modulus measurement of the third and fourth stages (σ_3 = 104 kPa and 208 kPa in Fig. 109). In the case of a triaxial test, the influence of fissures can be overemphasized by the fact that compression is uniaxial and by the small size of the sample; the pressuremeter test does not have the same drawback as the triaxial test in this respect, because the mass of soil which is tested is larger and the load is exerted in all radial directions.

The subgrade beside the runway seems to be much stronger than the subgrade under the runway center line. Indeed the Briaud pressuremeter modulus under the runway ranged from 1500 to 28,000 kPa and averaged 10,000 kPa (Holes 3, 4, 5, 6, 7, 8, 8A, 14, 15) whereas the modulus averaged about 30,000 kPa beside the runway (Holes 1, 2, 10, 11, 12). Also, when comparing the shape of the Briaud pressuremeter modulus profiles (Holes 3, 5, 6, 7, 15), it can be seen that there is a weak layer about 0.5 m thick immediately under the base course layer. These findings indicate a loss of strength of the subgrade under the runway due, probably,

to a combination of traffic loading and poor drainage. Frequent load applications to the pavement, induce high pore pressures which tend to loosen the subgrade material with time. This type of detailed strength information is easily obtained with a Briaud pressuremeter whereas, it is impossible to obtain with the plate test.

In the triaxial tests, the variation of the modulus with the cell pressure (σ_3) is small. The triaxial modulus (E_T) and the Briaud pressuremeter modulus (E) can be compared under the same σ_3 condition of 20 kPa (Section 6.3.6). The triaxial modulus E_T at σ_3 = 20 kPa is 22,000 kPa in Test No. 257 and 65,000 kPa in Test No. 258 (Fig. 109). At 1.2 m depth in Holes 10, 11, 12 (close to the samples holes) the average Briaud pressuremeter modulus is 28,600 kPa which is well within the range of values of the triaxial modulus (E_T).

The Briaud pressuremeter cyclic modulus (E_c) was measured during Test No. 144 (Appendix A). In order to determine the point at which to stop first loading and start the cycle, a non cyclic test (Test No. 143) was performed before Test No. 144 in a nearby hole. The cycles were started in Test No. 144 at the pressure corresponding to the end of the elastic phase in Test No. 143. This way of determining the point at which to start the cycles is acceptable but requires two tests rather than one (the single test procedure is explained in Section 4.4.6). In Test No. 144, 10 cycles were performed and the cyclic modulus increased slightly with the number of cycles; after 10 cycles it was 10% higher than after the first cycle (Fig. 103). Test No. 144 lasted about 20 minutes or 3.5 times longer than a test which would measure only the first cyclic modulus. The pressuremeter modulus ratio ($\frac{E_c}{E}$) was 1.4 and the average triaxial

modulus ratio ($\frac{E_{Tc}}{E_T}$) was 3.5. Since E and E_T are reasonnably close, this means that in the silty clay of Sarnia Airport the E_{Tc} values are about 2.5 times higher than the E_c values.

It is interesting to note that the blow count profile from the SPT test is reasonably parallel to the pressuremeter profile (Fig. 104 to 108) and that 500 N gives the order of magnitude of the Briaud pressuremeter modulus in kPa.

7.4 Ottawa Airport

7.4.1 The Site and the Soil

Ottawa International Airport is made up of two parts: an older, smaller airport (lower left part of Fig. 110) with runways 04-22 and 17-35 and a more recent airport with runways 07-25 and 14-32.

The taxiway Zoulou of the newer airport has a pavement made up of 100 mm of asphalt and 300 mm of base course. The subgrade is a silty sand with 20% silt, 60% sand and 20% gravel; the grain size curve is presented in Figure 111 (Hole 1). The in situ unit weight of this silty sand was measured with a nuclear densometer to be 21.4 kN/m^3. The moisture content was about 10% and the water table was deeper than 2 m.

Runway Mike and taxiways Uniform and Tango of the older airport have a pavement made up of 50 mm of asphalt and 100 mm of base course. The subgrade is a uniform sand. Grain size curves are shown in Figure 111 (Hole 5 and 6); the nuclear densometer gave an in situ unit weight of 16.6 kN/m^3. The moisture content was 10% and the water table was deeper than 2 m below the ground surface.

The samples which were used for the grain size analyses and the

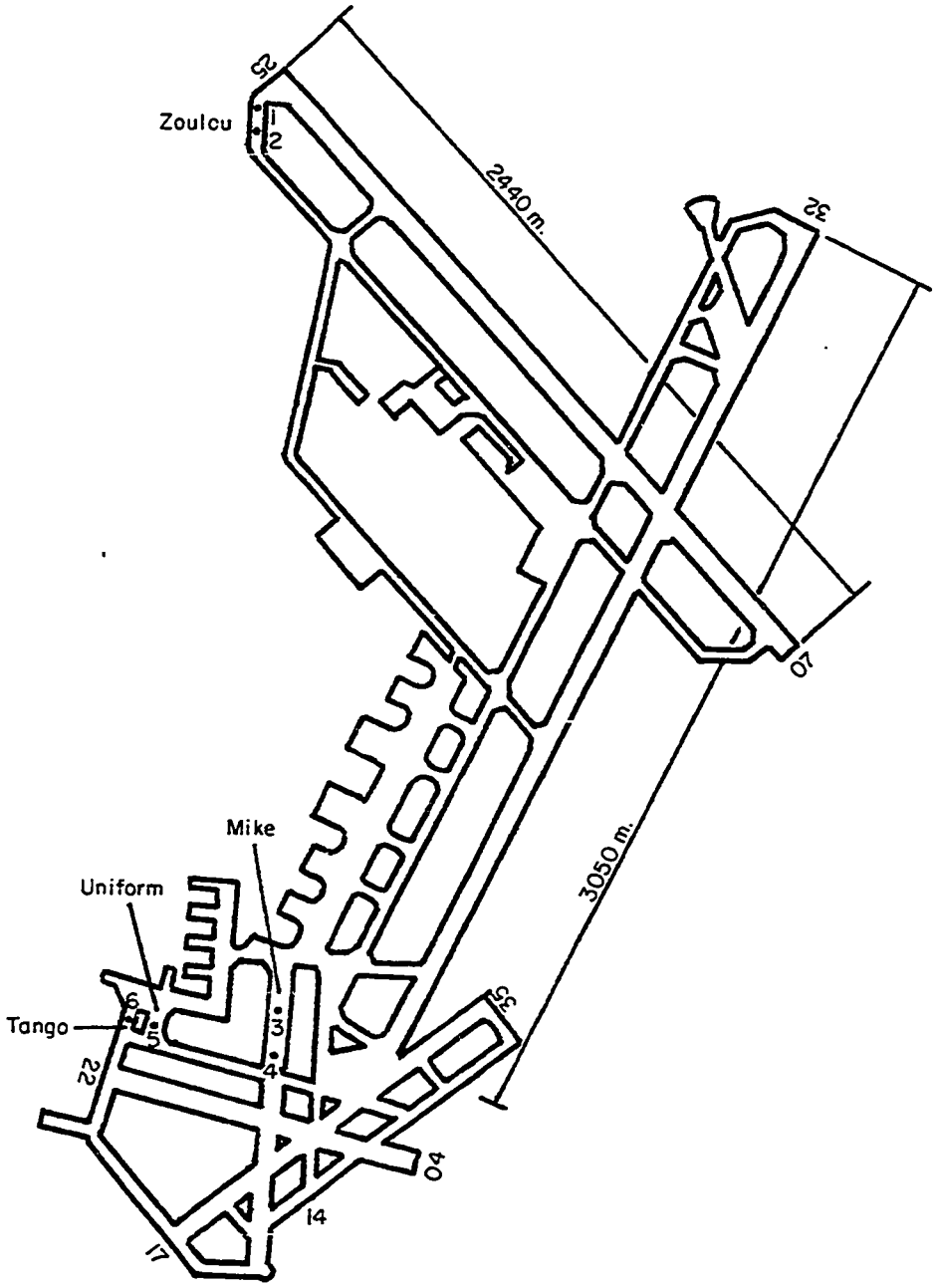

Fig. 110 - Ottawa International Airport - Location of Test Holes.

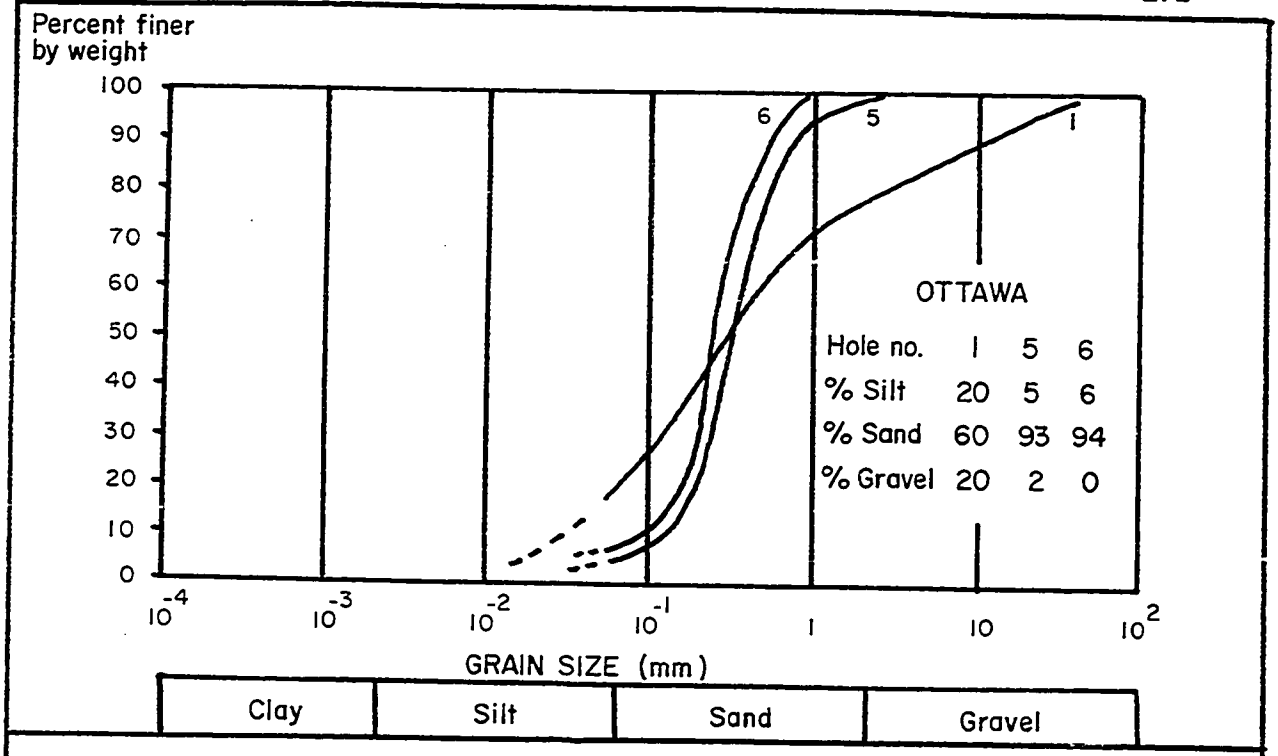

Fig. 111 - Ottawa International Airport. Grain Size Curves.

Hole No.	Old or New Airport	Pavement Bearing Strength S_p (kN)	Asphalt Thickness t_a (cm)	Base Course Thickness t_b (cm)	Equivalent Granular Thickness t (cm)	Subgrade Bearing Strength S_s (kN)
1	New	1709	10	30	50	851
2	New	1728	10	30	50	860
3	Old	412	5	10	20	312
4	Old	405	5	10	20	306
5	Old	601	5	10	20	455
6	Old	614	5	10	20	464

Fig. 112 - Ottawa International Airport. Summary of the McLeod Plate Test Results.

triaxial tests were taken at the edge of the pavement, right beside the pressuremeter borehole. A small 0.5 m deep pit was dug with a shovel, and bags were filled with disturbed samples. The in situ unit weight of the soil at the bottom of the pit was measured with a nuclear densometer. Moisture contents were determined in the laboratory.

7.4.2 The Testing Program

The testing program involved 34 Briaud pressuremeter tests in six different holes, six McLeod plate tests, and three triaxial tests.

The pressuremeter holes are numbered from 1 to 6; the holes were located on the runway or taxiway center lines as shown in Figure 110.

Holes 1A, 1 and 2 are on taxiway Zoulou of the new airport (Fig. 110). Hole 1A was made by driving the 34.92 mm diameter E rods; refusal to driving was encountered at 0.75 m depth and no tests were performed in this hole. Hole 1 is close to Hole 1A, and Holes 1 and 2 are 100 m apart. Holes 1 and 2 were made by driving the 34.92 mm E rods and the pressuremeter tests were performed starting at the bottom of the hole.

Holes 3 and 4 are located 100 m apart on runway Mike of the old airport; Hole 5 is on taxiway Uniform and Hole 6 on taxiway Tango. All four holes were made and tested in the same fashion as Holes 1 and 2.

A plate test was carried out about 2 m away from each pressuremeter hole, making six plate tests in all. Repetitive plate tests were done close to Holes 1 and 4; the other plate tests were non repetitive. The asphalt and base course thicknesses (t_a and t_b) under the plate at each test location are given in Figure 112.

The three multistage cyclic triaxial tests were performed on reconstructed specimens. Using the disturbed soil taken in the field, the

test specimens were made up to have the same water content and the same unit weight as the soil in situ. The required unit weight was obtained in the laboratory by vibration (Fig. 86).

7.4.3 The Test Results

The individual results of the Briaud pressuremeter tests are shown in Appendix A; Figures 113 to 116 are profiles of modulus versus depth. Figure 113 presents the profiles obtained at the new airport (Holes 1 and 2) while Figures 114 to 116 are the profiles from the old airport (Holes 3 to 6). At Ottawa Airport both the Briaud pressuremeter modulus (E) and the Briaud pressuremeter cyclic modulus (E_c) were measured. The E profiles are the solid lines in the figures while the E_c profiles are dotted.

The individual results of the six McLeod plate tests are given in Appendix B; Figure 112 summarizes the pavement bearing strengths (S_p) and the subgrade bearing strengths (S_s). The diameter (B) of the plate is indicated on the individual curves and varies from 0.457 m to 0.762 m. The parameters S_p and S_s have been calculated as described in Section 5.1.1. The thicknesses of the base course and asphalt layers listed in Figure 112 were obtained from the construction records and were used to calculate the equivalent granular thickness with a factor of 1 for the base course and 2 for the asphalt.

The individual results of the three multistage cyclic triaxial tests are shown in Appendix C; Figures 117 and 118 are profiles of the modulus versus the cell pressure σ_3. The samples were 100 mm in diameter and 200 mm high. Figure 117 presents the results of the test which was performed on the sample from taxiway Zoulou of the new airport; during this test, the cell leaked when the cell pressure was raised above 104 kPa

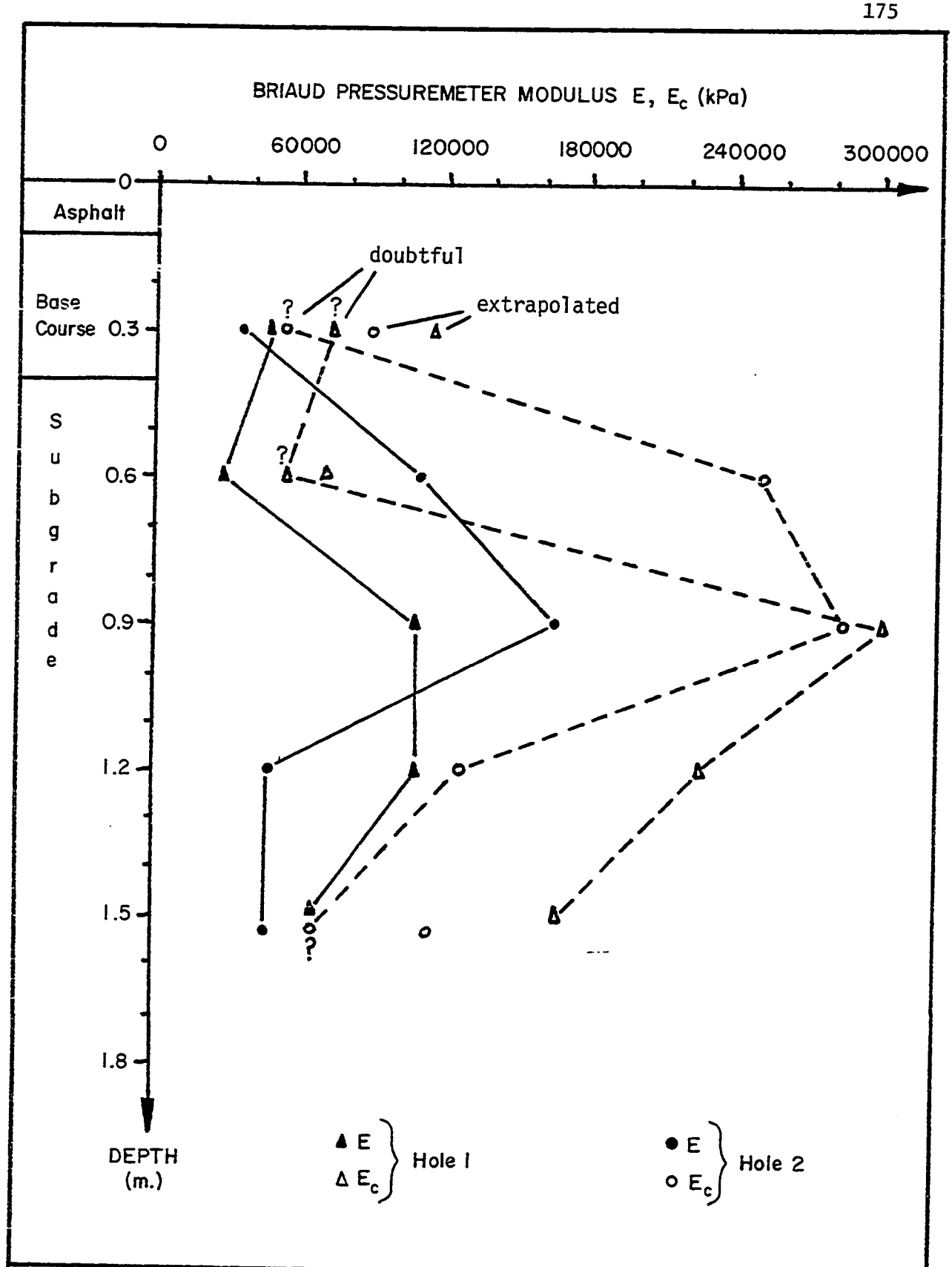

Fig. 113 - Ottawa International Airport - Briaud Pressuremeter. Moduli vs depth. Hole 1, 2 - New Airport.

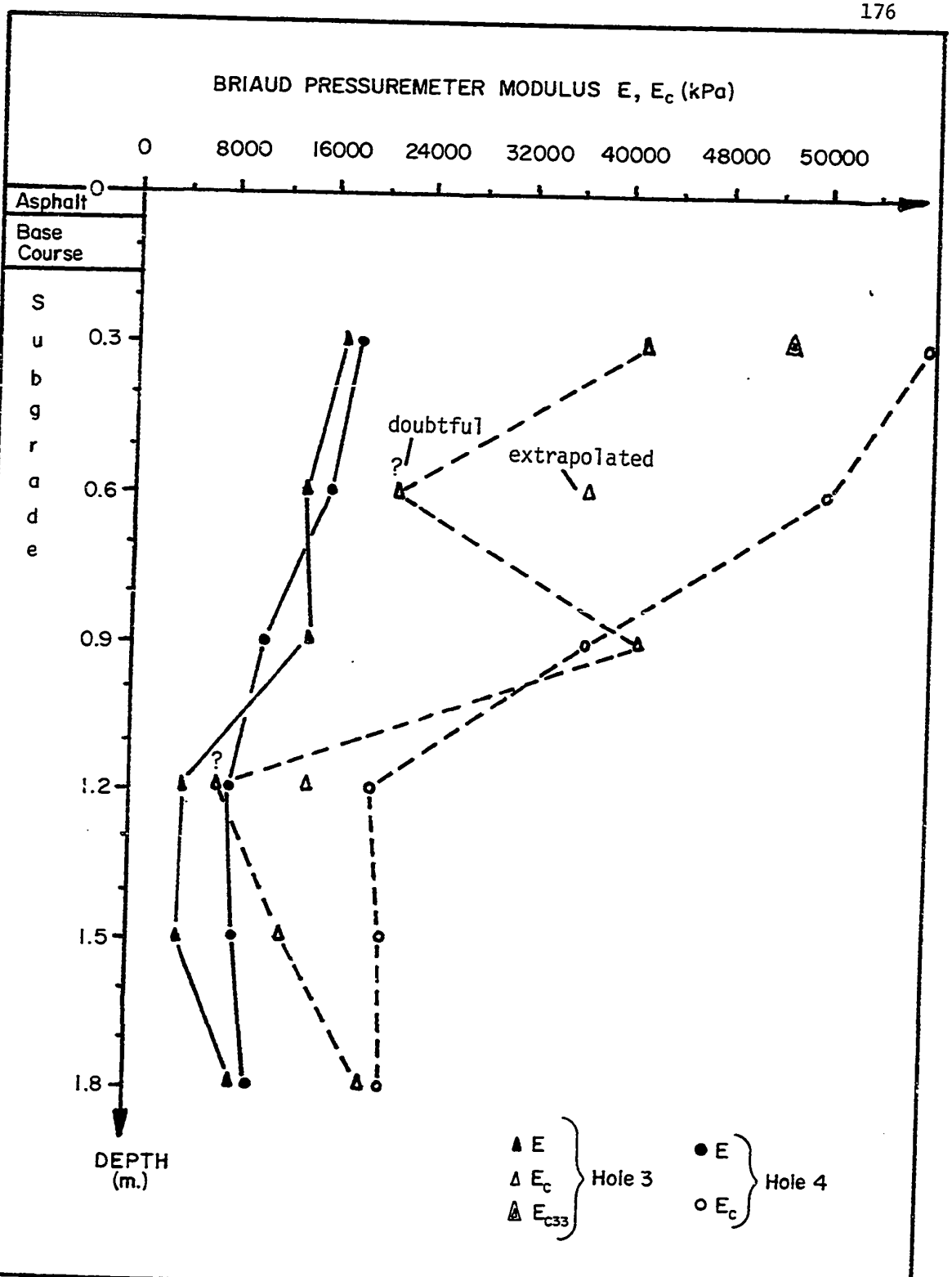

Fig. 114 - Ottawa International Airport - Briaud Pressuremeter. Moduli vs depth. Hole 3, 4 - Old Airport.

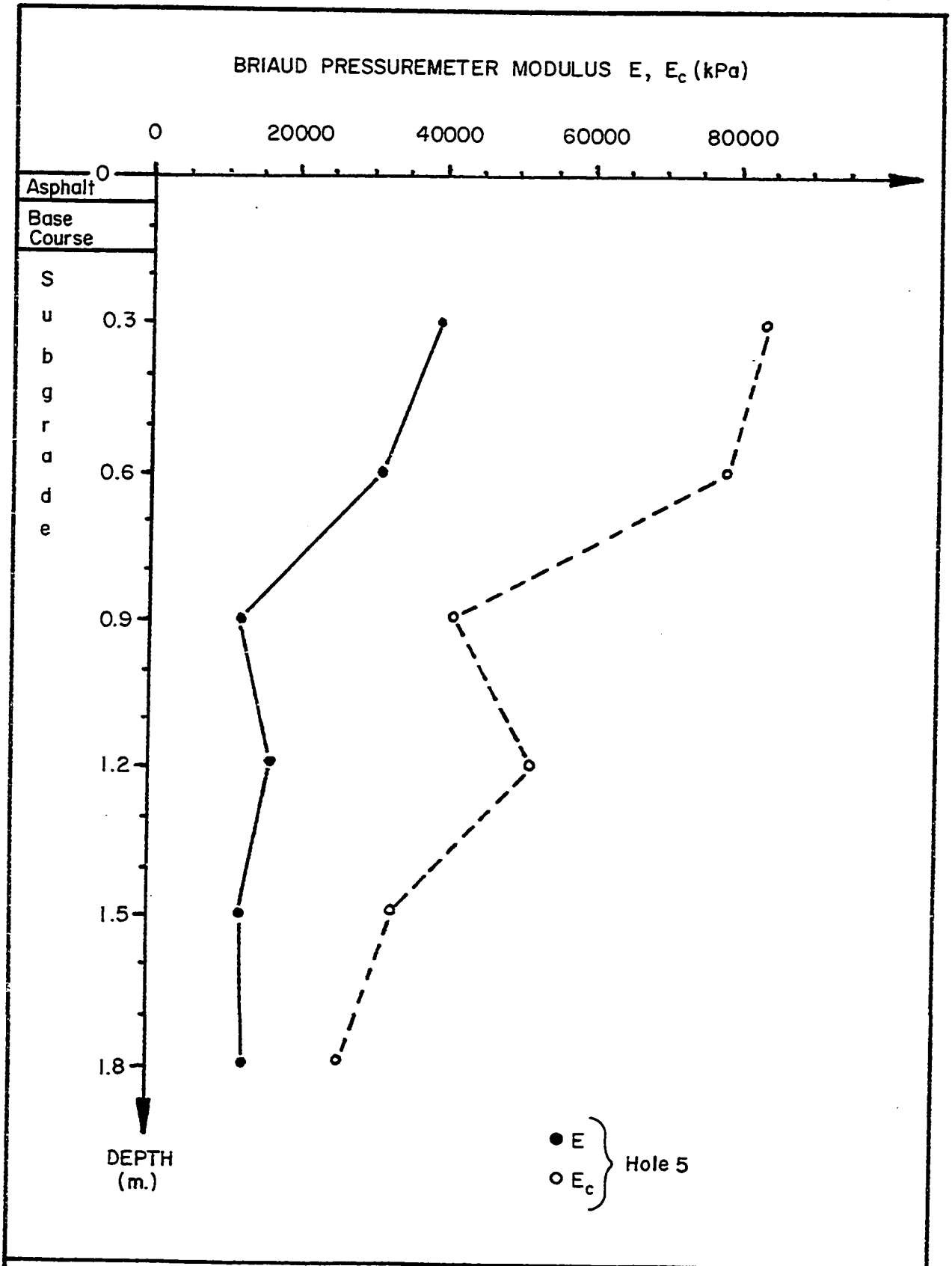

Fig. 115 - Ottawa International Airport - Briaud Pressuremeter. Moduli vs. depth. Hole 5 - Old Airport.

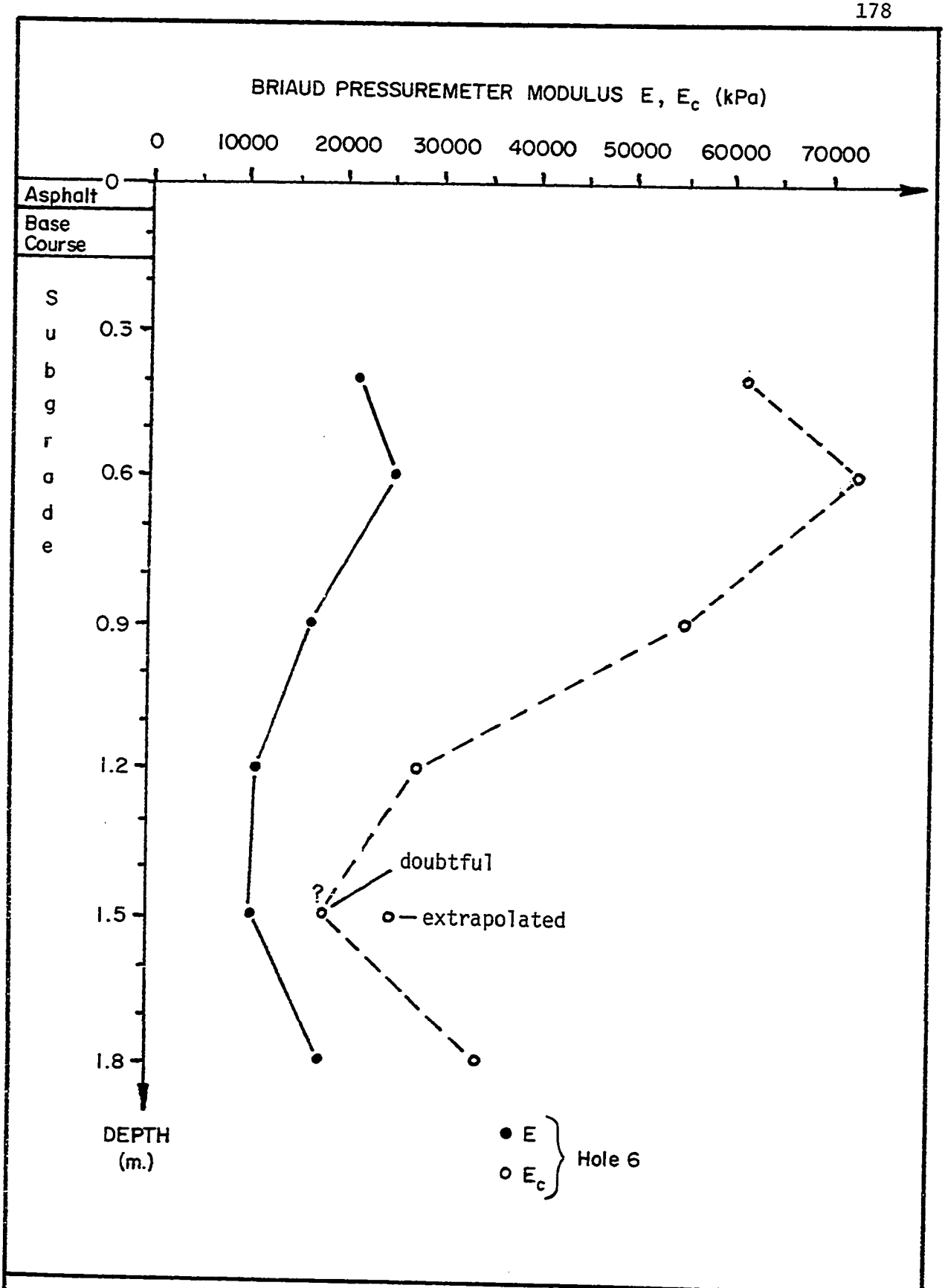

Fig. 116 - Ottawa International Airport - Briaud Pressuremeter. Moduli vs depth. Hole 6 - Old Airport.

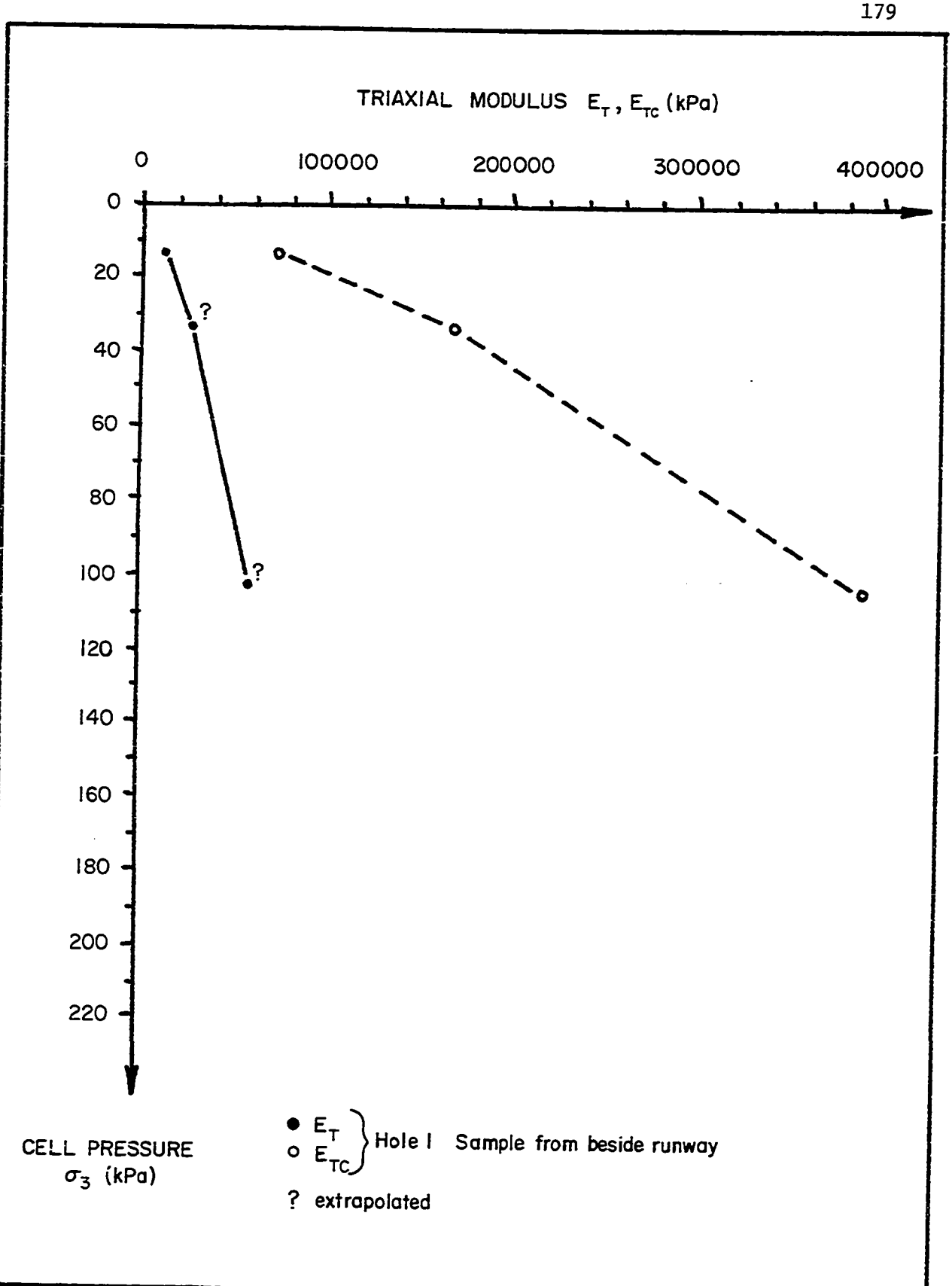

Fig. 117 - Ottawa International Airport - Triaxial Modulus vs Cell Pressure. Hole 1 - New Airport.

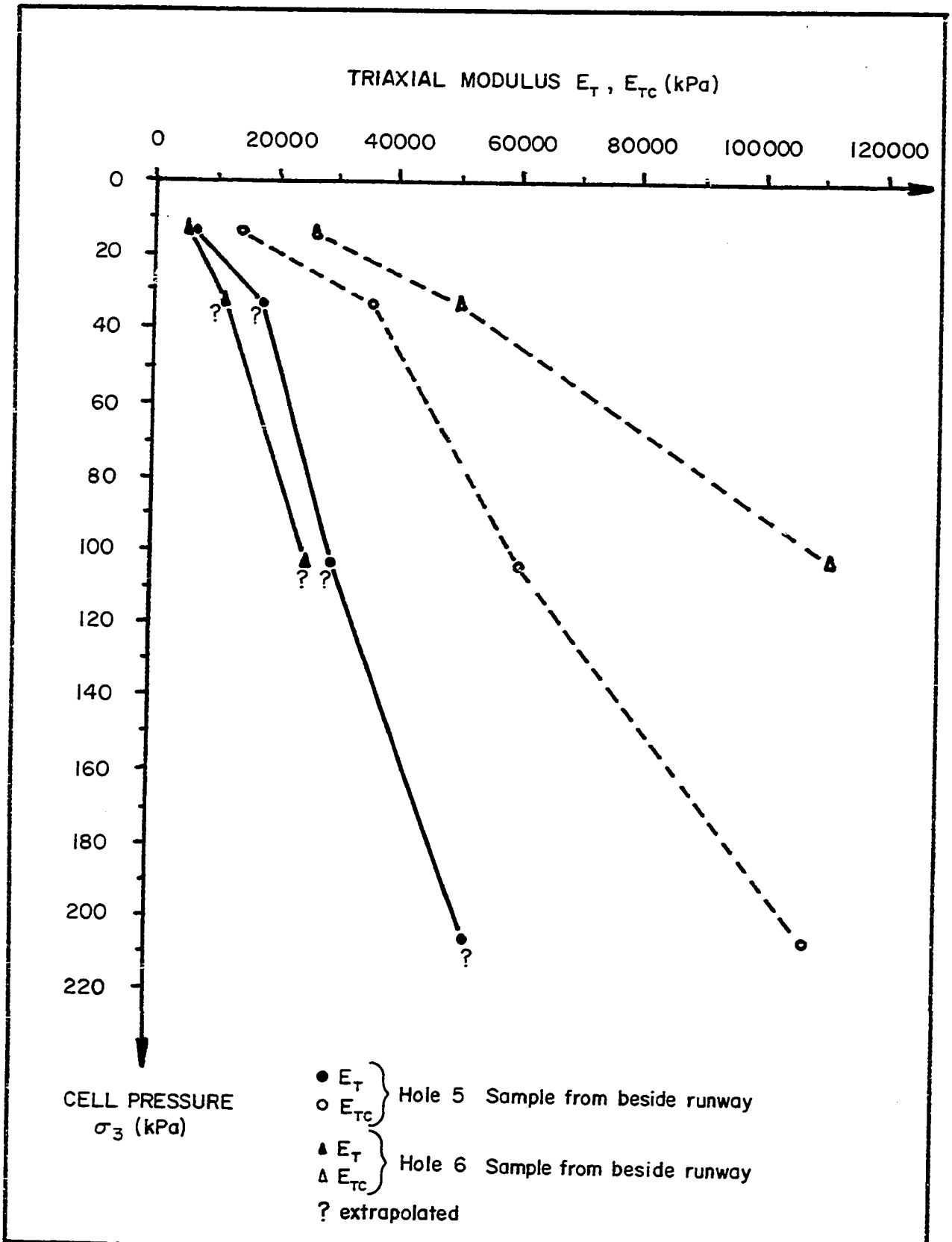

Fig. 118 - Ottawa International Airport - Triaxial Modulus vs. Cell Pressure. Hole 5, 6 - Old Airport.

and this is why there are only one E_T, three E_{Tc} and two extrapolated E_T values shown in Figure 117. The same problem with leakage occurred with the tests which were performed on the taxiway Tango sample; this problem was solved by the time the samples from taxiway Uniform were tested. Figure 118 gives the results of the tests which were performed on taxiway Tango and Uniform (old airport).

7.4.4 Discussion

The high quality of the Briaud pressuremeter tests which were run at Ottawa illustrate the benefit of the experience which was gained during the Sarnia testing program. In a few instances at Ottawa the hole was still too big (for example: Test No. 195). At Ottawa Airport, the Briaud pressuremeter cyclic modulus (E_c) was measured routinely. It will be recalled that the first attempt at measuring E_c took place during the sand box testing program; there, the cycle was started arbitrarily after an inflation of 10 cm^3 (Section 6.3.4). During the Sarnia testing program it was found that at 10 cm^3 the sheath had generally not come in contact with the wall of the cavity. Based on this experience, it was decided to increase the volume at which to start cycling to 60 cm^3 for the Ottawa testing program; this was done for the tests in Hole 1 and 2. By Hole 3 it was realized that although 60 cm^3 was an improvement, it was still not sufficient. Indeed, at an inflation of 60 cm^3 some tests had not yet reached the end of the elastic phase (Test No. 187). Then it became apparent that the volume at which cycling should be started had to be determined while the test was in progress; this procedure is outlined in Section 4.4.6 and was applied to the tests of Holes 4, 5 and 6.

The curve of Test No. 216 (Appendix A) is an example of what a Briaud pressuremeter test curve should look like. Examining the test curves, it can be seen that Hole 3 was too large at 1.2 and 1.5 m depth. As a result the E and E_c values for these two tests are too low. Because the cycling procedure was still evolving as described above, some of the E_c values for Holes 1, 2 and 3 are too low. Low values of E_c are the case for Hole 1 at 0.3 and 0.6 m depth (Test Nos. 183 and 187), for Hole 2 at 0.3 and 1.65 m depth (Tests Nos. 188 and 189), and for Hole 3 at 0.6, 1.2 and 1.5 m depth (Tests Nos. 197, 195 and 194). The pressuremeter curves of these tests are given in Appendix A. Whenever the E_c value was judged to be too low while the E value was found to be acceptable, a new E_c value was calculated by multiplying the acceptable E value by the average $\frac{E_c}{E}$ ratio of the neighboring two tests (Fig. 116).

The average value of the Briaud pressuremeter modulus E at Ottawa Airport was 75,000 kPa in the new airport and 15,000 kPa in the old airport. The average value of the Briaud pressuremeter cyclic modulus E_c was 200,000 kPa in the new airport and 40,000 kPa in the old airport. The average pressuremeter modulus ratio $(\frac{E_c}{E})$ for all the tests performed in the sand of Ottawa Airport was 2.63.

The shape of the Briaud pressuremeter modulus profile varies considerably (compare, for example, Fig. 115 and Fig. 105). Rare is the case where the subgrade can be considered to be uniform (Fig. 113 or Fig. 108). However, a weak layer such as the one which was found immediately below the base course in Sarnia was not found at Ottawa. The better condition of the subgrade at Ottawa may be due to a better drainage system or to the fact that for sands the absence of good drainage is not

as critical as for silty clays. The above findings could not have resulted from McLeod plate tests.

The shape of the McLeod plate test curves is reasonable and it seems that the test at Hole 4 (Test No. 340, Appendix B) was approaching failure. At Ottawa Airport the pavement bearing strengths (S_p) were 1709 and 1728 kN at the new airport and varied from 412 to 614 kN at the old airport. The subgrade bearing strength (S_s) were 851 and 860 kN at the new airport and varied from 312 to 464 kN at the old airport.

The triaxial test results show the large influence that σ_3 has on the modulus of deformation in a granular soil. The n value of Equation 27 can be calculated for each of the triaxial tests; the exponent n was found to be 0.83 for Test No. 253 (new airport) and an average of 0.75 for the Test Nos. 251 and 252 (old airport). The modulus ratio ($\frac{E_{Tc}}{E_T}$) averaged 4.36 for the three triaxial tests.

The triaxial modulus (E_T) and the Briaud pressuremeter modulus (E) should be compared at the same confining pressure, for example 20 kPa (Section 6.3.6). It must be remembered that the pressuremeter tests were at the runway centerline whereas the triaxial samples were taken at the edge of the pavement, 20 m away from the pressuremeter holes and at a depth of 0.5 m. One problem is to determine the depth of the pressuremeter test where the confining stress is equal to the triaxial cell pressure of 20 kPa (Fig. 117 and 118); the stress history of the sand immediately under the runway centerline is completely different from that of the sand near the pavement edge; on the other hand, the stress history of the sand near the pavement edge and the sand at depth below the runway centerline are probably more alike. Based on this reasoning,

it seems appropriate to compare the E_T values at 20 kPa cell pressure with the E values from the deeper pressuremeter tests. At Holes 1, 5 and 6, the deeper E values are 52,000, 13,000 and 11,000 kPa respectively; the corresponding E_T values at σ_3 = 20 kPa are 18,000, 10,000 and 7,000 kPa. Except at Hole 1, the E and E_T values are reasonably close to one another.

The average Briaud pressuremeter modulus ratio $(\frac{E_c}{E})$ was 2.63 and the average triaxial modulus ratio $(\frac{E_{Tc}}{E_T})$ was 4.36. Since E and E_T are reasonably close together, this means that for the sand of Ottawa Airport the E_{Tc} values are about 1.7 times higher than the E_c values.

7.5 Pavement Equivalent Briaud Pressuremeter Modulus

7.5.1 Definition

At each test location on a runway, one plate test is carried out on the pavement surface and six pressuremeter tests are performed at different depths in a borehole. The plate test result is characterized by a bearing strength value whereas the pressuremeter tests result is characterized by six moduli values which vary with depth. To facilitate comparing the plate test with the pressuremeter tests, the six moduli values must be reduced to one equivalent pressuremeter modulus by some appropriate method.

By definition, a fictitious homogeneous soil with a modulus E_e (Fig. 119) will be said to be equivalent to a layered soil with moduli E_1 to E_n (Fig. 120) if, under a certain load applied to the soil through a rigid circular plate of given diameter, the surface settlement (s) is the same for both soils. The modulus E_e is called the equivalent modulus. This definition is based on a settlement criterion; the reason a

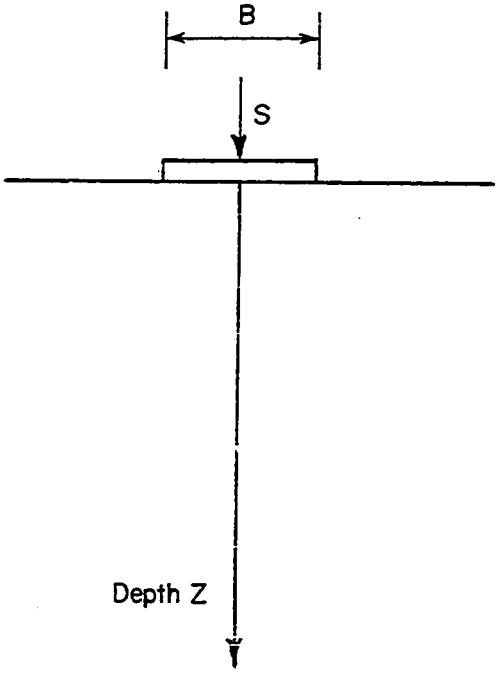

Fig. 119 - An Elastic Homogeneous Soil.

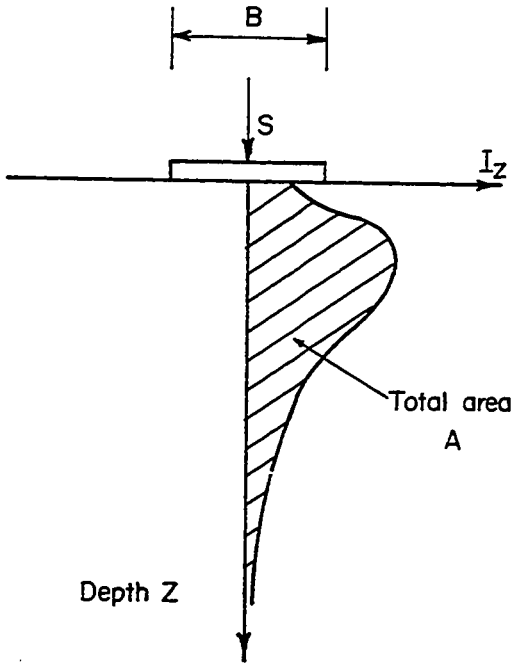

Fig. 121 - Homogeneous Soil. An I_z Curve

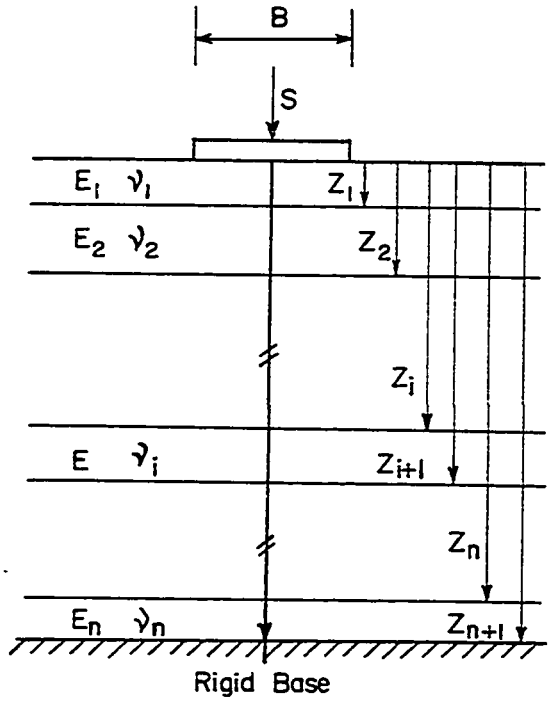

Fig. 120 - An Elastic Layered Soil.

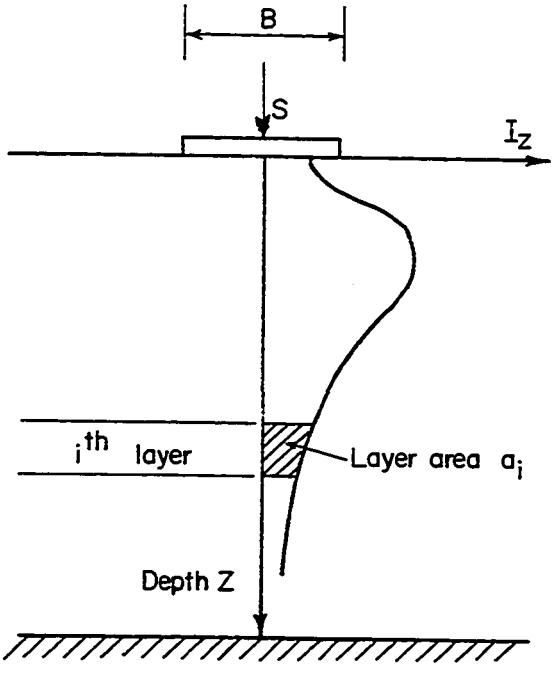

Fig. 122 - Layered Soil. An I_z Curve

settlement criterion is used is that both the McLeod plate test and the design of flexible pavements are controlled by the amount of deflection or settlement.

Four equivalent moduli are defined:

- the pavement equivalent Briaud pressuremeter modulus (E_{ep}) is the modulus of the fictitious homogeneous soil which is equivalent to the layered soil made of the pavement and the subgrade, and having the six Briaud pressuremeter moduli (E) as layer moduli.

- the pavement equivalent Briaud pressuremeter cyclic modulus (E_{cep}) is the modulus of the fictitious homogeneous soil which is equivalent to the layered soil made of the pavement and the subgrade, and having the six Briaud pressuremeter cyclic moduli (E_c) as layer moduli.

- the subgrade equivalent Briaud pressuremeter modulus (E_{es}) is the modulus of the fictitious homogeneous soil which is equivalent to the layered soil made of the subgrade only, and having the Briaud pressuremeter moduli (E) as layer moduli.

- the subgrade equivalent Briaud pressuremeter cyclic modulus (E_{ces}) is the modulus of the fictitious homogenous soil which is equivalent to the layered soil made of the subgrade only, and having the Briaud pressuremeter cyclic moduli (E_c) as layer moduli.

7.5.2 Derivation

In any soil, under any type of loading, the vertical settlement (s) is given by:

$$s = \int_0^\infty \varepsilon_z \, dz \quad \ldots\ldots\ldots\ldots\ldots\ldots\ldots\ldots \quad (30)$$

where ε_z is the vertical strain at the depth z. In a linear elastic isotropic soil, ε_z can be written:

$$\varepsilon_z = \frac{p}{E_z} I_z \quad \ldots\ldots\ldots\ldots\ldots\ldots\ldots\ldots\ldots\ldots \quad (31)$$

where E_z is the modulus of elasticity at the depth z,

I_z is the strain influence factor at the depth z,

p is the average contact pressure.

Then, since p does not depend upon z:

$$s = p \int_0^\infty \frac{I_z}{E_z} dz \quad \ldots\ldots\ldots\ldots\ldots\ldots\ldots\ldots\ldots\ldots \quad (32)$$

In the case of the homogeneous soil (Fig. 119) E_z is a constant equal to E_e:

$$s = \frac{p}{E_e} \int_0^\infty I_z \, dz = \frac{p}{E_e} A \quad \ldots\ldots\ldots\ldots\ldots\ldots\ldots \quad (33)$$

where A is the area under the strain influence factor curve (I_z curve) for the homogeneous soil and the type of loading being considered (Fig. 121). In the case of a layered soil (Fig. 120), E_z is a constant within each layer so that:

$$s = p \sum_1^n \frac{1}{E_i} \int_{z_i}^{z_{i+1}} I_z \, dz \quad \ldots\ldots\ldots\ldots\ldots\ldots\ldots \quad (34)$$

$$\text{If:} \quad a_i = \int_{z_i}^{z_{i+1}} I_z \, dz \quad \ldots \quad (35)$$

$$\text{then:} \quad s = p \sum_{1}^{n} \frac{a_i}{E_i} \quad \ldots \quad (36$$

where E_i is the modulus of elasticity of the i^{th} layer; z_i and z_{i+1} are the depth of the top and the bottom interface enclosing the i^{th} layer; and a_i represents the area under the I_z curve for the i^{th} layer and the type of loading being considered (Fig. 122).

Using Equations 33 and 36, the settlement is the same for both soils if:

$$\frac{1}{E_e} = \frac{1}{A} \sum_{1}^{n} \frac{a_i}{E_i} \quad \ldots \quad (37)$$

Equation 37 can be applied to the pressuremeter modulus profiles in order to obtain an equivalent modulus. The coefficients a_i and A must be determined; this means that the I_z curve must be found. The I_z curve depends on the type of loading, the value of the elastic constants for each layer and the roughness of the interfaces between layers. In the case of airport pavement design, 1) the type of loading varies since the tires of planes vary in size, 2) the pressuremeter moduli profile is different from one hole to another, and 3) the roughness of the interface can only be approximated. The net result is that the I_z curve is not unique.

The following sections study possible I_z curves as they relate to the determination of the pavement equivalent Briaud pressuremeter moduli.

7.5.3 Literature Survey

For a linear elastic homogeneous isotropic soil the strain distribution factor (I_z) varies in the same way as the vertical strain (ϵ_z) according to Equation 31. For a Poisson's ratio of 0.33 and a rigid circular plate, the I_z curve is given in Figure 123. Schmertmann (37) proposed a simplified I_z curve for evaluating settlements over sand; Schmertmann's curve is shown on Figure 123.

Hartman (p. 176, 177, 189 of (17)) studies the shape of the I_z curve for the case of a two layer elastic soil with a hard layer over a soft layer; Hartman found I_z curves simular to the one shown in Figure 123.

The area, A, under the I_z curve in the case of a linear elastic homogeneous isotropic soil and for both rigid and flexible circular plates is obtained from Equation 33 and the following formulae hold true:

$$\text{rigid plate} \qquad s = \frac{\pi}{4}(1-\nu^2)\, p\, \frac{B}{E_{e\ell}} \qquad \ldots\ldots\ldots\ldots \quad (38)$$

$$\text{flexible plate} \qquad s = (1-\nu^2)\, p\, \frac{B}{E_{e\ell}} \qquad \ldots\ldots\ldots\ldots \quad (39)$$

where s = settlement at the center of the plate

B = plate diameter

p = contact pressure

$E_{e\ell}$ = elastic modulus of the soil

then, rigid plate $$A = \frac{\pi}{4}(1-\nu^2)\, B \qquad \ldots\ldots\ldots\ldots\ldots\ldots \quad (40)$$

flexible plate $$A = (1-\nu^2)\, B \qquad \ldots\ldots\ldots\ldots\ldots\ldots \quad (41)$$

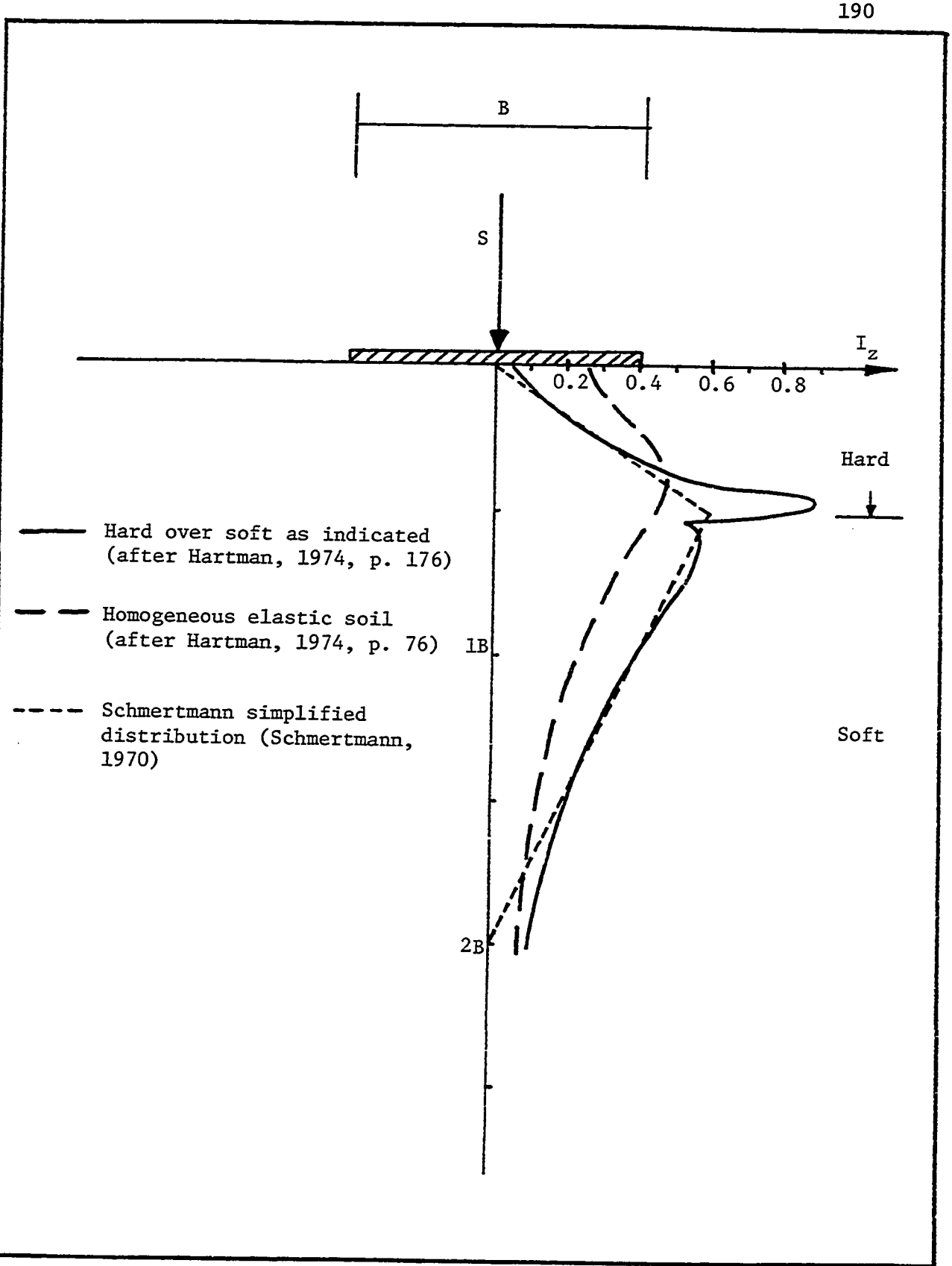

Fig. 123 - Examples of Strain Influence Factor (I_z) Curves.

It is interesting to note that in the case of Schmertmann's simplified I_z curve, A = 0.6 B which is equivalent to a ν of 0.49 for the case of rigid plate over an elastic soil.

Menard (p. 232 of (1)) proposed a relationship to find an equivalent modulus (E_e) for the case of a layered soil (with layer moduli E_1, E_2, $E_{3,4,5}$, $E_{6,7,8}$, $E_{9,16}$), provided the variation in moduli is not too great;

$$\frac{1}{E_e} = \frac{1}{4}\left(\frac{1}{E_1} + \frac{1}{0.85E_2} + \frac{1}{E_{3,4,5}} + \frac{1}{2.5\ E_{6,7,8}} + \frac{1}{2.5\ E_{9,16}}\right) \quad . \ . \ . \quad (42)$$

this equation can be written:

$$\frac{1}{E_e} = \frac{0.25}{E_1} + \frac{0.21}{E_2} + \frac{0.25}{E_{3,4,5}} + \frac{0.1}{E_{6,7,8}} + \frac{0.1}{E_{9,16}} \quad . \ . \ . \ . \ . \ . \ . \ . \quad (43)$$

In Equation 44 the coefficients (0.25, 0.21, 0.25, 0.1, 0.1) correspond to the $\frac{a_i}{A}$ of Equation 37; since the coefficients of Equation 44 are constant, Menard made the simplifying assumption that the I_z curve was unique for all conditions.

7.5.4 Calculations Based on Schmertmann's Simplified I_z Curve

As a first approximation the a_i and A coefficients can be evaluated from Schmertmann's simplified I_z curve in order to obtain E_{ep} and E_{cep} values. Since the shallowest test is below the asphalt layer, no asphalt modulus is measured which means that in order to calculate E_{ep} and E_{cep}, an asphalt modulus must be chosen. In this section of the thesis, an

asphalt modulus of 1500,000 kPa is used. Although chosen arbitrarily, this value of the modulus is conservative but realistic (p. 229 of (3)). In any event, as will be shown later, the magnitude of the asphalt modulus has a relatively small influence on the value of E_{ep} and E_{cep}.

Figure 124 is an example of how E_{ep} is calculated. The same procedure was used to find the other values of E_{ep} and E_{cep} which are listed on Figure 125.

If in the example of Figure 124 the value of the asphalt modulus is doubled (E_1 = 3,000,000 kPa), E_{ep} increases only 0.05% to 23,440 kPa (instead of 23,428 kPa for E_1 = 1,500,000 kPa). The influence of the value of E_1 on E_{ep} is very small. Of course, the thicker the asphalt layer and the stronger the underlying layers, the greater the influence of the asphalt modulus will be on E_{ep}. Even so, for the thick asphalt layer and the strong subgrade at Ottawa Hole 2, doubling the asphalt modulus increases E_{cep} by only 0.13%.

7.5.5 Multilayer Elastic Analysis: Procedure and Parameters

The equivalent pressuremeter modulus can be calculated by using a strain influence factor curve and Equation 37 as explained in Section 7.5.4. The modulus can also be calculated by finding the settlement (s) occurring for the particular load in the layered soil and using an equation such as Equation 38. The latter procedure is the one which is used here and is explained using Hole 1 at Ottawa Airport as an example (Fig. 126). The pavement and the subgrade are divided into layers. The boundary between layers is considered to be at the mid point between two consecutive pressuremeter tests. The Briaud pressuremeter moduli, the asphalt modulus and Poisson's ratios are fed into a computer program;

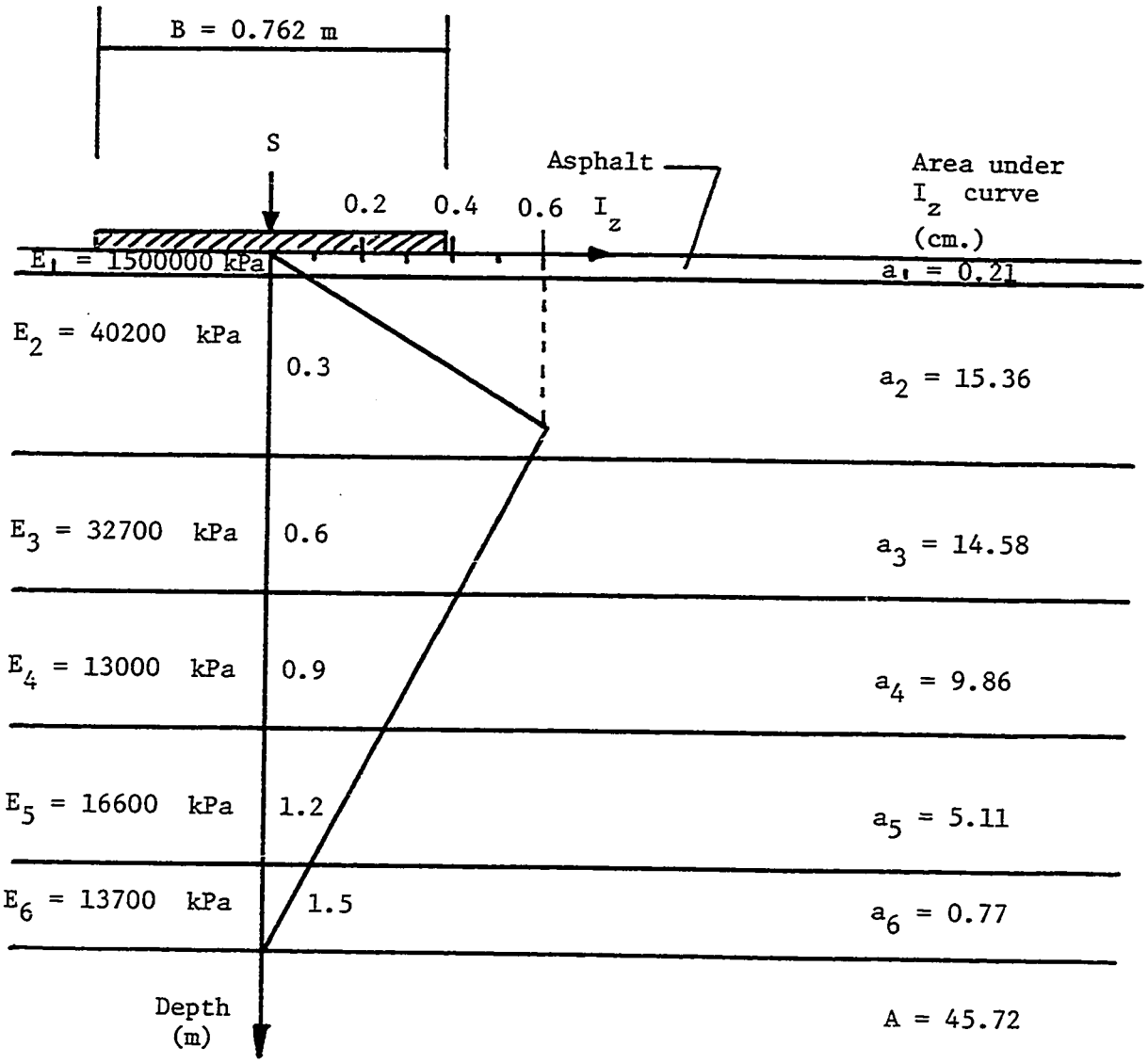

$$\frac{1}{E_{ep}} = \frac{1}{45.72}\left[\frac{0.21}{1500000} + \frac{15.36}{40200} + \frac{14.58}{32700} + \frac{9.86}{13000} + \frac{5.11}{16600} + \frac{0.77}{13700}\right]$$

$$E_{ep} = 23488 \text{ kPa.}$$

Fig. 124 - Sample Calculation of the Equivalent Pressuremeter Modulus Using Schmertmann Simplified Distribution. Ottawa: Old Airport. Hole No. 5. Briaud Pressuremeter Moduli.

Location	E_1 (E_{c1})	E_2 (E_{c2})	E_3 (E_{c3})	E_4 (E_{c4})	E_5 (E_{c5})	E_6 (E_{c6})	E_7 (E_{c7})	E_{ep} (E_{cep})
Sar. 3	1500000	6650	1405	2165	7900	9175	7695	2333
Sar. 5	1500000	6435	5810	17870	28195	21165	18220	8079
Sar. 6	1500000	10085	2755	10320	14180	8990	9110	5574
Sar. 7	1500000	16800(8A)	4240	7170	10245	8355	12770	7469
Sar. 15	1500000	15290	7490	5645	13140	17750	10485	9502
Ott. 1	1500000 (1500000)	47445 (114000)*	27500 (66000)*	106900 (298000)	100700 (224900)	64600 (166000)		45840 (111067)
Ott. 2	1500000 (1500000)	35435 (85000)*	109300 (251600)	163900 (283800)	45880 (126350)	47680 (115000)		61887 (145476)
Ott. 3	1500000 (1500000)	17500 (41200)	13900 (36000)*	14500 (41100)	4600 (13500)*	4110 (12500)	8430 (19370)	11703 (31345)
Ott. 4	1500000 (1500000)	18000 (65500)	16240 (55800)	11300 (36700)	7800 (19100)	8730 (21000)	9930 (21400)	13572 (42758)
Ott. 5	1500000 (1500000)	40200 (84100)	32700 (78700)	13000 (42000)	16600 (52500)	13700 (34000)	13200 (26000)	23428 (63228)
Ott. 6	1500000 (1500000)	21500 (60900)	25600 (72500)	16700 (55000)	11200 (27400)	10400 (25000)*	16900 (33800)	18785 (53145)

(8A) Modulus of hole 8A

* Recalculated according to Section 6.4.4.

Fig. 125 – Pavement Equivalent Briaud Pressuremeter Moduli and Cyclic Moduli for Ottawa and Sarnia Airport; Calculations Based on Schmertman Simplified Distribution.

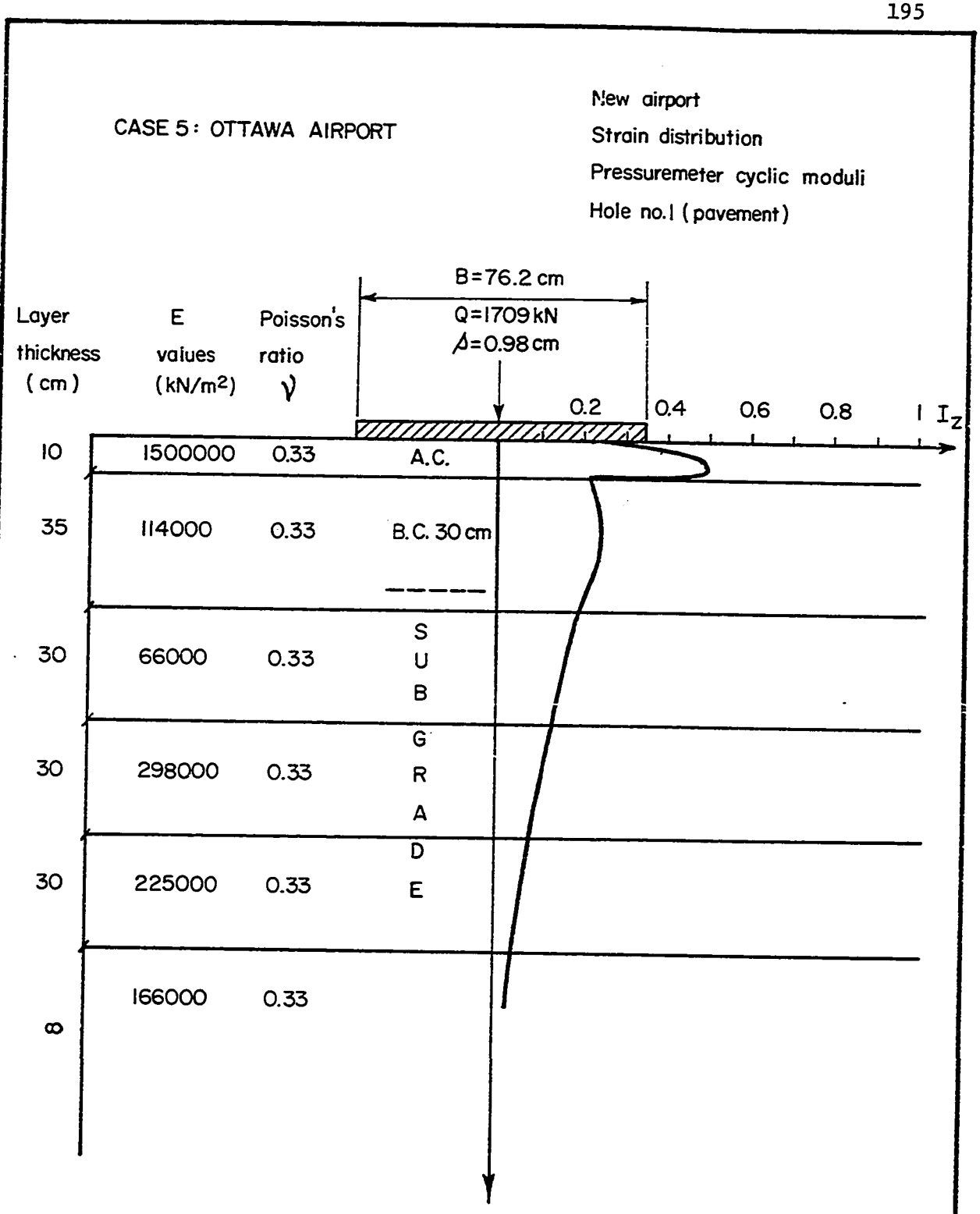

Fig. 126 - Plate Test Analysis. I_z Curve and Settlement. Ottawa: New Airport. Pressuremeter Cyclic Moduli. Hole No. 1. Pavement Test.

then the rigid McLeod plate (0.762 m in diameter) is placed on this multilayer elastic soil and that the plate is loaded with the bearing strength which has been measured in the field. The plate settlement (s) is calculated by the computer and the equivalent pressuremeter modulus is obtained from:

$$E_e = \frac{\pi}{4} (1 - \nu^2) \frac{Q}{sB} \quad \ldots\ldots\ldots\ldots\ldots\ldots\ldots\ldots\ldots\ldots \quad (44)$$

where E_e is the equivalent modulus (E_{ep}, E_{cep}, E_{es} or E_{ces} depending on the case),

ν is Poisson's ratio considered to be 0.33 in all cases,

Q is the load (S_p or S_s depending on the case)

B is the plate diameter (0.762 m)

and s is the settlement as calculated in the computer analysis.

The program also allowed the computer to calculate the strain influence factor I_z with depth (Fig. 126). The settlement (s), the equivalent modulus and the strain influence factor were obtained for all plate test locations.

The finite element program which was used was developed originally by E.L. Wilson and J.M. Duncan of the University of California; the program was modified later by J. P. Hartman at the University of Florida. The listing and user's manual of this program are given in Hartman (p. 348-364 of (17)). Hartman's program solves axisymmetric, plane strain stress-deformation problems in cross-anisotropic soils. Although the program can handle stress dependent moduli, the assumption of linear elasticity in each layer was made here. The assumption was also made that there

would be perfect adhesion between soil layers.

In all, twenty-six specific cases, including all plate test locations, were treated. Figure 127 shows a typical finite element grid; the vertical outer boundary and the horizontal lower boundary were placed on rollers and these boundaries were located at 10 plate radii from the center of the plate (this distance was found to be sufficient by Hartman (p. 67 of (17))). The grid spacing is very small close to the plate where the variation in the stress field is rapid. The number of elements was 390 for each of the 26 cases.

The results of all the cases which were analyzed are presented in Figure 126 and Appendix F. An asphalt modulus value of 1,500,000 kPa was used with three exceptions: Case 10 where the value was assumed to be 6,000,000 kPa, Case 11 where the value was taken as 600,000 kPa, Cases 4, 8, 9 where there was no asphalt layer. As discussed in Section 7.5.4, 1,500,000 kPa appears to be a reasonable asphalt modulus value.

In all cases, a Poisson's ratio of 0.33 was used. Making Poisson's ratio a constant is a simplifying assumption and is justified by the following comments:

1. The range of Poisson's ratio values for soils is about 0.2 to 0.5; 0.33 is therefore a reasonable average. (This average value of 0.33 was used to determine all pressuremeter moduli in this study).

2. the value of Poisson's ratio usually has a relatively small influence on the magnitude of the settlement (p. 52 of (10) and p. 160 of (26)).

3. having to choose a Poisson's ratio for each layer may lead to errors which are similar in magnitude to the error that is generated by choosing a single average value for all materials.

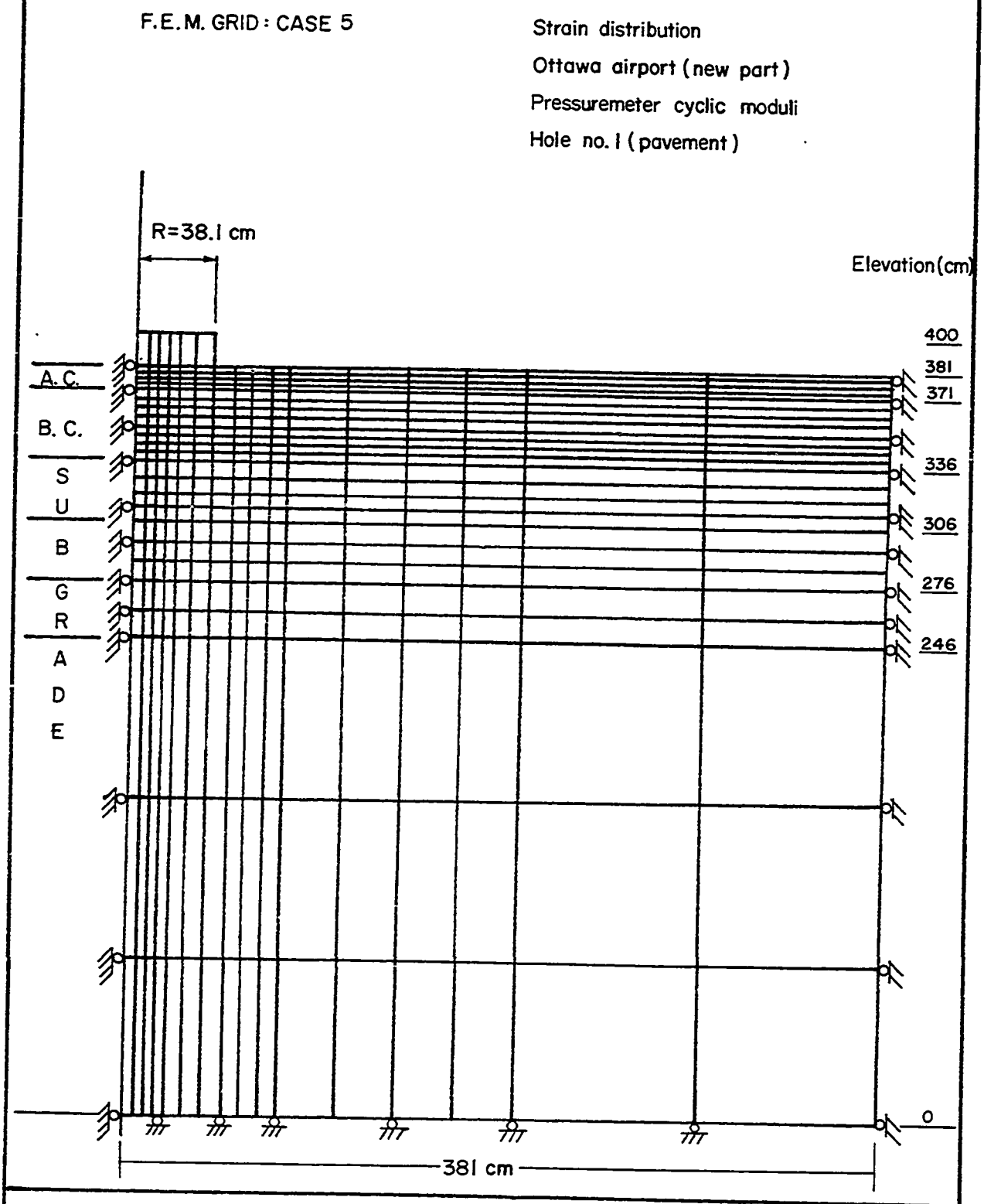

Fig. 127 - Grid for the Finite Element Analysis of the Plate Test. Ottawa: New Airport. Hole No. 1.

The following examples give some idea of the errors involved: for an homogeneous isotropic linear elastic soil, the settlement of a rigid plate is proportional to $(1 - \nu^2)$ (see Equation 38 for example). For the following Poisson's ratios the settlement is

$\nu = 0.2$ $\quad s = 96\ K_1$

$\nu = 0.33$ $\quad s = 89\ K_1$

$\nu = 0.5$ $\quad s = 75\ K_1$

where K_1 is a quantity which does not depend on Poisson's ratio. Fixing Poisson's ratio at 0.33 means the maximum error is in the order of 16% for this particular case.

In the case of soils having a modulus of elasticity which increases with depth, the following example gives an idea of the influence of Poisson's ratio on the settlement values. The data for the example comes from Figure 128 and the numbers which are given appear to represent reasonable values. Giroud (p. 281 of (14)) using the theory of elasticity and a circular uniformly distributed load found:

$\nu = 0.2$ $\quad s = 150\ K_2$

$\nu = 0.33$ $\quad s = 137\ K_2$

$\nu = 0.5$ $\quad s = 105\ K_2$

By choosing a Poisson's ratio of 0.33 the maximum error in this case is 23%.

In the case of layered soils where the modulus decreases with depth from one layer to the next, the following example gives an idea of the influence of Poisson's ratio on settlement. The data for the example are

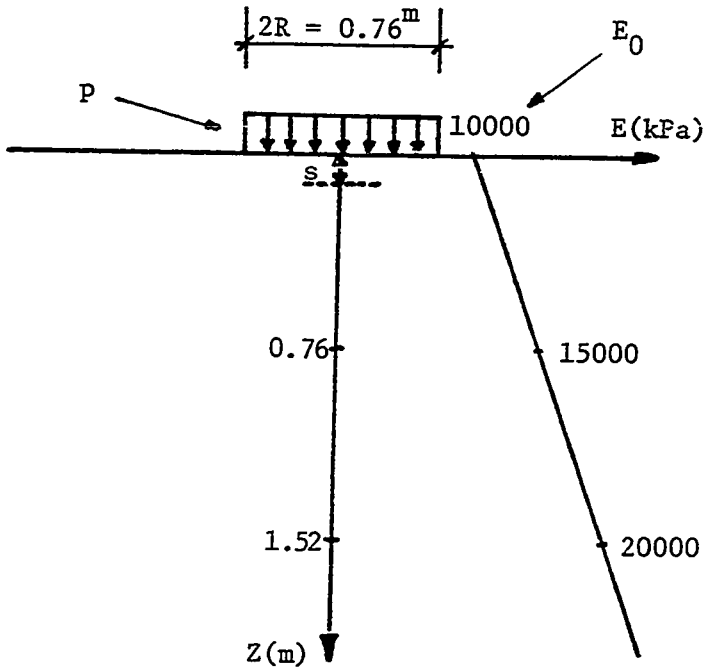

Fig. 128 - Influence of Poisson's Ratio on the Elastic Settlement. Case of a Soil with a Modulus of Elasticity Linearly Increasing with Depth (after Giroud, 1972).

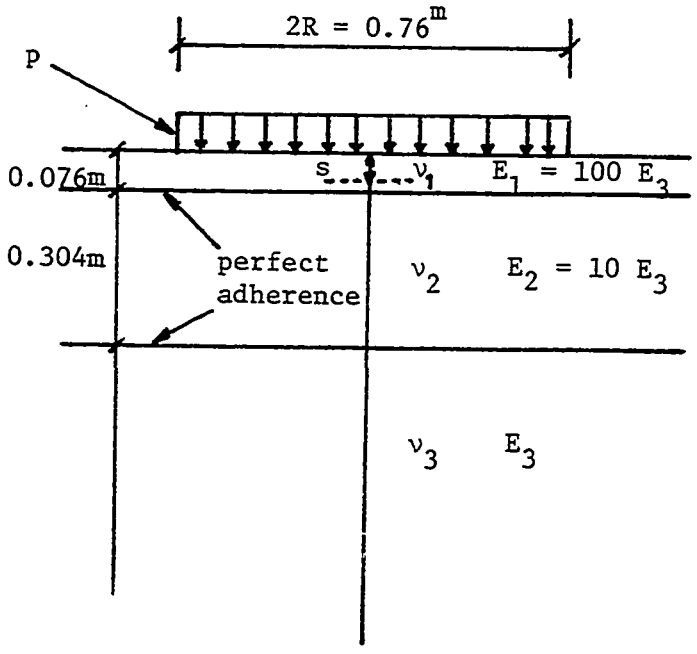

Fig. 129 - Influence of Poisson's Ratio on the Elastic Settlement. Case of a Multilayer Elastic Soil with Layer Moduli Decreasing with Depth (after Giroud, 1972).

given in Figure 129. Giroud (p. 260 of (14)) using the theory of elasticity and a circular, uniformly distributed load gives:

$$\nu_1 = \nu_2 = \nu_3 = 0.35 \qquad s = 65.6\ K_3$$

$$\nu_1 = \nu_2 = \nu_3 = 0.5 \qquad s = 65.0\ K_3$$

Choosing in this case a Poisson's ratio of 0.35 when the real ratio is 0.5 would result in a 1% error.

The Briaud pressuremeter moduli and cyclic moduli were used as deformation moduli for each layer. In the case of Sarnia Airport (Cases 1 to 4, 16 and 17) the layer moduli are the Briaud pressuremeter moduli since no cyclic moduli were measured at the location of the plate tests. At Ottawa Airport Cases 18 to 23 use Briaud pressuremeter moduli while Cases 5 to 15 and 24 to 28 use the Briaud pressuremeter cyclic moduli as layer moduli.

In a few instances at Ottawa Airport, it was necessary to ignore doubtful pressuremeter cyclic moduli values. The doubtful values were replaced by cyclic moduli which were calculated as described in the following example: referring to Figure 114, for Hole 3, the test at 0.6 m depth gave a cyclic modulus value which did not appear to be reasonable; the ratio of $\frac{E_c}{E}$ was calculated at 0.3 m and 0.9 m depth and the ratio of $\frac{E_c}{E}$ value was determined; this average value of $\frac{E_c}{E}$ was multiplied by the first loading modulus at 0.6 m depth to obtain a better estimate of the Briaud pressuremeter cyclic modulus (E_c) at 0.6 m depth.

The asphalt thickness which is used in the analysis is the thickness under the plate at the time of the McLeod plate test.

7.5.6 Multilayer Elastic Analysis: Results and Discussion

For each of the 26 cases which were studied, the settlement of the plate and the strain influence factors with depth were calculated by the computer. Then the equivalent pressuremeter moduli were calculated using Equation 44.

The settlement values and the strain influence factor curves of all cases are given on Figure 126 (Case 5) and Appendix F (other cases). A summary of the results and a list of the equivalent pressuremeter moduli are presented in Figure 130.

The calculated values of plate settlement varied from 0.61 cm to 3.55 cm and averaged about 2 cm when using the Briaud pressuremeter moduli as the layer moduli; they averaged slightly less than 1 cm when using the Briaud pressuremeter cyclic moduli as the layer moduli. The bearing strengths S_p and S_s are the loads which create a 12.5 mm settlement of the plate at the 10^{th} repetition of load and about 8.5 mm at the first application of the load. If the Briaud pressuremeter cyclic moduli are used as layer moduli, settlement of the plate can be predicted with reasonable accuracy.

In the case of Hole 7 at Ottawa Airport, a parametric study was performed which was based on Case 5 being taken as the reference case. In Case 5, the asphalt modulus is 1,500,000 kPa, the asphalt thickness is 10 cm and the calculated settlement is 0.98 cm. In Case 10, the asphalt modulus was four times larger (6,000,000 kPa) than for Case 5 and this lead to a settlement which was 21% smaller (0.77 cm). In Case 11 the asphalt modulus was 40% less than for Case 5 (600,000 kPa); this lead to a settlement which was 12% greater (1.1 cm). These calculations show that

Case	Location	S_p (kN)	S_s (kN)	s (cm)	E_{ep} (kPa)	E_{cep} (kPa)	E_{es} (kPa)	E_{ces} (kPa)	Observations
1	Sar 5	186		0.99	17756				
2	Sar 6	243		1.83	12196				
3	Sar 15	208		0.78	24492				
4	Sar 6		147	2.37			5697		
5	Ott 1	1709		0.98		160169			
6	Ott 2	1728		0.95		167063			
7	Ott 5	601		0.79		69873			
8	Ott 5		455	0.77				54272	
9	Ott 1		861	0.75				105439	
10	Ott 1	1709		0.77		203851			asphalt modulus = 6000000 kPa
11	Ott 1	1709		1.1		142696			asphalt modulus = 600000 kPa
12	Ott 1	1709		0.76		206533			asphalt thickness = 20 cm
13	Ott 1	1709		0.61		257320			asphalt thickness = 30 cm

Fig. 130 - Summary of the Results of the Multilayer Elastic Analysis for Equivalent Moduli and Settlement Calculations

Case	Location	S_p (kN)	S_s (kN)	s (cm)	E_{ep} (kPa)	E_{cep} (kPa)	E_{es} (kPa)	E_{ces} (kPa)	Observations
14	Ott 1	DC8 tire		0.26		196641			contact pressure = 1350 kPa
15	Barker (1977)	700		0.53		121300			
16	Sar 3	196		3.55	5068				
17	Sar 7	265		1.01	24086				
18	Ott 1	1709		2.05	76530				
19	Ott 2	1728		1.89	83931				
20	Ott 3	412		2.46	15375				
21	Ott 4	405		2.07	17961				
22	Ott 5	601		1.78	30995				
23	Ott 6	614		2.28	24722				
24	Ott 3	412		0.99		38204			
25	Ott 4	405		0.72		51638			
26	Ott 6	614		0.80		70457			

Fig. 130 - Summary of the Results of the Multilayer Elastic Analysis for Equivalent Moduli and Settlement Calculations. cont'd.

the influence of the asphalt modulus is indeed small but not necessarily negligible.

In Case 12, the asphalt thickness was assumed to be double that of Case 5 (20 cm); this increase in thickness lead to a calculated settlement which was 22% smaller (0.76 cm). In Case 13 the asphalt thickness was assumed to be triple that of Case 5 (30 cm); this leads to a 38% smaller settlement (0.61 cm). Both calculations show that the asphalt thickness has an appreciable influence on the settlement, an influence which is greater than that of the asphalt modulus.

In Case 14, a tire of the design plane (DC 8) was assumed to be applying a load to the pavement instead of the McLeod plate. The settlement of the tire was only a quarter (0.26 cm) of the settlement under the plate for the same soil and asphalt conditions. Although the stresses from the other wheels of the same landing gear will create additional settlement, this calculation indicates that the settlement under the plate is larger than the settlement under the wheel of a fairly large plane.

The equivalent modulus E_e is inversely proportional to the settlement s (Equation 44). As a result, in the above parametric study when s increased, E_e decreased, and when s decreased, E_e increased.

The curves of the strain influence factor versus depth (I_z curves) are given for each of the cases in Figure 126 and Appendix F. In all cases where the asphalt layer is present, the I_z curve is similar to the curve shown in Figure 126. With the peak I_z values being reached in the asphalt layer, the shape of the I_z curves is considerably different from the Schmertmann simplified I_z curve. The elastic I_z curve gives more weight to the asphalt modulus than does the Schmertmann I_z curve; as a

result, the equivalent modulus which is calculated from the elastic settlement is greater than the modulus which is calculated from the Schmertmann distribution.

7.6 Comparison

7.6.1 Comparison Between Equivalent Briaud Pressuremeter Moduli and the Pavement Bearing Strength

At each hole location, the test data is now reduced to the following parameters:

- one pavement bearing strength value S_p.
- one pavement equivalent Briaud pressuremeter modulus (E_{ep}) which was calculated using Schmertmann's simplified distribution.
- one pavement equivalent Briaud pressuremeter modulus (E_{ep}) which was calculated from an elastic settlement analysis.
- one pavement equivalent Briaud pressuremeter cyclic modulus (E_{cep}) which was calculated using Schmertmann's simplified distribution.
- one pavement equivalent Briaud pressuremeter cyclic modulus (E_{cep}) which was calculated from an elastic settlement analysis.

The S_p values are given in Figures 102 and 112. The E_{ep} (Schmertmann distribution) and E_{cep} (Schmertmann distribution) values are listed in Figure 125. The E_{ep} (elastic settlement) and E_{cep} (elastic settlement) values are listed in Figure 130.

Figure 131 shows S_p versus E_{ep} (Schmertmann distribution) for both the Sarnia Airport and the Ottawa Airport. The average (linear) relationship is:

$$E_{ep} = 32\ S_p \quad \ldots\ldots\ldots\ldots\ldots\ldots\ldots\ldots\ldots\ldots \quad (45)$$

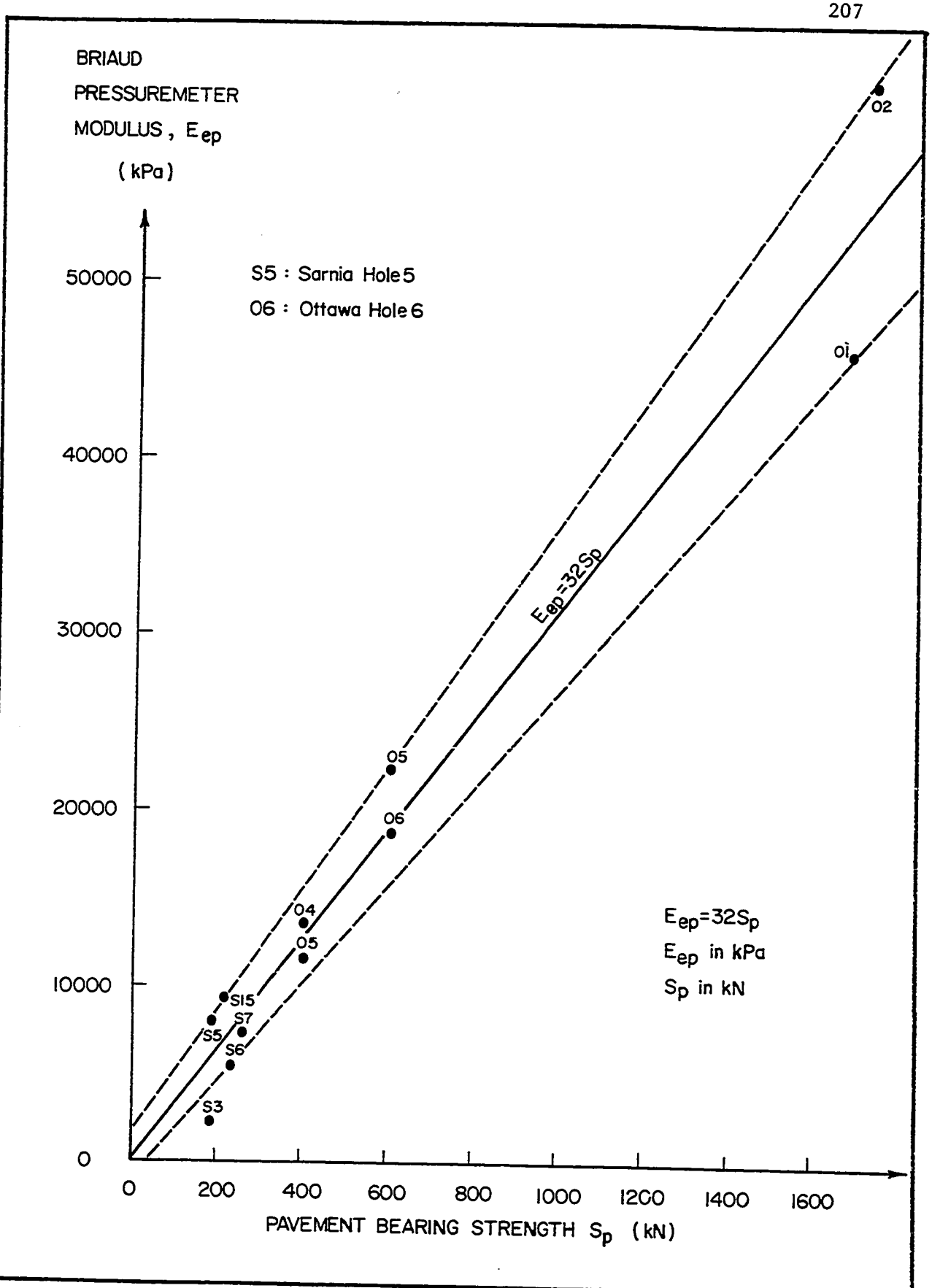

Fig. 131 - Pavement Equivalent Briaud Pressuremeter Modulus versus Pavement Bearing Strength (Schmertmann Strain Distribution)

with E_{ep} in kPa and S_p in kN. Figure 132 shows S_p versus E_{cep} (Schmertmann distribution) for Ottawa Airport; the average (linear) relationship is:

$$E_{cep} = 88\ S_p \quad \ldots\ldots\ldots\ldots\ldots\ldots\ldots\ldots \quad (46)$$

with E_{cep} in kPa and S_p in kN. Figure 133 shows S_p versus E_{ep} (elastic settlement) for the Sarnia and Ottawa Airports; the average (linear) relationship is:

$$E_{ep} = 55\ S_p \quad \ldots\ldots\ldots\ldots\ldots\ldots\ldots\ldots \quad (47)$$

with E_{ep} in kPa and S_p in kN. Figure 134 shows S_p versus E_{cep} (elastic settlement) for Ottawa Airport; the average (linear) relationship is:

$$E_{cep} = 100\ S_p \quad \ldots\ldots\ldots\ldots\ldots\ldots\ldots\ldots \quad (48)$$

with E_{cep} in kPa and S_p in kN.

7.6.2 Discussion

Figures 131 and 133 show the relationship between E_{ep} and S_p. The scatter of values is small in Figure 131 where the Schmertmann simplified distribution was used. The scatter is somewhat greater in Figure 133 where the multilayer elastic theory was used; in fact in Figure 133 the scatter is appreciable at low values of the Briaud pressuremeter modulus (Sarnia Airport). This large scatter may be due to the proposed borehole preparation creating more erratic disturbance in fine grained soils. The

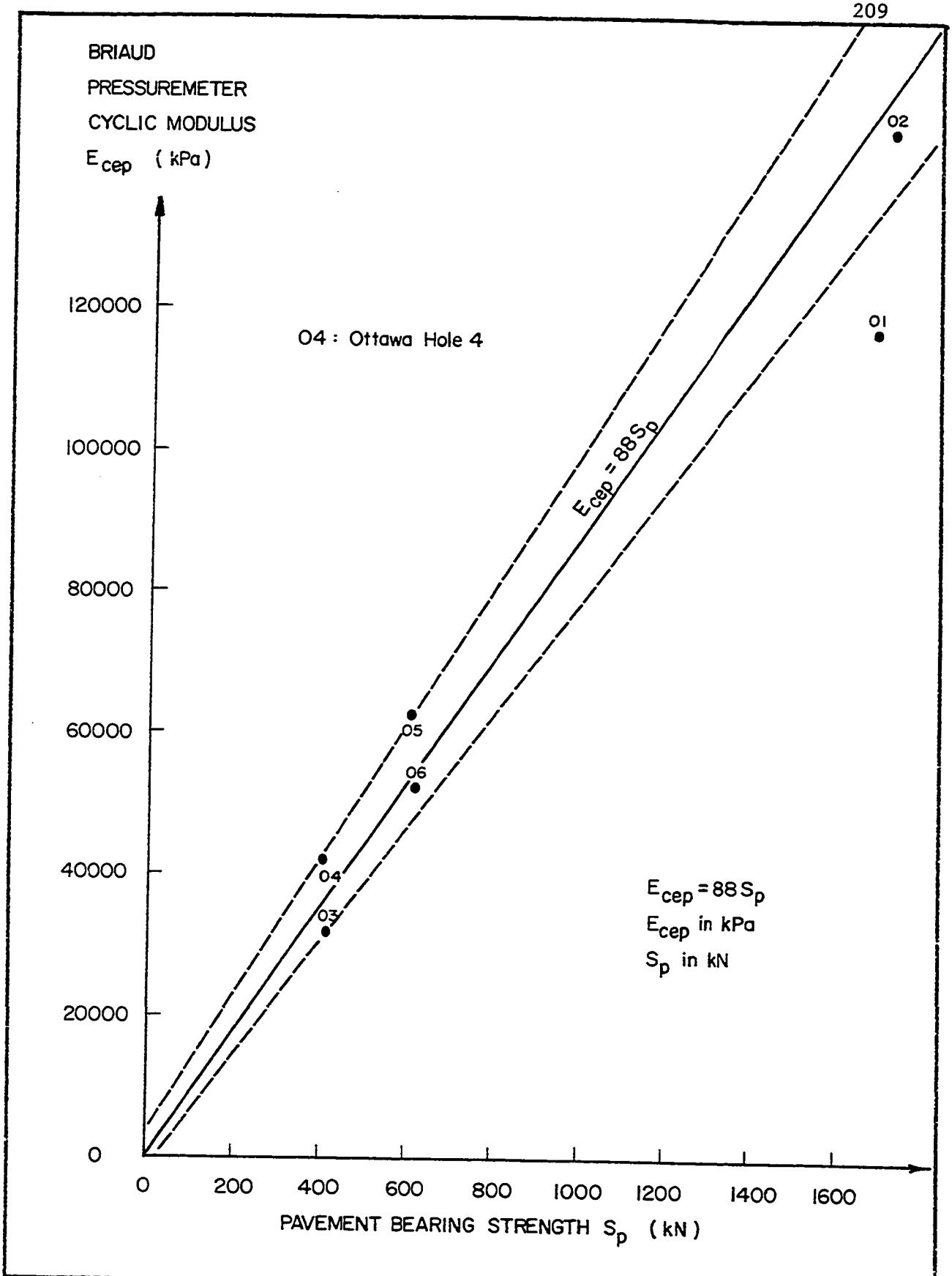

Fig. 132 - Pavement Equivalent Briaud Pressuremeter Cyclic Modulus versus Pavement Bearing Strength (Schmertmann Strain Distribution)

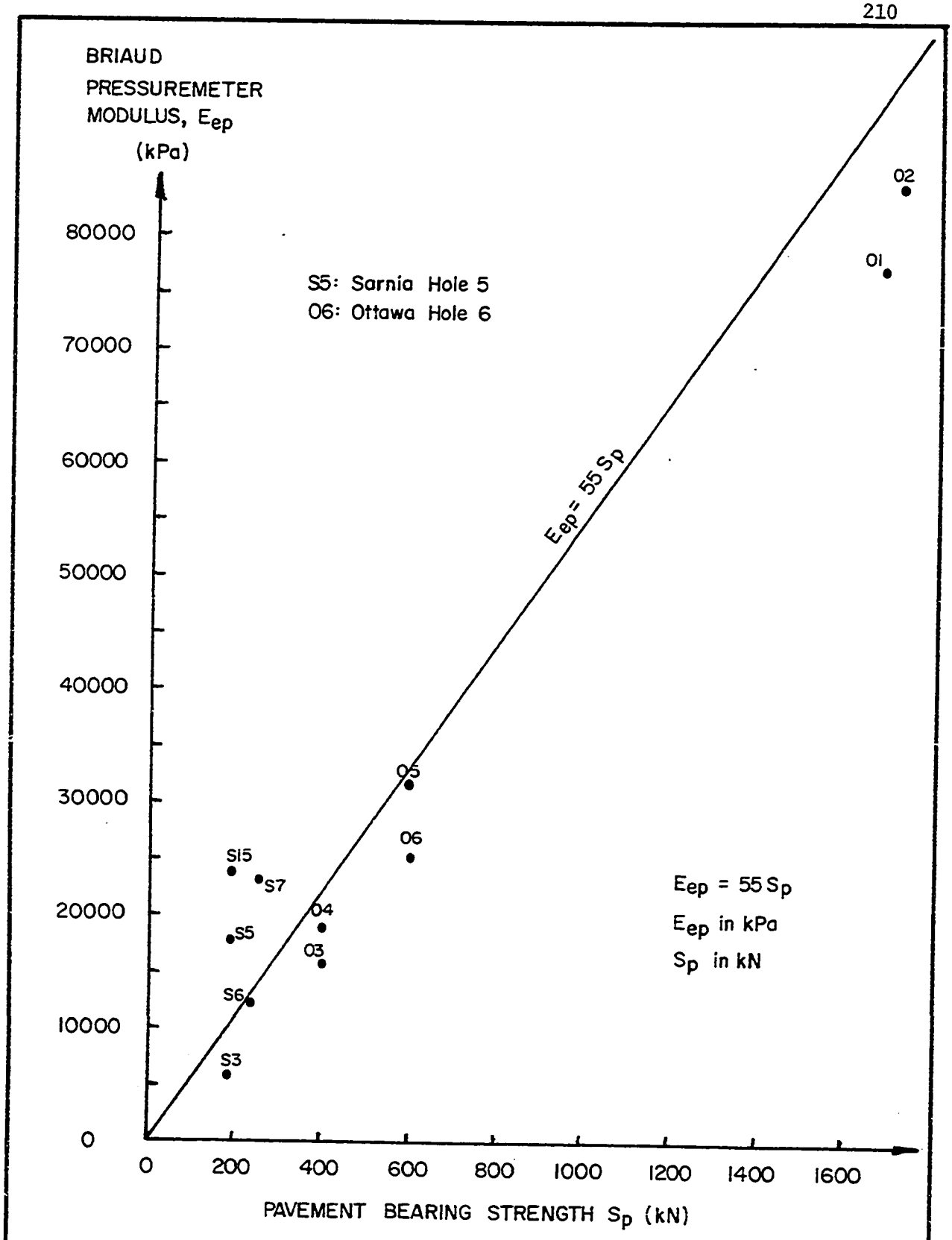

Fig. 133 - Pavement Equivalent Briaud Pressuremeter Modulus versus Pavement Bearing Strength (Multilayer Elastic Analysis).

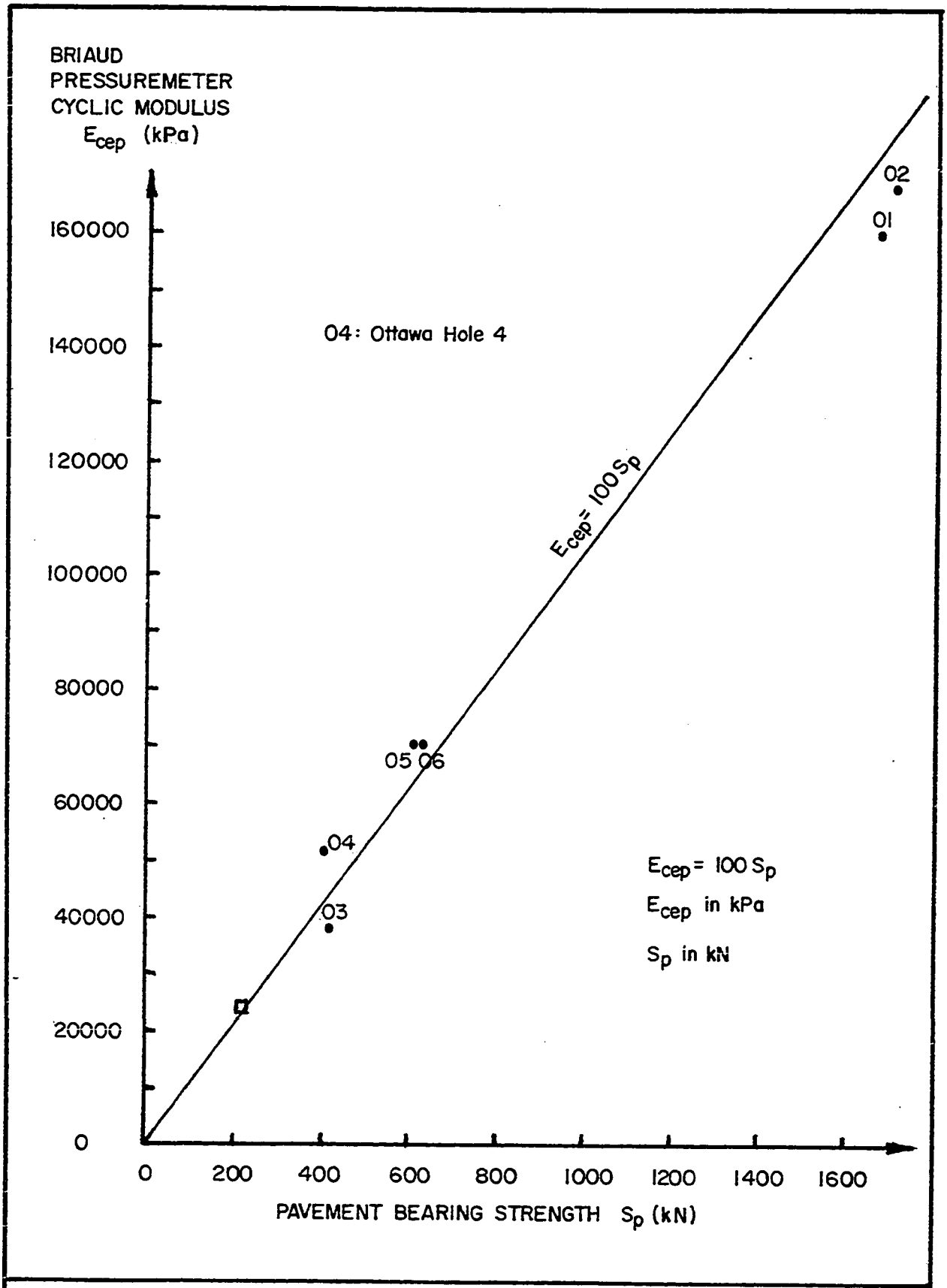

Fig. 134 – Pavement Equivalent Briaud Pressuremeter Cyclic Modulus versus Pavement Bearing Strength (Multilayer Elastic Analysis).

large scatter may also be due to the fact that the plate test and pressuremeter test results were not as reliable in Sarnia as in Ottawa; in Sarnia there were calibration problems for the jack which was used for the plate tests and a lack of experience for the pressuremeter tests.

Figures 132 and 134 show the relationship between E_{cep} and S_p; the scatter of the values is very small. There are no points shown for Sarnia Airport because the Briaud pressuremeter cyclic modulus was not measured in Sarnia. Values of the cyclic modulus, however, can be estimated as follows. Figure 133 illustrates the fact that the Sarnia points are mostly above an $E_{ep} = 55\ S_p$ line whereas the Ottawa points are below this line. The average $\frac{E_{cep}}{E_{ep}}$ ratio for Ottawa is 2.25; for Sarnia, this ratio was measured in only one test (Test No. 144, Appendix A) and found to be 1.4. Given that the average E_{ep} value for Sarnia is 16,700 kPa, an average E_{cep} value for Sarnia can be estimated from:

$$E_{cep} \text{ (average Sarnia)} = 1.4 \times 16{,}700 \simeq 23{,}400 \text{ kPa}$$

The average pavement bearing strength (S_p) for Sarnia is:

$$S_p \text{ (average Sarnia)} = 220 \text{ kN}$$

These E_{cep} and S_p values intersect at the square which is plotted on Figure 134; the square is located very close to the $E_{cep} = 100\ S_p$ line.

An inspection of Figures 131 to 134 inclusive leads to the conclusion that a linear relationship seems to exist between the pressuremeter moduli (E_{ep}, E_{cep}) and the pavement bearing strength (S_p). The fact that S_p and E_{ep} or S_p and E_{cep} are linearly proportional tends to prove

that similar σ_3 conditions exist during a plate test and a pressuremeter test.

An idea of the relative magnitude of the stresses involved in the soil which is affected by both the plate and the pressuremeter tests can be had by studying the results of Hole 1 of Ottawa Airport. The maximum contact pressure under the plate was 3750 kPa; at one plate radius below the plate (0.38 m depth), the vertical stress was 609 kPa and the radial stress was 187 kPa according to Newmark's charts based on a Boussinesq analysis (p. 142 of (48)). At 0.38 m depth the maximum radial pressure exerted by the pressuremeter probe in the elastic range of the test was about 1400 kPa (Test No. 183, Appendix A). The contact pressure of a DC 8-63 (the design plane for Ottawa Airport) is 1350 kPa.

Equation 44 can be applied to the plate results in order to evaluate Equations 45 to 48:

$$E_e = \frac{\pi}{4} (1 - \nu^2) \frac{Q}{sB} \quad \ldots\ldots\ldots\ldots\ldots\ldots\ldots \quad (44)$$

In this study $\nu = 0.33$, $B = 0.762$ m and Q is the load on the plate (S_p for the McLeod plate test). The settlement s is usually 8.5 mm at the first load application (Section 2.1.1) and is 12.5 mm at the 10^{th} load repetition or:

for the first S_p application $\qquad E_e = 108\ S_p \quad \ldots\ldots \quad (49)$

for the 10th S_p application $\qquad E_e = 73.5\ S_p \quad \ldots\ldots \quad (50)$

The experimental Equations 45, 46, 47, 48 and the theoretical Equations 49, 50 are all of the form:

$$E = K S_p$$

The K value of Equation 48, which involves the pavement equivalent Briaud pressuremeter cyclic modulus (E_{cep}) is 100 while the K value of Equation 49, which involves the equivalent modulus of elasticity, is 108. The closeness of these two K values tends to prove that the Briaud pressuremeter cyclic modulus measures a 'modulus of elasticity' of the soil.

The K value of Equation 47 which involves the pavement equivalent Briaud pressuremeter modulus (E_{ep}) is 55. This shows that the Briaud pressuremeter modulus is much smaller than a 'modulus of elasticity' of the soil.

7.7 Conclusions

The results of 11 McLeod plate tests and 93 Briaud pressuremeter tests, performed in a silty clay (Sarnia Airport) and in a sand (Ottawa Airport), show that there is a linear relationship between the pavement bearing strength (S_p) and the pavement equivalent Briaud pressuremeter cyclic modulus (E_{cep}):

$$E_{cep} = 100\ S_p \quad \ldots\ldots\ldots\ldots\ldots\ldots\ldots\ldots\ldots\ldots \quad (48)$$

with E_{cep} in kPa and S_p in kN. This simple relationship enables E_{cep} to replace S_p. Since S_p is used for flexible runway pavement design, the

design could be based on E_{cep} instead. It is concluded therefore that, on the basis of the evidence presented in this thesis, the Briaud pressuremeter test can be used as the basis of the traffic load design of flexible airfield pavements.

It was found in this chapter that the settlements measured in the field under the McLeod plate are in close agreement with the settlements calculated using the theory of elasticity and the Briaud pressuremeter cyclic moduli.

It was also found that the triaxial cyclic modulus (E_{Tc}) was 1.7 times higher than E_c in a silty clay and 2.5 times than E_c in a sand.

CHAPTER 8

THE BRIAUD PRESSUREMETER TEST AND THE CANADIAN PLATE TEST DESIGN

8.1 General

It has been shown in Chapter 7 that there is a relationship between the pavement bearing strength (S_p) and the pavement equivalent Briaud pressuremeter cyclic modulus (E_{cep}). The traffic load design of flexible airport pavements in Canada is based on the pavement bearing strength (Section 2.1.1). It is therefore possible to base the design on the pavement equivalent Briaud pressuremeter cyclic modulus by substituting E_{cep} for S_p in the procedure.

In this chapter, first, the McLeod plate test results of Sarnia and Ottawa Airports are used to give an example of the traffic load design of flexible airport pavement in Canada; second, the Briaud pressuremeter cyclic modulus design chart is presented; third, traffic load design procedures for new and existing flexible airport pavements, using the Briaud pressuremeter cyclic modulus design chart, are proposed.

8.2 Evaluation of Ottawa and Sarnia Airports

Sarnia Airport can be evaluated from the results of the McLeod plate tests. The evaluation follows the procedure described in Section 2.1.1. The five subgrade bearing strengths (S_s) for Sarnia Airport are given in Figure 102; the lower quartile factor is 1.75 which means that the in situ S_s value for Sarnia is three quarters of the way between the

lowest and the second lowest S_s values. Thus:

$$S_s = 100 + \frac{3}{4}(111 - 100) = 108 \text{ kN}$$

The silty clay of Sarnia is classified as CL according to the Unified Soil Classification System; for a CL soil the spring reduction factor is 25%. Therefore:

$$S_s = 108 \times 0.75 = 81 \text{ kN}$$

Given that the design plane, the Convair 440, has an ALR classification of six and Sarnia Airport had an average pavement equivalent granular thickness of 560 mm after overlay, the minimum acceptable S_s value (Fig. 5) for the Convair 440 to land safely is:

$$S_s \text{ (min)} = 65 \text{ kN}$$

The factor of safety of runway 14-32 at Sarnia Airport is:

$$F = \frac{S_s}{S_{s(min)}} = 1.27$$

Two S_s values are available for the new section of Ottawa Airport (Fig. 112). The lower quartile factor is 1 and the in situ S_s value is:

$$S_s = 851 \text{ kN}$$

The silty sand underlying the pavements of the new section is classified

as SM according to the Unified Soil Classification System; for an SM soil the spring reduction factor is 45%. Therefore:

$$S_s = 851 \times 0.55 = 468 \text{ kN}$$

The design plane for the new section, the DC 8-63, has an ALR rating of 12. The new runways have an average pavement equivalent granular thickness of 500 mm (Section 7.4.1) and for this thickness, the minimum acceptable S_s value for the DC 8-63 to land safely is (Fig. 5):

$$S_s(\text{min}) = 210 \text{ kN}$$

The factor of safety of taxiway Zoulou at Ottawa Airport is:

$$F = \frac{S_s}{S_{s(\text{min})}} = \frac{468}{210} = 2.23.$$

In the case of the older section at Ottawa Airport, four S_s values are available (Fig. 112). The lower quartile factor is 1.5 and the in situ S_s value is:

$$S_s = 306 + 0.5\ (312-306) = 309 \text{ kN}$$

The sand underlying the older pavements is classified as SP according to the Unified Soil Classification System, which means that the spring reduction factor is 20%. Therefore,

$$S_s = 309 \times 0.8 = 247 \text{ kN}$$

The design plane for the old section, the DC 3, has an ALR classification of 4. Given that the pavement equivalent granular thickness of this section of the airport is 200 mm (Section 7.4.1), the minimum acceptable S_s value for the DC-3 to land safely is (Fig. 5):

$$S_s(\text{min}) = 75 \text{ kN}$$

The factor of safety of the pavement of the old section of Ottawa Airport is:

$$F = \frac{S_s}{S_s(\text{min})} = \frac{247}{75} = 3.29$$

8.3 Briaud Pressuremeter Cyclic Modulus Design Chart

In Section 7.6.1 a linear relationship was found between the pavement equivalent Briaud pressuremeter cyclic modulus E_{cep} and the pavement bearing strength (S_p). This relationship is:

$$E_{cep} = 100\ S_p \quad \ldots\ldots\ldots\ldots\ldots\ldots\ldots\ldots \quad (48)$$

with E_{cep} in kPa and S_p in kN. The parameter S_p is obtained from a plate test performed on the pavement. The parameter E_{cep} is an equivalent modulus for the combined subgrade, base course and asphalt layer. The parameter which is used in the Canadian runway design is the subgrade bearing strength S_s; the value of S_s is obtained, in theory, from a plate test performed on the subgrade. The equivalent Briaud pressuremeter subgrade cyclic modulus E_{ces} is for the subgrade alone. It seems

reasonable to assume that the factor 100 relating E_{cep} and S_p also applies between E_{ces} and S_s making:

$$E_{ces} = 100\ S_s \quad \ldots\ldots\ldots\ldots\ldots\ldots\ldots\ldots\ldots\ldots\ldots\ldots \quad (51)$$

with E_{ces} in kPa and S_s in kN. The assumption that the factor of 100 can be applied to E_{ces} and S_s is based on the reasoning that

1) Both sets of parameters, E_{cep} and S_p, and E_{ces} and S_s, are obtained in the same manner.
2) Since Equation 48 is true for many different soil profiles (the profiles of the 6 holes of Ottawa Airport for example), the equation should be true for the subgrade.
3) In the two cases where E_{ces} and S_s have been calculated (Fig. 130 and 135) a factor of 120 was found.

This last point can be represented by the equation

$$E_{ces} = 120\ S_s \quad \ldots\ldots\ldots\ldots\ldots\ldots\ldots\ldots\ldots\ldots\ldots\ldots \quad (52)$$

A factor of 100 is preferred over 120 because the S_s values leading to Equation 52 are not direct field measurements (Section 2.1.1) and 120 is based on only two comparisons.

The foregoing discussion leads to the conclusion that the Transport Canada design chart (Fig. 5) can be based on the subgrade equivalent Briaud pressuremeter cyclic modulus E_{ces} rather than the subgrade bearing strength S_s (Fig. 136).

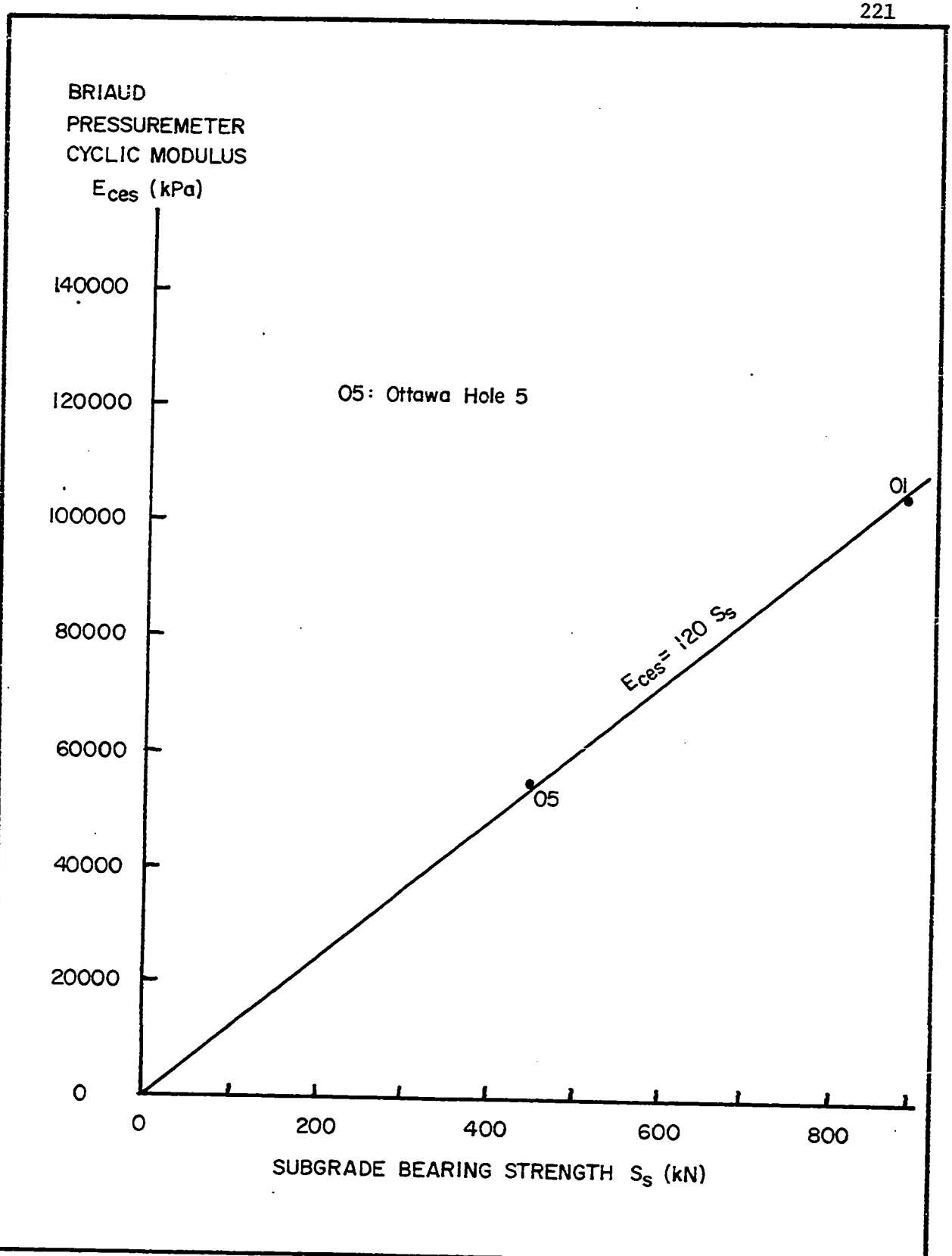

Fig. 135 – Subgrade Equivalent Briaud Pressuremeter Cyclic Modulus versus Subgrade Bearing Strength (Multilayer Elastic Analysis).

February 1979

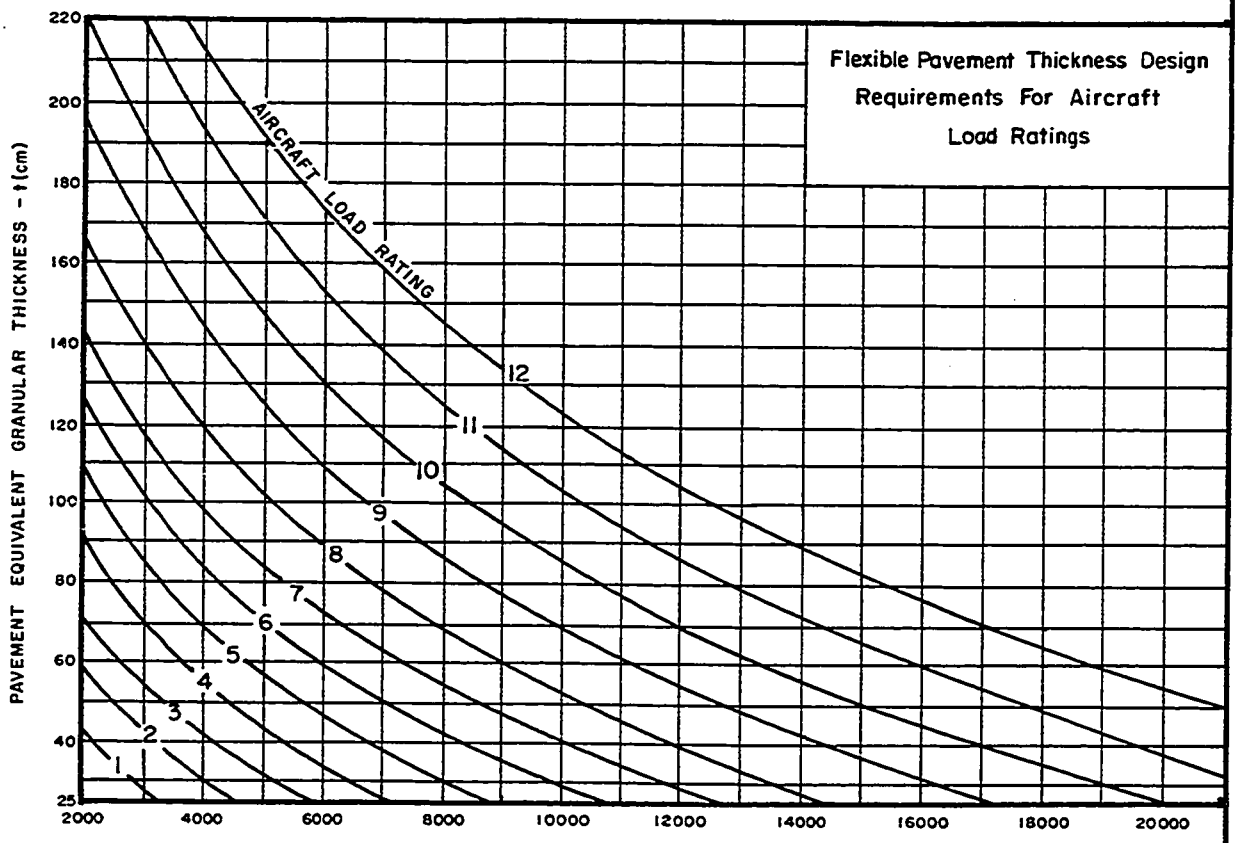

Fig. 136 - Thickness Design Chart Based on the Briaud Pressuremeter Test for Airfield Flexible Pavement.

8.4 Design Procedure Based on the Briaud Pressuremeter Test

The design procedure using the chart of Figure 136 is the same as the procedure which is described in Section 2.1.1 except that the Briaud pressuremeter test replaces the McLeod plate test. The following procedure can be followed to design new airfield flexible pavements:

1) Briaud pressuremeter tests are performed along the proposed runway according to the procedure described in Chapter 4. The test holes should be spaced about 100 m apart and at each hole location a test should be performed at 0.3 m intervals down to 1.5 m.

2) The data is reduced and plotted in the form of curves using the computer program of Section 4.5.3.

3) The equivalent Briaud pressuremeter subgrade cyclic modulus (E_{ces}) is calculated by the procedure described in Section 7.5.5 and 7.5.6 for each test hole location. An arbitrary but reasonable subgrade bearing strength (S_s) should be used for the analysis. An S_s value of 100 kN is recommended. The E_{ces} value depends only on the ratio of the subgrade bearing strength (S_s) to the calculated settlement (s). The ratio $\frac{S_s}{s}$ is a constant for a given linearly elastic multilayer soil. Therefore, the modulus E_{ces} and consequently the equivalent granular thickness of the pavement (t) do not depend on the arbitrary value of S_s.

4) The E_{ces} values are multiplied by the applicable spring reduction factor and the lower quartile factored E_{ces} value is determined. The lower quartile E_{ces} is considered to be the in situ E_{ces} value.

5) The Aircraft Load Rating of the design plane is obtained (Fig. 137) and the chart of Figure 136 is used to determine the required equivalent granular thickness.

6) If base course material is available from different borrow pits, it may be desirable to prepare pavement test sections with the different base course materials and to test them with the pressuremeter.

For the evaluation and design of overlays for existing pavements the following procedure should be followed:

1) Briaud pressuremeter tests are performed along the runway according to the procedure which is described in Chapter 4. At each hole location, a test is performed immediately below the asphalt layer and subsequent tests are performed at 0.3 m intervals down to a depth of about 1.8 m. The test holes should be about 100 m apart.

2) The data is reduced and test curves are plotted using the computer program of Section 4.5.3.

3) Only the results of tests in the subgrade should be considered. The equivalent Briaud pressuremeter subgrade cyclic modulus for each test hole location is calculated by the procedure which is described in Sections 7.5.5 and 7.5.6. An arbitrary but reasonable subgrade bearing strength value (S_s) should be used for the analysis. An S_s value of 100 kN is recommended. The arbitrary choice of S_s has no influence on the results as explained previously in this section.

4) The E_{ces} values are multiplied by the spring reduction factor as

Aircraft	Tire Pressure (MPa)	Max. Weight (kN)	Min. Weight (kN)	Weight Range (kN)	Aircraft Load Rating
Concorde	1.38	1800	770	990-1250 1250-1500 1500-(1830)	10 11 12
DC-8-63	1.38	1590	710	850-1050 1050-1290 1290-1560 1560-(1850)	9 10 11 12
B-747-200	1.34	3660	1730	1890-2390 2390-2930 2930-3560 3560-	9 10 11 12
L-1011	1.28	2080	1070	1390-1660 1660-2030 2030-(2490)	10 11 12
DC-10-20/30	1.14	2480	1050	1340-1680 1680-2020 2020-2480 2480-	9 10 11 12
B-747-100	1.48	3280	1590	1860-2340 2340-2890 2890-(3600)	9 10 11
B-747-200	1.41	3590	1630	1910-2410 2410-2960 2960-(3600)	9 10 11
B-747SR	1.28	3280	1530	1670-2050 2050-2420 2420-2870 2870-(3510)	8 9 10 11
DC-8	1.28	1460	663	685- 867 867-1060 1060-1260 1260-(1610)	8 9 10 11
SUPER HERCULES	1.28	1230	494	623- 792 792- 974 974-1180 1180-(1420)	8 9 10 11
AIRBUS A-300B4	1.25	1470	845	921-1100 1100-1310 1310-(1650)	9 10 11
B-707-320/420	1.24	1490	600	649- 881 881-1110 1110-1340 1340-(1570)	8 9 10 11
DC-10-10	1.19	1930	1050	1380-1630 1630-(2480)	10 11
B-727	1.16	850	390	476- 587 587- 712 712- (876)	9 10 11

Fig. 137 - Aircraft Load Ratings for Specific Aircrafts (Transport Canada Manual, AK-68-12)

Aircraft	Tire Pressure (MPa)	Max. Weight (kN)	Min. Weight (kN)	Weight Range (kN)	Aircraft Load Rating
TU-114	0.93	1710	990	916-1130 1130-1370 1370-(1910)	9 10 11
IL-62	0.93	1620	920	1070-1320 1320-(1820)	10 11
SUPER VC-10	0.85	1450	690	694- 841 841-1030 1030-1290 1290-	8 9 10 11
CONVAIR 990	1.21	1090	494	565- 712 712- 921 921-(1330)	8 9 10
B-707-120B	1.17	1150	570	716- 885 885-1080 1080-(1300)	8 9 10
ELECTRA-P3	1.17	560	254	325- 400 400- 507 507- (649)	8 9 10
DC-9-51	1.17	543	288	325- 400 400- 507 507- (649)	8 9 10
B-747SR	1.08	2680	1530	1620-1930 1930-2320 2320-(2890)	8 9 10
Convair 880	1.03	854	387	436- 552 552- 676 676- 818 818-(1010)	7 8 9 10
B-747SR /	0.94	2330	1530	1580-1880 1880-2260 2260-(2780)	8 9 10
Vanguard	0.91	652	365	374- 454 454- 556 556- (672)	8 9 10
DC-7-7C	0.90	636	347	374- 490 490- 601 601- (712)	8 9 10
Super Constellation L-1049	0.90	623	325	369- 463 463- 565 565- (712)	8 9 10
BAC-1-11-500	1.10	450	240	338- 418 418- (520)	8 9
B-737	1.02	494	260	298- 383 383- 485 485- (623)	7 8 9

Fig. 137 - Aircraft Load Ratings for Specific Aircrafts (Transport Canada Manual, AK-68-12) cont'd.

Aircraft	Tire Pressure (MPa)	Max. Weight (kN)	Min. Weight (kN)	Weight Range (kN)	Aircraft Load Rating
Hercules C130E	0.66	689	325	383- 498 498- 623 623- (814)	7 8 9
Viscount	0.90	325	187	191- 240 240- 316 316- (436)	6 7 8
DC-9-15	0.88	407	219	276- 356 356- (436)	7 8
TU-104	0.83	712	400	436- 543 543- 645 645- (747)	6 7 8
IL-18	0.79	623	356	374- 458 458- 543 543- (645)	6 7 8
DC-6B Super	0.72	472	241	311- 387 387- (485)	7 8
Argosy 650	0.50	410	200	240- 294 294- 356 356- 414	6 7 8
DC-4-M2	0.62	365	209	267- 329 329- (391)	6 7
Convair 440/640	0.48	245	—	178- 222 222- (343)	5 6
Gulfstream G159	0.83	157	100	120- (178)	5
Dash-7	0.69	191	116	142- (196)	5
Friendship-Fokker	0.55	201	113	116- 165 165- (214)	4 5
HS-748	0.50	200	110	129- 173 173- (218)	4 5
Dart Herald	0.40	191	—	173- (214)	5
Convair Canso	0.37	138	—	102- (147)	5
DH-125	0.67	90	50	76- (133)	4
DC-3	0.34	120	76	107- (151)	4
Lockheed 18	0.26	90	—	44- 71 71- (98)	2 3
King Air	0.38	44	—	0- 36 36- (67)	1 2
Apache/Aztec	0.41	27	—	0- (31)	1
Dove	0.32	40	28	0- 40	1
Beech-18	0.31	40	—	0- 40	1

Fig. 137 - Aircraft Load Ratings for Specific Aircrafts (Transport Canada Manual, AK-68-12) cont'd.

required and the lower quartile modified E_{ces} value is determined. This latter E_{ces} value is considered to be the in situ E_{ces} value.

5) The Aircraft Load Rating for the design plane is obtained (Fig. 137). This in situ E_{ces} value and the design chart of Figure 135 are used to determine the required equivalent granular thickness (t).

6) This required thickness (t_1) is compared to the equivalent granular thickness of the existing pavement (t_2). An overlay is necessary if t_1 is greater than t_2; the overlay thickness is:

$$t \text{ (overlay)} = \frac{t_1 - t_2}{\text{equivalency factor}} \quad \ldots\ldots\ldots\ldots \quad (53)$$

Equivalency factors are given in Section 240 of (42).

The above design procedure points out two advantages of the pressuremeter tests over the plate test. The first advantage is that pressuremeter tests can be carried out readily in situ before building the pavement; pressuremeter test results allow the engineer to really design the pavement rather than check his estimate as is done with the plate test (Section 2.1.1). The second advantage is that the subgrade modulus is measured directly whereas with the McLeod procedure the subgrade bearing strength (S_s) is estimated from the pavement bearing strength (S_p) by means of an empirical relationship.

CHAPTER 9

THE BRIAUD PRESSUREMETER TEST AND MULTILAYER ELASTIC DESIGN

9.1 General

The multilayer elastic theory approach to pavement design seems to be coming into greater and greater use. It appears, however, that evaluation of the moduli of deformation has not kept pace with the rapid advance in theory and computational capabilities (Section 2.1.5).

In this regard, the Briaud pressuremeter test represents a real improvement in the ability of engineers to evaluate and select moduli of elasticity.

This chapter discusses 13 cases where multilayer elastic pavement analysis has been carried out using the program BISAR. Calculations have been performed in the usual way (Section 2.1.4) except that the first loading or cyclic Briaud pressuremeter moduli were used as the elastic layer moduli. One case consists of having the leg of the design plane loading the pavement and of calculating, under this loading, three quantities: the maximum tensile horizontal strain (ε_h) at the lower face of the asphalt layer, the maximum compressive vertical strain (ε_v) at the top of the subgrade and the maximum settlement (s) of the pavement surface (Fig. 1). The 13 cases studied involve different design planes and different elastic moduli for the layers constituting the pavement and the subgrade at Sarnia and Ottawa Airports. The computed strains are compared with the strain values which are reported in the literature (Fig. 10 and 11).

9.2 Selection of the Multilayer Elastic Parameters

The BISAR program was developed by the Shell Oil Company (10). The imput parameters are: the design plane (load and geometry), the characteristics of the layers (thickness, modulus of elasticity, Poisson's ratio), and the location at which the strains are to be calculated. In all cases, the hypothesis of perfect adherence between layers is made since this assumption is thought to simulate reality (4).

The 13 cases are presented in Figure 139 and Appendix G. The design planes are the Convair 440 for Sarnia Airport (Fig. 138), the DC-8-63 for the new section of Ottawa Airport and the DC-3 for the older section of Ottawa Airport.

The actual thickness of the asphalt layer was measured at Sarnia Airport and was taken from construction records in the case of Ottawa Airport. At Sarnia two different thicknesses of asphalt had to be considered: 5 cm before the overlay and 17.5 cm after the overlay. In all cases, the boundary betwen layers was assumed to be at the midpoint between two consecutive pressuremeter test.

The deformation parameter for the various soil layers are given with the results of each case on the individual figures. A Poisson's ratio of 0.33 was chosen for all cases as recommended by Claessen et al. (10) (Section 2.1.4). The asphalt modulus was taken to be 1,500,000 kPa as a reasonable value (p. 235 of (3)). In cases 4, 6, 9 and 12 a higher asphalt modulus (6,000,000 kPa) was considered for comparison purposes.

For Sarnia Airport (Cases 1 and 2) a representative Briaud pressuremeter modulus was obtained for each layer by averaging the moduli which were obtained in Holes 5, 6, 7 and 15. A Briaud pressuremeter cyclic

DESIGN PLANES

SARNIA AIRPORT

Convair 440

gross weight: 219 kN
wheel arrangement: dual
load on each leg: 100 kN
tire pressure: 480 kN/m^2
contact area per tire: 1021 cm^2

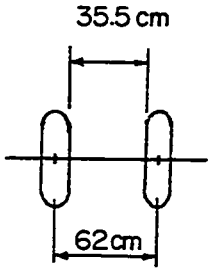

OTTAWA AIRPORT

New Airport: DC 8-63

gross weight: 1580 kN
wheel arrangement: dual tandem
load on each leg: 766 kN
tire pressure: 1350 kN/m^2
contact area per tire: 1415 cm^2

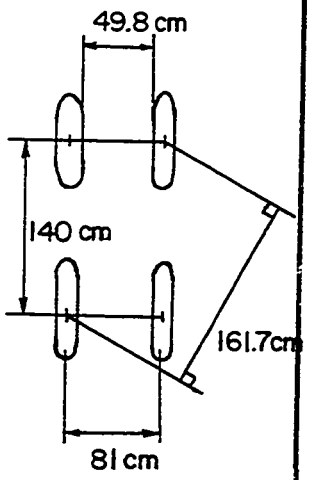

Old Airport: DC 3

gross weight: 112 kN
wheel arrangement: single
load on each leg: 56 kN
tire pressure: 310 kN/m^2
contact area per tire: 1784 cm^2

Fig. 138 - Load and Geometry Data of the Design Planes.

CASE 8: OTTAWA AIRPORT

New airport
Pressuremeter cyclic moduli
Design plane: DC 8-63
$\varepsilon_H = 1.66 \times 10^{-3}$
$\varepsilon_V = 3.04 \times 10^{-3}$
$A = 0.39$ cm

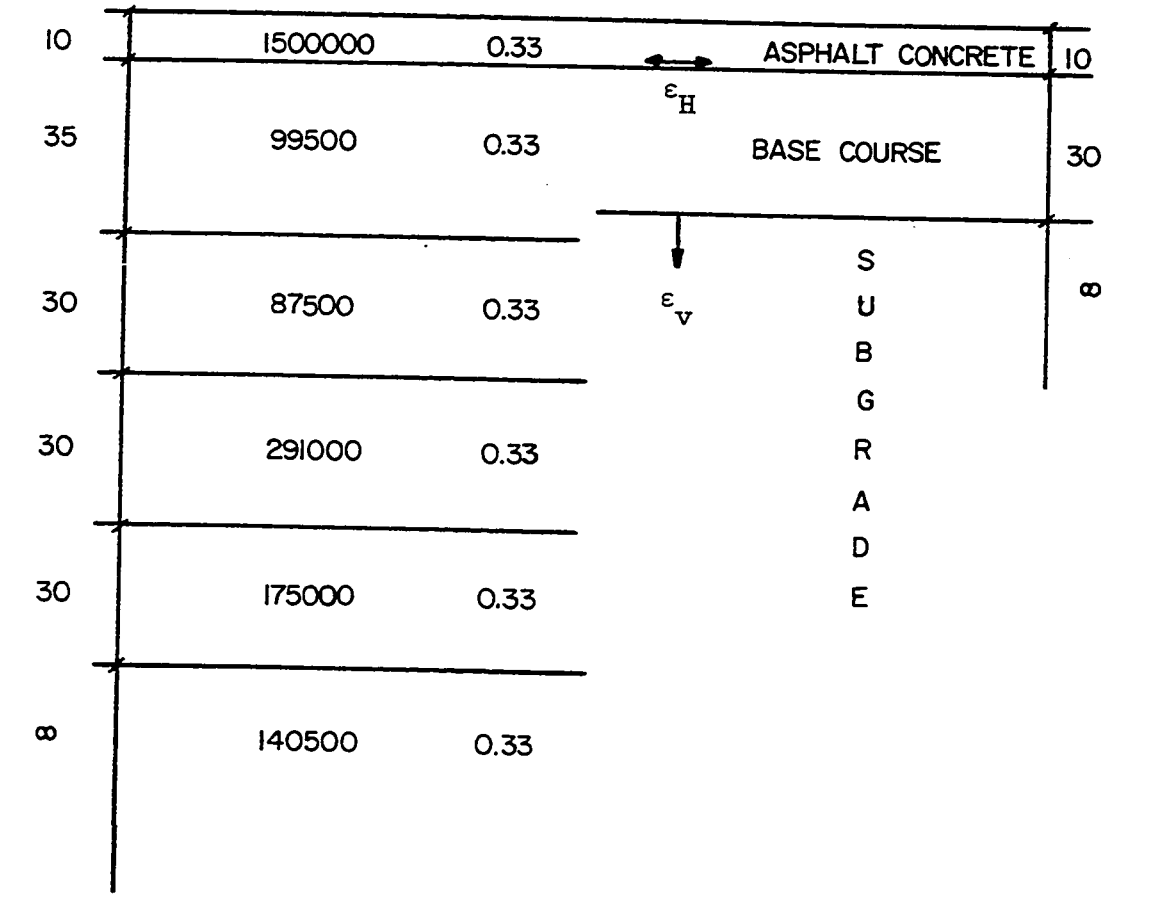

Fig. 139 - Multilayer Plastic Analysis. Ottawa: New Airport. Pressuremeter Cyclic Moduli. Asphalt Modulus: 1500000 kPa.

modulus profile was obtained by simply doubling the first loading modulus (Cases 3 to 7). For Case 7, a base course modulus of 300,000 kPa was chosen arbitrarily for comparison purposes. At Ottawa Airport, doubtful values of the pressuremeter cyclic moduli were replaced by interpolated values in a few instances as explained in Section 7.5.5. A representative Briaud pressuremeter cyclic modulus profile was obtained by averaging the cyclic moduli of Holes 1 and 2 in the case of the newer section of Ottawa Airport (Cases 8, 9, 10) and Holes 3 to 6 for the older section at Ottawa Airport (Cases 11, 12, 13). In Cases 10 and 13 an arbitrary base course modulus of 300,000 kPa was used for comparison purposes.

9.3 Results

The computer program BISAR is extremely easy to use; about 10 minutes are required to input the data and a typical run costs about three dollars (1978).

The results of Case 8 are given in Figure 139, the other 12 cases are considered in Appendix G. The results of a typical case (Fig. 139) consist of two strain values and a settlement prediction. The loading is taken to be from the entire wheel assembly of one leg of the design plane (Fig. 138); strains and settlement are calculated for static conditions. The quoted values of the horizontal tensile strain at the bottom of the asphalt layer (ε_h), the vertical compressive strain at the top of the subgrade (ε_v), and the vertical settlement (s) for each case are the maximum values which occur under the loading being considered. The results are summarized in tabular form in Figure 140. They give information on the influence of the following factors on ε_h, ε_v and s:

Case	Airport	Plane	First loading or cyclic pressuremeter modulus	Asphalt Modulus (kPa)	Asphalt Thickness (cm)	Strain ε_H 10^{-3}	Strain ε_V 10^{-3}	Settle-ment s (cm)	Observations
1	Sarnia	Convair 440	First Loading	1500000	5	2.92	12.7	1.1	
2	Sarnia	Convair 440	First Loading	1500000	17.5	1.01	4.81	0.52	~ case 1
3	Sarnia	Convair 440	Cyclic	1500000	5	1.91	6.89	0.61	
4	Sarnia	Convair 440	Cyclic	6000000	5	1.05	5.9	0.50	~ case 3
5	Sarnia	Convair 440	Cyclic	1500000	17.5	0.81	3.1	0.31	~ case 3
6	Sarnia	Convair 440	Cyclic	6000000	17.5	0.3	1.8	0.21	~ case 3
7	Sarnia	Convair 440	Cyclic	1500000	17.5	0.28	1.71	0.20	~ case 3 E_{base} = 300000 kPa
8	Ottawa (new)	DC8-63	Cyclic	1500000	10	1.66	3.04	0.39	
9	Ottawa (new)	DC8-63	Cyclic	6000000	10	0.9	2.29	0.31	~ case 8
10	Ottawa (new)	DC8-63	Cyclic	1500000	10	0.66	2.86	0.28	~ case 8 E_{base} = 300000 kPa
11	Ottawa (old)	DC 3	Cyclic	1500000	5	0.44	3.03	0.22	
12	Ottawa (old)	DC 3	Cyclic	6000000	5	0.39	2.4	0.19	~ case 11
13	Ottawa (old)	DC 3	Cyclic	1500000	5	0.08	2.63	0.17	~ case 11 E_{base} = 300000 kPa

Fig. 140 - Summary of the Results of the Multilayer Elastic Analyses: Strain Calculations

first loading or cyclic Briaud pressuremeter modulus, asphalt thickness, asphalt modulus, and base course modulus.

9.4 Discussion

Comparison of Cases 1 and 3 and Cases 2 and 5 indicates that the use of the first loading pressuremeter modulus rather than the cyclic pressuremeter modulus leads to higher strains and settlement values. In the cases which are reported, the strains and settlement values which were obtained when using the first loading pressuremeter modulus vary from 1.2 to 1.9 times the values obtained when using the cyclic pressuremeter modulus.

Comparison of Cases 1 and 2 and Cases 3 and 5 shows that increasing the asphalt thickness (overlaying) leads to lower strains and settlement values. In the cases which are reported, the asphalt thickness was multiplied by 3.5 (from 5 cm to 17.5 cm); as a result the strains and settlement values corresponding to the thicker asphalt layer were equal on average to only 40% of the values for the thinner asphalt layer.

Comparison of Cases 3 and 4, 5 and 6, 8 and 9, and 11 and 12 shows that increasing the asphalt modulus leads to lower strains and settlement values. In the cases reported, the asphalt modulus was multiplied by four (from 1,500,000 kPa to 6,000,000 kPa); as a result the asphalt strain ε_h was reduced by approximately one half and the subgrade strain ε_v and the settlement s were reduced by approximately one quarter. Cases 11 and 12 are proof that an increase in asphalt modulus alone leads to only a minor decrease in strains and settlement values.

Comparison of Cases 5 and 7, 8 and 10, and 11 and 13 shows that increasing the base course modulus leads to lower strains and settlement

values. In the cases reported, the base course modulus was increased from the cyclic pressuremeter value to 300,000 kPa; the resulting decrease in strains and settlement was similar to the one obtained by increasing the asphalt modulus from 1,500,000 kPa to 6,000,000 kPa.

In the multilayer elastic design of pavements, a limit is placed on the strain (ε_h) to which the asphalt can be subjected. Figure 10 gives several asphalt limiting strain curves; the limiting strain depends on the number of load repetitions and the modulus of the asphalt. The asphalt modulus which was used as a reference for this study is 1,500,000 kPa. A conservative estimate of the number of load repetitions for Sarnia and Ottawa Airport is probably 5,000 which corresponds to about 12 landings or take-offs of the design plane per day over a period of one year. For a dense bitumen macadam (Fig. 10a) and the foregoing load repetitions and asphalt modulus, the limiting strain ε_h is about 0.8×10^{-3}. In actual fact, the asphaltic concrete which is used at Sarnia and Ottawa Airport would have a limiting strain about 40% higher than 0.8×10^{-3} (of the order of 1.1×10^{-3})(Fig. 10b). This means that if the maximum tensile strain in the asphalt is 1.1×10^{-3} or less under the static load of the design plane, the asphalt layer will perform satisfactorily for at least 5,000 passes of the design plane.

The limiting strain in the subgrade (ε_v) depends mainly on the number of load repetitions as shown in Figure 11. For 5,000 repetitions, Figure 11 gives 2×10^{-3} as a reasonable estimate of subgrade limiting strain. This means, that if the subgrade strain ε_v is 2×10^{-3} or less under the static load of the design plane, the subgrade also will perform satisfactorily for at least 5,000 passes of the design plane.

In the 13 cases which are reported, the asphalt strain ε_h varies between 0.08×10^{-3} and 2.92×10^{-3}, the subgrade strain ε_v varies from 1.71×10^{-3} to 12.7×10^{-3} and the settlement s varies from 0.17 cm to 1.1 cm. The use of the first loading pressuremeter modulus as soil layer modulus leads to the highest strain values; these values are much greater than the limiting strain values (see for example Case 1). Since the first loading modulus leads to unacceptably high estimates of strain, the cyclic pressuremeter modulus is to be preferred for multilayer elastic analyses.

The pavement at Sarnia Airport had to be overlaid because of an increase in Convair 440 traffic. At this site, then, only the overlaid pavement should be used to compare the calculated strains induced by the Convair 440 with the limiting strains. Also, only one asphalt modulus need be considered when making the comparisons.

Given the above conditions, only three cases can be considered: Cases 5, 8 and 11. Case 5 gives the calculated strains for Sarnia Airport:

$$\varepsilon_h = 0.81 \times 10^{-3} \qquad \varepsilon_v = 3.1 \times 10^{-3}$$

Case 8 gives the strains for the newer section of Ottawa Airport:

$$\varepsilon_h = 1.66 \times 10^{-3} \qquad \varepsilon_v = 3.04 \times 10^{-3}$$

Case 11 gives the strains for the older section of Ottawa Airport:

$$\varepsilon_h = 0.44 \times 10^{-3} \qquad \varepsilon_v = 3.03 \times 10^{-3}$$

The limiting strains are:

$$\varepsilon_h = 1.1 \times 10^{-3} \qquad \varepsilon_v = 2 \times 10^{-3}$$

The calculated strains are not far from the limiting strain. The calculated asphalt strains straddle the limiting strain value while the subgrade strain is consistently higher than the limiting strain. These results indicate that the Briaud pressuremeter cyclic modulus is compatible with the use of a limiting strain criterion for pavement design. On the basis of this evidence, it seems reasonable to conclude that the Briaud pressuremeter can measure, in situ, the moduli necessary for multilayer elastic pavement design. The Briaud pressuremeter cannot, as yet, measure the modulus of the asphalt; this limitation may yield to further research.

9.5 Design Procedure Based on the Briaud Pressuremeter Test

The following procedure should be followed to design new airport flexible pavements.

1) Briaud pressuremeter tests should be performed according to the procedure which is described in Chapter 4. At each location along the proposed runway, a test is performed every 0.3 m down to 1.5 m. The test holes should be about 100 m apart.
2) The field data should be reduced and the results plotted in the form of curves using the computer program of Section 4.5.3. A Briaud pressuremeter cyclic modulus profile is drawn for each hole location.

3) The subgrade at each hole location is divided into layers; the boundaries of the various layers should be taken to be the mid-point between two consecutive pressuremeter tests. A reasonable base course and asphalt layer thickness is selected either by experience or by using Figure 141 as a guide (Section 320 of (42)).

4) Elastic deformation parameters are selected for each layer. However, Poisson's ratio is chosen to be 0.33 for all layers. The modulus of elasticity for each subgrade layer is taken to be the corresponding Briaud pressuremeter cyclic modulus. For the base course layer, the modulus of elasticity is assumed to be equal to the Briaud pressuremeter cyclic modulus which is measured in a test embankment. The modulus of elasticity of the asphalt layer is chosen to be 1,500,000 kPa for all cases.

5) The design plane characteristics are determined; these characteristics include the tire pressure, the contact area per tire and the wheel arrangement (see, for example, Fig. 138).

6) Input the data and run the BISAR program in order to obtain the two strains ε_h and ε_v, (Fig. 1) at each hole location.

7) Apply a spring influence factor, if necessary, to all ε_h and ε_v values; then find the lower quartile value for both modified ε_h (ε_{hq}) and modified ε_v (ε_{vq}).

8) Estimate the equivalent number of passes of the design plane during the intended service life of the pavement. Find the allowable strains ε_{ha} and ε_{va} from Figure 10 and 11 or their equivalent.

MINIMUM LAYER THICKNESSES FOR FLEXIBLE PAVEMENTS

Component Layer	DESIGN AIRCRAFT TIRE PRESSURE				
	Less than 0.4 MPa	0.4 MPa to 0.7 MPa	0.7 MPa to 1.0 MPa	1.0 MPa to 1.4 MPa	Above 1.4 MPa
Asphaltic Concrete Surface Course (Hot Mix)	5.0 cm	6.5 cm	9.0 cm	10.5 cm	12.5 cm
Crushed Gravel or Crushed Stone Base Course	15 cm	25 cm	23 cm	30 cm	38 cm
Selected Granular Sub-base Course	As required in addition to the asphalt and base layers to provide: (a) The total pavement equivalent granular thickness required for structural support; (b) Total pavement depth required for partial frost protection.				

Fig. 141 - Minimum Layer Thicknesses of Flexible Pavements for Different Aircraft Tire Pressure (from Transport Canada Manual AK-68-12).

9) If the lower quartile strains are approximately the same as the allowable strains, the design is satisfactory. If the lower quartile strains are smaller than the allowable strains, start the design again at Step 3 and use a thinner base course. If the lower quartile strains are larger than the allowable strains, start again at Step 3 but assume a thicker base course.

10) If the ε_h and ε_v values which were obtained in Step 6 vary considerably along the runway it may be economical to consider a runway with a varying thickness of base course.

For the evaluation and the design of overlays of existing pavements, the following procedure should be followed:

1) Briaud pressuremeter tests should be performed according to the procedure described in Chapter 4. At each hole location a first test is performed immediately below the asphalt layer; the subsequent tests are performed at 0.3 m intervals down to a depth of about 1.8 m. The test holes should be about 100 m apart.

2) The field data is reduced and curves plotted using the computer program of Section 4.5.3. A Briaud pressuremeter cyclic modulus profile is drawn for each borehole.

3) The base course and subgrade at each hole location is divided into layers with the boundary between layers corresponding to the midpoint between two consecutive pressuremeter tests. The thickness of the asphalt layer is known from measurements made during the field test program.

4) Elastic parameters are selected for each layer with the Poisson's ratio fixed at 0.33. In the case of the subgrade and base course

layers, the modulus of elasticity is taken to be the corresponding Briaud pressuremeter cyclic modulus. The modulus of elasticity of the asphalt layer is taken to be 1,500,000 kPa.

5) The characteristics of the design plane such as tire pressure, contact area per tire and wheel arrangement are obtained: (see, for example: Fig. 138).

6) Input the data and run the program BISAR in order to estimate the two strains ε_h and ε_v (Fig. 1) at each hole location.

7) If the pressuremeter tests have not been performed during the spring, apply a spring influence factor to all ε_h and ε_v. Then, find the lower quartile value of the adjusted ε_h and ε_v values (ε_{hq} and ε_{vq}).

8) Plot ε_{vq} on the allowable subgrade strain versus number of passes curve (see, for example, Fig. 11); the point will determine the remaining life of the pavement (as the number of load repetitions N_v). Then, plot ε_{hq} on the allowable asphalt strain versus number of passes curve (for example, Fig. 10a); the point will determine the remaining life of the pavement (as the number of load repetitions N_h). The smaller of the two numbers N_h and N_v is the remaining life of the pavement.

9) If the remaining life of the pavement is unsatisfactory, the pavement must be overlaid. Start again at Step 3 with a thicker asphalt layer until the required service life is obtained.

This design procedure makes more direct, and therefore better, use of the pressuremeter results than the design procedure described in Section 8.4. For this reason, the procedure outlined here is the recommended

design method. However, this recommended procedure must be employed with caution since the allowable subgrade and asphalt strains have not yet been determined, and since a test is needed to determine the asphalt modulus accurately.

CHAPTER 10

CONCLUSIONS

10.1 The Briaud Pressuremeter Test

A special pressuremeter has been developed for use in pavement design. The probe is short (active length = 230 mm), is monocellular and has a diameter of 32 mm. The control unit is simple, and strain controlled tests can be performed readily using a standard procedure to measure cyclic pressuremeter moduli of the soil in situ. Throughout the thesis, the new equipment and test are referred to as the "Briaud" pressuremeter test to emphasize the fact that the test is different from other pressuremeter tests and that the conclusions which have been reached for pavement design may not hold true for other pressuremeters and other test procedures. The Briaud pressuremeter and test provide a practical, inexpensive and useful way of designing new pavements or assessing existing pavements.

A standard procedure for making the borehole has been evolved. The procedure called the rod driving method is applicable to all soil types and consists of driving E rods into the soil, withdrawing the rods and inserting the pressuremeter probe into the hole. Although this method may not keep disturbance to the soil to a minimum, the method does have a number of advantages over other more involved methods which would reduce disturbance. When considering the test results in the literature and the tests results in this thesis, it seems that, on average, the disturbance to the soil induced by the rod driving method or by the direct

insertion of the probe results in soil modulus changes of the order of 30%. Disturbance is particularly important in soft and loose soils.

A standard procedure for running the pressuremeter test has been established and allows the Briaud pressuremeter first loading modulus (E) and the Briaud pressuremeter cyclic modulus (E_c) to be measured. The ratio $\frac{E_c}{E}$ averaged 1.75 in two deposits of clay and 2.63 in a deposit of sand. Consolidated undrained triaxial tests were performed on samples which were taken close to the location of the pressuremeter tests. During the triaxial tests, two moduli were measured: the triaxial first loading modulus (E_T) and the triaxial cyclic modulus (E_{Tc}). When comparing the pressuremeter moduli and the triaxial moduli at similar confining pressures it was found that E and E_T were always reasonably close and that E_{Tc} was consistently much greater than E_c.

10.2 The Critical Depth Problem

The Briaud pressuremeter test measures moduli close to the surface. Because pressuremeter theory assumes that plane strain conditions are created in the soil, it was important to determine whether or not the proximity of the surface would create a deformation process different from that of a plane strain. The results of 84 Briaud pressuremeter tests and 20 Menard GA pressuremeter tests in both sand and clay, and the results of a computer simulation, show that even at the shallowest testing depth (about 0.3 m), there is negligible influence of the surface during the elastic phase of the test. This conclusion does not hold true at the limit pressure. This indicates that the critical depth depends on the volume displaced by the apparatus and not only on the original diameter

of the apparatus as seems to be the case for piles.

During the study, the pressuremeter moduli were found to vary with depth; this phenomenon was attributed to such factors as changes in minor principal stress level and variations in the soil strength with depth; the variations were not due to a critical depth phenomenon.

As far as limit pressure is concerned, the results of 20 Ménard GA pressuremeter tests in dense and compact sand show the existence of a critical depth at about 1.2 m depth.

10.3 Comparison Between the Briaud Pressuremeter Test and the McLeod Plate Test

A total of 11 McLeod plate tests and 93 Briaud pressuremeter tests were performed at Ottawa and Sarnia Airports with their respective sand and clay subgrades. At each test location the plate yields one bit of information (the value of S_p which is the load leading to 12.5 mm deflection of the plate after 10 load repetitions) whereas the pressuremeter test gives six results (a vertical profile of six moduli through the base course layers and into the subgrade). The engineer can assess a pavement in much more detail with the profile of the six pressuremeter moduli than with the one plate bearing strength.

At any one hole location, the six pressuremeter moduli can be reduced to one equivalent modulus by calculating the settlement of the McLeod plate. The settlement is calculated over a multilayer elastic soil in which the layer moduli are the pressuremeter moduli. The detailed procedure is given in Section 7.5. The pavement equivalent Briaud pressuremeter modulus (E_{ep}) is obtained when the Briaud pressuremeter

moduli (E) are used in the layers and the pavement equivalent Briaud pressuremeter cyclic modulus (E_{cep}) is obtained when the Briaud pressuremeter cyclic moduli (E_c) are used. It was found that, on average (Fig. 133 and 134):

$$E_{ep} = 55\ S_p \quad \ldots\ldots\ldots\ldots\ldots\ldots\ldots\ldots \quad (47)$$

and $$E_{cep} = 100\ S_p \quad \ldots\ldots\ldots\ldots\ldots\ldots\ldots\ldots \quad (48)$$

with E_{ep} and E_{cep} in kPa and S_p in kN.

Since S_p is used in Canada for the design of flexible airfield pavements, and since there is a (linear) relationship between E_{cep} and S_p, it can be concluded that the Briaud pressuremeter test can replace the McLeod plate test as the basis of the traffic load design of flexible airfield pavements.

The McLeod plate test can be analyzed using elastic theory to compute a modulus of elasticity for the soil. The basic equation is:

$$E_e = 108\ S_p \quad \ldots\ldots\ldots\ldots\ldots\ldots\ldots\ldots \quad (49)$$

with E_e in kPa and S_p in kN. Comparing Equation 48 and Equation 49, it is apparent that $E_{cep} = E_e$ within 8%. This means that the Briaud pressuremeter cyclic modulus (E_c) measures a modulus which is compatible with the theory of elasticity. Indeed, the settlements measured in the field under the McLeod plate were found in close agreement with the settlements calculated using the theory of elasticity and the E_c values.

10.4 The Design Procedures Based on the Briaud Pressuremeter Test

Two procedures, based on the Briaud pressuremeter test, are proposed for the design of flexible airfield pavements. The first procedure is empirical and is identical to the procedure based on the McLeod plate test except that a pressuremeter parameter replaces the plate parameter. The second procedure is based on multilayer elastic theory with the modulus of the various layers being measured by the pressuremeter.

The empirical design method makes use of a chart such as Figure 136. This chart was derived from the Transport Canada chart for pavement design based on plate tests (Fig. 5); the subgrade bearing strength (S_s) was converted to an equivalent Briaud pressuremeter cyclic modulus (E_{ces}) through the use of Equation 51. The step by step procedure of the empirical design method is given in Section 8.4.

The theoretical design method makes use of the Briaud pressuremeter cyclic moduli (E_c). The method allows the strains ε_h and ε_v (Fig. 1) under one leg of the design plane to be calculated; the design is satisfactory when both ε_h and ε_v are less than the maximum allowable strain values. The step by step procedure of the theoretical design method is given in Section 9.5. This theoretical design method was used in this thesis to calculate the strains ε_v and ε_h under the loading of the design planes at Sarnia and Ottawa Airports. The calculated strains compare favorably with strains reported in the literature.

Both empirical and theoretical designs have a procedure for the design of new pavements and a procedure for the evaluation and the design of overlays for existing pavements.

The theoretical design procedure is recommended over the empirical procedure because the theoretical procedure has two advantages: 1) it makes a more direct use of the pressuremeter moduli, 2) it analyses more easily and more logically the pavement and subgrade response to the loading developed by a complicated wheel arrangement. However, the theoretical design is not yet complete or proven (Section 9.5). It is therefore suggested that the empirical design be used during a transition period while the theoretical design is developed and tested further.

10.5 Recommendations for Further Research

A major improvement to the apparatus would be to replace the hand pump by an electric pump running on a car battery; this would ensure a more controlled rate of inflation of the probe.

The preparation of the borehole requires a drilling machine. The feasibility of using a portable equipment, such as a power auger, for making the borehole should be investigated. It may be possible to apply a vibrator to the top of the pressuremeter rods in order to vibro-drive the probe to the required depth in the ground without predrilling a hole. This insertion technique would have many practical advantages but a new study would have to be made of the disturbance created in the soil and the effect of this disturbance on Equation 48.

Equation 48 is based on only six test points (Fig. 134). Many other plate-pressuremeter comparisons on different airport sites are needed to confirm the validity of this equation. Also, further comparisons should tell if the scatter of results which was obtained at Sarnia Airport was due to varying amounts of disturbance to the soil when making

the borehole for the pressuremeter tests, or due to lack of precision in the tests technique.

A method of determining the asphalt modulus is needed. This may be done by measuring the Briaud pressuremeter cyclic modulus (E_c) in a thick (23 cm or more) test specimen of the asphalt. The variation of E_c as a function of some asphalt characteristics such as its Marshall stability resistance could be studied in the laboratory. For an asphalt modulus of 1,500,000 kPa, the volume injected in the probe between 0 kPa and 2000 kPa would be only about 0.7 cm^3. This small volume change would be impossible to measure with the existing Briaud pressuremeter since one division on the volumeter is 1 cm^3 and the volume corrections are about 10 cm^3 at 2000 kPa.

The multilayer theoretical design method should be completed by establishing realistic ε_h and ε_v allowable strain criteria. This could be done by calculating the strains ε_h and ε_v by the method described in Section 9.5 for any airport that has been tested with the Briaud pressuremeter. The calculated strains would then be compared with the actual performance of that airport in order to set allowable strain criteria.

When the Briaud pressuremeter test is used extensively, it would be valuable to store the data on a computer. This would facilitate information retrieval and allow the evolution of the different layers of pavement at any airport to be followed.

The Briaud pressuremeter test has other potential applications. It could be used for the design and evaluation of airfield rigid pavements and highway pavements. It could also be used for compaction control and for the control of foundation beds.

LIST OF REFERENCES

1. Baguelin, F., Jezequel, J.-F., and Shields, D., The Pressuremeter and Foundation Engineering, Trans Tech Publications, Clausthal, Germany, 1978.

2. Barker, W., "Nonlinear Finite Element Analysis of Heavily Loaded Airfield Pavement Systems", Proceedings of the Symposium on Applications of the Finite Element Method in Geotechnical Engineering, Vol. 2, U. S. Army Engineer Waterways Experiment Station, Vicksburg, MS., U.S.A., 1972, pp. 657-693.

3. Barker, W., Brabston, W., and Chou, Y., "A General System for the Structural Design of Flexible Pavements", Proceedings of the Fourth International Conference on the Structural Design of Asphalt Pavements, Vol. 1, University of Michigan, Ann Arbor, MI, U.S.A., 1977, pp. 209-248.

4. Bleyenberg, W., et al., "Fully Monitored Motorway Trials in the Netherlands Corroborate Linear Elastic Design Theory", Proceedings of the Fourth International Conference on the Structural Design of Asphalt Pavements, Vol. 1, University of Michigan, Ann Arbor, MI, U.S.A., 1977, pp. 75-98.

5. Bowes, W. H., and Russell, L. T., "Axi-Symmetric Solids", Stress Analysis by the Finite Element Method for Practicing Engineers, Lexington Books, Lexington, MA, U.S.A., 1975, pp. 125-142.

6. Briaud, J.-L., and Shields, D. H., "The Pressuremeter: Application to Pavement Design", Report for Research Contract KAC-77-003, Transport Canada, Ottawa, ON., Canada, 1978.

7. Carlo, J. C., "Programme d' Exploitation de l'Essai Pressiometrique Menard: Notice d' Analyse", Rapport Interne, Laboratoire Regional des Ponts et Chaussées, St Brieuc, France, 1977.

8. Chantereau, M., and Leger, Ph., "The Catologue of Structure of the Direction des Routes et de la Circulation Routière Francaise", Proceedings of the Third International Conference on the Structural Design of Asphalt Pavements, Vol. 1, London, England, 1972, pp. 990-1000.

9. Circulaire du Ministere des Transports 2483 DBS/6, "Dimensionnement des Chaussees d' Aérodromes et Détermination des Charges Admissibles, Service Technique des Bases Aeriennes, Paris, France, 1970, pp. 45-105.

10. Claessen, A. E. M., et al., "Asphalt Pavement Design: the Shell Method", Proceedings of the Fourth International Conference on the Structural Design of Asphalt Pavements, Vol. 1, University of Michigan, Ann Arbor, MI., U.S.A., 1977, pp. 39-74.

11. Deschenes, J.-H., "Bearing Capacity of Footings Close to Slope of Cohesionless Soils", Ph.D. Thesis, University of Ottawa, Ottawa, ON., Canada, 1978.

12. Federal Aviation Administration Manual AC 150/4320-6B, "Airport Pavement Design and Evaluation," Washington, D.C., U.S.A., 1974.

13. Fourth International Conference on the Structural Design of Asphalt Pavements, Proceedings, Vol. 1 and 2, University of Michigan, Ann Arbor, MI., U.S.A., 1977.

14. Giroud, J.-P., Tables pour le Calcul des Fondations, Tome 1, Dunod, Paris, France, 1972.

15. Gschwendt, I. and Poliacek, I., "Design of Flexible Pavements in Czechoslovakia: Recent Research Works", Proceedings of the Third International Conference on the Structural Design of Asphalt Pavements, Vol. 1, London, England, 1972, pp. 1018-1030.

16. Haile, G., "Foundation Performance of a Tower Silo", a Master's Thesis, University of Ottawa, ON., Canada, 1977.

17. Hartman, J. P., "Finite Element Parametric Study of Vertical Strain Influence Factors and the Pressuremeter Test", Ph.D. Thesis, University of Florida, Gainesville, FL., U.S.A., 1974.

18. Jezequel, J.-F., Lemasson, H., Touze, J., "Le Pressiomètre Ménard: Quelques Problemes de Mise en ceuvre et leur Influence sur les Valeurs Pressiometriques", Bulletin de Liaison des Laboratoires des Ponts et Chaussees No. 32, Paris, France, 1968, pp. 97-120.

19. Jezequel, J.-F., "Site de Caudan: Résultats des Essais d'Expansion", Rapport Interne, Laboratoire Regional des Ponts et Chaussées, Saint-Brieuc, France, 1977.

20. Kasianchuk, D. A. and Argue, G. H., "A Comparison of Plate Load Testing with the Wave Propagation Technique", Proceedings of the Third International Conference on the Structural Design of Asphalt Pavements, Vol. 1, London, England, pp. 444-454.

21. Kunio Suyama, Tsumeo Imai, "Studies of Subgrade Reaction Coefficient K Value of Soil Ground", OYO Technical Note, OYO Corporation, Tokyo, Japan, 1976, pp. 2014.

22. Lacroix, D., "French Policy and Procedures for Airfield Pavement Load Evaluation" (presented at the 1977 American Society of Civil Engineers Annual Convention), Service Technique des Bases Aeriennes, Paris, France, 1977.

23. Ladanyi, B., and Saint-Pierre, R., "Evaluation of Creep Properties of Sea Ice by Means of a Borehole Dilatometer", prepared for the IAHR Symposium on Ice Problems, Lulea, Sweden, August, 1978.

24. Lai, P., "Measurement of Density by Various Methods in a Cohesionless Quartz Sand", a Master's Thesis, University of Ottawa, Ottawa, ON., Canada, 1977.

25. Laier, J., "Effects of Pressuremeter Probe Length/Diameter Ratio and Borehole Disturbance on Pressuremeter Test Results in Dry Sand", Ph.D. Thesis, University of Florida, Gainesville, FL., U.S.A., 1973.

26. Lambe, T. W., and Whitman, R. V., Soil Mechanics, John Wiley and Sons, New York, N.Y., U.S.A., 1969.

27. Lemée, E., and Saintilan, D., "Exploitation de l' Essai Pressiométrique Normal par Methode Numérique", Rapport Interne, Laboratoire Régional des Ponts et Chaussées, Saint-Brieuc, France, 1973.

28. McLeod, N. W., "Airport Runway Evaluation in Canada", Internal Report, Transport Canada, Ottawa, ON., Canada, August 1947.

29. Ménard, L., "Calcul de la Force Portante des Fondations sur la Base des Résultats des Essais Pressiométriques", Sol-Soils, Vol. 2, Longjumeau, France, 1963, p. 10.

30. Ménard, L., "Comparaison entre le CBR et les Résultats du Minipressiomètre", Rapport Interne: Techni-Route, Technique Louis Ménard, Longjumeau, France, 1968.

31. Ménard, L., "Chantier Experimental de Neeltje Jans", Rapport Interne, Technique Louis Ménard, Longjumeau, France, 1976.

32. Ménard, L., "Dynamic Consolidation: Miscellaneous Jobs", Rapport Interne P/7000 an, Technique Louis Ménard, Longjumeau, France, 1977.

33. Mittal, H. K., and Morgenstern, N. R., "Parameters for the Design of Tailings Dams", Canadian Geotechnical Journal, Vol. 12, Montreal, PQ, Canada, 1975, pp. 235-261.

34. Monismith, C. L., "Design Theory", Proceedings of the Third International Conference of Structural Design of Asphalt Pavements, Vol. 2, London, England, 1972, pp. 144-170.

35. Rao, H. A. B., "Evaluation of Flexible Pavements by Nondestructive Tests", Proceedings of the Third International Conference on the Structural Design of Asphalt Pavements, Vol. 1, London, England, 1972, pp. 903-910.

36. Roy, M., et al., "In Situ Measurements of the Properties of Sensitive Clays by Pressuremeter Test", Proceedings of the Specialty Conference on In Situ Measurement of Soil Properties, American Society of Civil Engineers, Vol. 1, Raleigh, NC, U.S.A., 1975, pp. 350-372.

37. Schmertmann, J., "Static Cone to Compute Static Settlement over Sand", Journal of the Soil Mechanics and Foundations Division, American Society of Civil Engineers, Vol. 96, No. SM3, pp. 1011-1043.

38. Scott, J. D. (ed.), Canadian Foundation Engineering Manual, Canadian Geotechnical Society, Montreal, PQ, Canada, 1978, Part 3, p. 9.

39. Serota, S., and Lowther, G., "A New and Simple Penetration Pressuremeter", Ground Engineering, Vol. 9, No. 1, London, England, 1976, pp. 29-31.

40. Shields, D., and Bauer, G., "Determination of the Modulus of Deformation of a Sensitive Clay Using Laboratory and In Situ Tests", Proceedings of the Specialty Conference on In Situ Measurement of Soil Properties, American Society of Civil Engineers, Vol. 1, Raleigh, NC, U.S.A., 1975, pp. 450-476.

41. Third International Conference on the Structural Design of Asphalt Pavements, Proceedings, Vol. 1 and 2, London, England, 1972.

42. Transport Canada Manual AK-68-12, "Pavement Design and Rehabilitation", Transport Canada, Ottawa, ON, Canada, 1976.

43. Transport Canada Manual AK-68-31, "Pavement Bearing Strength: Measurement and Analysis", Transport Canada, Ottawa, ON, Canada, 1978.

44. Van Til, C. J., and Vallerga, B. A., "Application of a Theoretical Procedure to Airfield Pavement Evaluation and Overlay Design", Proceedings of the Third International Conference on the Structural Design of Asphalt Pavements, Vol. 1, London, England, 1972, pp. 1236-1243.

45. Wester, K., "Strengthening Existing Pavements", Proceedings of the Third International Conference on the Structural Design of Asphalt Pavements, Vol. 2, London, England, 1972, pp. 337-346.

46. Windle, D., and Wroth, C. P., "The Use of a Self-Boring Pressuremeter to Determine the Undrained Properties of Clays", Ground Engineering, Vol. 10, No. 6, London, England, pp. 37-46.

47. Wong, K. S., and Duncan, J. M., "Hyperbolic Stress Strain Parameters for Nonlinear Finite Element Analysis of Stresses and Movements in Soil Masses", Report No. TE-74-3, University of California, Berkeley, CA, U.S.A., 1974.

48. Wu, T. H., Soil Mechanics, Allyn and Bacon Inc., Boston, MA, U.S.A., 1976.

49. Yoder, E. J. Principles of Pavement Design, 1st ed., John Wiley and Sons, New York, NY, U.S.A., 1959, p. 337.

50. Yoder, E. J., and Witezak, M. W., Principles of Pavement Design, 2nd ed., John Wiley and Sons, New York, NY, U.S.A., 1975.

51. Mitchell, J. K., Fundamentals of Soil Behavior, John Wiley and Sons, New York, 1976, p229.

52. Poulos, H. G., and Davis, E.H., Elastic Solutions For Soil and Rock Mechanics, John Wiley and Sons, New York, 1974, p.186.

APPENDIX A

PRESSUREMETER TESTS CURVES

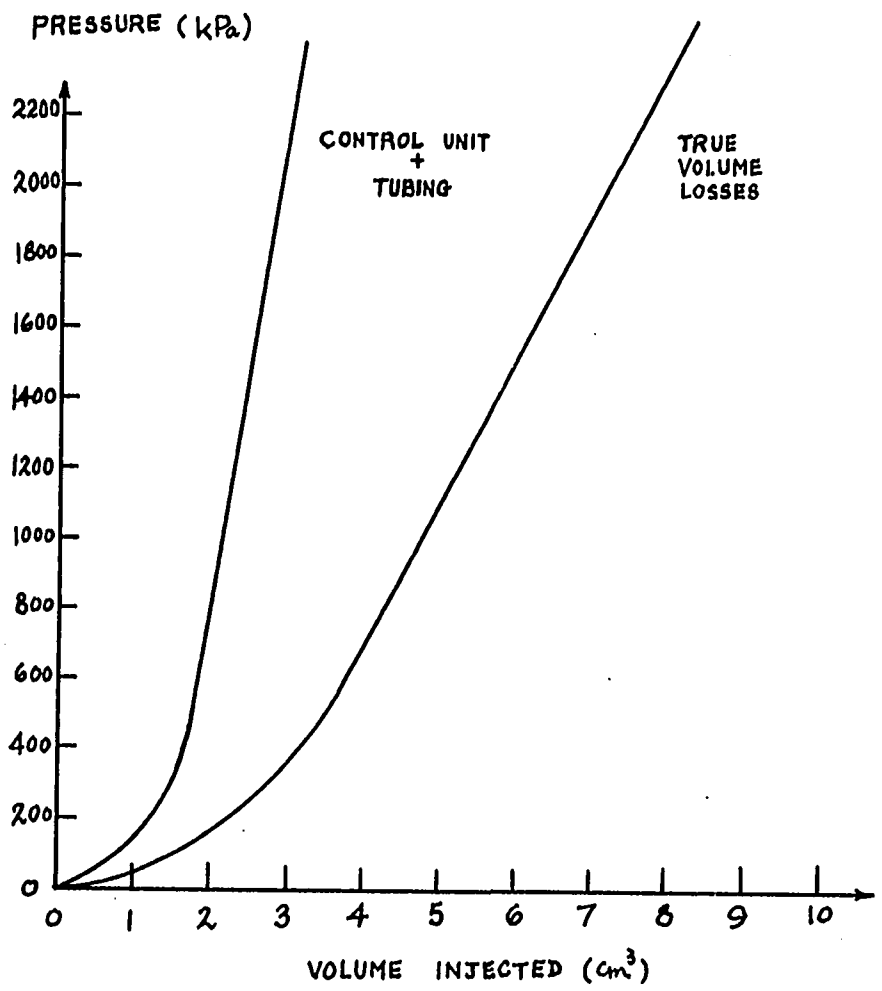

Fig. 142 - Test No. 3. Sand Box. Ménard GA Pressuremeter. Calibration of Volume Losses.

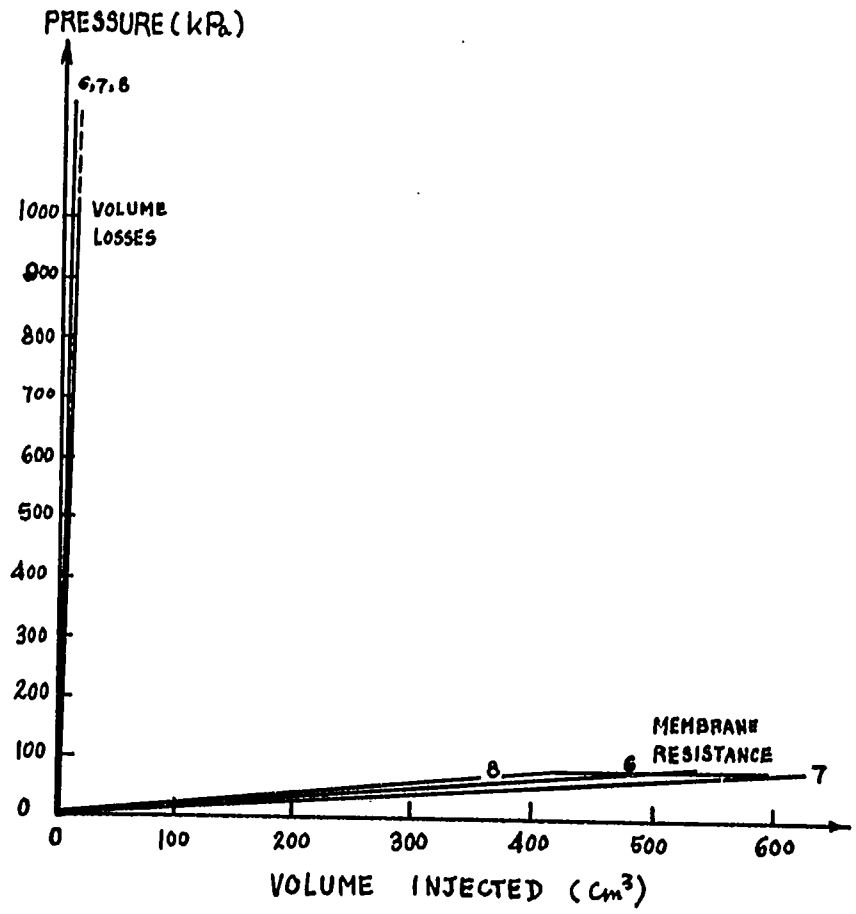

Fig. 143 - Test Nos. 6,7,8. Sand Box. Ménard GA Pressuremeter. Volume Losses and Membrane Resistance.

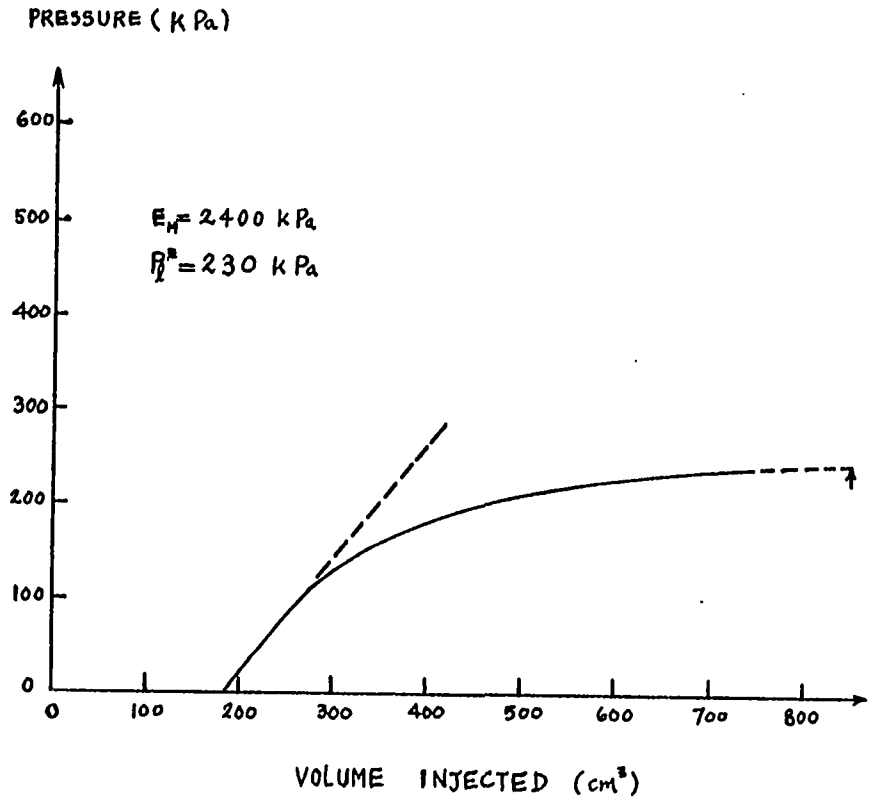

Fig. 144 - Test No. 9. Sand Box. Menard GA Pressuremeter Test. Buried Probe. I_D = 63%. Depth = 1.49 m.

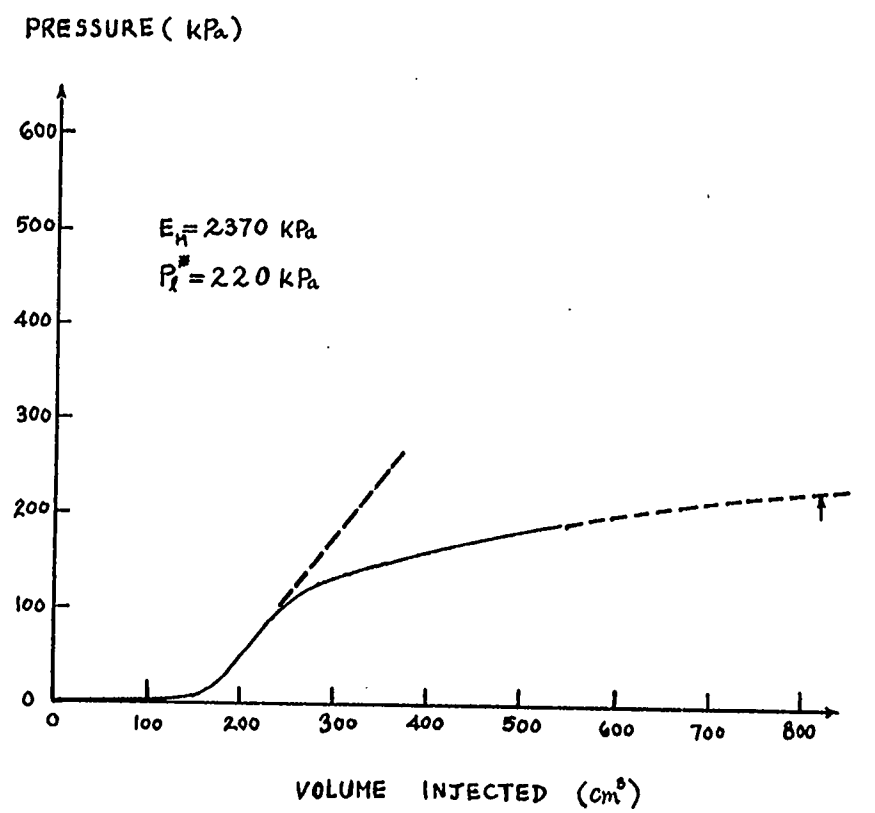

Fig. 145 - Test No. 10. Sand Box. Menard GA Pressuremeter Test. Buried Probe. I_D = 64%. Depth = 1.45 m.

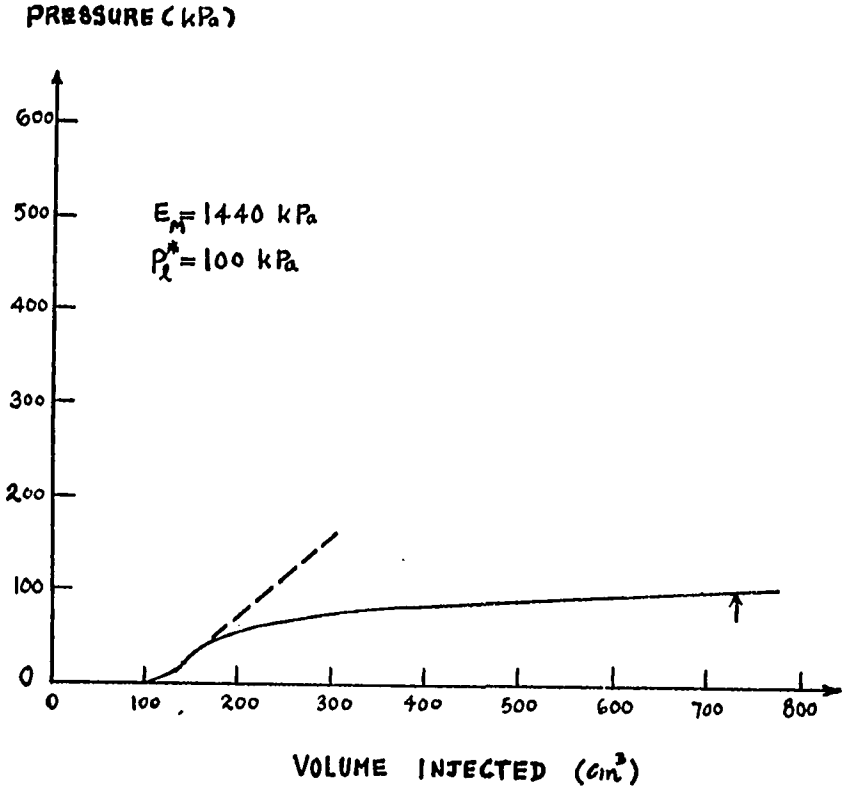

Fig. 146 - Test No. 11. Sand Box. Menard GA Pressuremeter Test. Buried Probe. I_D = 63%. Depth = 0.65 m.

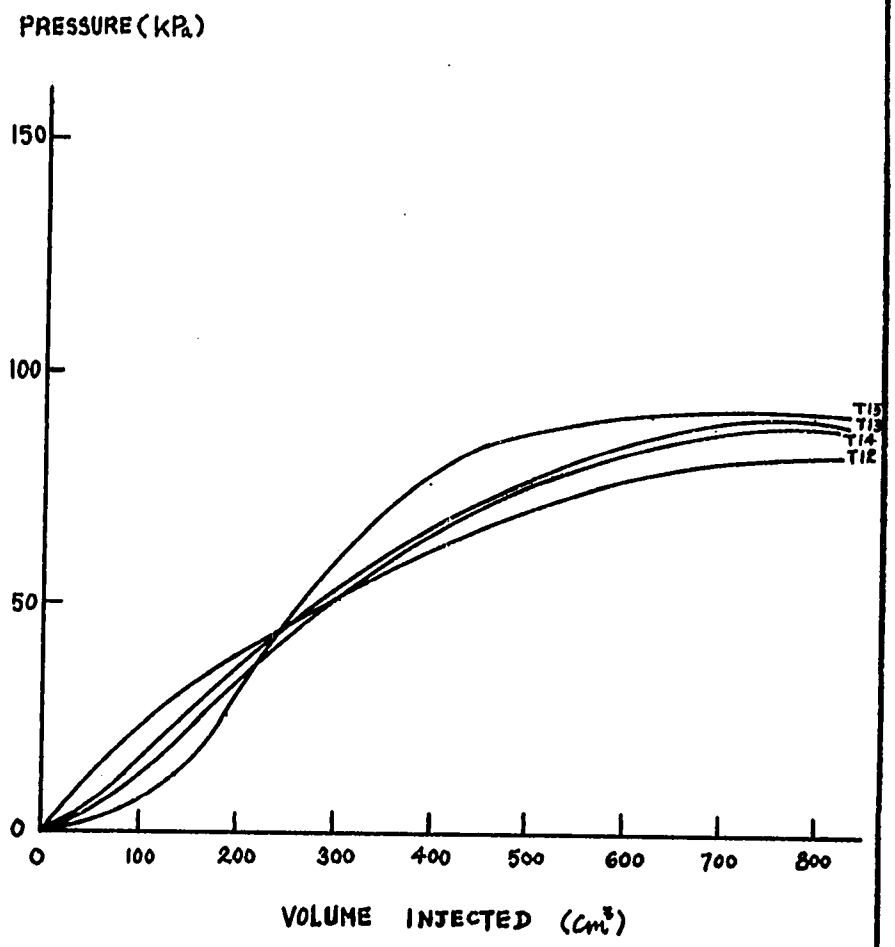

Fig. 147 - Test Nos. 12,13,14,15. Sand Box. Menard GA Pressuremeter. Calibration of Membrane Resistance (4 different probes).

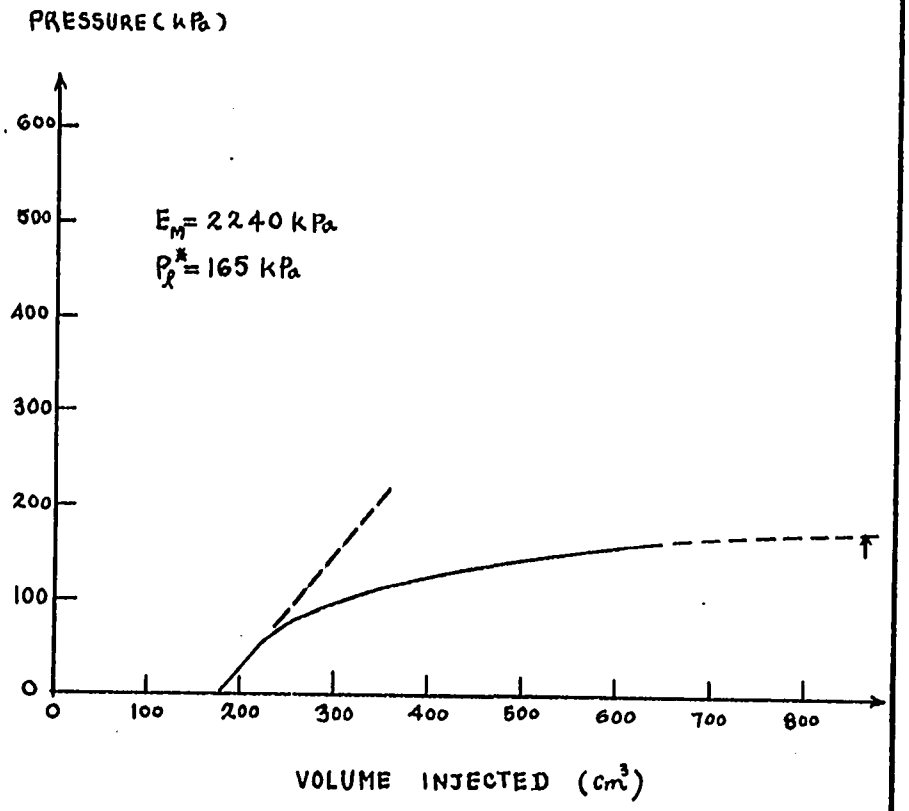

Fig.148 - Test No. 16. Sand Box. Menard GA Pressuremeter Test. Buried Probe. I_D = 59%. Depth = 1.22 m.

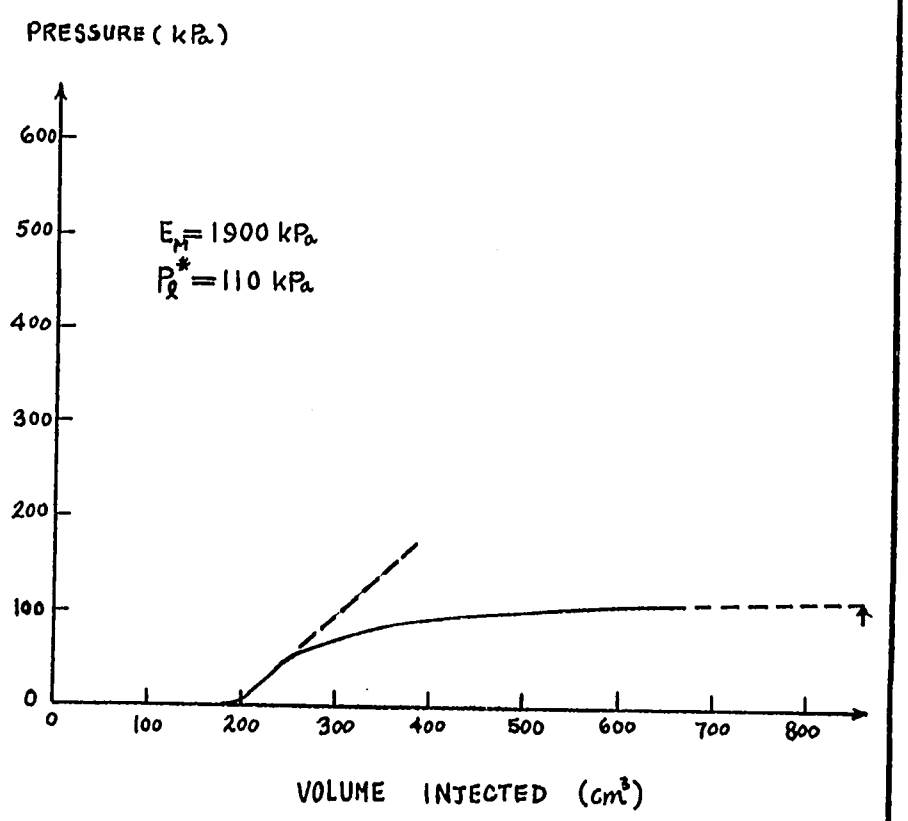

Fig. 149 - Test No. 17. Sand Box. Menard GA Pressuremeter Test. Buried Probe. I_D = 53%. Depth = 0.92 m.

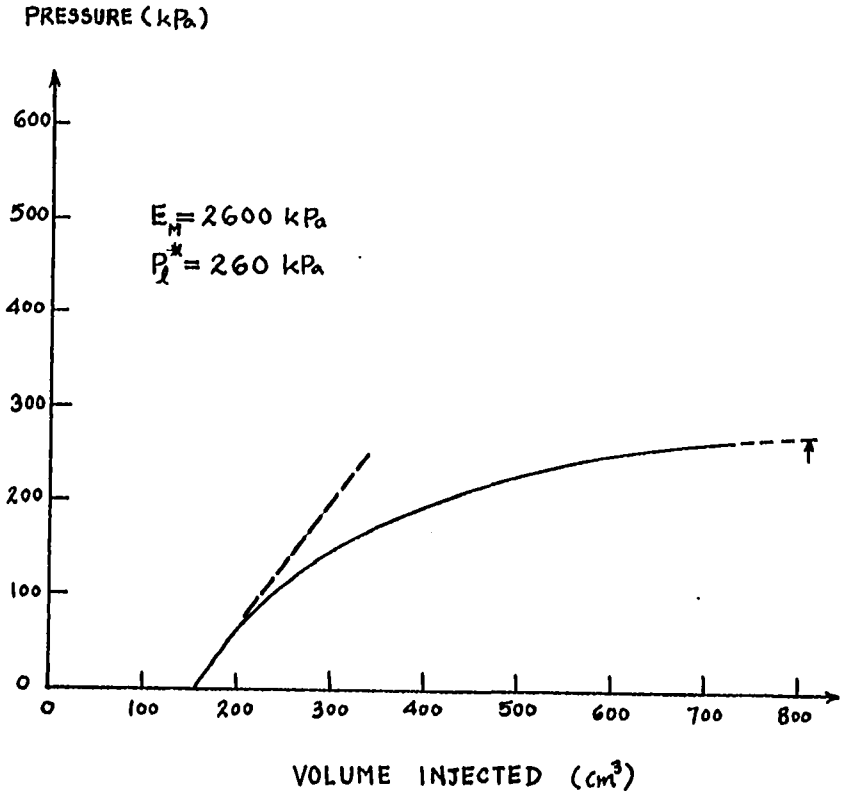

Fig. 150 - Test No. 18. Sand Box. Menard GA Pressuremeter Test. Buried Probe. I_D = 66%. Depth = 1.89 m.

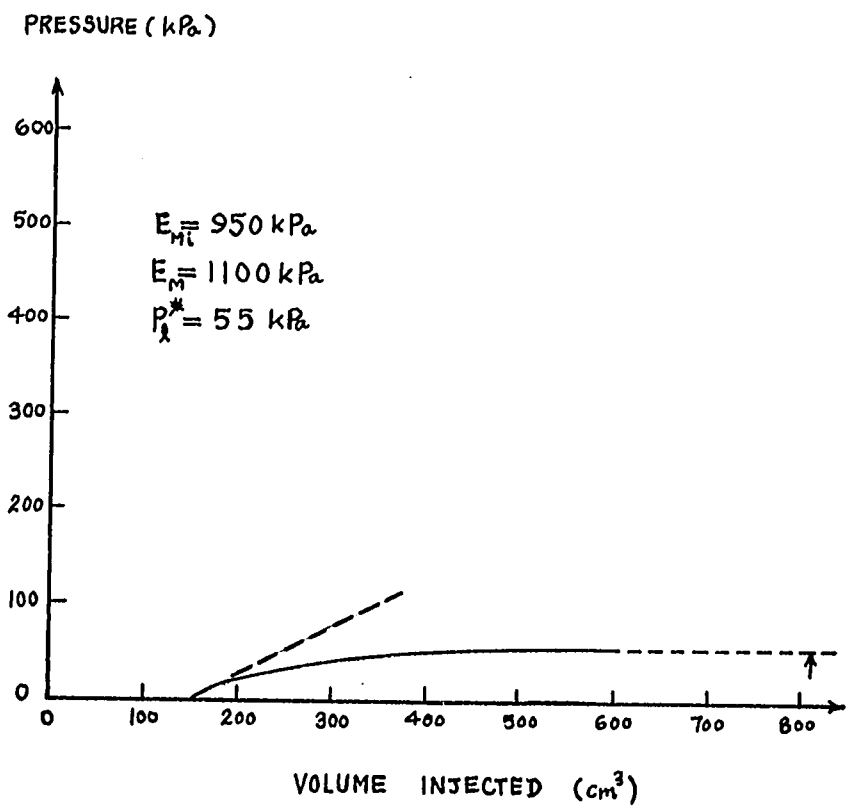

Fig. 151 - Test No. 19. Sand Box. Menard GA Pressuremeter Test. Buried Probe. I_D = 50%. Depth = 0.32 m.

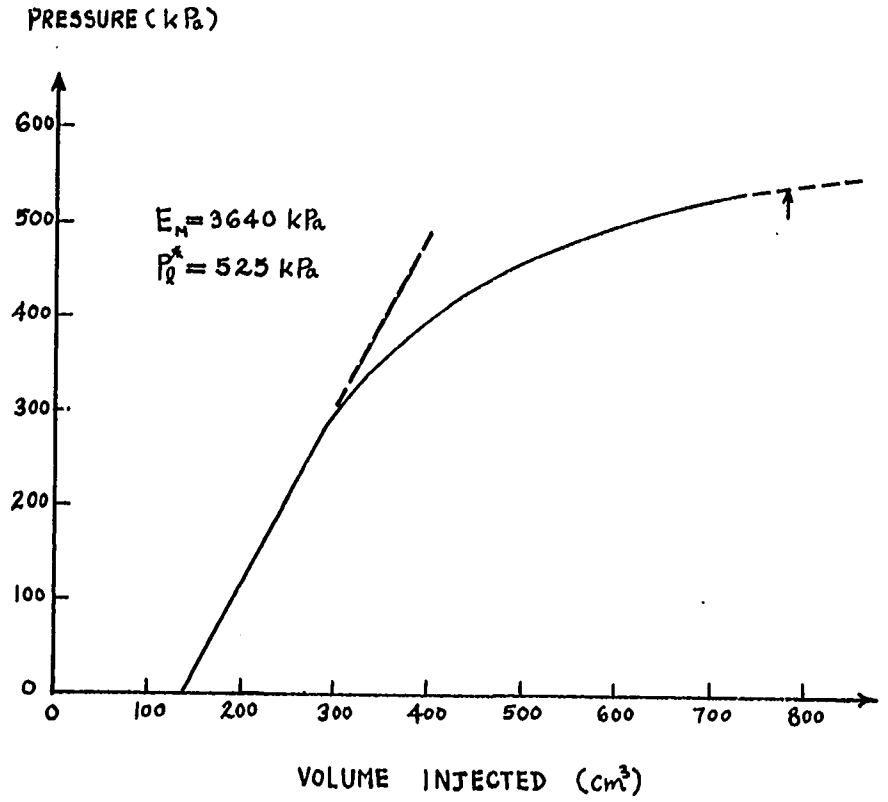

Fig. 152 - Test No. 20. Sand Box. Menard GA Pressuremeter Test. Buried Probe. I_D = 93%. Depth = 1.53 m.

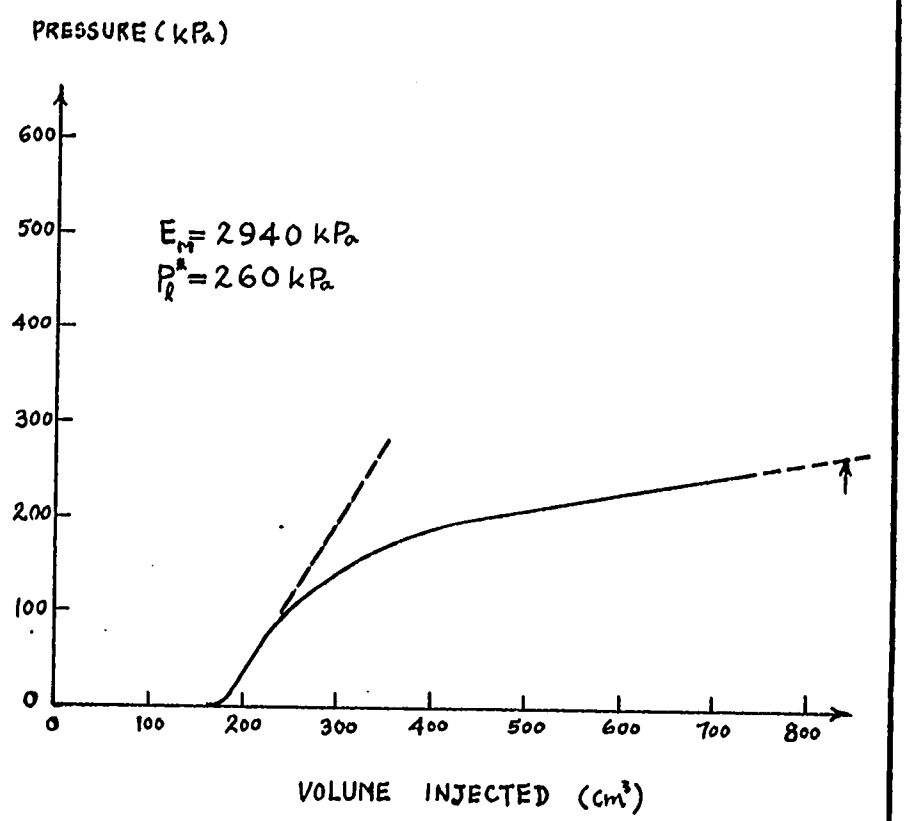

Fig. 153 - Test No. 21. Sand Box. Menard GA Pressuremeter Test. Buried Probe. I_D = 94%. Depth = 0.61 m.

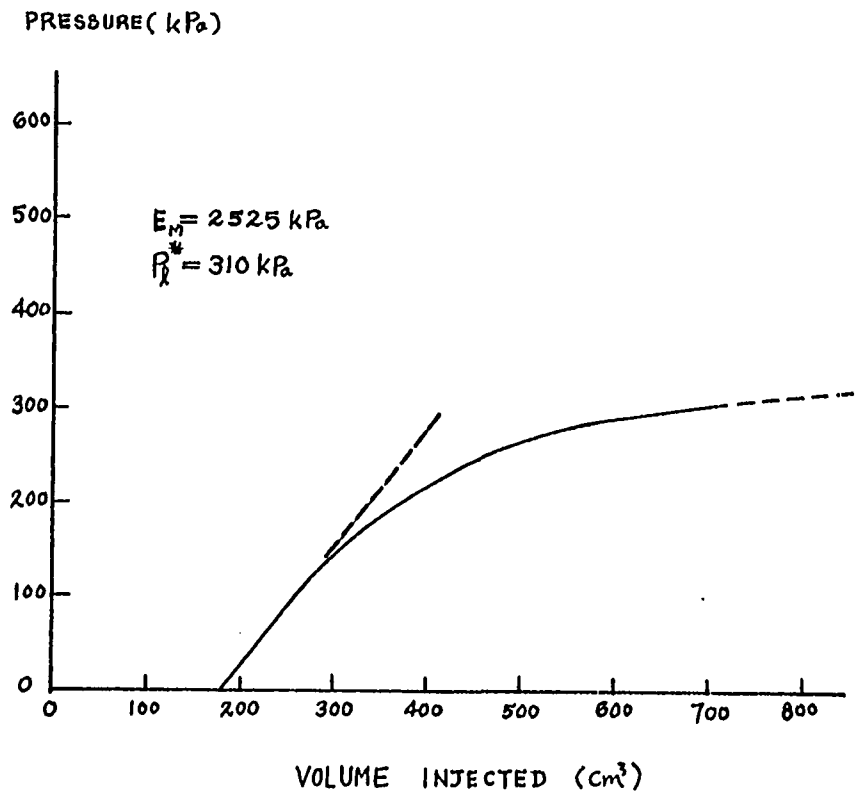

Fig. 154 - Test No. 22. Sand Box. Menard GA Pressuremeter Test. Buried Probe. I_D = 94%. Depth = 0.91 m.

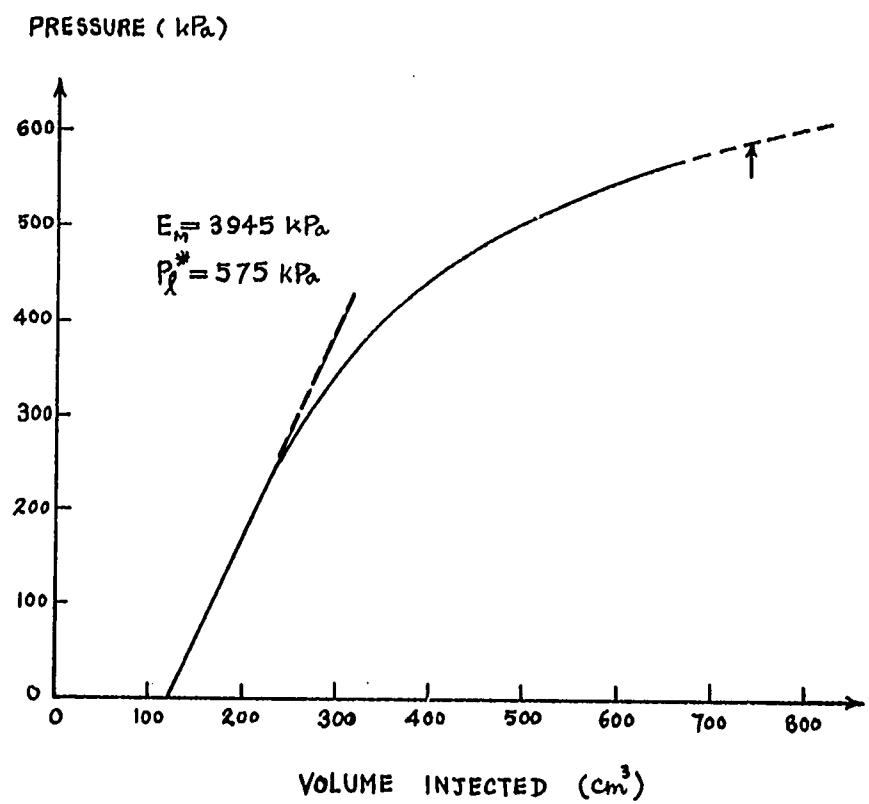

Fig. 155 - Test No. 23. Sand Box. Menard GA Pressuremeter Test. Buried Probe. I_D = 93%. Depth = 1.83 m.

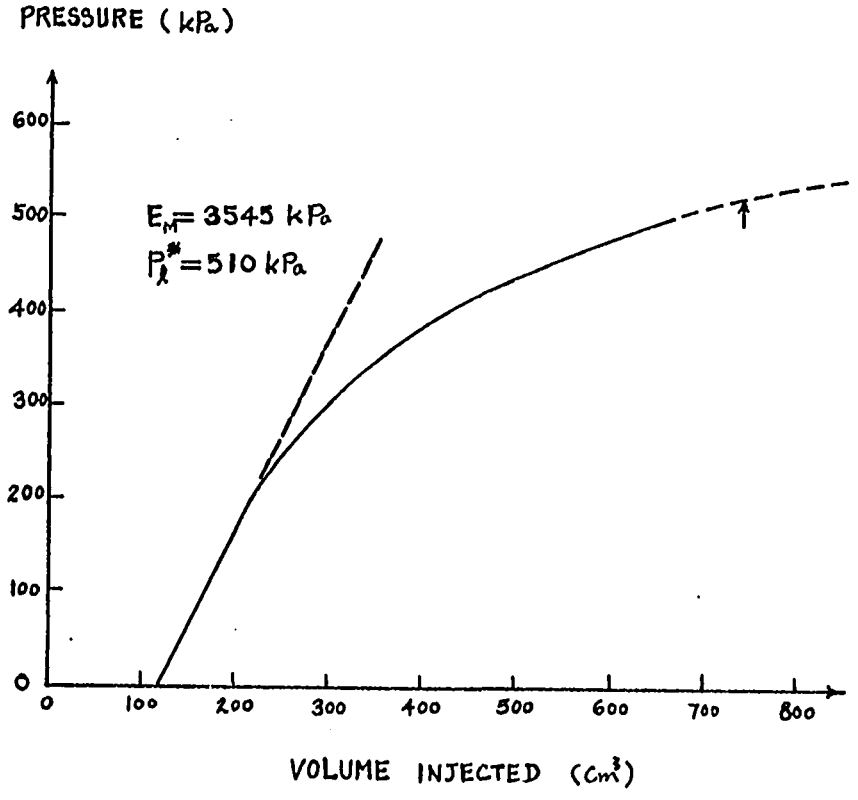

Fig. 156 - Test No. 24. Sand Box. Menard GA Pressuremeter Test. Buried Probe. I_D = 95%. Depth = 1.22 m.

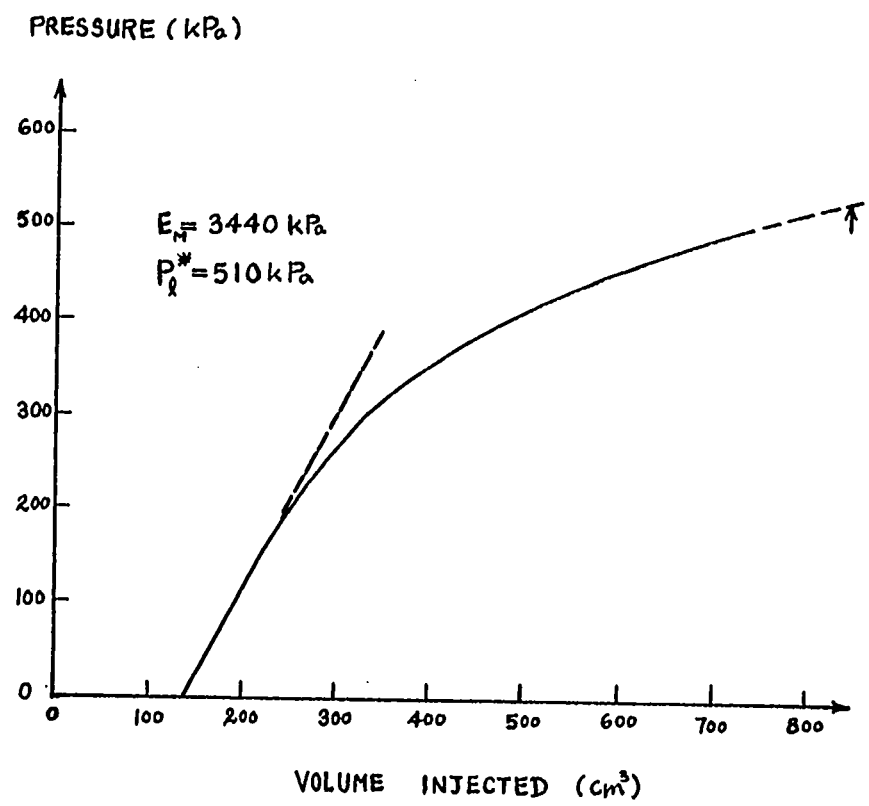

Fig. 157 - Test No. 25. Sand Box. Menard GA Pressuremeter Test. Buried Probe. I_D = 95%. Depth = 1.22 m.

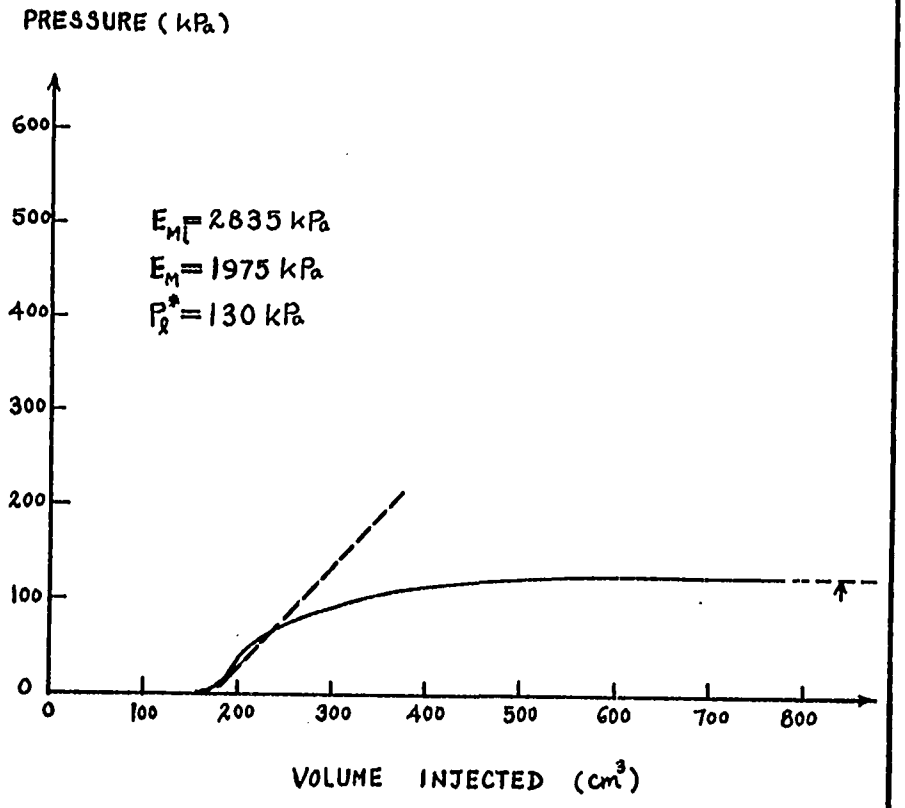

Fig. 158 - Test No. 26. Sand Box. Menard GA Pressuremeter Test. Buried Probe. I_D = 92%. Depth = 0.31 m.

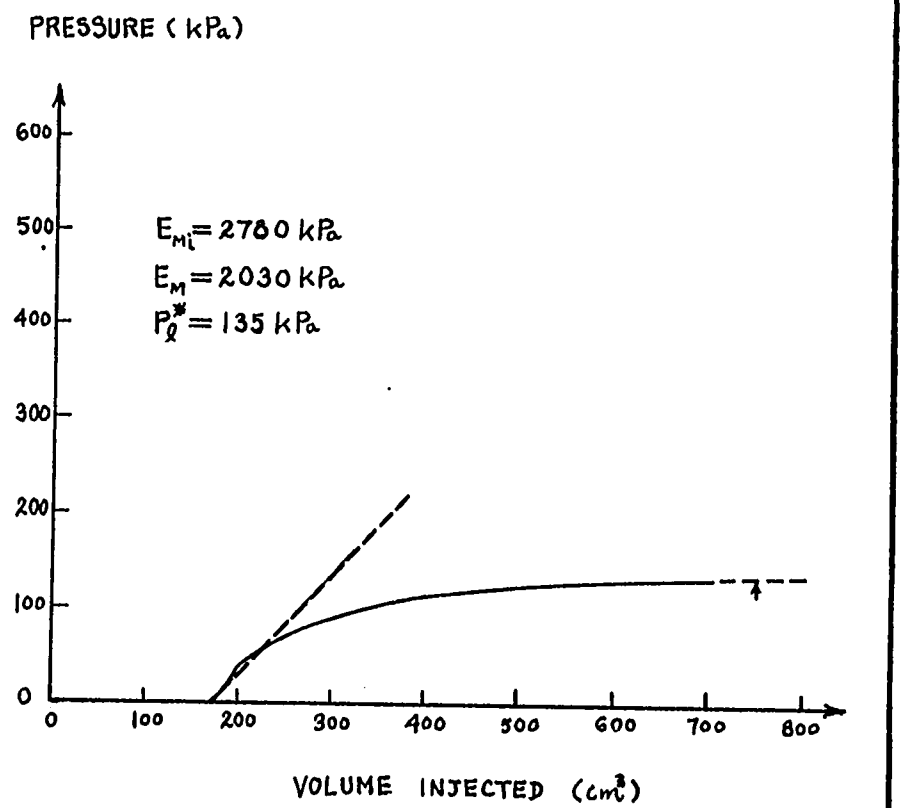

Fig. 159 - Test No. 27. Sand Box. Menard GA Pressuremeter Test. Buried Probe. I_D = 92%. Depth = 0.31 m.

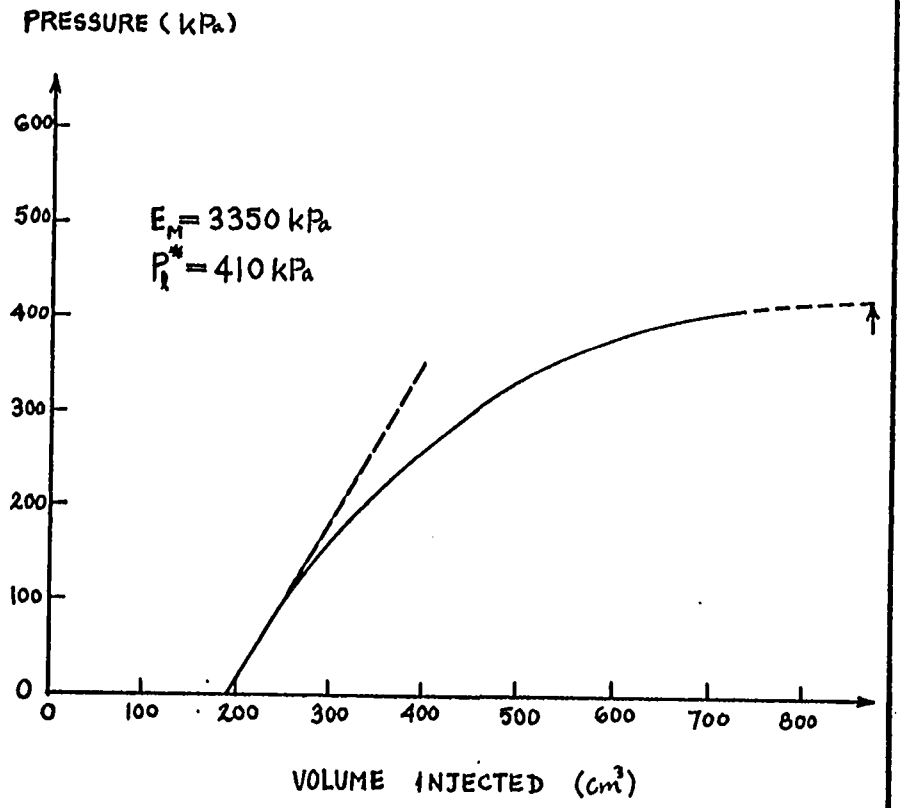

Fig. 160 - Test No. 28. Sand Box. Menard GA Pressuremeter Test. Buried Probe. I_D = 95%. Depth = 0.91 m.

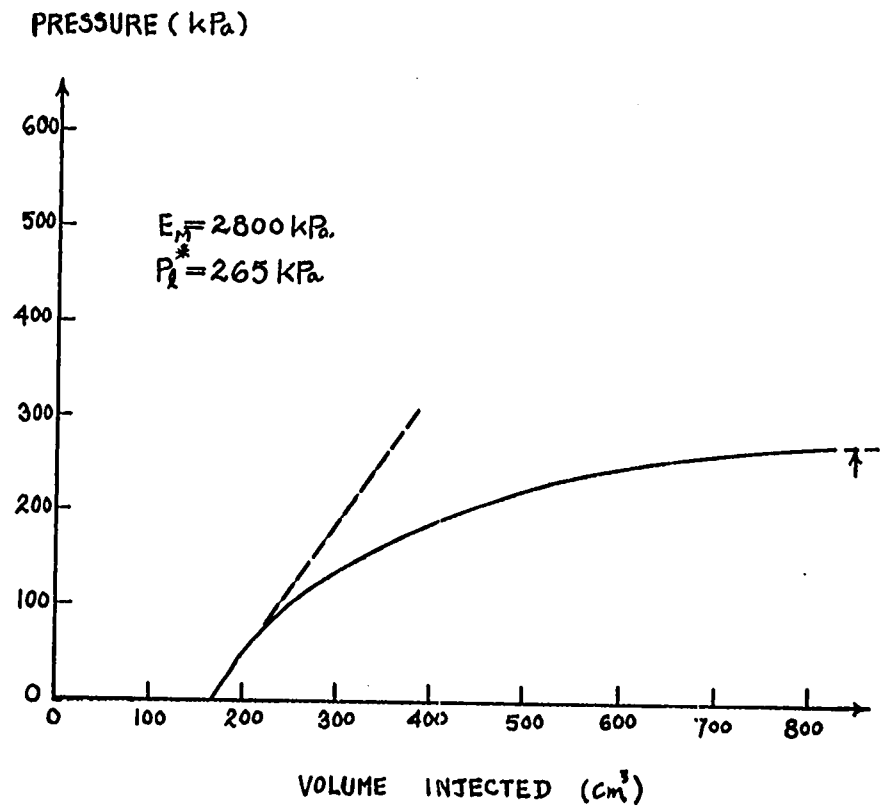

Fig. 161 - Test No. 29. Sand Box. Menard GA Pressuremeter Test. Buried Probe. I_D = 64%. Depth = 1.27 m.

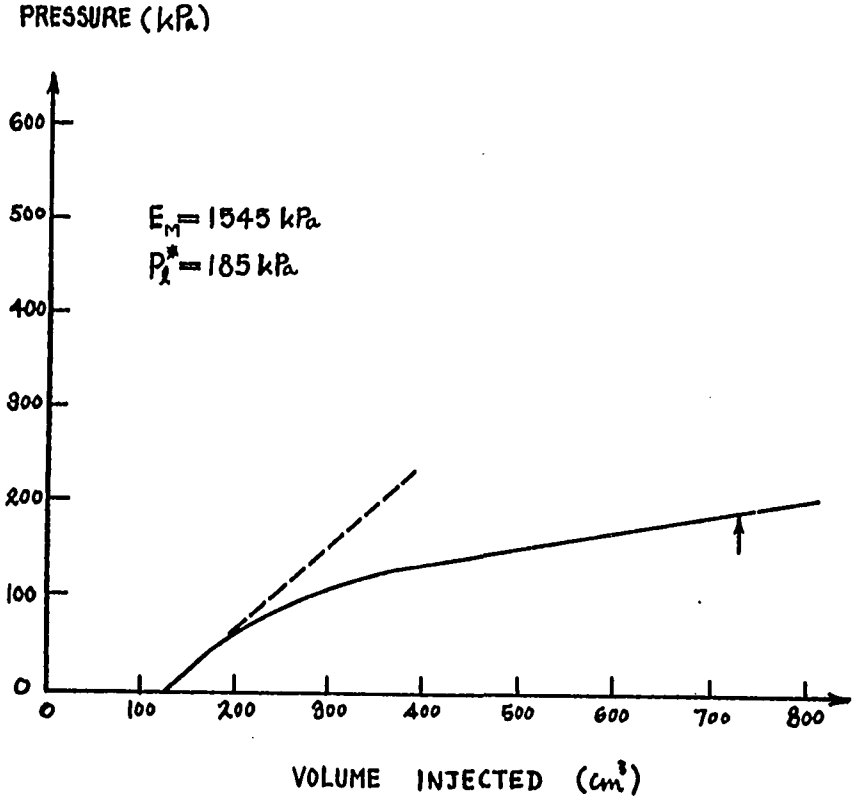

Fig. 162 - Test No. 30. Sand Box. Menard GA Pressuremeter Test. Buried Probe. I_D = 64%. Depth = 0.94 m.

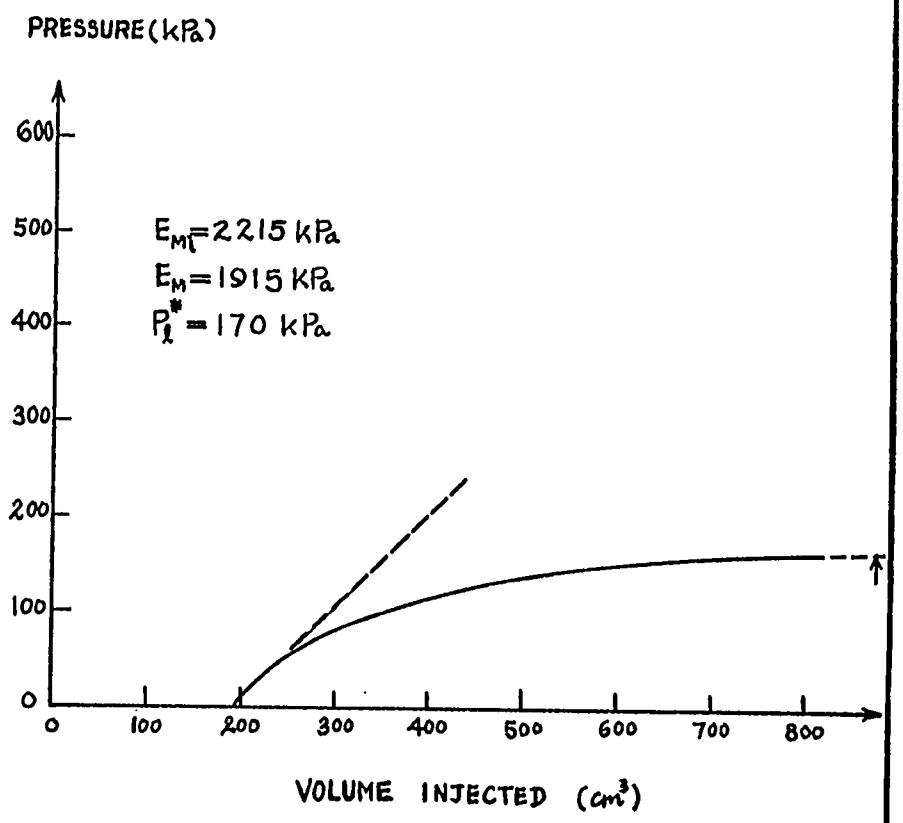

Fig. 163 - Test No. 31. Sand Box. Menard GA Pressuremeter Test. Buried Probe. I_D = 74%. Depth = 0.61 m.

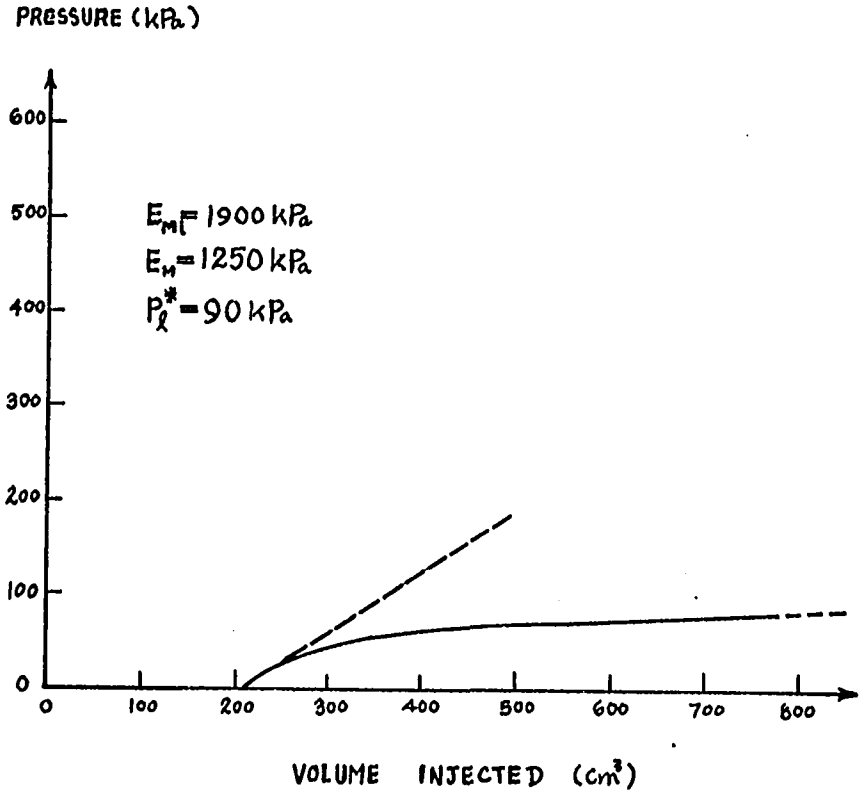

Fig. 164 – Test No. 32. Sand Box. Menard GA Pressuremeter Test. Buried Probe. I_D = 69%. Depth = 0.30 m.

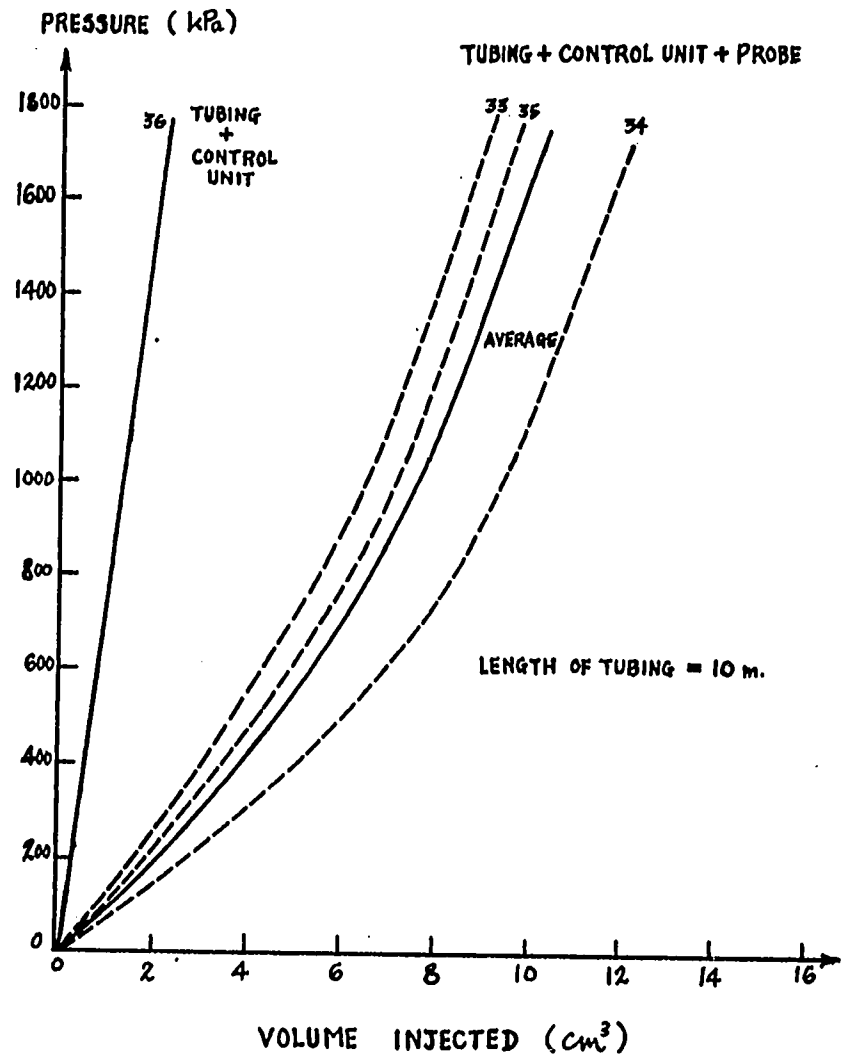

Fig. 165 – Test Nos. 33, 34, 35, 36. Sand Box. Briaud Pressuremeter. Calibration of Volume Losses.

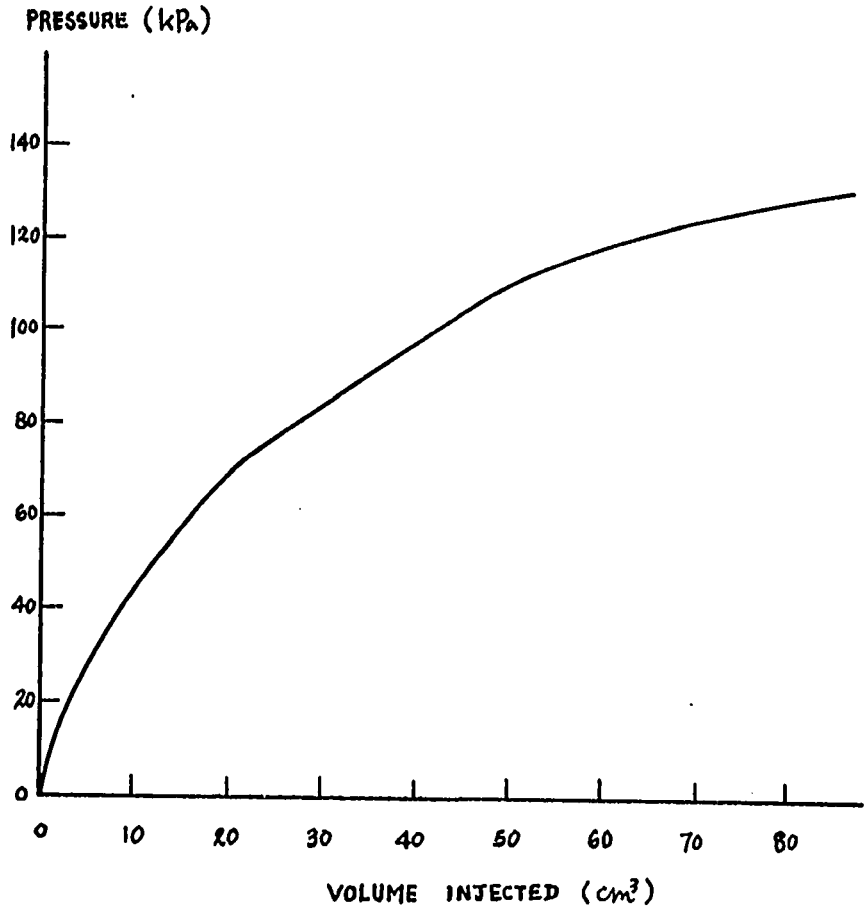

Fig.166 - Test No. 37 - Sand Box. Briaud Pressuremeter. Calibration of Membrane Resistance.

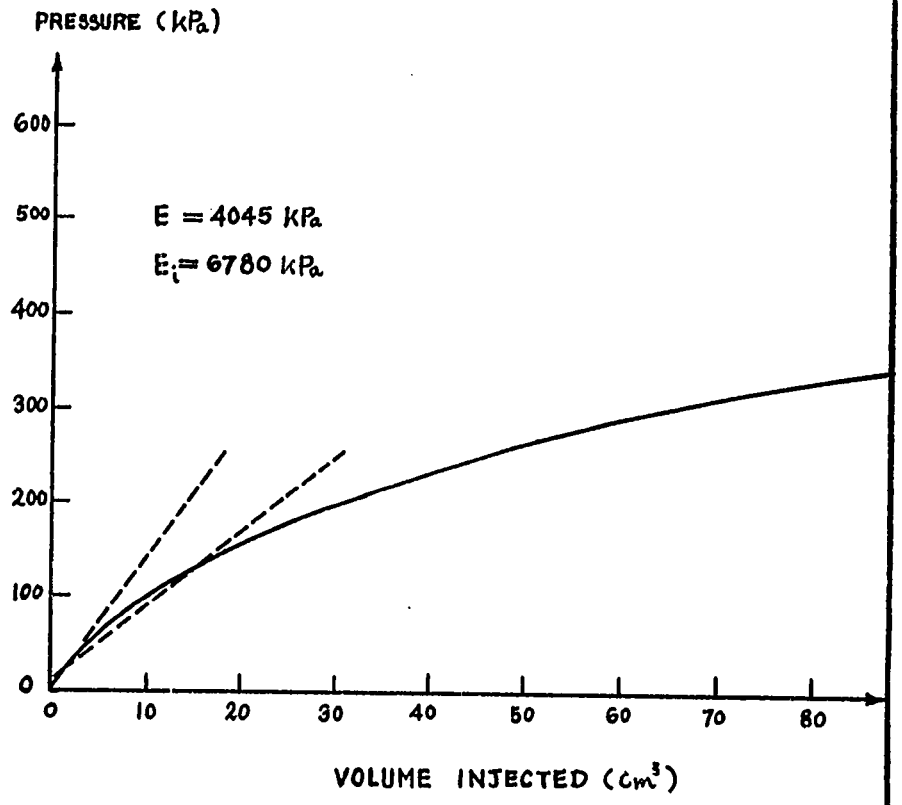

Fig.167 - Test No. 46 - Sand Box. Briaud Pressuremeter Test. Buried Probe. I_D = 65%. Depth = 1.83 m

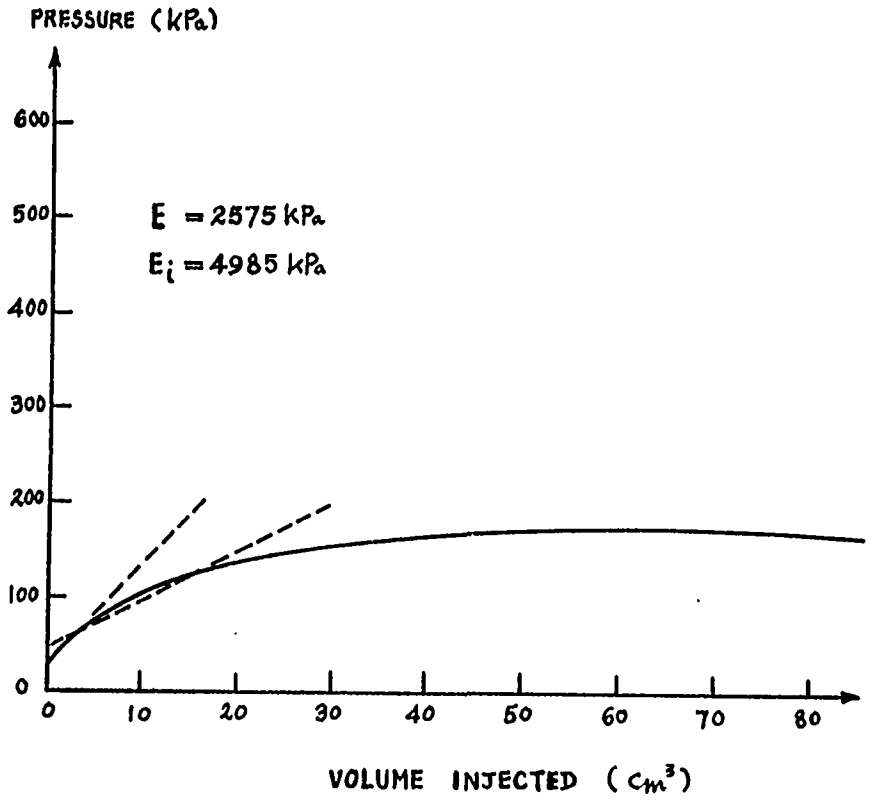

Fig.168 - Test No. 47 - Sand Box. Briaud Pressuremeter Test. Driven Probe. I_D = 65%. Depth = 0.30 m.

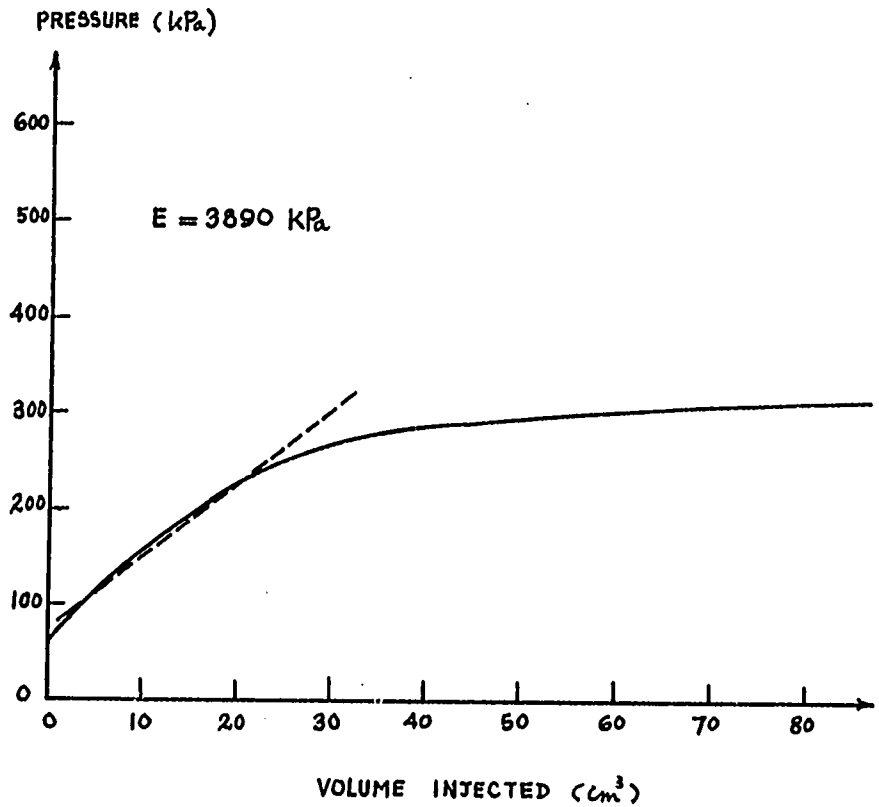

Fig. 169 - Test No. 48 - Sand Box. Briaud Pressuremeter Test. Driven Probe. I_D = 70%. Depth = 0.61 m.

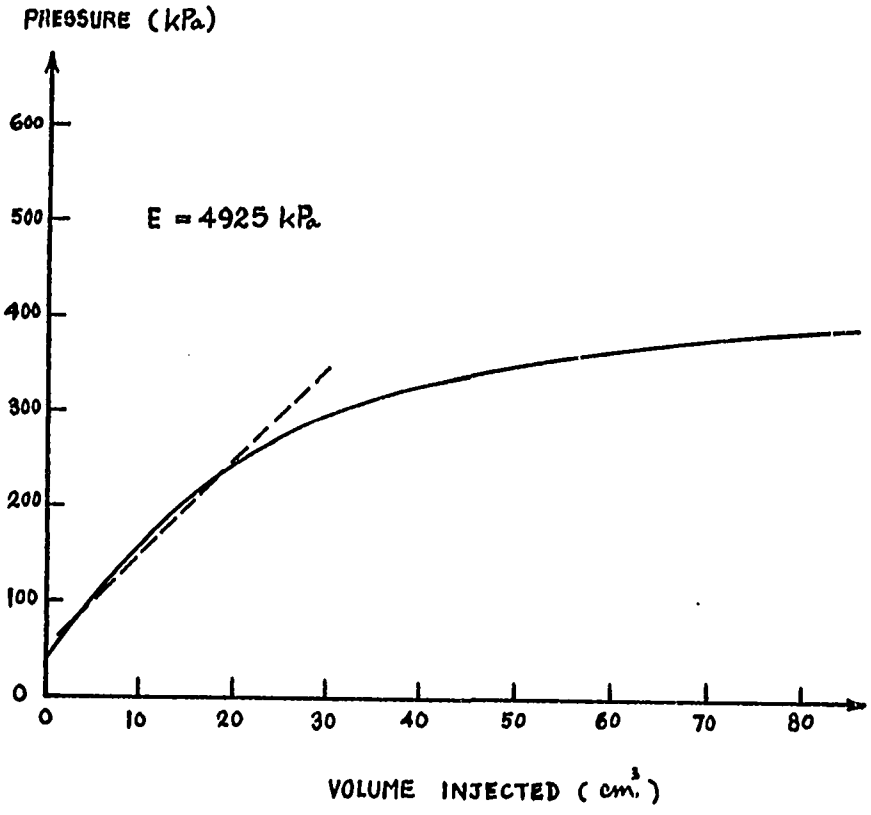

Fig.170 - Test No. 49 - Sand Box. Briaud Pressuremeter Test. Driven Probe. I_D = 70%. Depth = 0.91 m.

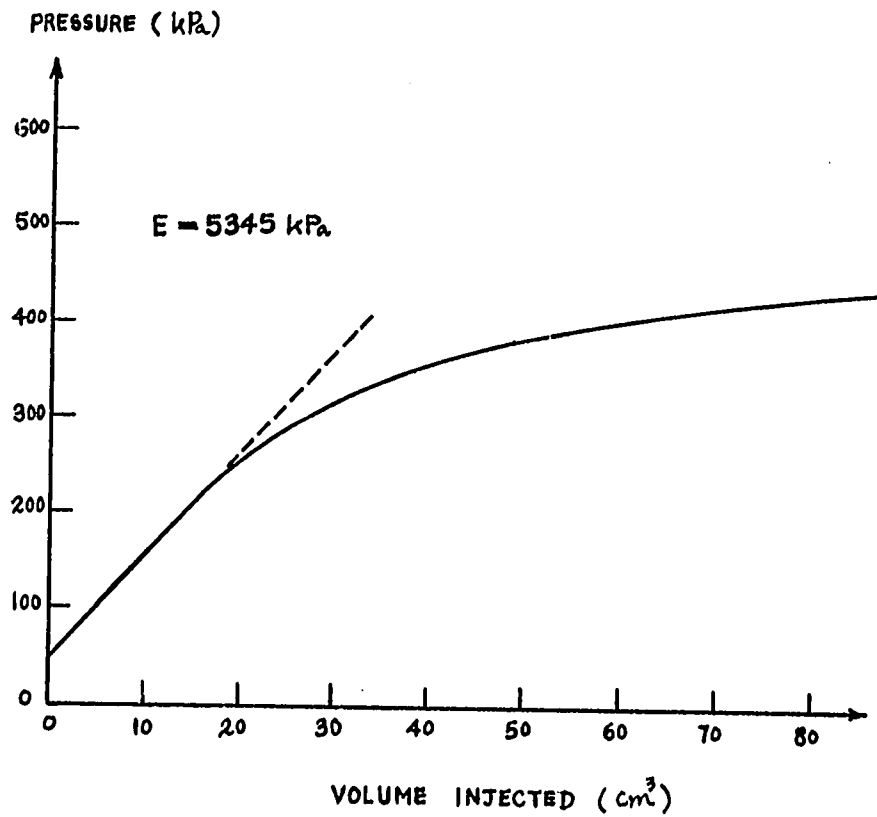

Fig.171 - Test No. 50 - Sand Box. Briaud Pressuremeter Test. Driven Probe. I_D = 70%. Depth = 1.22 m.

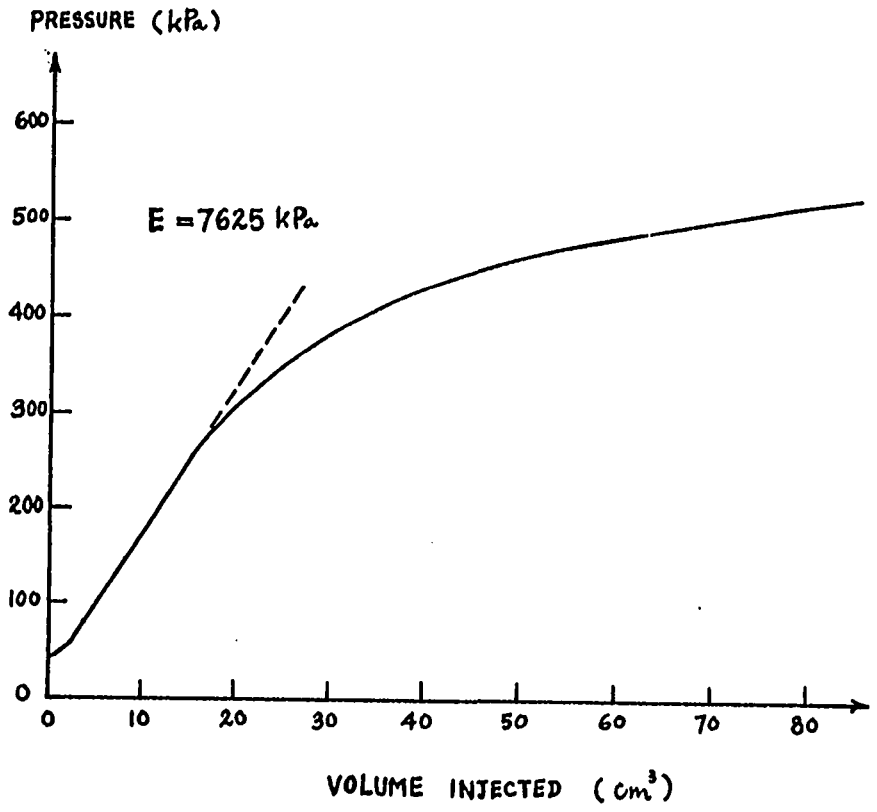

Fig. 172 - Test No. 51 - Sand Box. Briaud Pressuremeter Test. Driven Probe. I_D = 70%. Depth = 1.52 m.

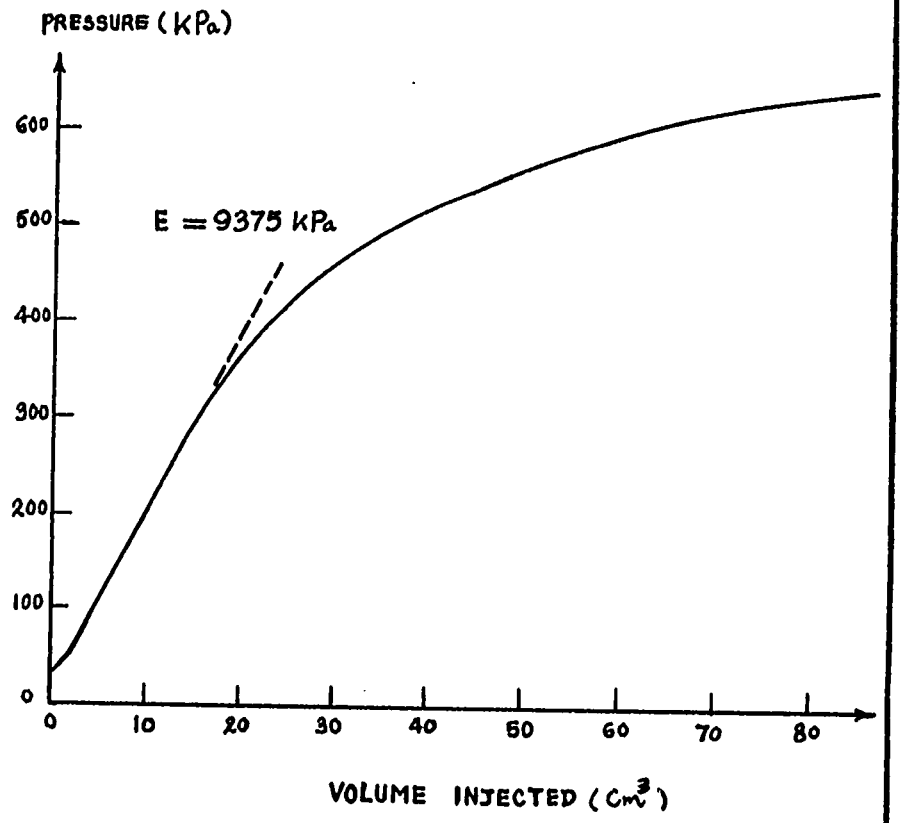

Fig. 173 - Test No. 52 - Sand Box. Briaud Pressuremeter Test. Driven Probe. I_D = 70%. Depth = 1.83 m.

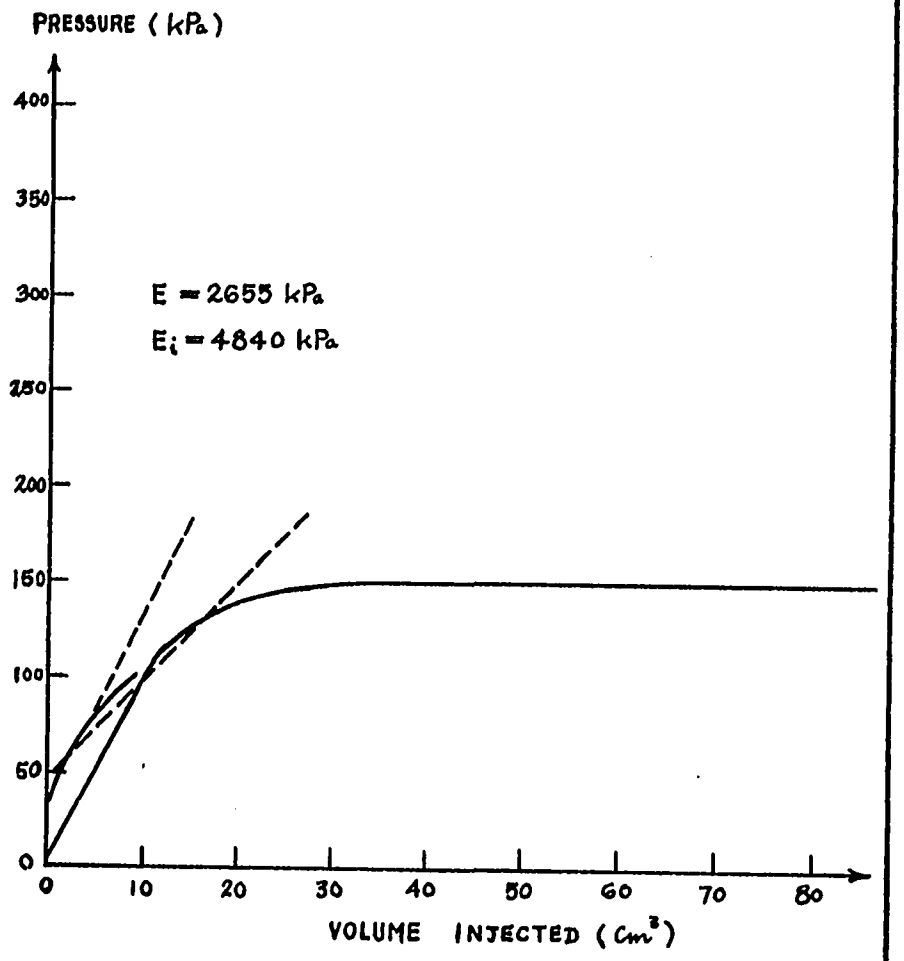

Fig.174 - Test No. 53 - Sand Box. Briaud Pressuremeter Test. Driven Probe. I_D = 70%. Depth = 0.3 m.

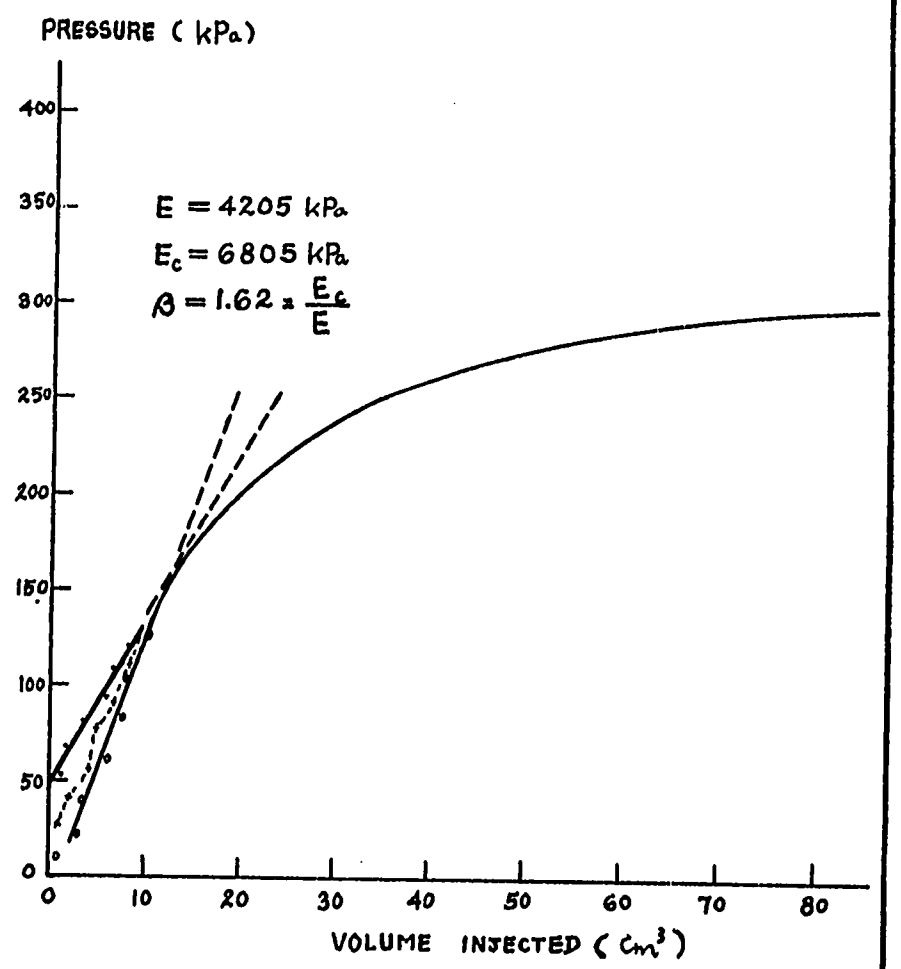

Fig.175 - Test No. 54 - Sand Box. Briaud Pressuremeter Test. Driven Probe. I_D = 70%. Depth = 0.61 m.

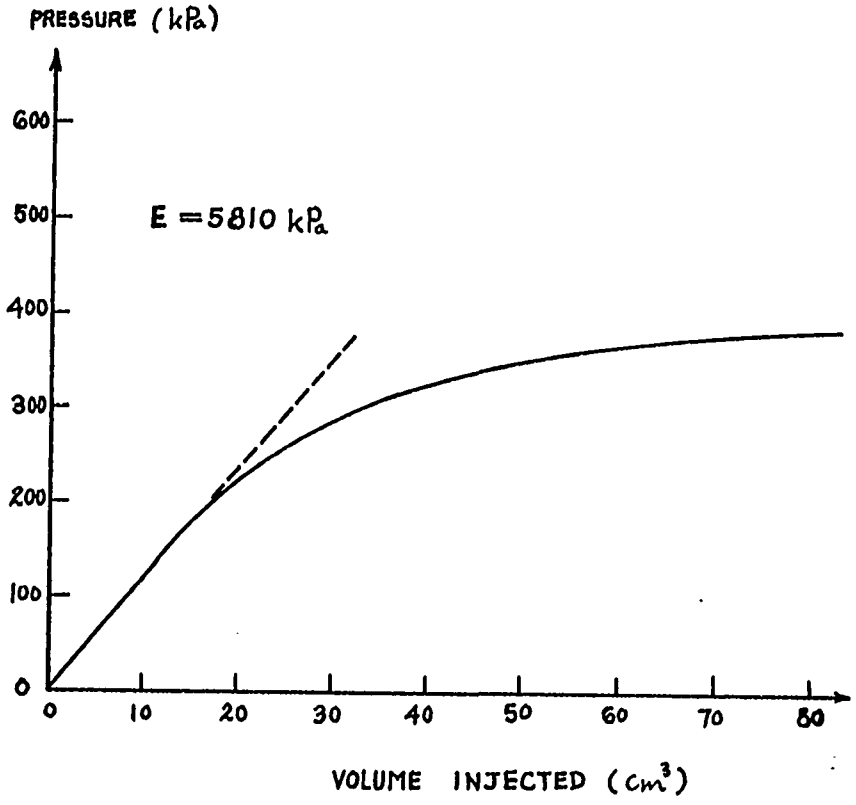

Fig.176 - Test No. 55 - Sand Box. Briaud Pressuremeter Test. Driven Probe. I_D = 70%. Depth = 0.91 m.

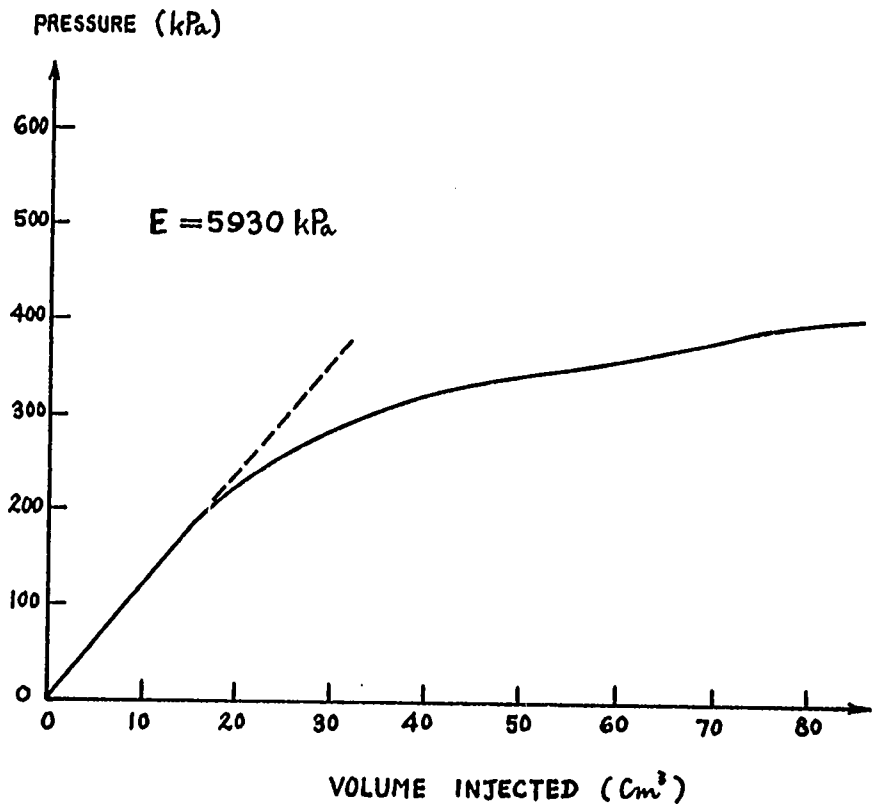

Fig.177 - Test No. 56 - Sand Box. Briaud Pressuremeter Test. Driven Probe. I_D = 70%. Depth = 1.22 m.

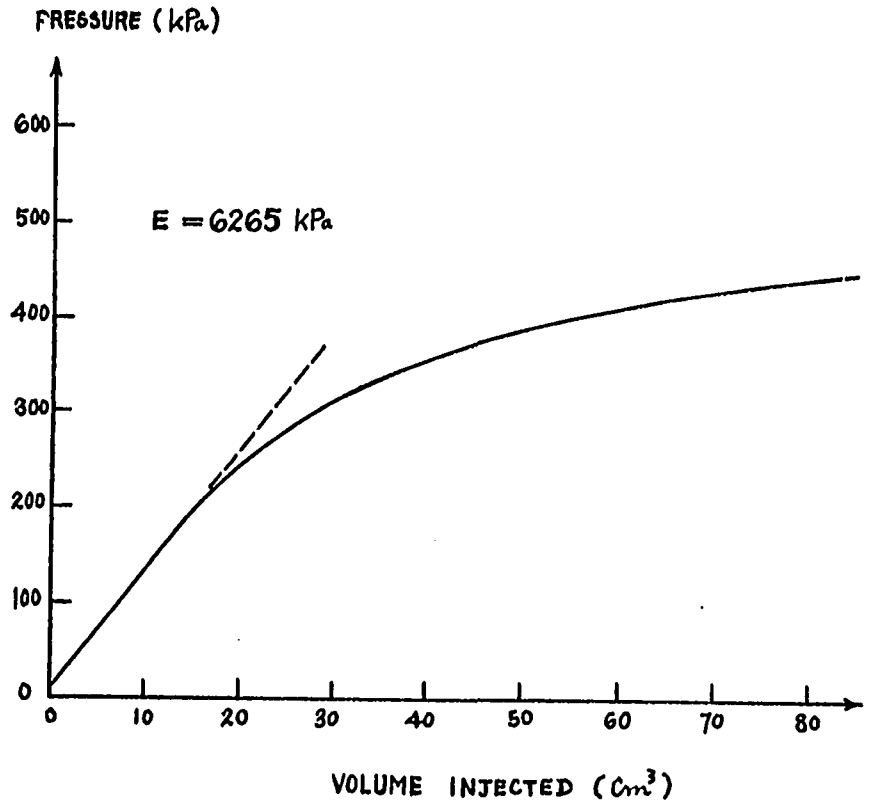

Fig. 178 - Test No. 57 - Sand Box. Briaud Pressuremeter Test. Driven Probe. I_D = 70%. Depth = 1.52 m.

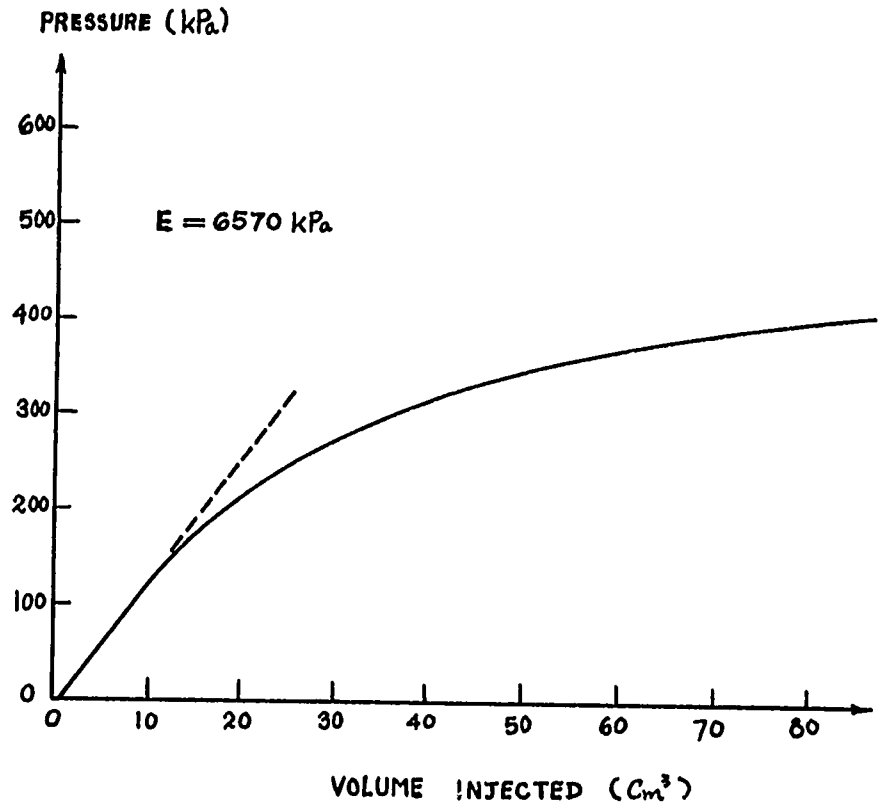

Fig. 179 - Test No. 58 - Sand Box. Briaud Pressuremeter Test. Driven Probe. I_D = 70%. Depth = 1.83 m.

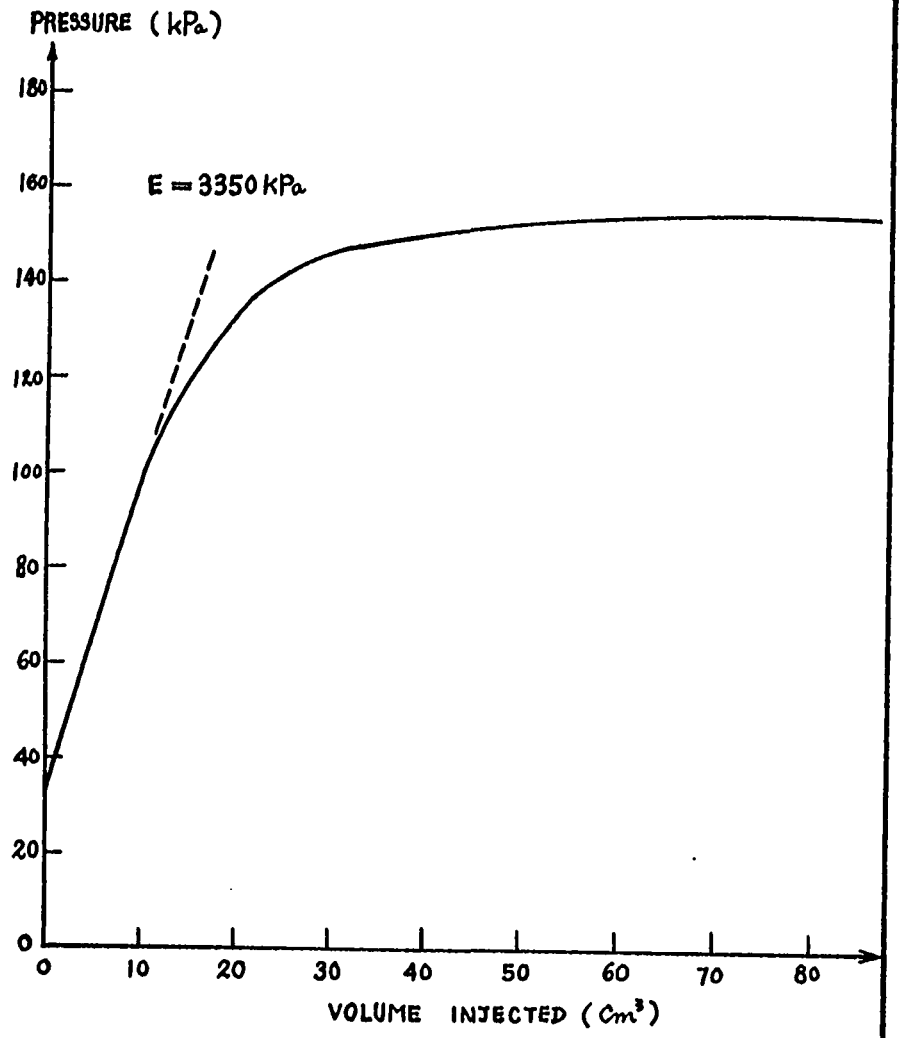

Fig.180 - Test No. 59 - Sand Box. Briaud Pressuremeter Test. Driven Probe. I_D = 70%. Depth = 0.3 m.

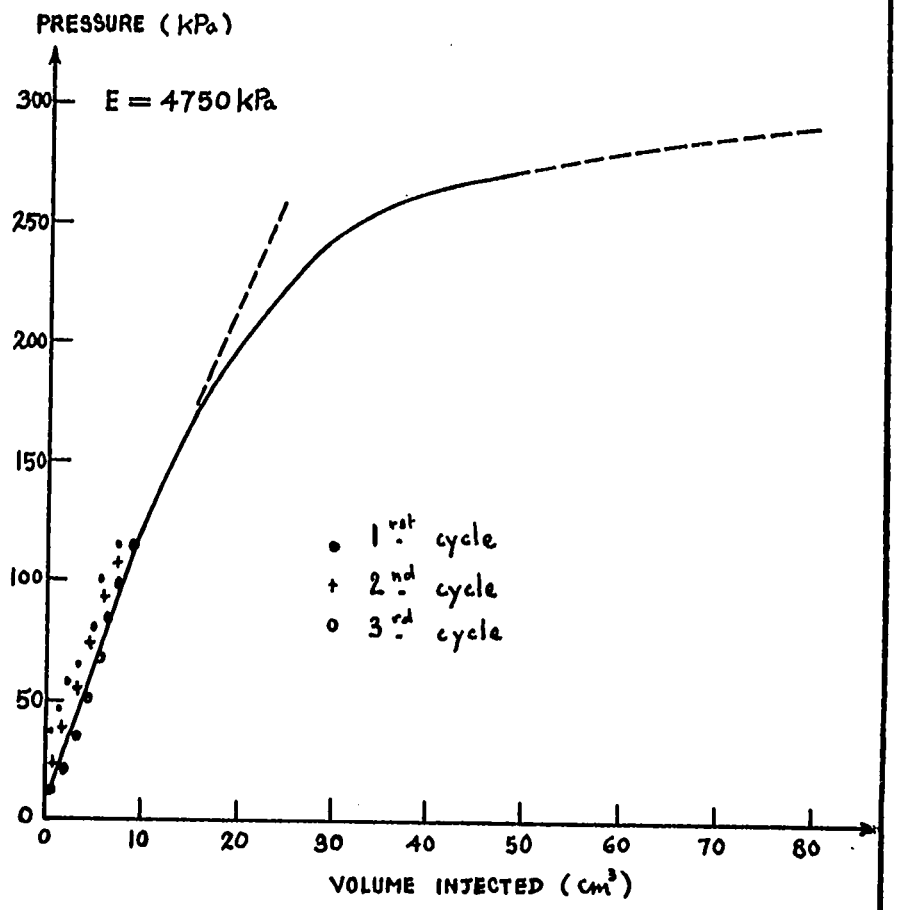

Fig.181 - Test No. 60 - Sand Box. Briaud Pressuremeter Test. Driven Probe. I_D = 70%. Depth = 0.61 m.

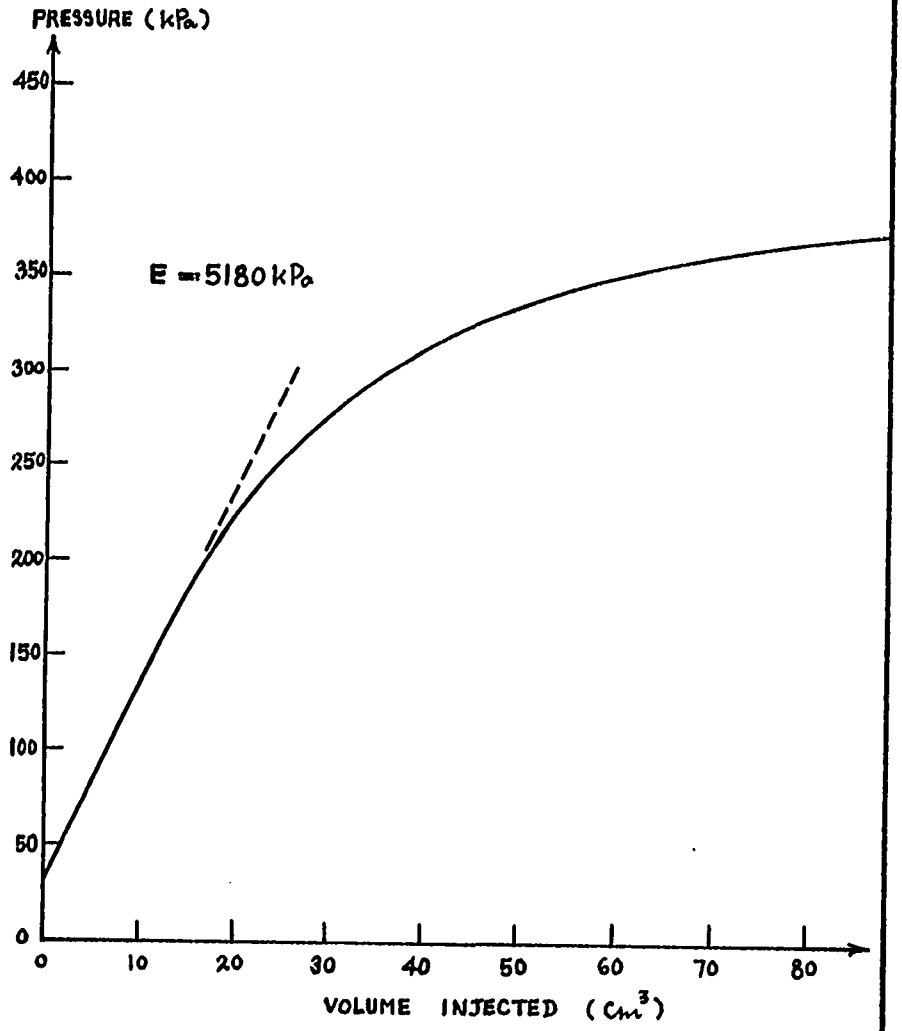

Fig. 182 - Test No. 61 - Sand Box. Briaud Pressuremeter Test. Driven Probe. I_D = 70%. Depth = 0.91 m.

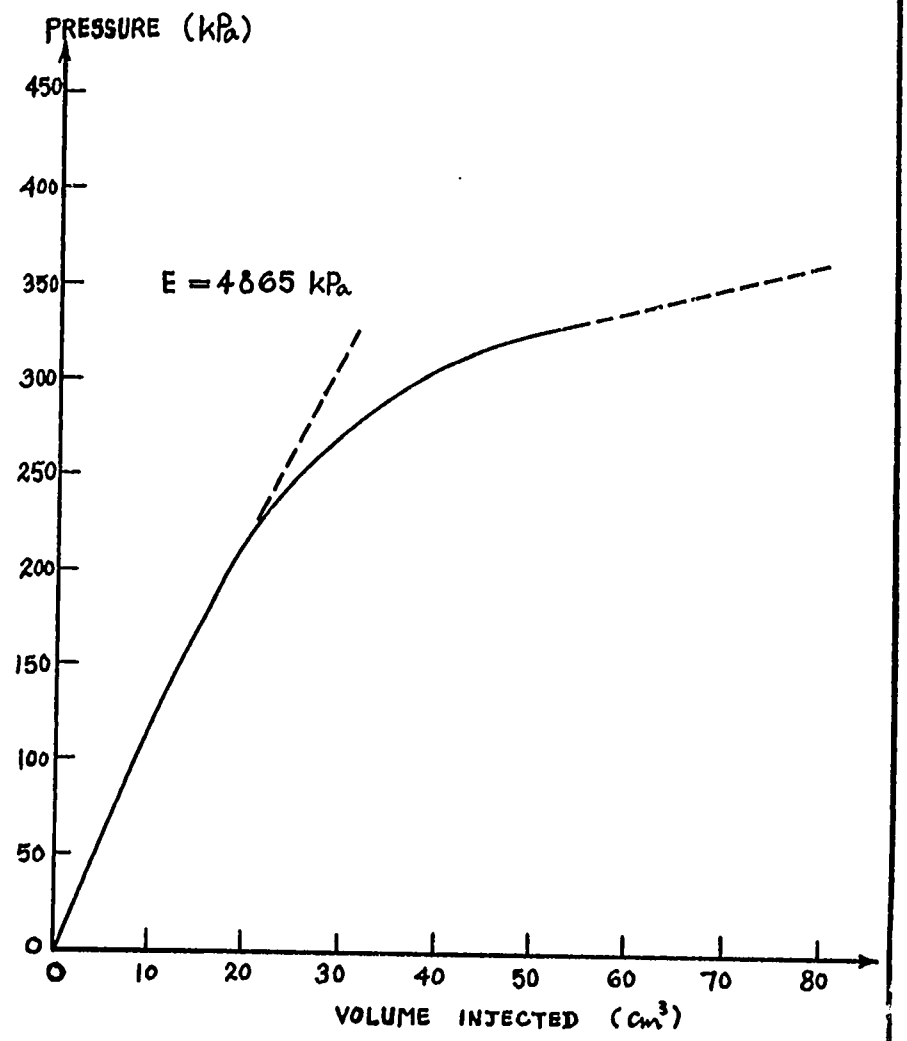

Fig. 183 - Test No. 62 - Sand Box. Briaud Pressuremeter Test. Driven Probe. I_D = 70%. Depth = 1.22 m.

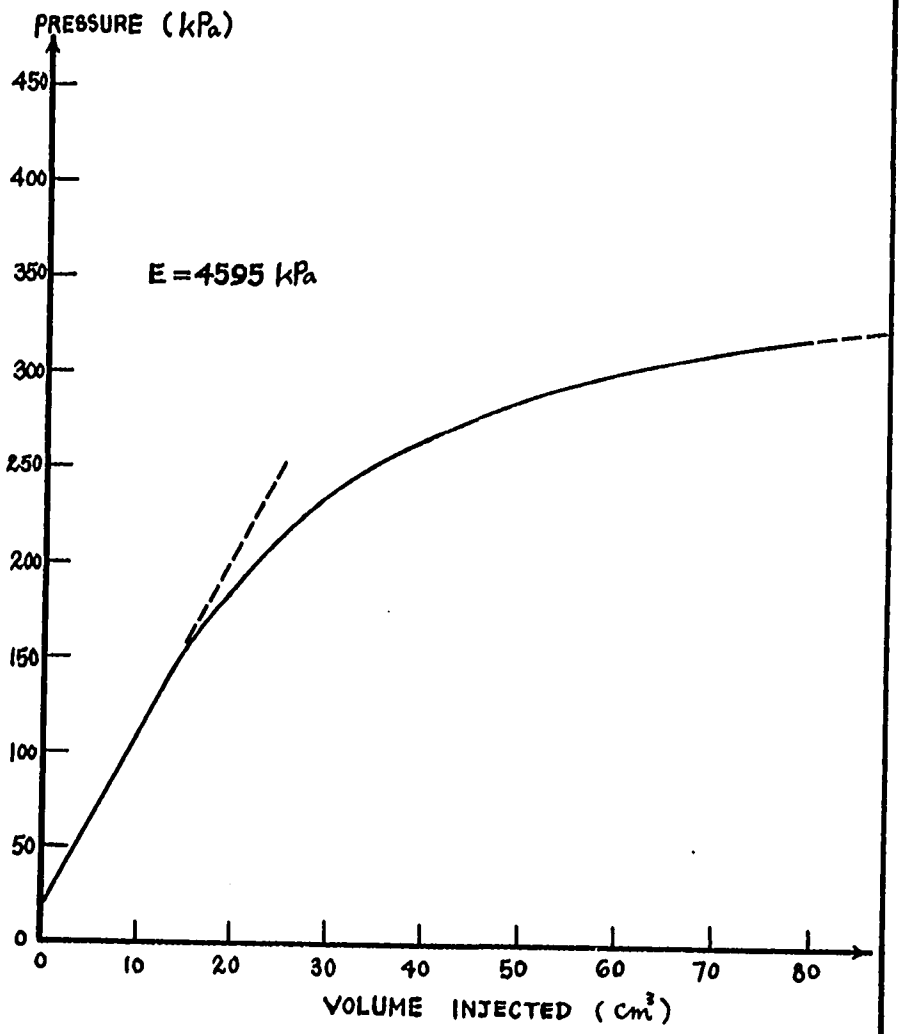

Fig. 184 – Test No. 63 – Sand Box. Briaud Pressuremeter Test. Driven Probe. I_D = 70%. Depth = 1.52 m.

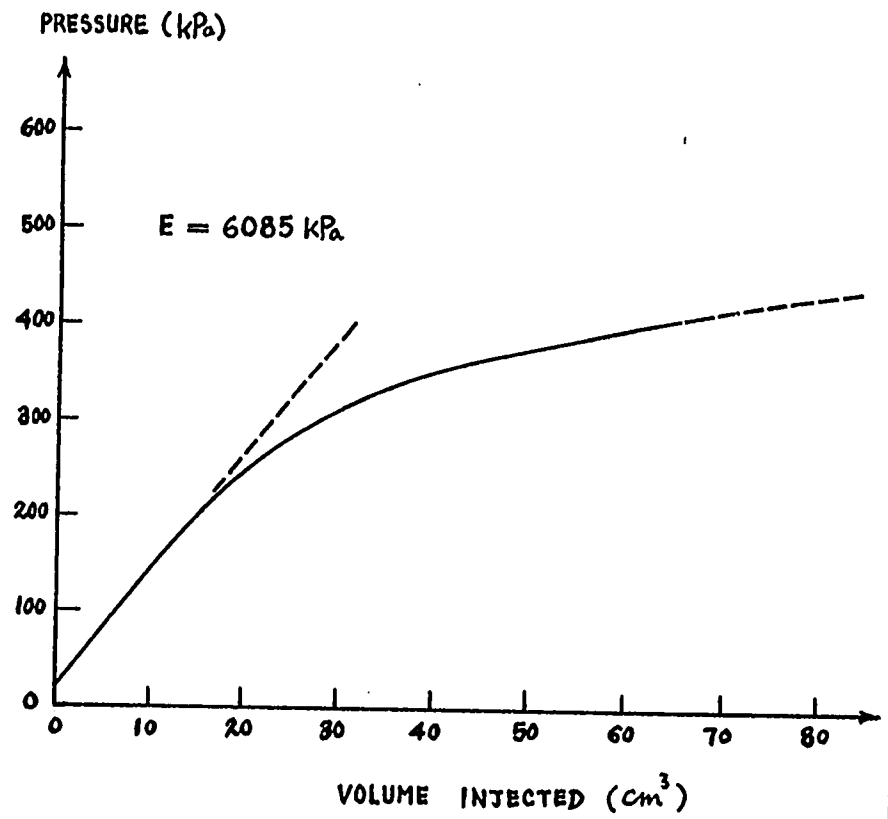

Fig. 185 – Test No. 64 – Sand Box. Briaud Pressuremeter Test. Driven Probe. I_D = 70%. Depth = 1.83 m.

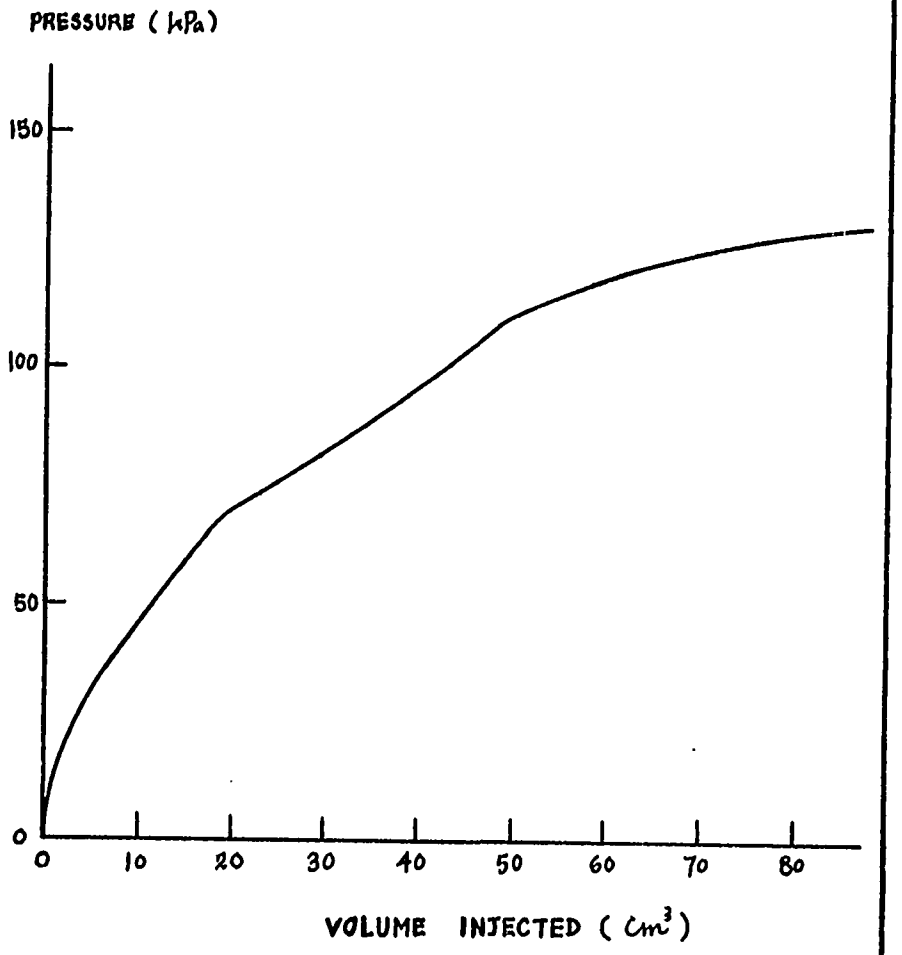

Fig. 186 - Test No. 65 - Sand Box. Briaud Pressuremeter Test. Calibration of Membrane Resistance.

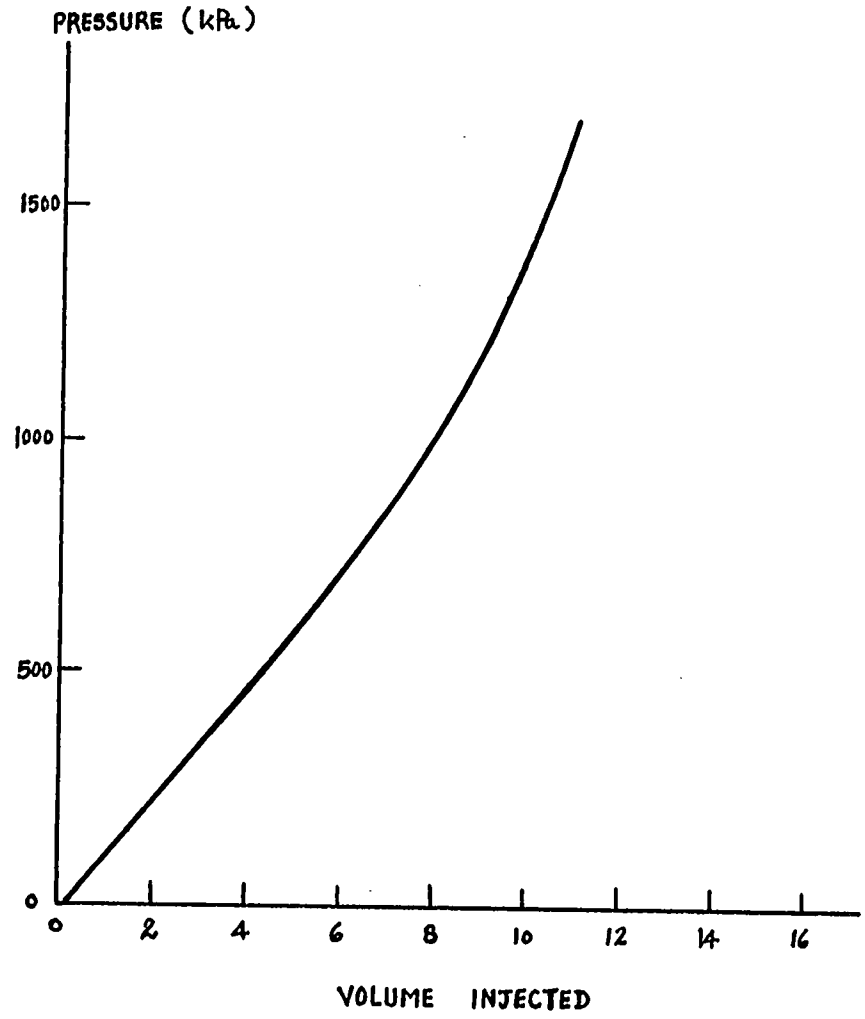

Fig. 187 - Test No. 65 - Sand Box. Briaud Pressuremeter Test. Calibration of Volume Losses.

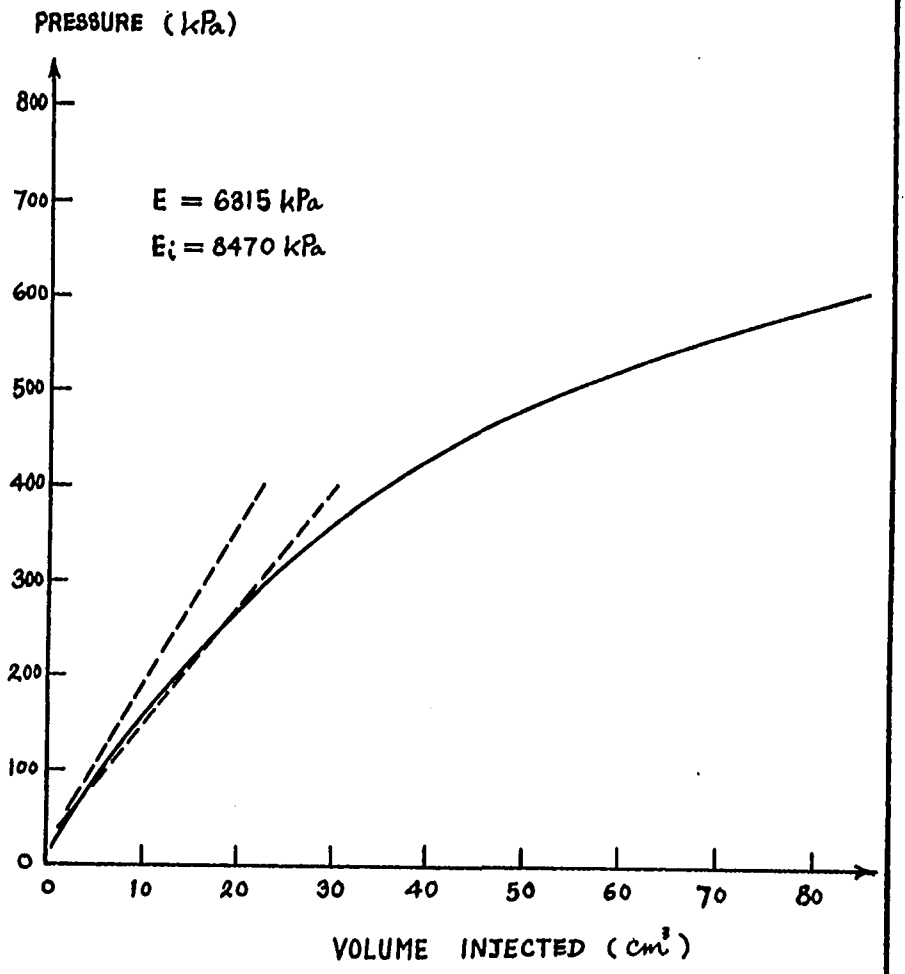

Fig. 188 - Test No. 66 - Sand Box. Briaud Pressuremeter Test. Buried Probe. I_D = 95%. Depth = 1.83 m.

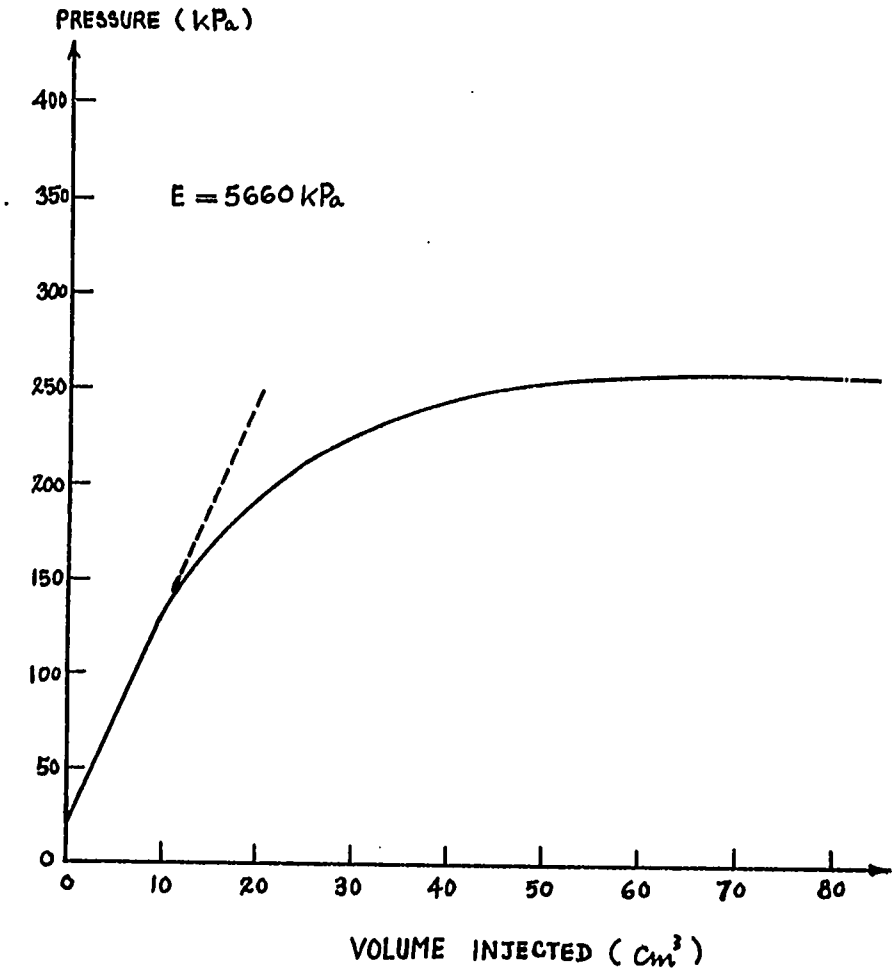

Fig. 189 - Test No. 67 - Sand Box. Briaud Pressuremeter Test. Driven Probe. I_D = 95%. Depth = 0.3 m.

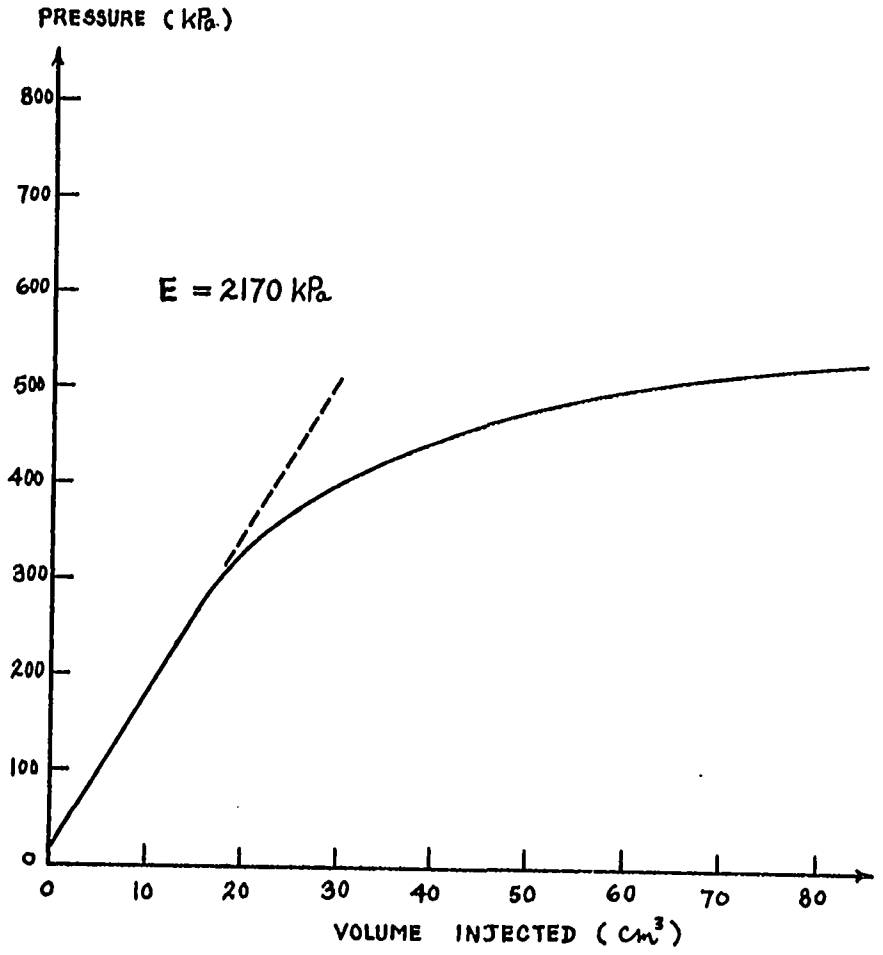

Fig. 190 - Test No. 68 - Sand Box. Briaud Pressuremeter Test. Driven Probe. I_D = 95%. Depth = 0.61 m.

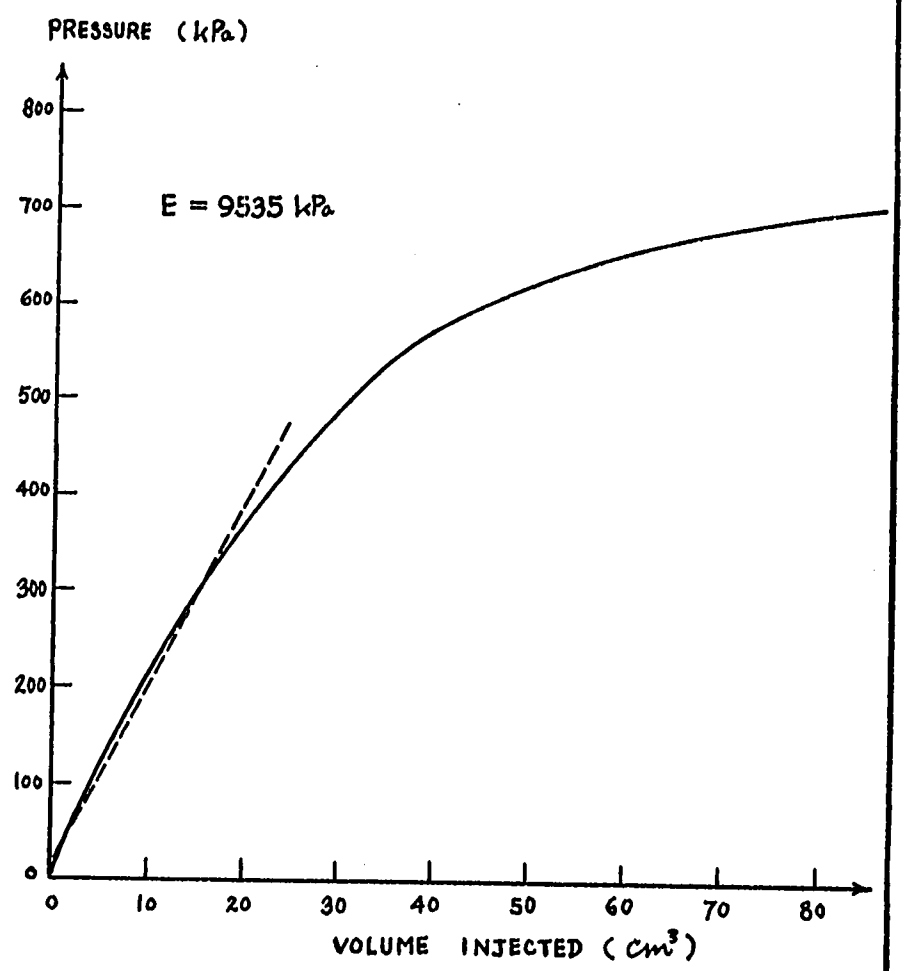

Fig. 191 - Test No. 69 - Sand Box. Briaud Pressuremeter Test. Driven Probe. I_D = 95%. Depth = 0.91 m.

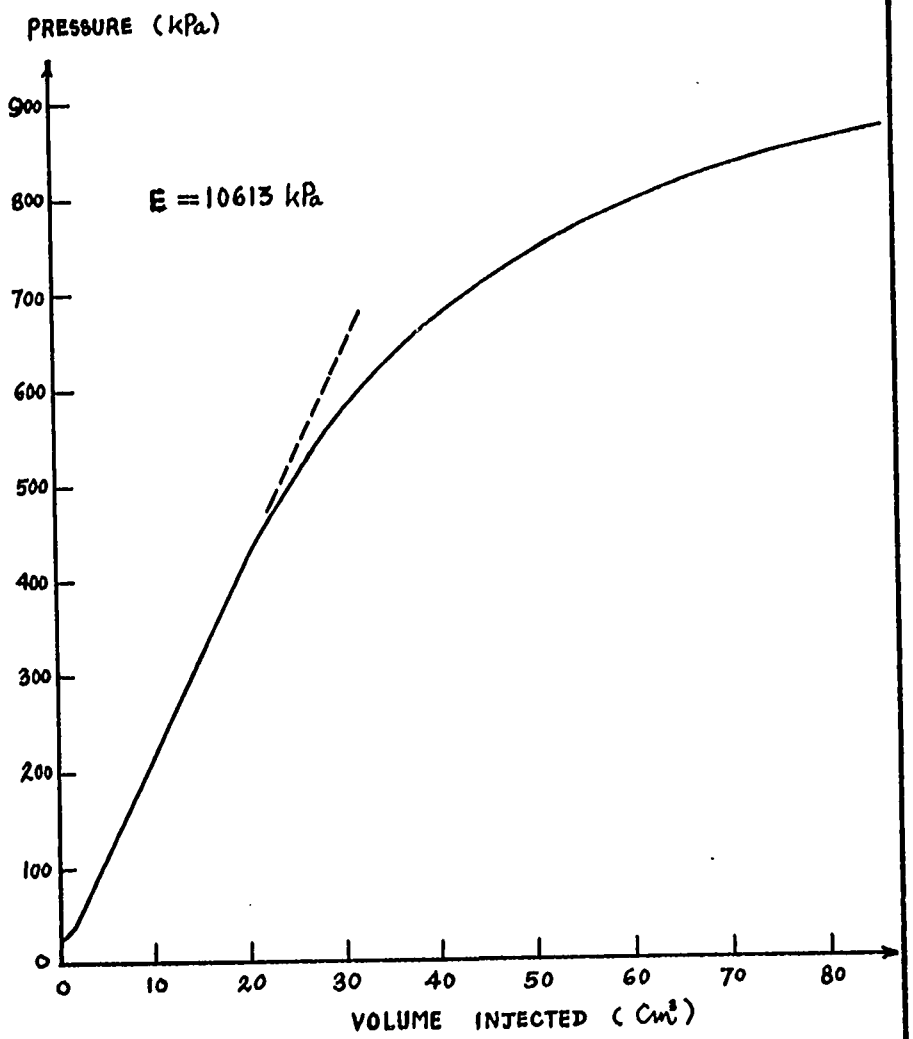

Fig.192 - Test No. 70 - Sand Box. Briaud Pressuremeter Test. Driven Probe. I_D = 95%. Depth = 1.22 m.

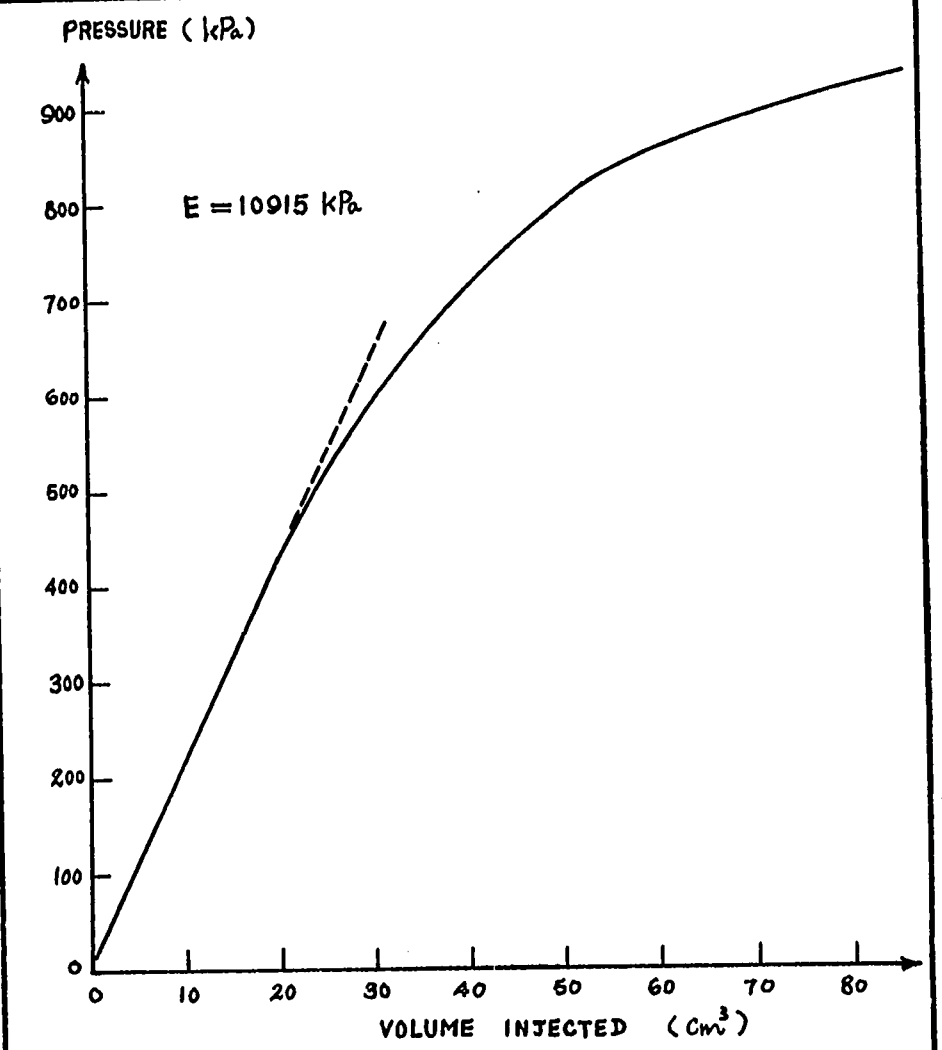

Fig.193 - Test No. 71 - Sand Box. Briaud Pressuremeter Test. Driven Probe. I_D = 95%. Depth = 1.52 m.

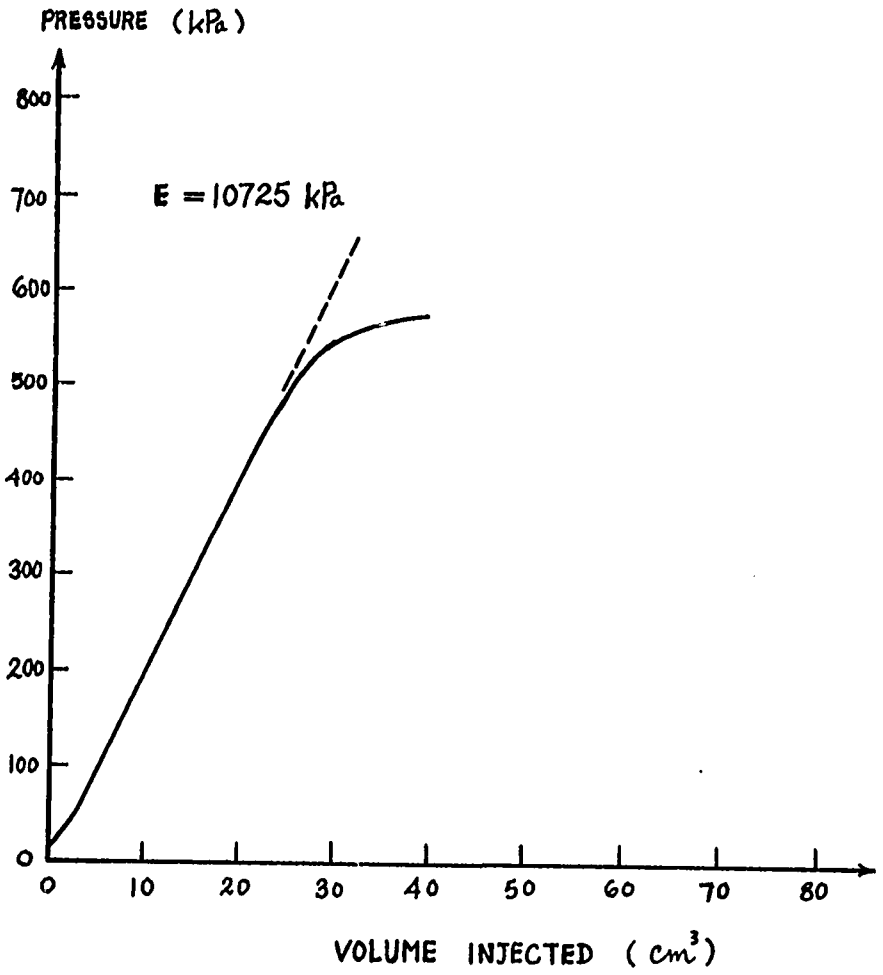

Fig. 194 - Test No. 72 - Sand Box. Briaud Pressuremeter Test. Driven Probe. I_D = 95%. Depth = 1.83 m.

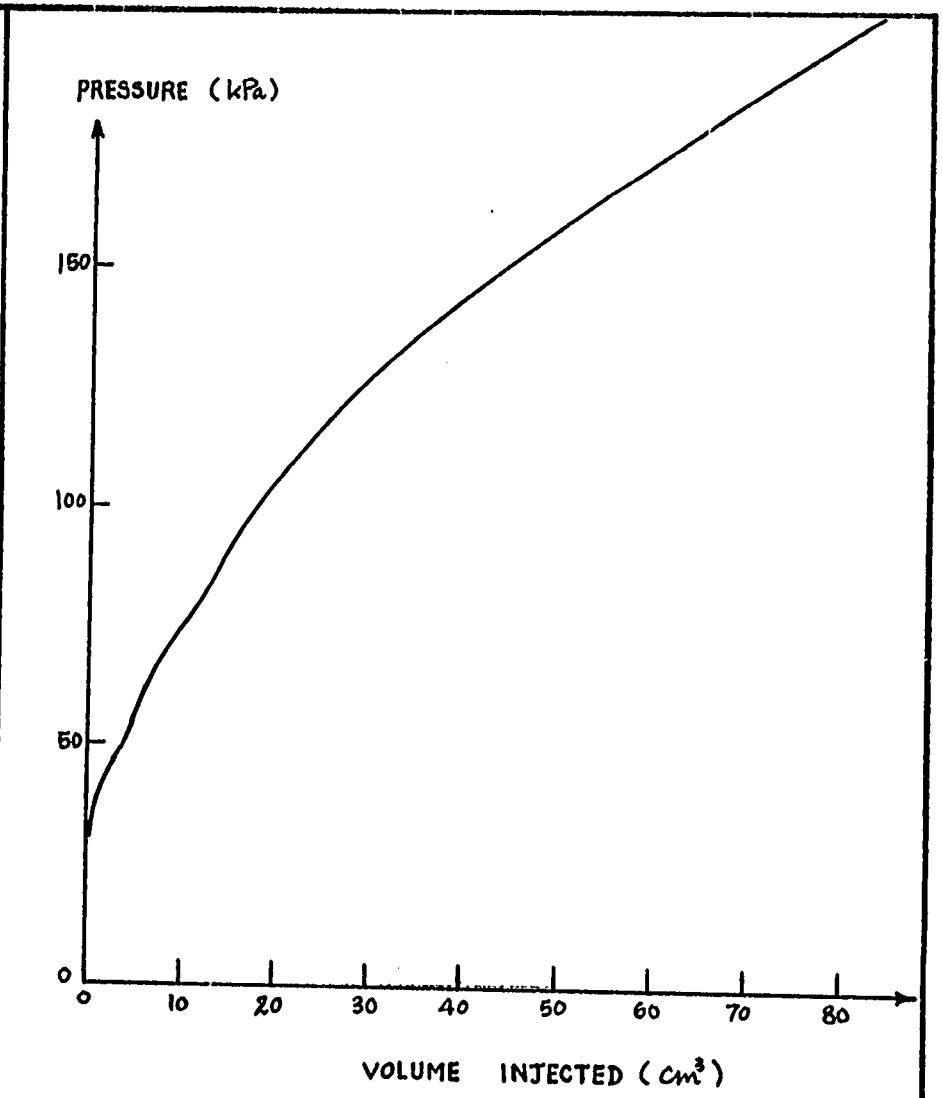

Fig.195 - Test No. 73 - Sand Box. Briaud Pressuremeter Test. Calibration of Membrane Resistance.

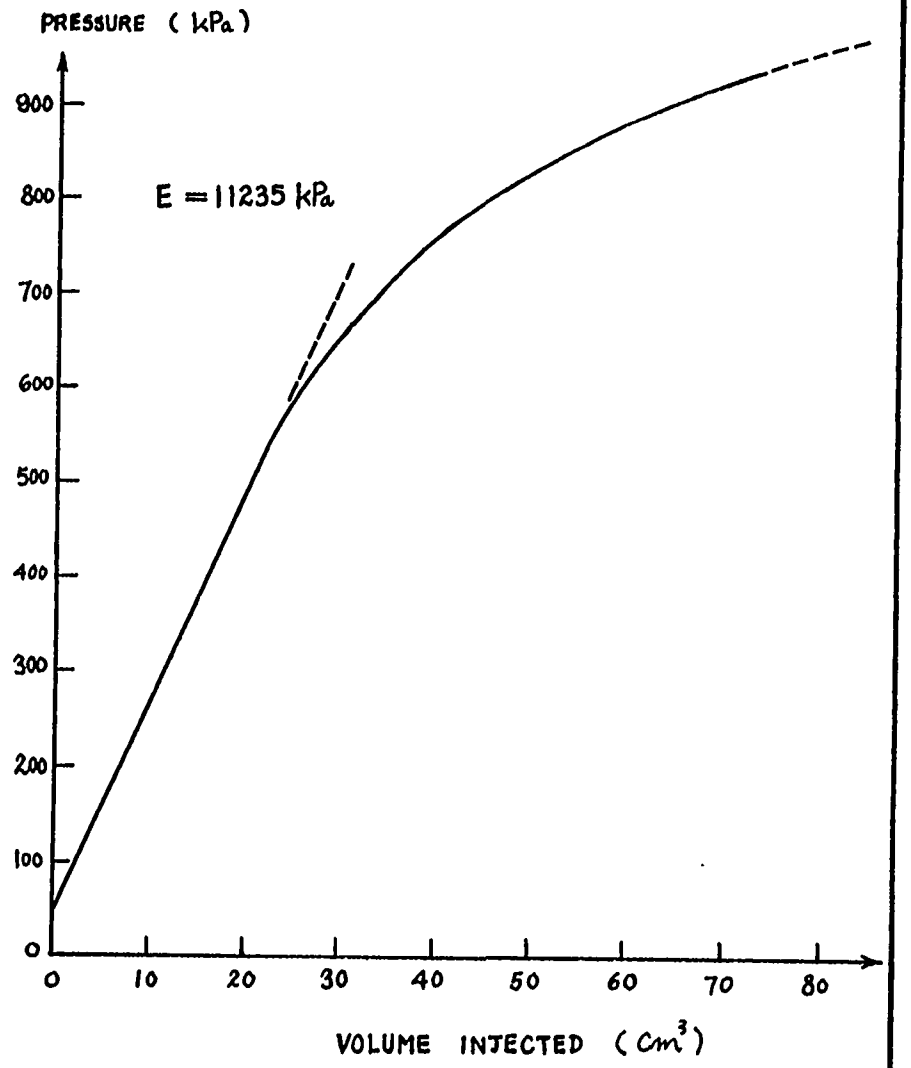

Fig.196 - Test No. 74 - Sand Box. Briaud Pressuremeter Test. Driven Probe. I_D = 95%. Depth = 1.83 m.

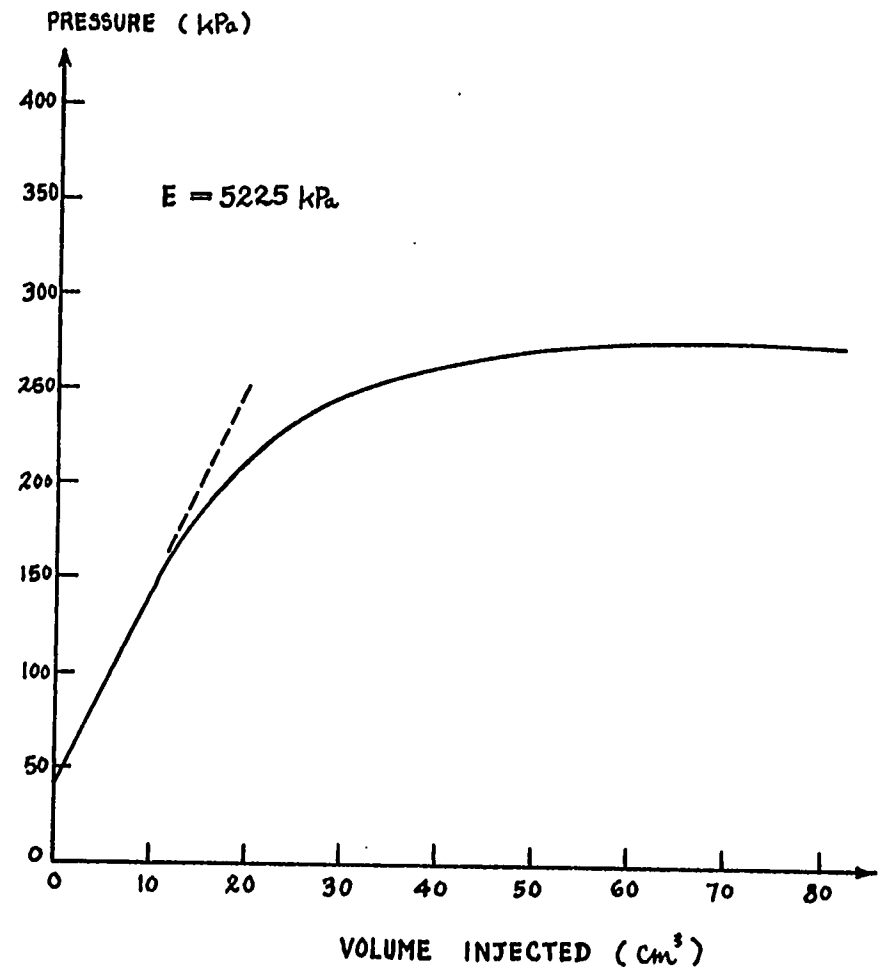

Fig.197 - Test No. 75 - Sand Box. Briaud Pressuremeter Test. Driven Probe. I_D = 95%. Depth = 0.30 m.

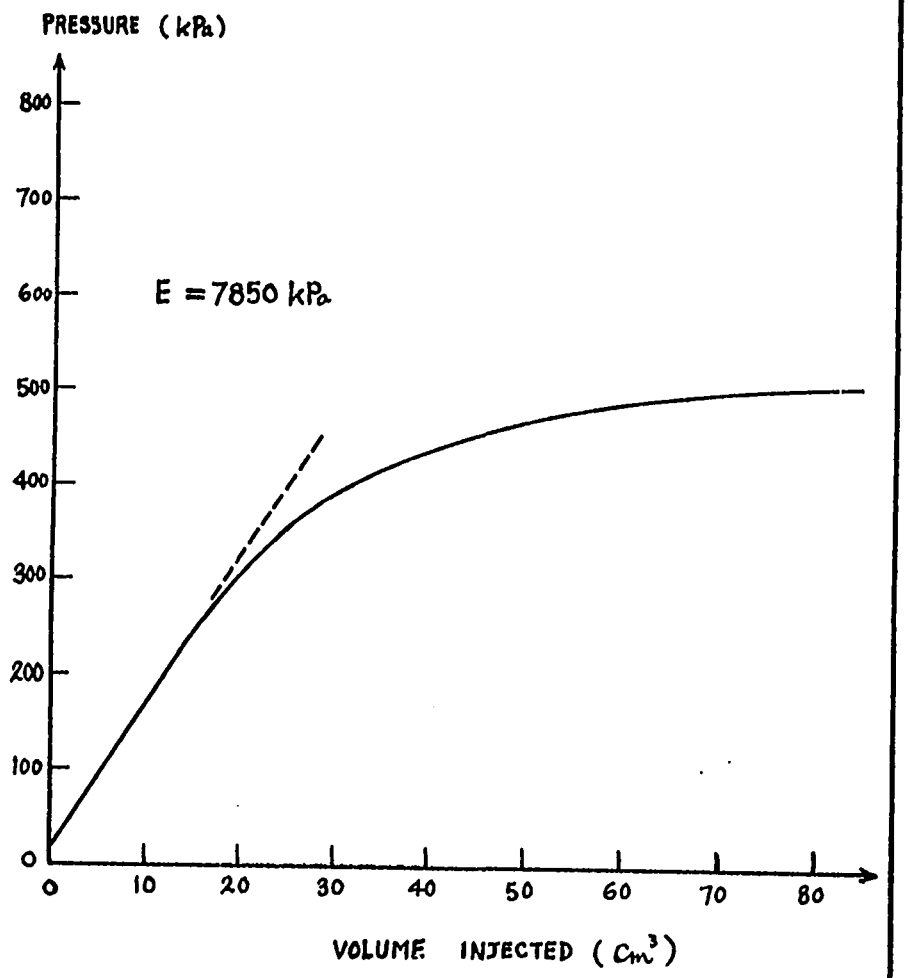

Fig. 198 - Test No. 76 - Sand Box. Briaud Pressuremeter Test. Driven Probe. I_D = 95%. Depth = 0.61 m.

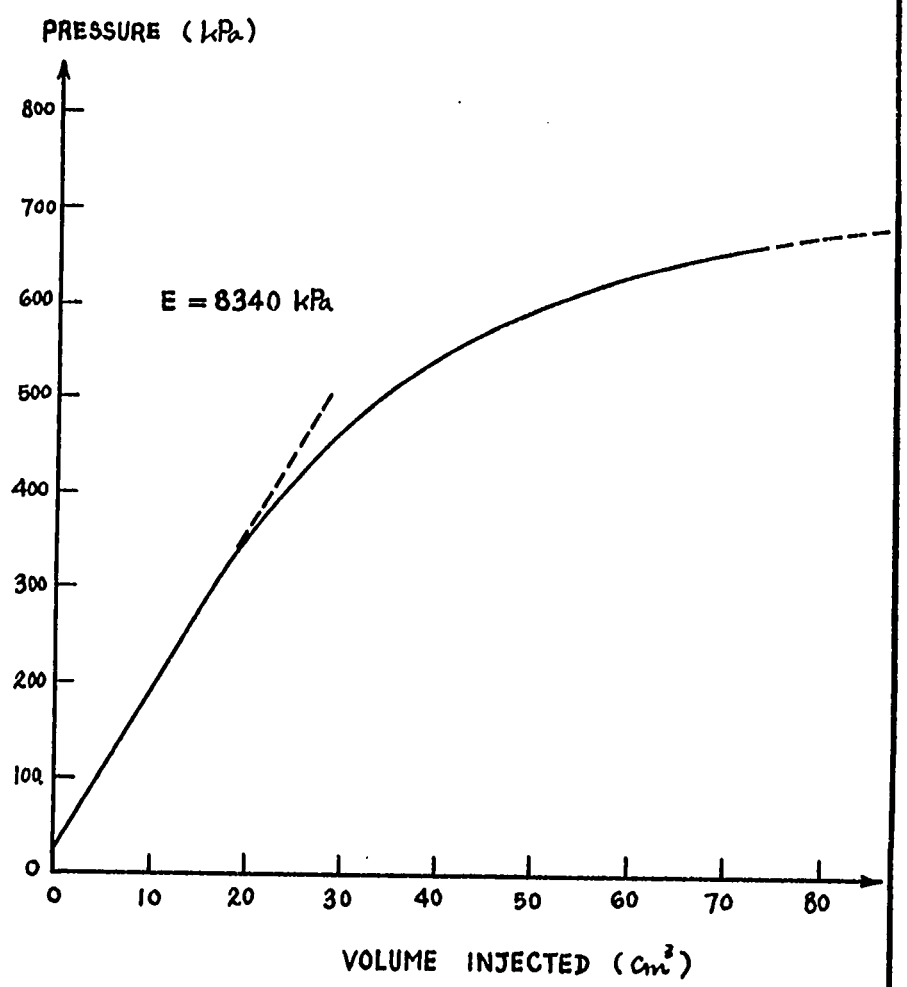

Fig. 199 - Test No. 77 - Sand Box. Briaud Pressuremeter Test. Driven Probe. I_D = 95%. Depth = 0.91 m.

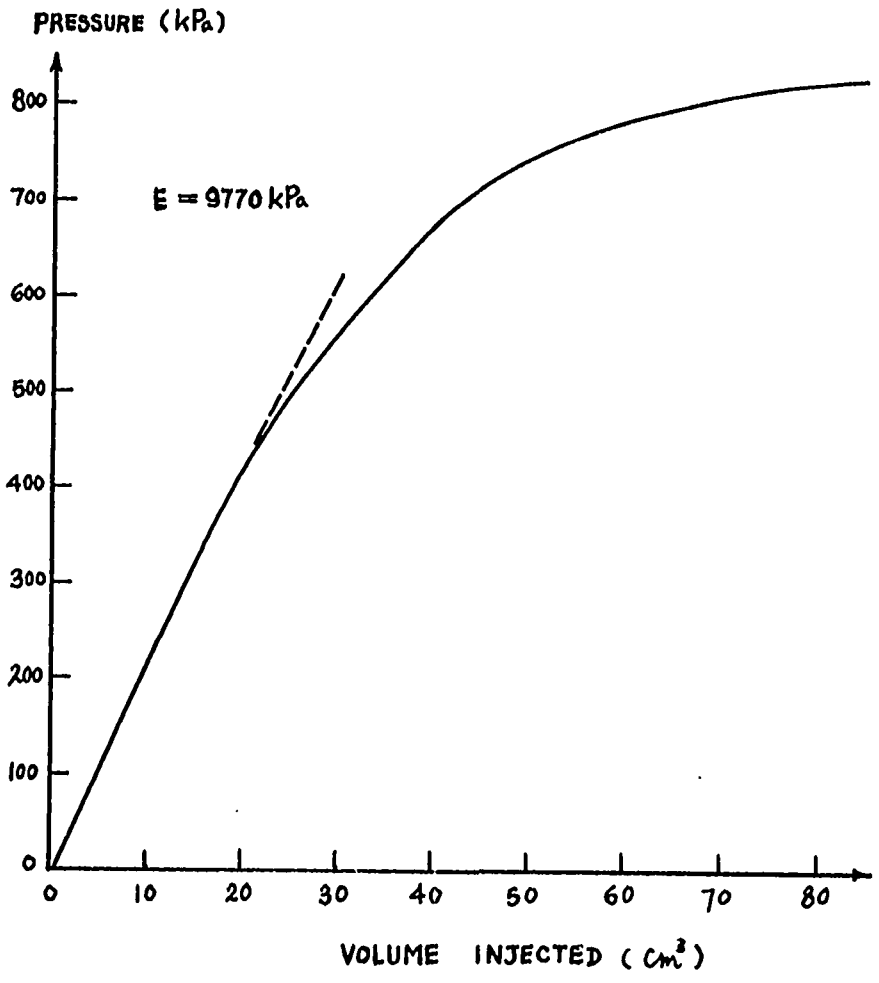

Fig. 200 - Test No. 78 - Sand Box. Briaud Pressuremeter Test. Driven Probe. I_D = 95%. Depth = 1.22 m.

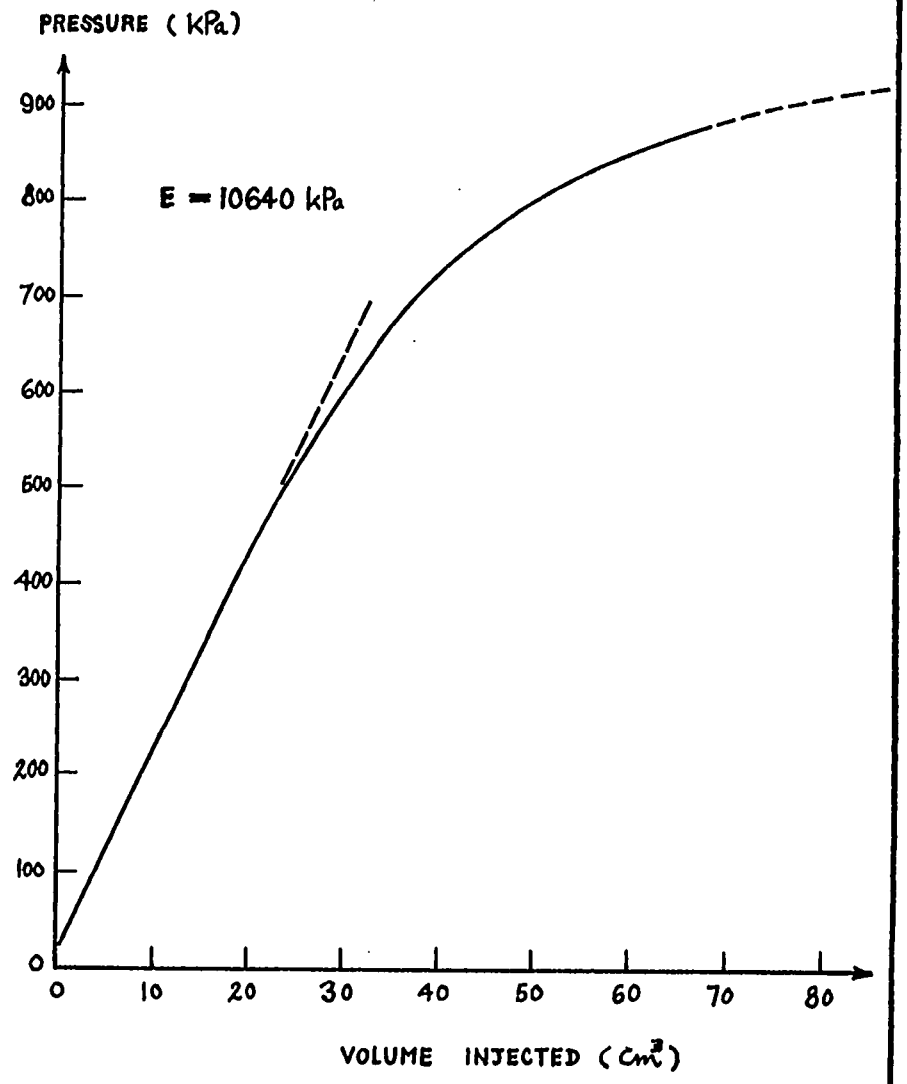

Fig. 201 - Test No. 79 - Sand Box. Briaud Pressuremeter Test. Driven Probe. I_D = 95%. Depth = 1.52 m.

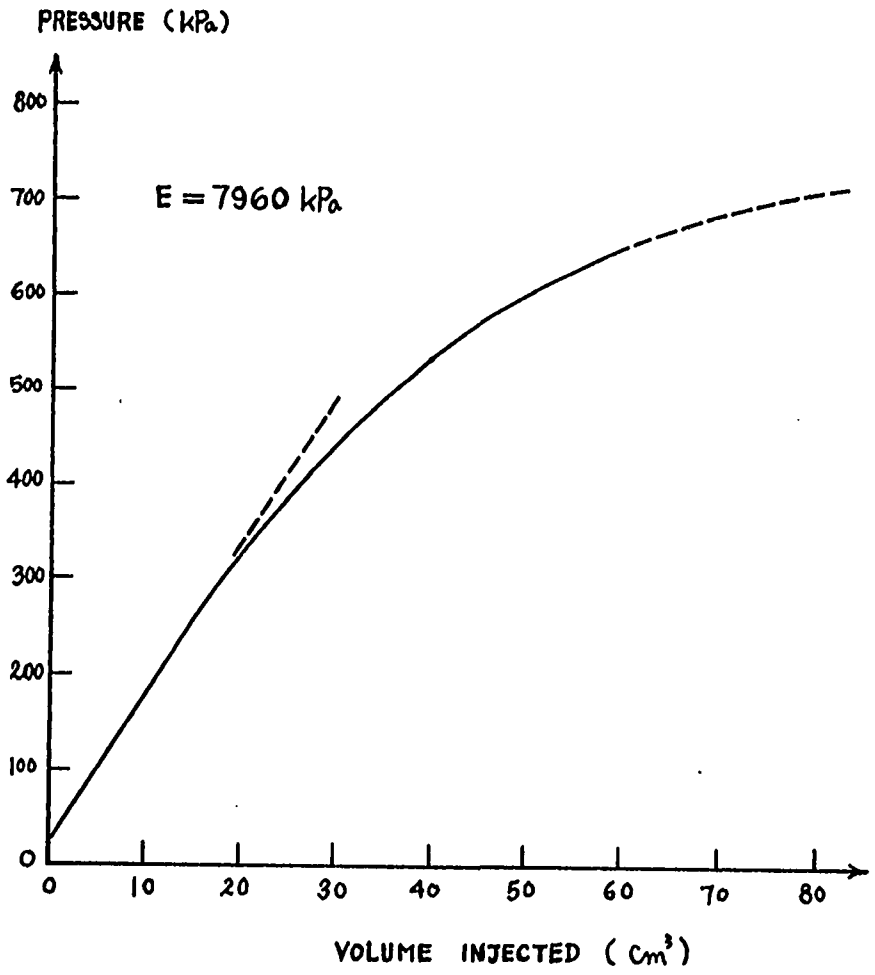

Fig.202 - Test No. 80 - Sand Box. Briaud Pressuremeter Test. Driven Probe. I_D = 95%. Depth = 1.83 m.

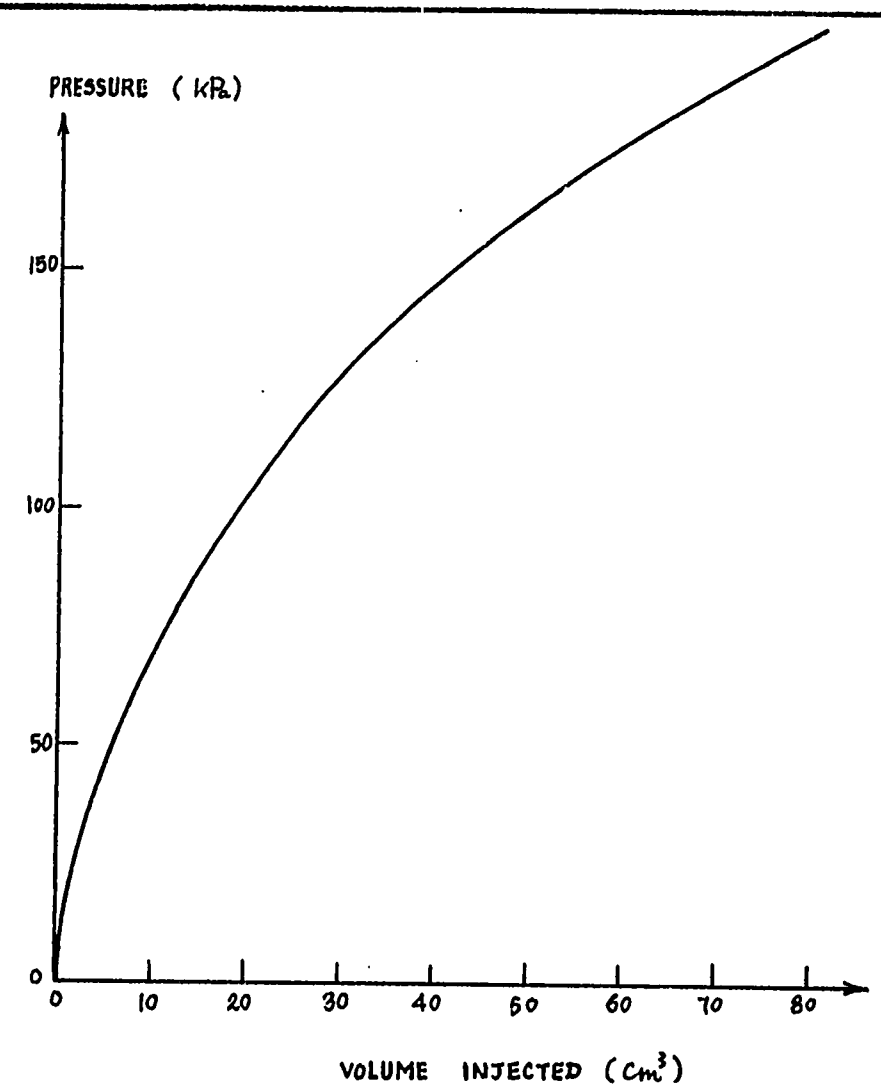

Fig.203 - Test No. 81 - Sand Box. Briaud Pressuremeter Test. Calibration of Membrane Resistance.

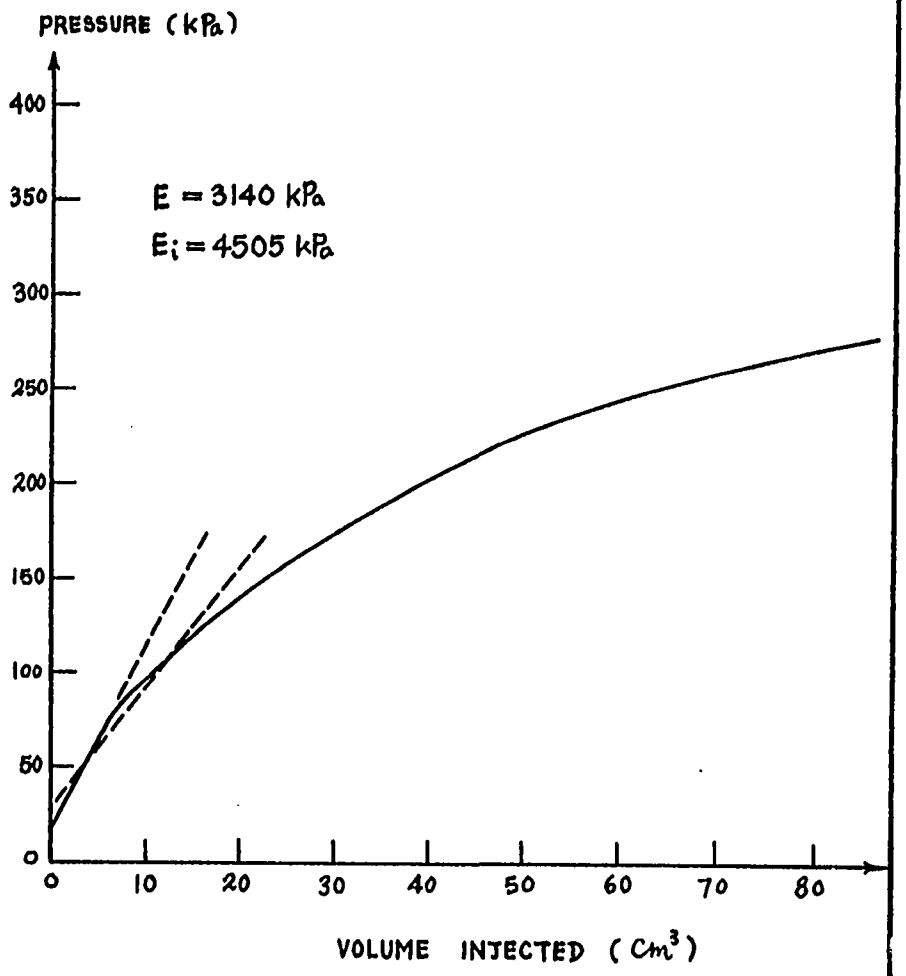

Fig.204 – Test No. 82 – Sand Box. Briaud Pressuremeter Test. Buried Probe. I_D = 66%. Depth = 1.26 m.

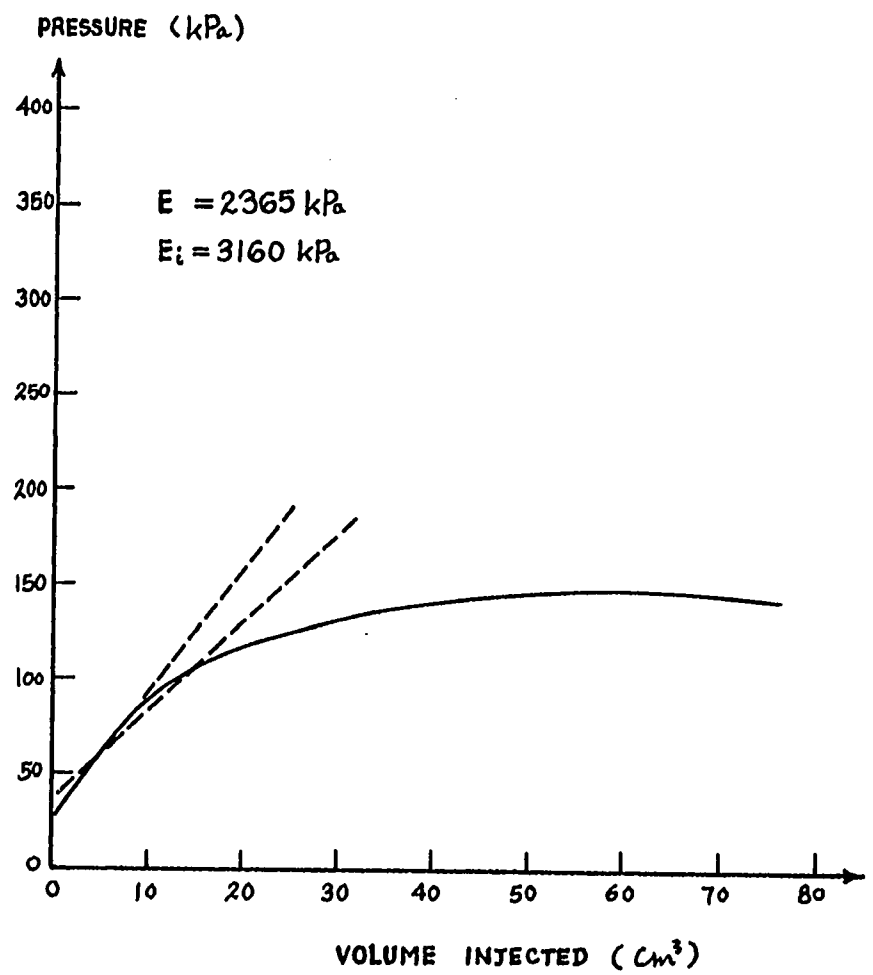

Fig. 205 – Test No. 83 – Sand Box. Briaud Pressuremeter Test. Driven Probe. I_D = 66%. Depth = 0.30 m.

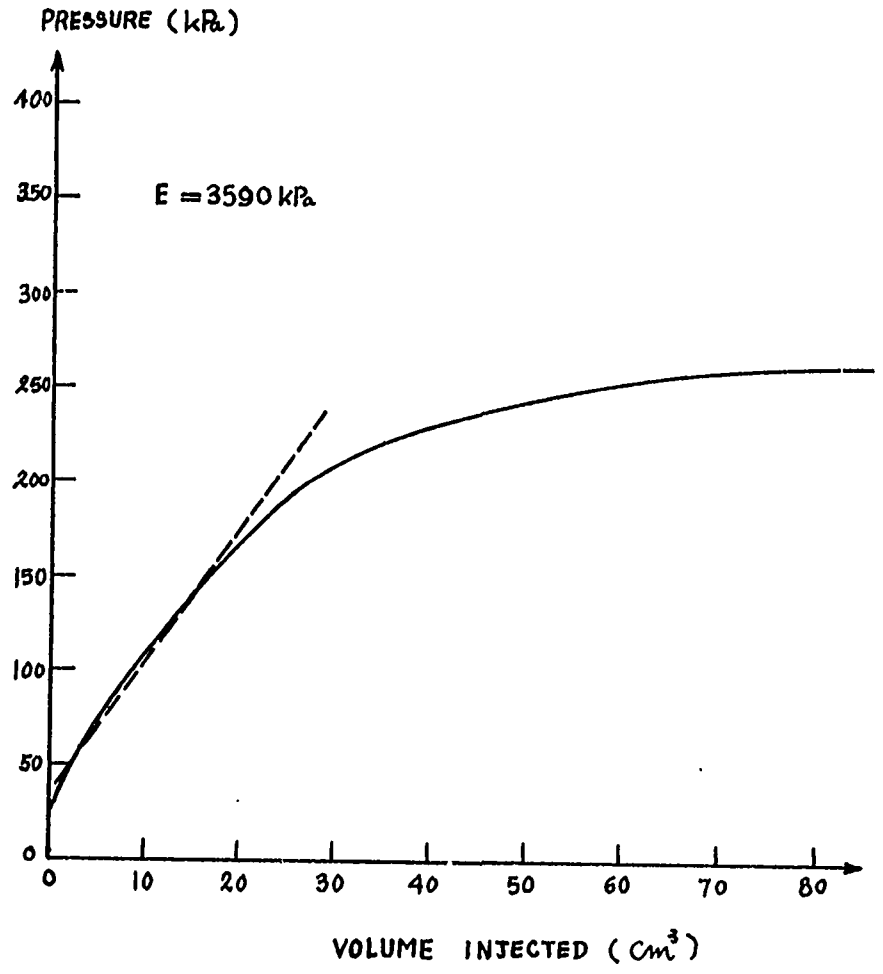

Fig. 206 – Test No. 84 – Sand Box. Briaud Pressuremeter Test. Driven Probe. I_D = 66%. Depth = 0.61 m.

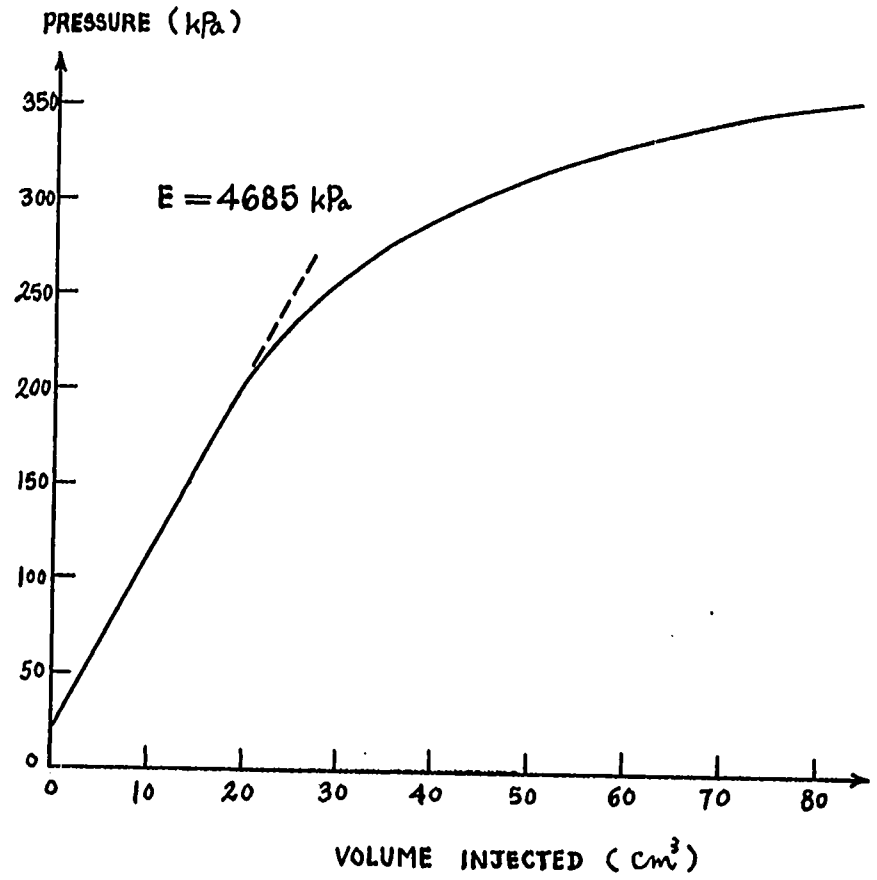

Fig. 207 – Test No. 85 – Sand Box. Briaud Pressuremeter Test. Driven Probe. I_D = 66%. Depth = 0.91 m.

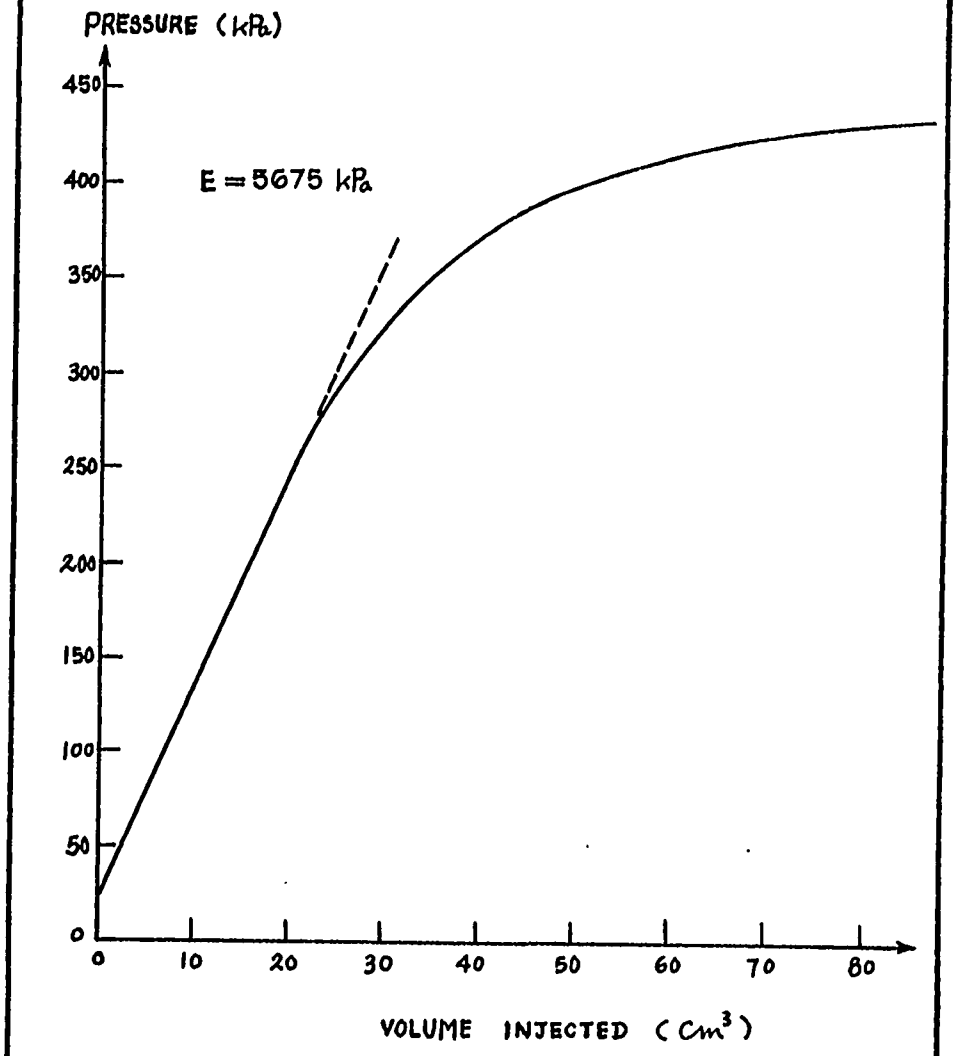

Fig. 208 - Test No. 86 - Sand Box. Briaud Pressuremeter Test. Driven Probe. I_D = 66%. Depth = 1.22 m.

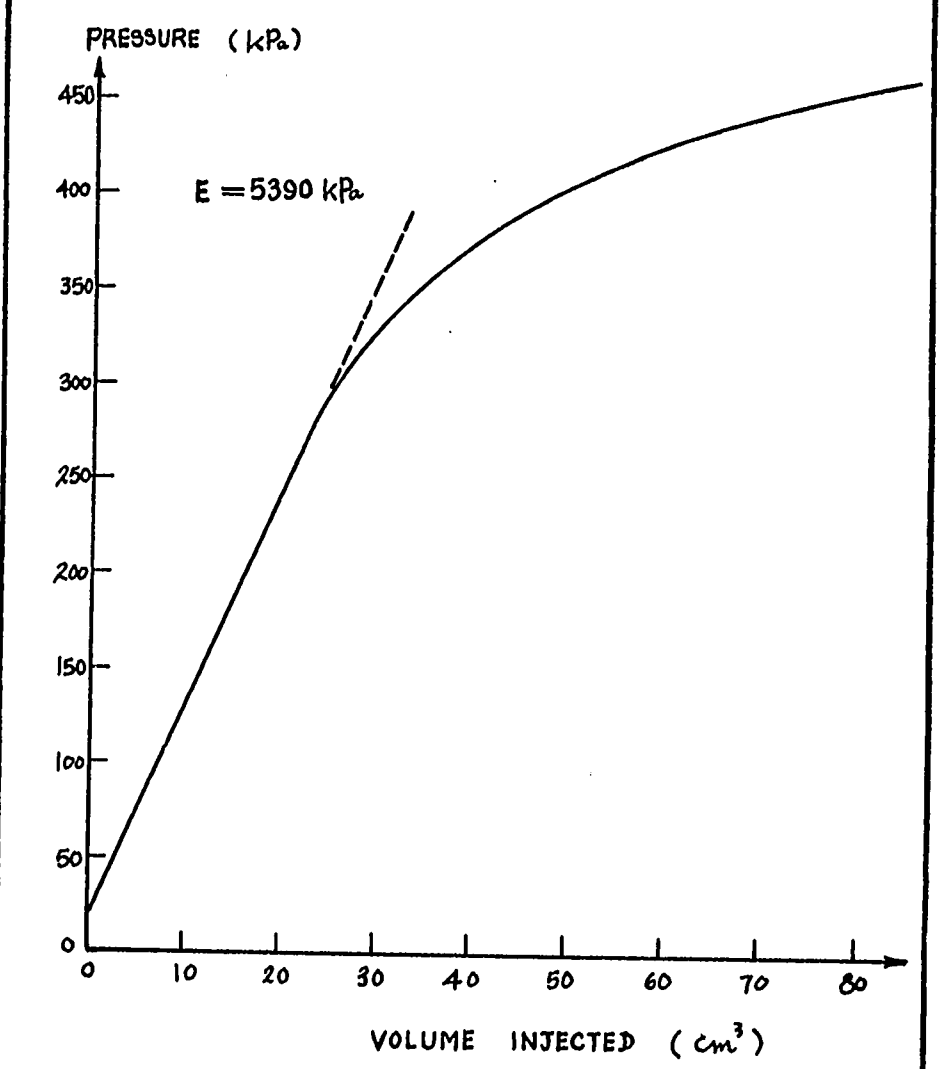

Fig. 209 - Test No. 87 - Sand Box. Briaud Pressuremeter Test. Driven Probe. I_D = 75%. Depth = 1.52 m.

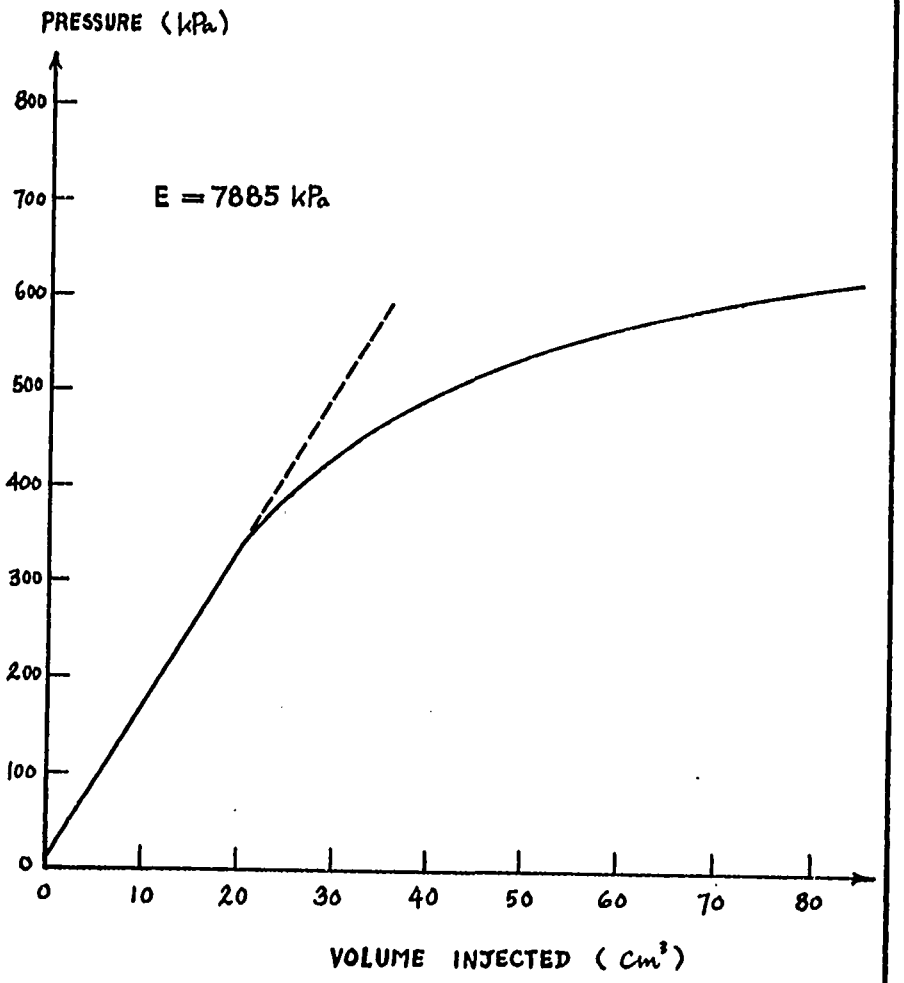

Fig.210 - Test No. 88 - Sand Box. Briaud Pressuremeter Test. Driven Probe. I_D = 75%. Depth = 1.73 m.

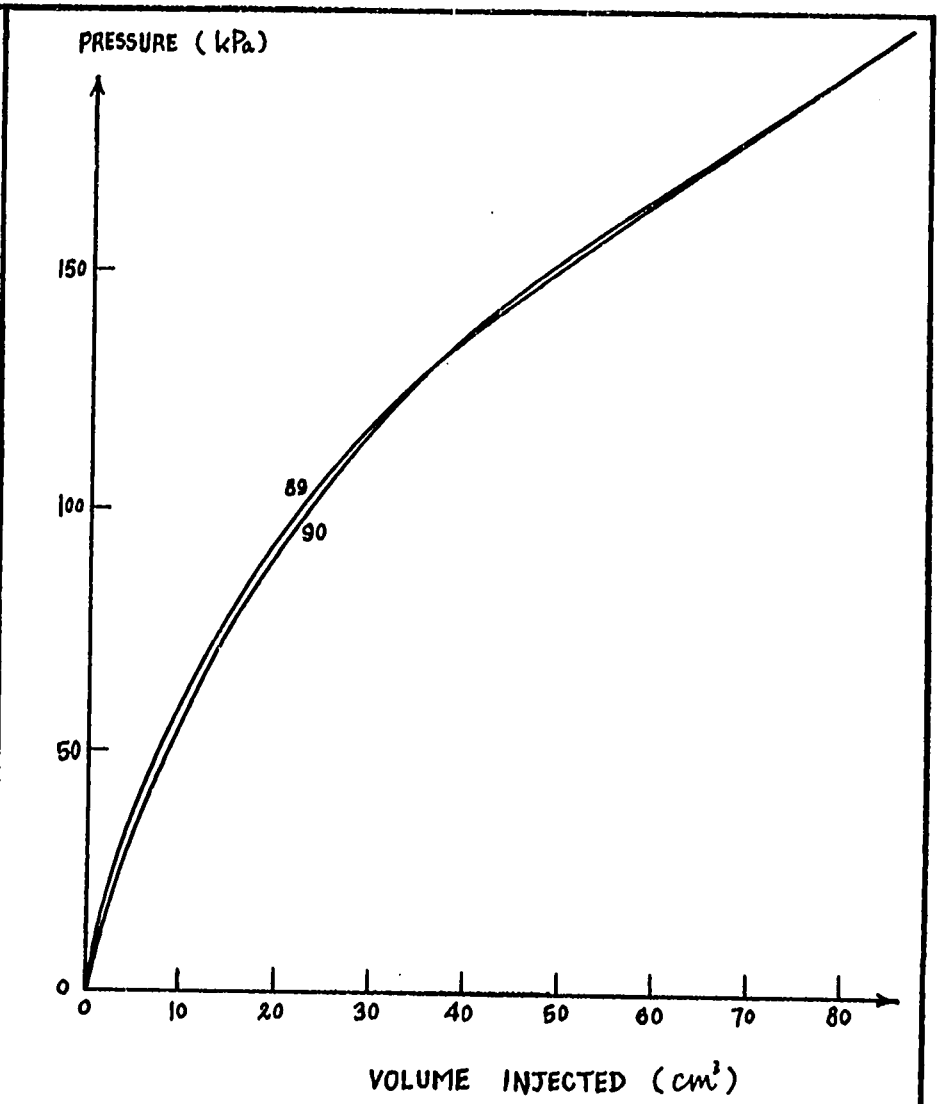

Fig.211 - Test Nos. 89 and 90 - Sand Box. Briaud Pressuremeter Test. Calibration of Membrane Resistance.

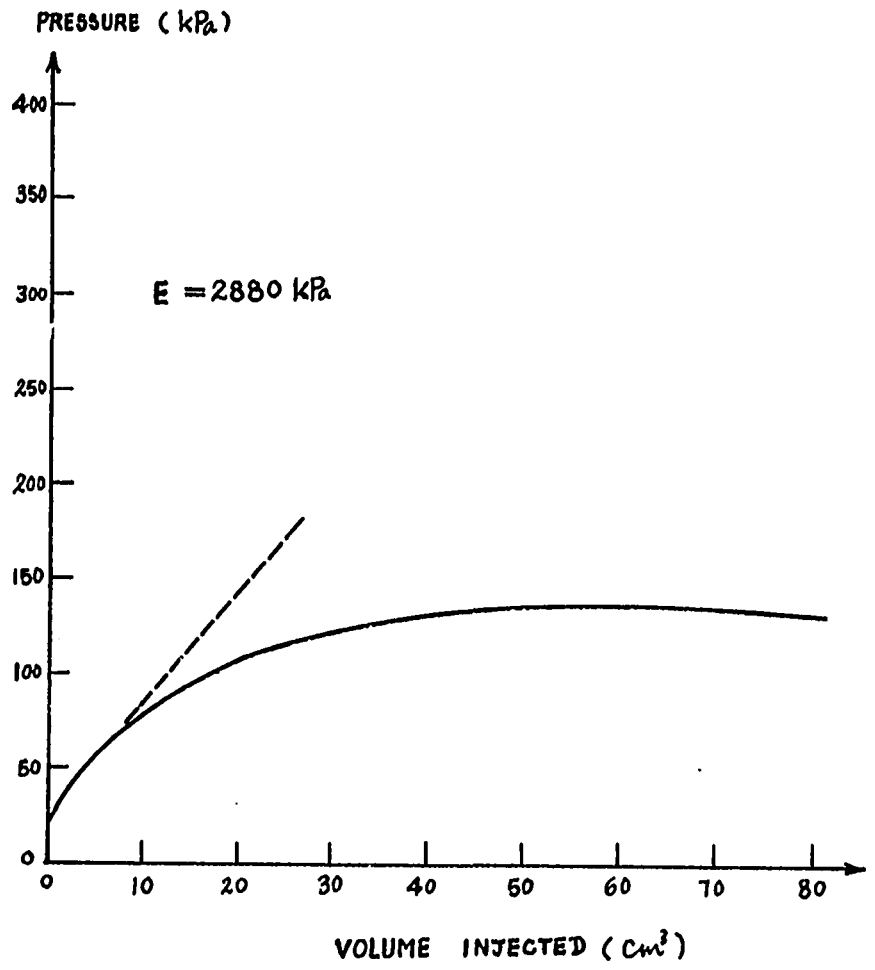

Fig. 212 - Test No. 91 - Sand Box. Briaud Pressuremeter Test. Driven Probe. I_D = 66%. Depth = 0.30 m.

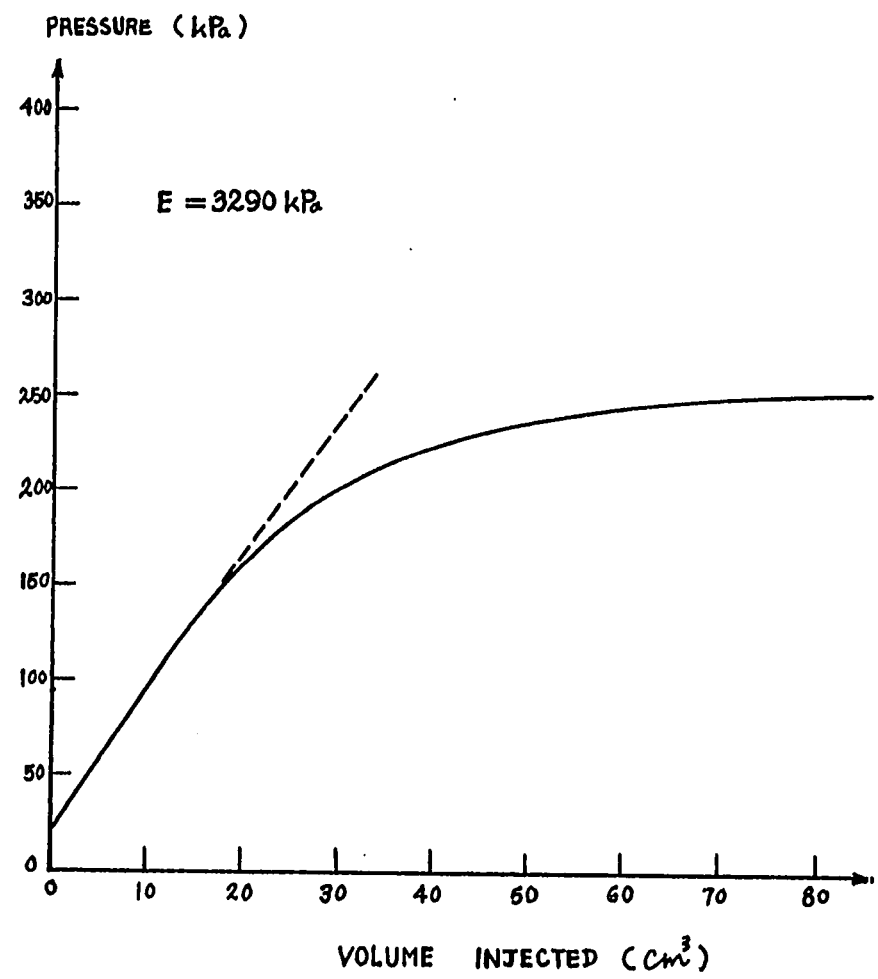

Fig. 213 - Test No. 92 - Sand Box. Briaud Pressuremeter Test. Driven Probe. I_D = 66%. Depth = 0.61 m.

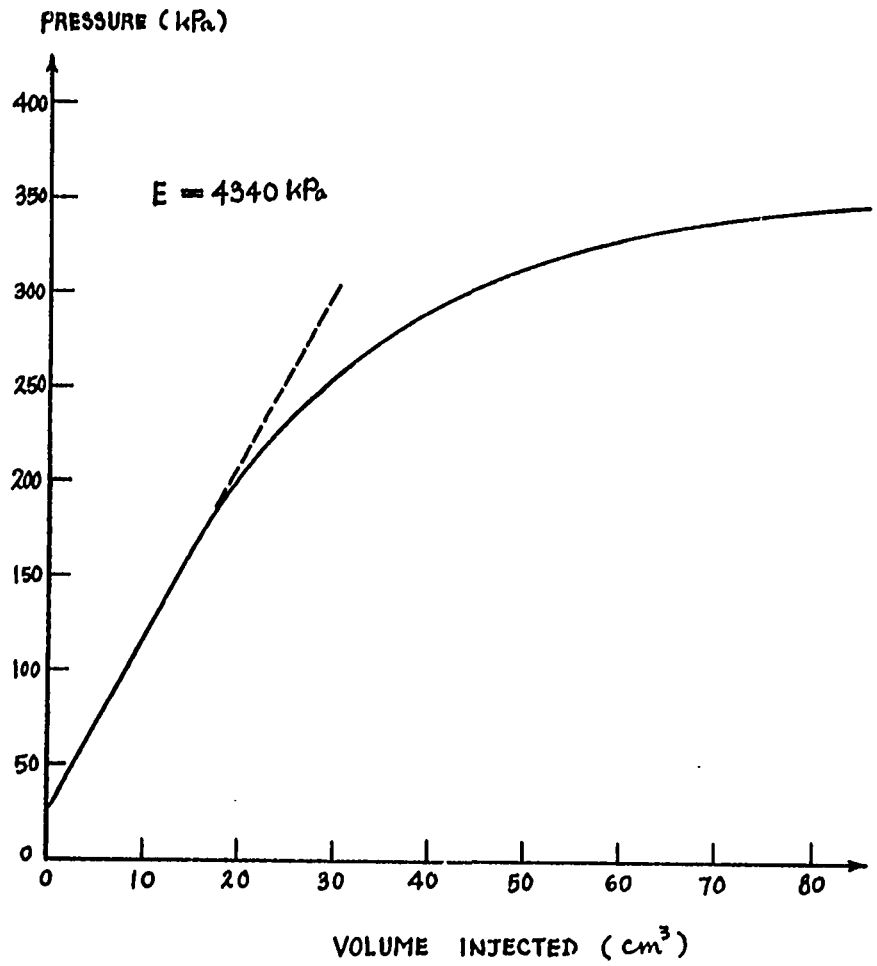

Fig. 214 - Test No. 93 - Sand Box. Briaud Pressuremeter Test. Driven Probe. I_D = 66%. Depth = 0.91 m.

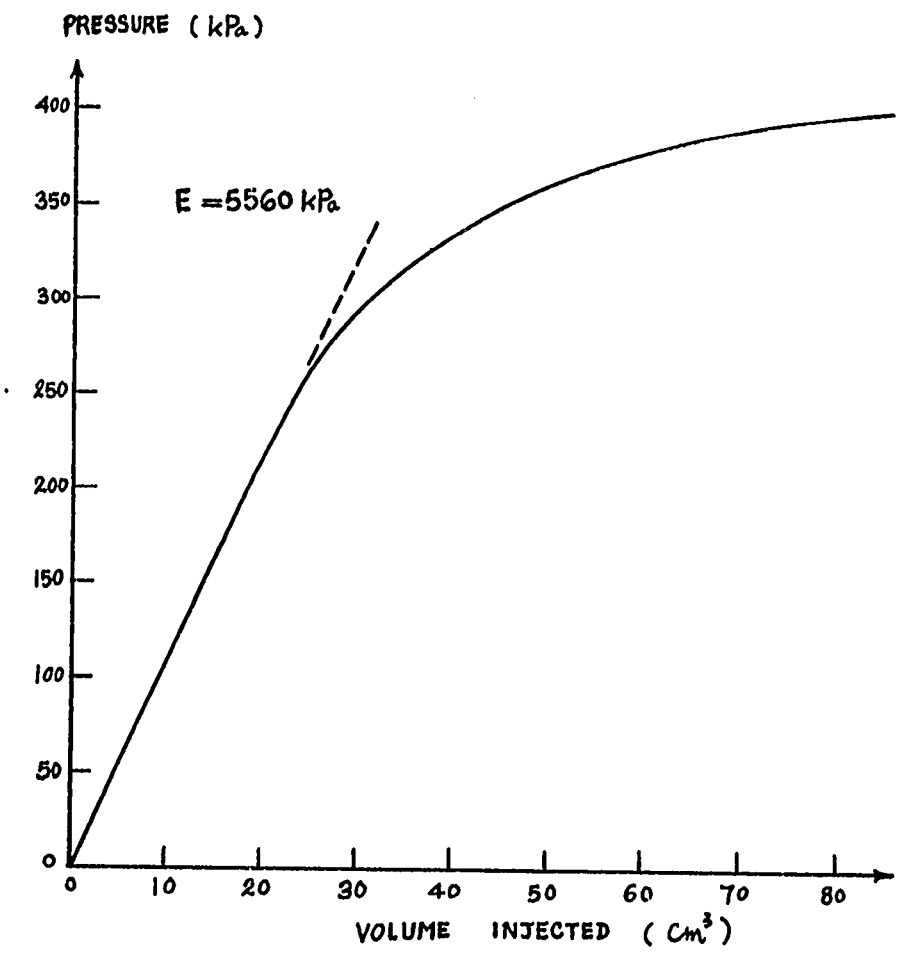

Fig. 215 - Test No. 94 - Sand Box. Briaud Pressuremeter Test. Driven Probe. I_D = 66%. Depth = 1.22 m.

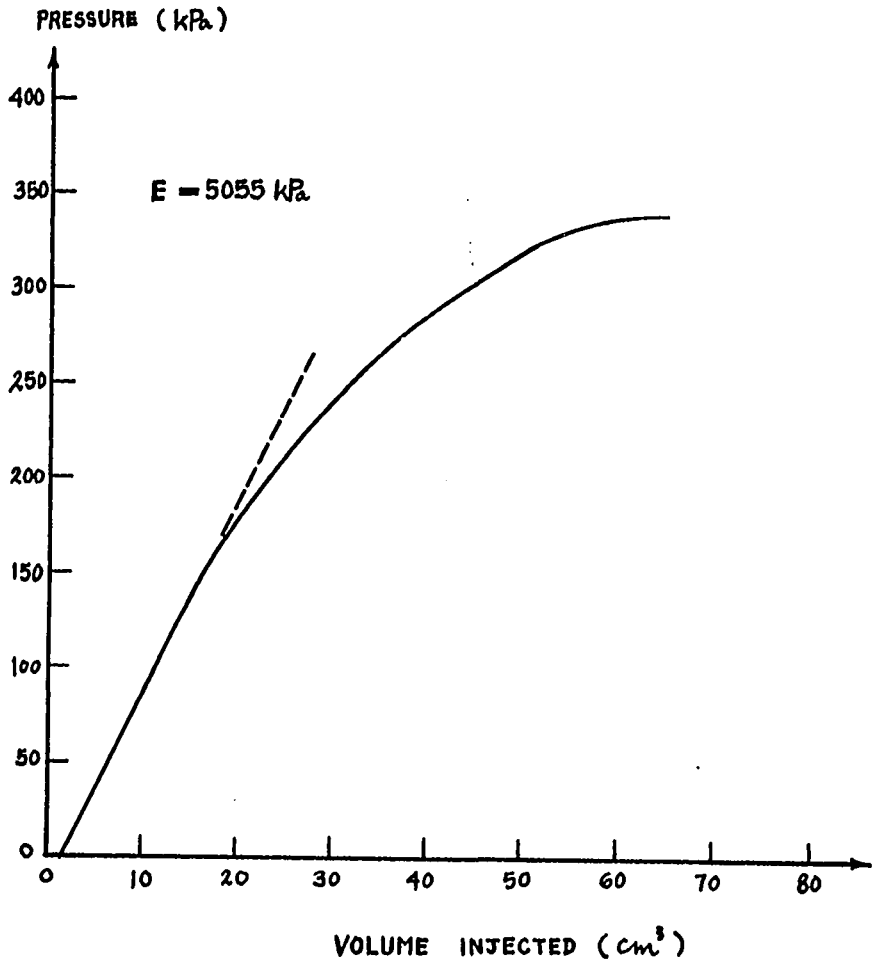

Fig.216 - Test No. 95 - Sand Box. Briaud Pressuremeter Test. Driven Probe. I_D = 66%. Depth = 1.52 m.

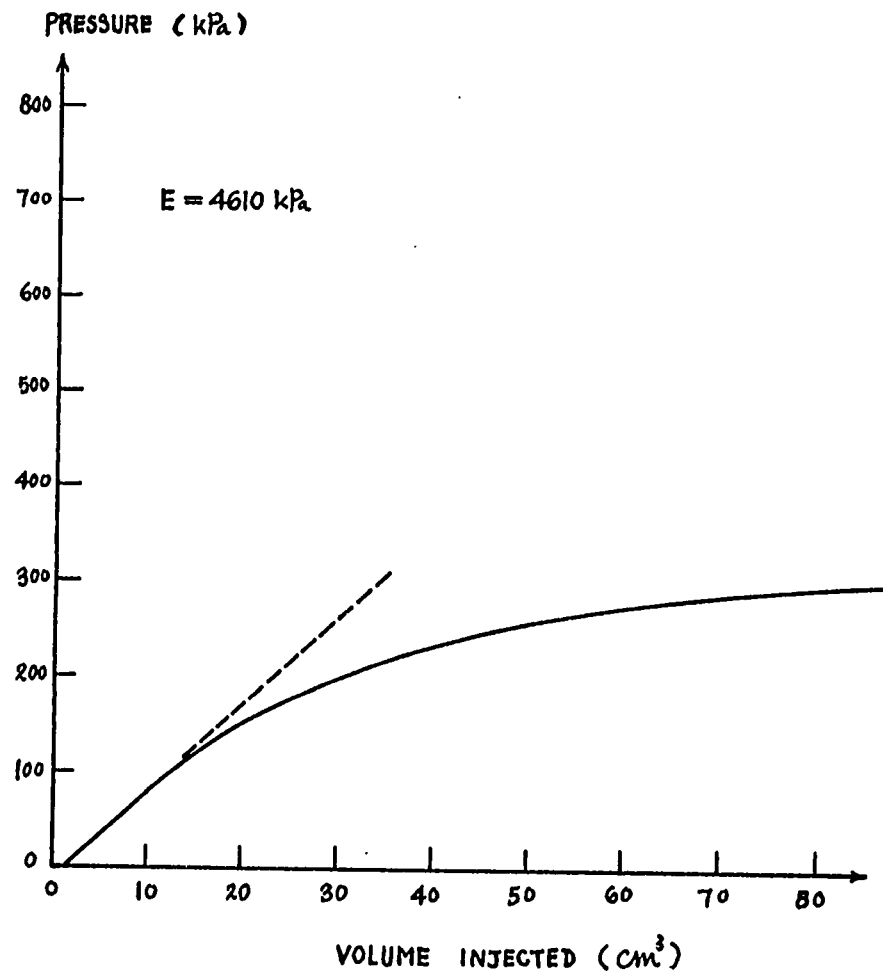

Fig.217 - Test No. 96 - Sand Box. Briaud Pressuremeter Test. Driven Probe. I_D = 66%. Depth = 1.83 m.

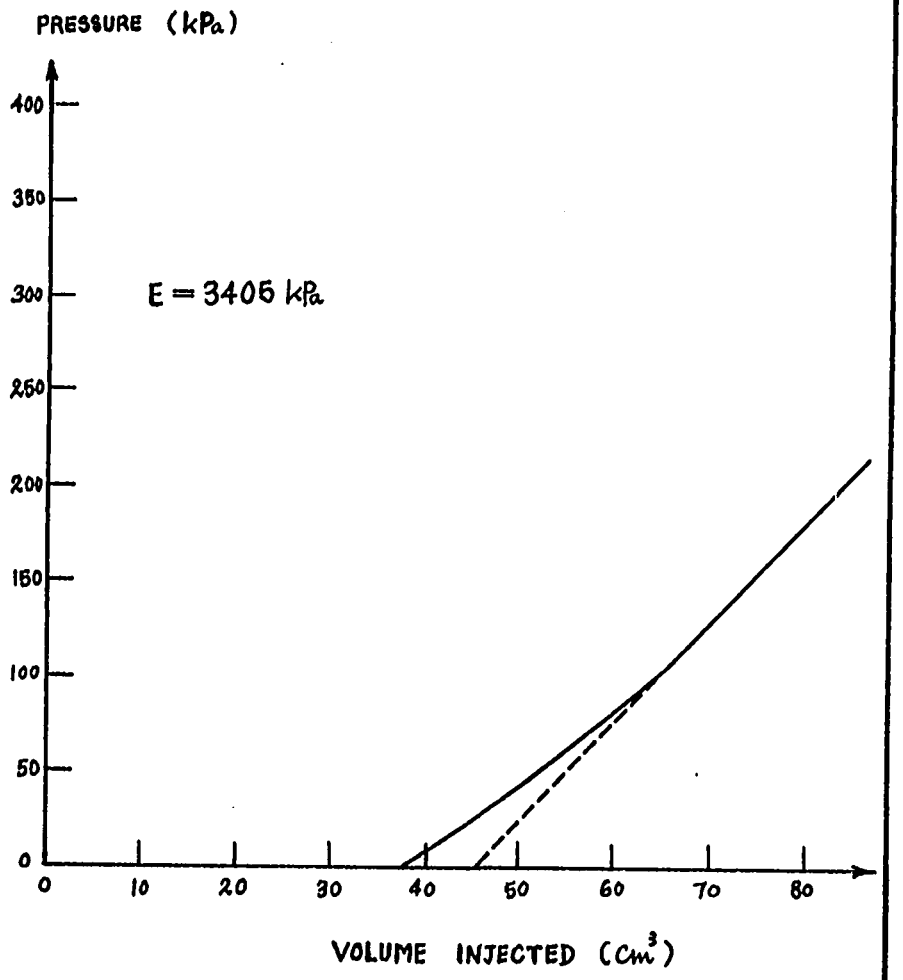

Fig. 218 - Test No. 98 - Sarnia Airport. Briaud Pressuremeter Test. Hole 1A. Hole: Hand Auger. Depth = 0.3 m.

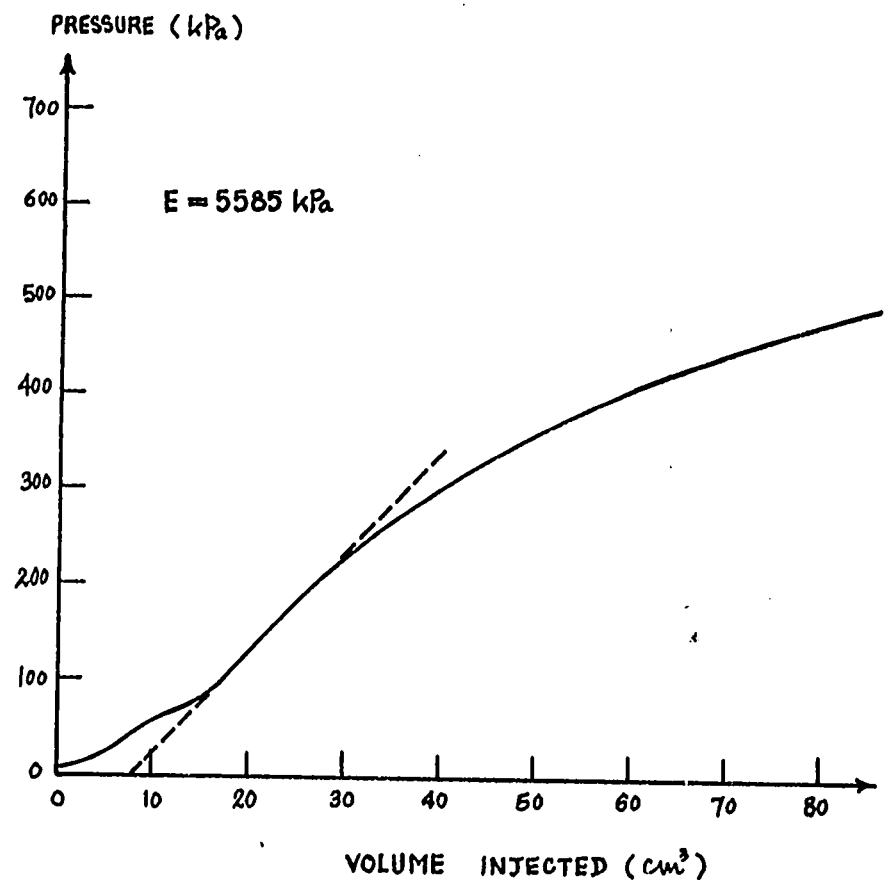

Fig. 219 - Test No. 99 - Sarnia Airport. Briaud Pressuremeter Test. Hole 1. Hole: Hand Auger. Depth = 0.3 m.

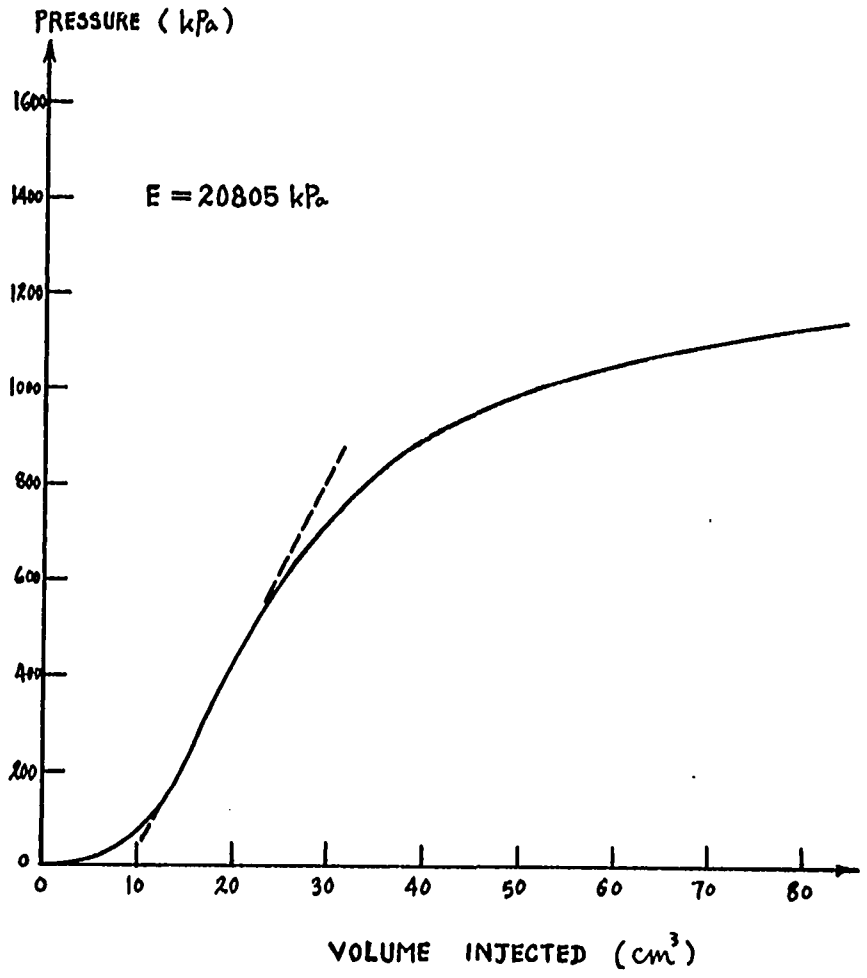

Fig. 220 - Test No. 100 - Sarnia Airport. Briaud Pressuremeter Test. Hole 1. Hole: Hand Auger. Depth = 0.6 m.

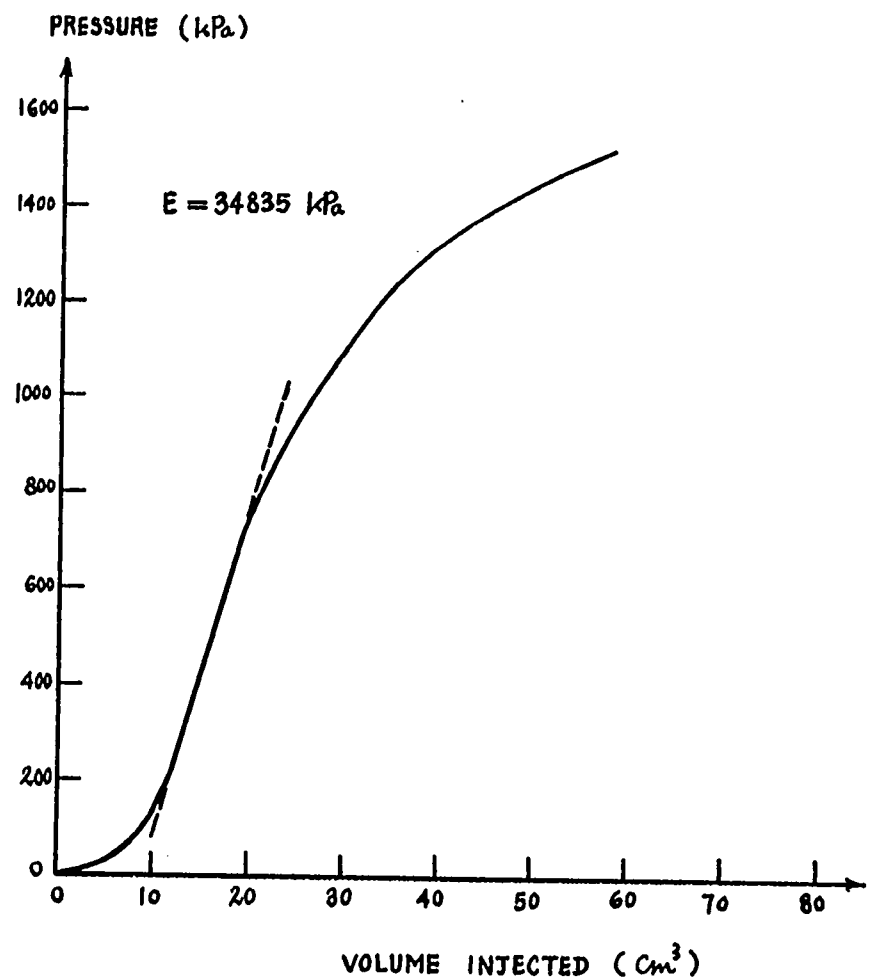

Fig. 221 - Test No. 101 - Sarnia Airport. Briaud Pressuremeter Test. Hole 1. Hole: Hand Auger. Depth = 0.9 m.

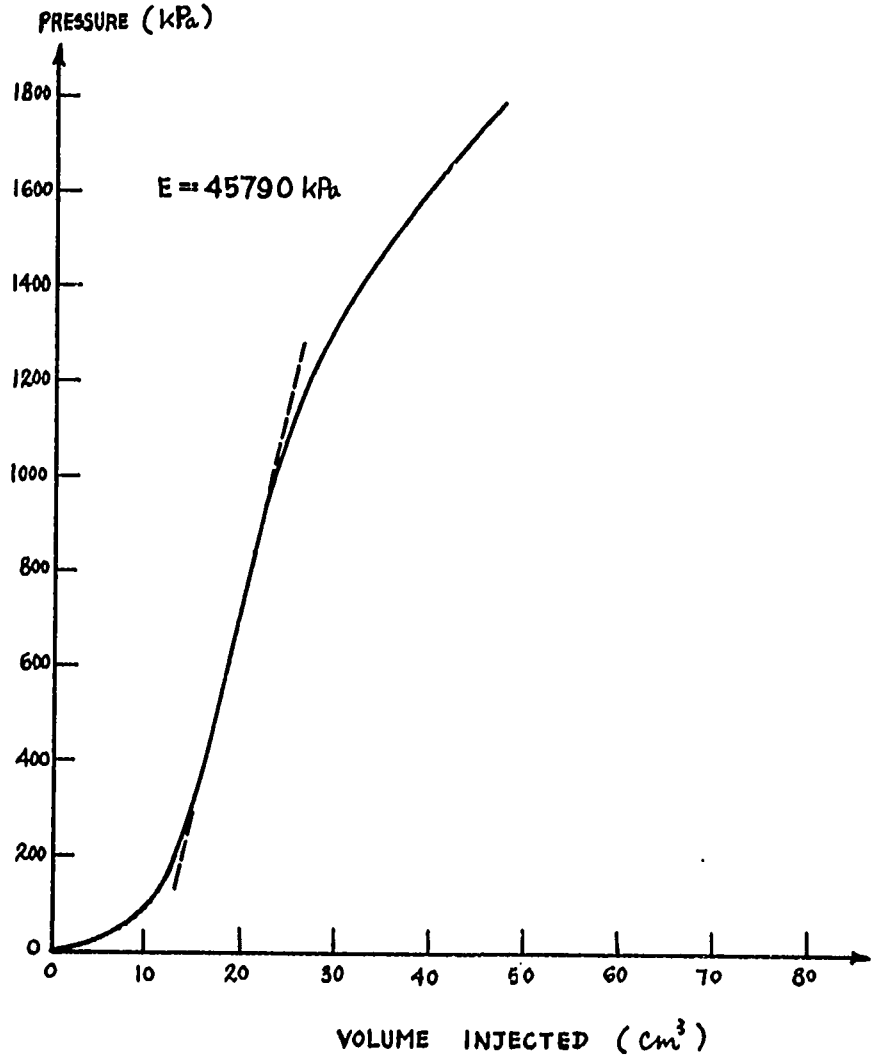

Fig. 222 - Test No. 102 - Sarnia Airport. Briaud Pressuremeter Test. Hole 1. Hole: Hand Auger. Depth = 1.2 m.

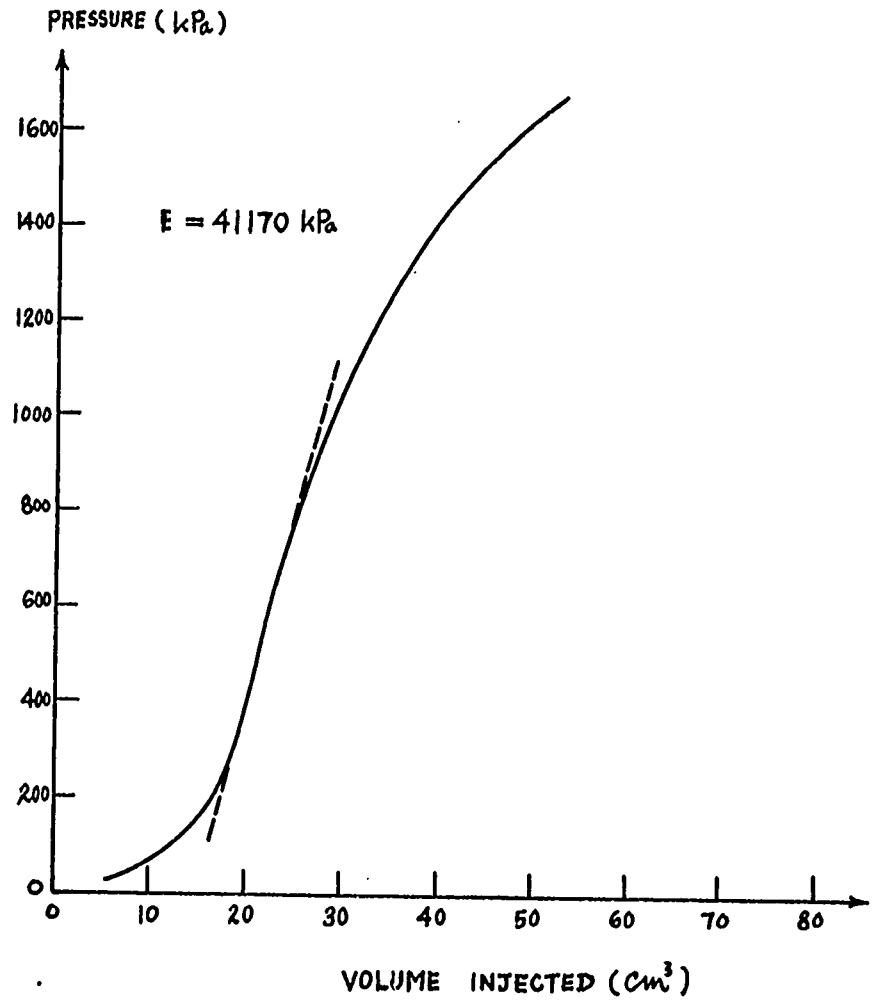

Fig. 223 - Test No. 103 - Sarnia Airport. Briaud Pressurement Test. Hole 1. Hole: Hand Auger. Depth = 1.5 m.

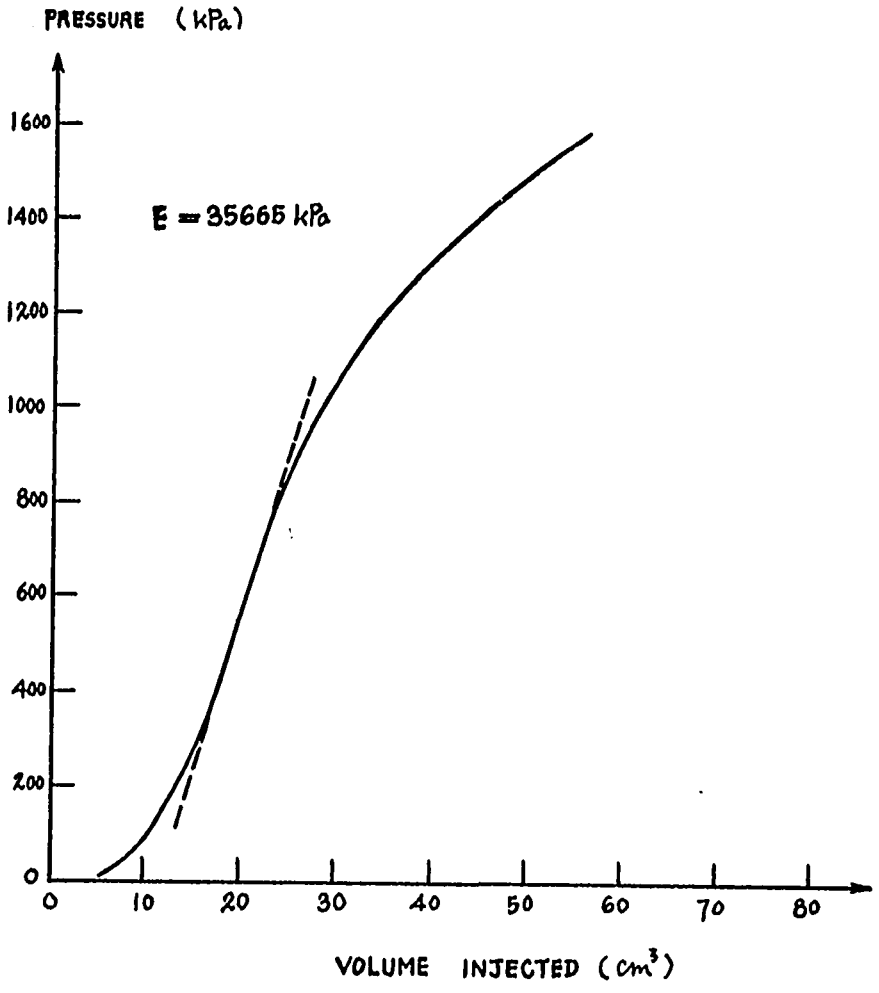

Fig.224 - Test No. 104 - Sarnia Airport. Briaud Pressuremeter Test. Hole 1. Hole: Hand Auger. Depth = 1.8 m.

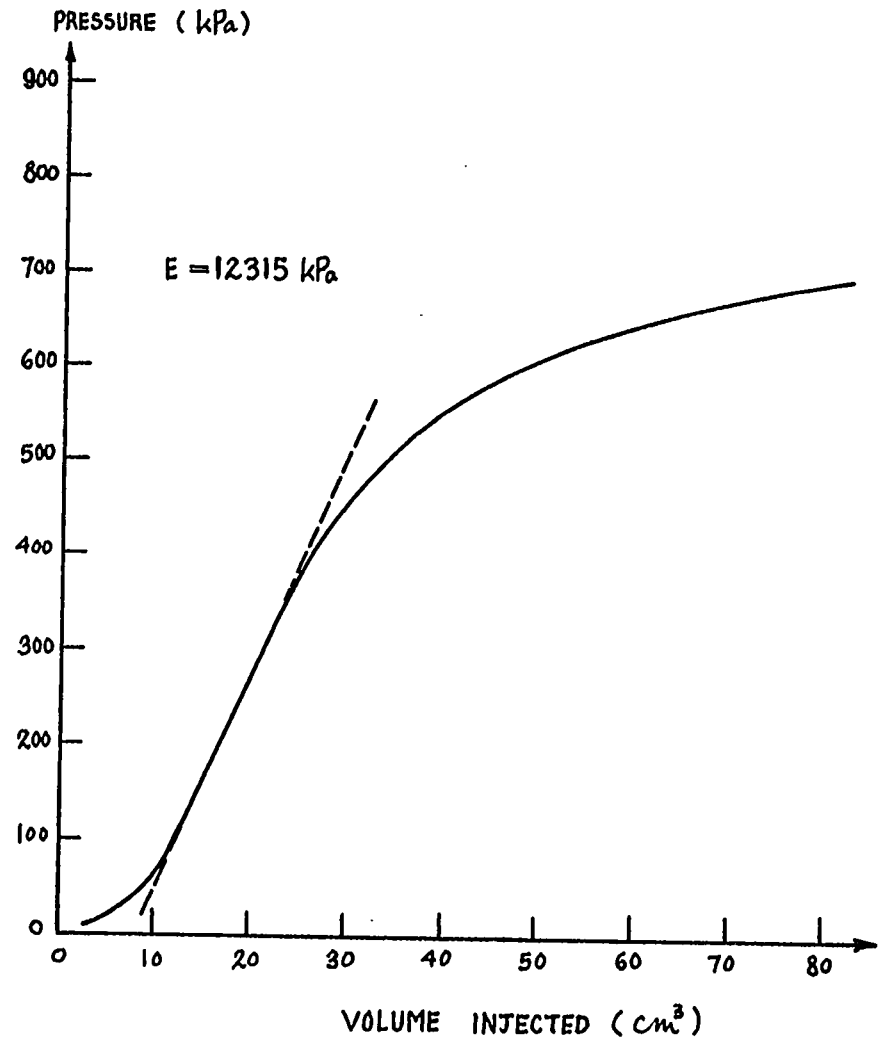

Fig.225 - Test No. 105 - Sarnia Airport. Briaud Pressuremeter Test. Hole 2. Hole: Rod Driving. Depth = 0.3 m.

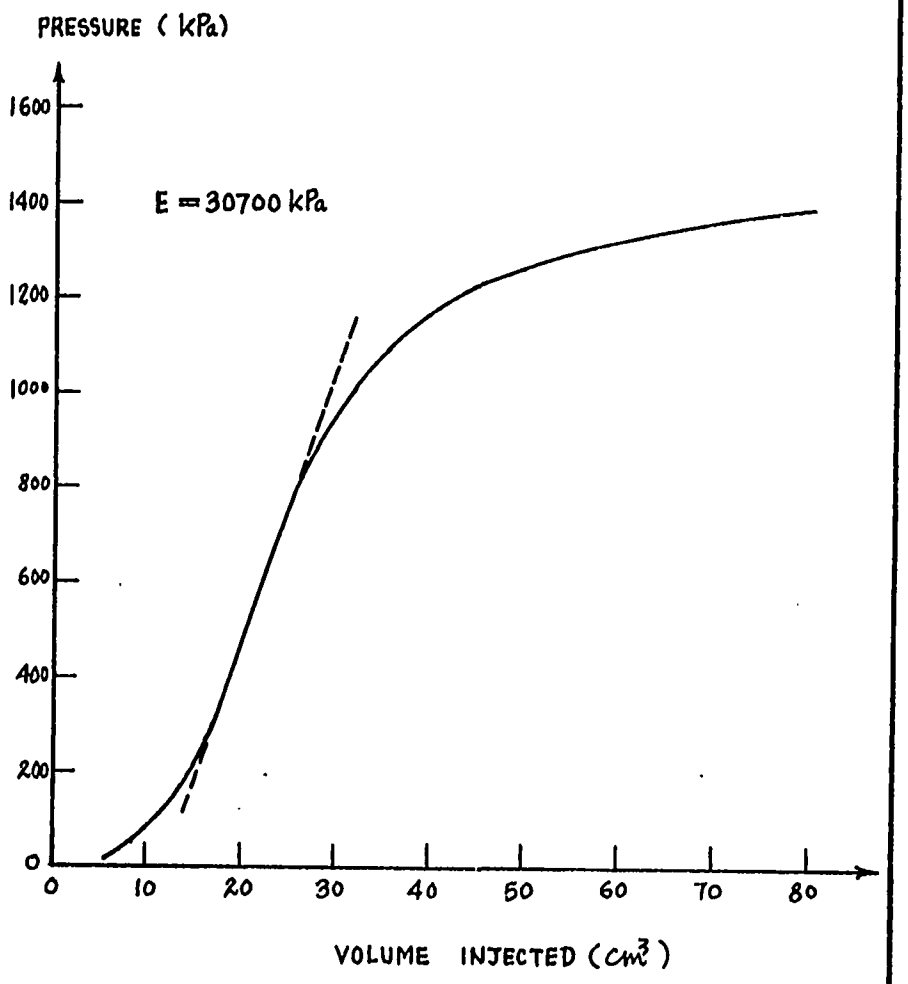

Fig.226 - Test No. 106 - Sarnia Airport. Briaud Pressuremeter Test. Hole 2. Hole: Rod driving. Depth = 0.6 m.

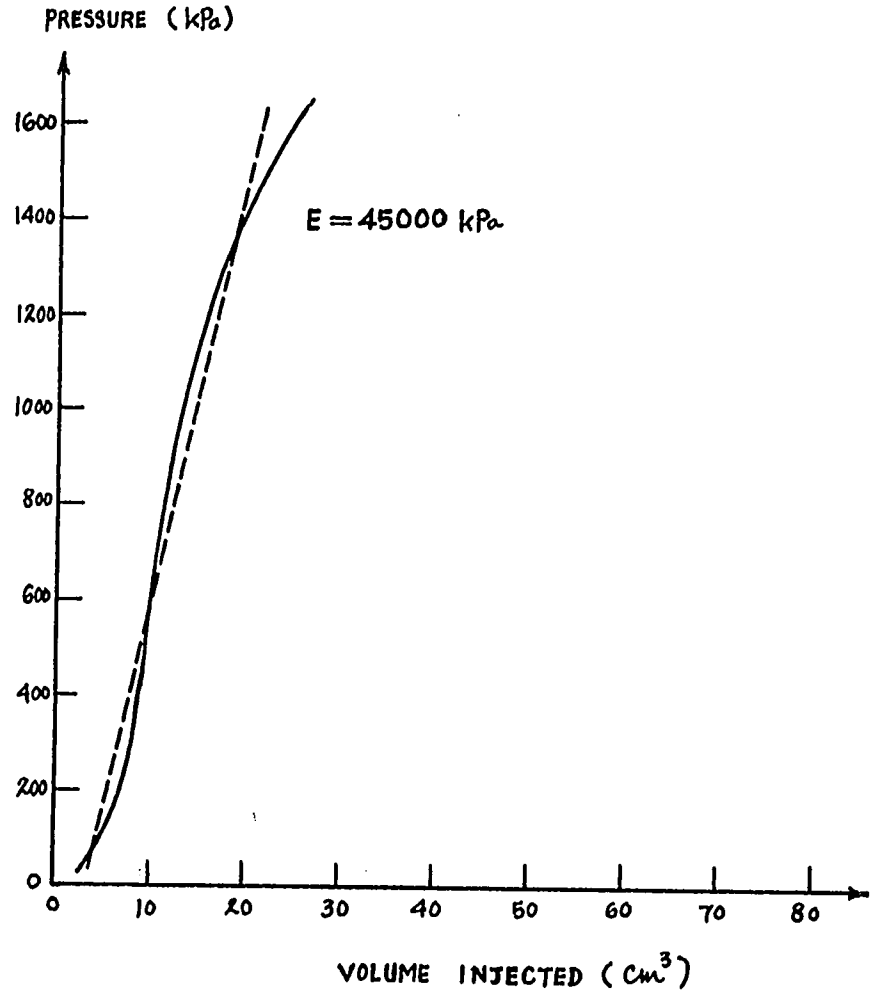

Fig.227 - Test No. 107 - Sarnia Airport. Briaud Pressuremeter Test. Hole 2. Hole:Rod Driving. Depth = 0.9 m.

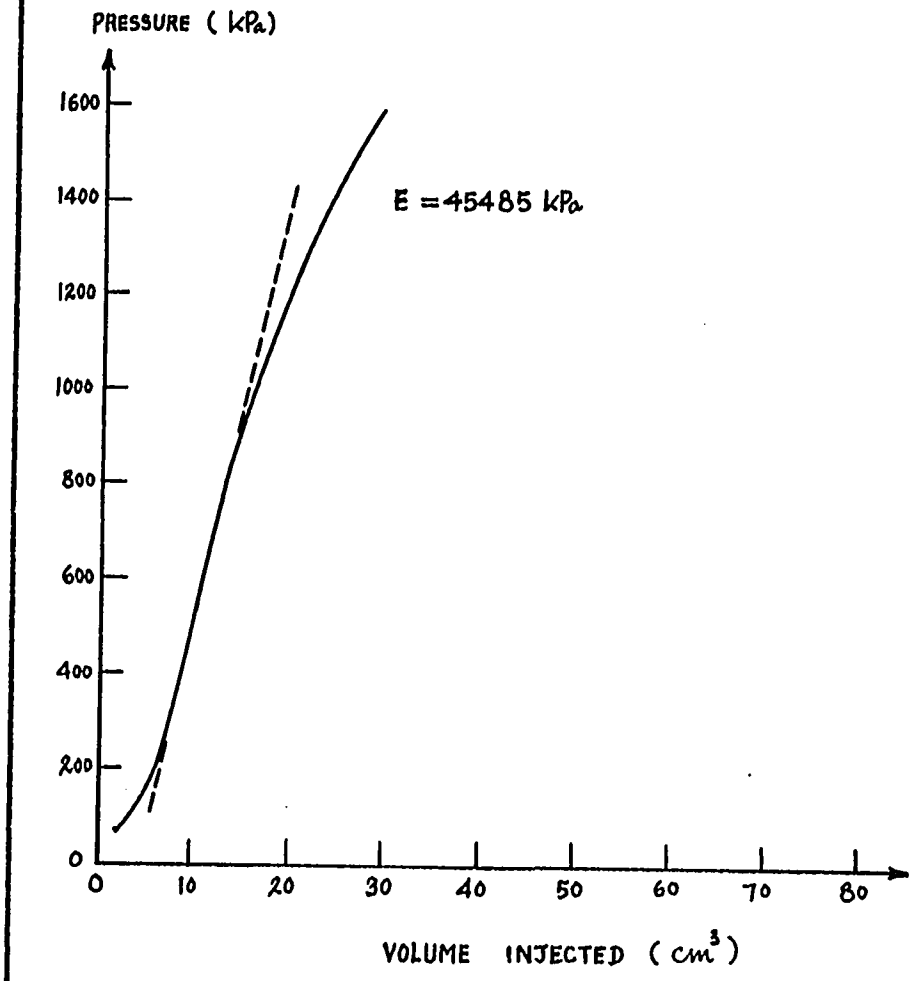

Fig. 228 - Test No. 108 - Sarnia Airport. Briaud Pressuremeter Test. Hole 2. Hole:Rod Driving. Depth = 1.2 m.

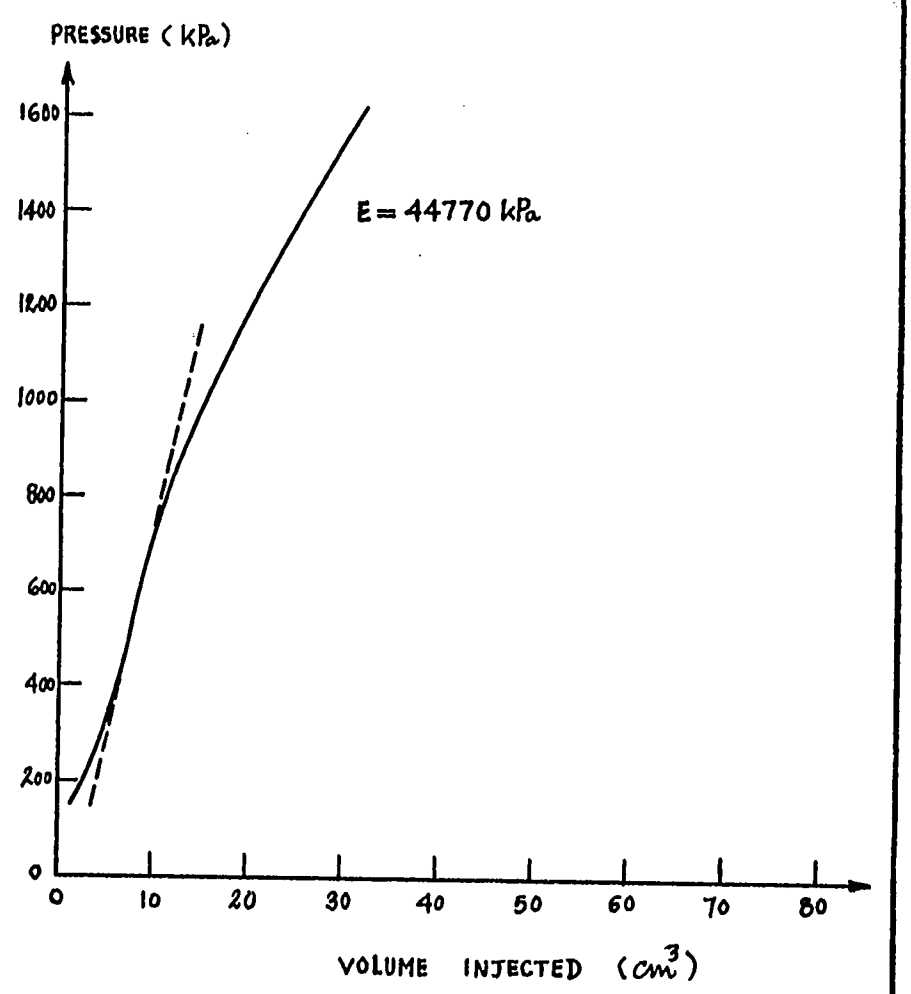

Fig. 229 - Test No. 109 - Sarnia Airport. Briaud Pressuremeter Test. Hole 2. Hole:Rod Driving. Depth = 1.5 m.

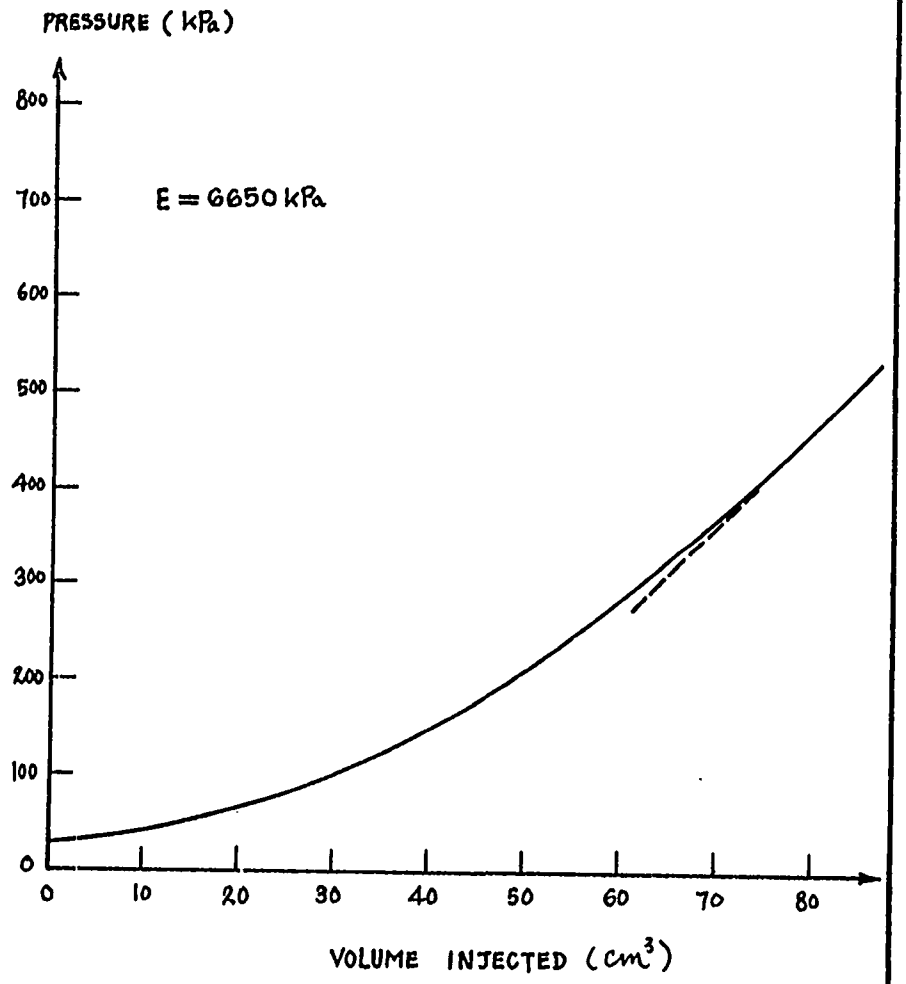

Fig. 230 – Test No. 110 – Sarnia Airport. Briaud Pressuremeter Test. Hole 3. Hole:Rod Driving. Depth = 0.2 m.

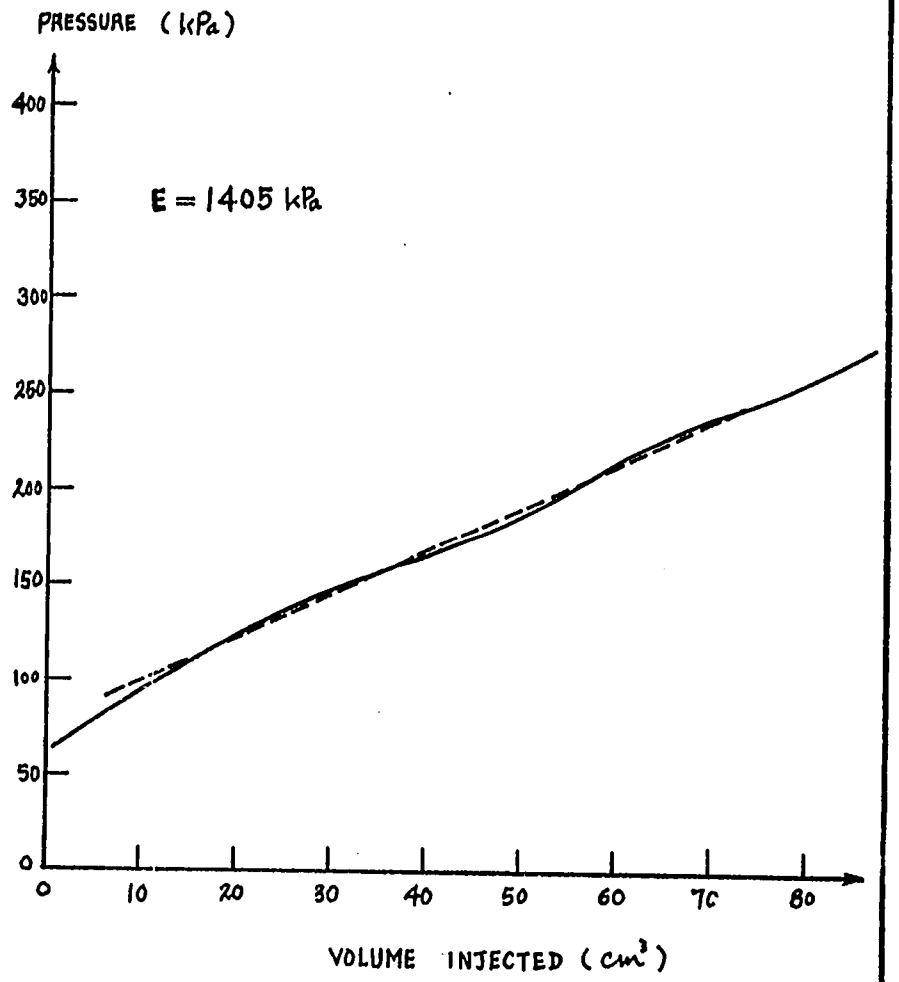

Fig. 231 – Test No. 111 – Sarnia Airport. Briaud Pressuremeter Test. Hole 3. Hole:Rod Driving. Depth = 0.6 m.

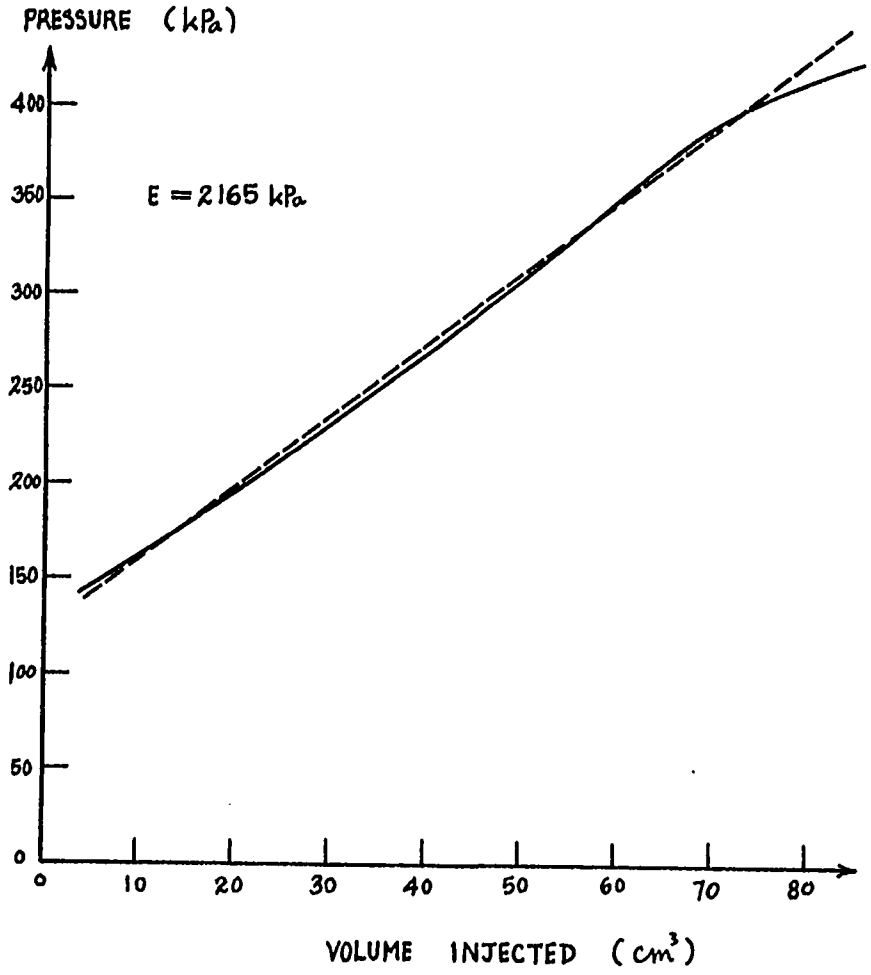

Fig. 232 - Test No. 112 - Sarnia Airport. Briaud Pressuremeter Test. Hole 3. Hole:Rod Driving. Depth = 0.9 m.

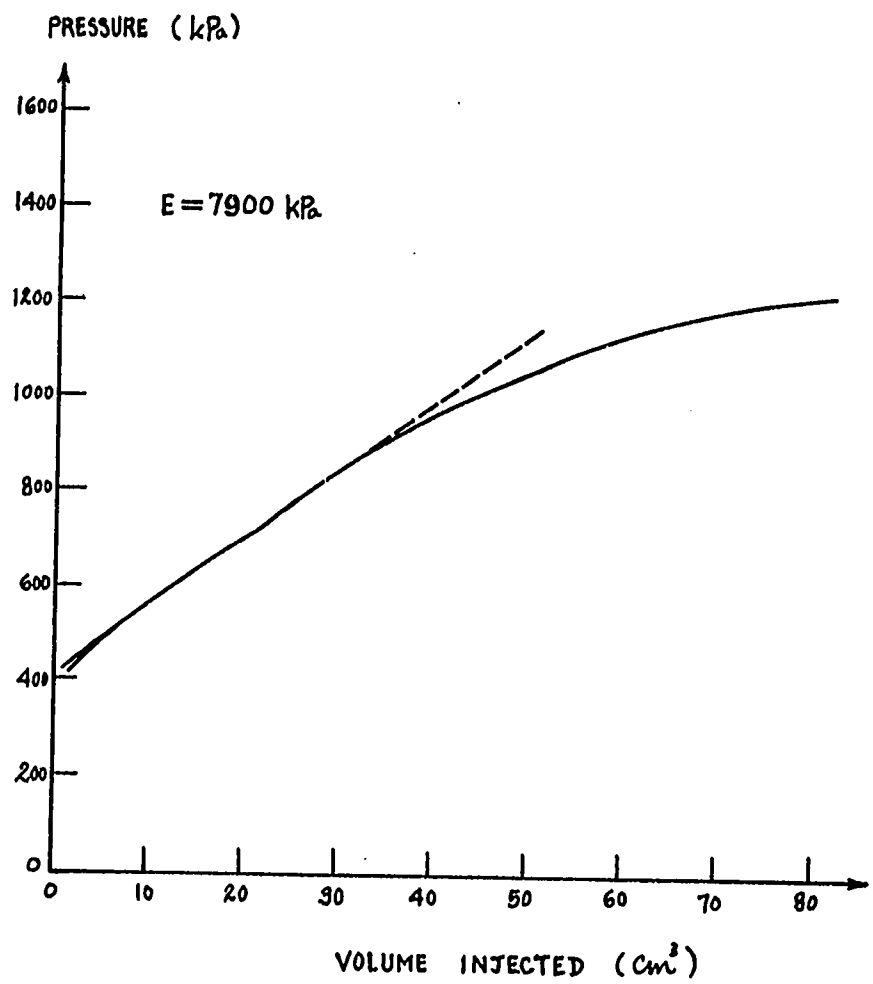

Fig. 233 - Test No. 113 - Sarnia Airport. Briaud Pressuremeter Test. Hole 3. Hole:Rod Driving. Depth = 1.2 m.

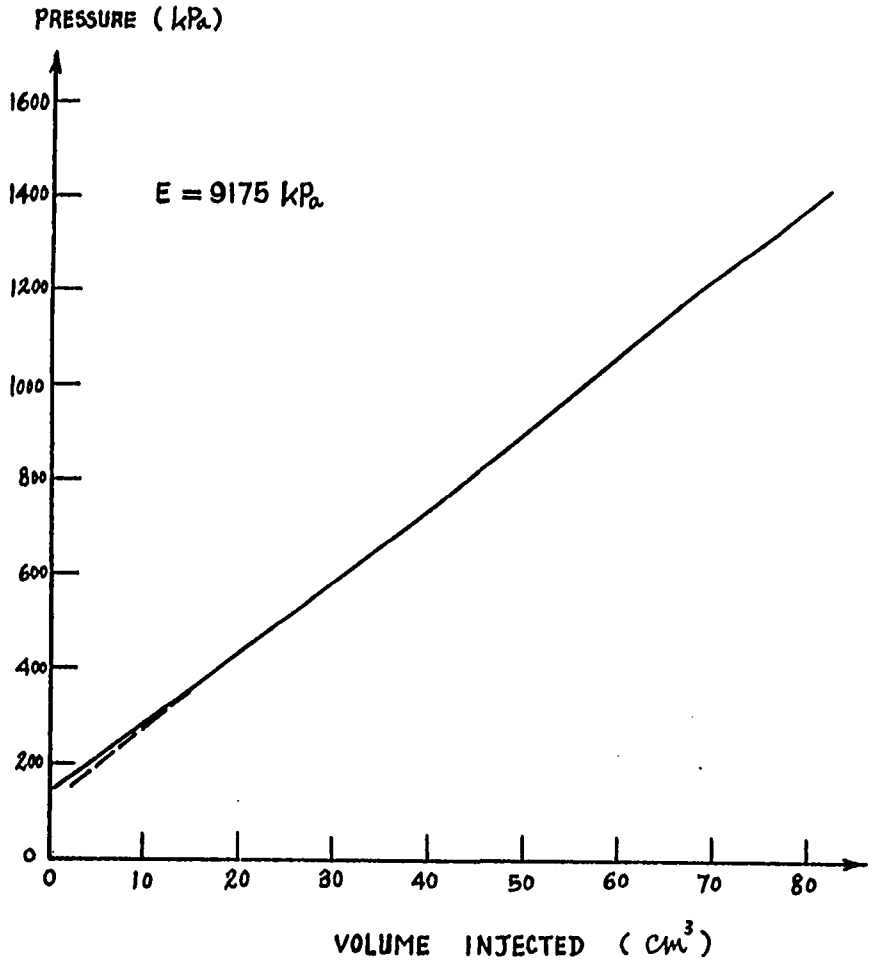

Fig. 234 - Test No. 114 - Sarnia Airport. Briaud Pressuremeter Test. Hole 3. Hole:Rod Driving. Depth = 1.5 m.

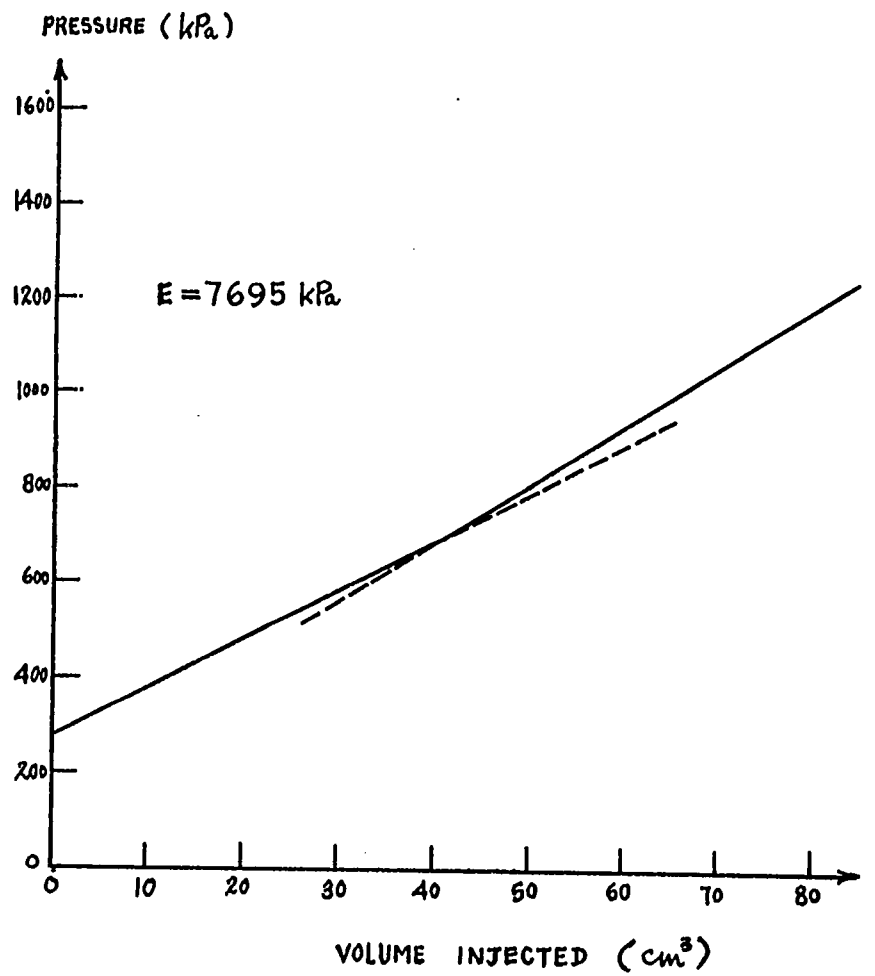

Fig. 235 - Test No. 115 - Sarnia Airport. Briaud Pressuremeter Test. Hole 3. Hole:Rod Driving. Depth = 1.8 m.

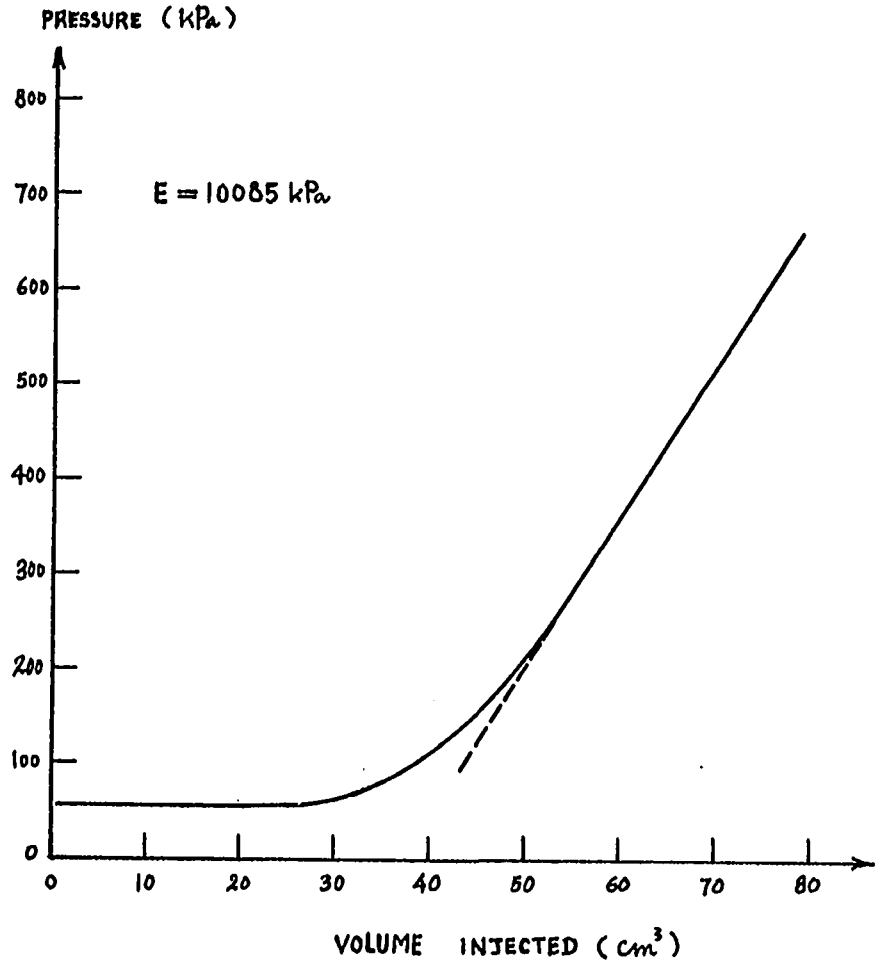

Fig. 236 - Test No. 116 - Sarnia Airport. Briaud Pressuremeter Test. Hole 6. Hole:Rod Driving. Depth = 0.2 m.

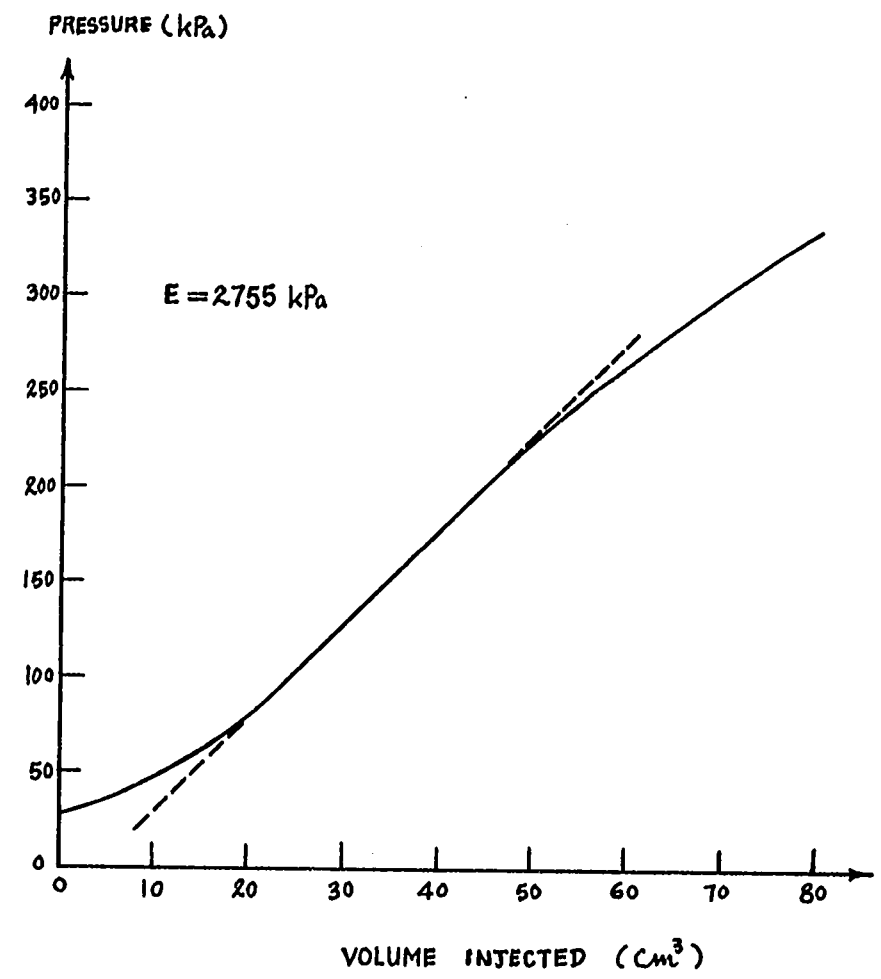

Fig. 237 - Test No. 117 - Sarnia Airport. Briaud Pressuremeter Test. Hole 6. Hole:Rod Driving. Depth = 0.6 m.

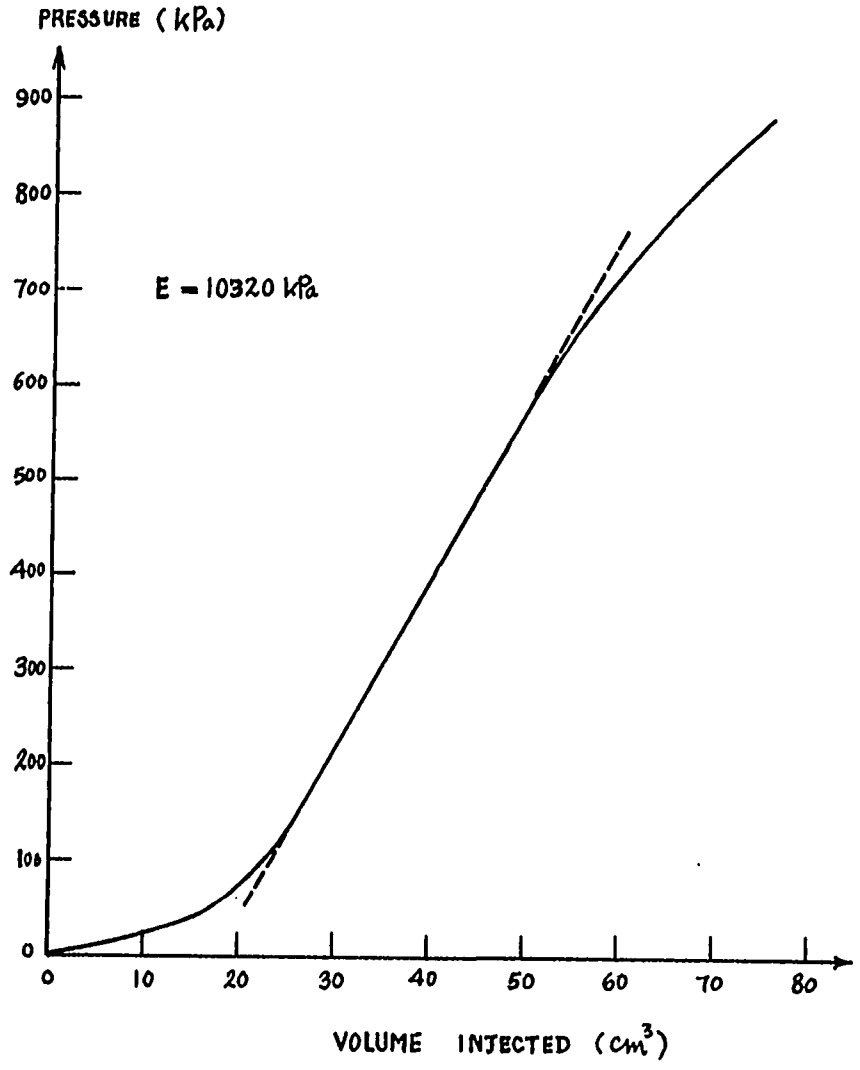

Fig. 238 - Test No. 118 - Sarnia Airport. Briaud Pressuremeter Test. Hole 6. Hole:Rod Driving. Depth = 0.9 m.

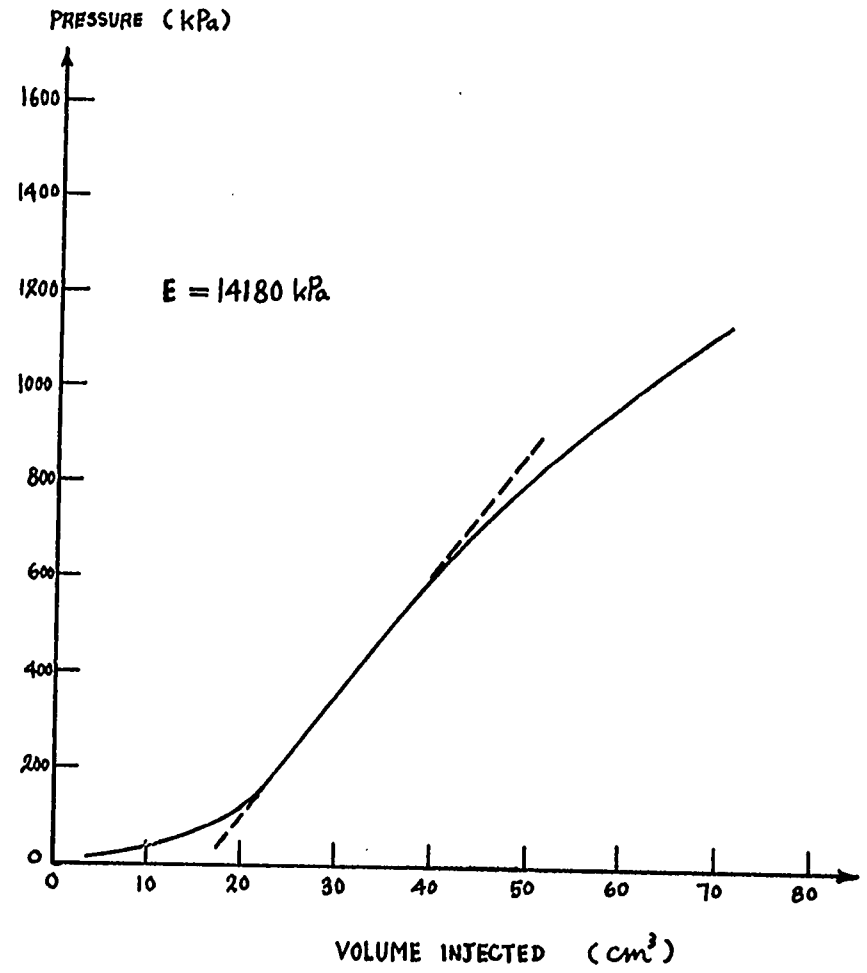

Fig. 239 - Test No. 119 - Sarnia Airport. Briaud Pressuremeter Test. Hole 6. Hole:Rod Driving. Depth = 1.2 m.

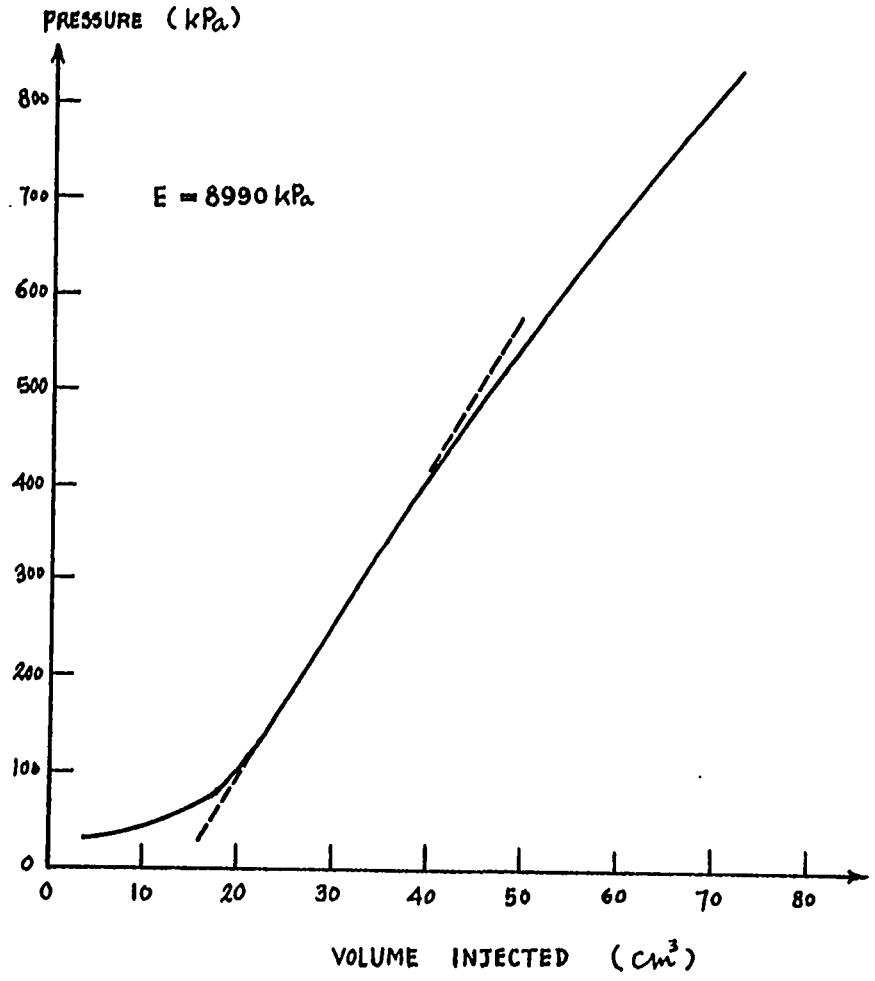

Fig. 240 - Test No. 120 - Sarnia Airport. Briaud Pressuremeter Test. Hole 6. Hole:Rod Driving. Depth = 1.5 m.

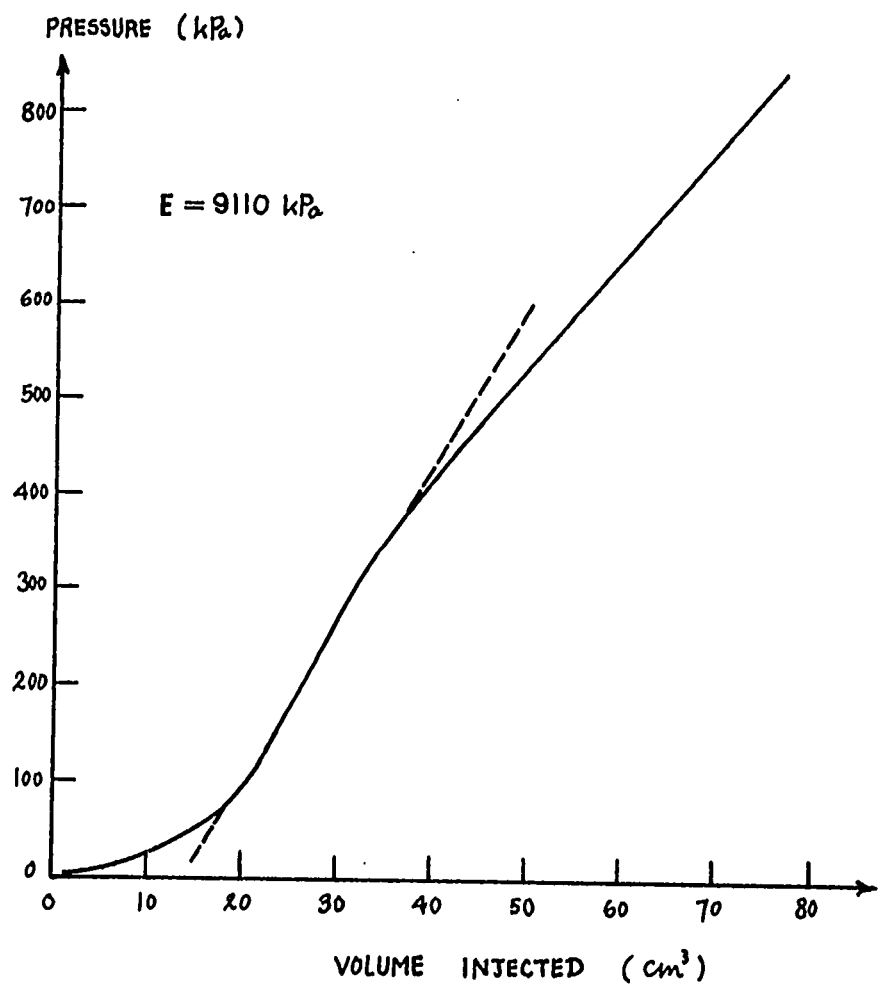

Fig. 241 - Test No. 121 - Sarnia Airport. Briaud Pressuremeter Test. Hole 6. Hole:Rod Driving. Depth = 1.8 m.

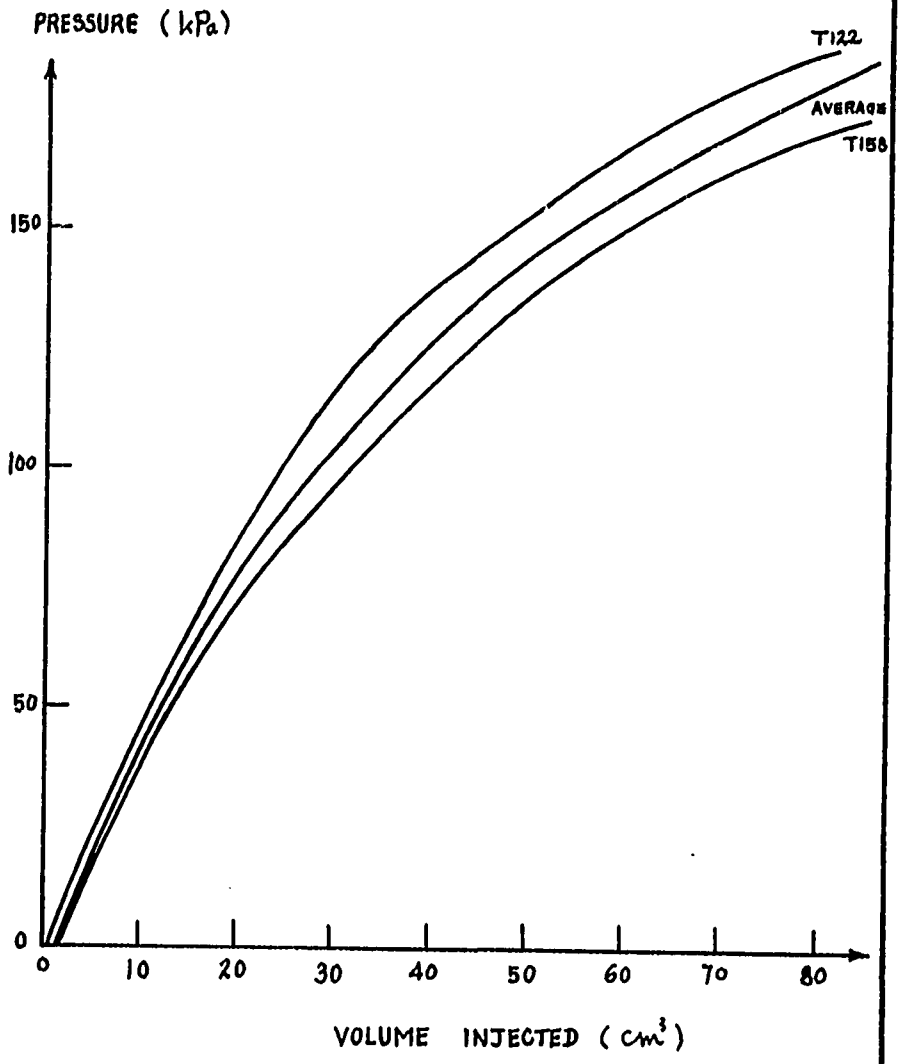

Fig. 242 - Test No. 122 - Sarnia Airport. Briaud Pressuremeter Test. Calibrations of Membrane Resistance.

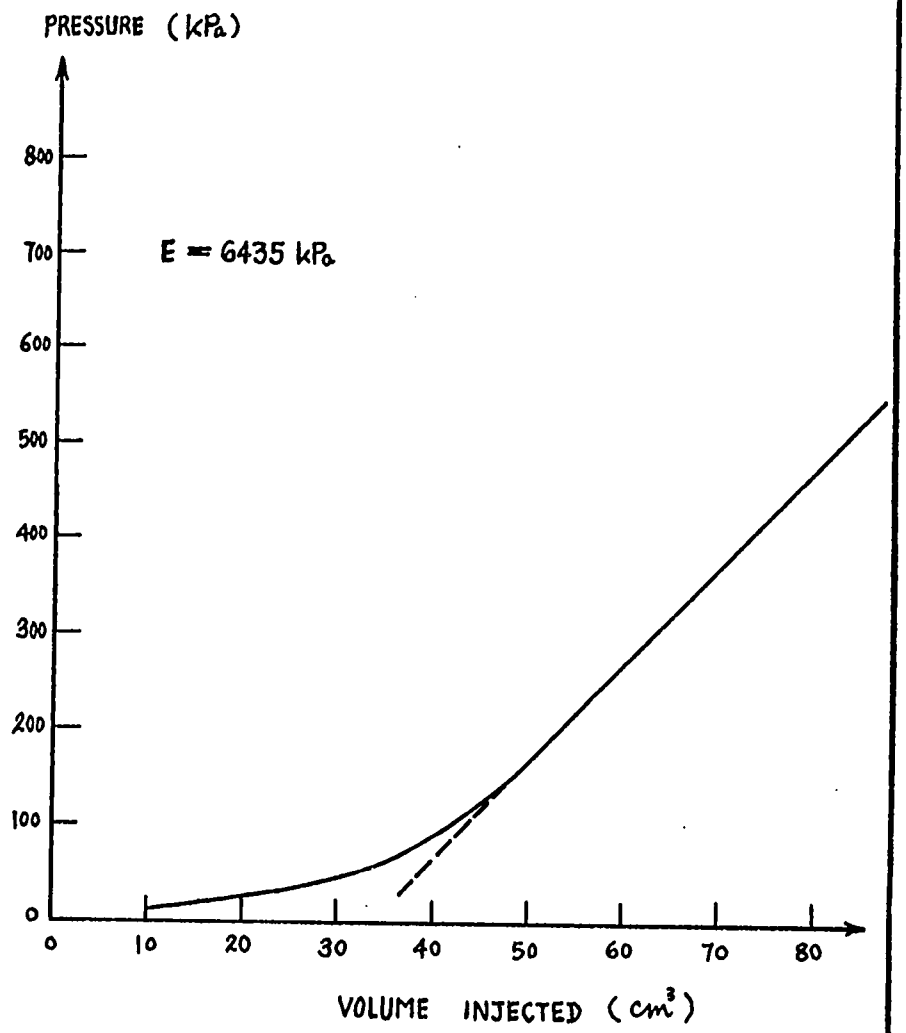

Fig. 243 - Test No. 123 - Sarnia Airport. Briaud Pressuremeter Test. Hole 5. Hole:Rod Driving. Depth = 0.2 m.

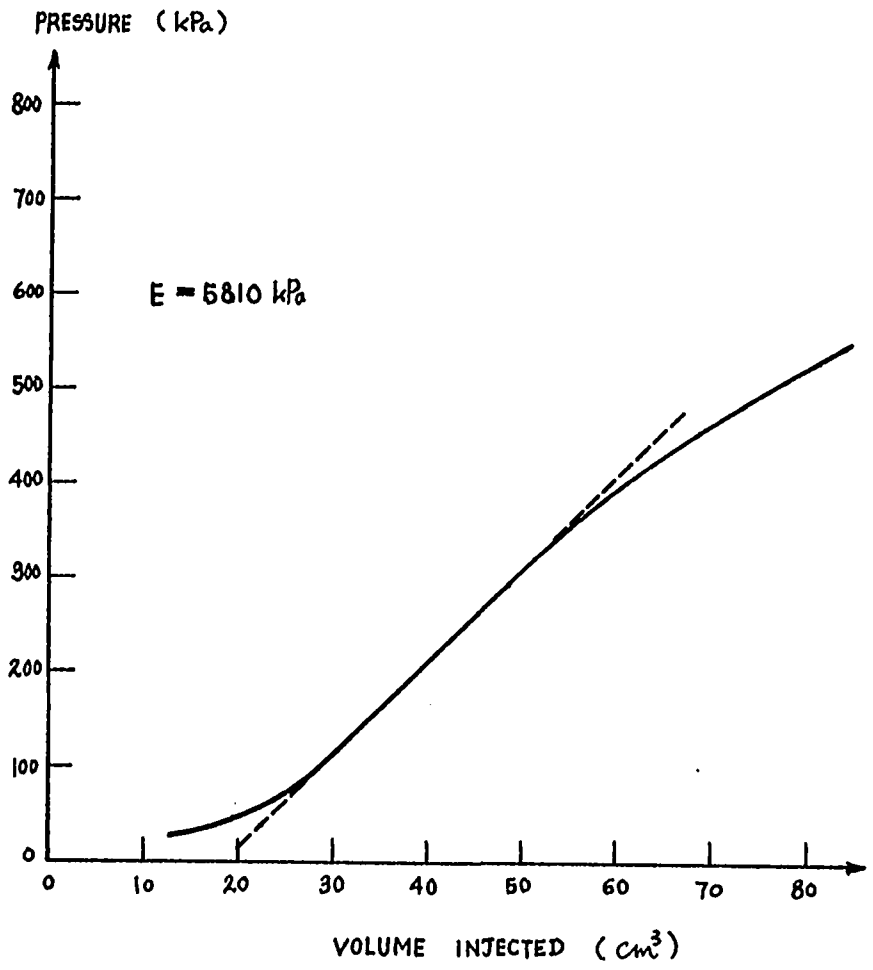

Fig. 244 - Test No. 124 - Sarnia Airport. Briaud Pressuremeter Test. Hole 5. Hole:Rod Driving. Depth = 0.6 m.

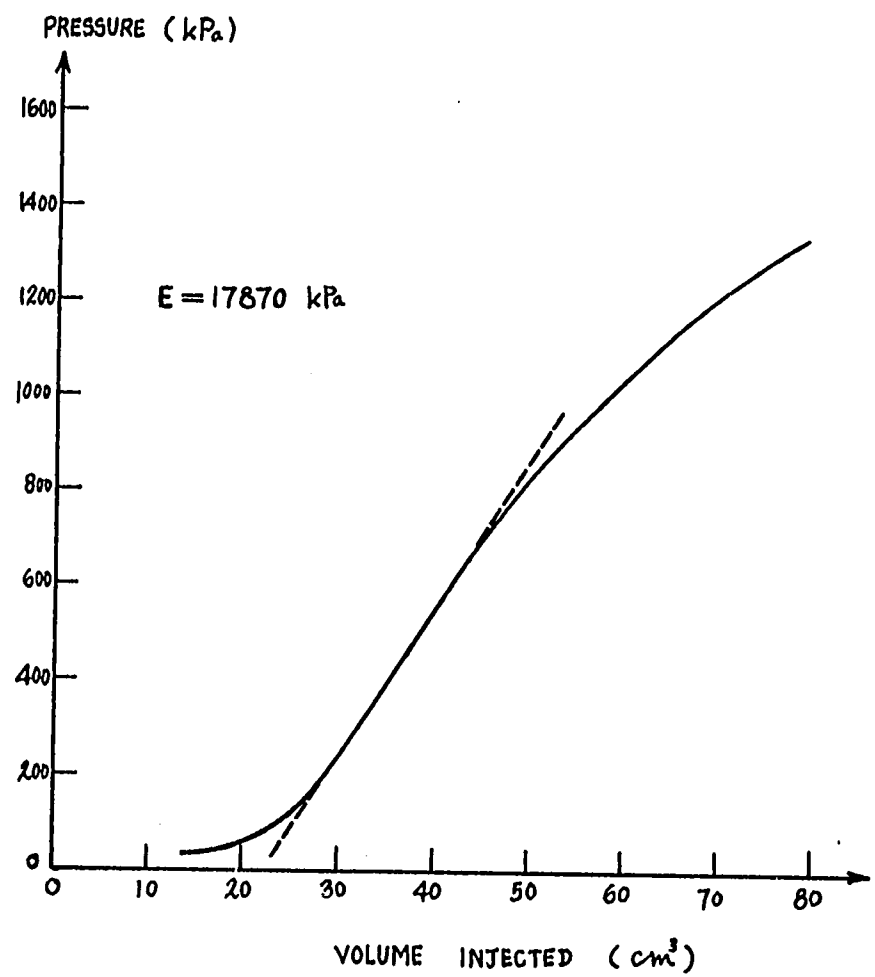

Fig. 245 - Test No. 125 - Sarnia Airport. Briaud Pressuremeter Test. Hole 5. Hole:Rod Driving. Depth = 0.9 m.

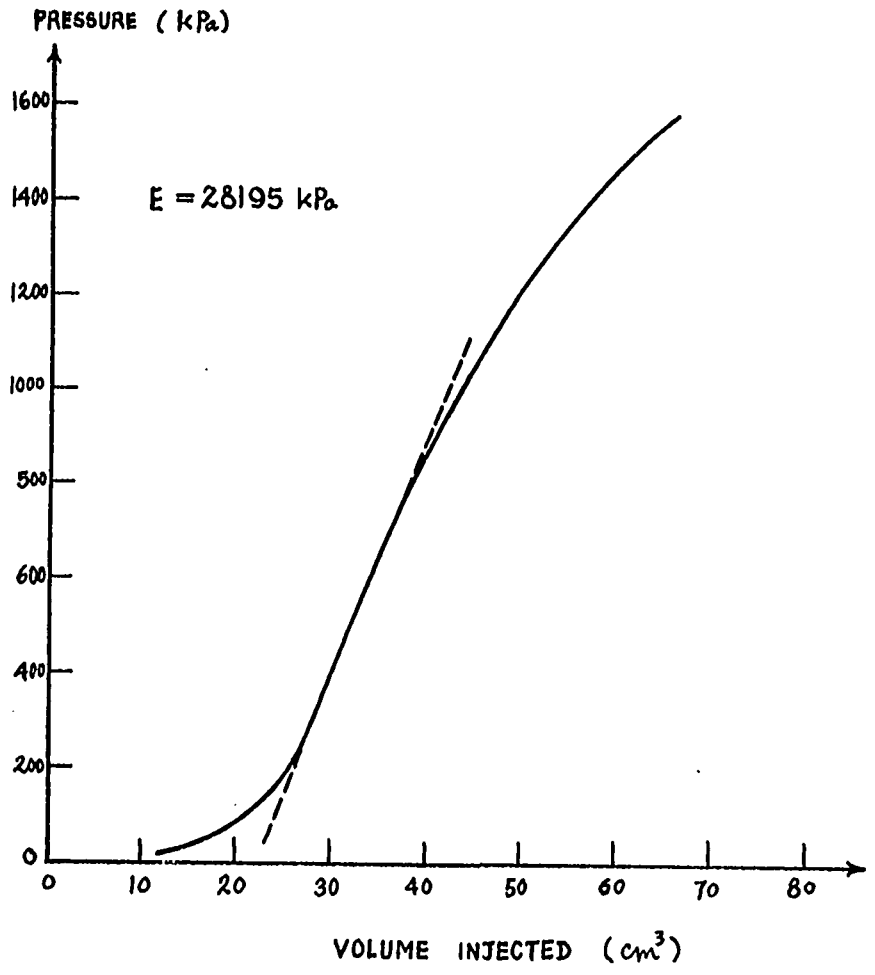

Fig.246 - Test No. 126 - Sarnia Airport. Briaud Pressuremeter Test. Hole 5. Hole:Rod Driving. Depth = 1.2 m.

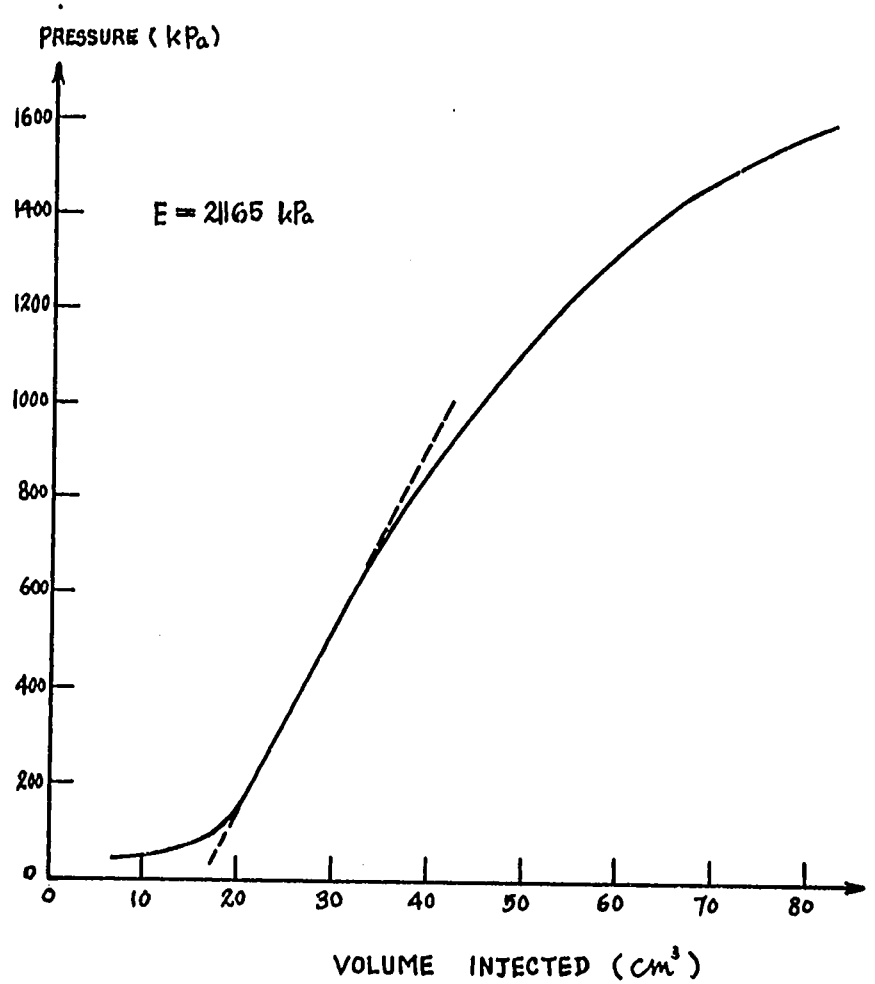

Fig.247 - Test No. 127 - Sarnia Airport. Briaud Pressuremeter Test. Hole 5. Hole:Rod Driving. Depth = 1.5 m.

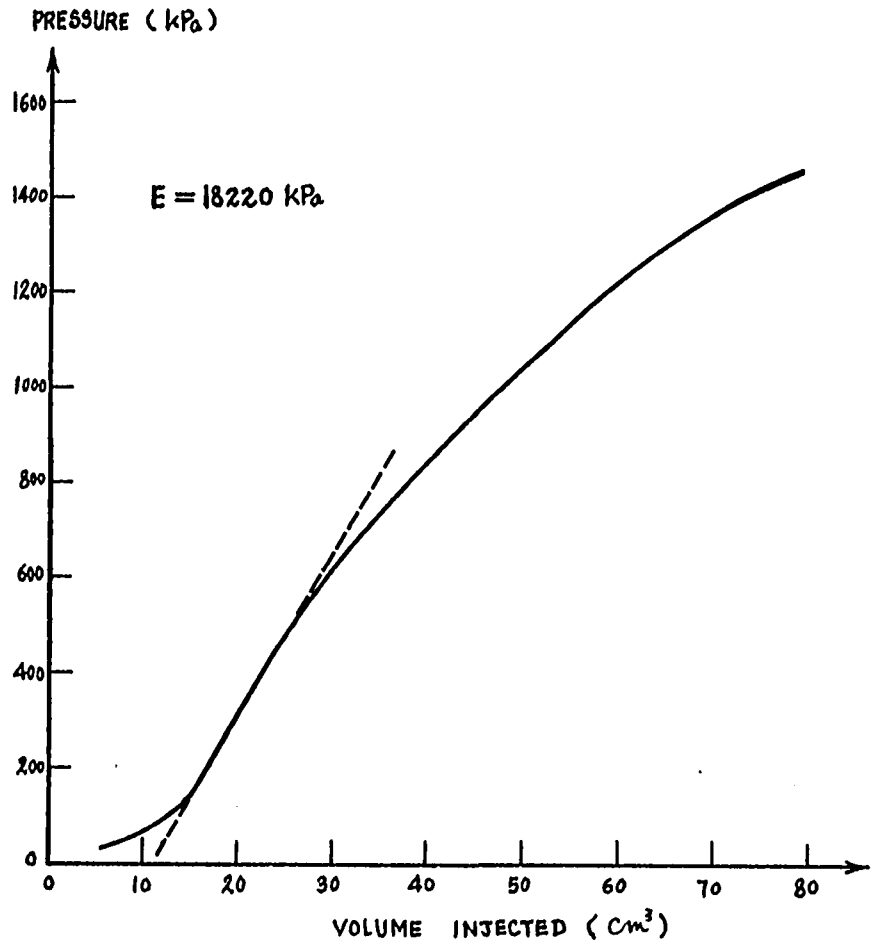

Fig. 248 - Test No. 128 - Sarnia Airport. Briaud Pressuremeter Test. Hole 5. Hole:Rod Driving. Depth = 1.8 m.

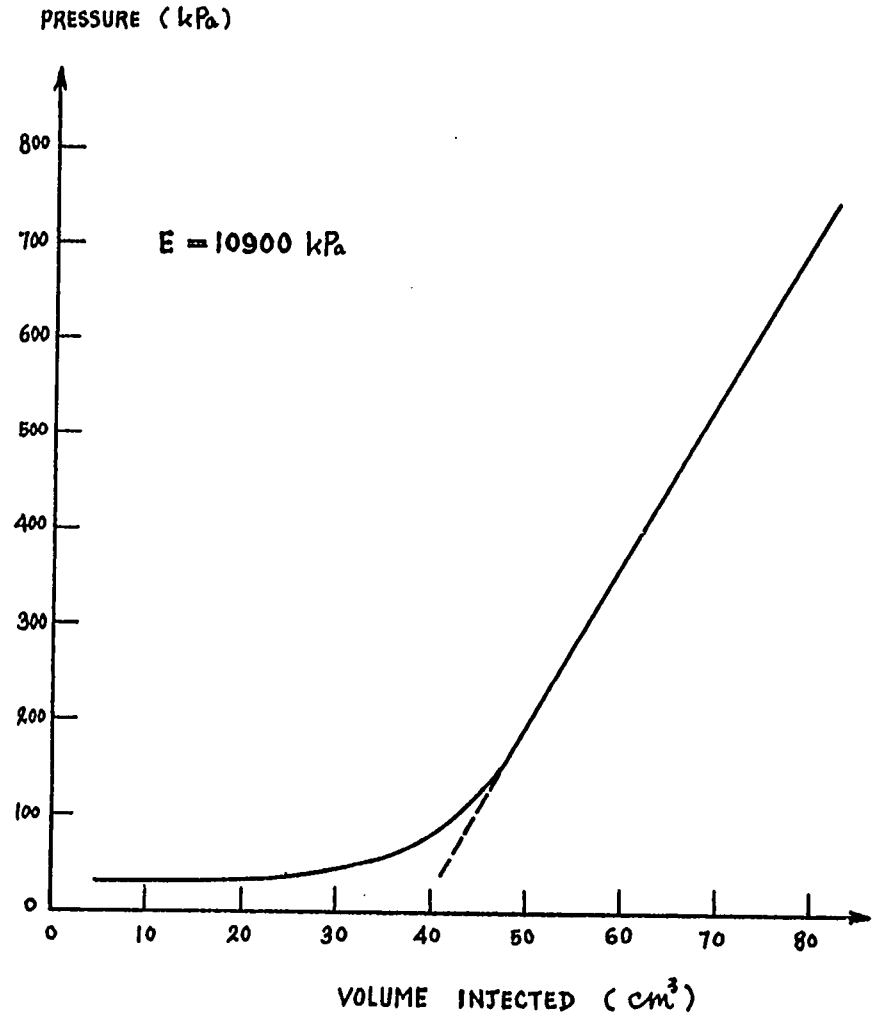

Fig. 249 - Test No. 129 - Sarnia Airport. Briaud Pressuremeter Test. Hole 4. Hole:Rod Driving. Depth = 0.2 m.

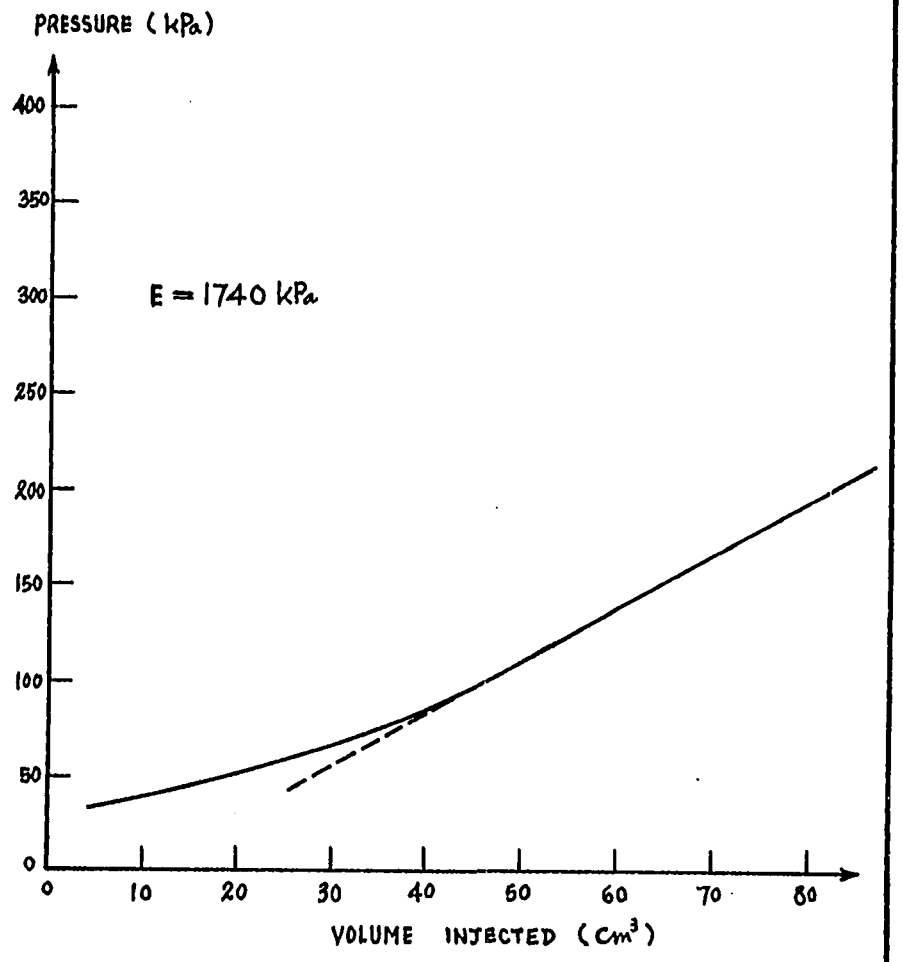

Fig.250 - Test No. 130 - Sarnia Airport. Briaud Pressuremeter Test. Hole 4. Hole:Rod Driving. Depth = 0.6 m.

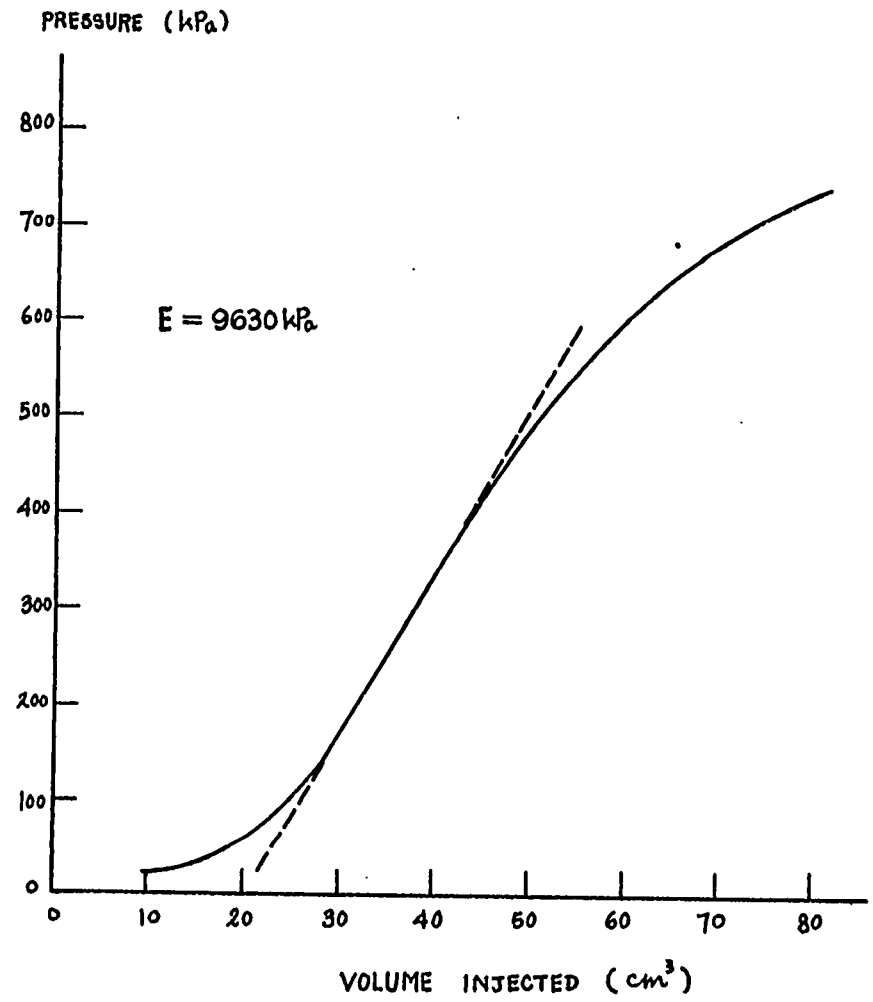

Fig.251 - Test No. 131 - Sarnia Airport. Briaud Pressuremeter Test. Hole 4. Hole:Rod Driving. Depth = 0.9 m.

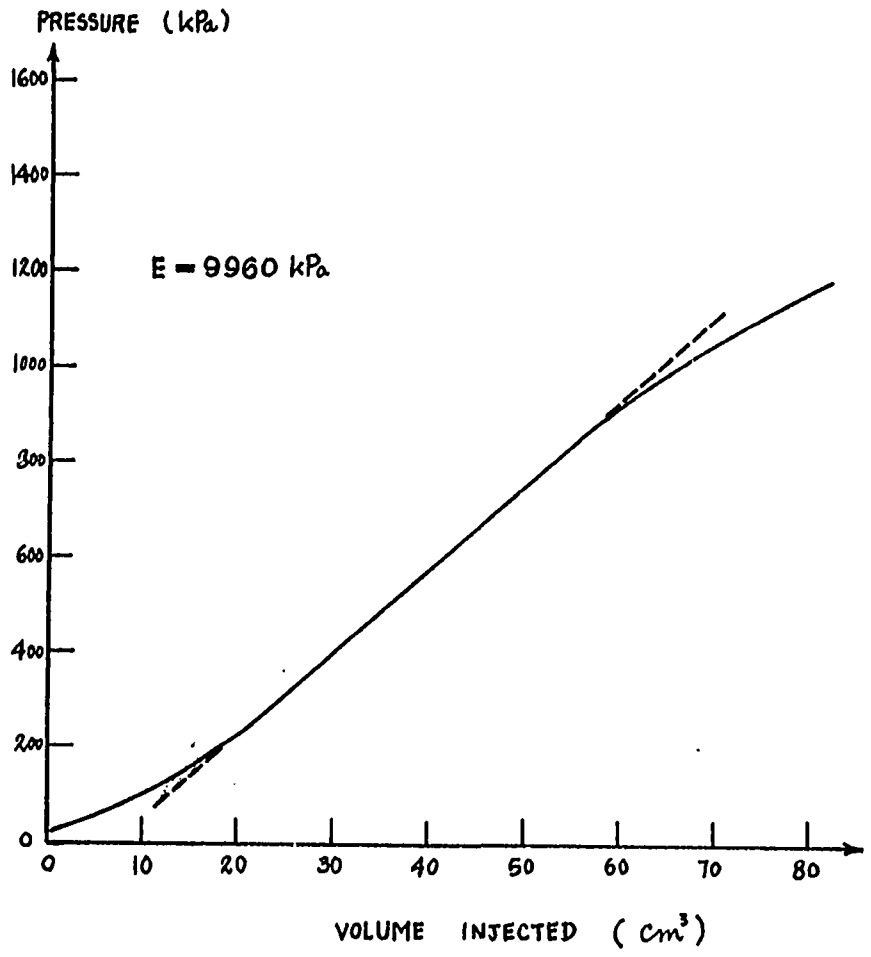

Fig. 252 – Test No. 132 – Sarnia Airport. Briaud Pressuremeter Test. Hole 4. Hole:Rod Driving. Depth = 1.2 m.

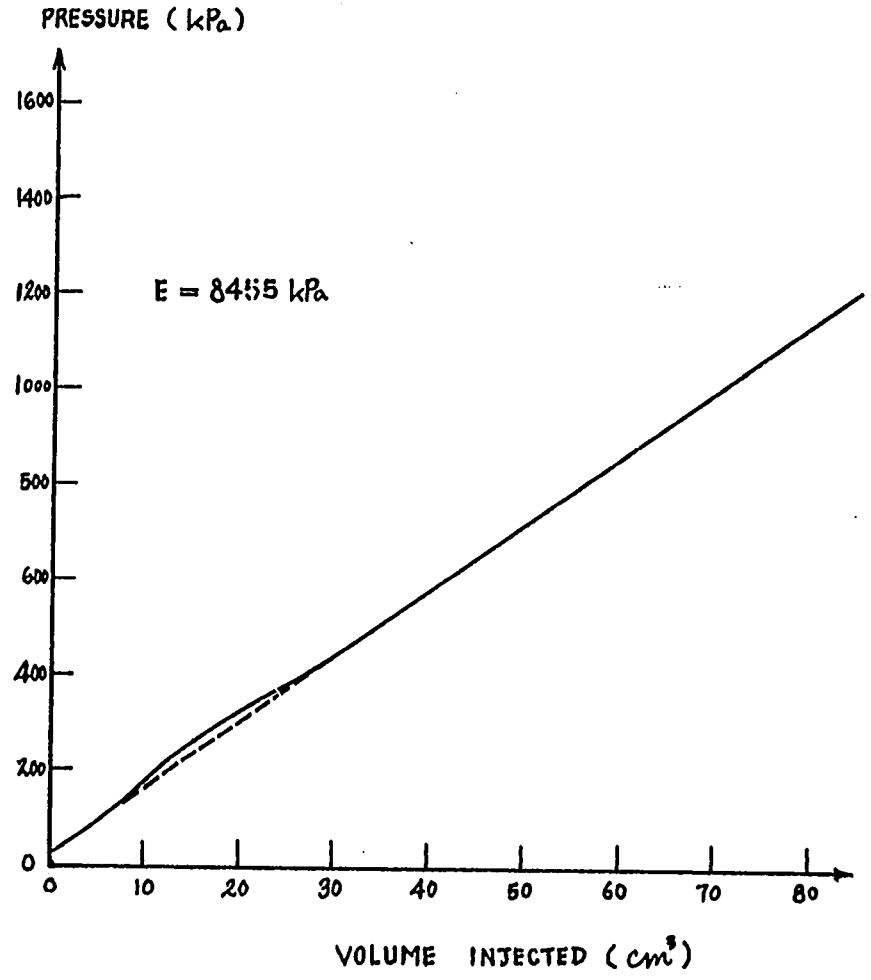

Fig. 253 – Test No. 133 – Sarnia Airport. Briaud Pressuremeter Test. Hole 4. Hole:Rod Driving. Depth = 1.5 m.

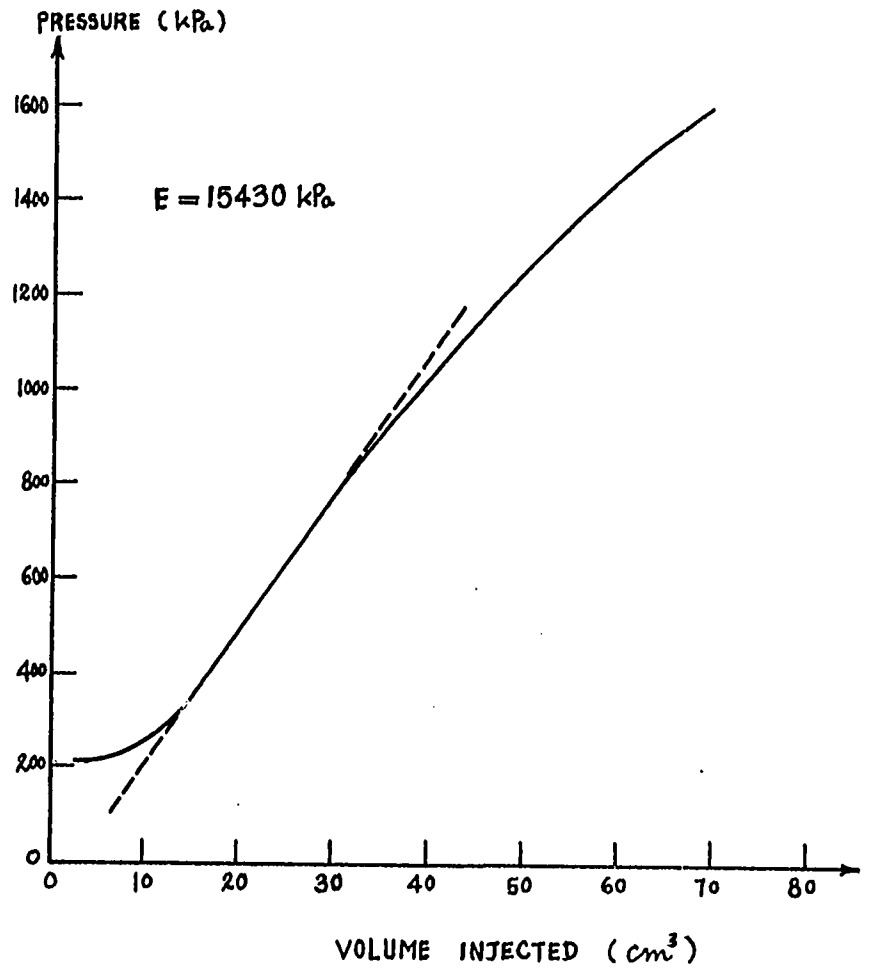

Fig. 254 – Test No. 134 – Sarnia Airport. Briaud Pressuremeter Test. Hole 4. Hole:Rod Driving. Depth = 1.8 m.

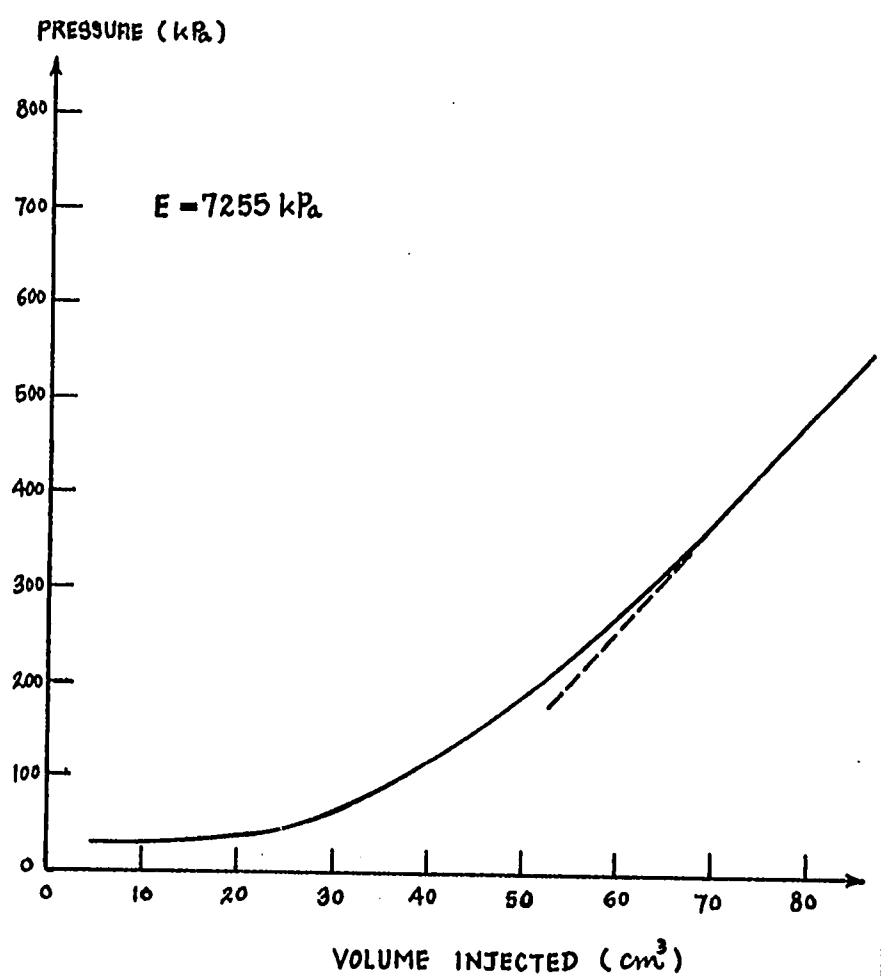

Fig.255 – Test No. 135 – Sarnia Airport. Briaud Pressuremeter Test. Hole 7. Hole:Rod Driving. Depth = 0.27 m.

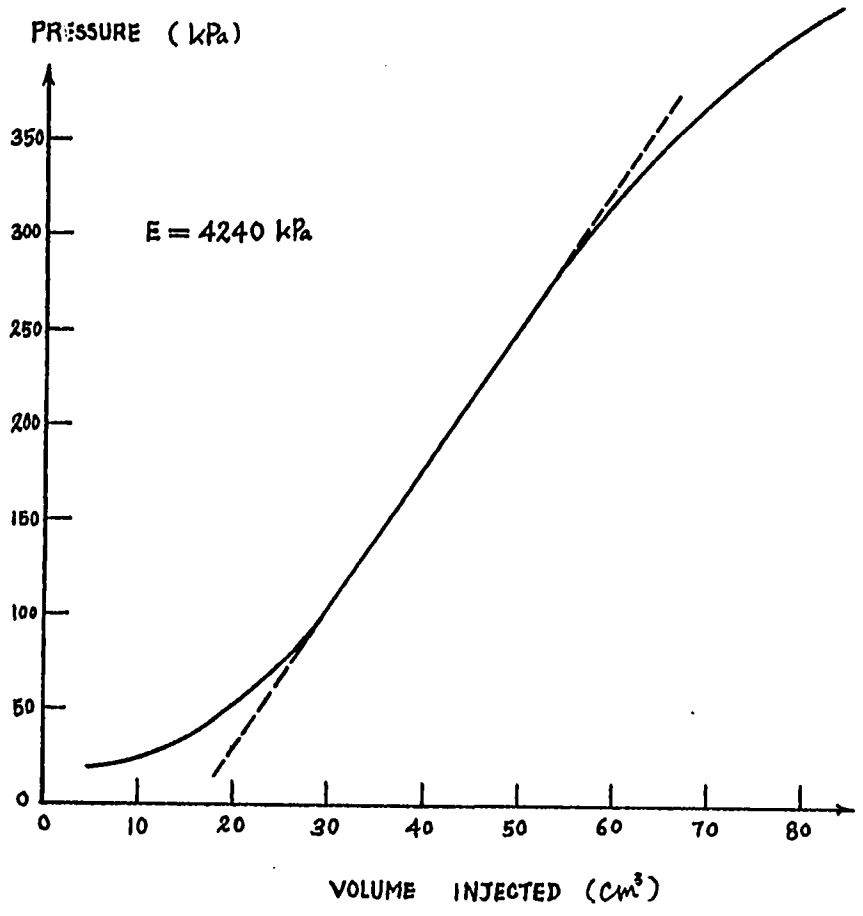

Fig. 256 - Test No. 136 - Sarnia Airport. Briaud Pressuremeter Test. Hole 7. Hole:Rod Driving. Depth = 0.6 m.

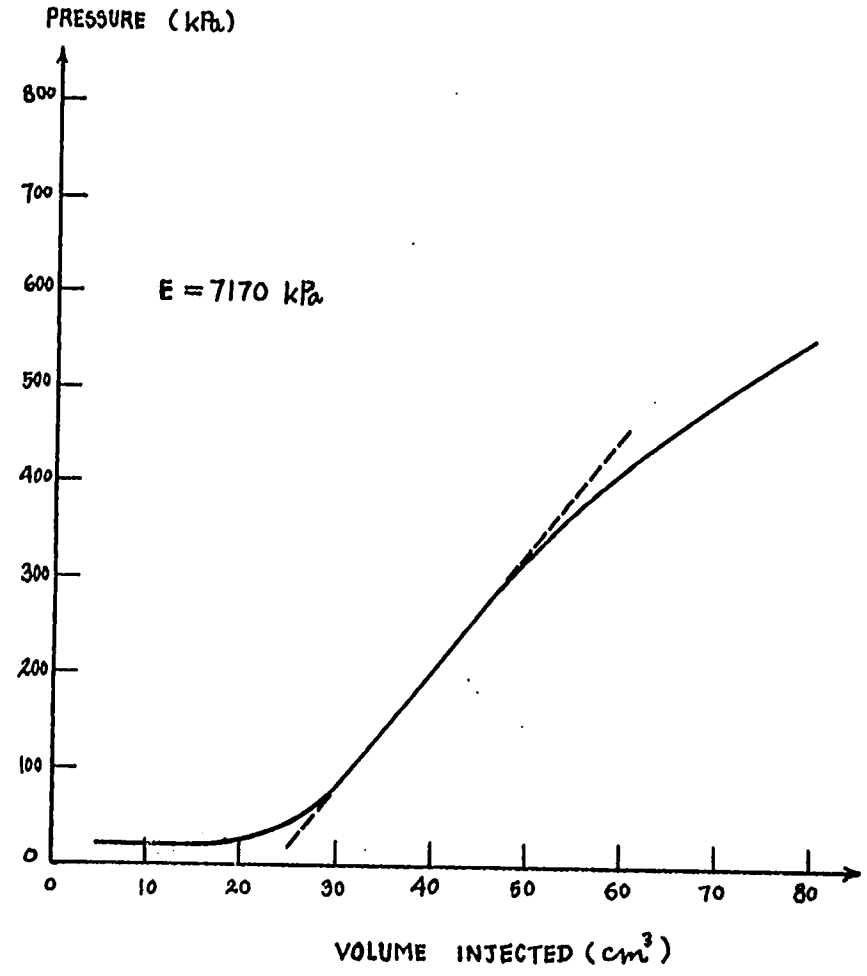

Fig. 257 - Test No. 137 - Sarnia Airport. Briaud Pressuremeter Test. Hole 7. Hole:Rod Driving. Depth = 0.9 m.

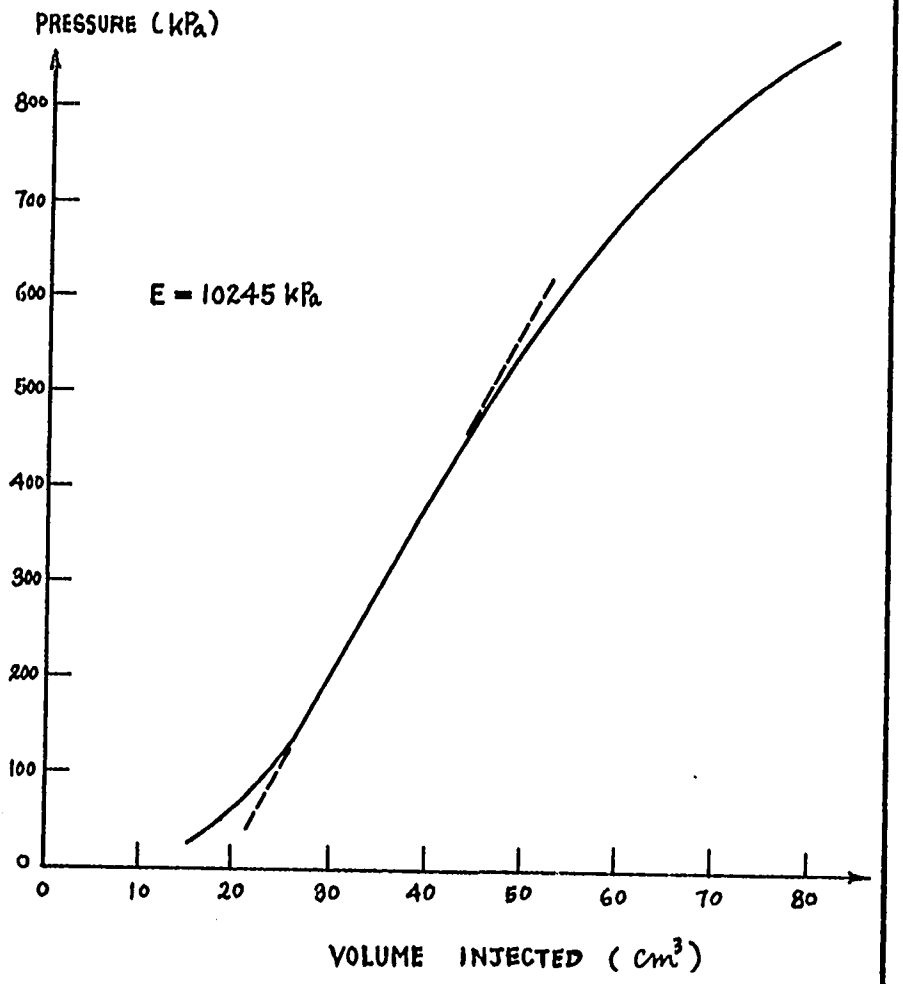

Fig.258 - Test No. 138 - Sarnia Airport. Briaud Pressuremeter Test. Hole 7. Hole:Rod Driving. Depth = 1.2 m.

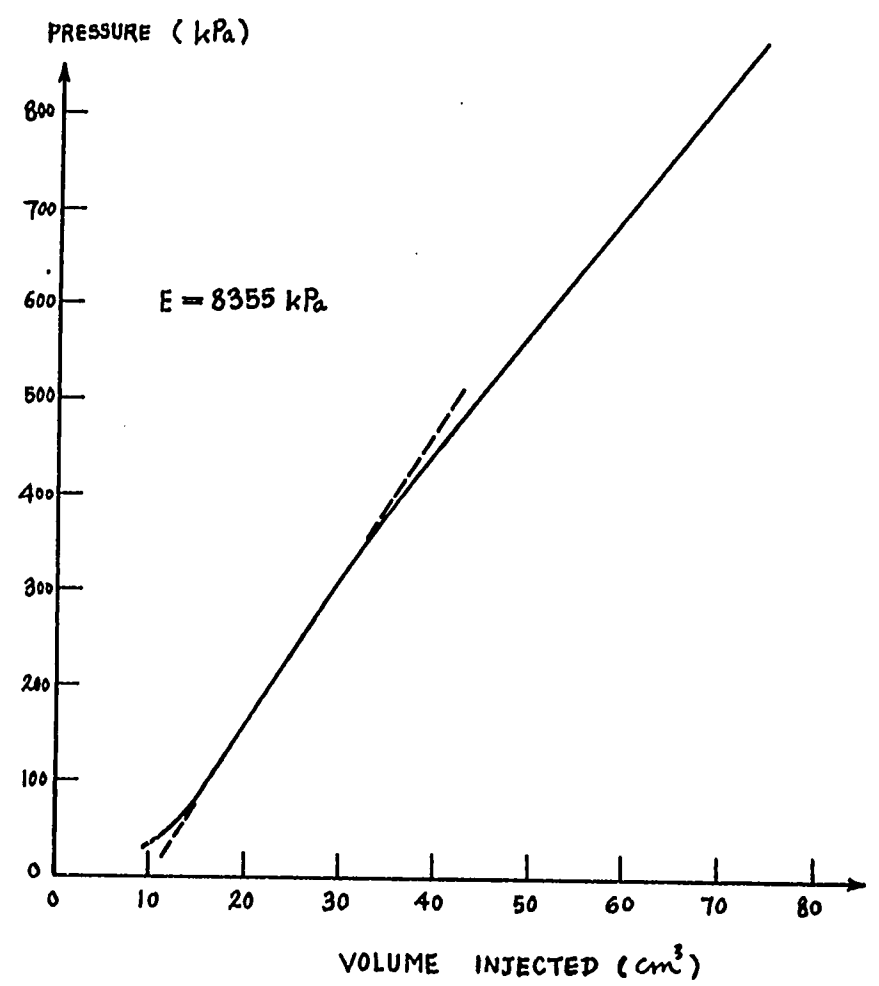

Fig.259 - Test No. 139 - Sarnia Airport. Briaud Pressuremeter Test. Hole 7. Hole:Rod Driving. Depth = 1.5 m.

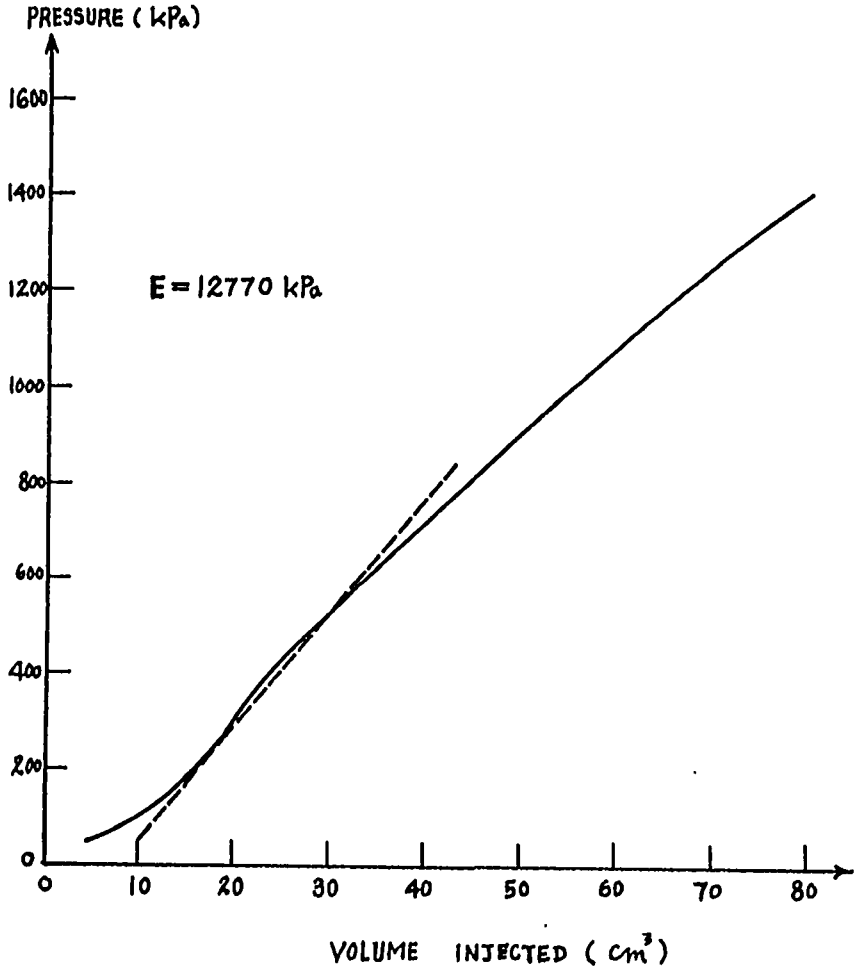

Fig. 260 - Test No. 140 - Sarnia Airport. Briaud Pressuremeter Test. Hole 7. Hole:Rod Driving. Depth = 1.8 m.

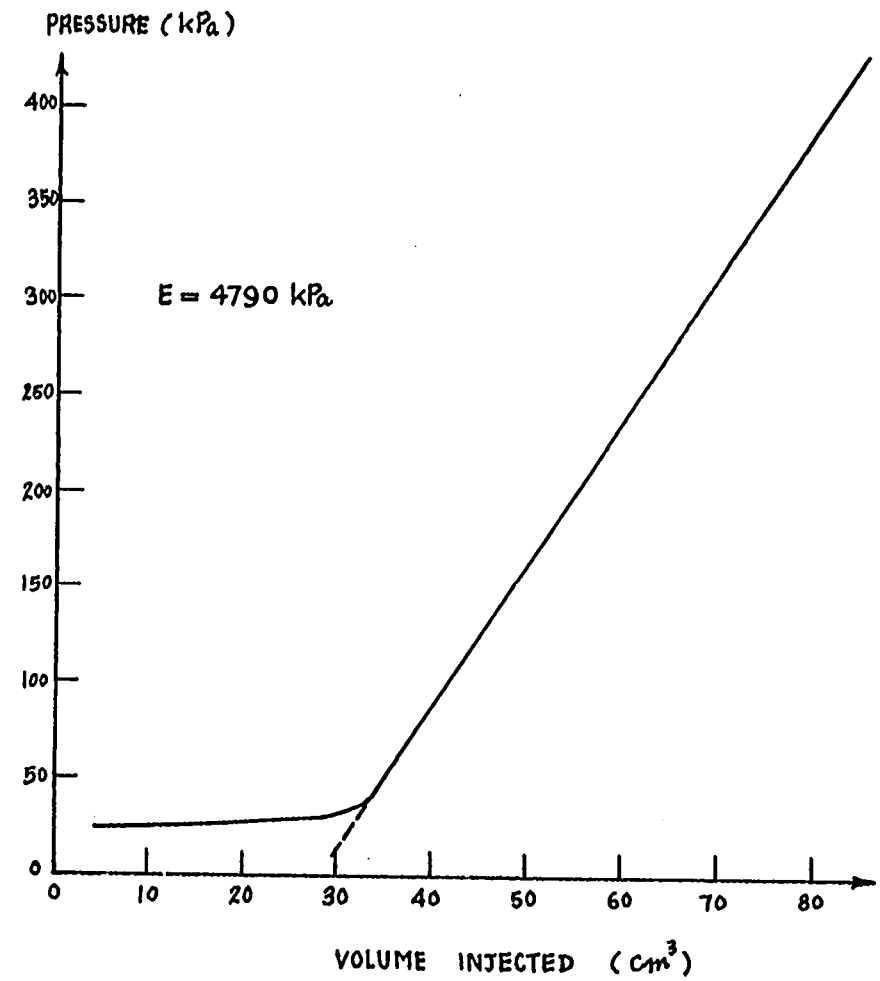

Fig. 261 - Test No. 141 - Sarnia Airport. Briaud Pressuremeter Test. Hole 8. Hole:Rod Driving. Depth = 0.27 m.

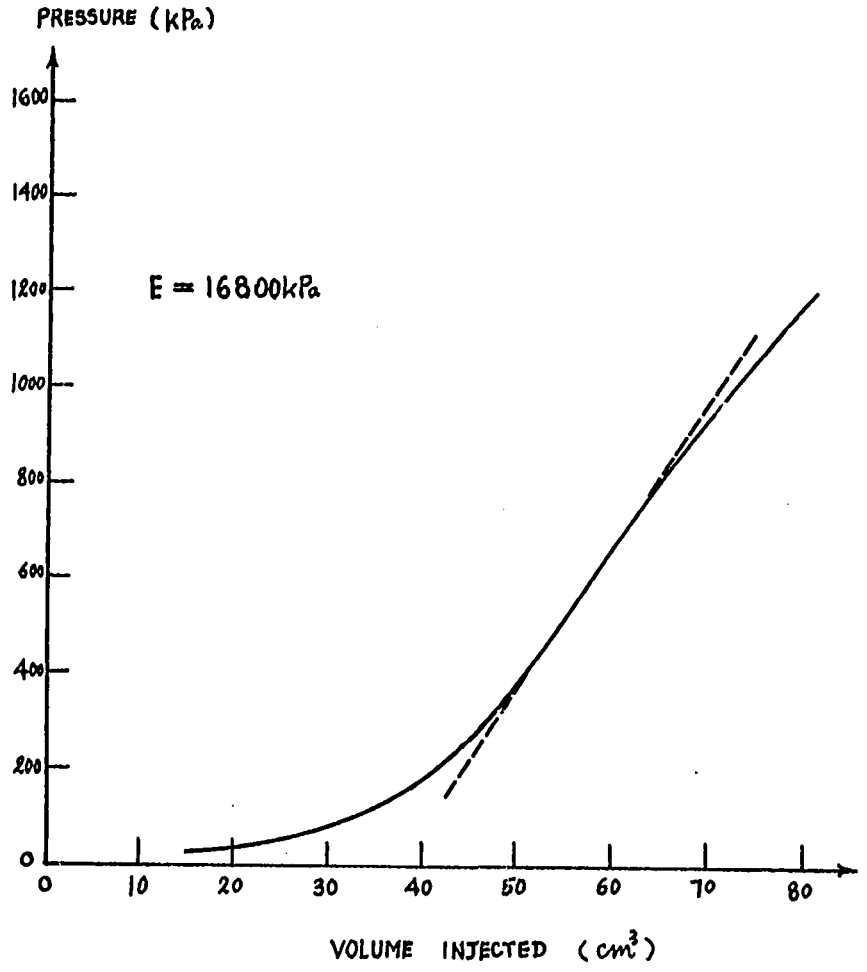

Fig. 262 - Test No. 142 - Sarnia Airport. Briaud Pressuremeter Test. Hole 8A. Hole:Rod Driving Depth = 0.3 m.

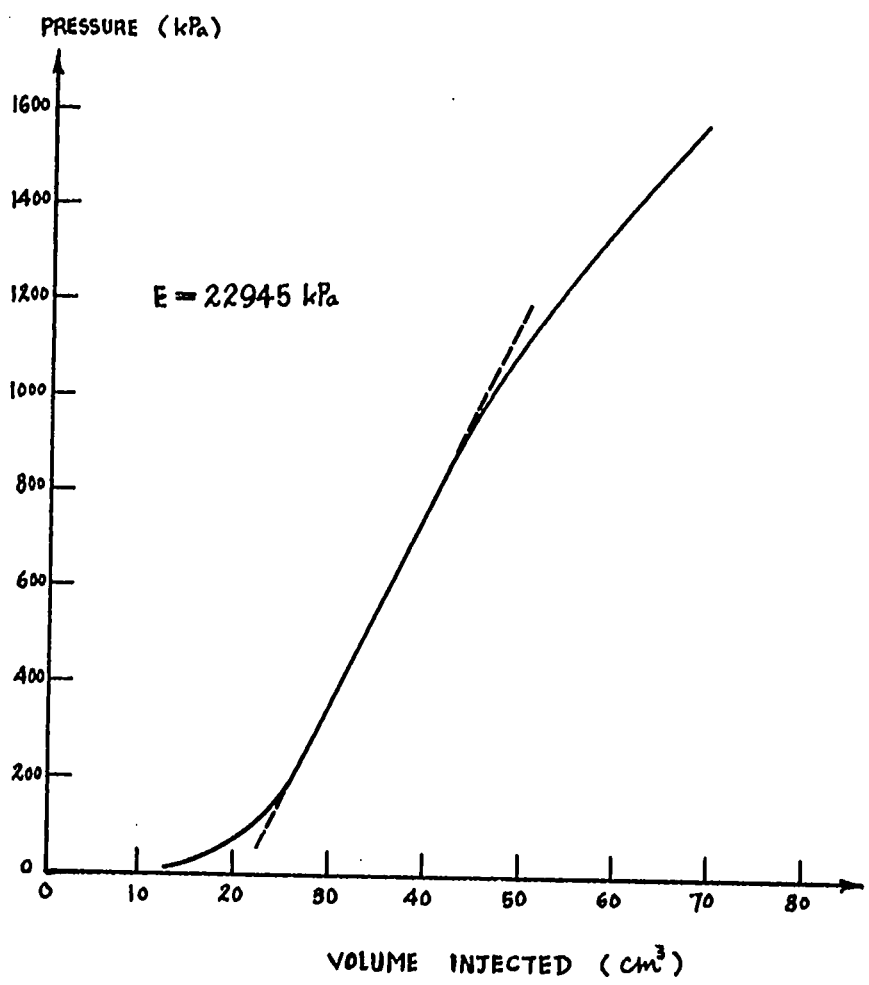

Fig. 263 - Test No. 143 - Sarnia Airport. Briaud Pressuremeter Test. Hole 10. Hole:Rod Driving Depth = 1.2 m.

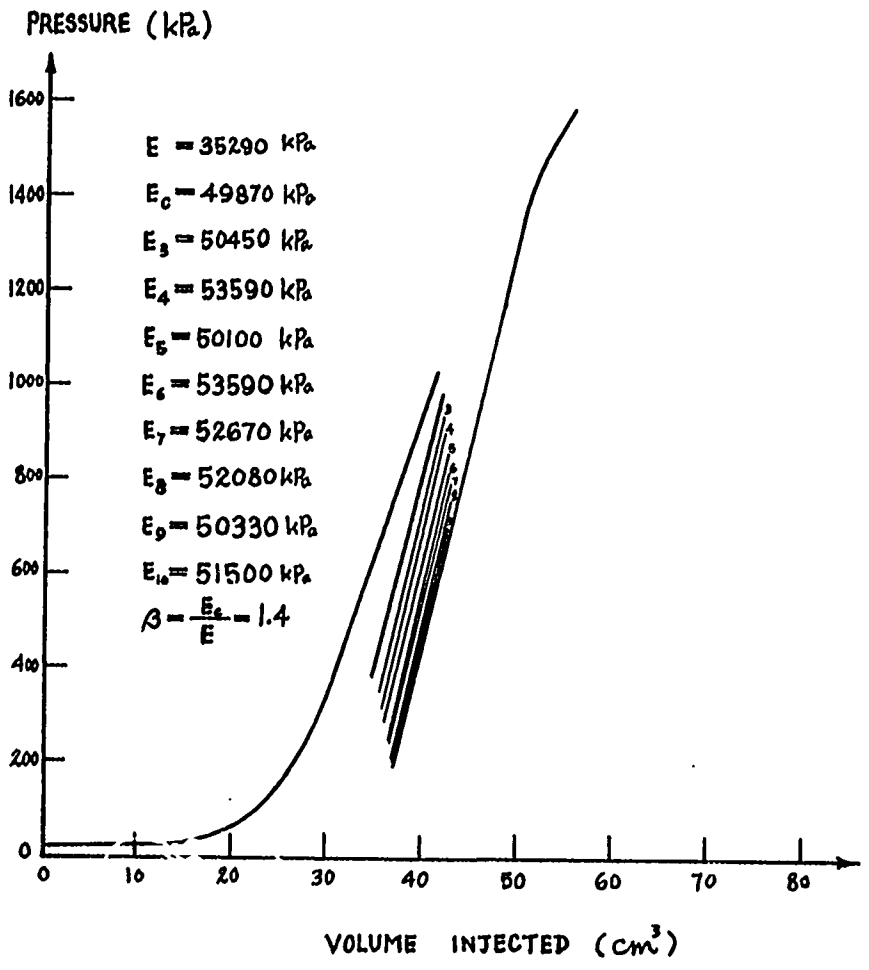

Fig. 264 - Test No. 144 - Sarnia Airport. Briaud Pressuremeter Test. Hole 11. Hole:Rod Driving Depth = 1.2 m.

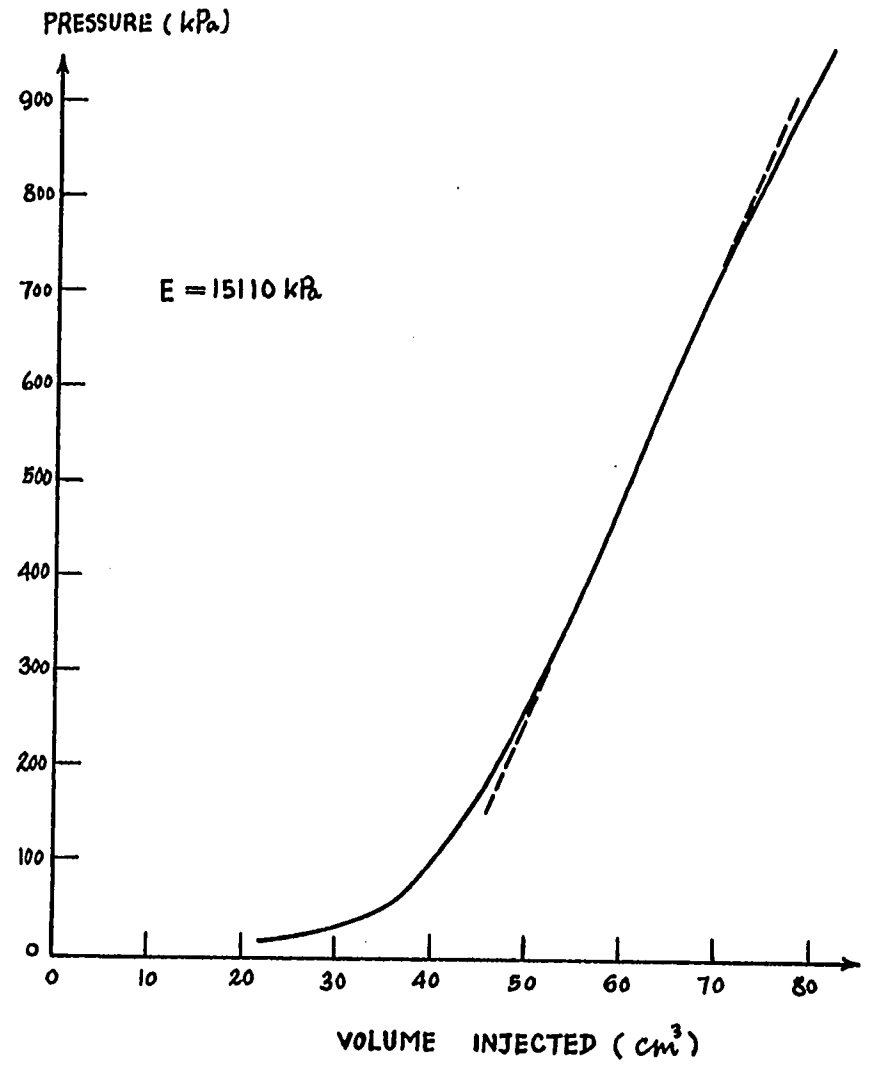

Fig. 265 - Test No. 145 - Sarnia Airport. Briaud Pressuremeter Test. Hole 14. Hole:Rod Driving Depth = 0.27 m.

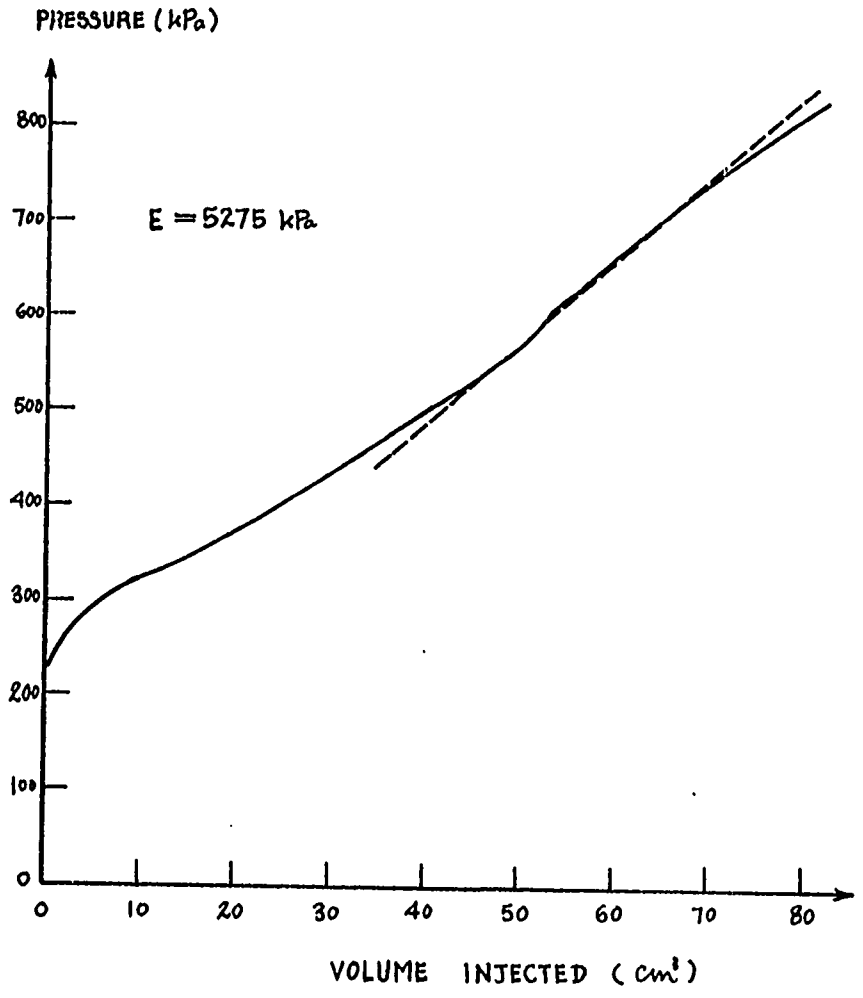

Fig.266 - Test No. 146 - Sarnia Airport. Briaud Pressuremeter Test. Hold 14. Hole:Rod Driving Depth = 1.8 m.

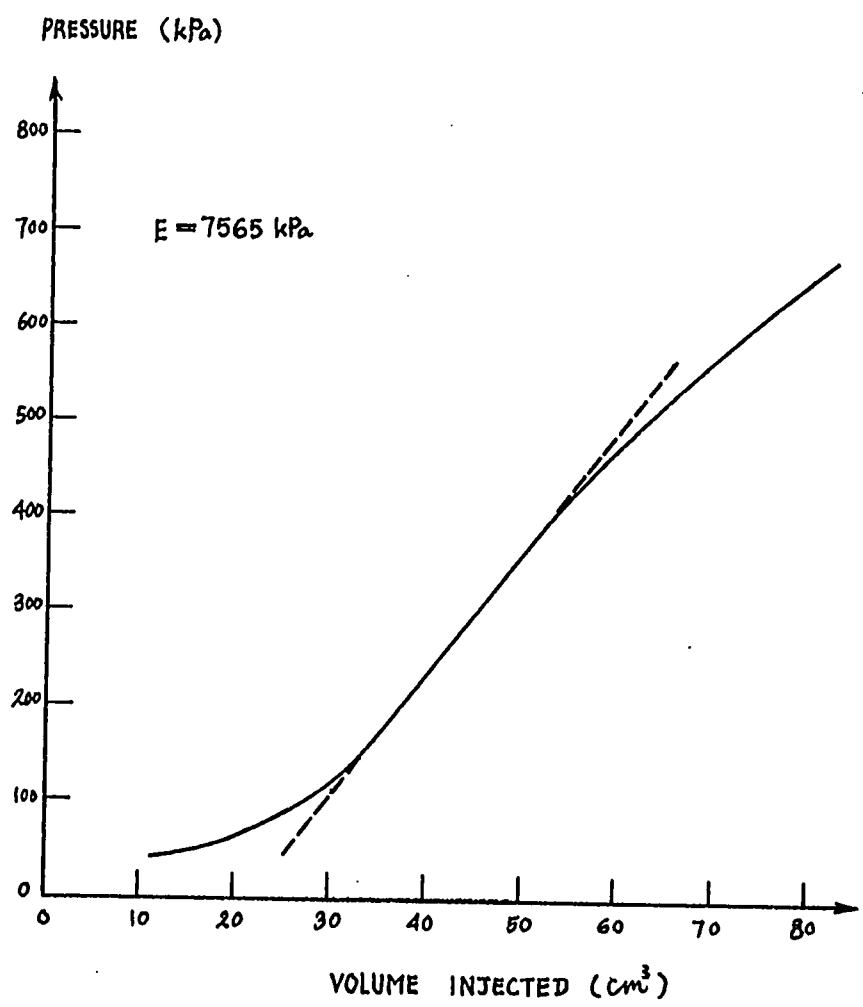

Fig.267 - Test No. 147 - Sarnia Airport. Briaud Pressuremeter Test. Hole 14. Hole:Rod Driving Depth = 1.5 m.

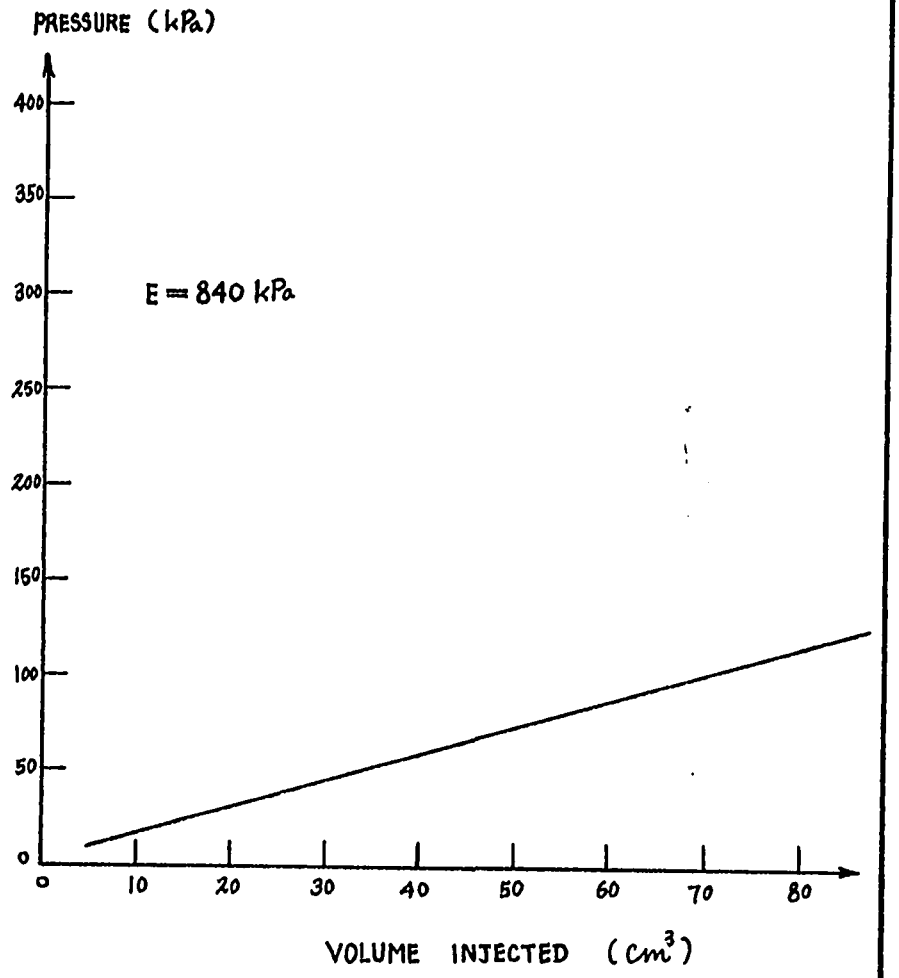

Fig. 268 – Test No. 148 – Sarnia Airport. Briaud Pressuremeter Test. Hole 14. Hole:Rod Driving Depth = 1.2 m.

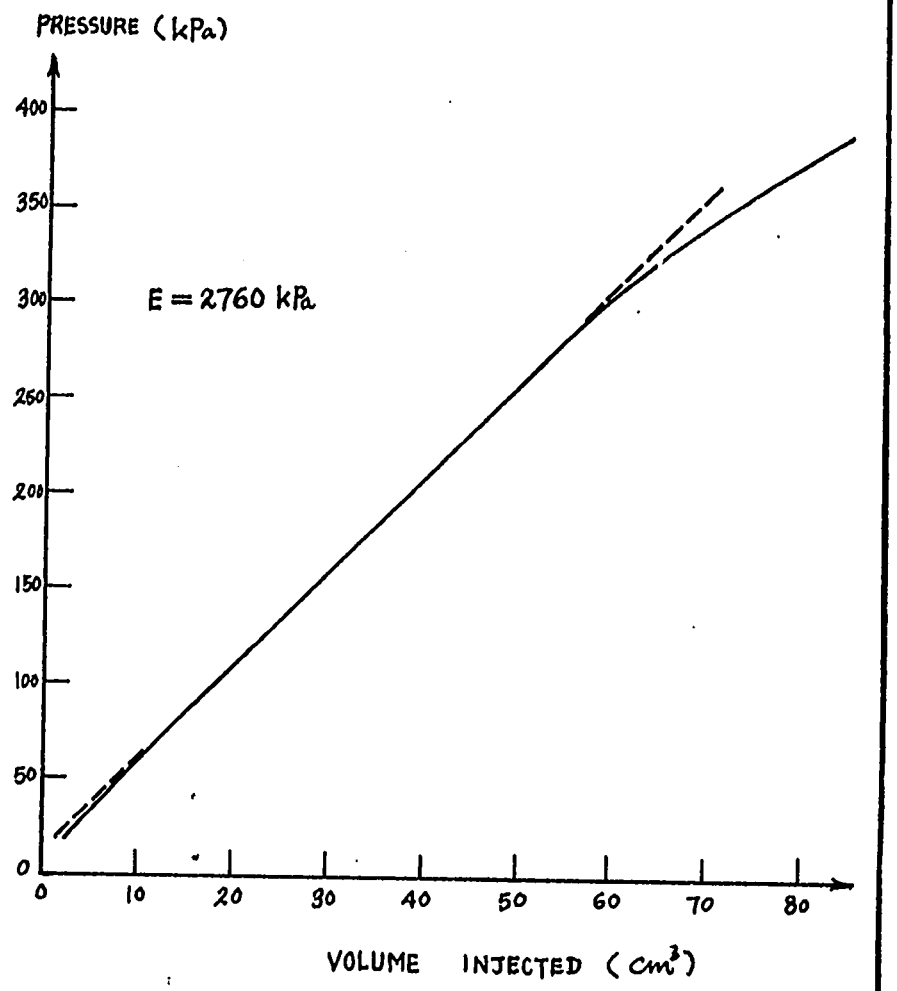

Fig. 269 – Test No. 149 – Sarnia Airport. Briaud Pressuremeter Test. Hole 14. Hole:Rod Driving Depth = 0.9 m.

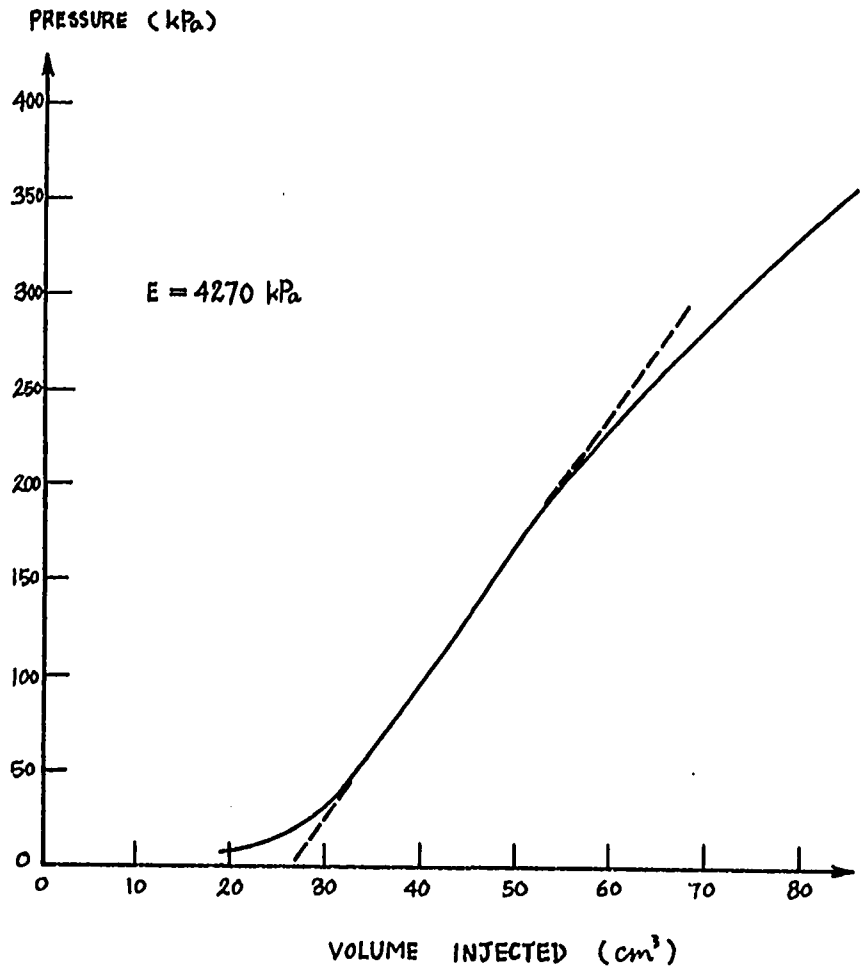

Fig.270 - Test No. 150 - Sarnia Airport. Briaud Pressuremeter Test. Hole 14. Hole:Rod Driving Depth = 0.6 m.

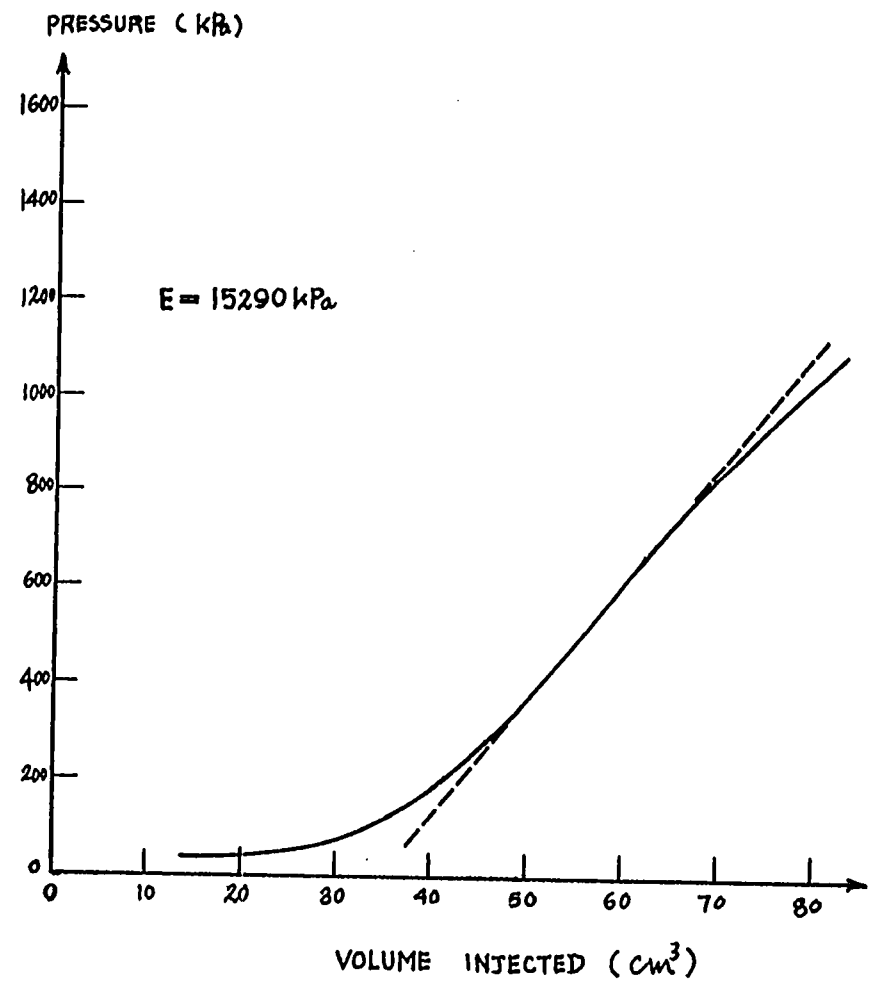

Fig.271 - Test No. 151 - Sarnia Airport. Briaud Pressuremeter Test. Hole 15. Hole:Rod Driving Depth = 0.33 m.

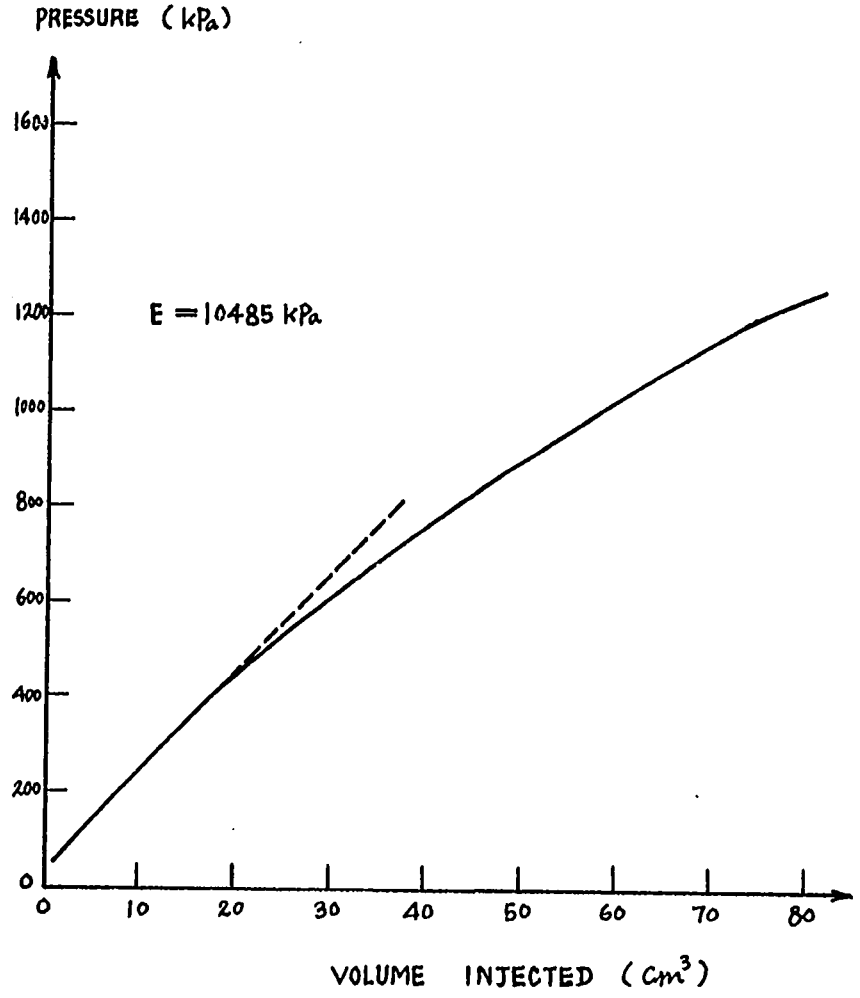

Fig. 272 - Test No. 152 - Sarnia Airport. Briaud Pressuremeter Test. Hole 15. Hole:Rod Driving Depth = 1.8 m.

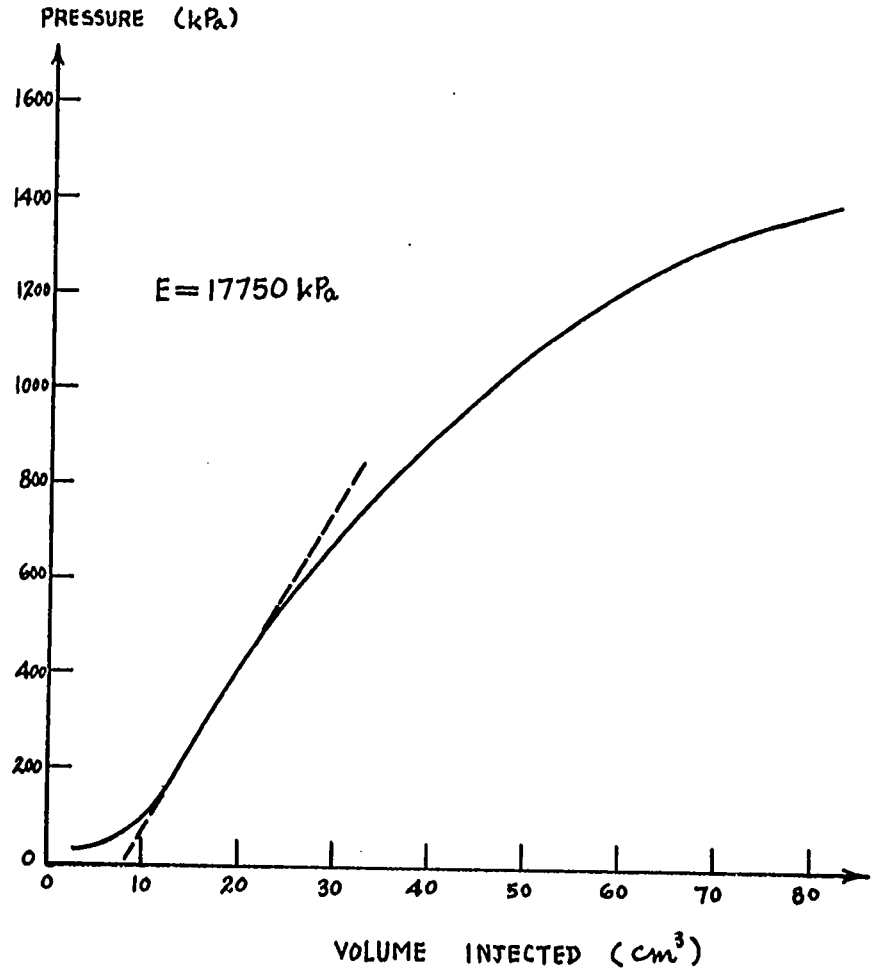

Fig. 273 - Test No. 153 - Sarnia Airport. Briaud Pressuremeter Test. Hole 15. Hole:Rod Driving Depth = 1.5 m.

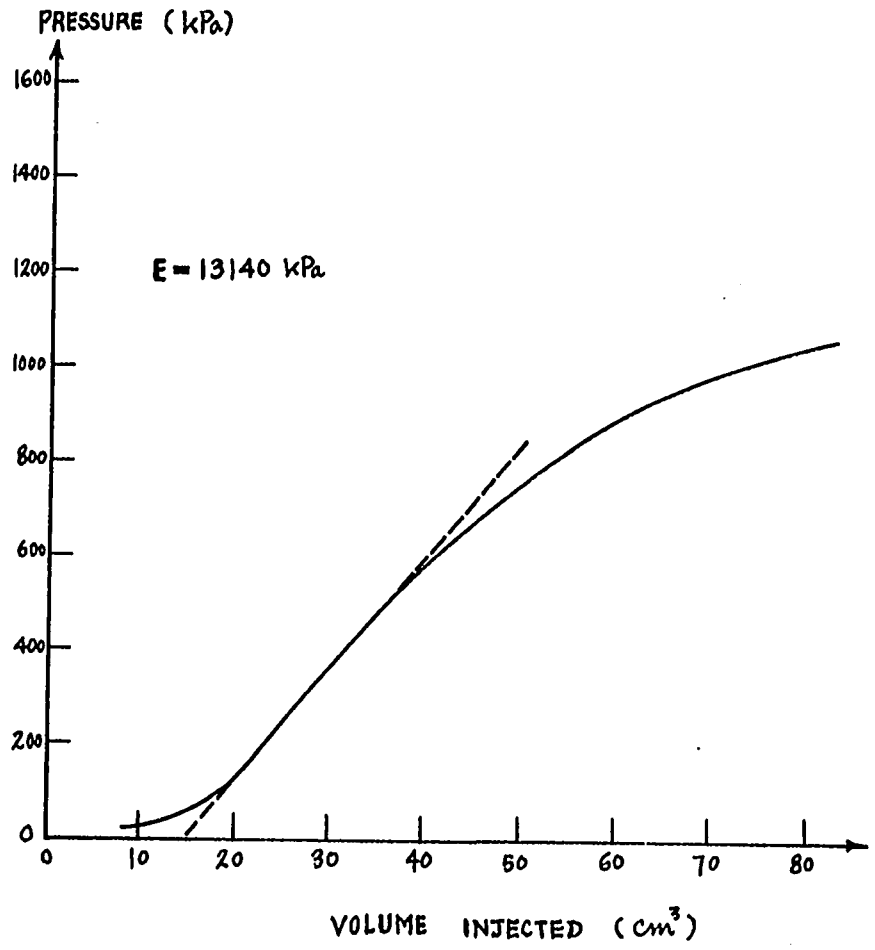

Fig. 274 - Test No. 154 - Sarnia Airport. Briaud Pressuremeter Test. Hole 15. Hole:Rod Driving Depth = 1.2 m.

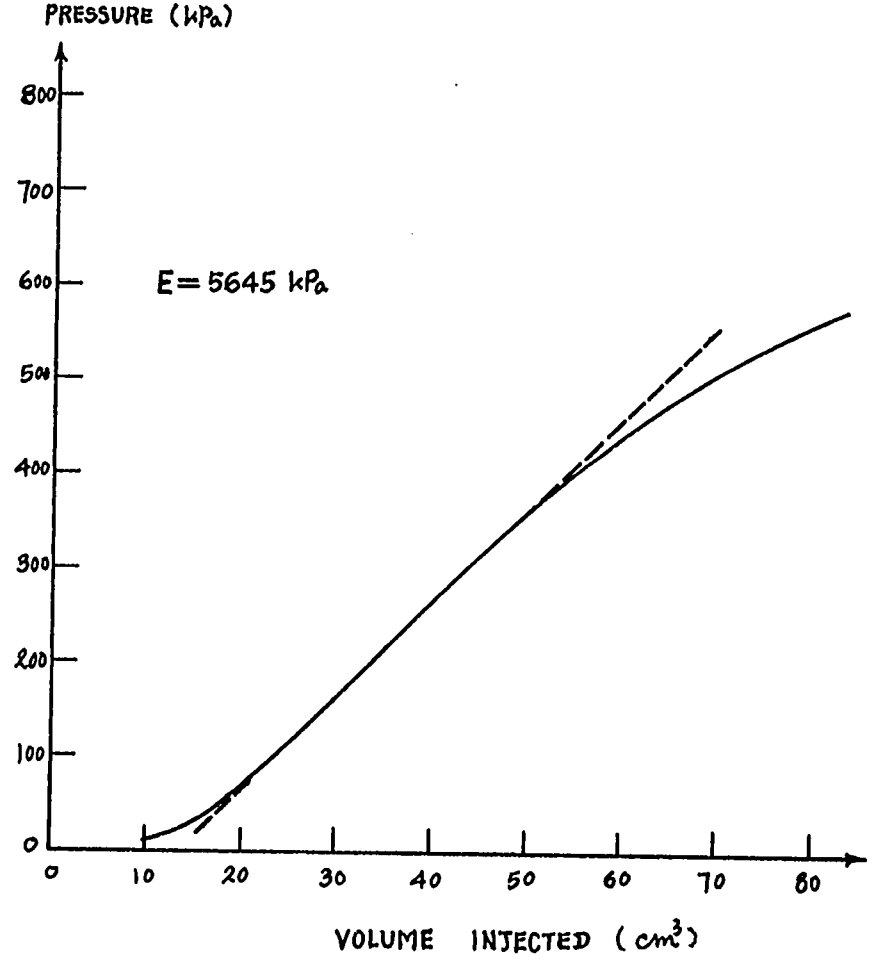

Fig. 275 - Test No. 155 - Sarnia Airport. Briaud Pressuremeter Test. Hole 15. Hole:Rod Driving Depth = 0.9 m.

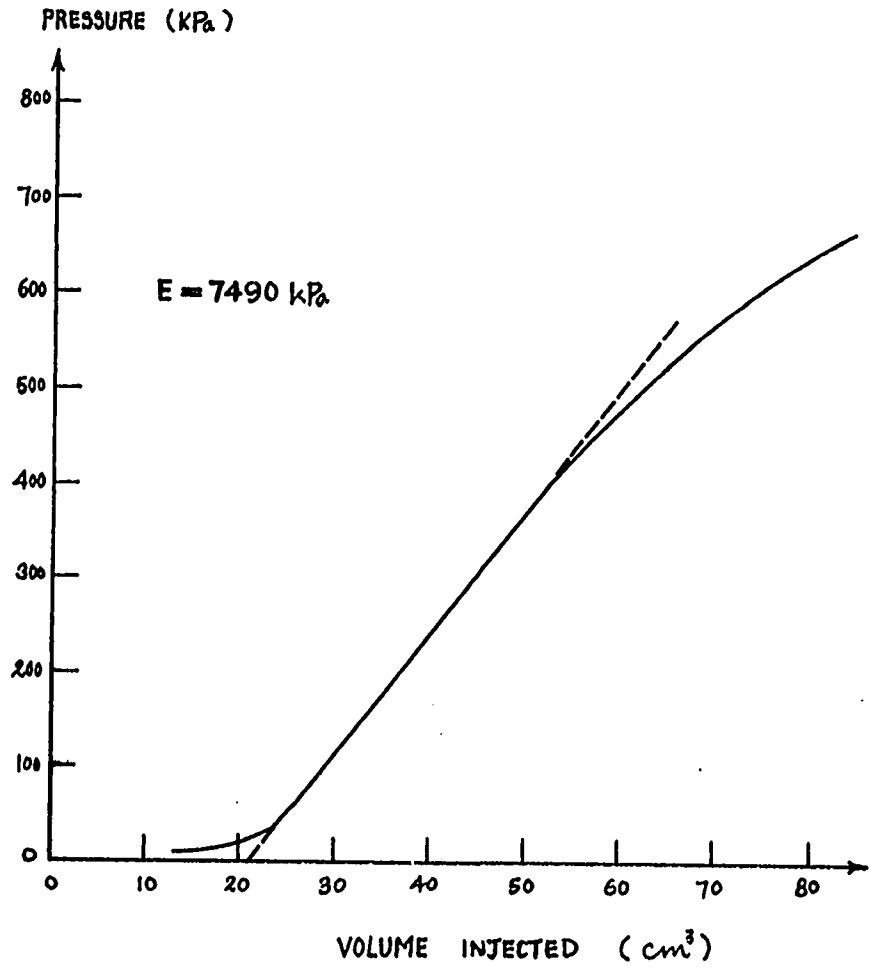

Fig. 276 - Test No. 156 - Sarnia Airport. Briaud Pressuremeter Test. Hole 15, Hole:Rod Driving Depth = 0.6 m.

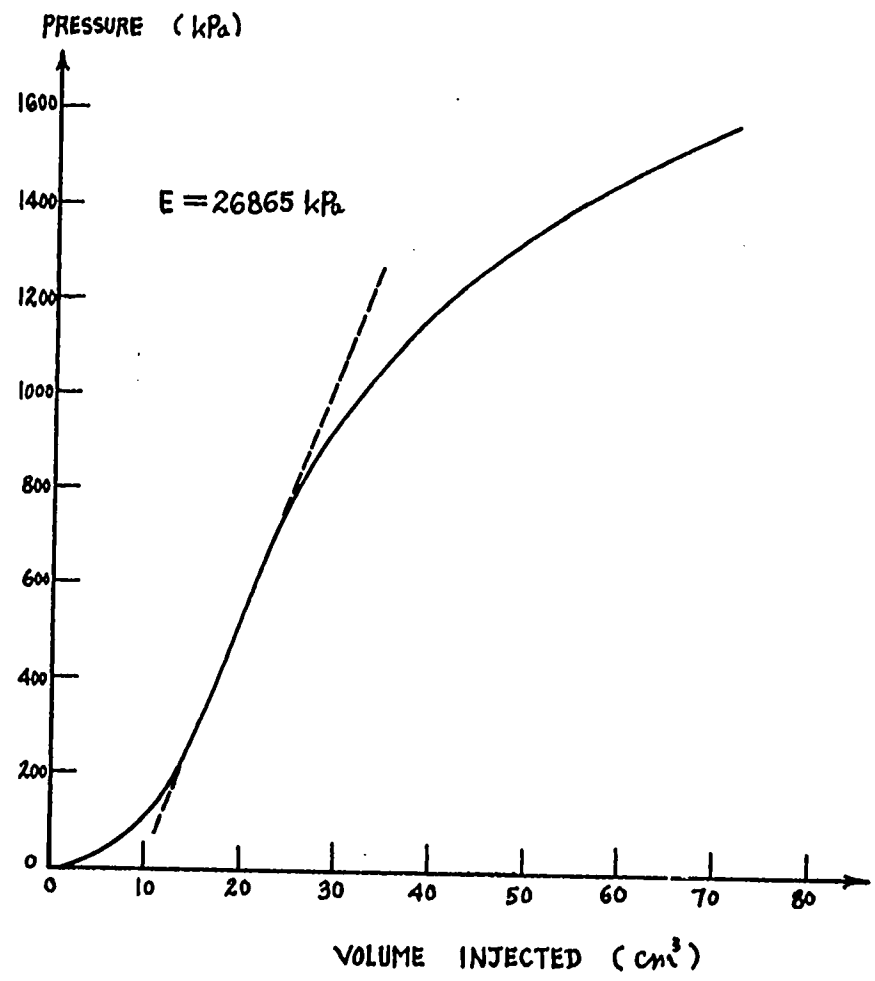

Fig. 277 - Test No. 157 - Sarnia Airport. Briaud Pressuremeter Test. Hole 12. Hole:Hand Auger Depth = 1.2 m.

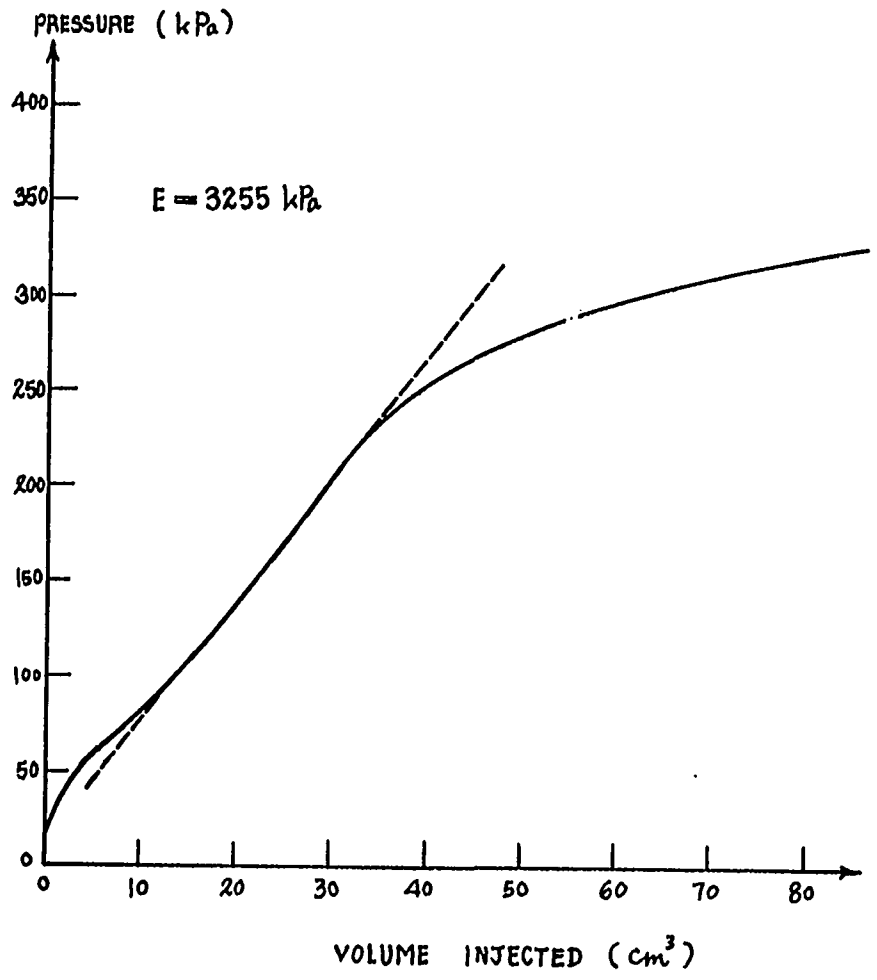

Fig. 278 - Test No. 159 - Fraser's Clay. Briaud Pressuremeter. Hole 1. Hole: Hand Auger. Before Slab. Depth = 0.3 m.

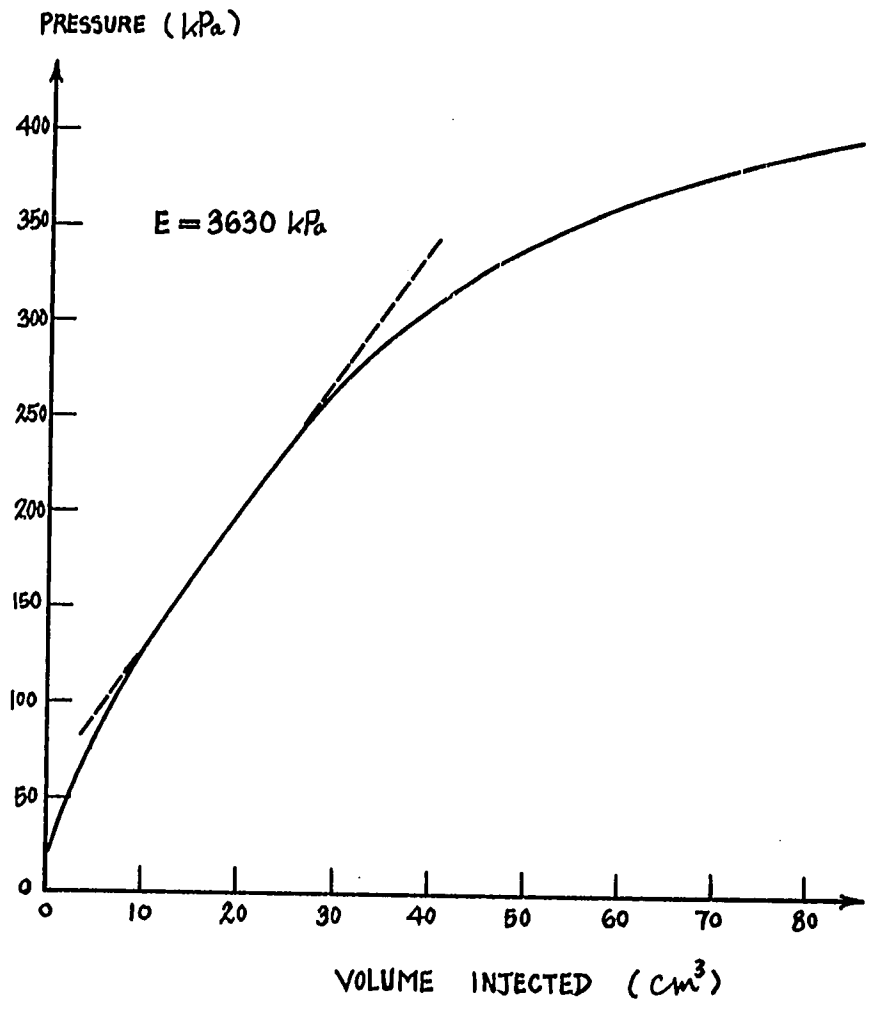

Fig. 279 - Test No. 160 - Fraser's Clay. Briaud Pressuremeter Test. Hole 1. Hole: Hand Auger. Before Slab. Depth = 0.6 m.

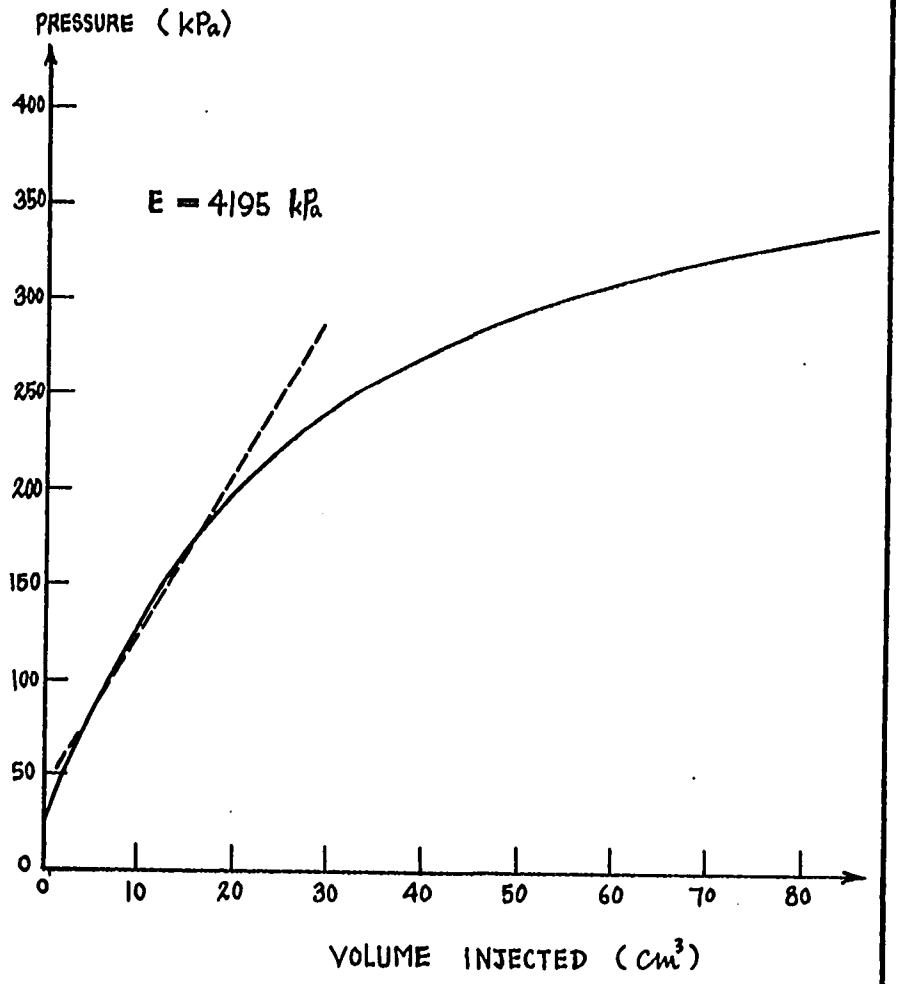

Fig. 280 - Test No. 161 - Fraser's Clay. Briaud Pressuremeter Test. Hole 1. Hole: Hand Auger. Before Slab. Depth = 0.9 m.

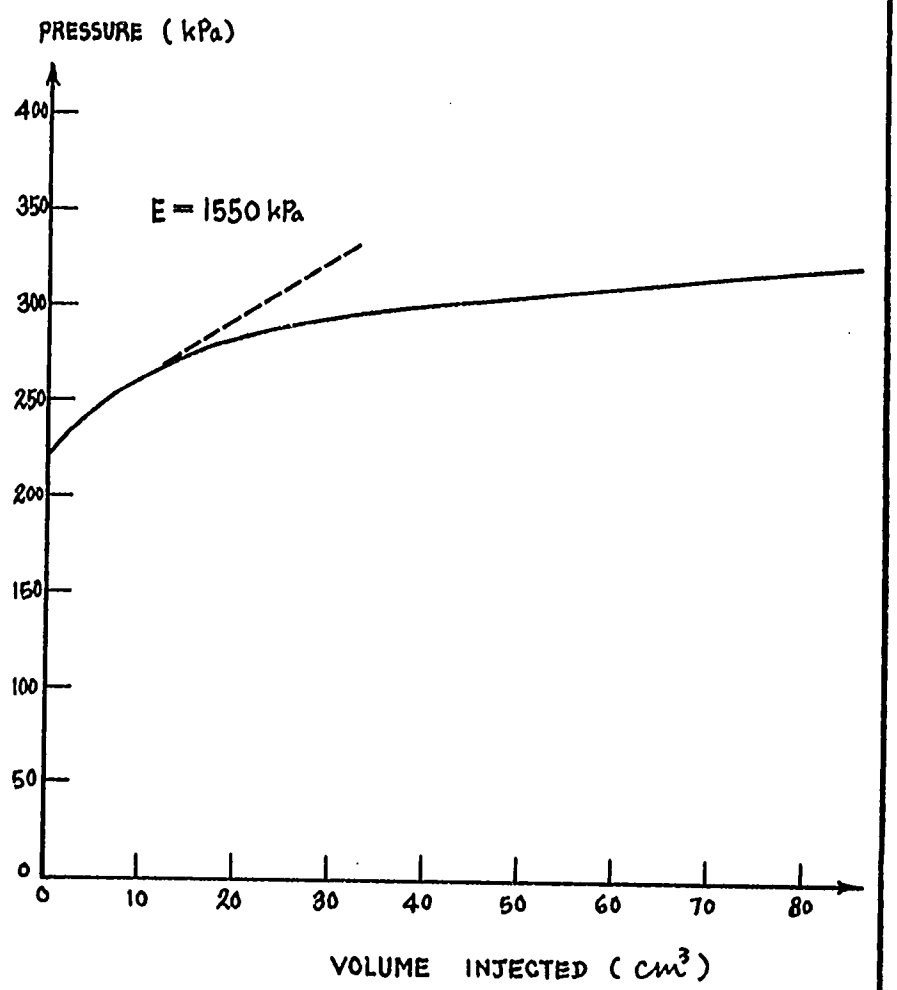

Fig. 281 - Test No. 162 - Fraser's Clay. Briaud Pressuremeter Test. Hole 1. Hole: Pushed Probe. Before Slab. Depth = 3.0 m.

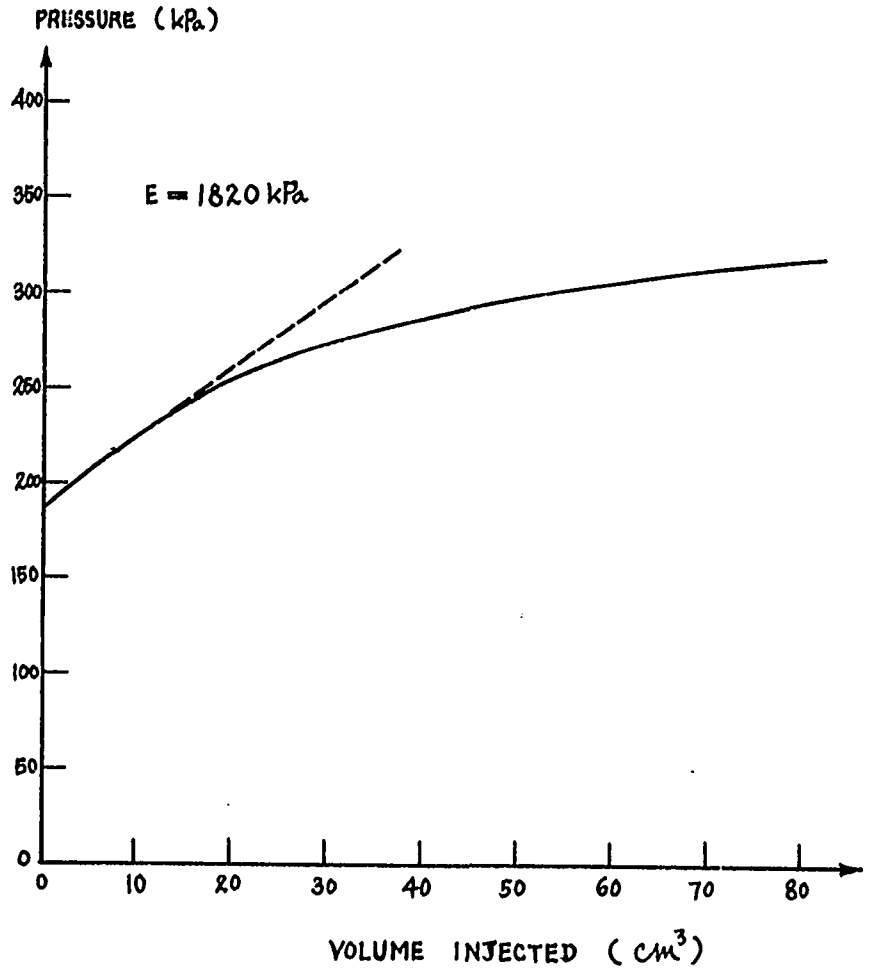

Fig. 282 - Test No. 163 - Fraser's Clay. Briaud Pressuremeter Test. Hole 1. Hole: Pushed Probe. Before Slab. Depth = 2.7 m.

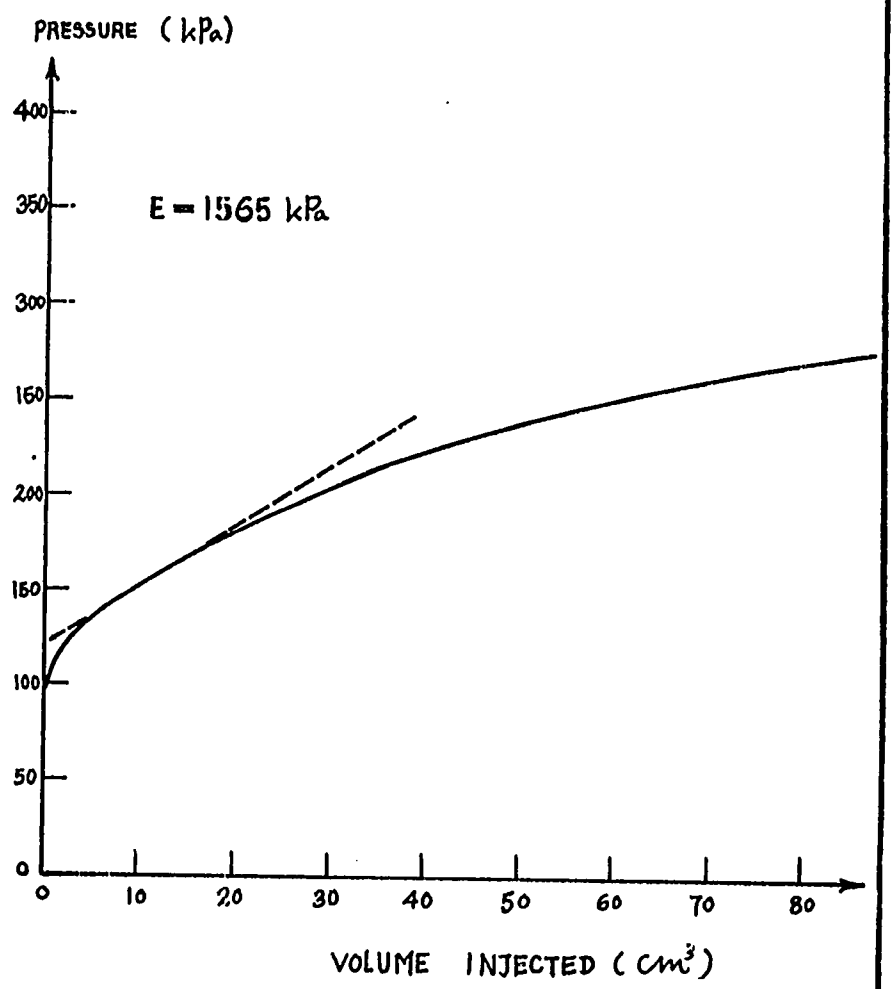

Fig. 283 - Test No. 164 - Fraser's Clay. Briaud Pressuremeter Test. Hole 1. Hole: Pushed Probe. Before Slab. Depth = 2.4 m.

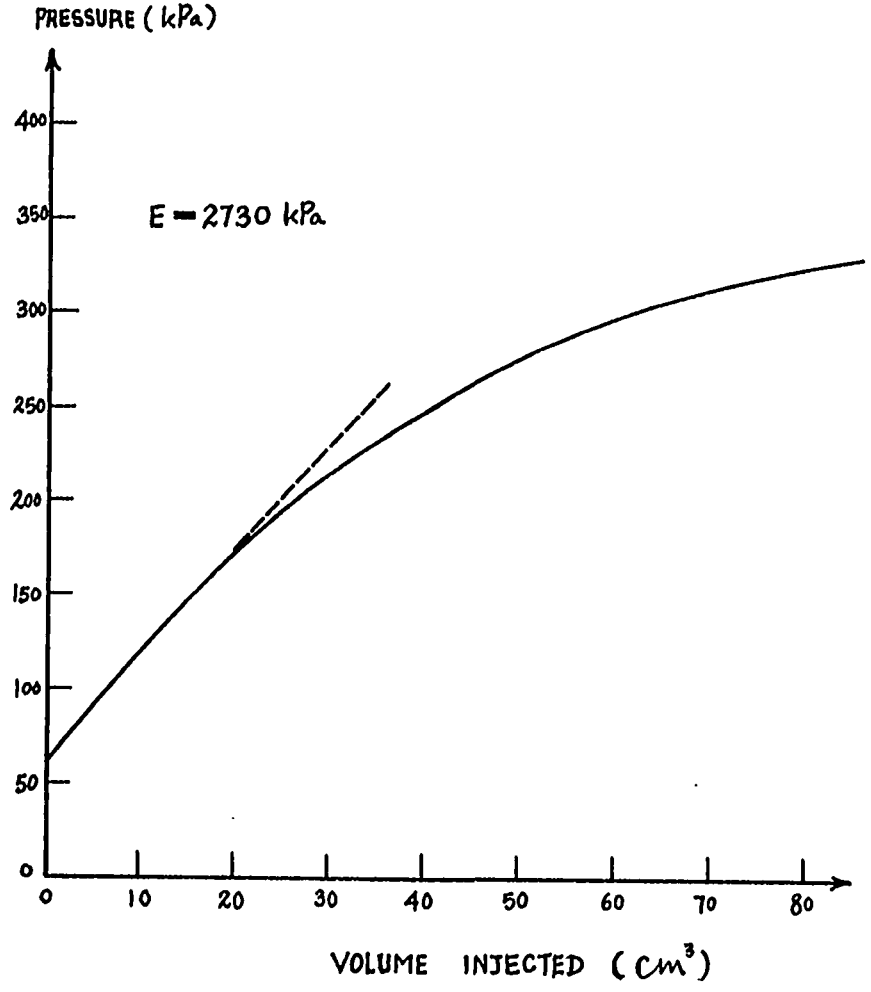

Fig.284 - Test No. 165 - Fraser's Clay. Briaud Pressuremeter Test. Hole 1. Hole: Hand Auger. Before Slab. Depth = 2.1 m.

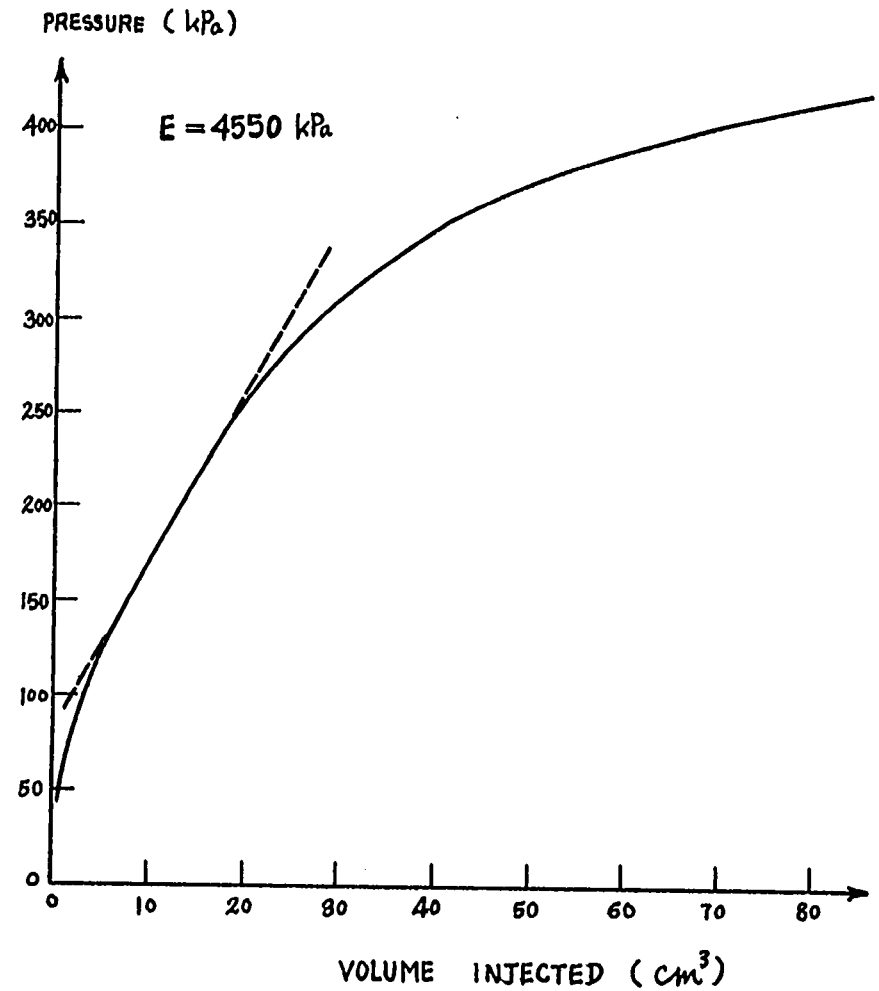

Fig.285 - Test No. 166 - Fraser's Clay. Briaud Pressuremeter Test. Hole 1. Hole: Hand Auger. Before Slab. Depth = 1.8 m.

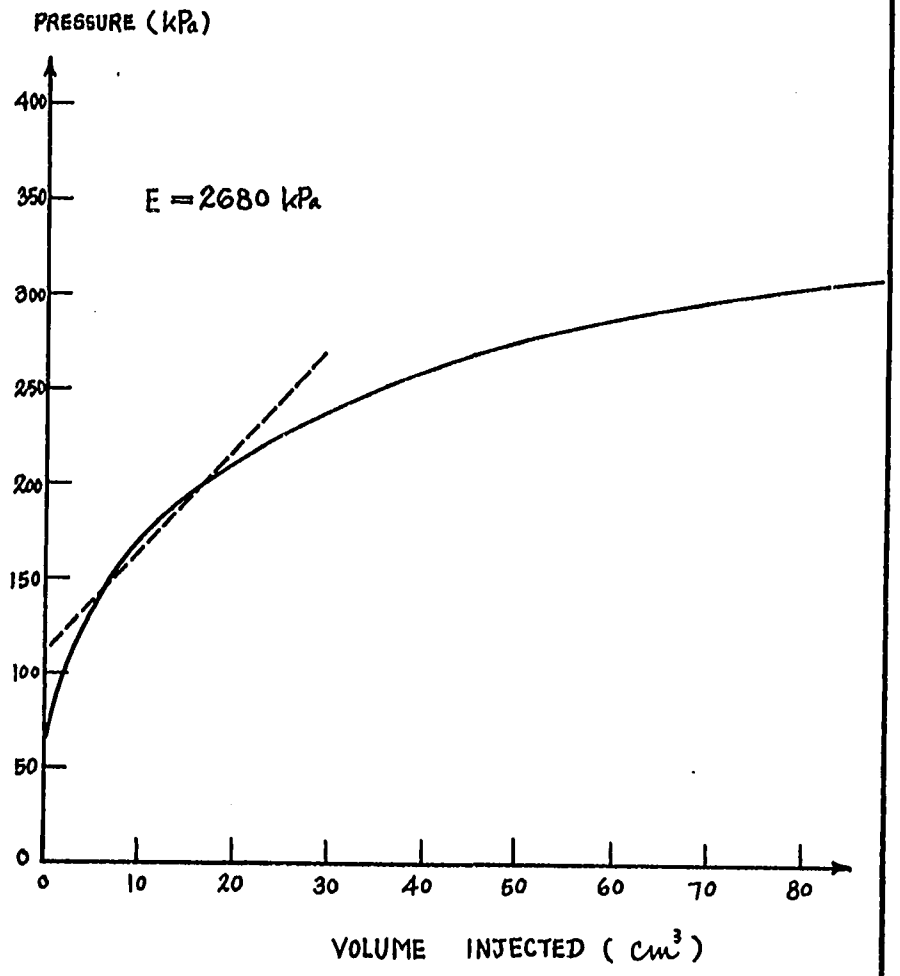

Fig. 286 - Test No. 167 - Fraser's Clay. Briaud Pressuremeter Test. Hole 1. Hole: Hand Auger. Before Slab. Depth = 1.5 m.

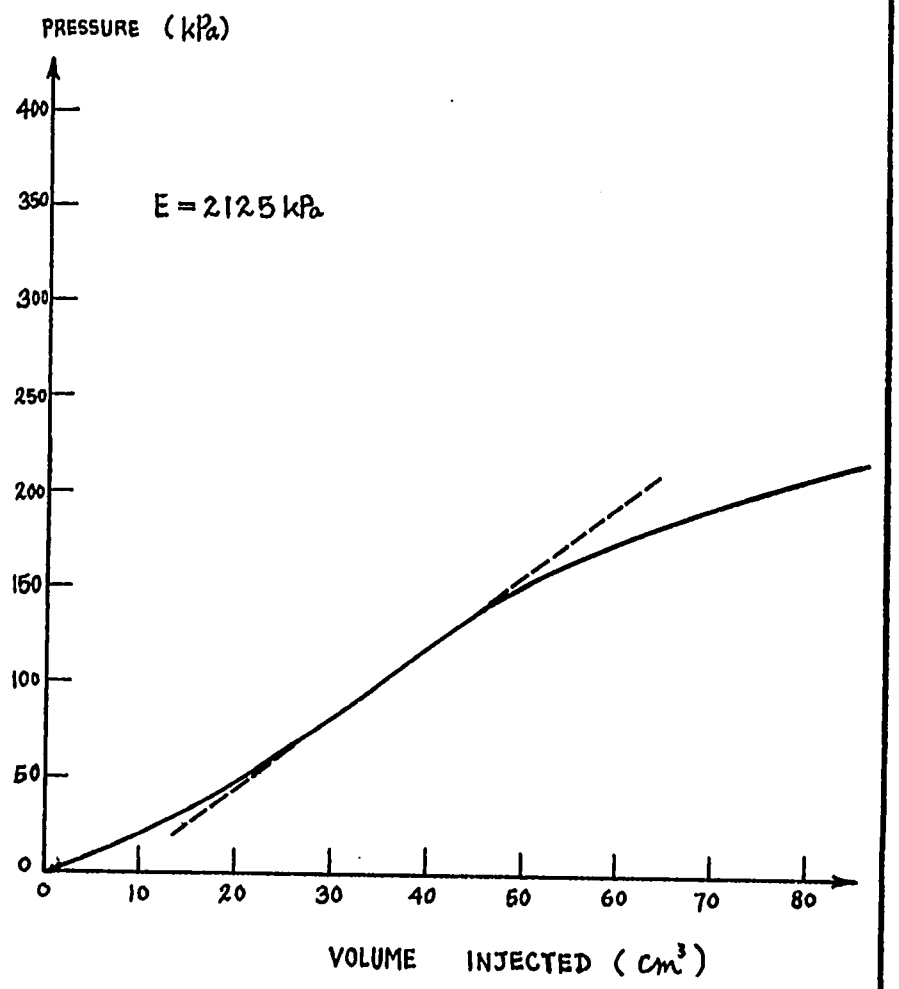

Fig. 287 - Test No. 168 - Fraser's Clay. Briaud Pressuremeter Test. Hole 1. Hole: Hand Auger. Before Slab. Depth = 1.2 m.

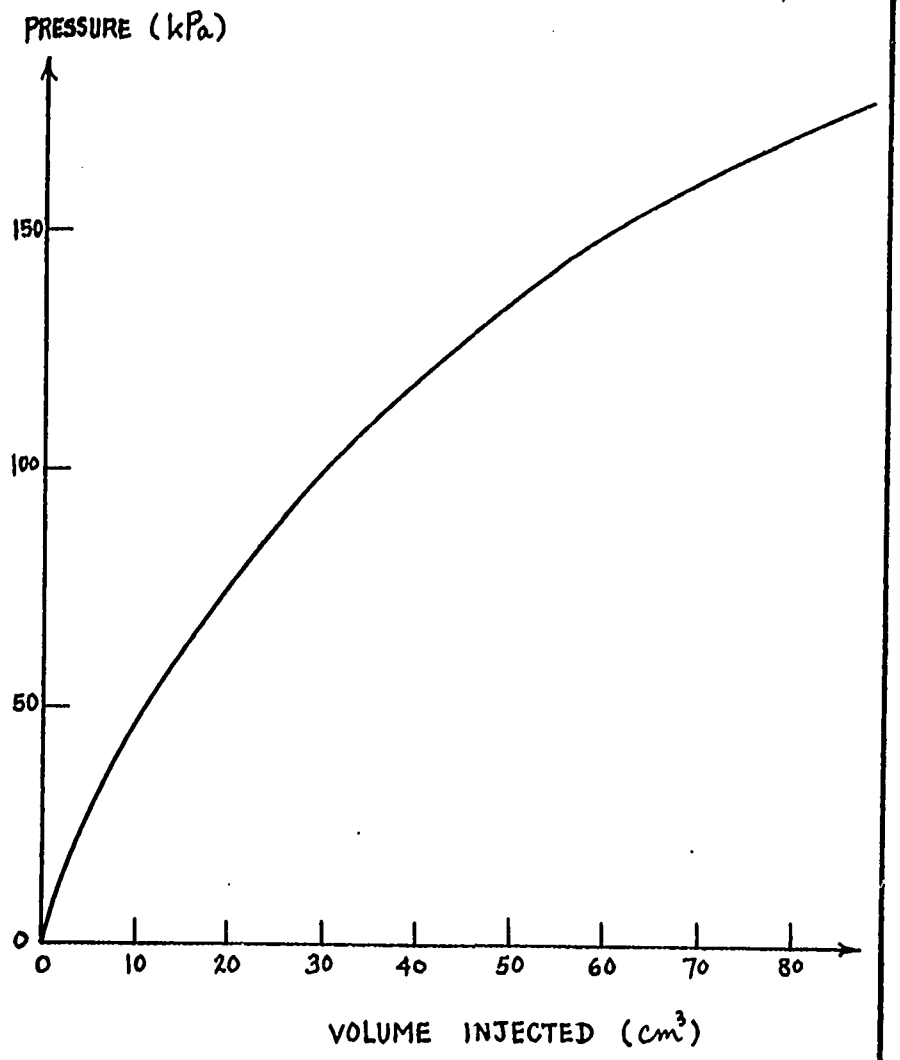

Fig. 288 - Test Nos. 169 and 180 - Fraser's Clay. Briaud Pressuremeter. Calibration of Membrane Resistance.

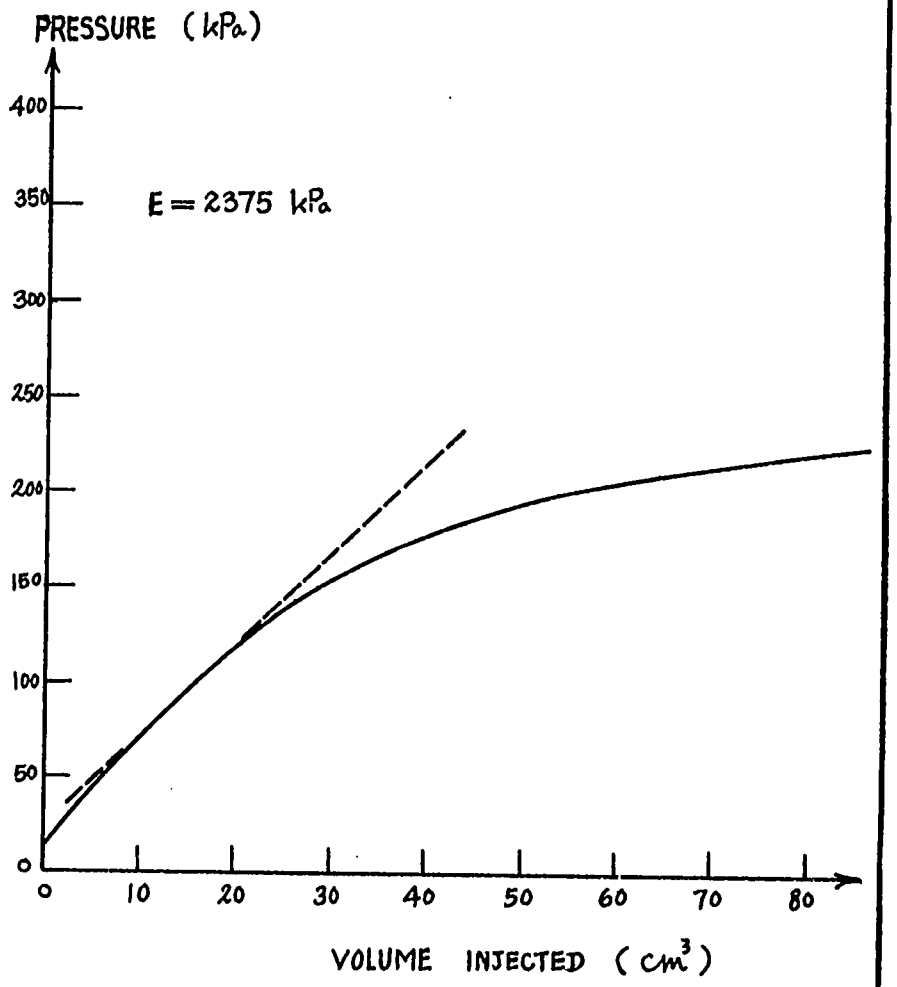

Fig. 289 - Test No. 170 - Fraser's Clay. Briaud Pressuremeter Test. Hole 2. Hole: Hand Auger. Before Slab. Depth = 0.3 m.

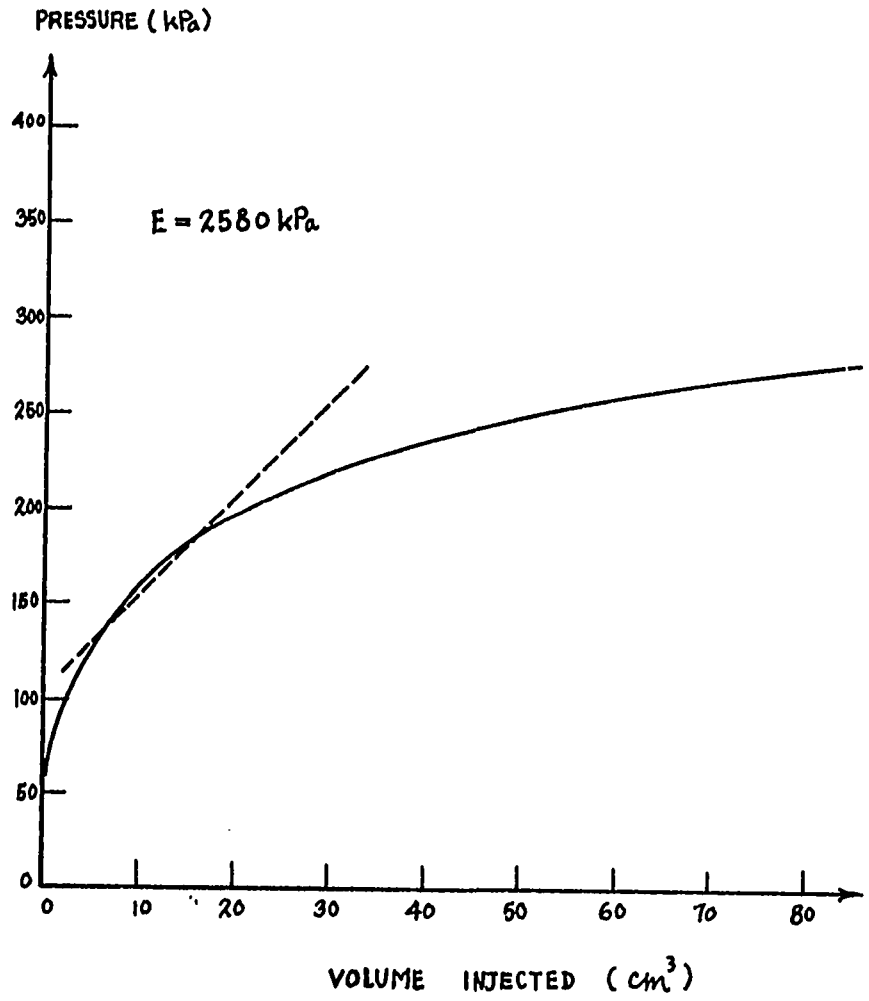

Fig. 290 - Test No. 171 - Fraser's Clay. Briaud Pressuremeter Test. Hole 2. Hole: Hand Auger. Before Slab. Depth = 0.6 m.

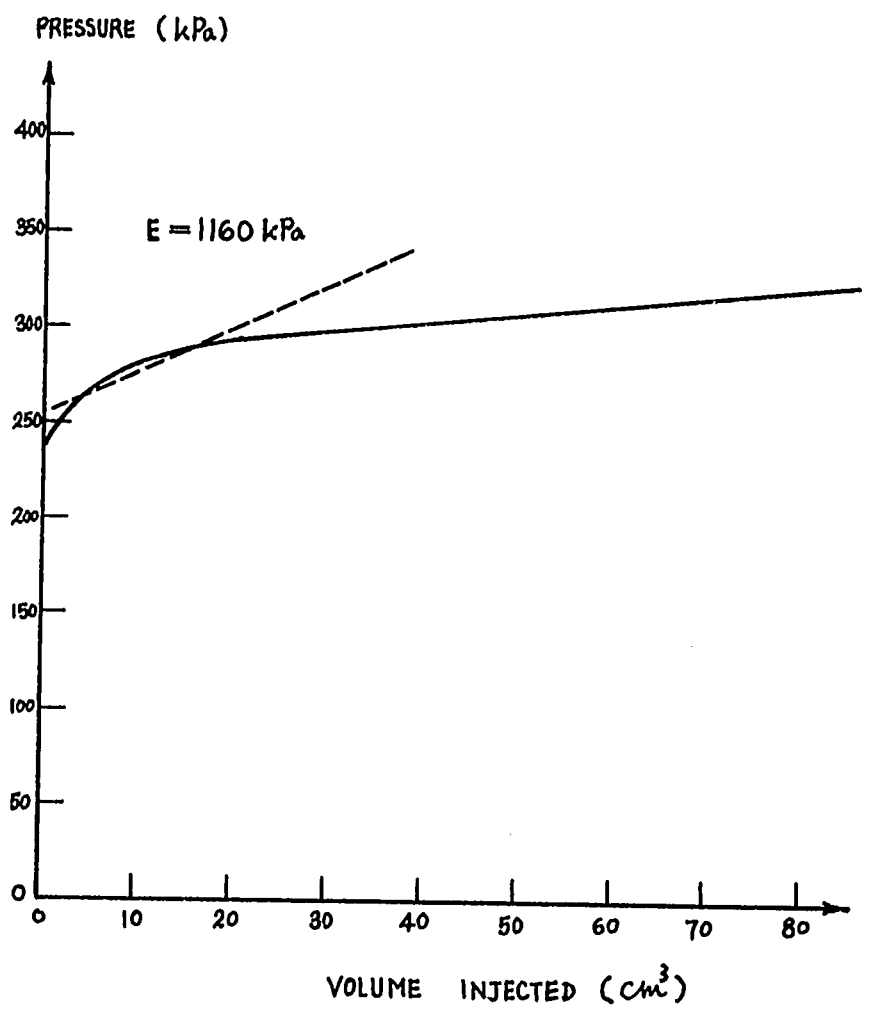

Fig. 291 - Test No. 172 - Fraser's Clay. Briaud Pressuremeter Test. Hole 2. Hole: Pushed Probe. Before Slab. Depth = 3 m.

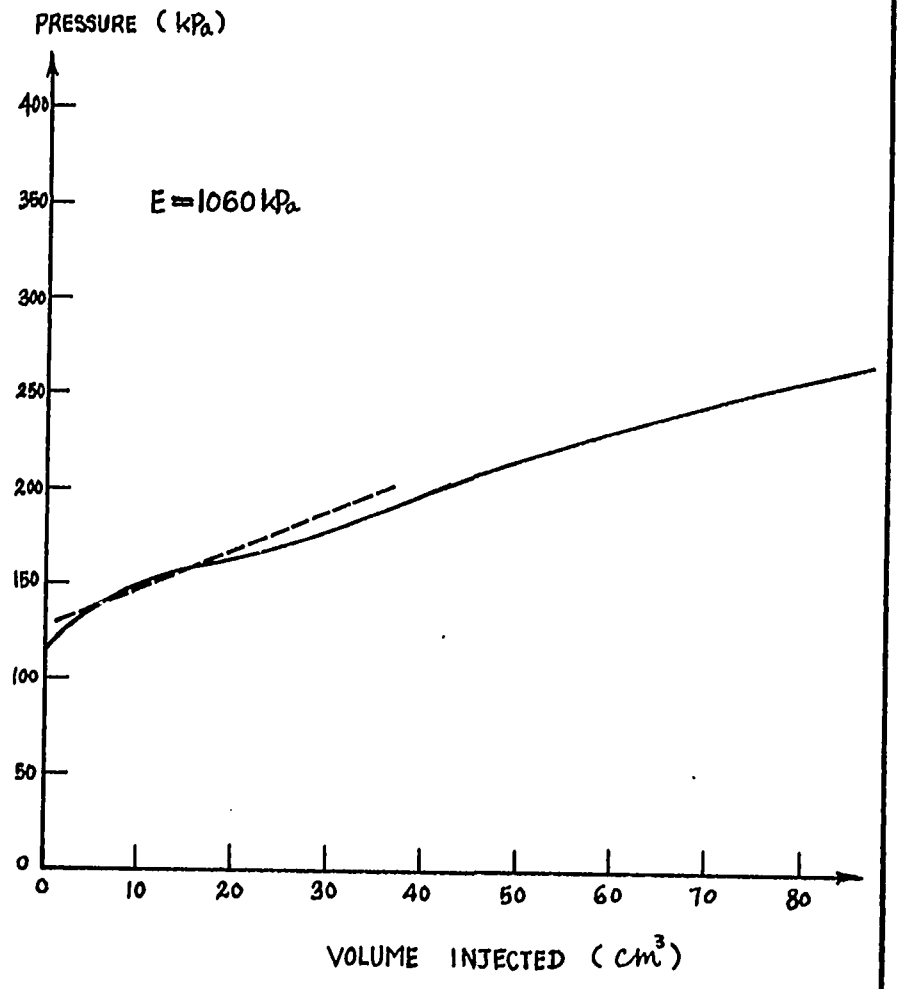

Fig. 292 - Test No. 173 - Fraser's Clay. Briaud Pressuremeter Test. Hole 2. Hole: Pushed Probe. Before Slab. Depth = 2.7 m.

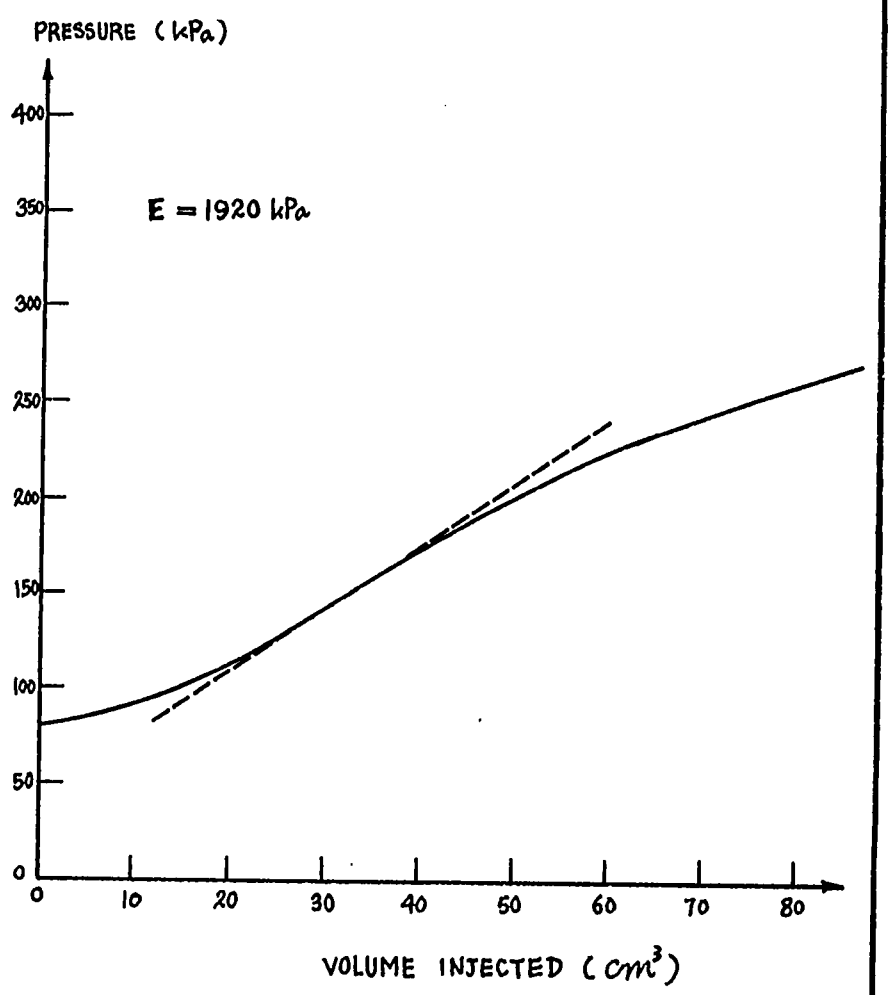

Fig. 293 - Test No. 174 - Fraser's Clay. Briaud Pressuremeter Test. Hole 2. Hole: Pushed Probe. Before Slab. Depth = 2.4 m.

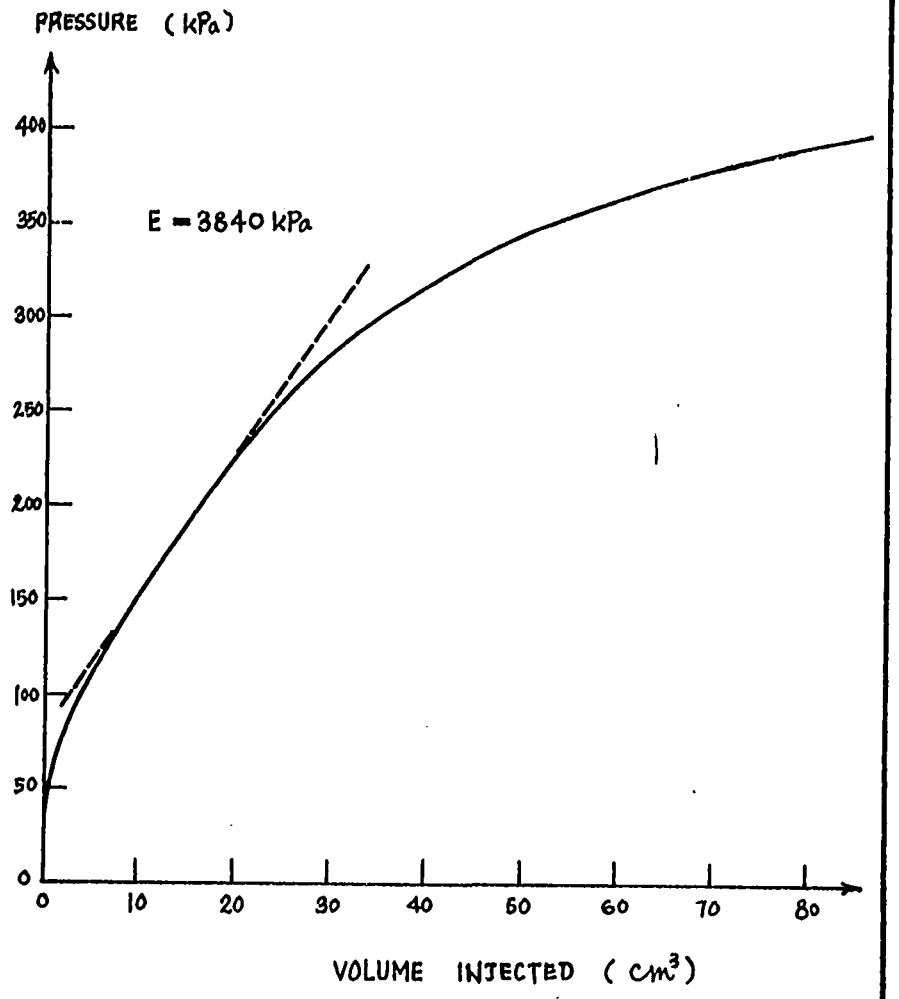

Fig. 294 - Test No. 175 - Fraser's Clay. Briaud Pressuremeter Test. Hole 2. Hole: Hand Auger. Before Slab. Depth = 2.1 m.

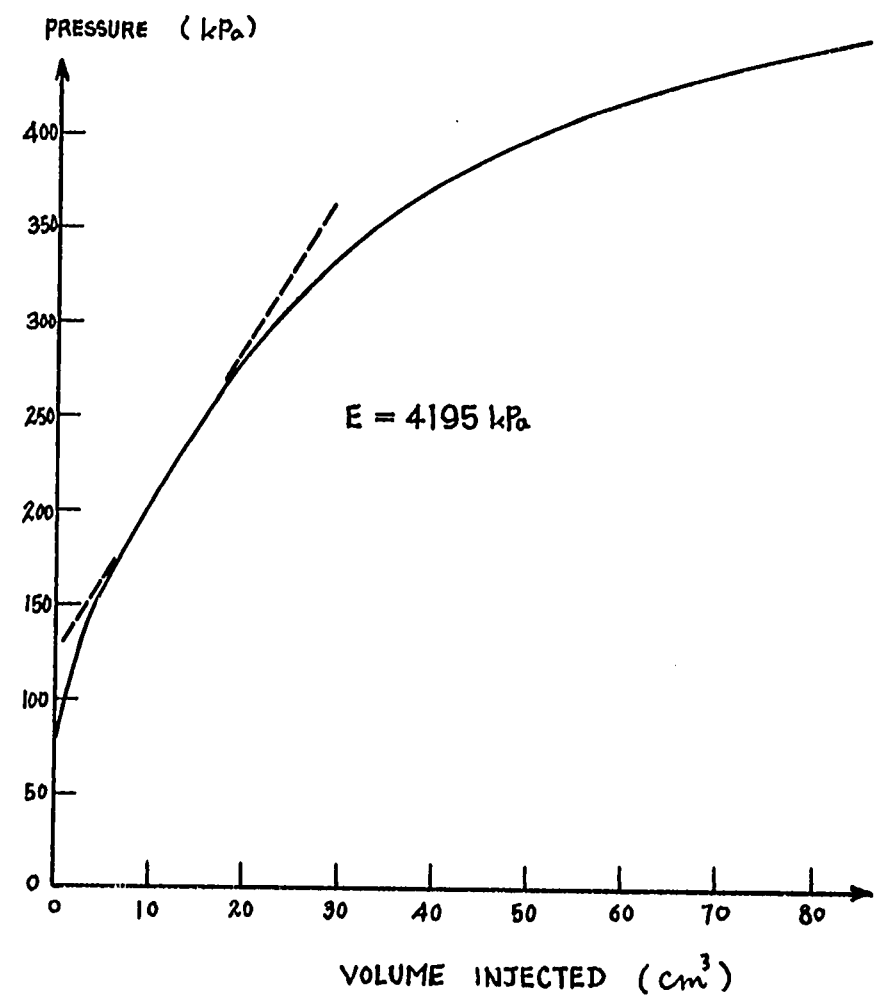

Fig. 295 - Test No. 176 - Fraser's Clay. Briaud Pressuremeter Test. Hole 2. Hole: Hand Auger. Before Slab. Depth = 1.8 m.

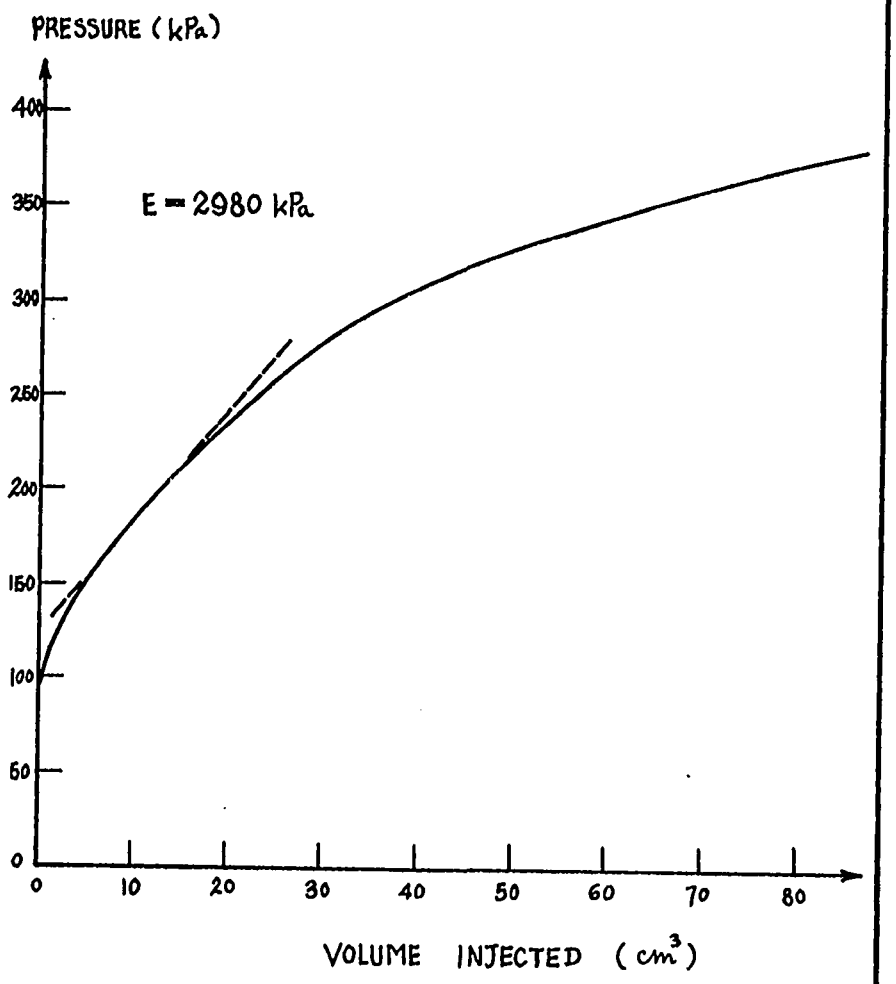

Fig. 296 - Test No. 177 - Fraser's Clay. Briaud Pressure meter Test. Hole 2. Hole: Hand Auger. Before Slab. Depth = 1.5 m.

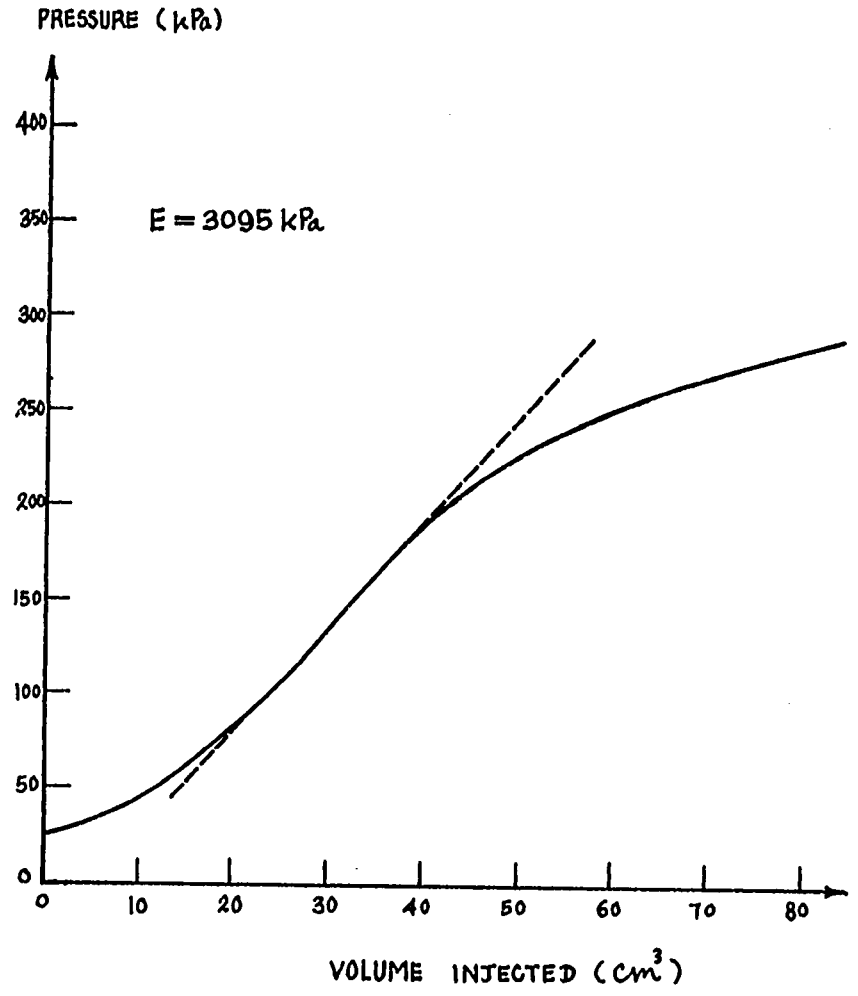

Fig. 297 - Test No. 178 - Fraser's Clay. Briaud Pressure-meter Test. Hole 2. Hole: Hand Auger. Before Slab. Depth = 1.2 m.

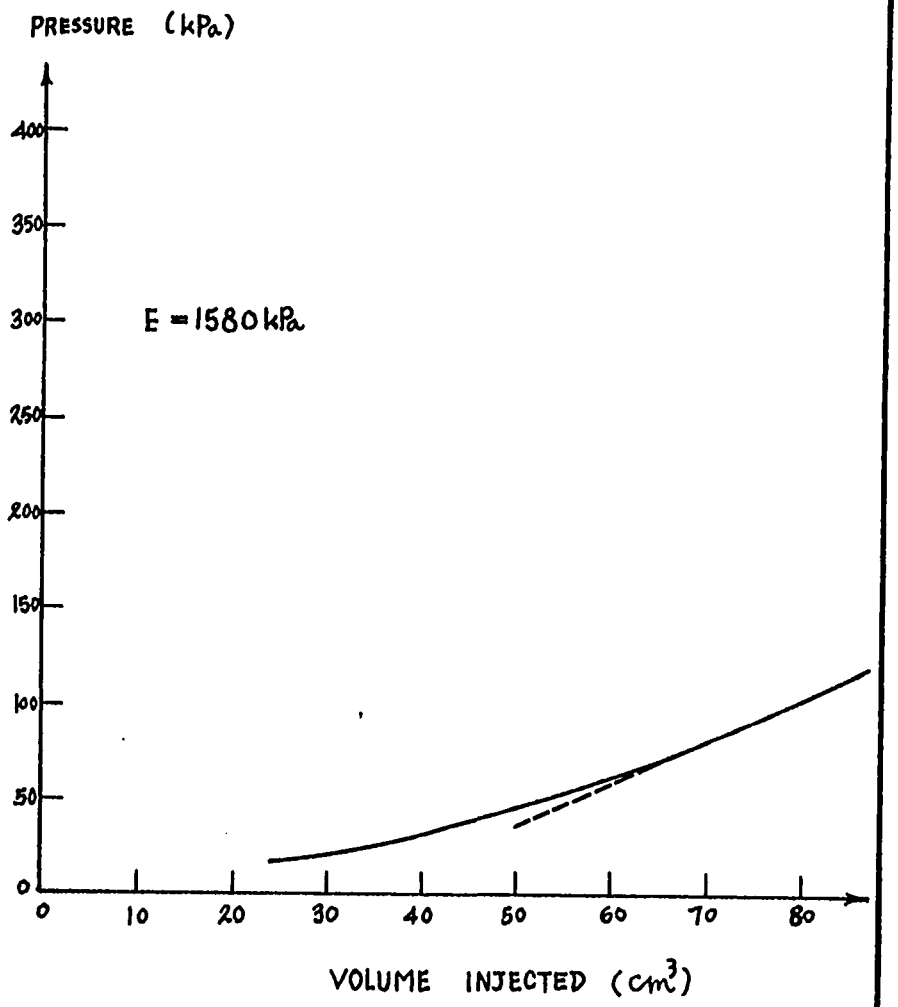

Fig. 298 - Test No. 179 - Fraser's Clay. Briaud Pressuremeter Test. Hole 2. Hole: Hand Auger. Before Slab. Depth = 0.9 m.

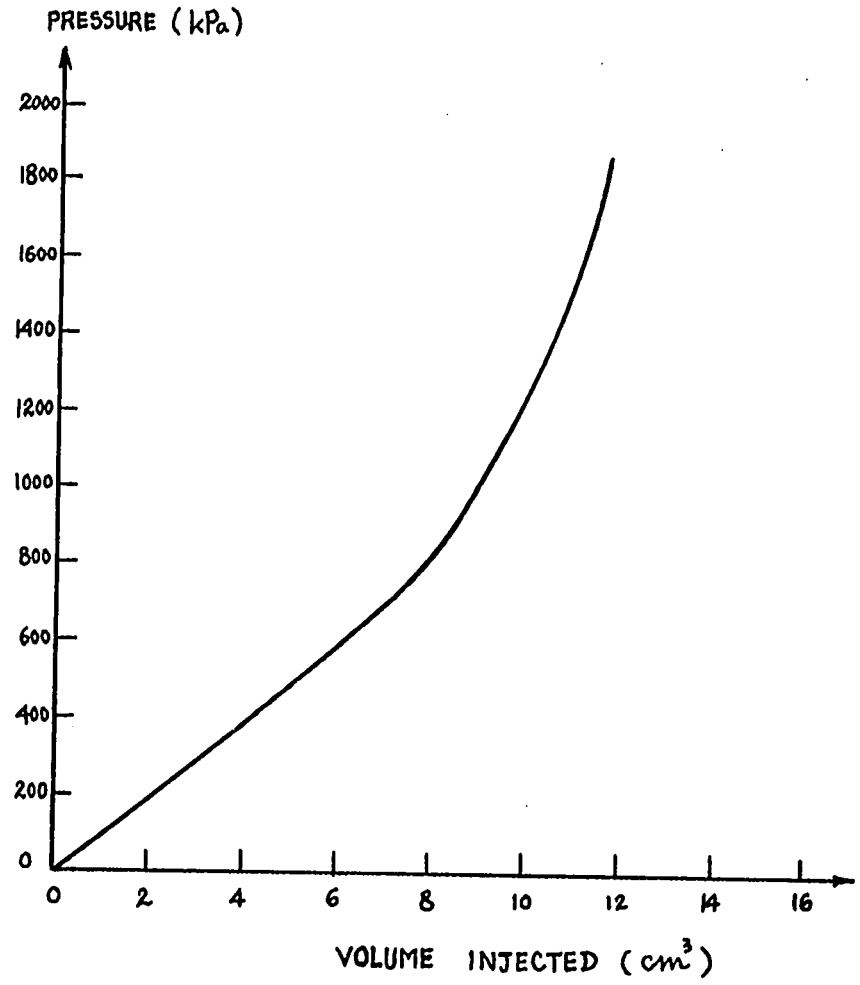

Fig. 299 - Test No. 181 - Ottawa Airport. Briaud Pressuremeter. Calibration of Volume Losses.

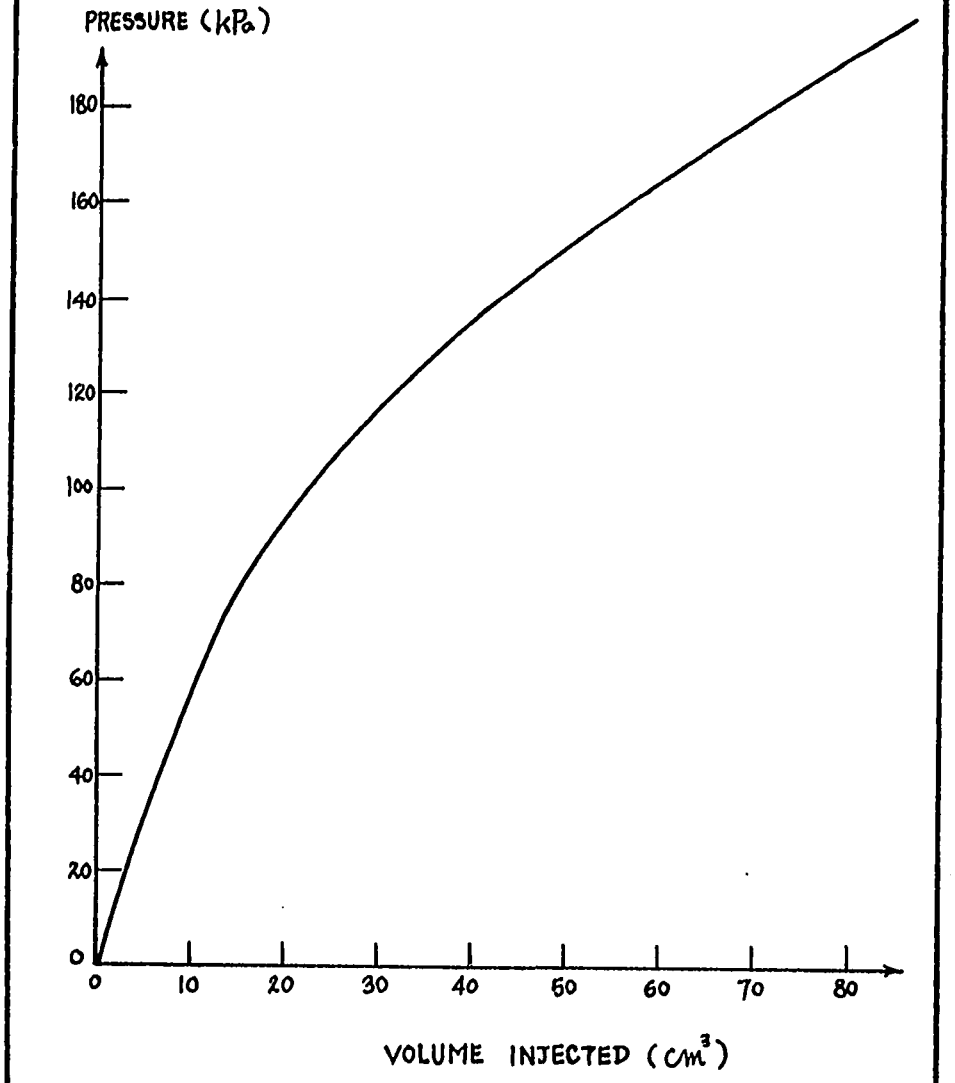

Fig. 300 - Test No. 182 - Ottawa Airport. Briaud Pressure-meter. Calibration of Membrane Resistance.

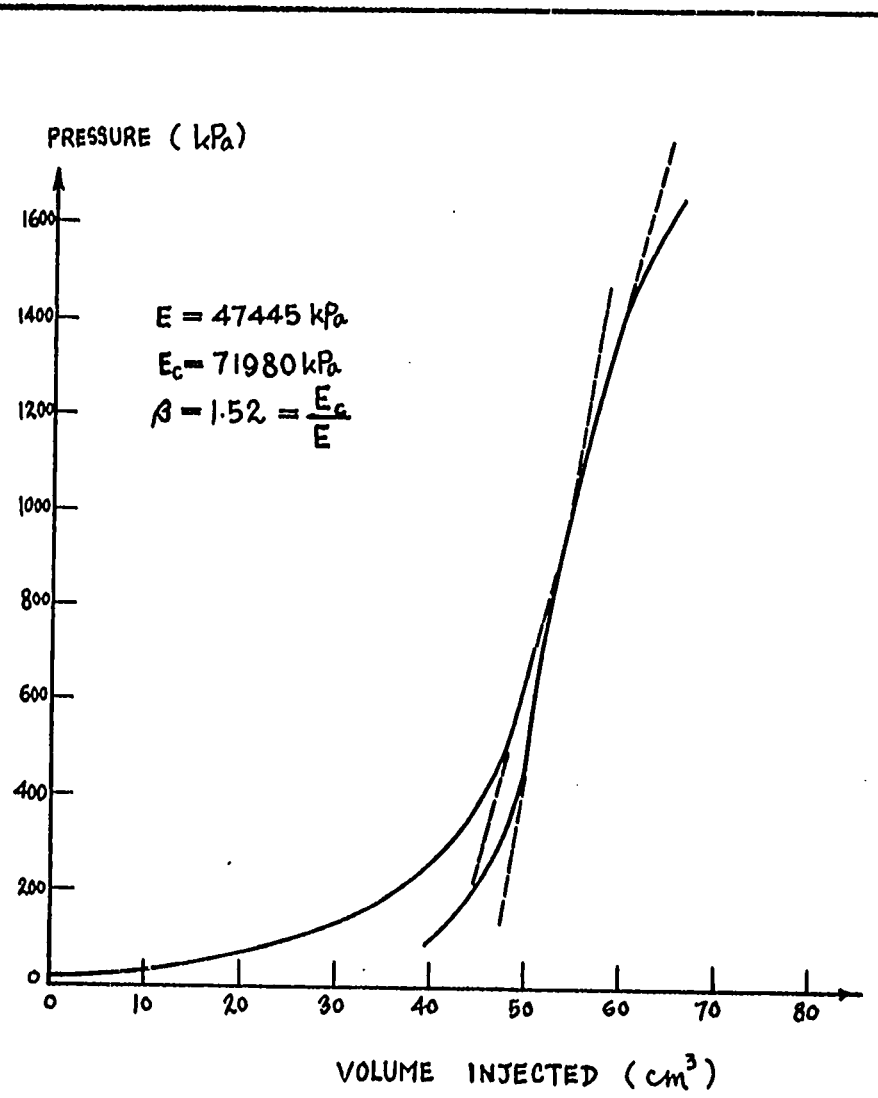

Fig. 301 - Test No. 183 - Ottawa Airport. Briaud Pressure-meter Test. Hole 1. Hole: Rod Driving. Depth = 0.3 m.

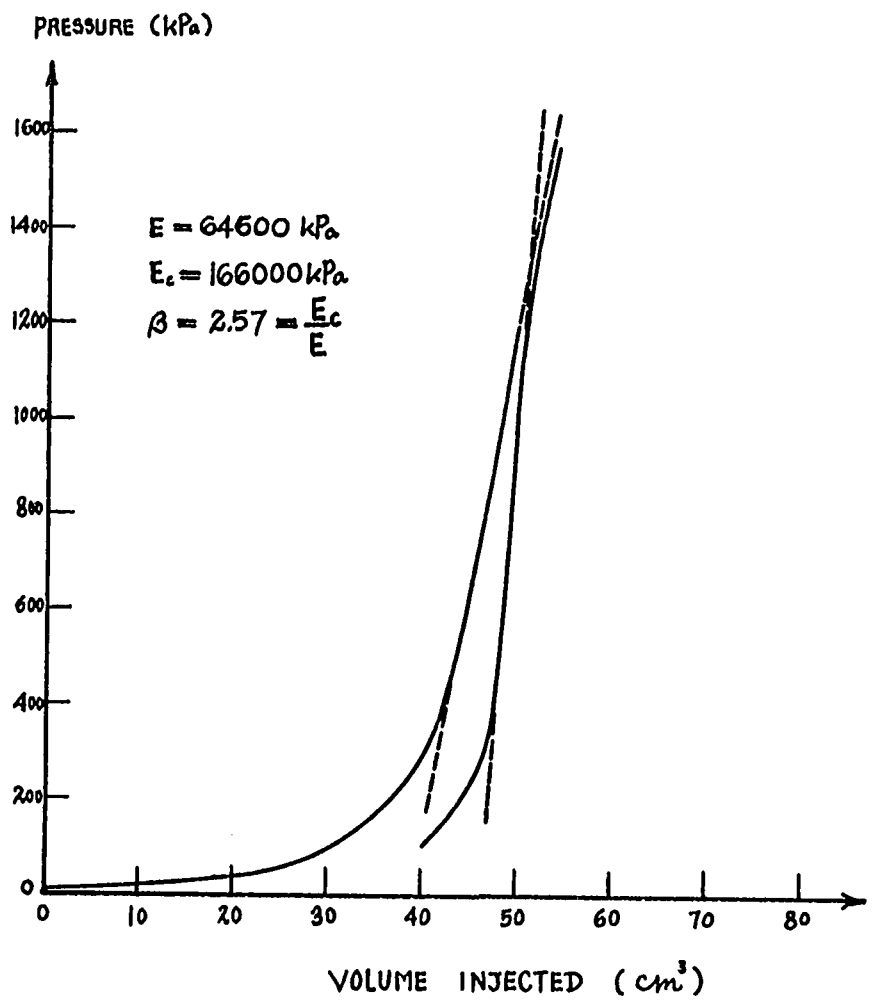

Fig.302 - Test No. 184 - Ottawa Airport. Briaud Pressuremeter Test. Hole 1. Hole: Rod Driving. Depth = 1.5 m.

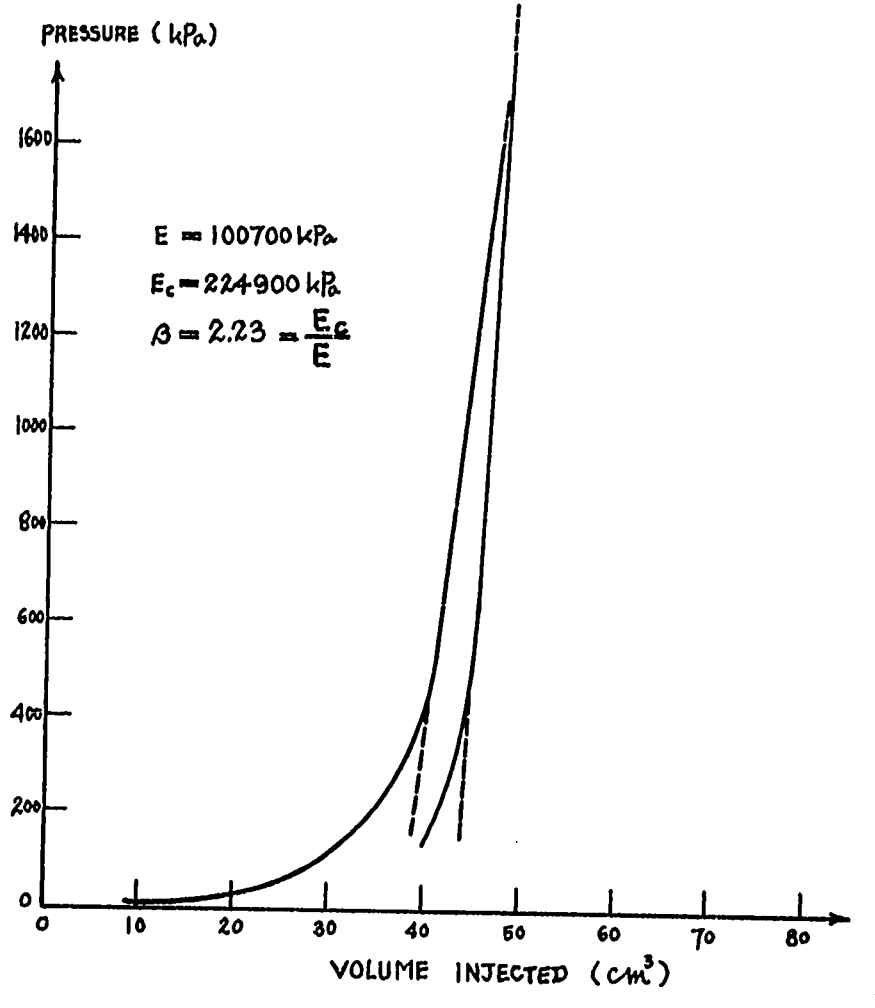

Fig.303 - Test No. 185 - Ottawa Airport. Briaud Pressuremeter Test. Hole 1. Hole: Rod Driving. Depth = 1.2 m.

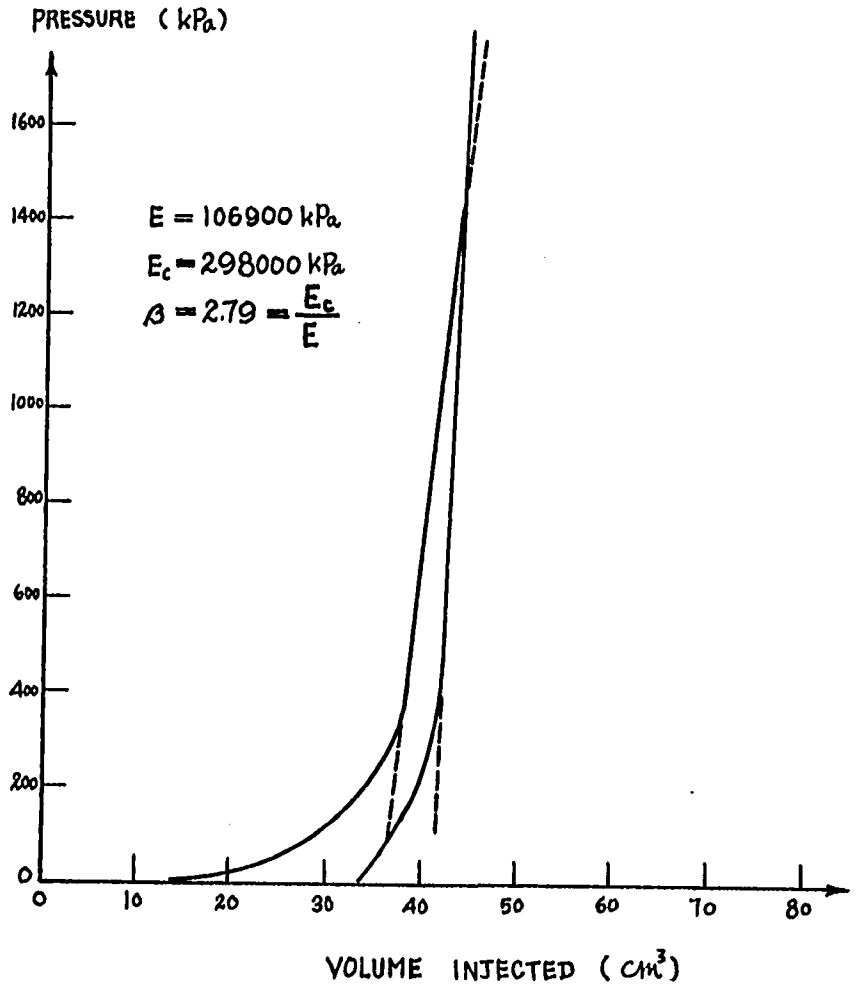

Fig. 304 - Test No. 186-Ottawa Airport. Briaud Pressuremeter Test. Hole 1. Hole: Rod Driving. Depth = 0.9 m.

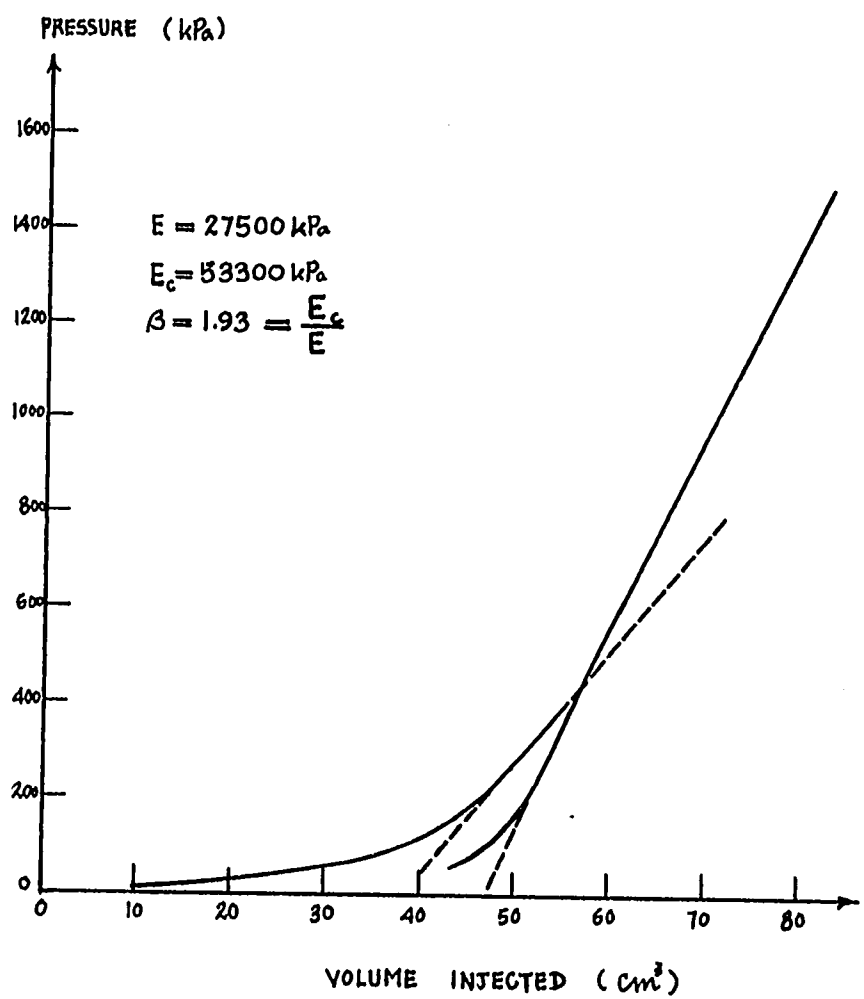

Fig. 305 - Test No. 187-Ottawa Airport. Briaud Pressuremeter Test. Hole 1. Hole: Rod Driving. Depth = 0.6 m.

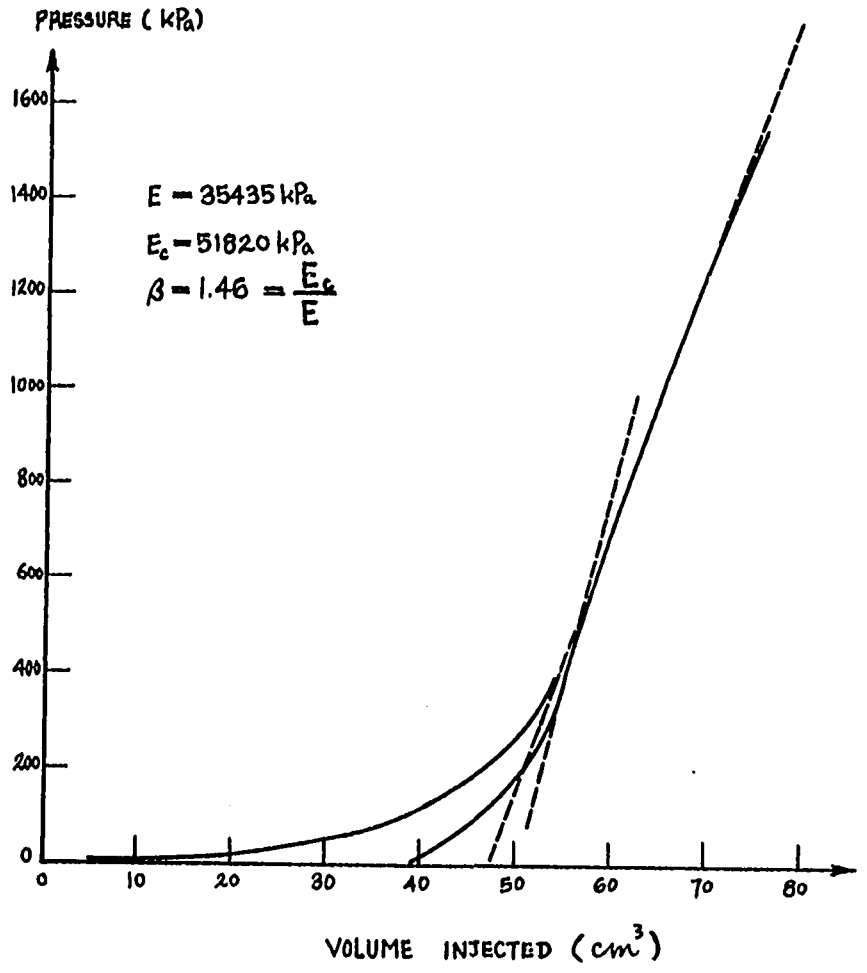

Fig. 306 - Test No. 188-Ottawa Airport. Briaud Pressuremeter Test. Hole 2. Hole: Rod Driving. Depth = 0.3 m.

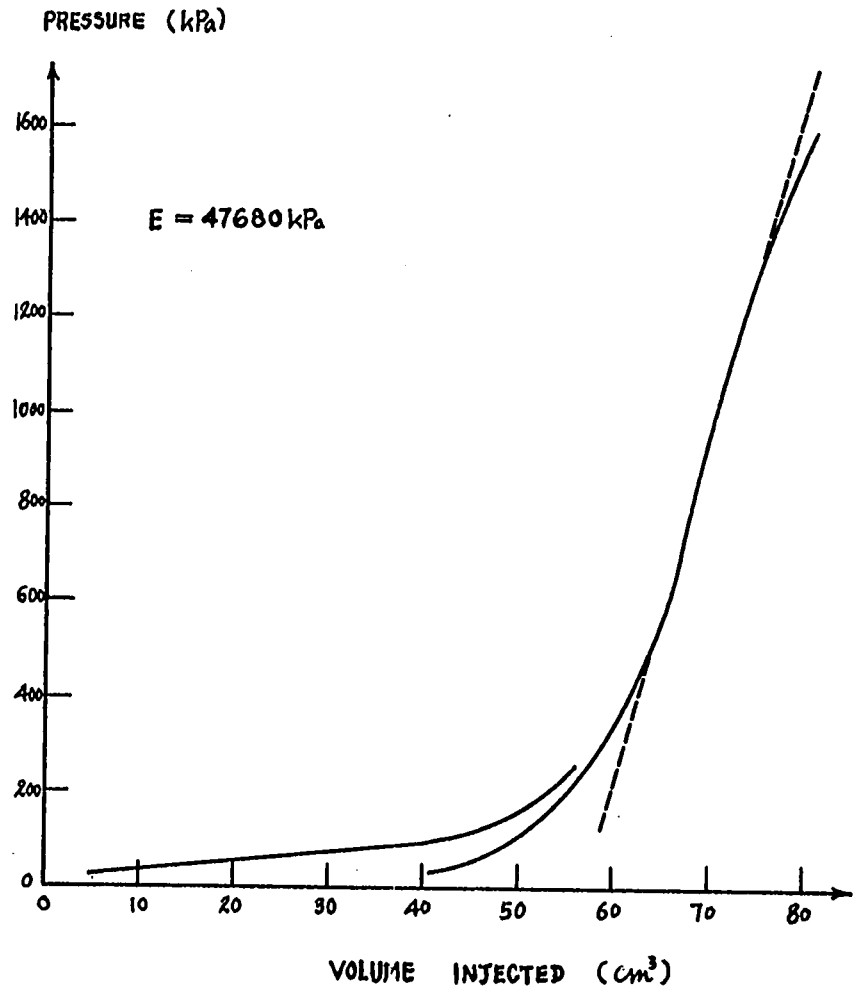

Fig. 307 - Test No. 189-Ottawa Airport. Briaud Pressuremeter Test. Hole 2. Hole: Rod Driving. Depth = 1.6 m.

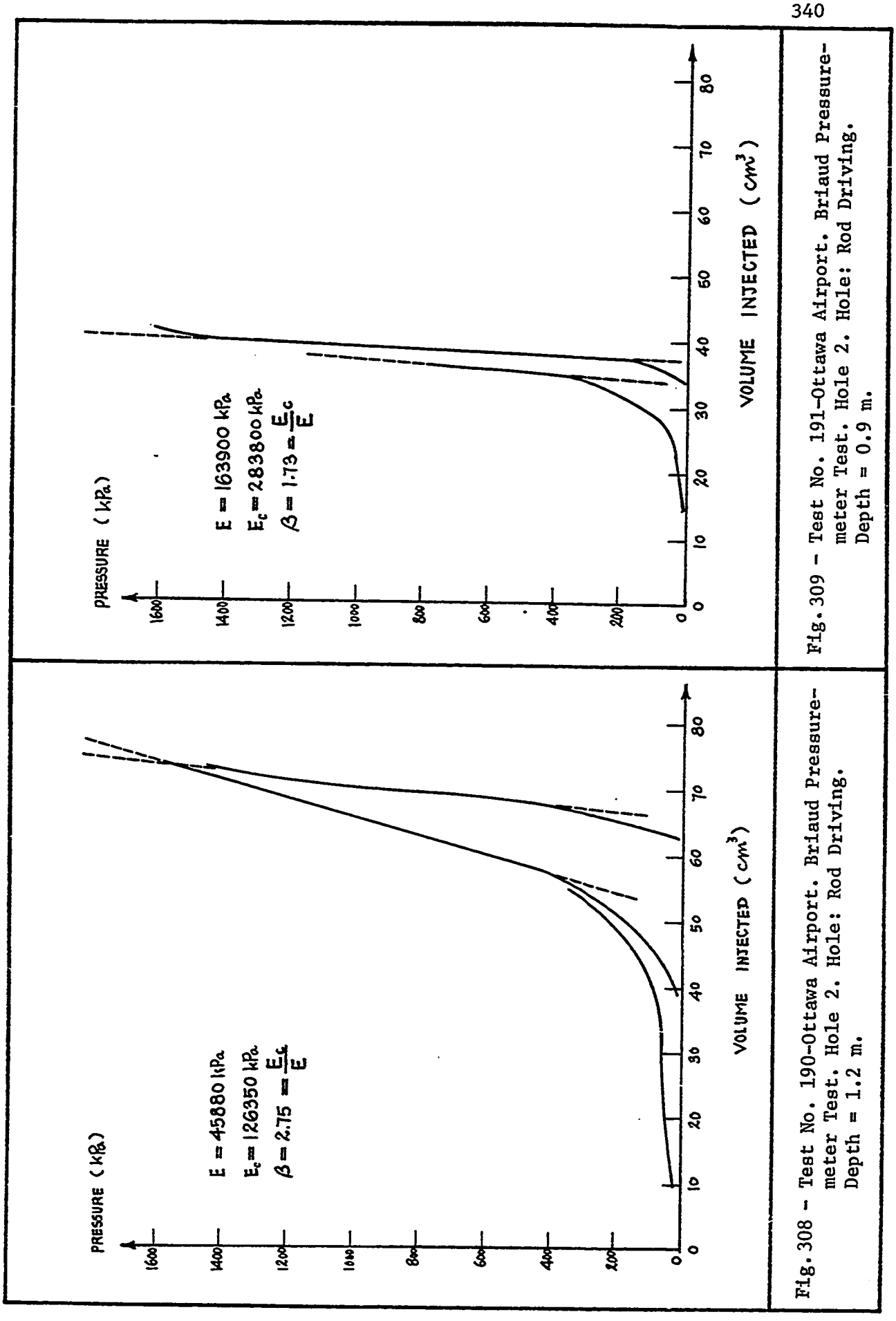

Fig. 308 - Test No. 190-Ottawa Airport. Briaud Pressuremeter Test. Hole 2. Hole: Rod Driving. Depth = 1.2 m.

Fig. 309 - Test No. 191-Ottawa Airport. Briaud Pressuremeter Test. Hole 2. Hole: Rod Driving. Depth = 0.9 m.

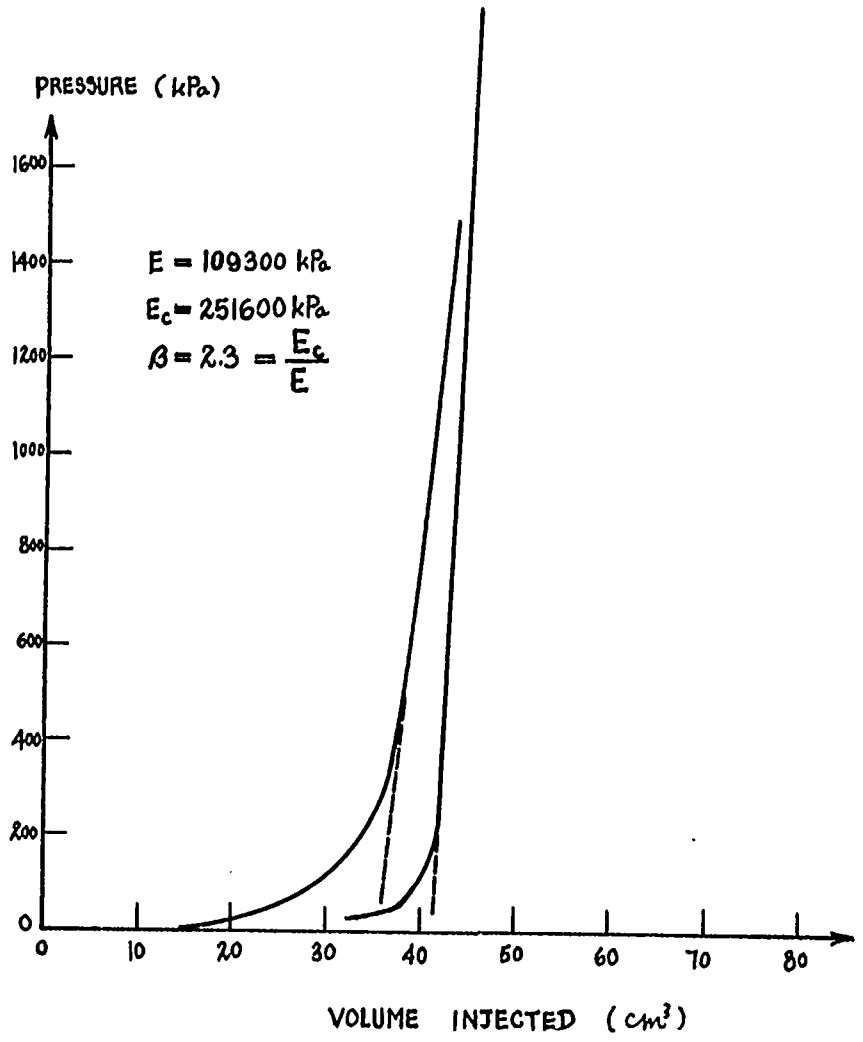

Fig.310 - Test No. 192-Ottawa Airport. Briaud Pressuremeter Test. Hole 2. Hole: Rod Driving. Depth = 0.6 m.

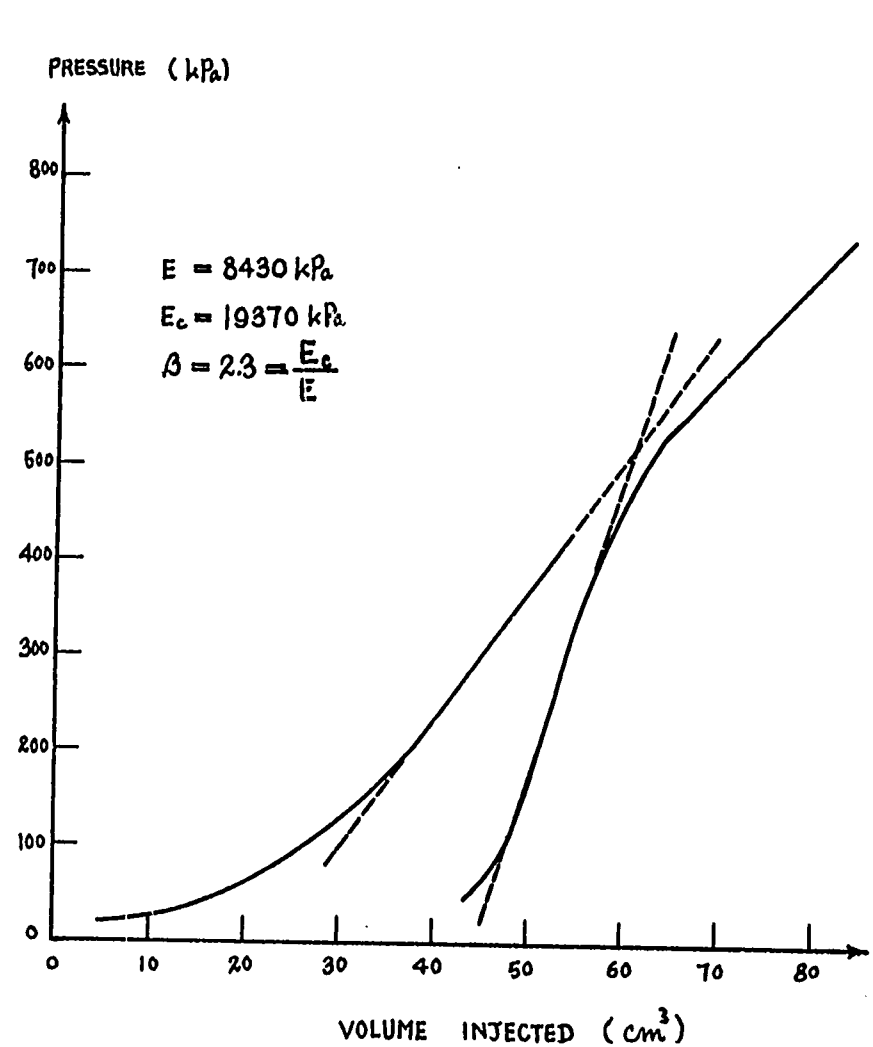

Fig. 311 - Test No. 193-Ottawa Airport. Briaud Pressuremeter Test. Hole 3. Hole: Rod Driving. Depth = 1.8 m.

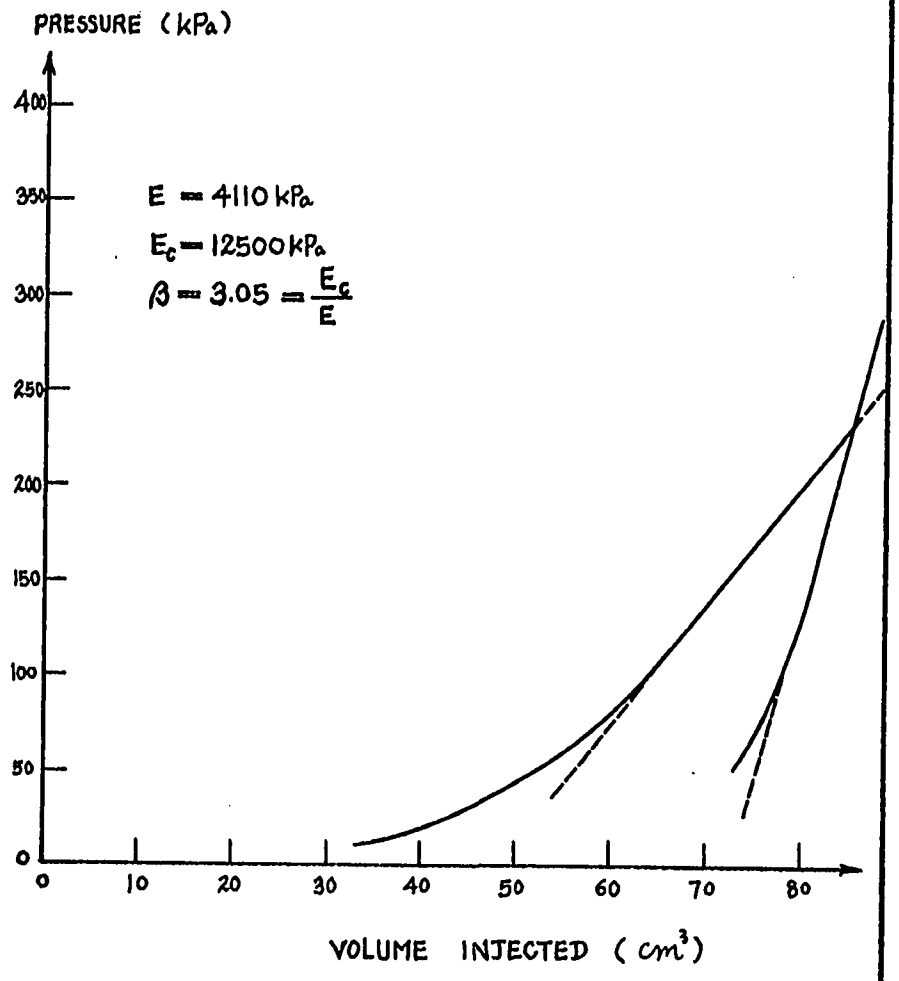

Fig. 312 - Test No. 194-Ottawa Airport. Briaud Pressuremeter Test. Hole 3. Hole: Rod Driving. Depth = 1.5 m.

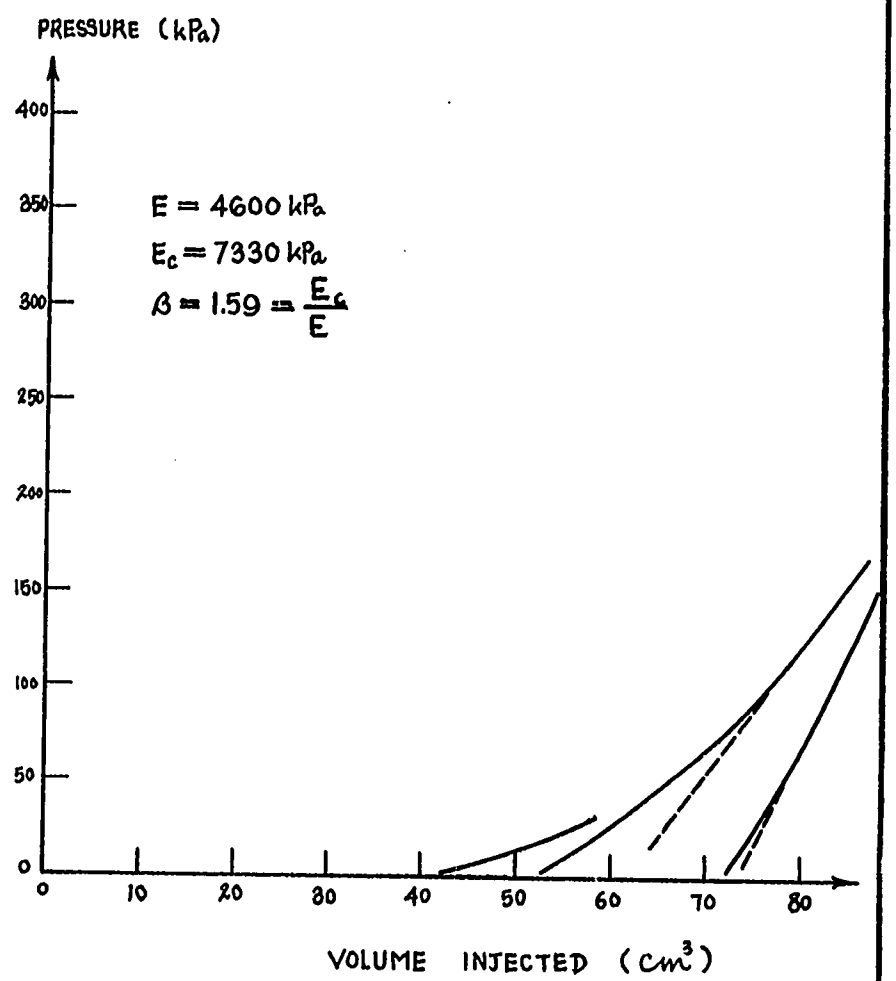

Fig. 313 - Test No. 195-Ottawa Airport. Briaud Pressuremeter Test. Hole 3. Hole: Rod Driving. Depth = 1.2 m.

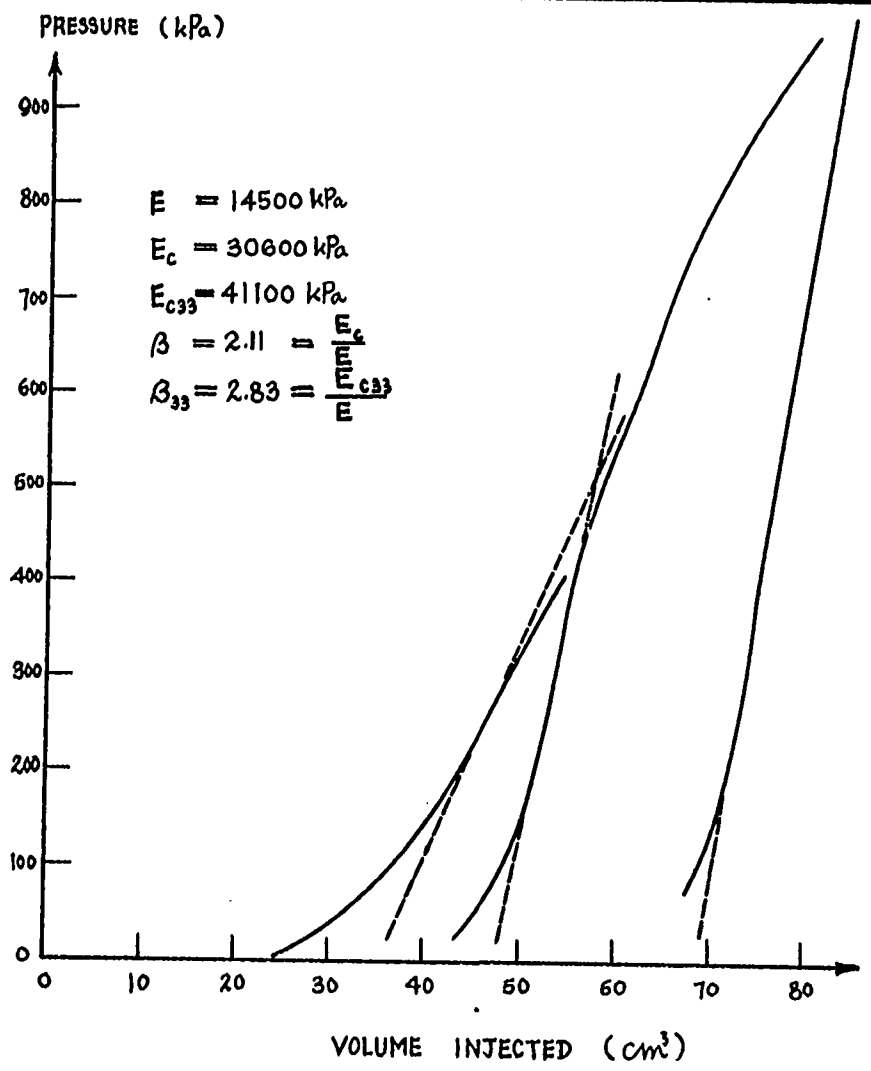

Fig. 314 - Test No. 196-Ottawa Airport. Briaud Pressuremeter Test. Hole 3. Hole: Rod Driving. Depth = 0.9 m.

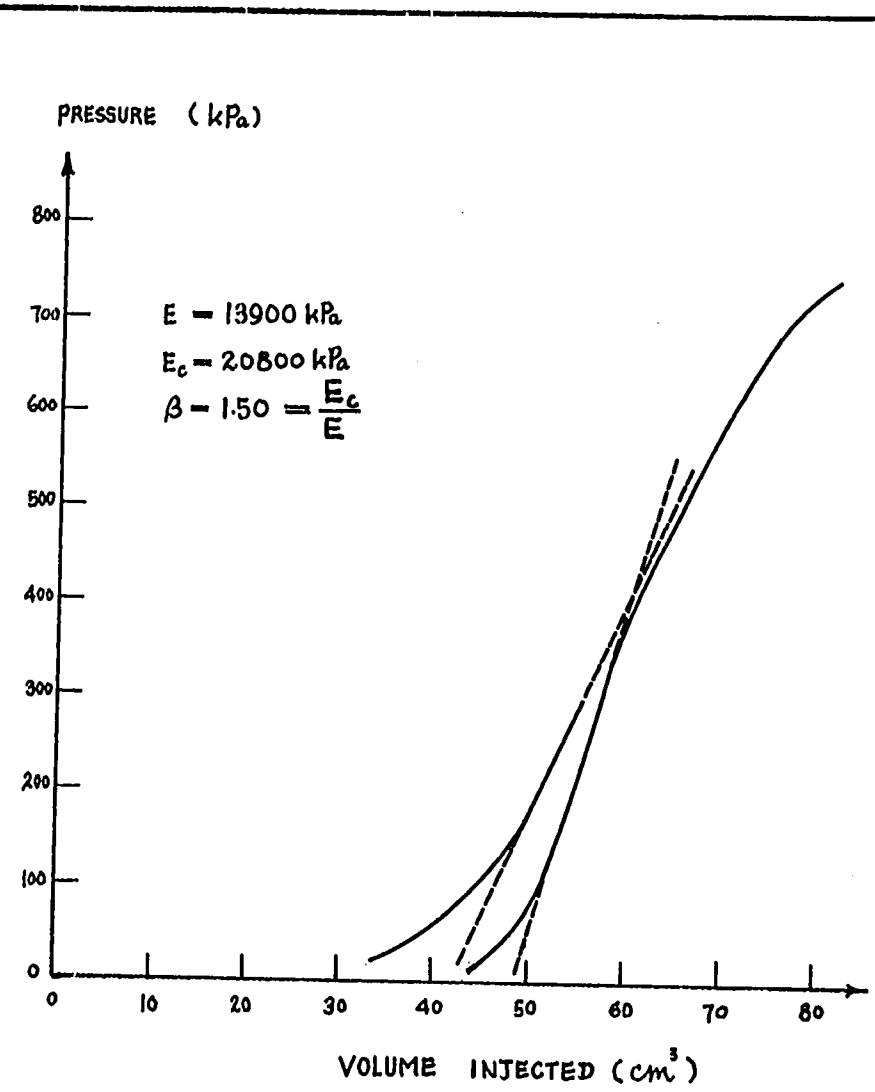

Fig. 315 - Test No. 197-Ottawa Airport. Briaud Pressuremeter Test. Hole 3. Hole: Rod Driving. Depth = 0.6 m.

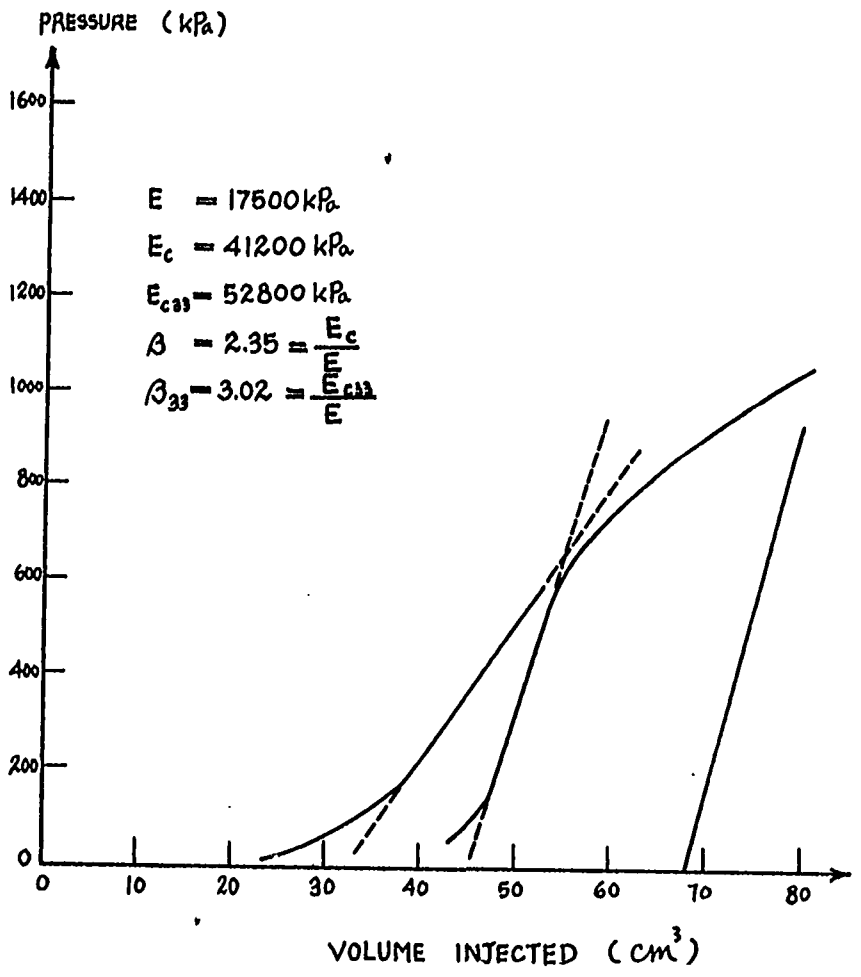

Fig. 316- Test No. 198-Ottawa Airport. Briaud Pressuremeter Test. Hole 3. Hole: Rod Driving. Depth = 0.3 m.

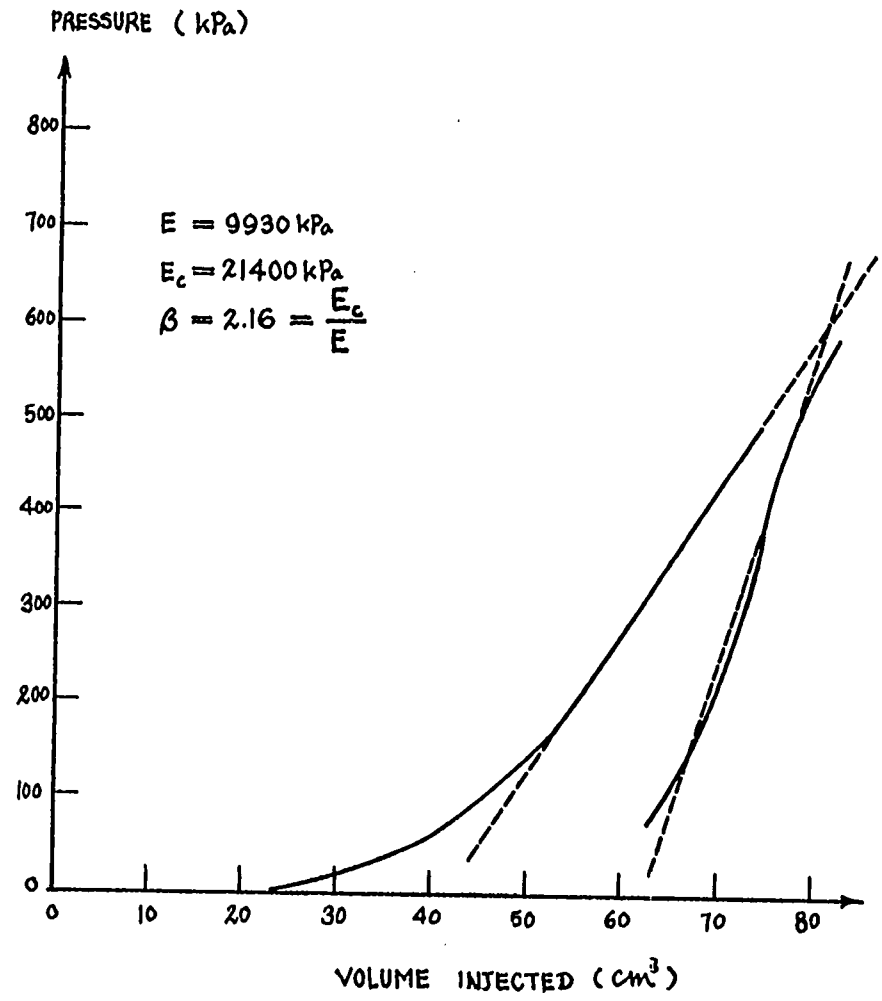

Fig.317 - Test No. 199-Ottawa Airport. Briaud Pressuremeter Test.Hole 4. Hole: Rod Driving. Depth = 1.8 m.

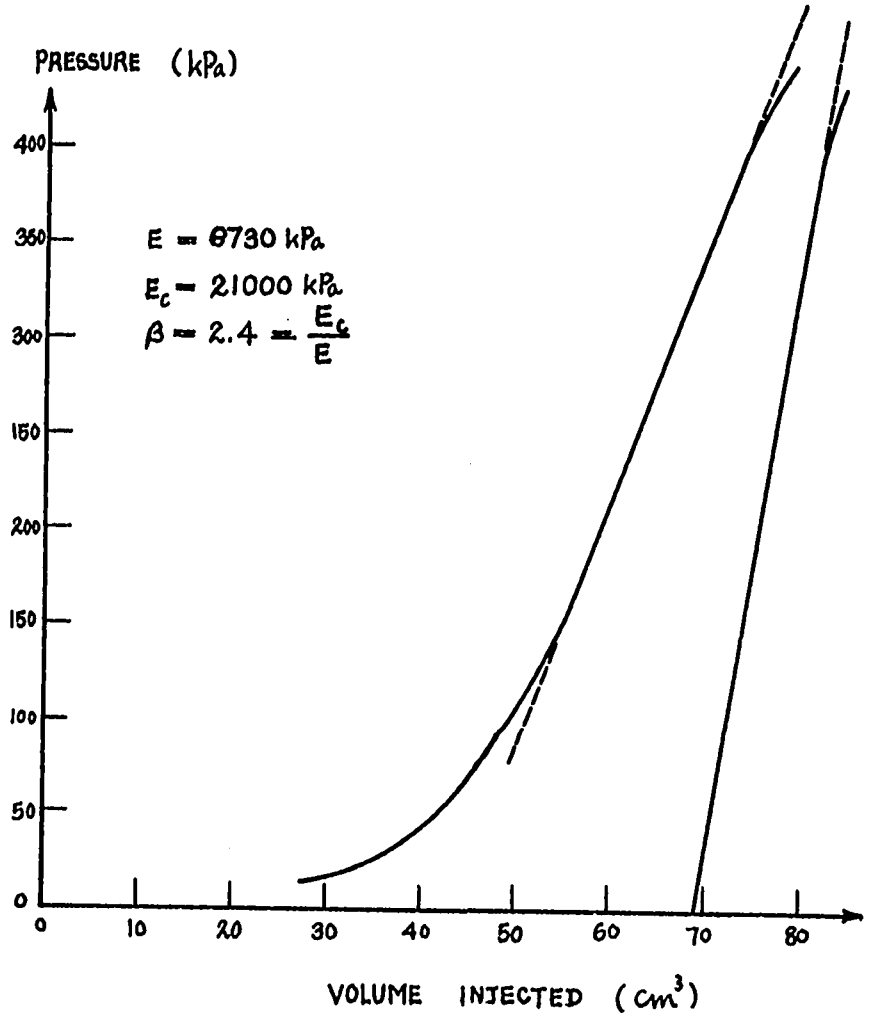

Fig. 318 - Test No. 200-Ottawa Airport. Briaud Pressuremeter Test. Hole 4. Hole: Rod Driving. Depth = 1.5 m.

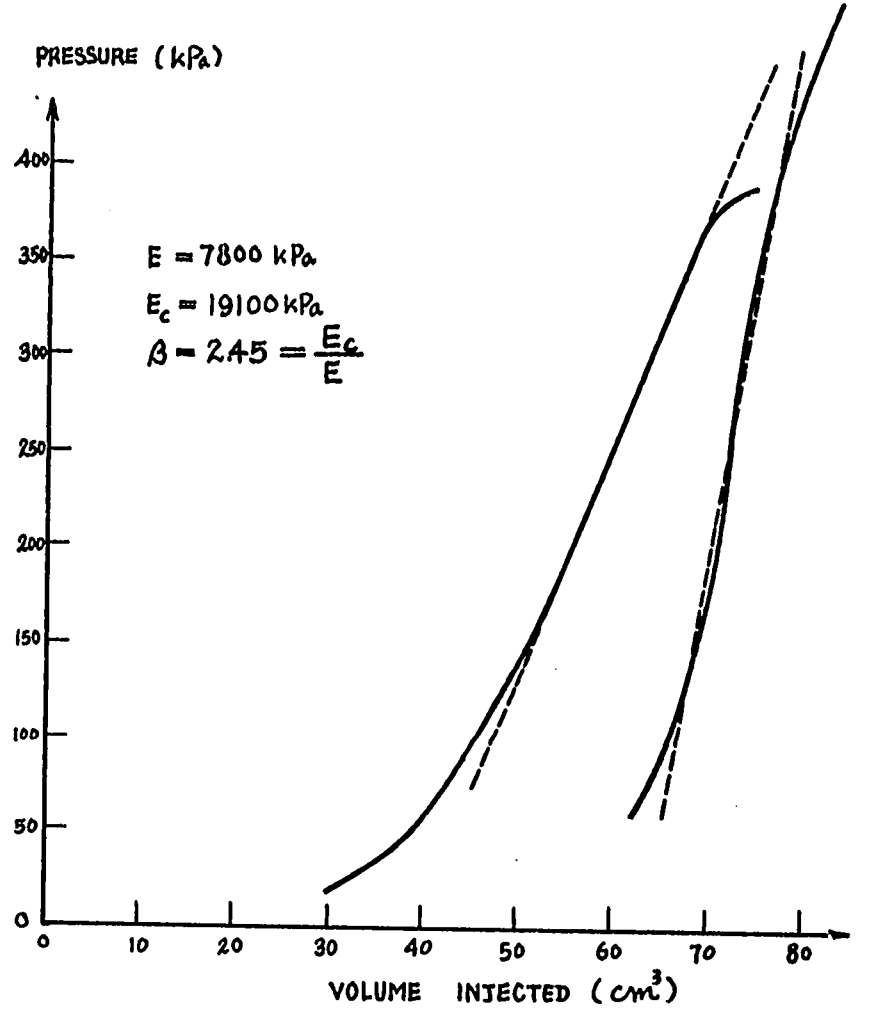

Fig. 319 - Test No. 201-Ottawa Airport. Briaud Pressuremeter Test. Hole 4. Hole: Rod Driving. Depth = 1.2 m.

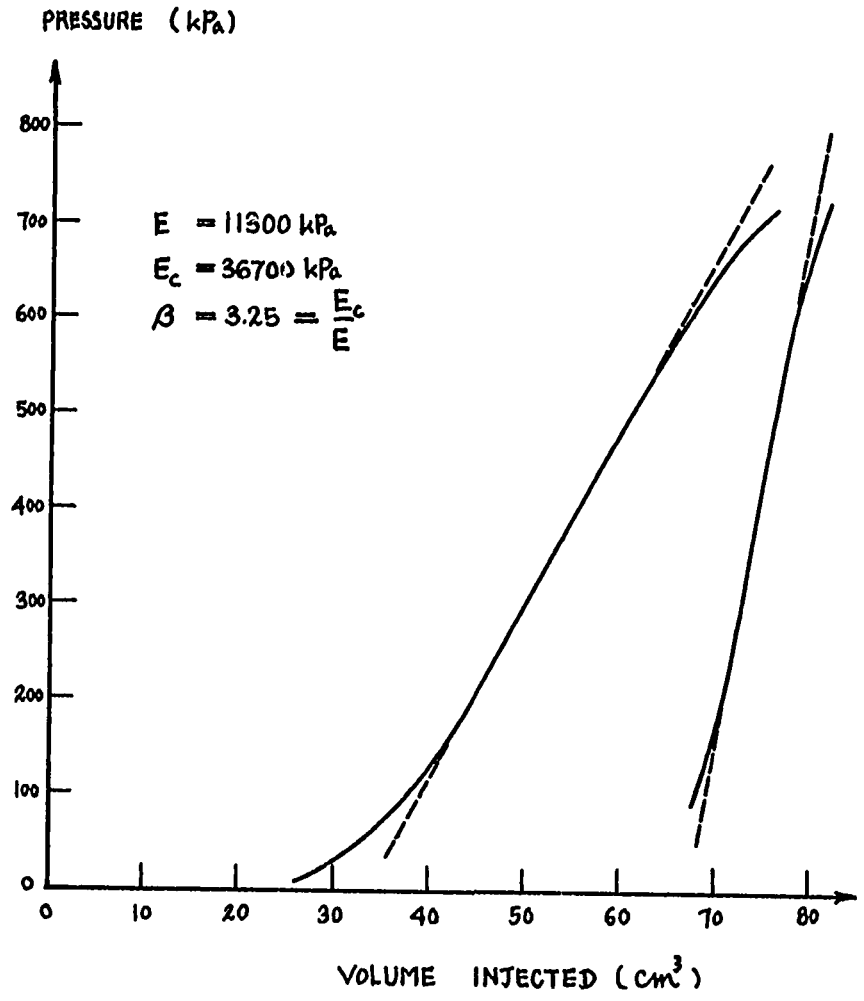

Fig. 320 - Test No. 202-Ottawa Airport. Briaud Pressuremeter Test. Hole 4. Hole: Rod Driving. Depth = 0.9 m.

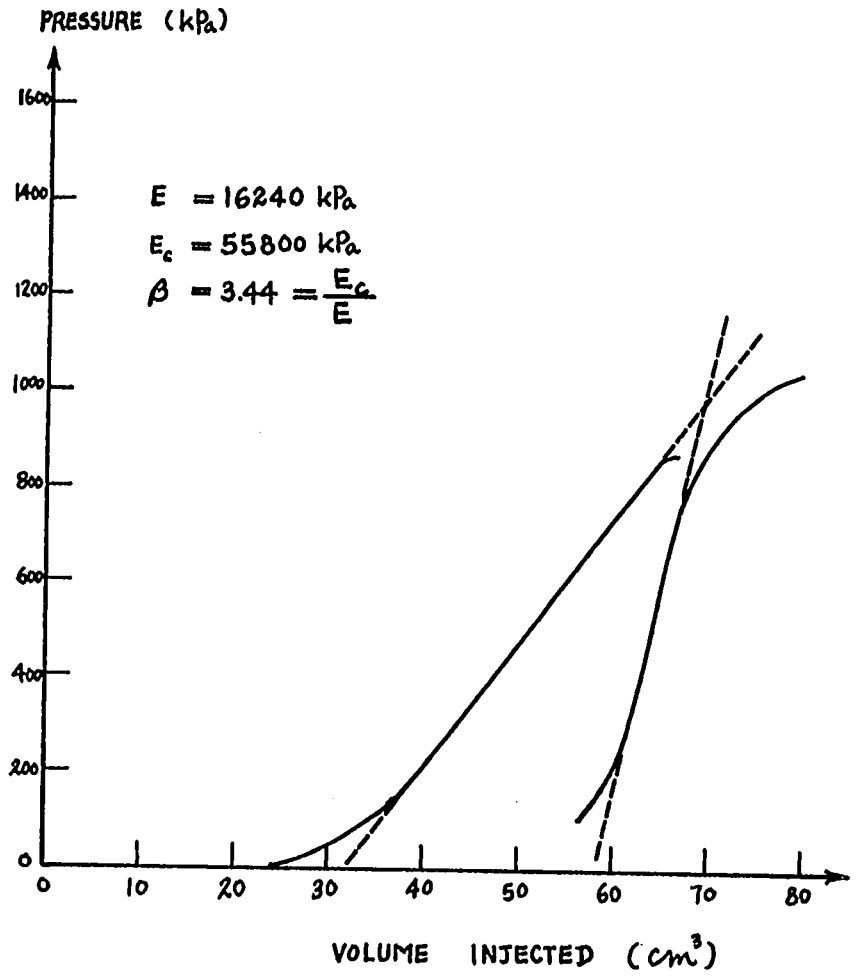

Fig. 321 - Test No. 203-Ottawa Airport. Briaud Pressuremeter Test. Hole 4. Hole: Rod Driving. Depth = 0.6 m.

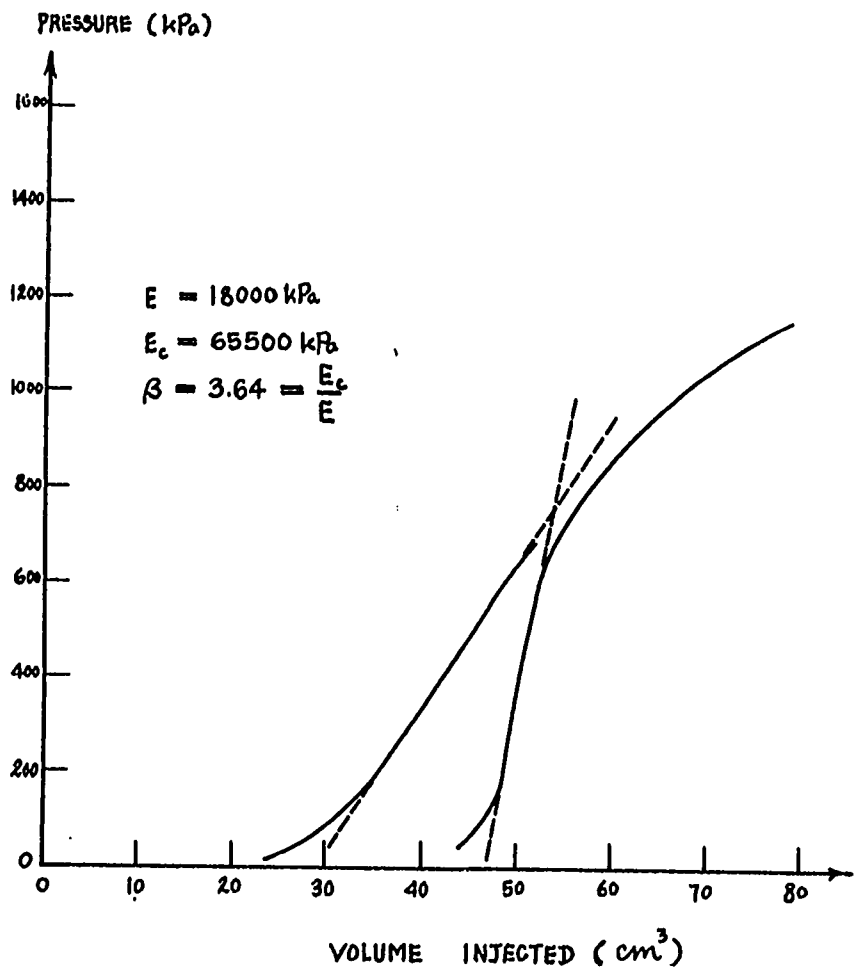

Fig. 322 - Test No. 204-Ottawa Airport. Briaud Pressuremeter Test. Hole 4. Hole: Rod Driving. Depth = 0.3 m.

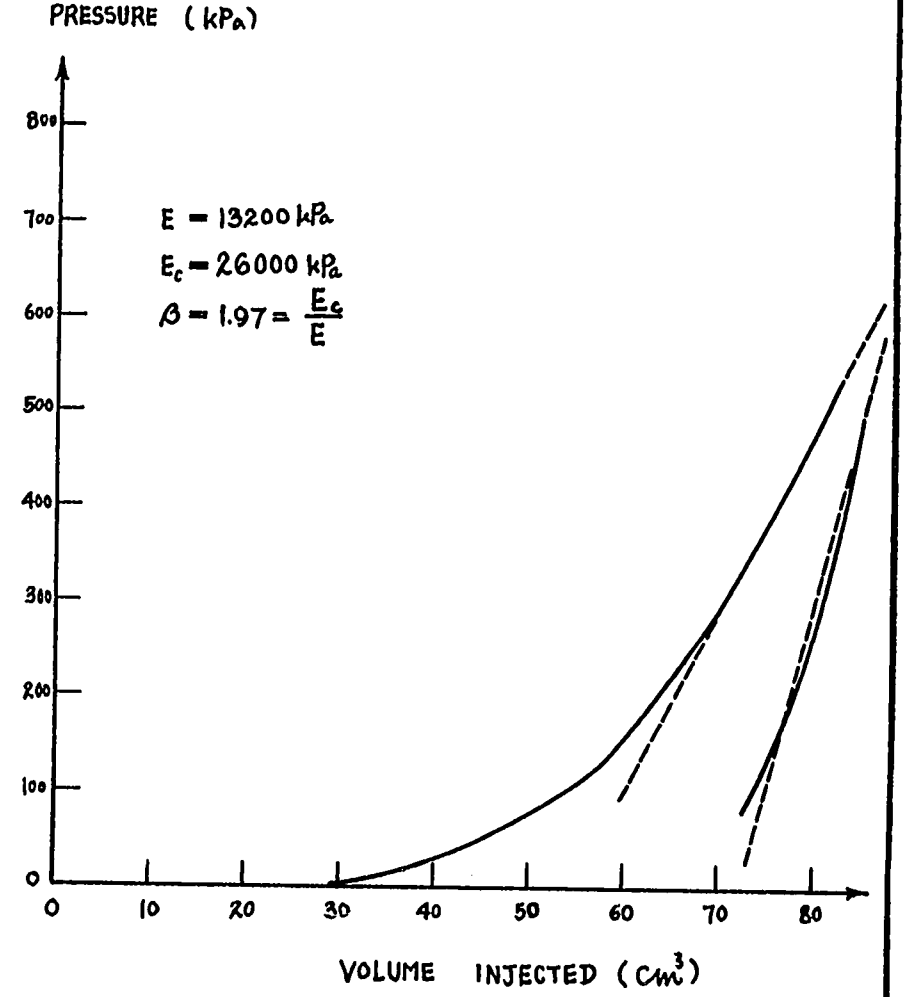

Fig. 323- Test No. 205-Ottawa Airport. Briaud Pressuremeter Test. Hole 5. Hole: Rod Driving. Depth = 1.8 m.

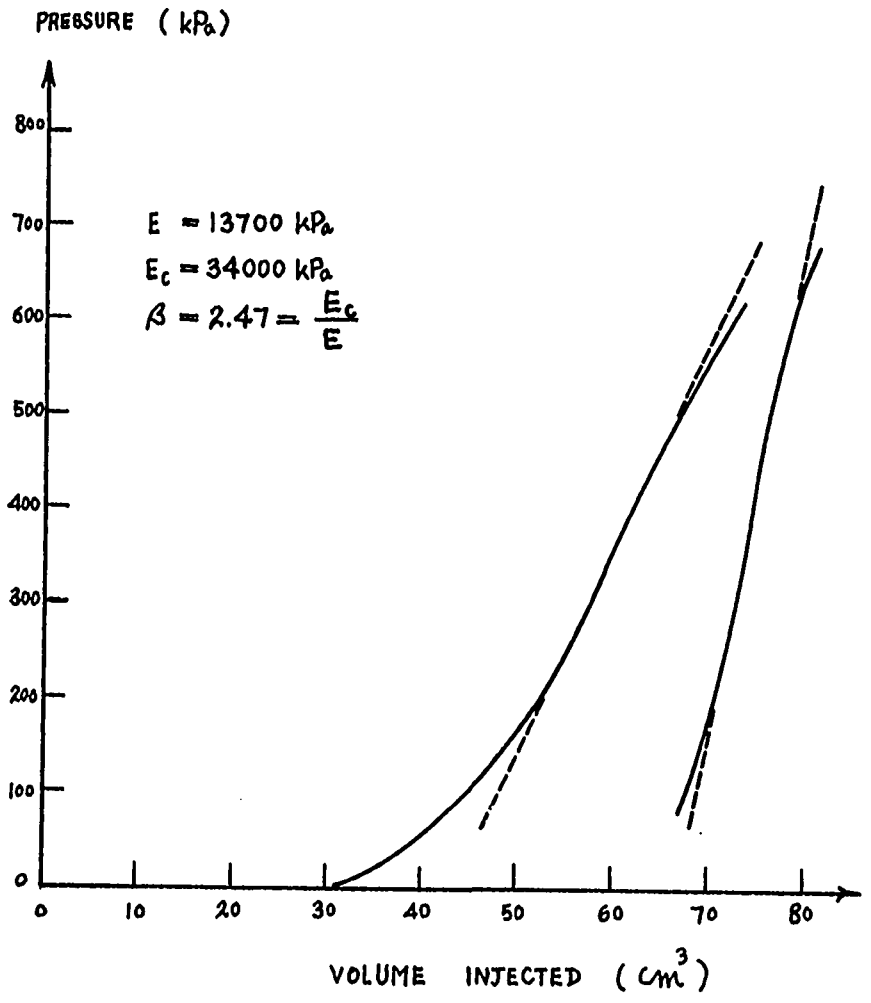

Fig.324 - Test No. 206-Ottawa Airport. Briaud Pressuremeter Test. Hole 5, Hole: Rod Driving. Depth = 1.5 m.

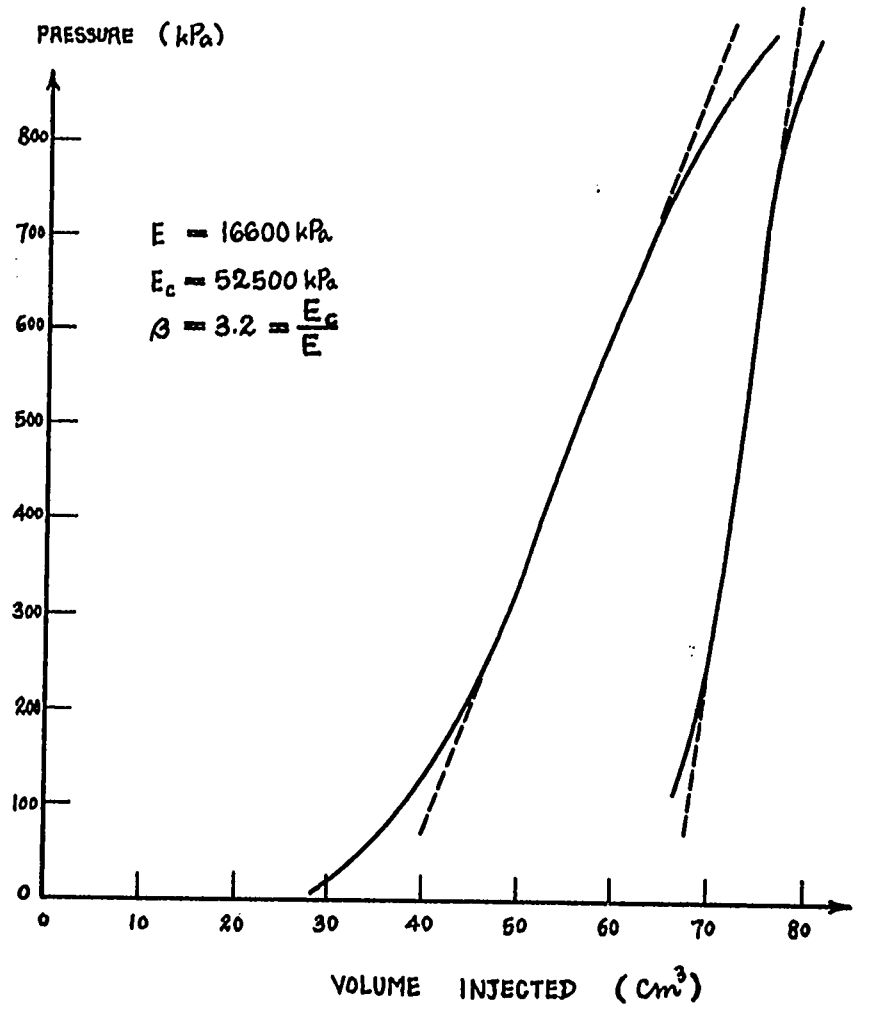

Fig.325 - Test No. 207-Ottawa Airport. Briaud Pressuremeter Test. Hole 5, Hole:Rod Driving. Depth = 1.2 m.

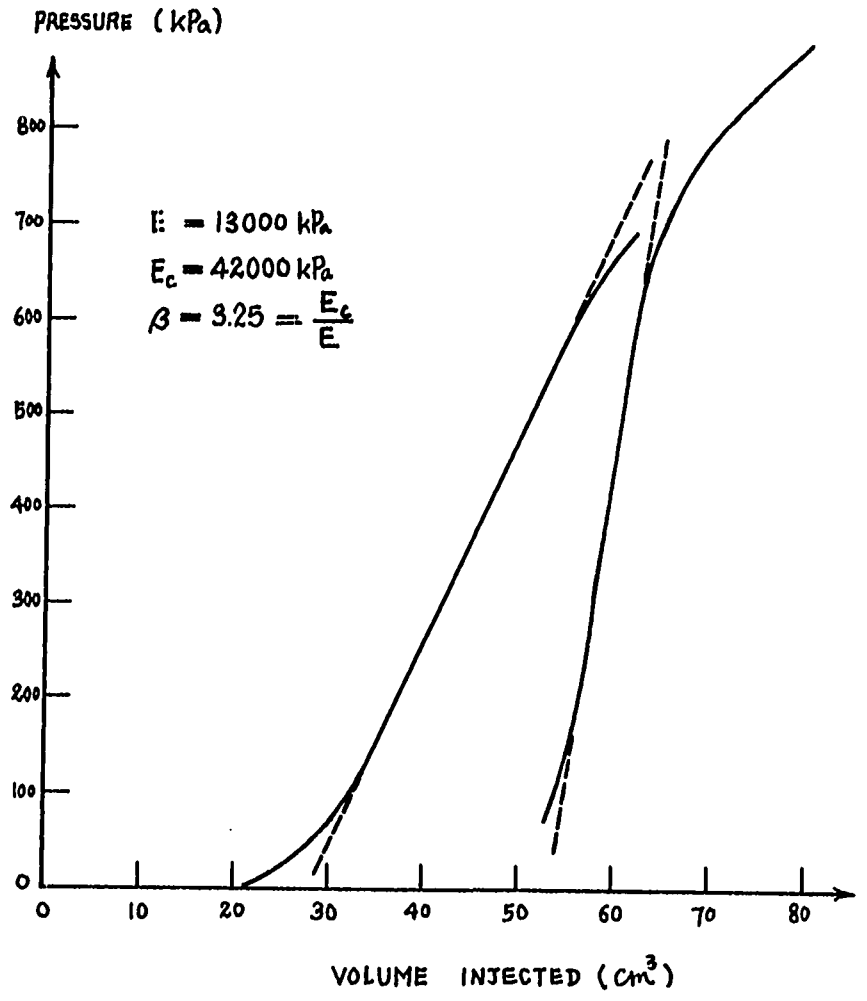

Fig. 326 - Test No. 208-Ottawa Airport. Briaud Pressuremeter Test. Hole 5. Hole: Rod Driving. Depth = 0.9 m.

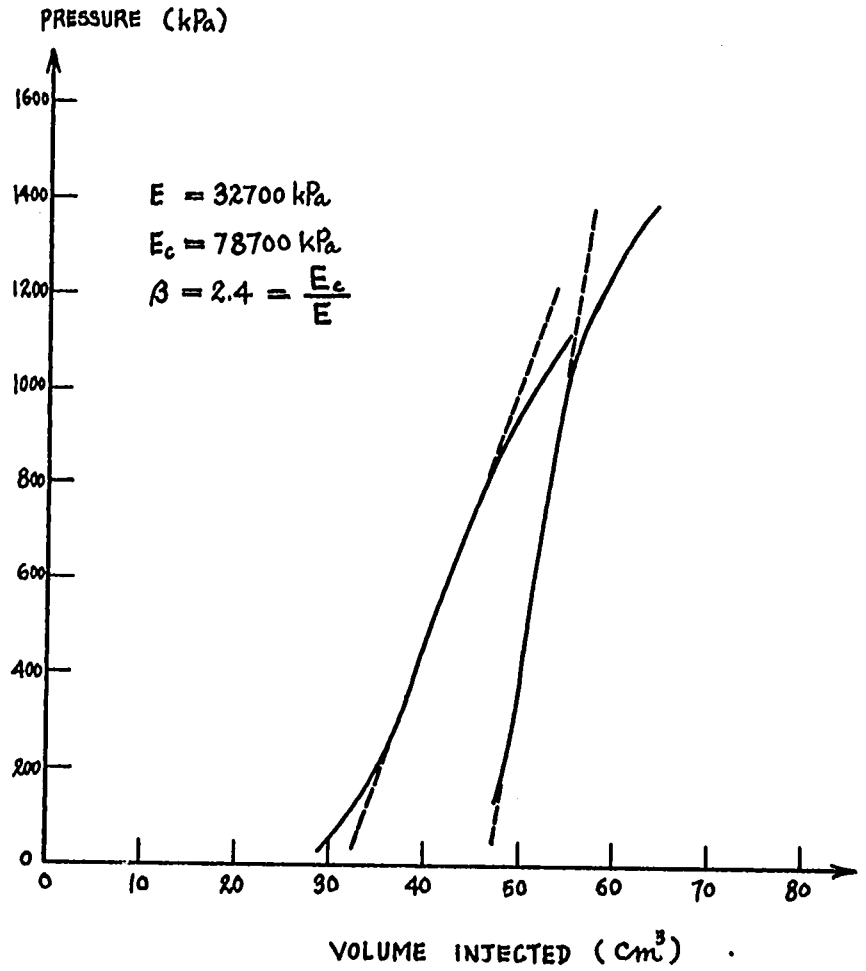

Fig. 327 - Test No. 209-Ottawa Airport. Briaud Pressuremeter Test. Hole 5. Hole: Rod Driving. Depth = 0.6 m.

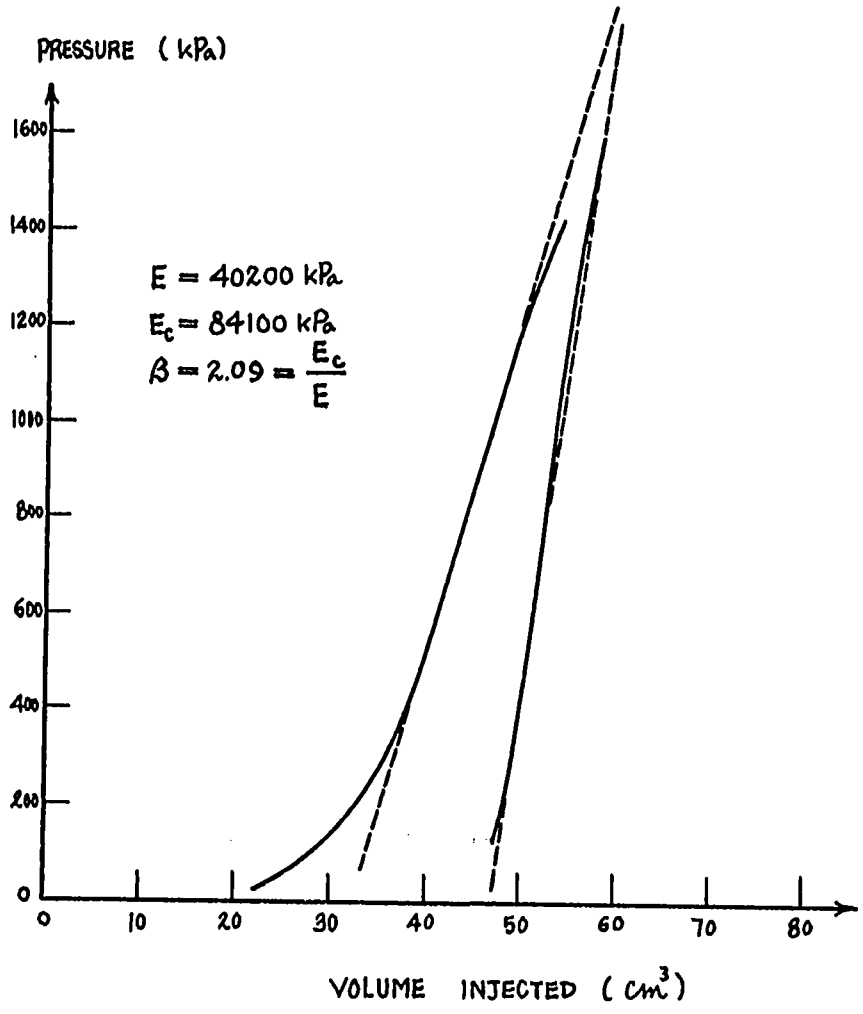

Fig. 328 - Test No. 210-Ottawa Airport. Briaud Pressuremeter Test. Hole 5. Hole: Rod Driving. Depth = 0.33 m.

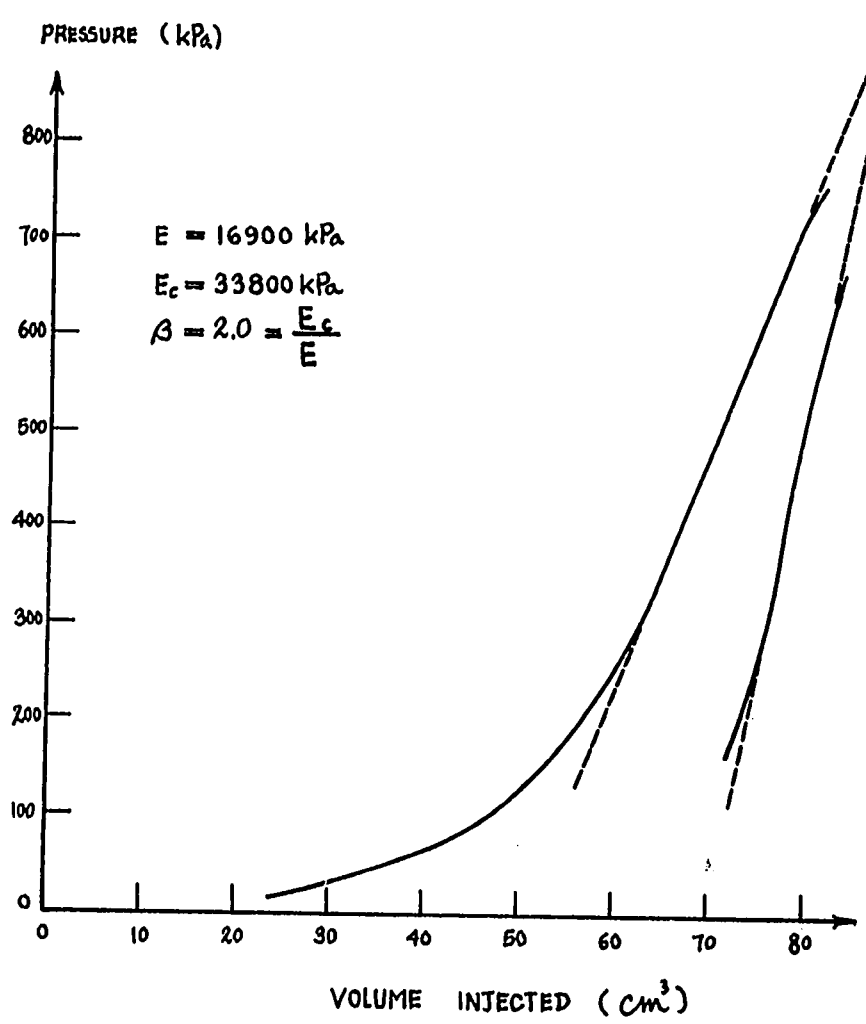

Fig. 329 - Test No. 211-Ottawa Airport. Briaud Pressuremeter Test. Hole 6. Hole: Rod Driving. Depth = 1.8 m.

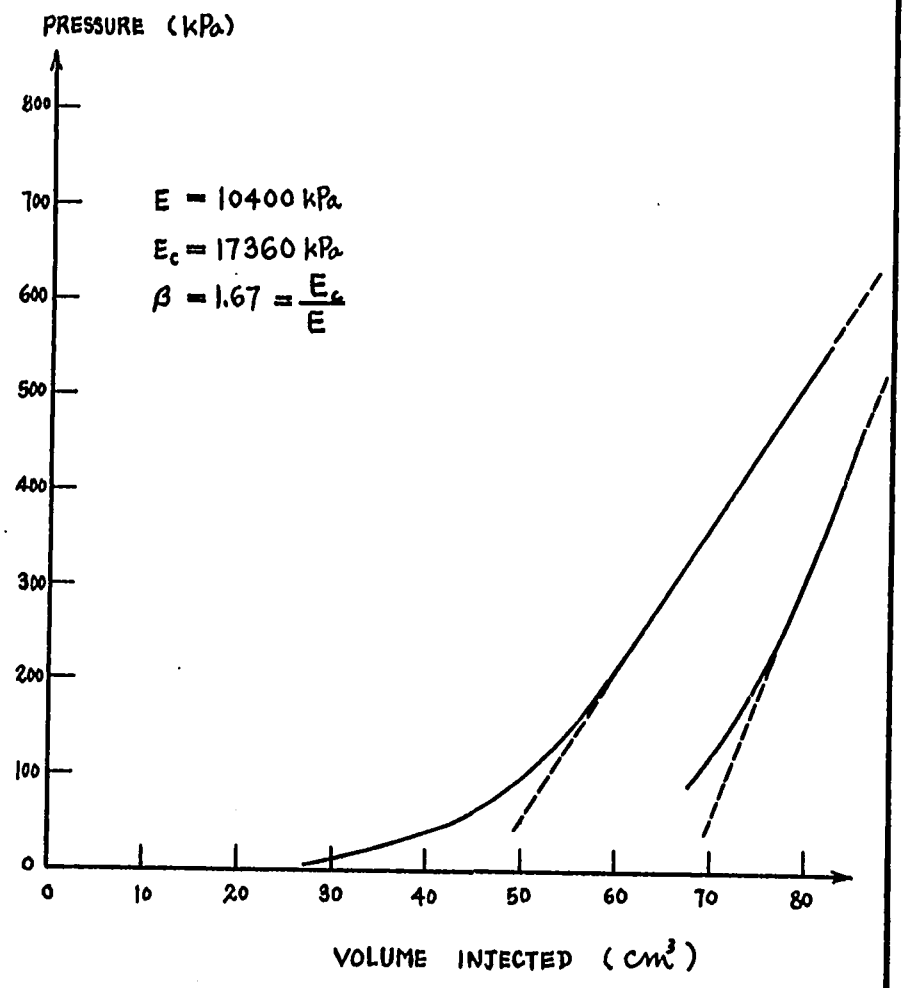

Fig. 330 - Test No. 212-Ottawa Airport. Briaud Pressuremeter. Hole 6. Hole: Rod Driving. Depth = 1.5 m.

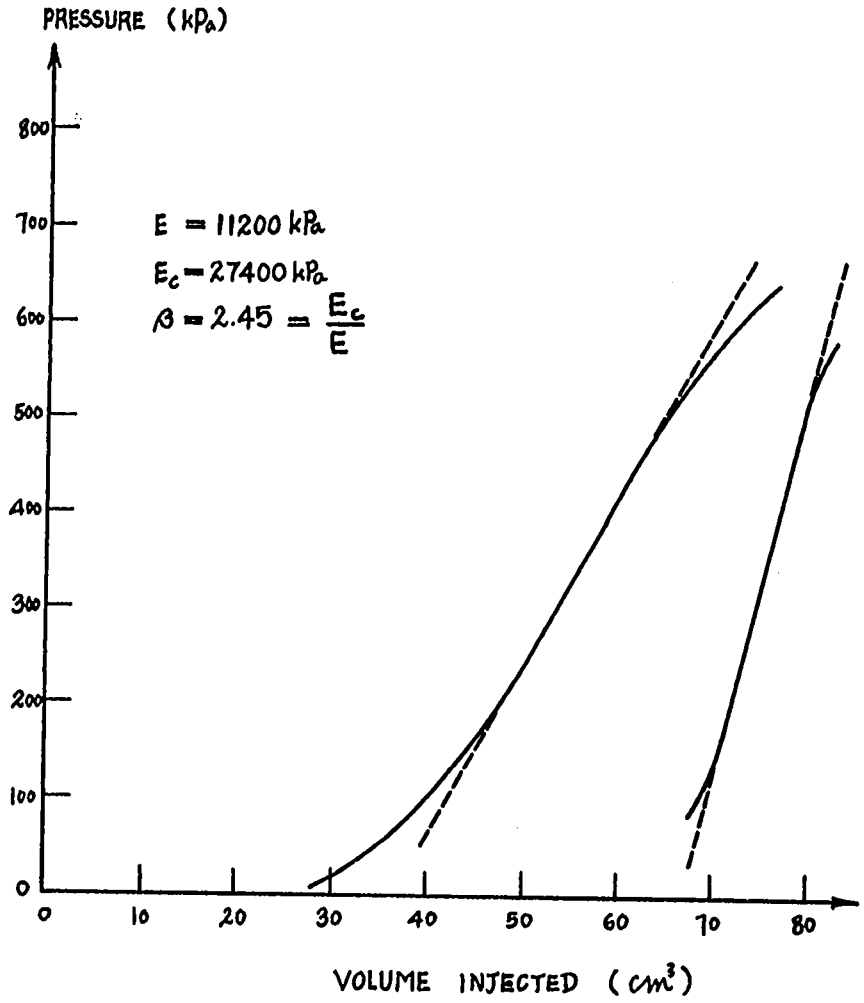

Fig. 331 - Test No. 213-Ottawa Airport. Briaud Pressuremeter Test. Hole 6. Hole: Rod Driving. Depth = 1.2 m.

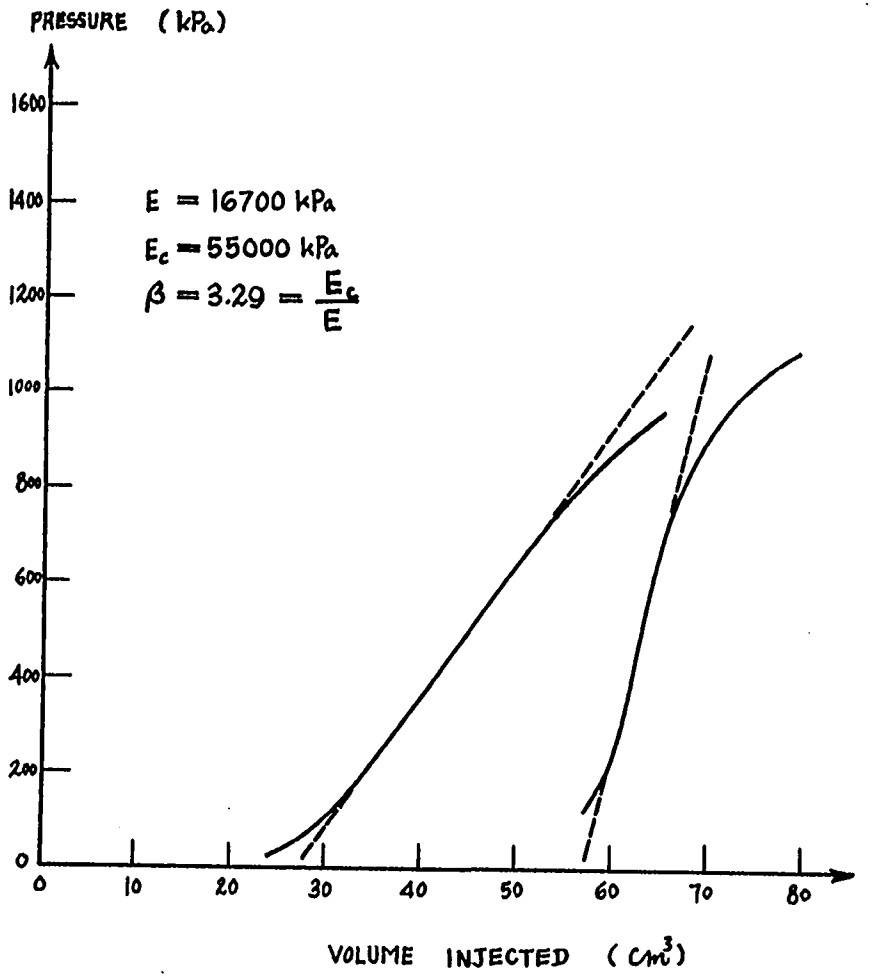

Fig. 332 - Test No. 214-Ottawa Airport. Briaud Pressuremeter Test. Hole 6. Hole: Rod Driving. Depth = 0.9 m.

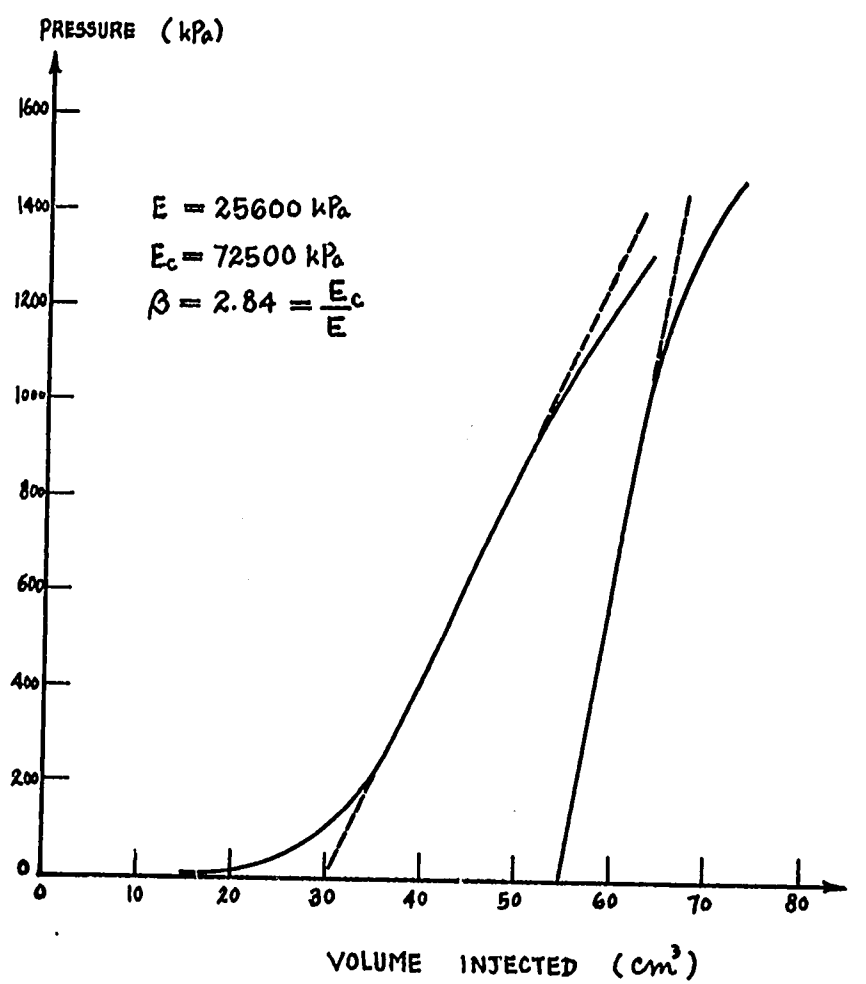

Fig.333 - Test No. 215-Ottawa Airport. Briaud Pressuremeter Test. Hole 6. Hole: Rod Driving. Depth = 0.6 m.

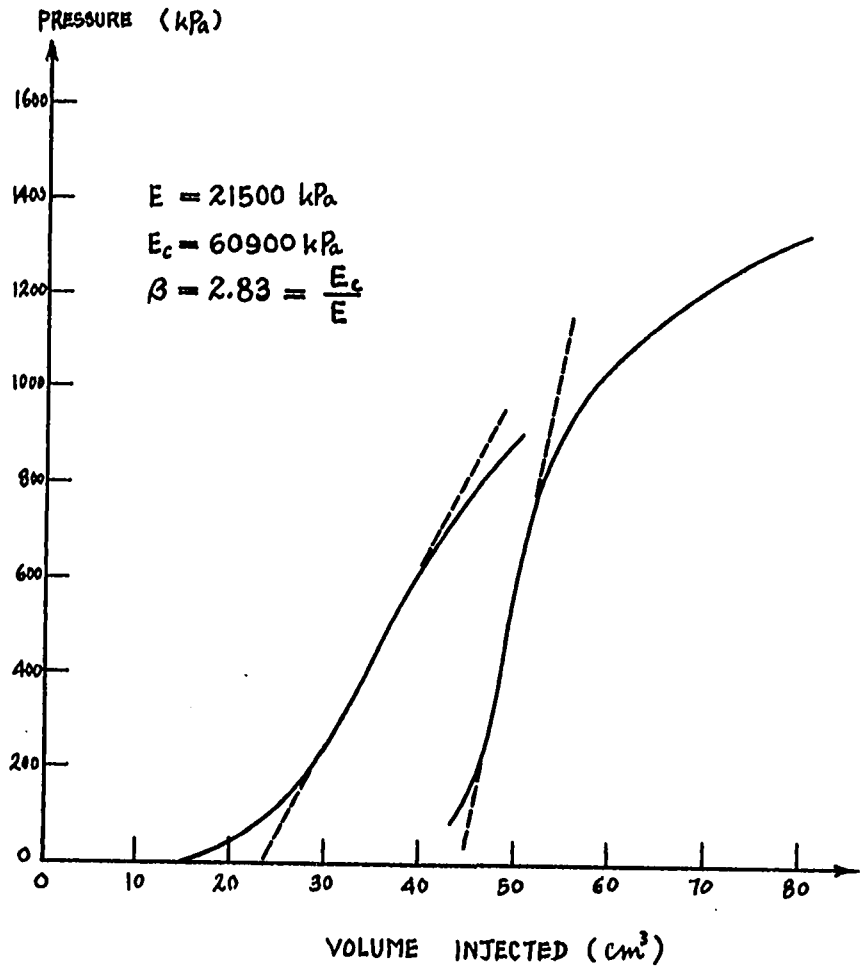

Fig. 334 - Test No. 216-Ottawa Airport. Briaud Pressuremeter Test. Hole 6. Hole: Rod Driving. Depth = 0.41 m.

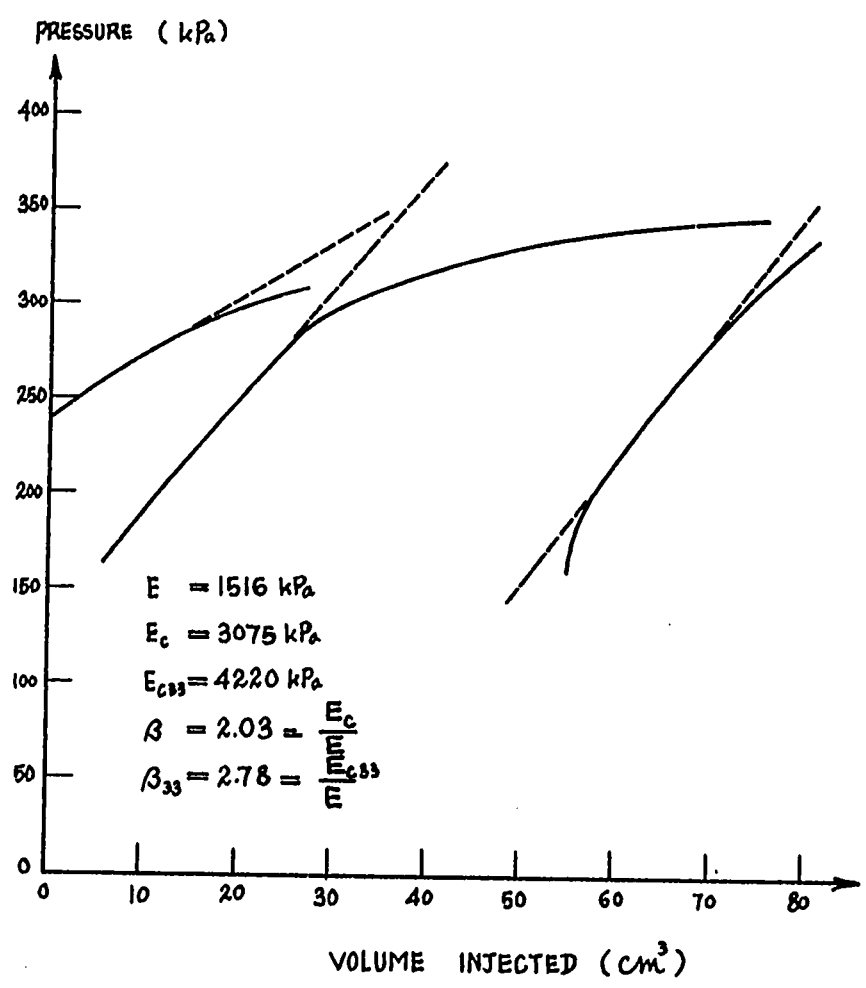

Fig. 335 - Test No. 219-Fraser's Clay. Briaud Pressuremeter Test. Hole 7. Hold: Rod Driving. After Slab. Depth = 2.7 m.

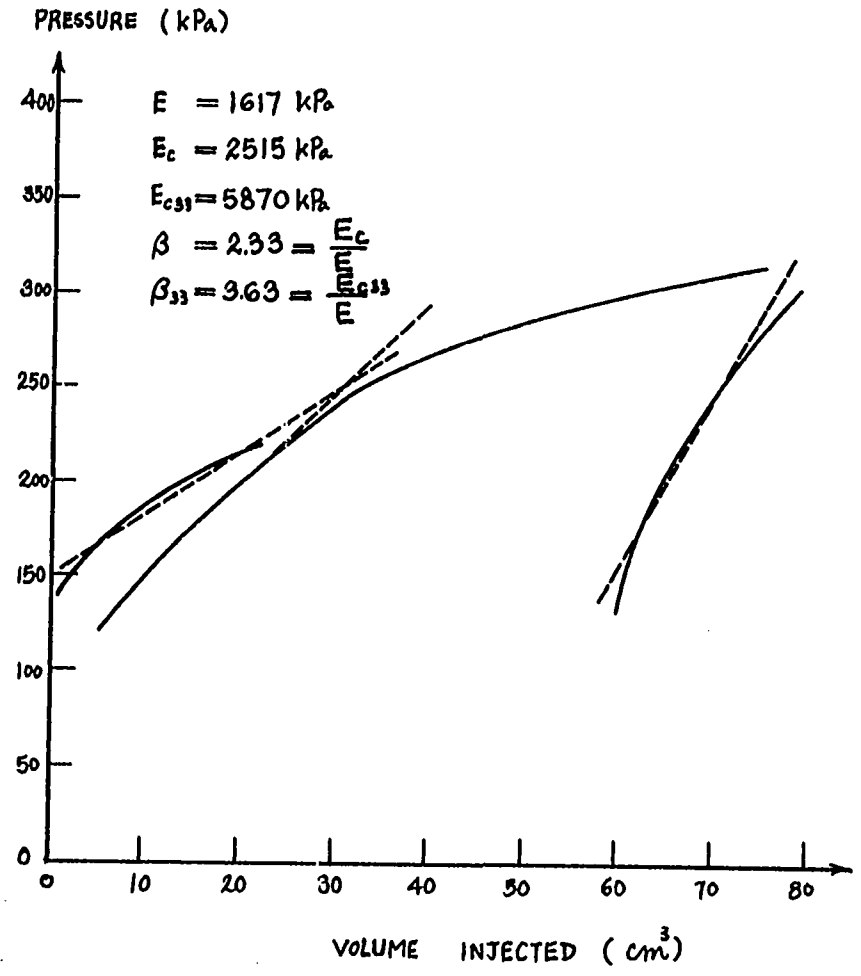

Fig.336 - Test No. 220-Fraser's Clay. Briaud Pressuremeter Test. Hole 7. Hole: Rod Driving. After Slab. Depth = 2.4 m.

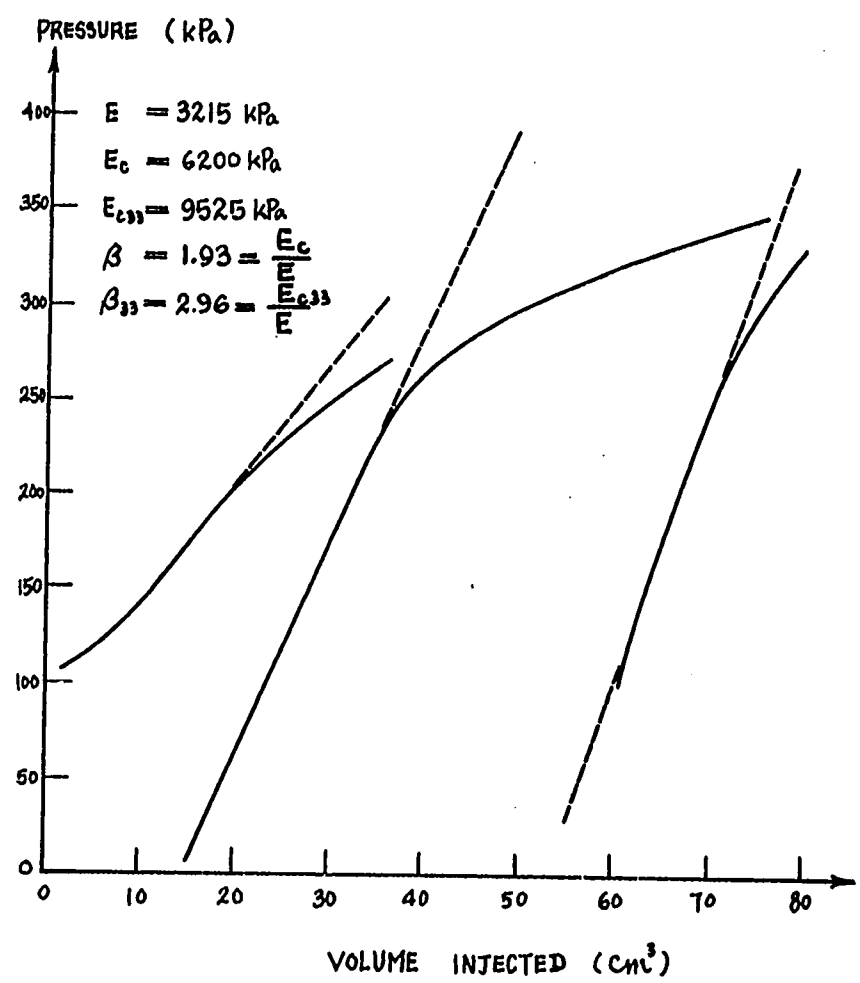

Fig.337 - Test No. 221-Fraser's Clay. Briaud Pressuremeter Test. Hole 7. Hole: Rod Driving. After Slab. Depth = 2.1 m.

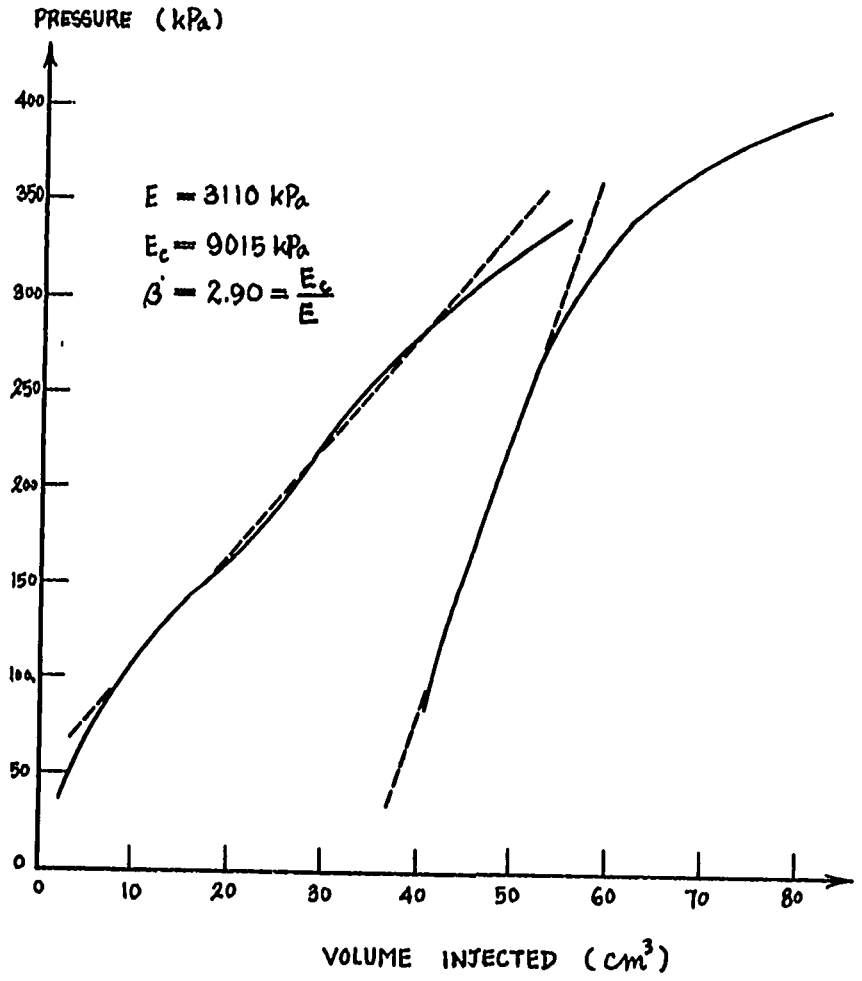

Fig.338 - Test No. 222-Fraser's Clay. Briaud Pressuremeter Test. Hole 7. Hole: Rod Driving. After Slab. Depth = 1.8 m.

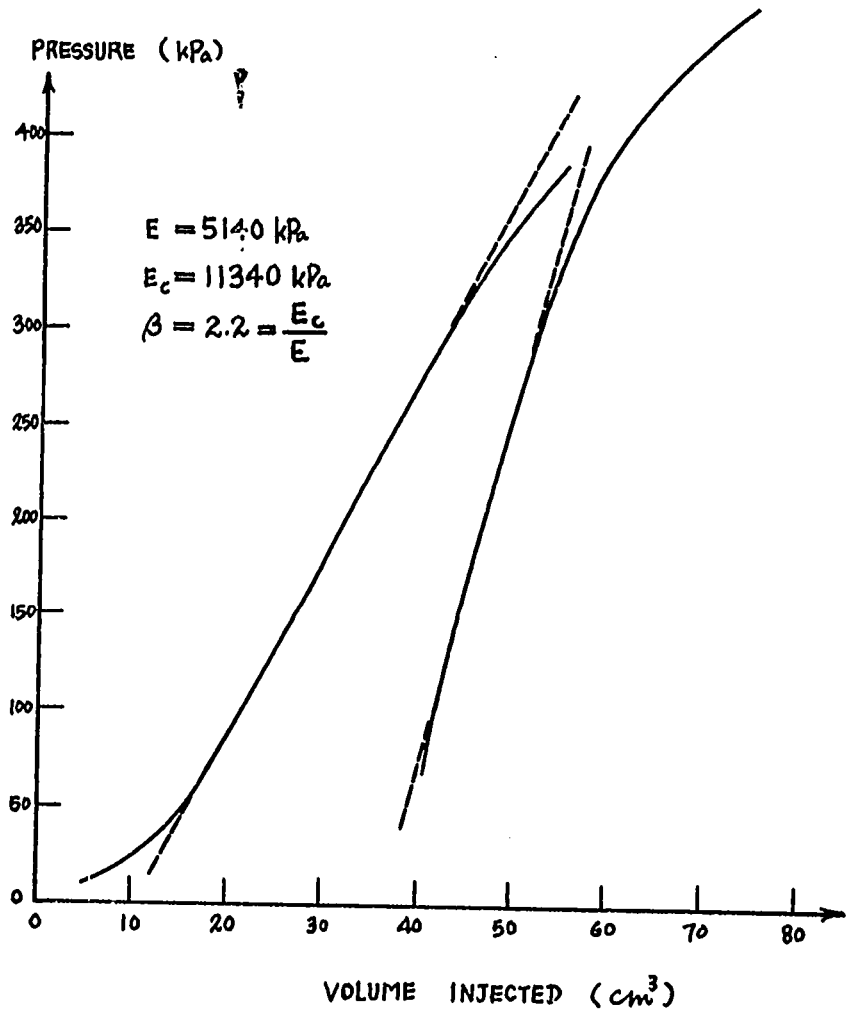

Fig.339 - Test No. 223-Fraser's Clay. Briaud Pressuremeter Test. Hole 7. Hole: Rod Driving. After Slab. Depth = 1.5 m.

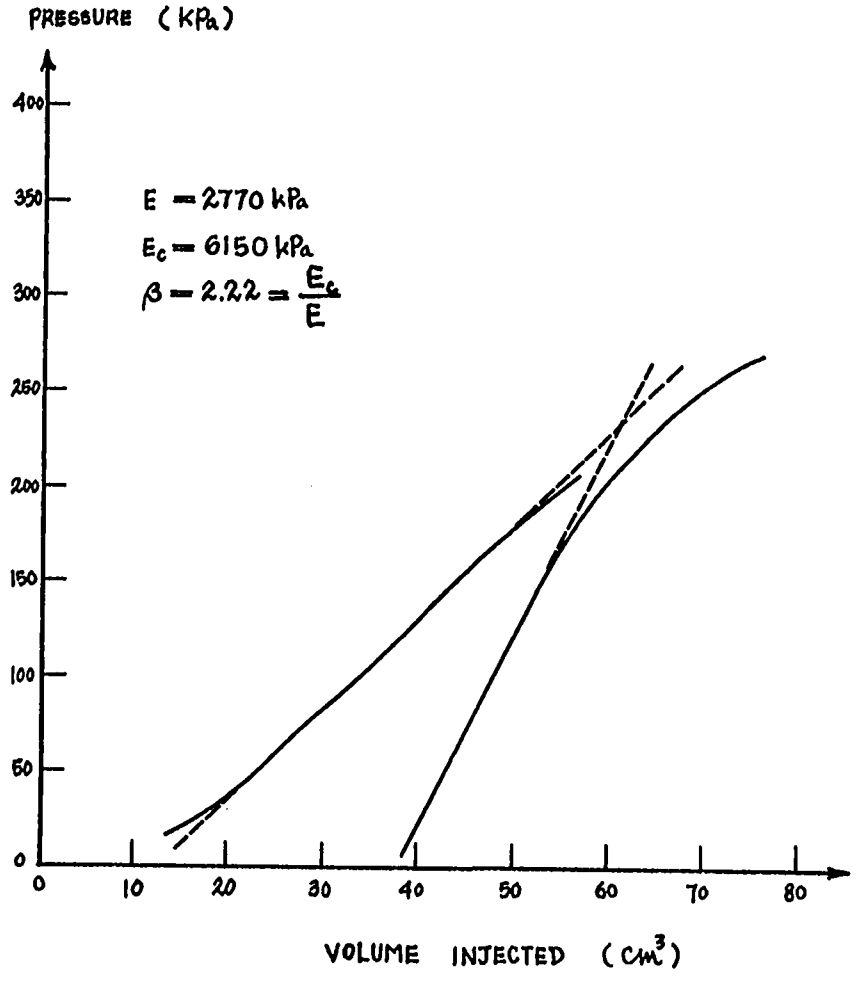

Fig. 340 - Test No. 224-Fraser's Clay. Briaud Pressuremeter Test. Hole.7. Hole: Rod Driving. After Slab. Depth = 1.2 m.

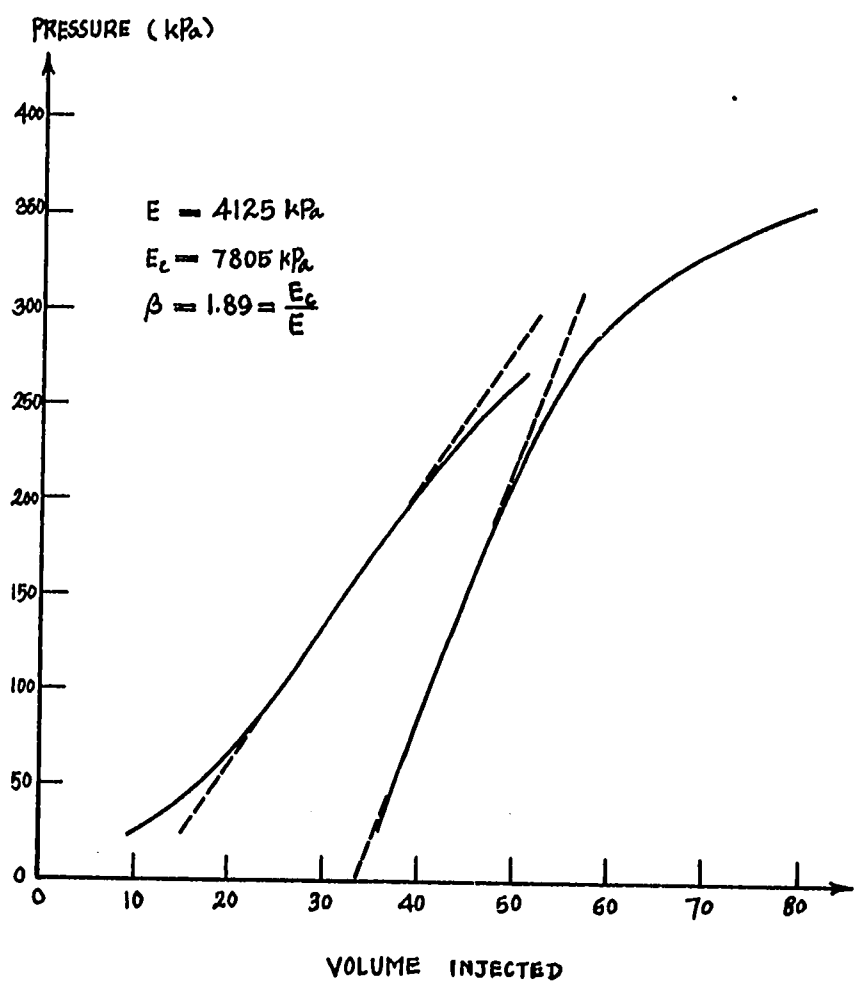

Fig. 341 - Test No. 225-Fraser's Clay. Briaud Pressuremeter Test. Hole 7. Hole: Rod Driving. After Slab. Depth = 0.9 m.

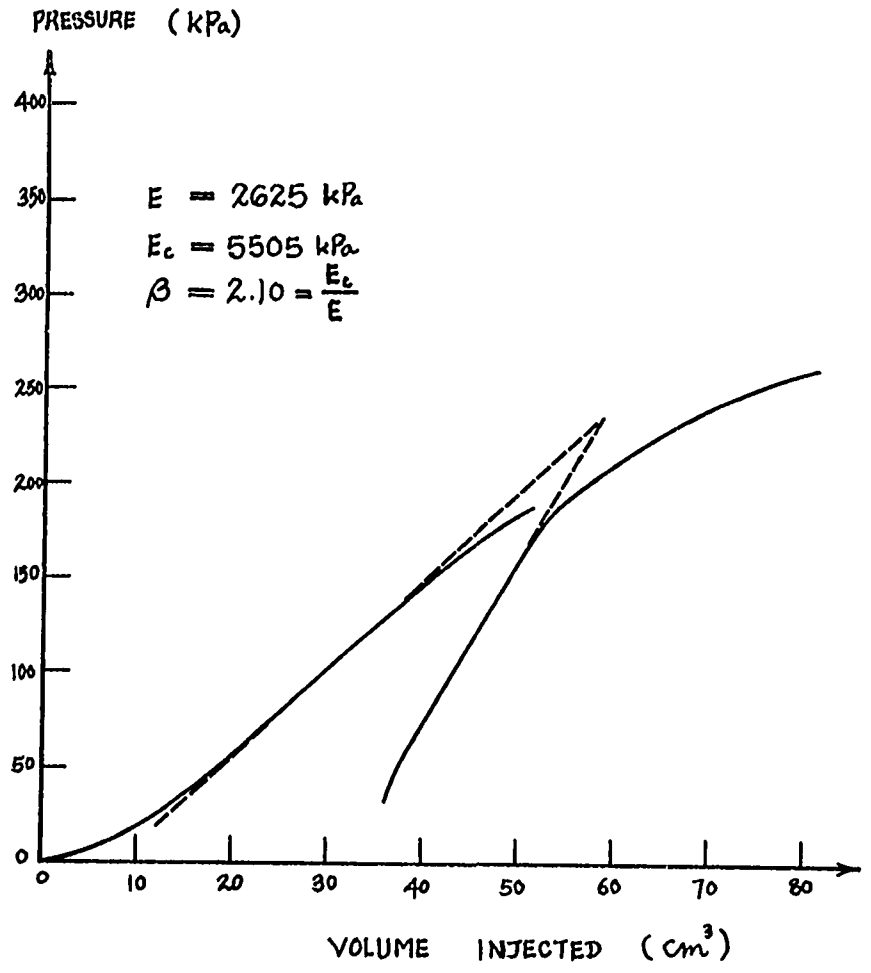

Fig. 342 - Test No. 226-Fraser's Clay. Briaud Pressuremeter Test. Hole 7. Hole: Rod Driving. After Slab. Depth = 0.6 m.

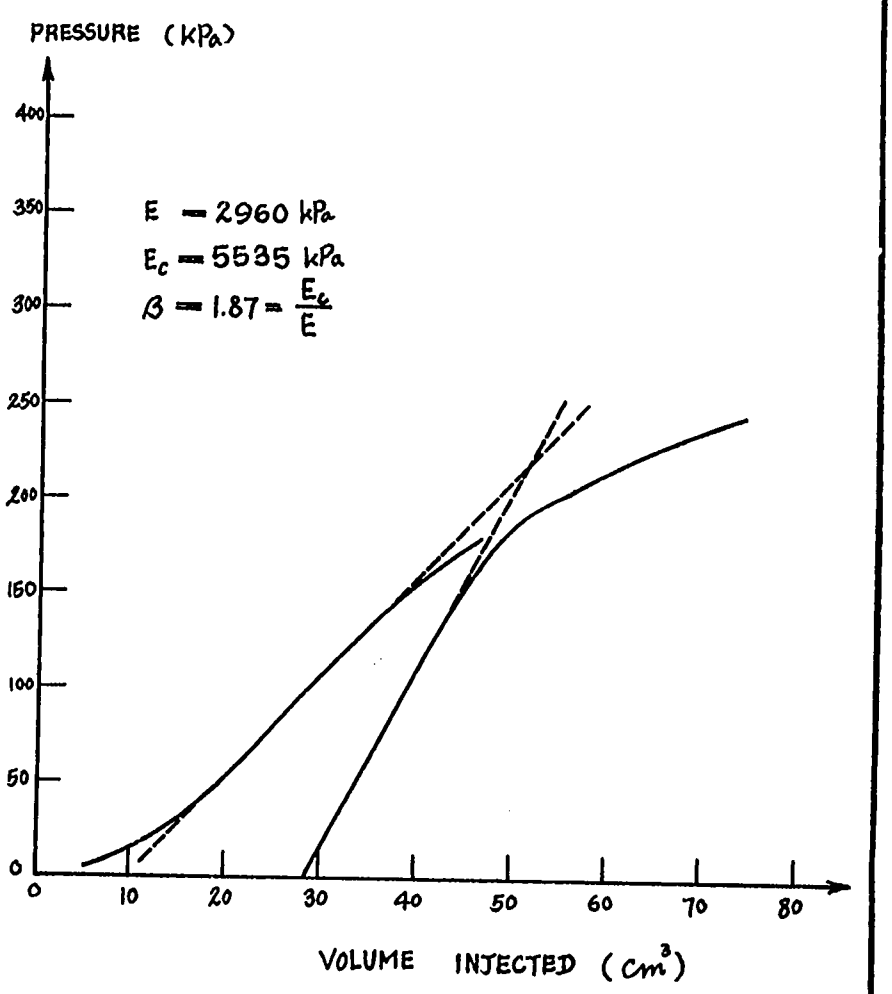

Fig. 343 - Test No. 227-Fraser's Clay. Briaud Pressuremeter Test. Hole 7. Hole: Rod Driving. After Slab. Depth = 0.3 m.

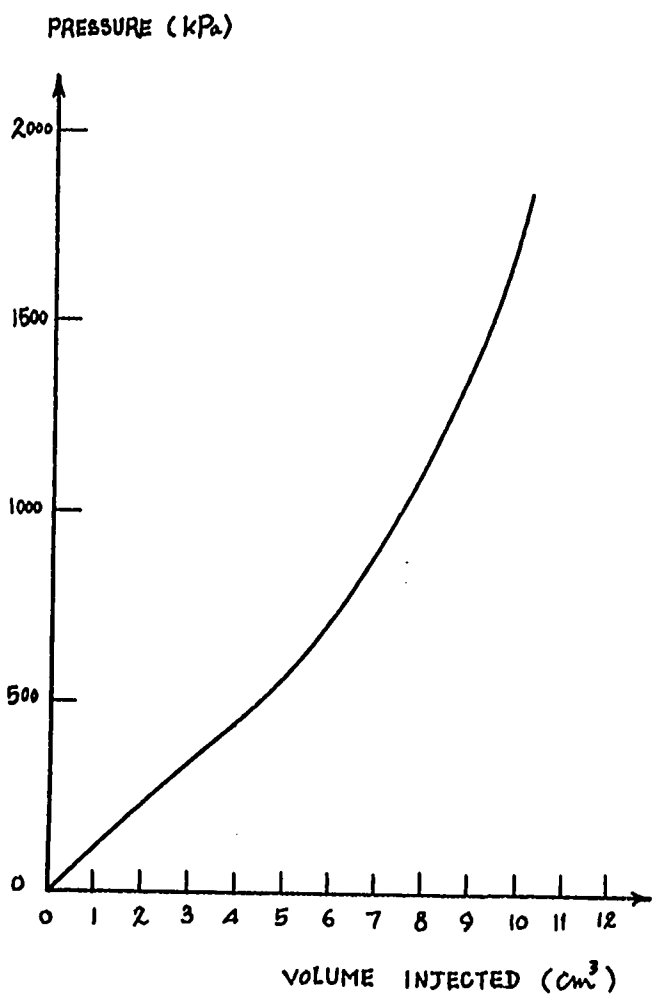

Fig. 344 - Test No. 228-Fraser's Clay. Briaud Pressuremeter. Calibration of Volume Losses.

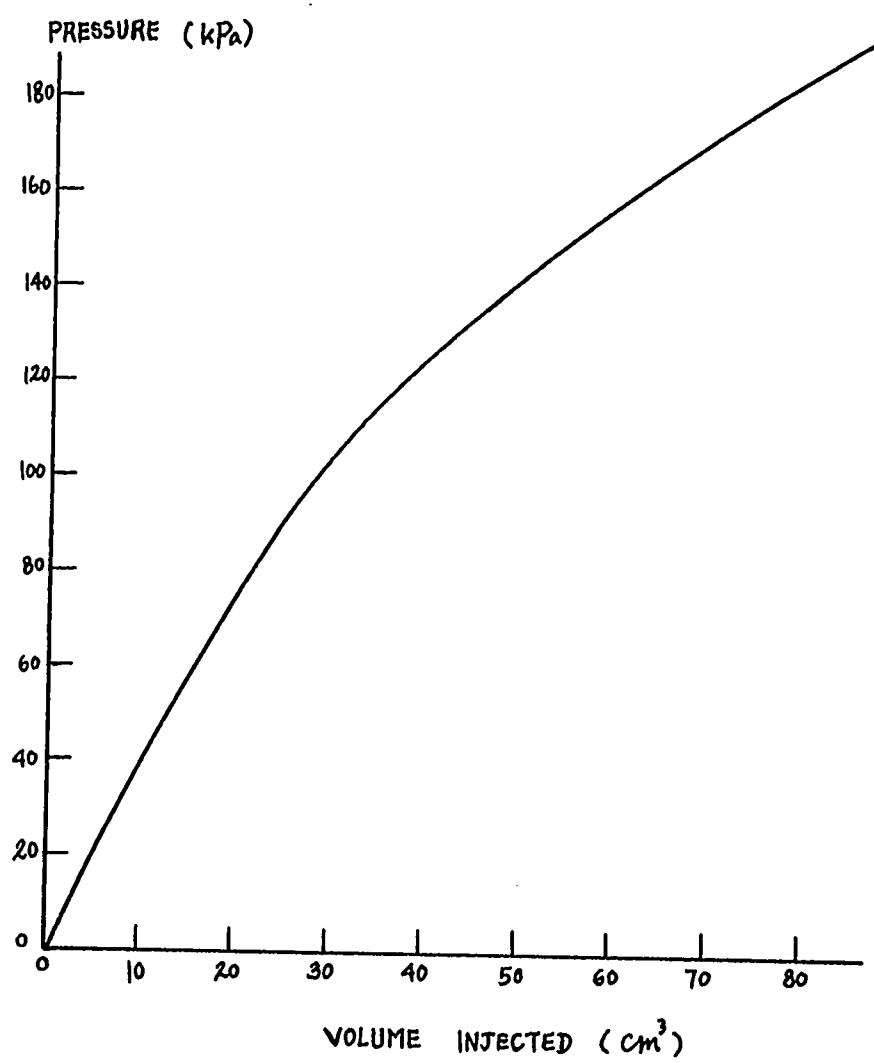

Fig. 345 - Test No. 229-Fraser's Clay. Briaud Pressuremeter. Calibration of Membrane Resistance.

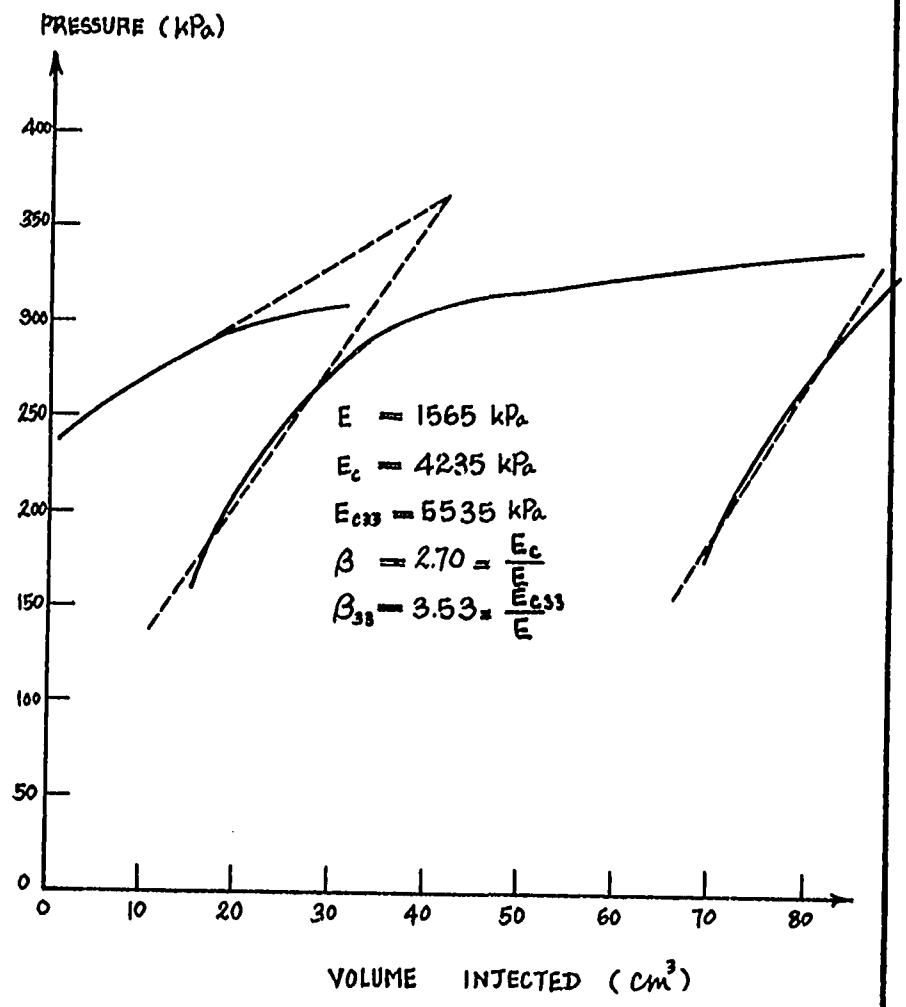

Fig. 346 - Test No. 230-Fraser's Clay. Briaud Pressuremeter Test. Hole 6. Hole: Hand Auger. After Slab. Depth = 2.7 m.

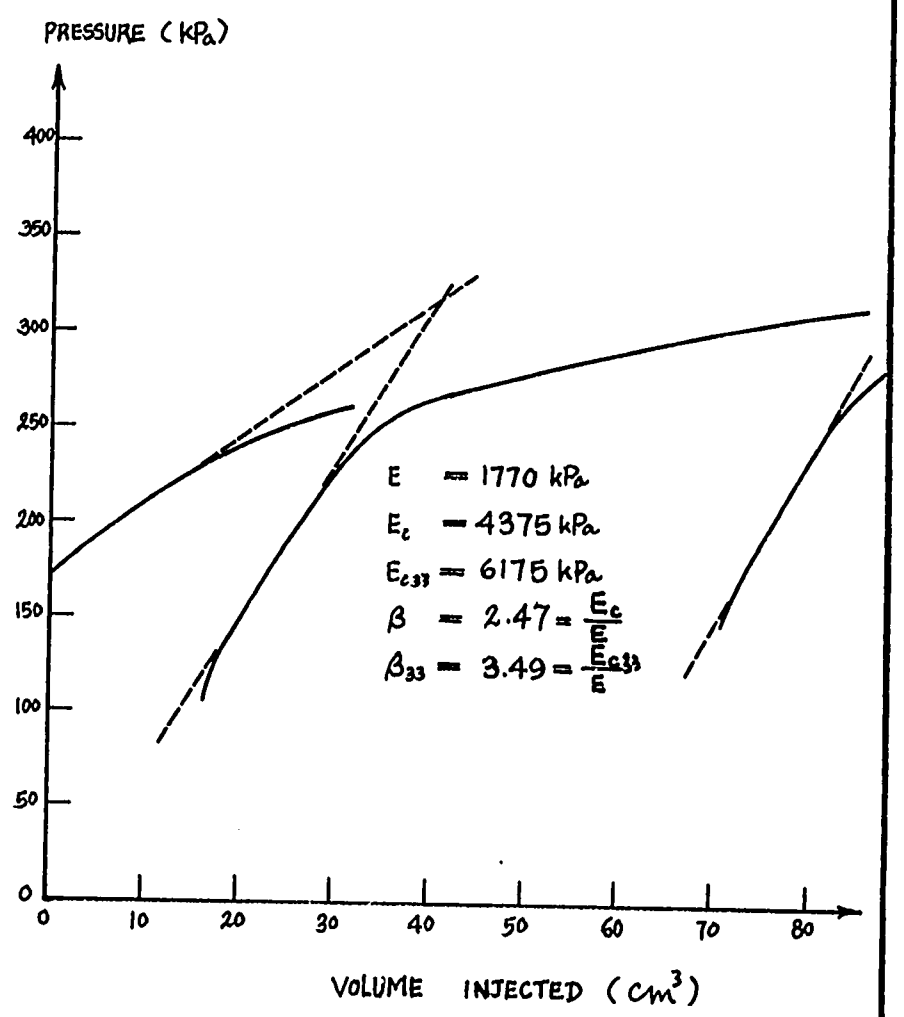

Fig. 347 - Test No. 231-Fraser's Clay. Briaud Pressuremeter Test. Hole 6. Hole: Hand Auger. After Slab. Depth = 2.4 m.

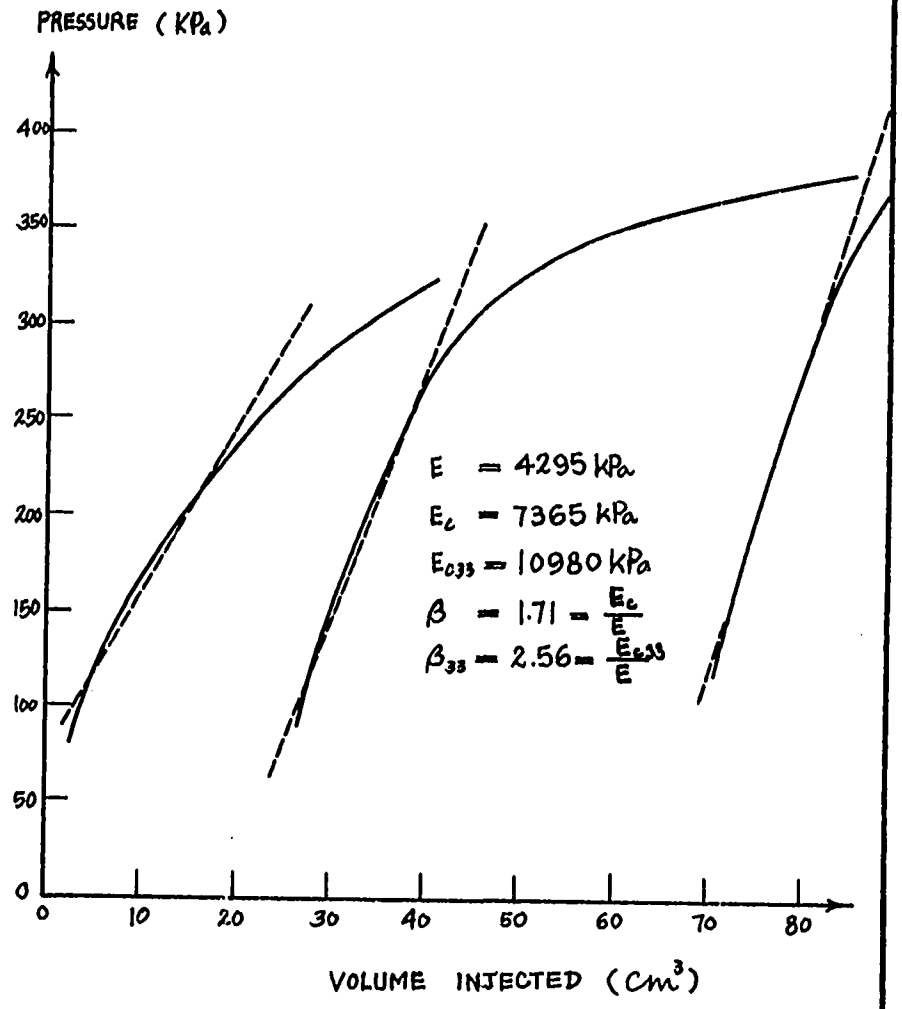

Fig.348 – Test No. 232-Fraser's Clay. Briaud Pressuremeter Test. Hole 6. Hole: Hand Auger. After Slab. Depth = 2.1 m.

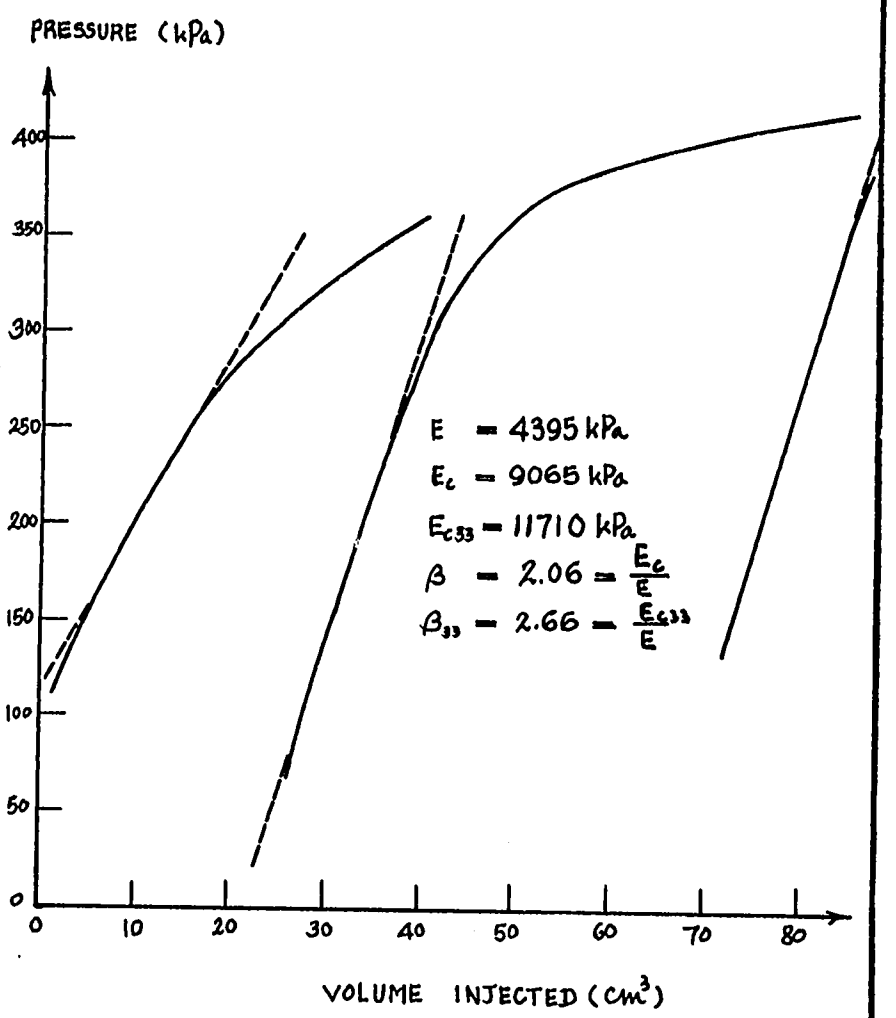

Fig.349 – Test No. 233-Fraser's Clay. Briaud Pressuremeter Test. Hole 6. Hole: Hand Auger. After Slab. Depth = 1.8 m.

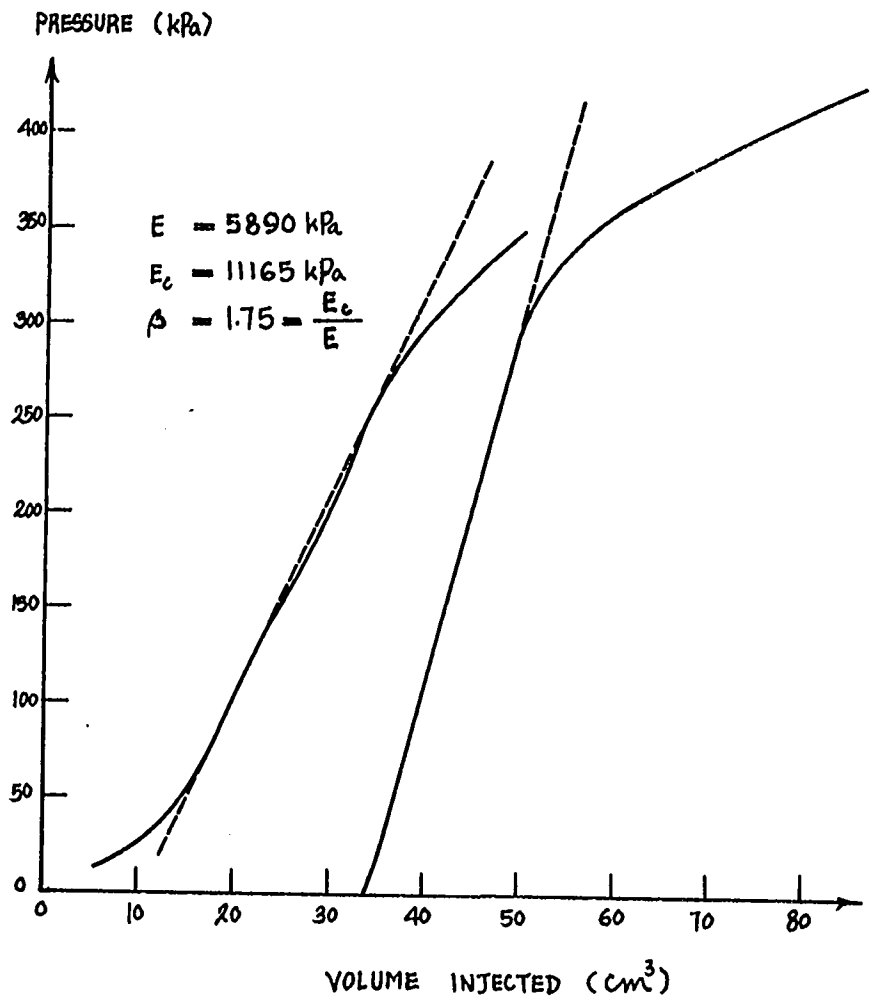

Fig. 350 - Test No. 234-Fraser's Clay. Briaud Pressuremeter Test. Hole 6. Hole: Hand Auger. After Slab. Depth = 1.5 m.

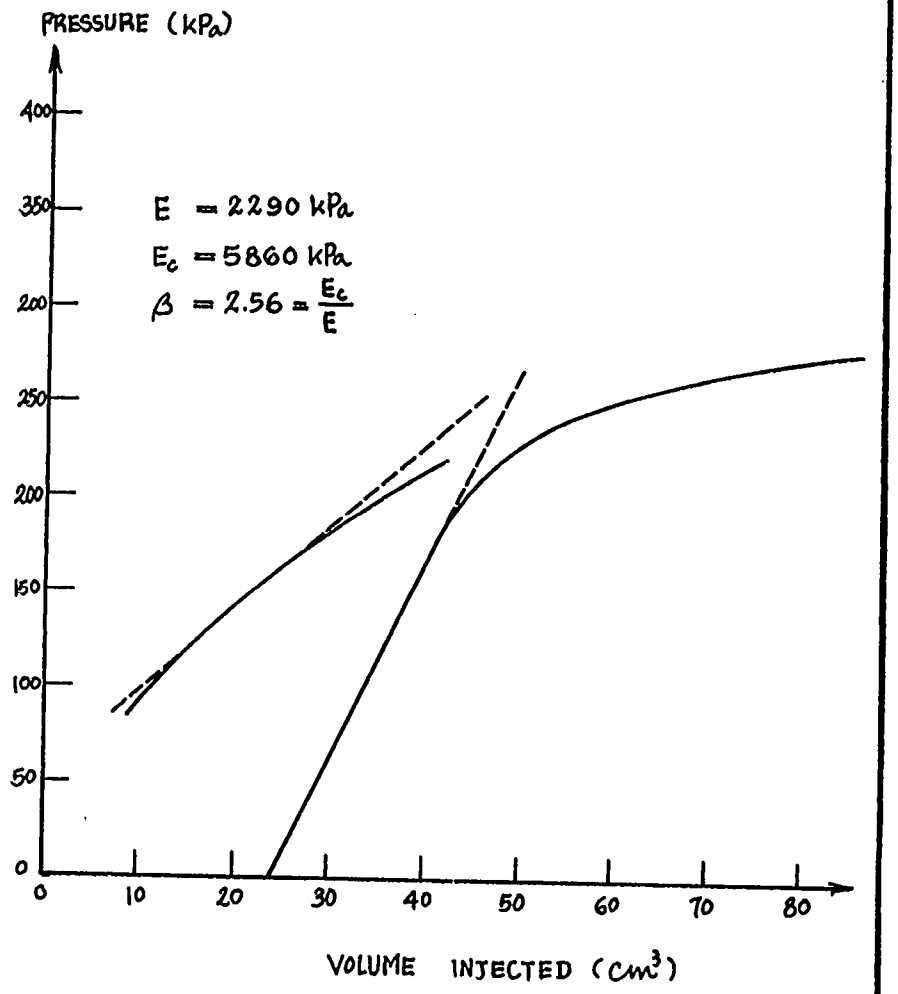

Fig. 351 - Test No. 235-Fraser's Clay. Briaud Pressuremeter Test. Hole 6. Hole: Hand Auger. After Slab. Depth = 1.2 m.

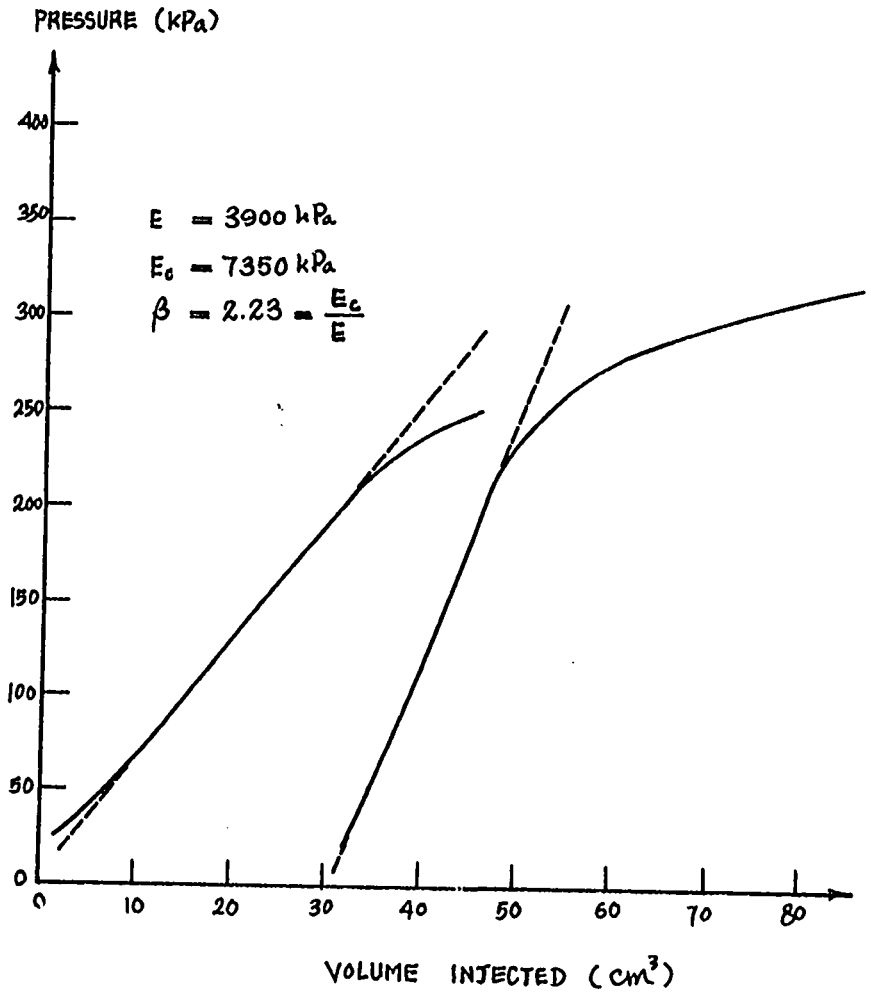

Fig. 352 - Test No. 236-Fraser's Clay. Briaud Pressuremeter Test. Hole 6. Hole: Hand Auger. After Slab. Depth = 0.9 m.

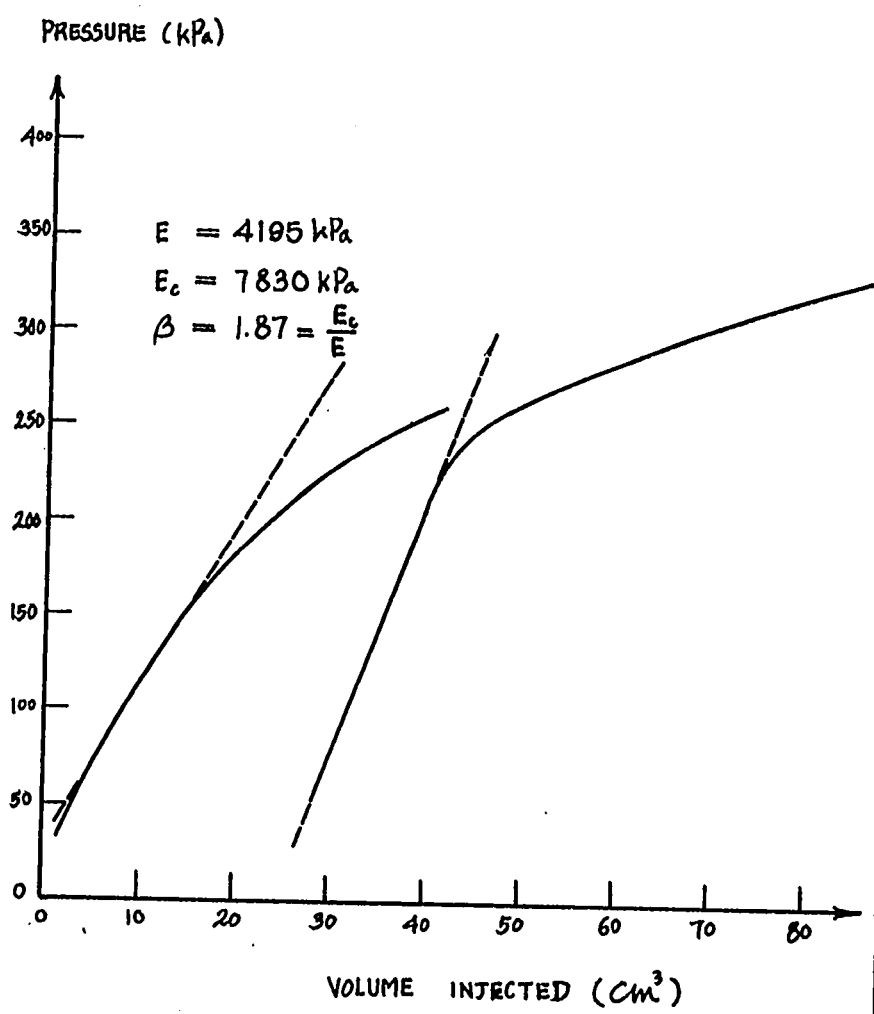

Fig. 353 - Test No. 237-Fraser's Clay. Briaud Pressuremeter Test. Hole 6. Hole: Hand Auger. After Slab. Depth = 0.6 m.

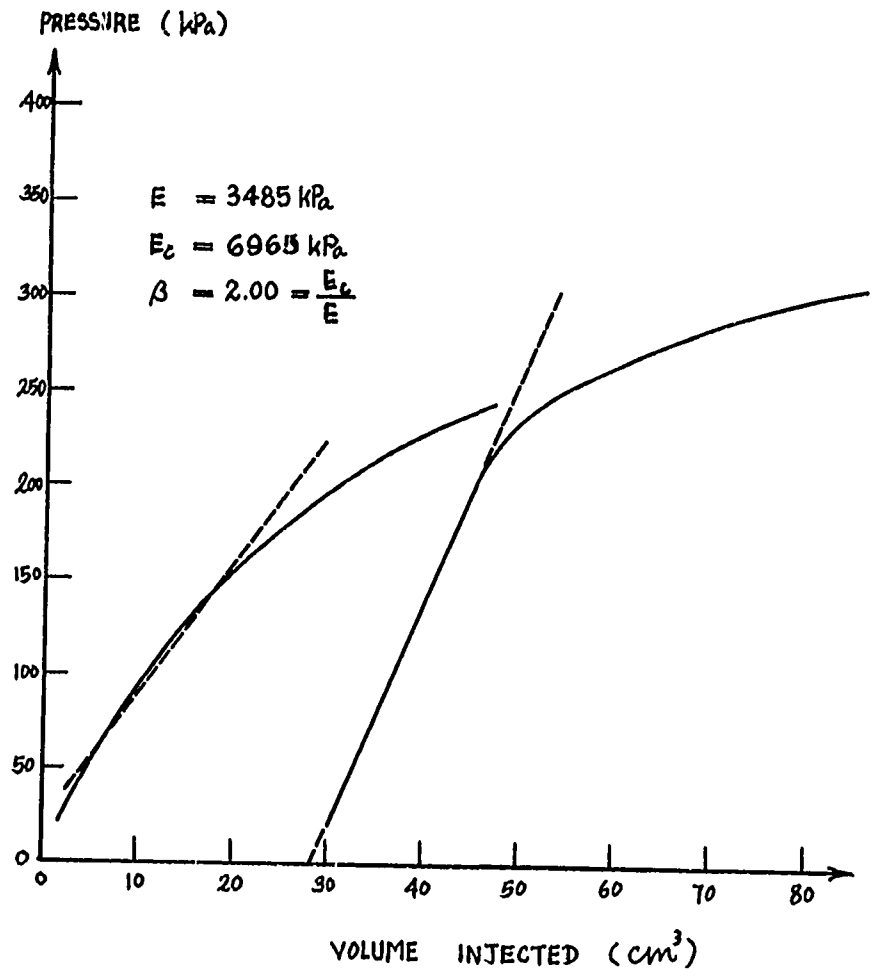

Fig. 354 - Test No. 238-Fraser's Clay. Briaud Pressuremeter Test. Hole 6. Hole::Hand Auger. After Slab. Depth = 0.3 m.

APPENDIX B

PLATE TESTS CURVES

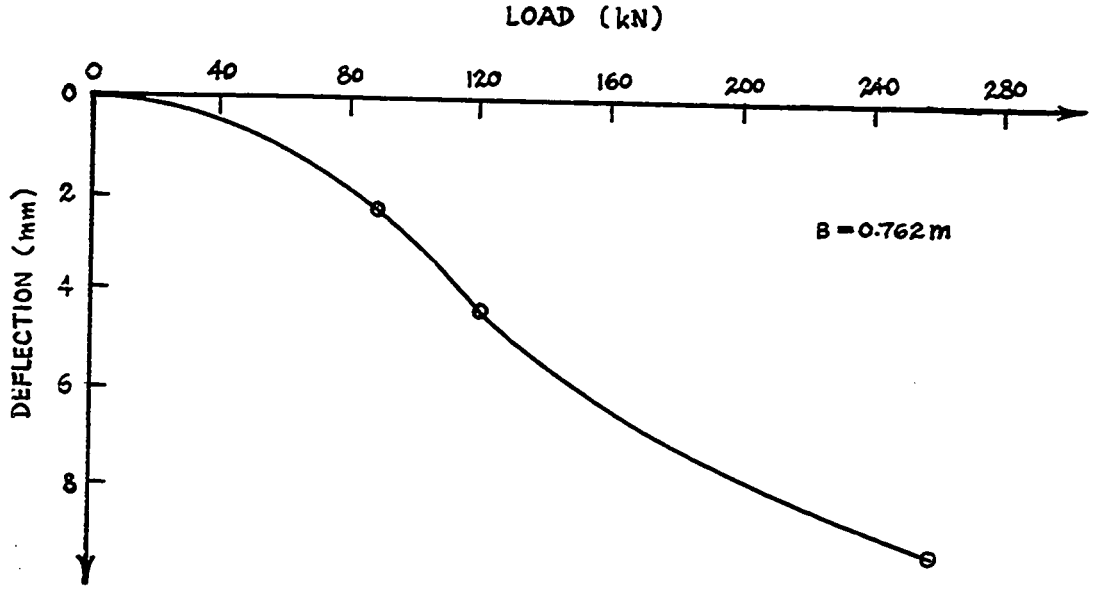

Fig. 355 - Test No. 334-Repetitive McLeod Plate Test. Sarnia Airport. Hole 7. Load vs. Deflection of First Loading.

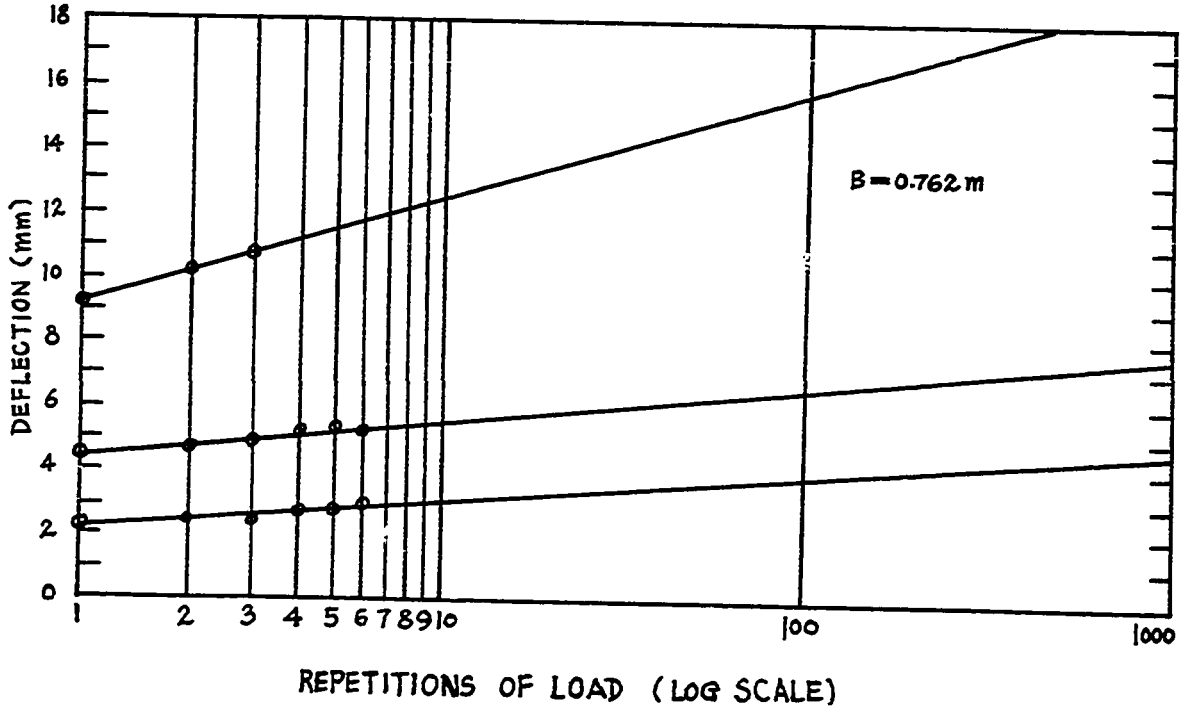

Fig. 356 - Test No. 334-Repetitive McLeod Plate Test. Sarnia Airport. Hole 7. Deflection vs. Repetition of Load.

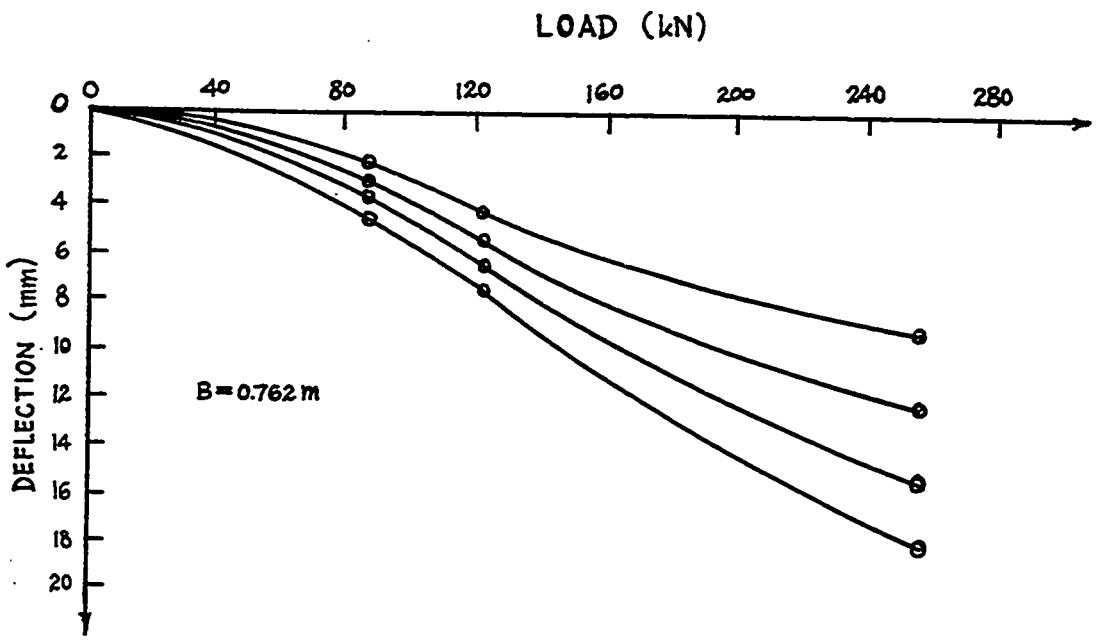

Fig.357 - Test No. 334-Repetitive McLeod Plate Test. Sarnia Airport. Hole 7. Load vs. Deflection at 1, 10, 100 and 600 repetitions.

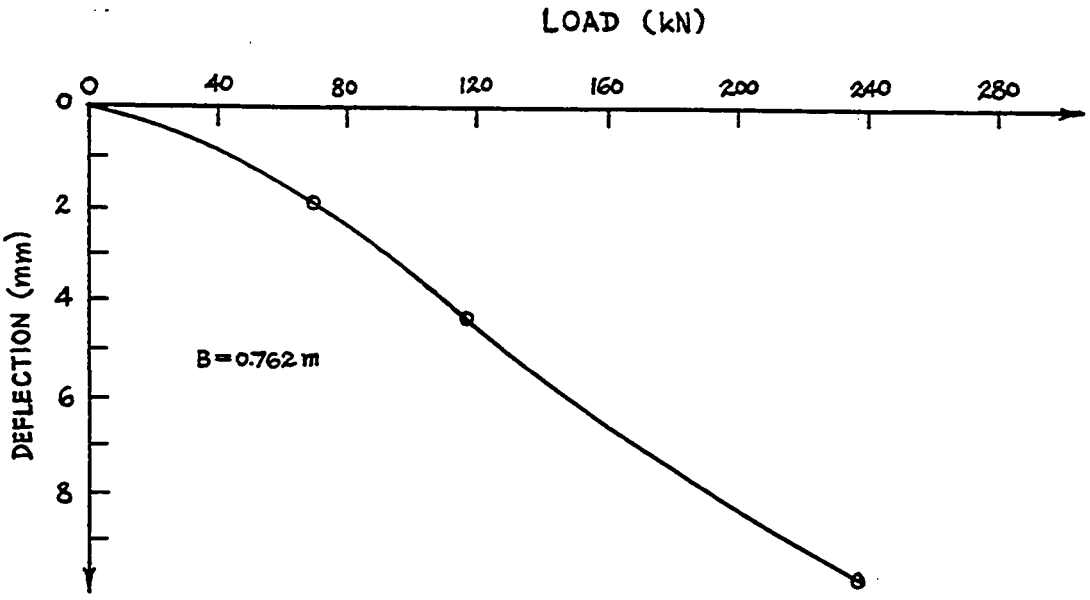

Fig.358 - Test No. 335-Repetitive McLeod Plate Test. Sarnia Airport. Hole 6. Load vs. Deflection of First Loading.

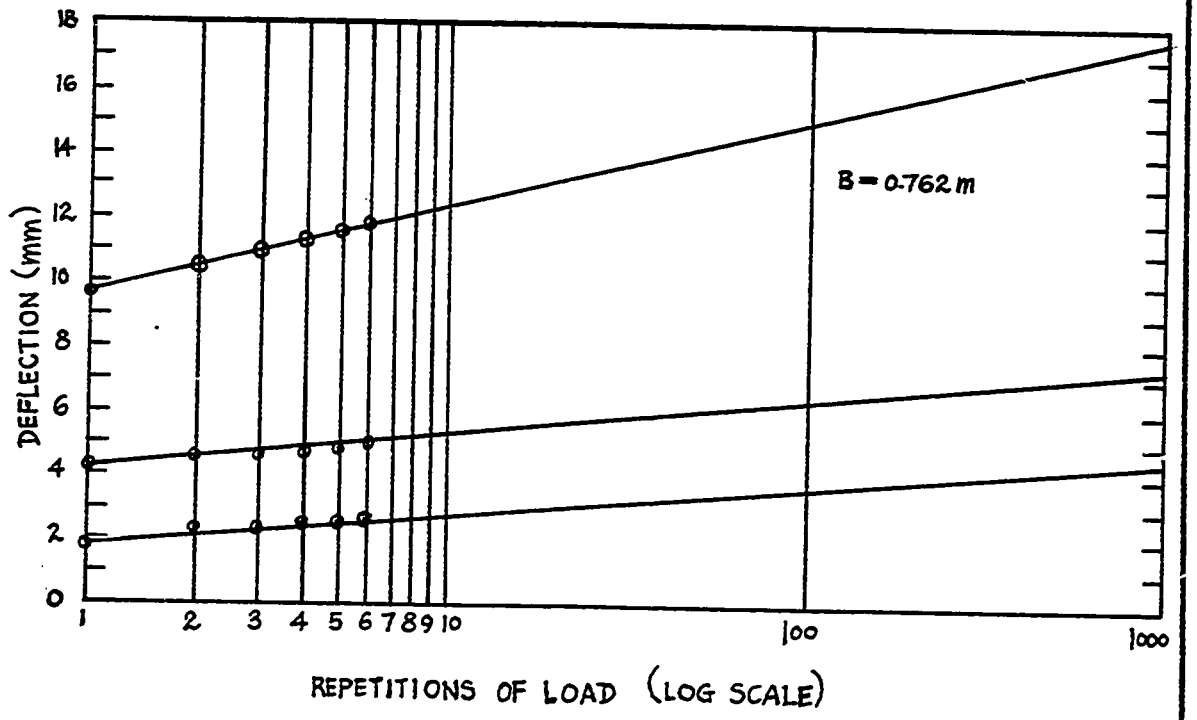

Fig. 359 - Test No. 335-Repetitive McLeod Plate Test. Sarnia Airport. Hole 6. Deflection vs. Repetition of Load.

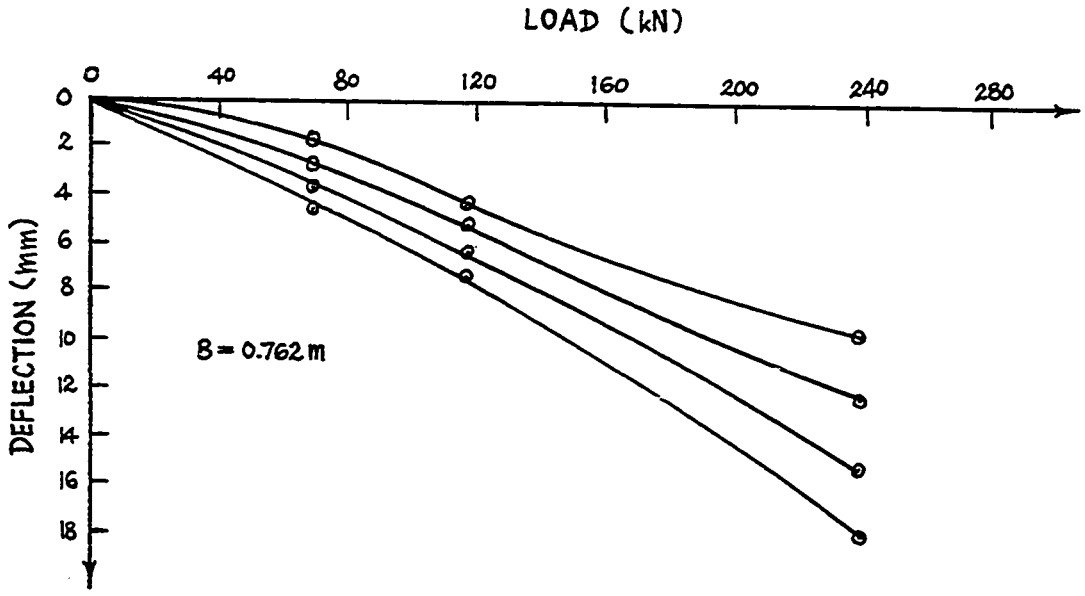

Fig. 360 - Test No. 335-Repetitive McLeod Plate Test. Sarnia Airport. Hole 6.

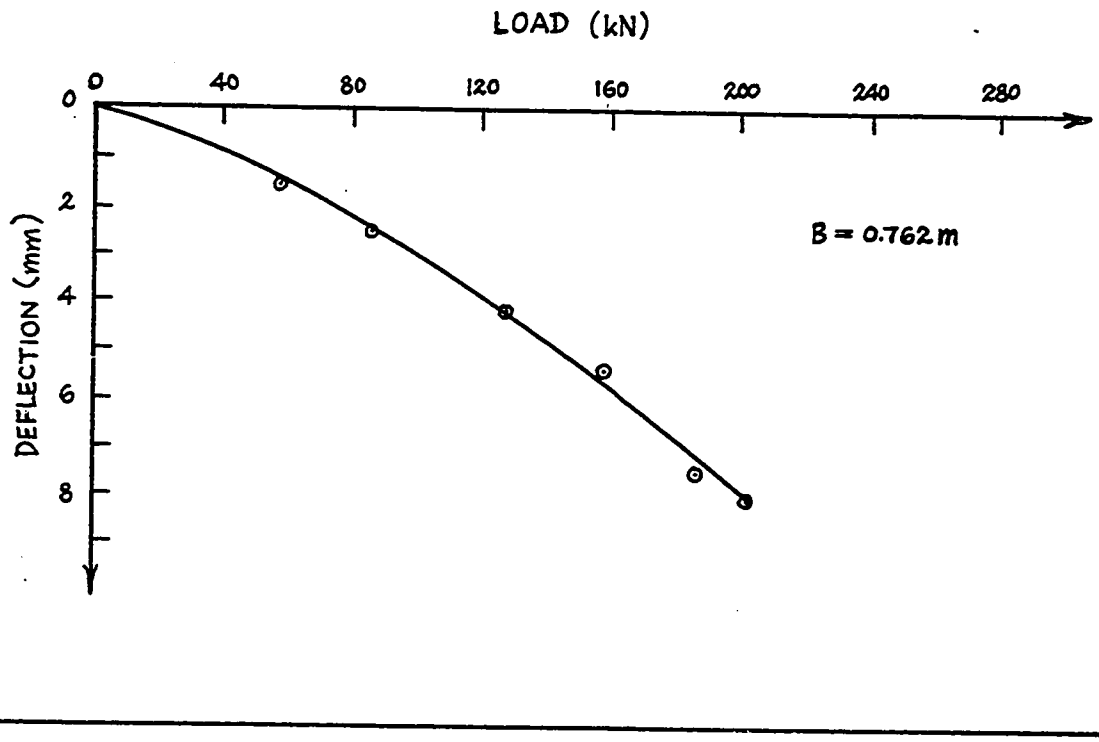

Fig.361 - Test No. 336-Non Repetitive McLeod Plate Test. Sarnia Airport. Hole 15. Load vs. Deflection.

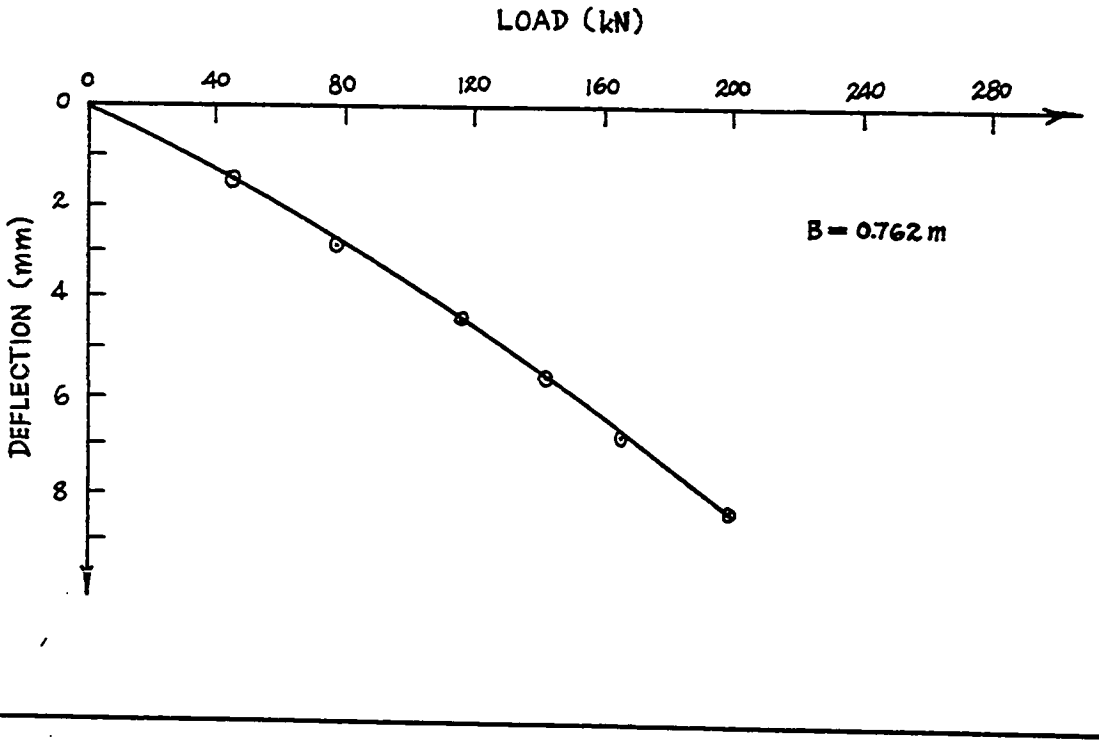

Fig. 362 - Test No. 337-Non Repetitive McLeod Plate Test. Sarnia Airport. Hole 3. Load vs. Deflection.

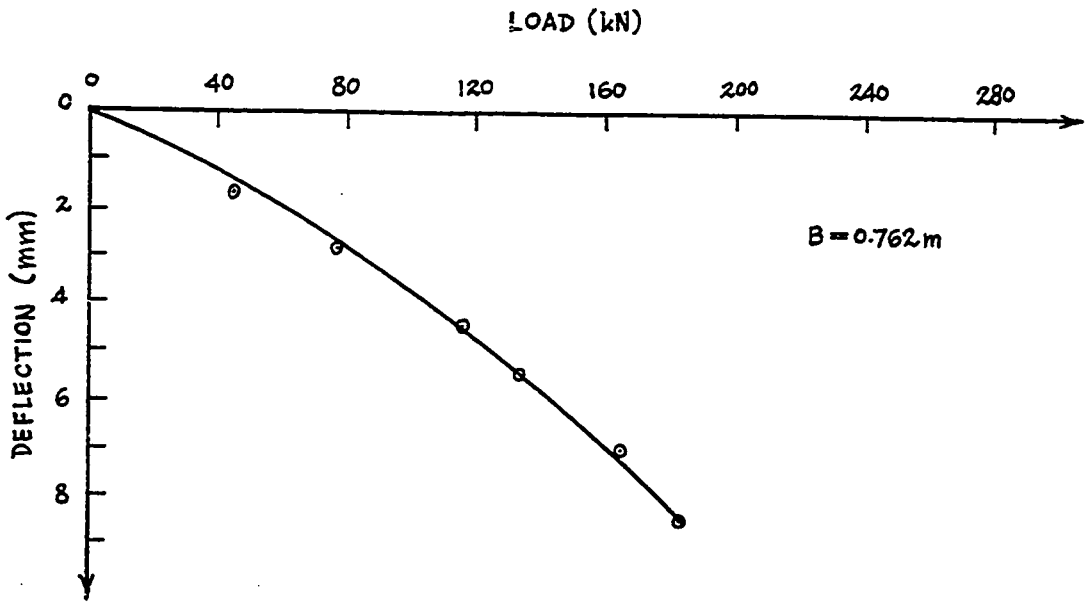

Fig. 363 - Test No. 338-Non Repetitive McLeod Plate Test. Sarnia Airport. Hole 5. Load vs. Deflection.

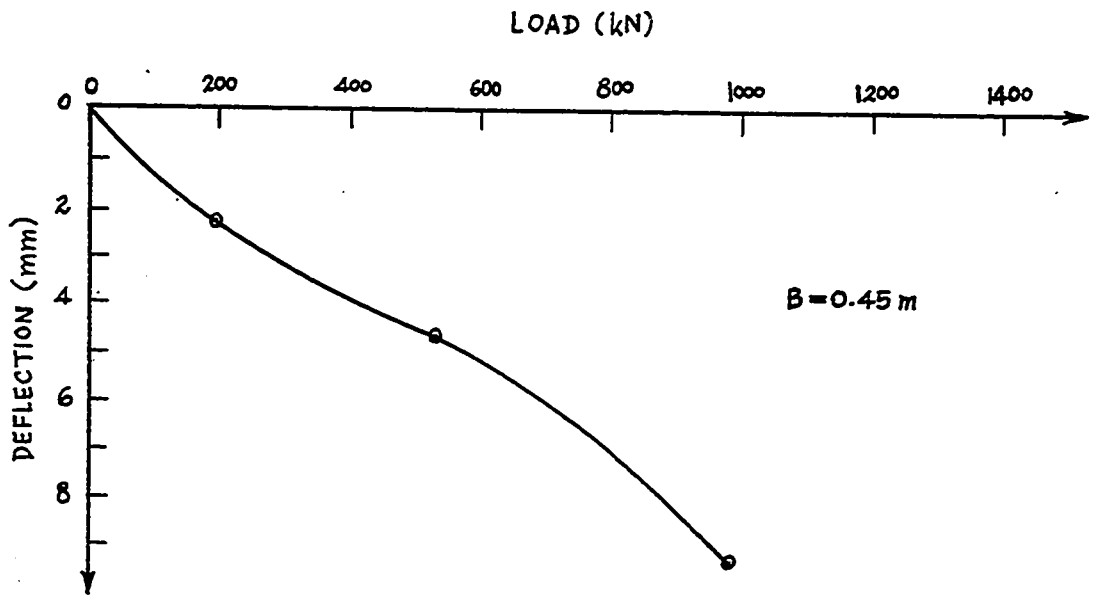

Fig.364 - Test No. 339-Repetitive McLeod Plate Test. Ottawa Airport. Hole 1. Load vs. Deflection at First Loading.

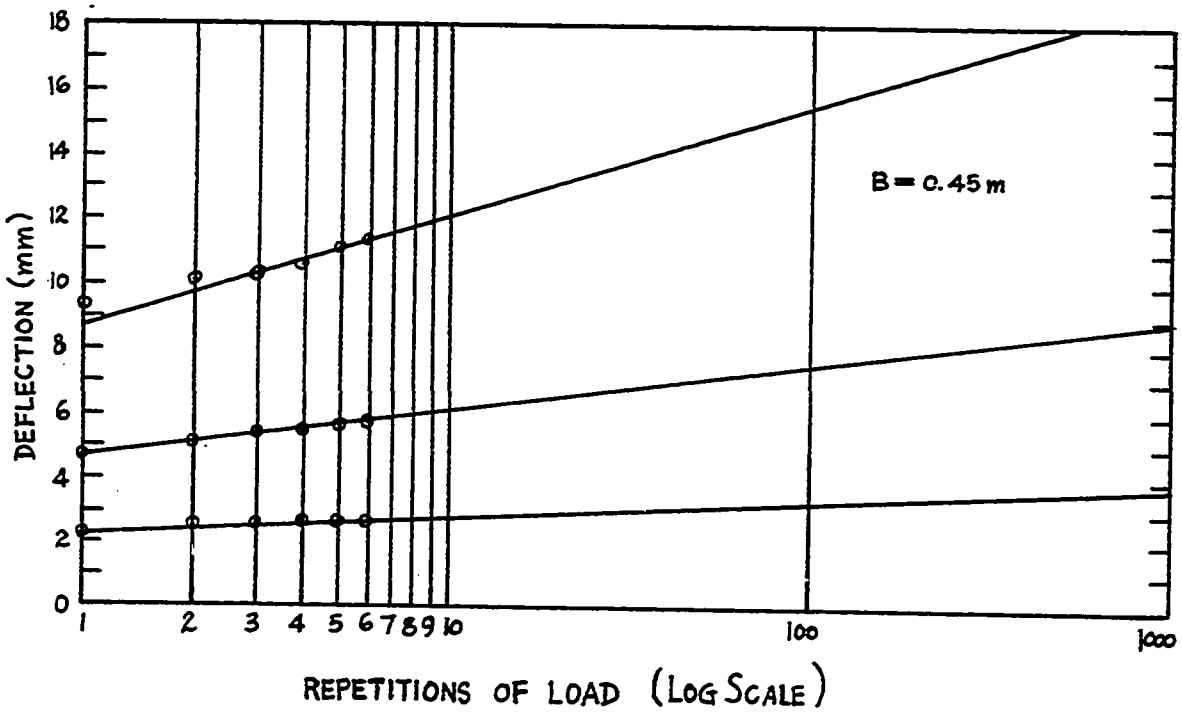

Fig.365 - Test No. 339-Repetitive McLeod Plate Test. Ottawa Airport. Hole 1. Deflection vs. Repetition of Load.

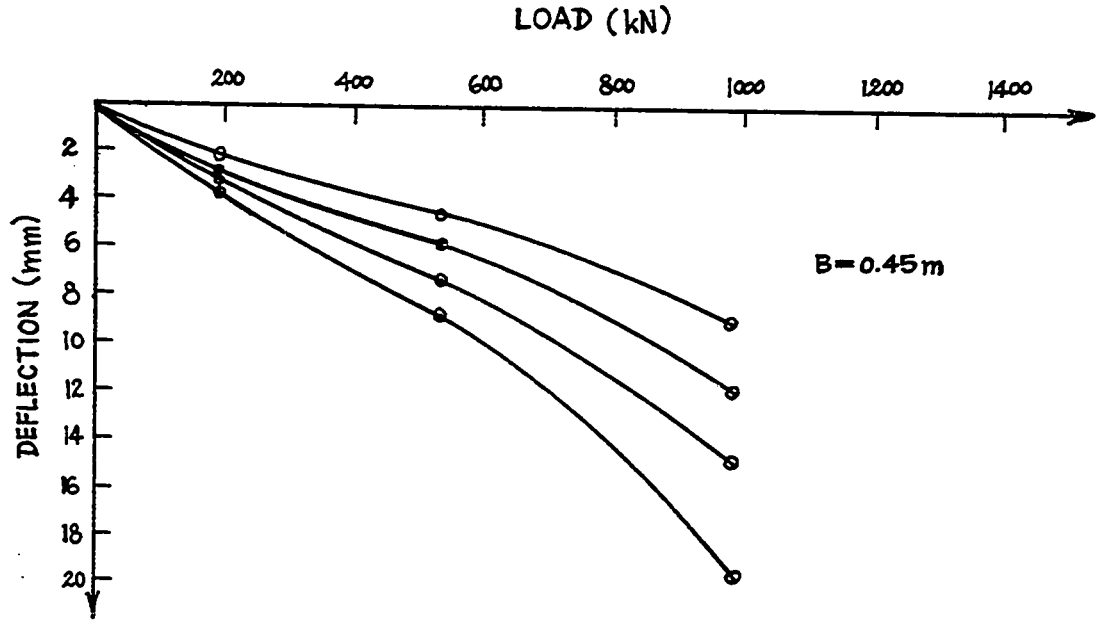

Fig.366 - Test No. 339-Repetitive McLeod Plate Test. Ottawa Airport. Hole 1. Load vs. Deflection at 1, 10, 100, 1000 repetitions.

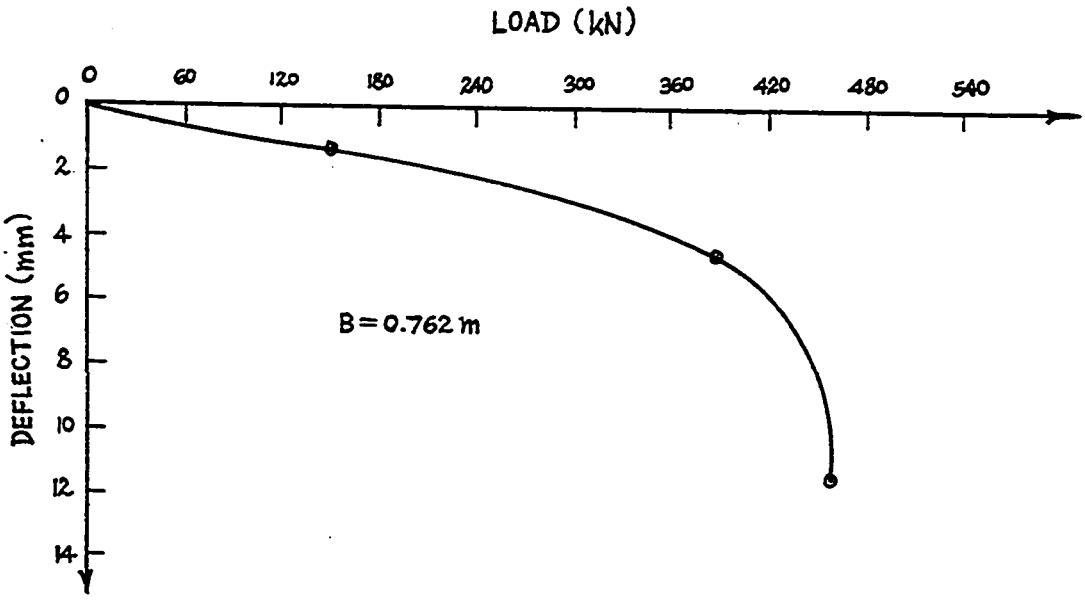

Fig.367 - Test No. 340-Repetitive McLeod Plate Test. Ottawa Airport. Hole 4. Load vs. Deflection of First Loading.

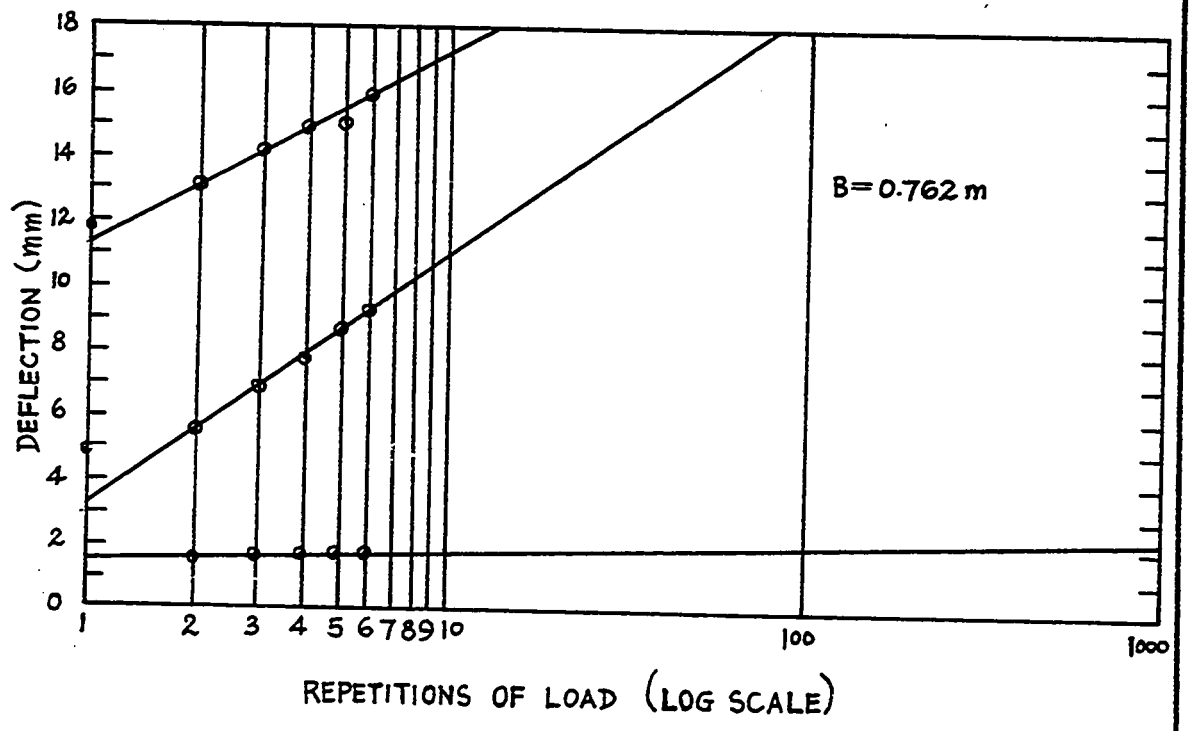

Fig. 368 - Test No. 340-Repetitive McLeod Plate Test. Ottawa Airport. Hole 4. Deflection vs. Repetition of Load.

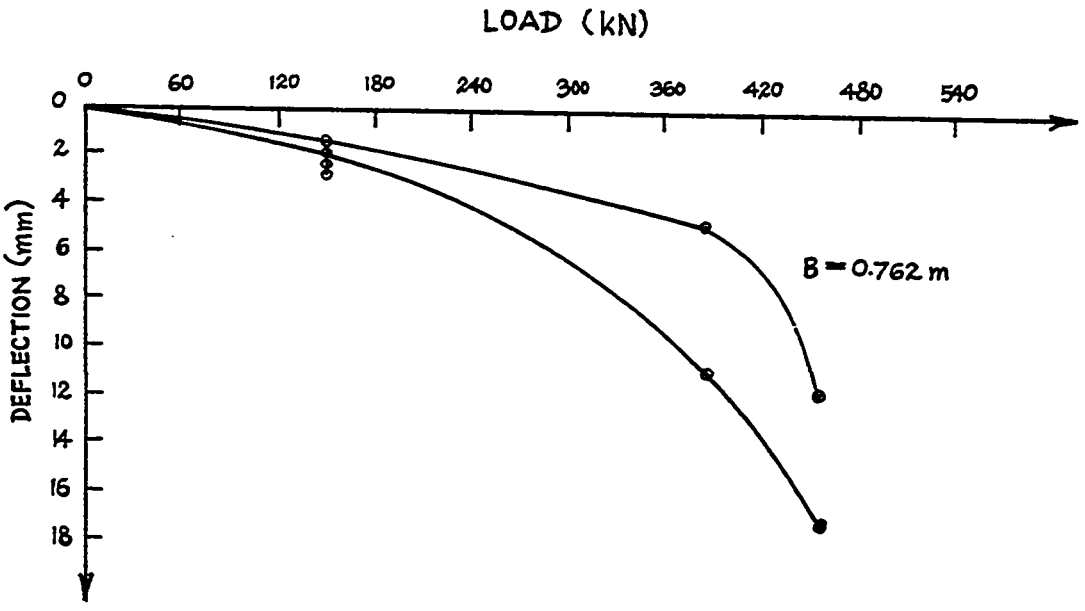

Fig. 369 - Test No. 340-Repetitive McLeod Plate Test. Ottawa Airport. Hole 4. Load vs. Deflection at 1, 10, 100, 1000 repetitions.

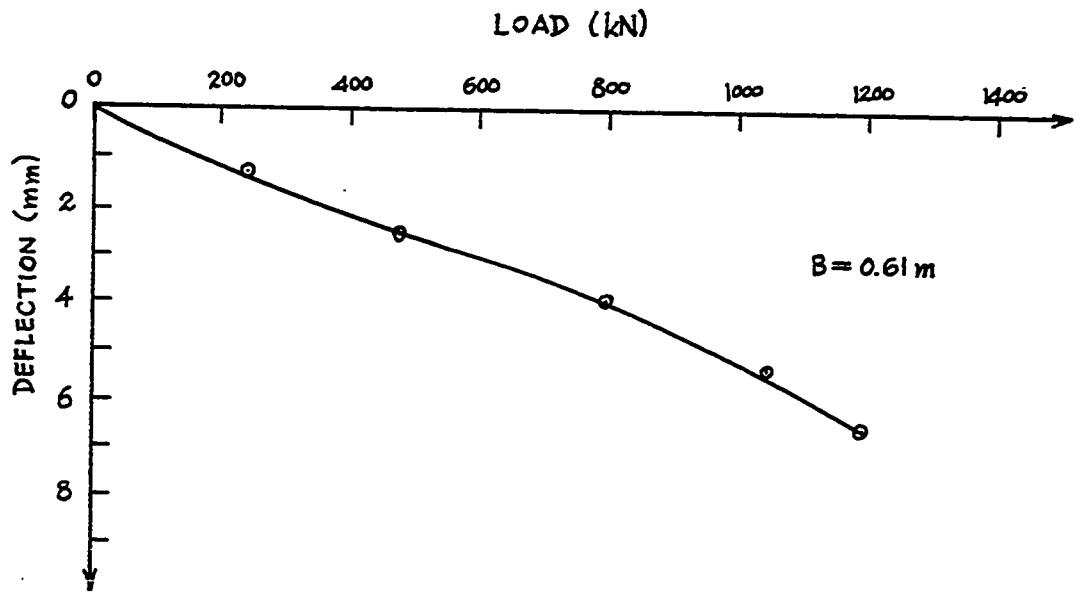

Fig.370 - Test No. 341-Non Repetitive McLeod Plate Test. Ottawa Airport. Hole 2. Load vs. Deflection.

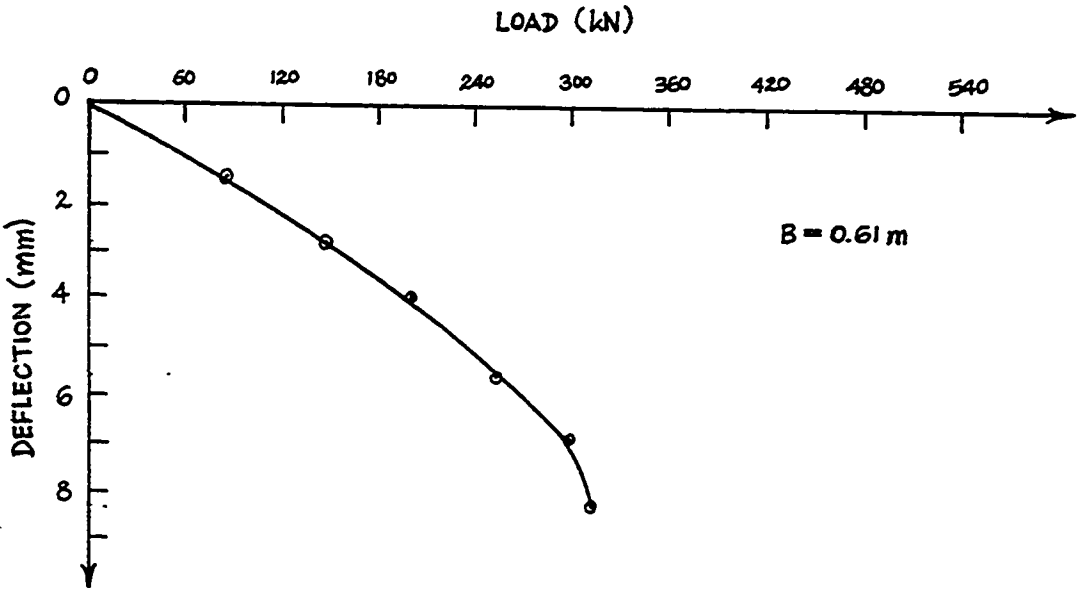

Fig. 371 - Test No. 342-Non Repetitive McLeod Plate Test. Ottawa Airport. Hole 3. Load vs. Deflection.

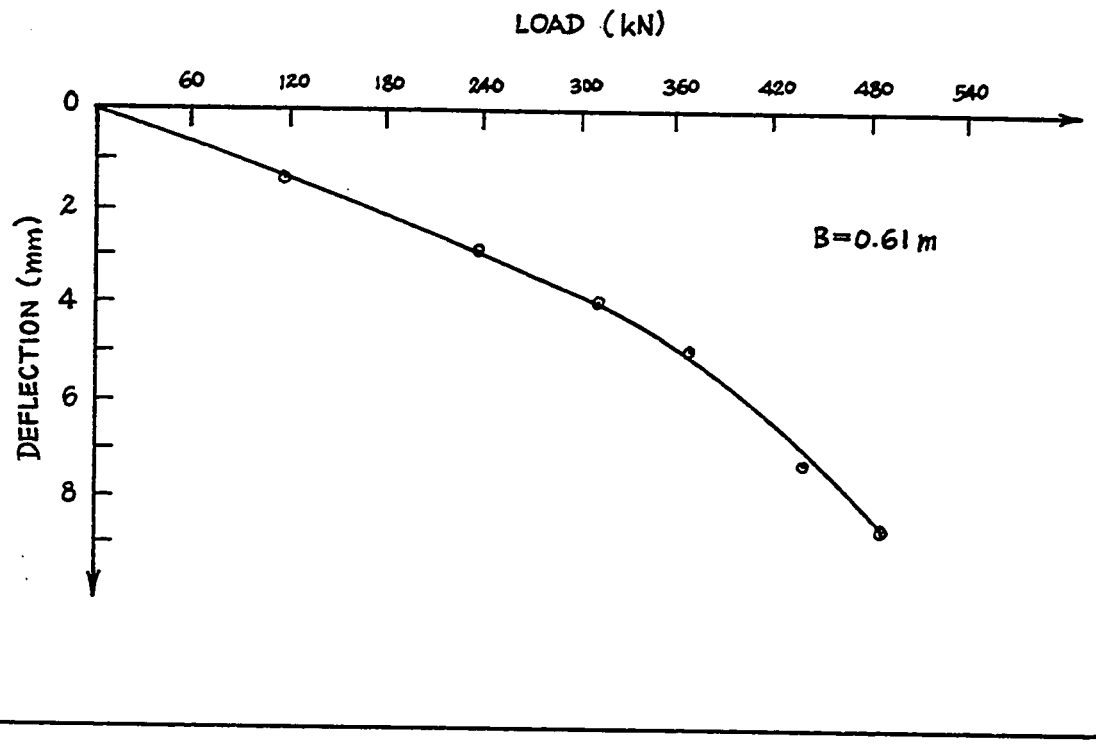

Fig.372 - Test No. 343-Non Repetitive McLeod Plate Test. Ottawa Airport. Hole 5. Load vs. Deflection.

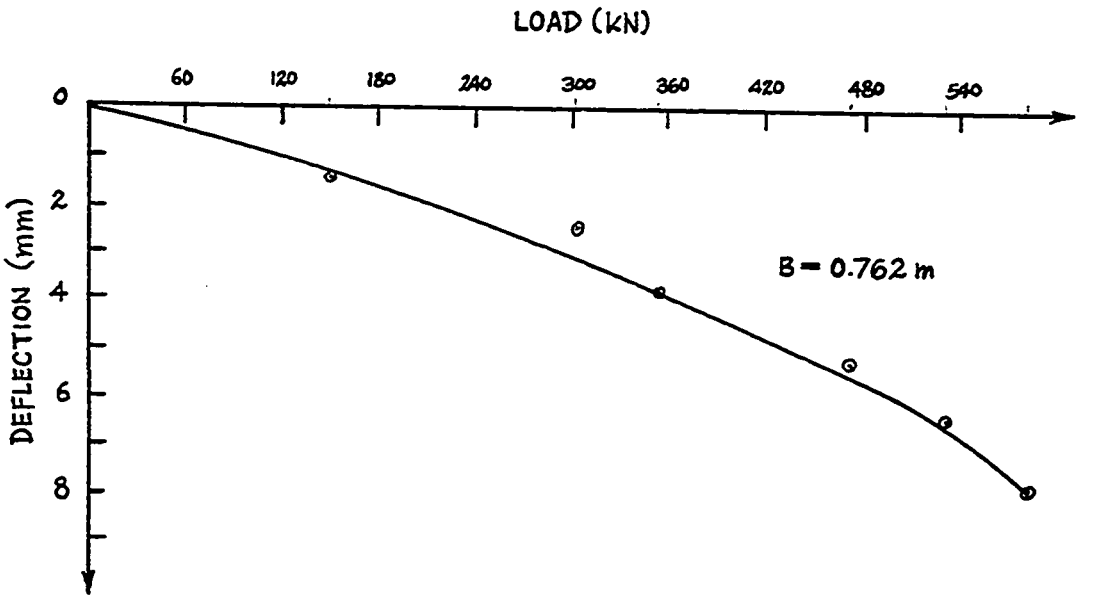

Fig.373 - Test No. 344-Non Repetitive McLeod Plate Test. Ottawa Airport. Hole 6. Load vs. Deflection.

APPENDIX C

TRIAXIAL TESTS CURVES

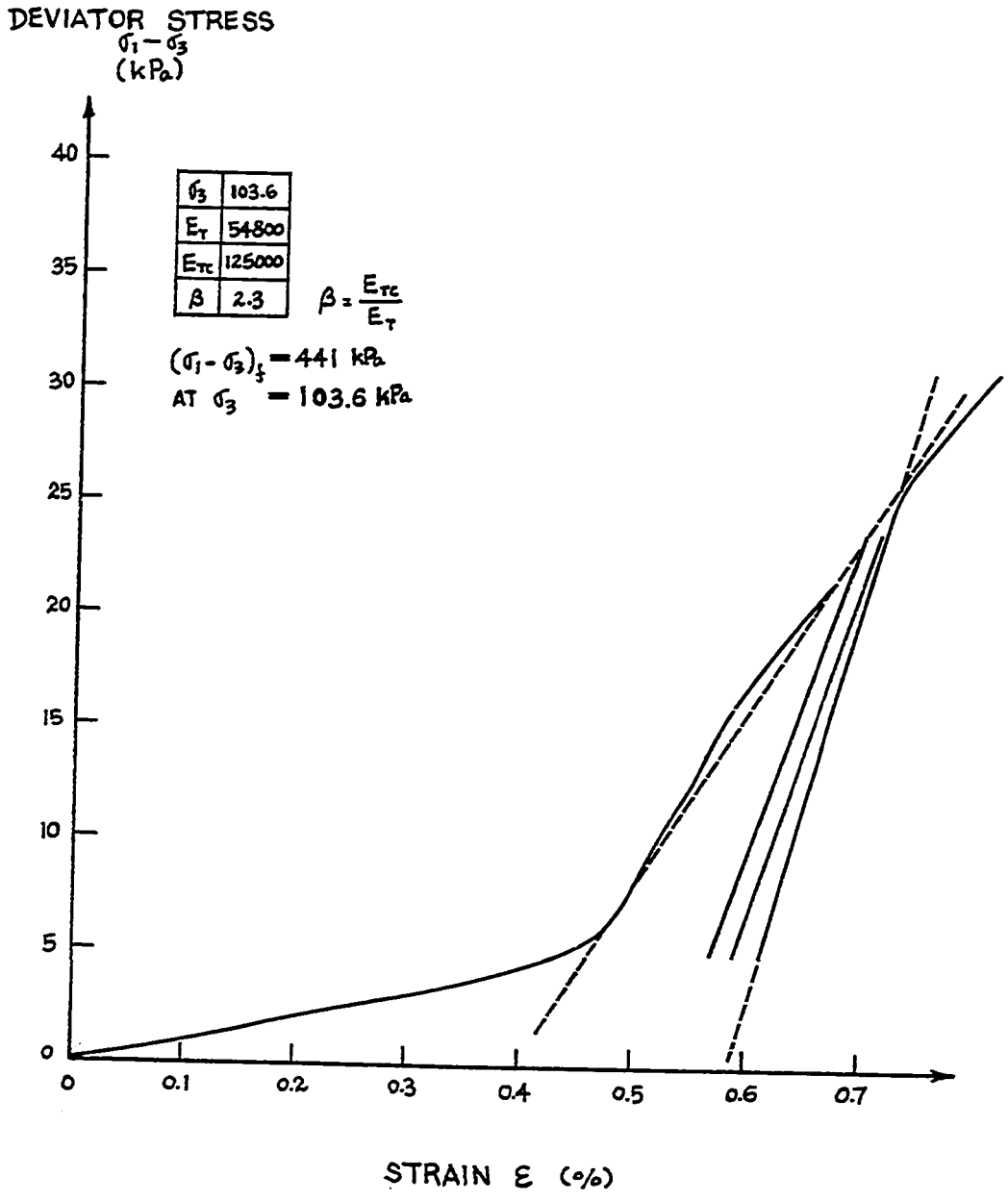

Fig. 374 - Test No. 218. Cyclic Triaxial Test. Sand Box. I_D = 93%. Sample Vibrated.

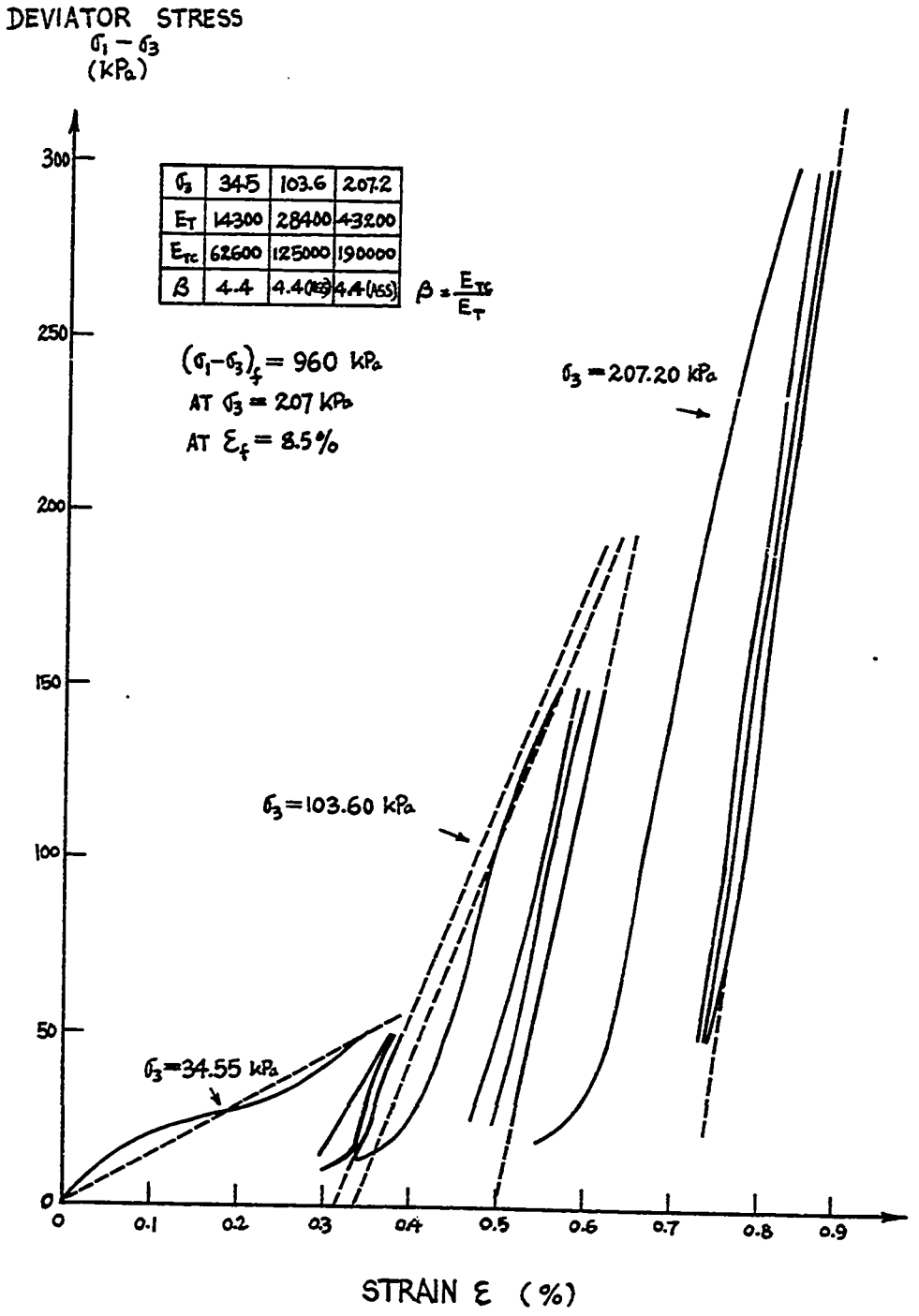

Fig. 375 - Test No. 247 Multistage Cyclic Triaxial Test. Sand Box. I_D = 95%. Sample Rained.

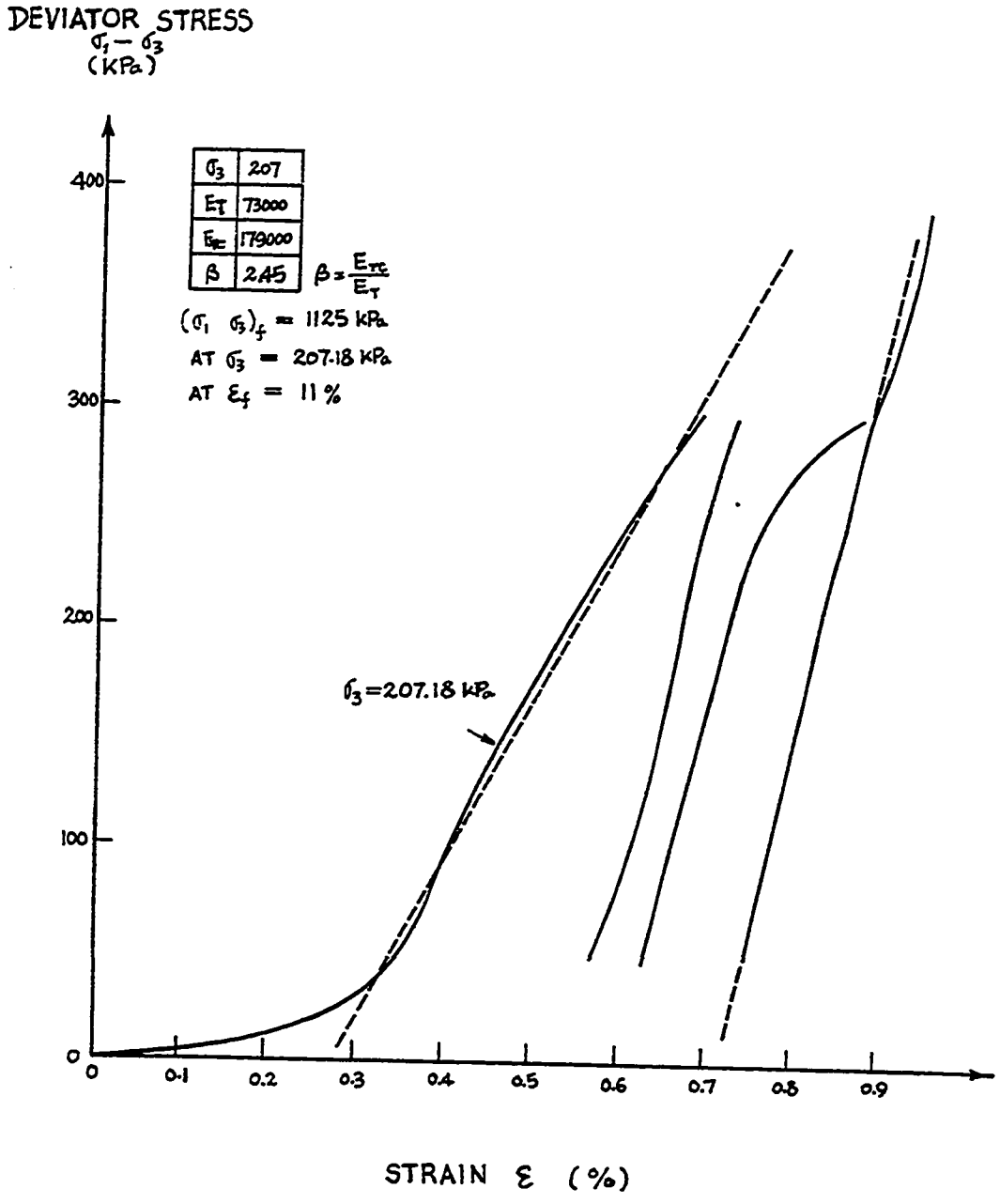

Fig. 376 - Test No. 248 Cyclic Triaxial Test. Sand Box. I_D = 95%. Sample Rained.

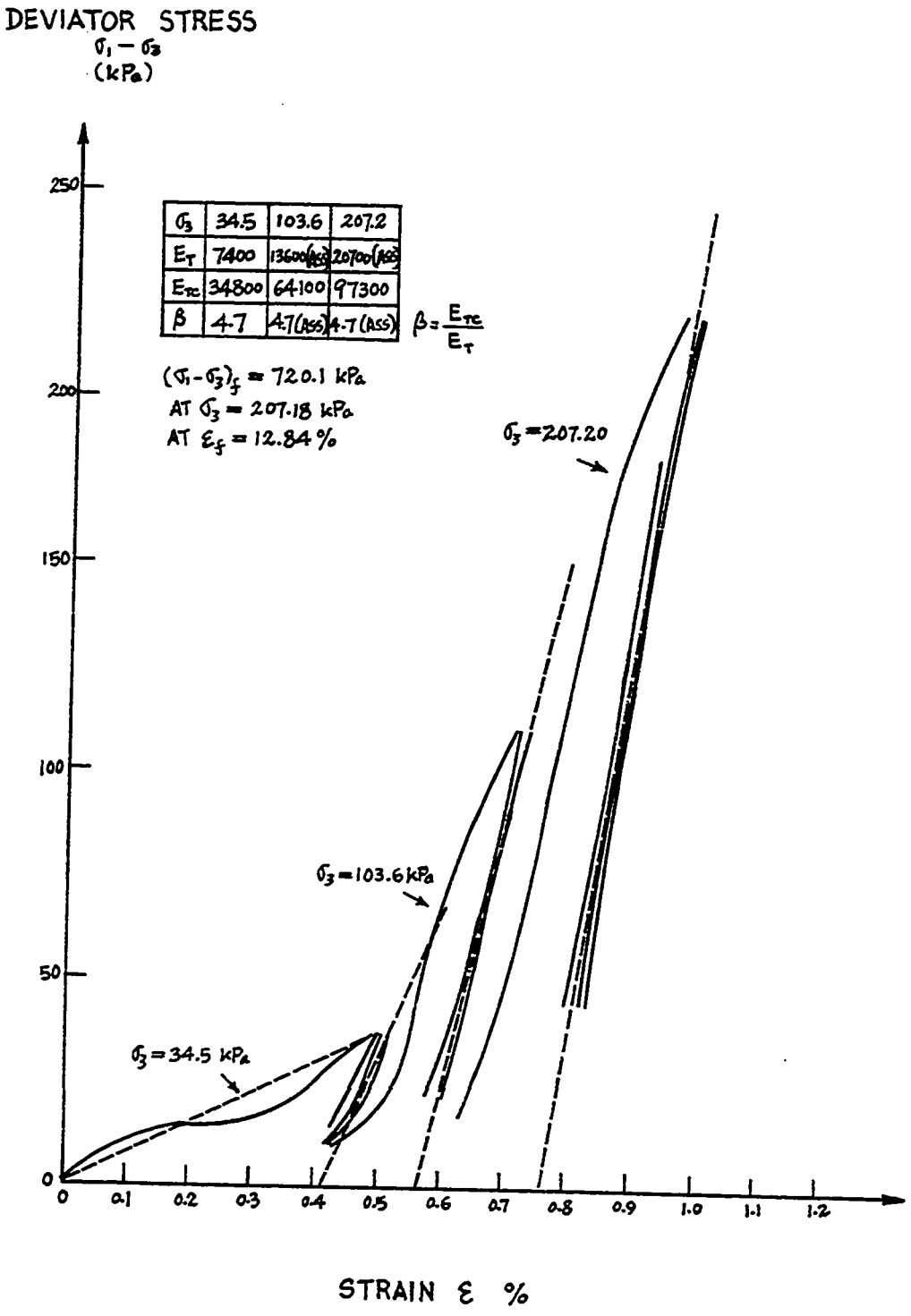

Fig.377 - Test No. 249 Multistage Cyclic Triaxial Test. Sand Box. I_D = 65%. Sample Rained.

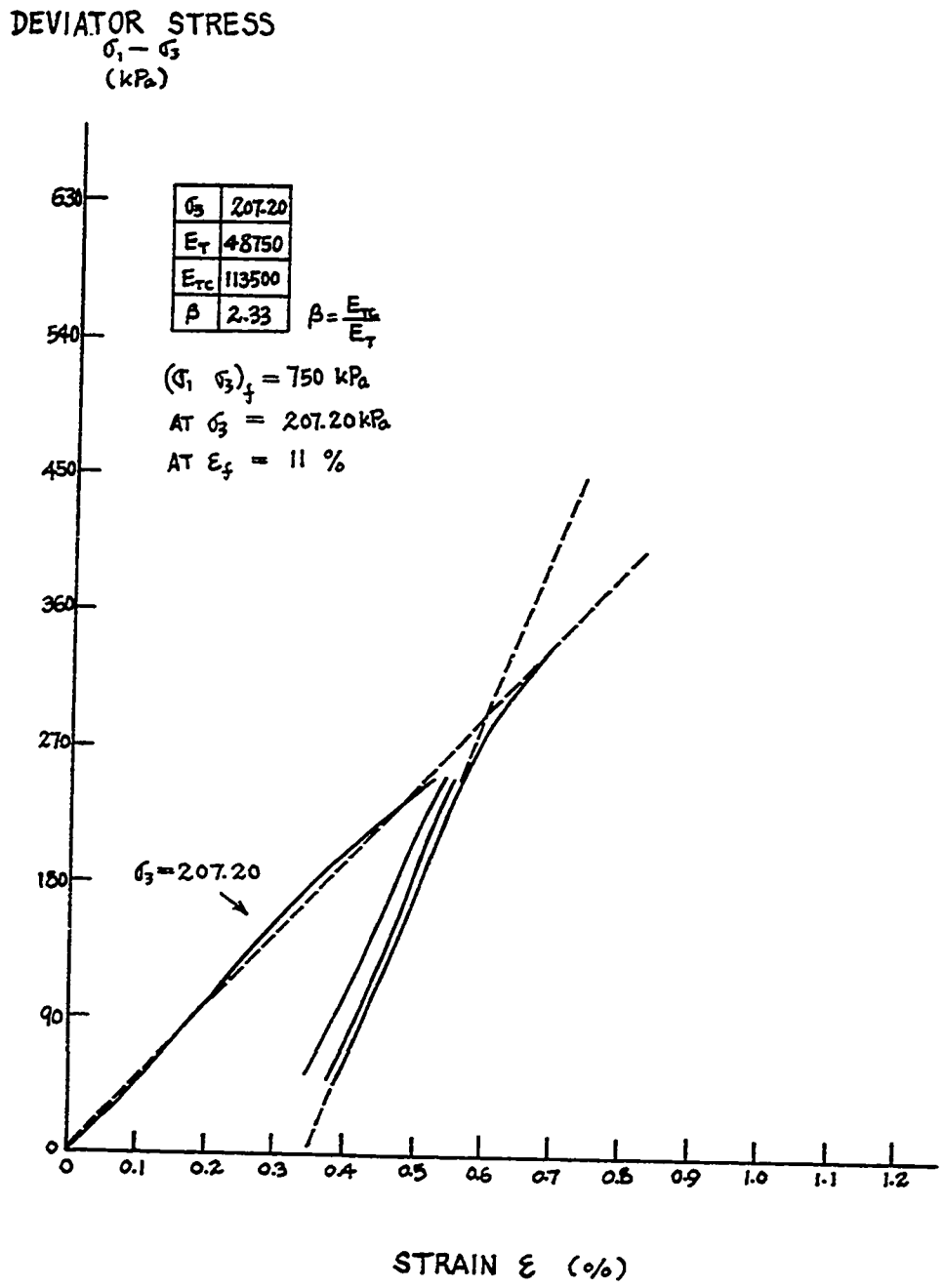

Fig. 378 - Test No. 250 Cyclic Triaxial Test. Sand Box. I_D = 65%. Sample Rained.

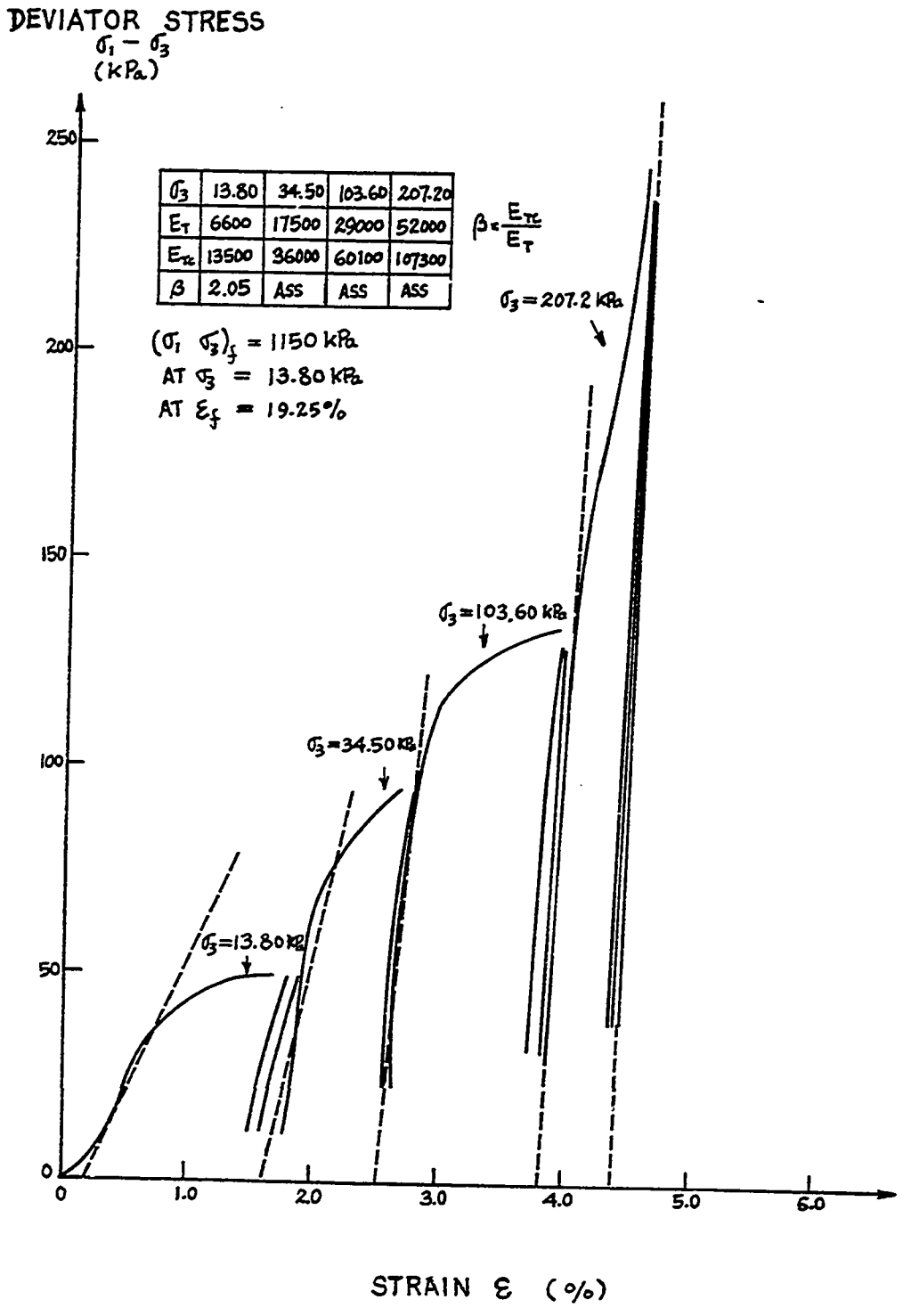

Fig. 379 – Test No. 251 Multistage Cyclic Triaxial Test. Ottawa Airport. Hole No. 5. Sample Vibrated.

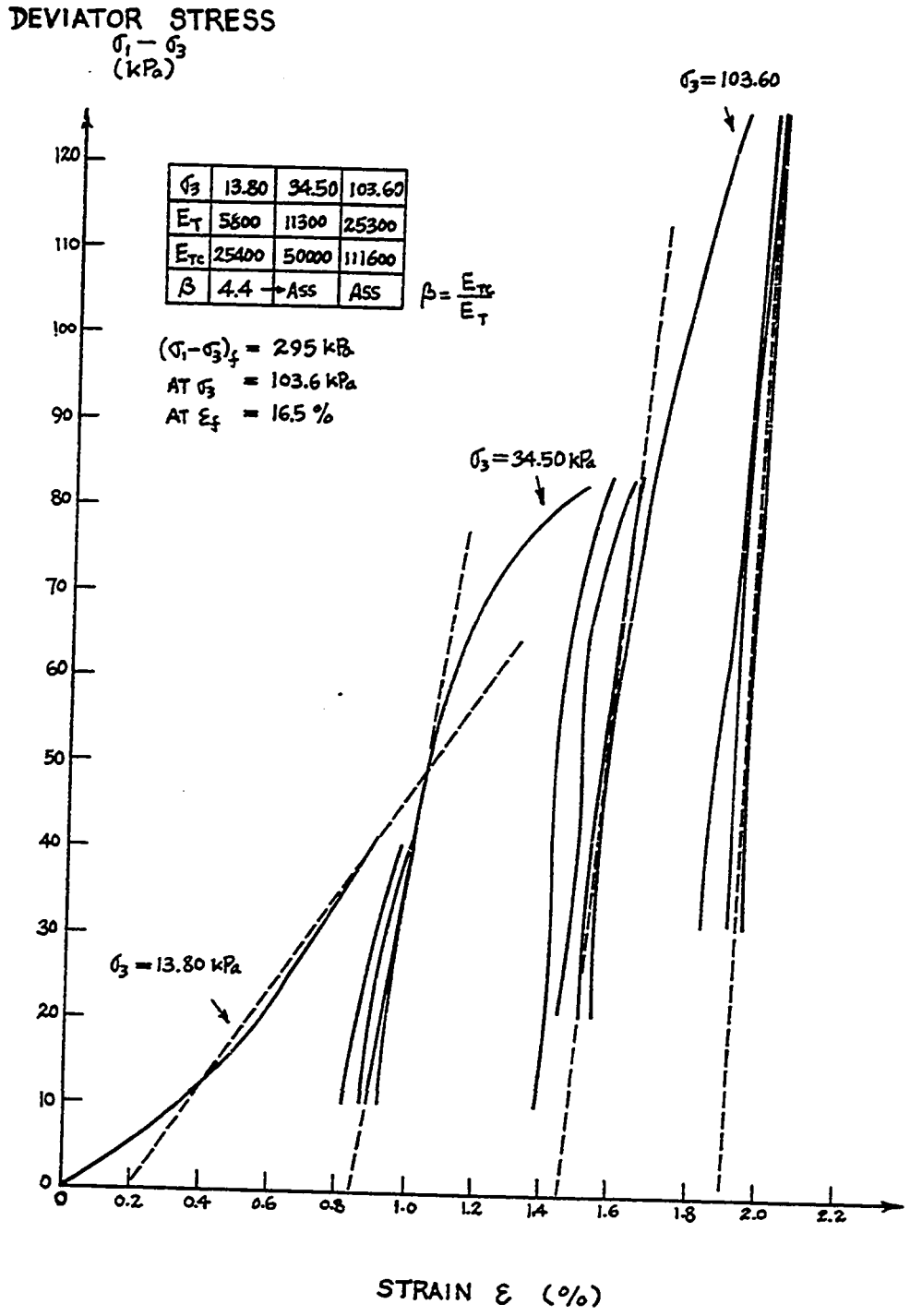

Fig.380 - Test No. 252 Multistage Cylic Triaxial Test. Ottawa Airport. Hole No. 6. Sample Vibrated.

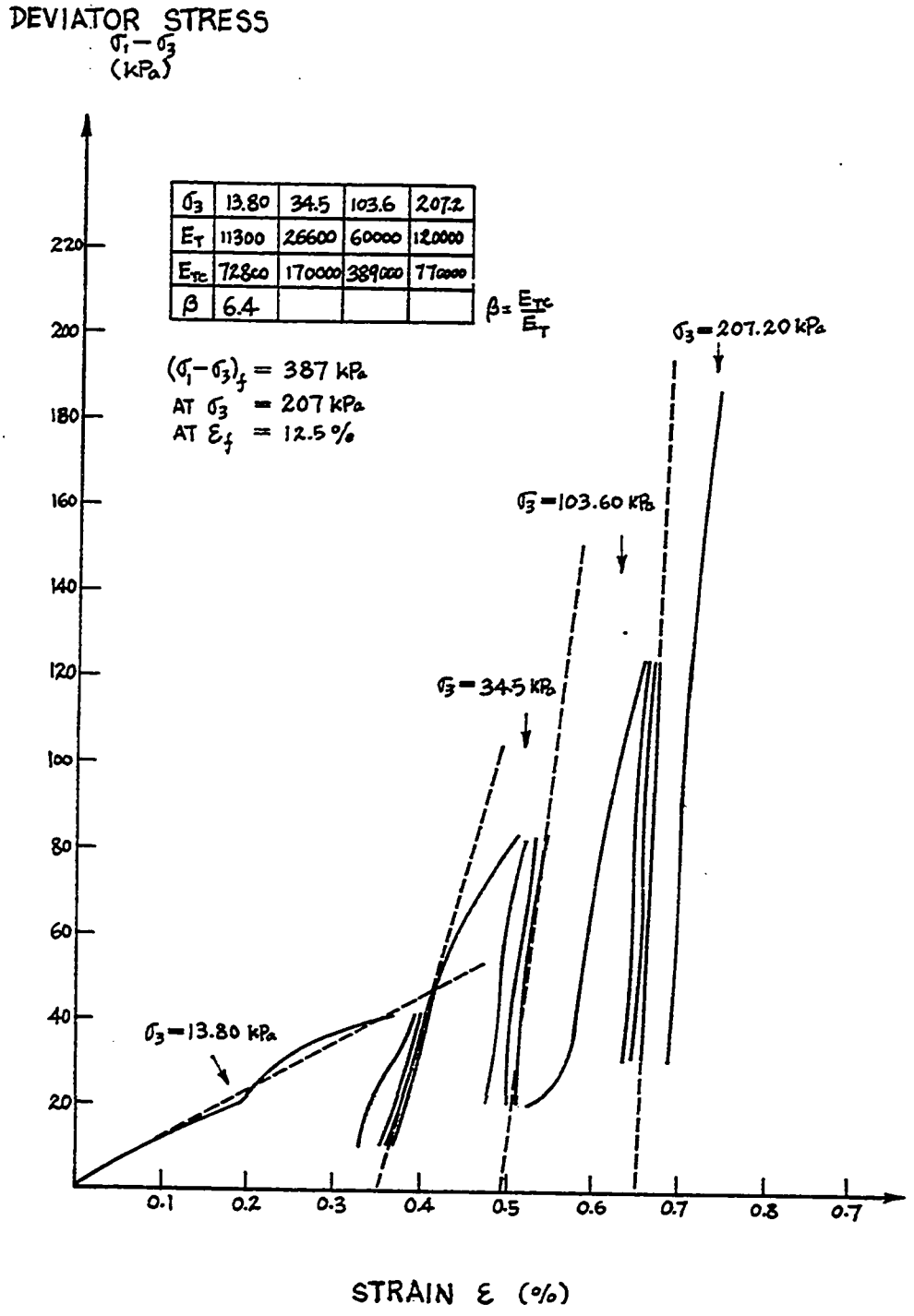

Fig. 381 – Test No. 253. Multistage Cyclic Triaxial Test. Ottawa Airport. Hole No. 1. Sample Vibrated.

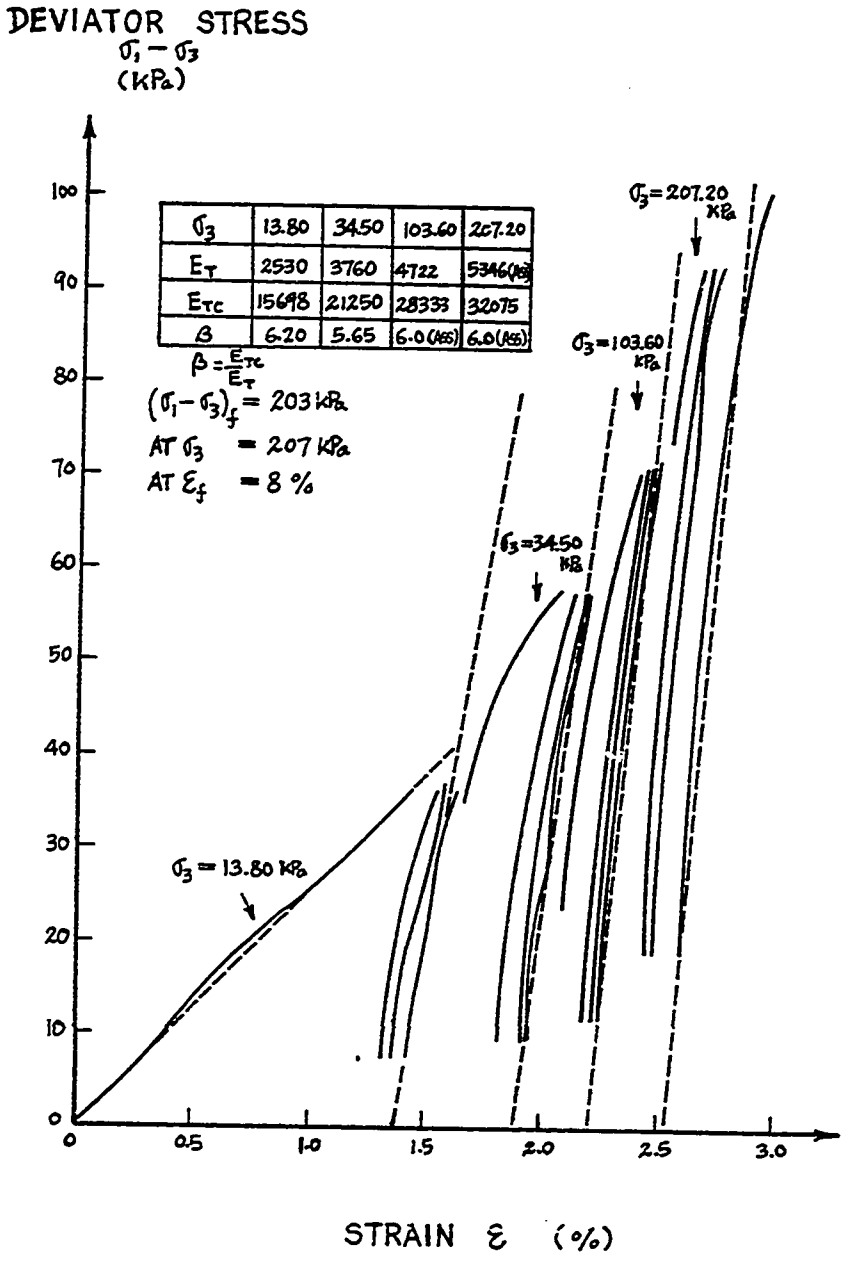

σ_3	13.80	34.50	103.60	207.20
E_T	2530	3760	4722	5346 (kPa)
E_{TC}	15698	21250	28333	32075
β	6.20	5.65	6.0 (Ave)	6.0 (Ave)

Fig. 382 - Test No. 255 Multistage Cyclic Triaxial Test. Fraser's Clay. Depth = 1.0 m. Shelby Tube Sample.

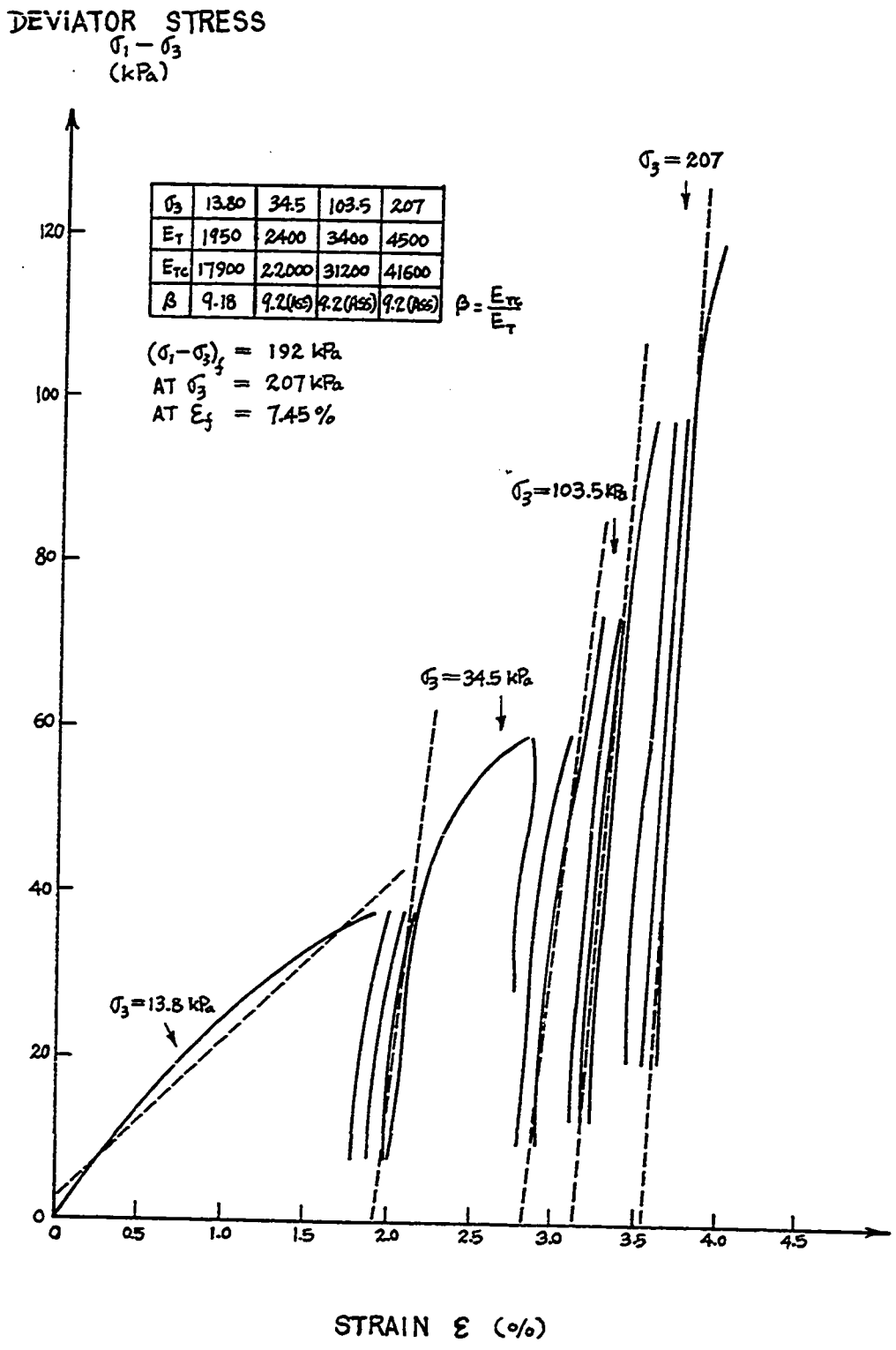

Fig. 383 - Test No. 256 Multistage Cyclic Triaxial Test. Fraser's Clay. Depth = 1.8 m. Shelby Tube Sample.

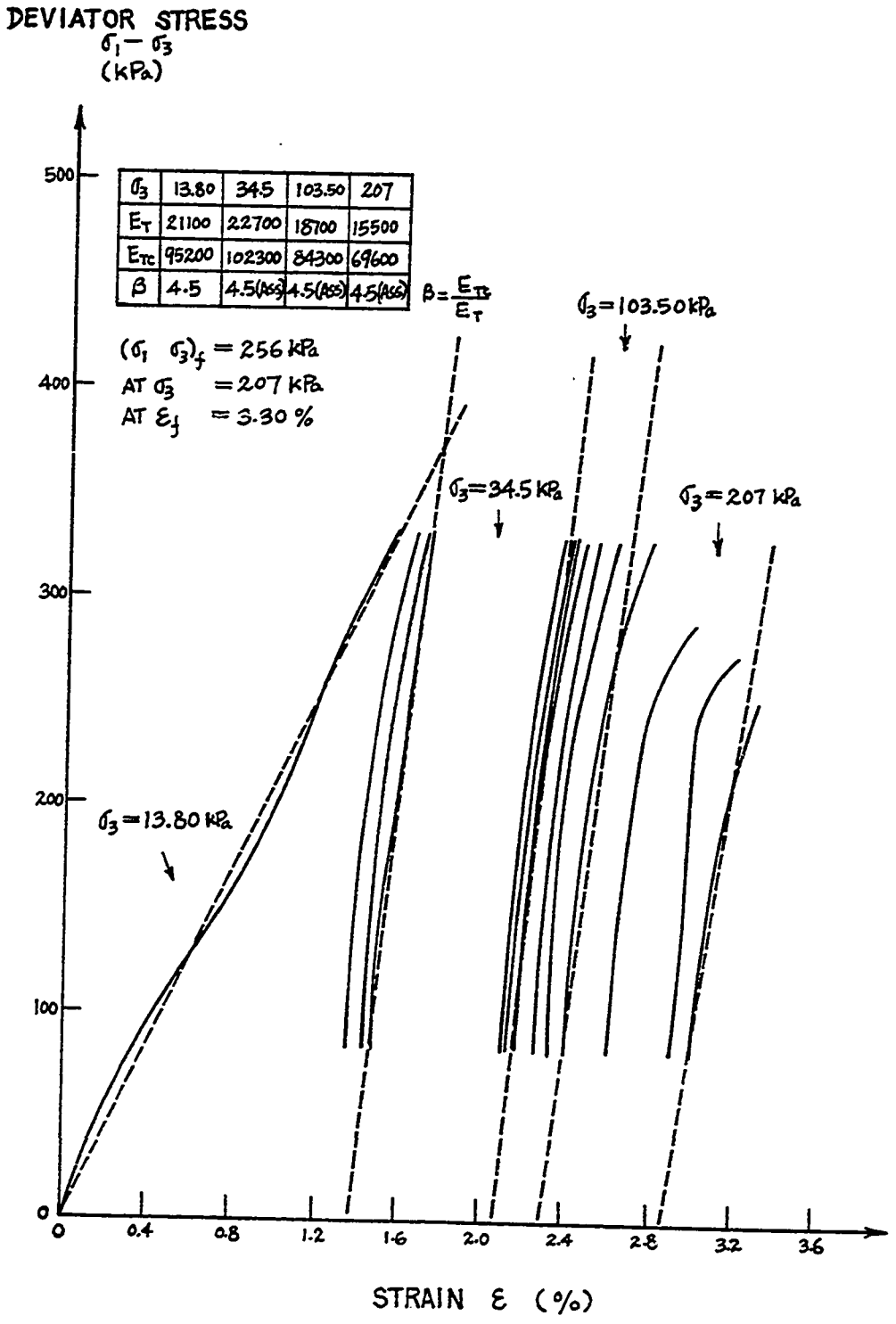

Fig.384 - Test No. 257 Multistage Cyclic Triaxial Test. Sarnia Airport. Hole No. 10. Depth: 1.2 m. Shelby Tube Sample.

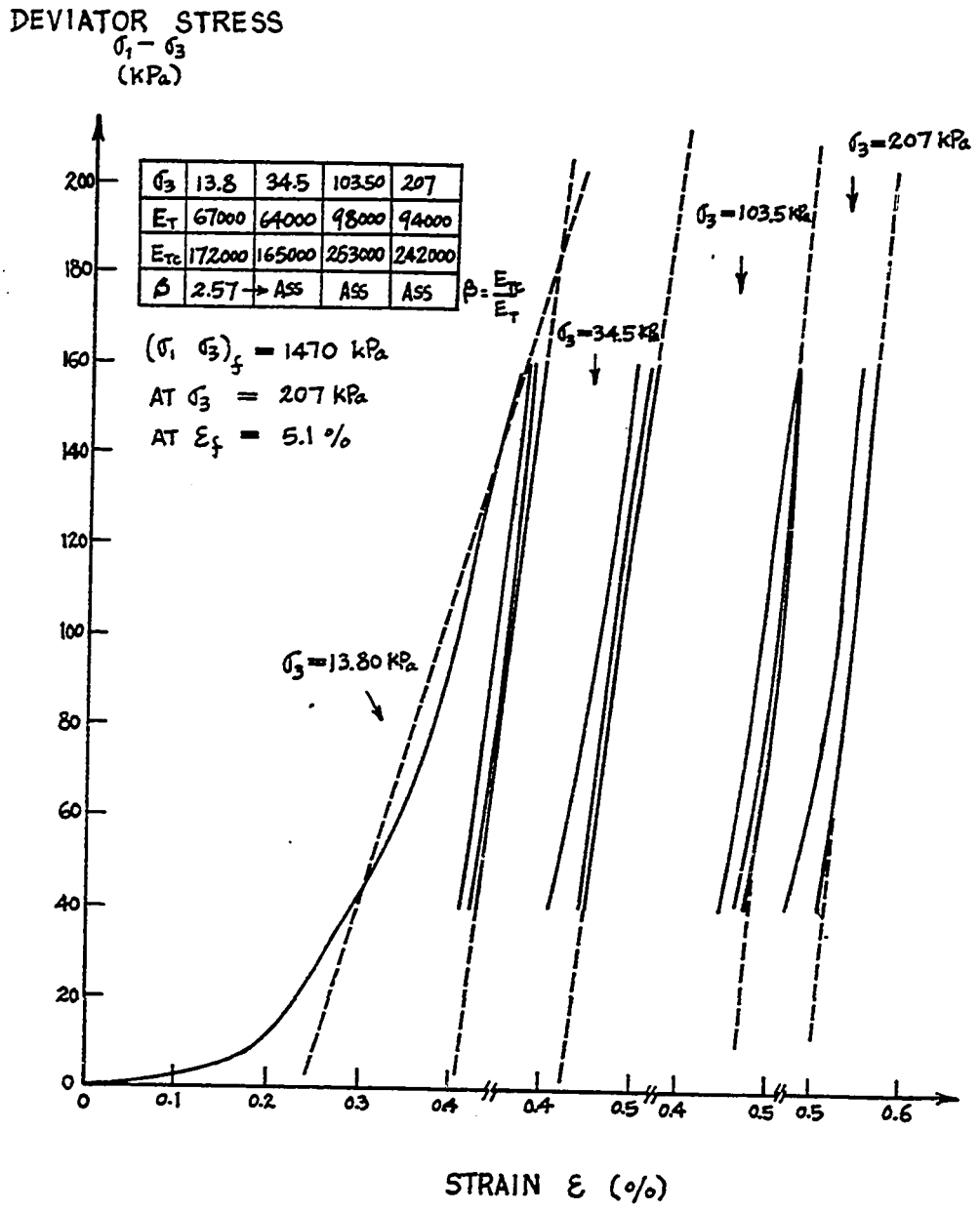

Fig. 385 - Test No. 258 Multistage Cyclic Triaxial Test. Sarnia Airport. Hole No. 10. Depth: 1.2 m. Shelby Tube Sample.

APPENDIX D

LISTING OF THE PROGRAM FOR THE REDUCTION OF PRESSUREMETER TEST DATA

```
 0: "file 5:TAPE 1":
 1: "NB:uses data file 0,trk1":
 2: "Menard":
 3: dim I[25],P[25],V[25]
 4: dim A$[7],B$[11],E$[17]
 5: dim Q$[1]
 6:
 7: trk 1;ldf 0,r1,r4
 8: trk 0
 9: "Ottawa"→A$
10: " Test "→B$
11: " Calibration "→E$
12: fmt 9,16"*";wrt 16,9
13: ent "Chantier?",A$
14: 1→N;.7→H;ent "niveau mano(m)?",N,"hauteur sonde(m)?",H
15: fmt "niv mano=",f3.1," m",/,"haut sonde=",f3.1," m"
16: wrt 16,N,H
17: N-H→L
18: "e"→Q$;ent "essai ou calibration?(e/c)",Q$
19: if Q$="e";gto "essai"
20: "etalonnage":
21: dsp "etalonnage choisi";wait 3000
22: ent "No. Etalon",B$[14,17]
23: prt A$;prt B$
24: "p"→Q$
25: ent "etalonnage:pression/volume?(p/v)",Q$
26: if Q$="p";gto "pression"
27: "volume":
28: prt "Etalon. Volume"
29: gsb "donnee"
30: 2000→Y;15→X
31: gsb "graphique"
32: plt 1,e10,0,1
33: for I=1 to N
34: P[I]/V[I]→P[I]
35: next I
36: fmt "Coefficients";wrt 16
37: "coeff vol":
38: 1→P;N→D
39: cll 'moindre'(P,D)
40: fmt "A=",e13.4,/,"+-",e13.4,/,"B=",e13.4,/,"+-",e13.4
41: wrt 16,A,I,B,J
42: fmt "C.D.=",f8.5;wrt 16,R
43: fmt 1,3x,"Regression",/," #  y=P/V  delta"
44: fmt 2,f2.0,f7.1,f7.1
45: cfg 5;gsb "command"
46: if Q$#"o";gto "coeff vol"
47:
48: "evaluation volume":
49: -A/2B→r3;B→r4
50: for P=0 to Y by Y/300
51: r3+√(r3*r3+P/r4)→V
52: plt V,P
53: next P
54: csiz 1.7;plt 0,Y,1;cplt 12,-2;lbl A$,E$
55: cplt -19,-2;lbl "-- volume --"
```

```
 56: plt 1e10,0,1
 57: fmt 16"*";wrt 16
 58:
 59: "o"→Q$;ent "etalonnage pression?(o/n)",Q$
 60: if Q$#"o";gto "fin etalon"
 61: "pression":
 62: prt "Etalon. Membrane"
 63: gsb "donnee"
 64: for I=1 to N
 65: P[I]+9.8e-3*L→P[I]
 66: next I
 67: 100→X;250→Y
 68: gsb "graphique"
 69: plt 1e10,0,1
 70:
 71: for I=1 to N
 72: P[I]*P[I]→X
 73: ln(V[I]/P[I])→P[I]
 74: X→V[I]
 75: next I
 76: fmt "coefficients";wrt 16
 77: 1→P;N→D
 78: "coeff press":
 79: cll 'moindre'(P,D)
 80: fmt "A=",f9.4,/,"B=",e12.4,/,"C.D=",f8.5
 81: wrt 16,A,B,R
 82: fmt 1,"Regression",/," # y=lnV/P  del"
 83: fmt 2,f2.0,f7.3,f7.3
 84: cfg 5;gsb "command"
 85: if Q$#"o";gto "coeff press"
 86:
 87: "evaluation press":
 88: A→r1;B→r2
 89: for P=0 to Y by Y/300
 90: Pexp(r2P↑2+r1)→V
 91: plt V,P
 92: next P
 93: csiz 1.7;plt 0,Y,1;cplt 12,-2;lbl A$,E$
 94: cplt -19,-2;lbl "-- membrane --"
 95: plt 1e10,0,1
 96:
 97:
 98: "fin etalon":
 99: fmt 16"*";wrt 16
100: trk 1;rcf 0,r1,r4
101: trk 0
102: dsp "etalonnage fini:CONTINUE=essai"
103: stp
104:
105:
106:
107: "essai":
108: dsp "essai choisi";wait 3000
109: ent "No. Essai",B$[7]
110: prt A$,B$
111: 0→Z;ent "Profondeur?",Z
```

```
112: fmt f4.2," m";wrt 16,Z
113: gsb "donnee"
114: "valeurs corrigees":
115: fmt 16".",/,"Correct.Memb.",/,"Pc*ex(A+BPc^2)=V";wrt 16
116: fmt "  A=",f7.4,/,"  B=",f8.4;wrt 16,r1,r2
117: fmt "Correct.Volume",/,"aVc+bVc^2=P";wrt 16
118: fmt "  a=",f8.2,/,"  b=",f8.4,/,16".";wrt 16,-2r4*r3,r4
119: fmt /,"Valeur Correcte",/," #   Vc      Pc";wrt 16
120: fmt f2.0,f6.1,f8.0
121: for I=1 to N
122: "membrane":
123: V[I]→C
124: for J=1 to 10
125: (1/(1+2r2C^2))(V[I]/exp(r2C^2+r1)+2r2C^3)→Q
126: if abs(Q-C)<=.01;Q→C;jmp 3
127: Q→C
128: next J
129: P[I]→P
130: P[I]-C+9.8*(Z+L+H)→P[I]
131: "volume":
132: V[I]-r3-√abs(r3*r3+P/r4)→V[I]
133: wrt 16,I,V[I],P[I]
134: next I
135:
136: 100→X;2000→Y;ent "Graphique: Pmax=?",Y
137: gsb "graphique"
138: plt 1e10,0,1
139: "Regres":
140: fmt 1,"  Regression",/," #   y=Pc  delta"
141: fmt 2,f2.0,f7.1,f7.1
142: sfg 5;gsb "command"
143: "pente":
144: cll 'moindre'(P,D)
145: fmt "Pente=",e10.2,/,"  +-",e12.2
146: wrt 16,B,J
147: fmt "C.D.=",f7.5;wrt 16,R
148: 1.33(360+V[P]+V[D])B→E
149: fmt "E= ",f10.0;wrt 16,E
150: cfg 5;gsb "command"
151: if Q$≠"o";gto "pente"
152: plt V[P],A+BV[P];plt V[D],A+BV[D]
153: plt 1e10,0,1
154: "fin":fmt 16"+";wrt 16;wrt 16;spc 3
155: "o"→Q$;ent "autre Pente?(o/n)",Q$
156: if Q$="o";gto "Regres"
157: csiz 1.7,1.1;plt 0,Y,1;cplt 6,-2;lbl A$,B$
158: plt 0,Y;cplt 6,-4
159: flt 2
160: 0→E;ent "module?",E
161: if E<=0;jmp 2
162: lbl "E=",E," MPa";cplt -15,-1;gto -2
163: "o"→Q$;ent "prochain  essai?(o/n)",Q$
164: if Q$="o";gto "essai"
165: dsp "FIN:RUN";end
166:
167: "command":
```

```
168: if flg5;gto 182
169: wrt 16.1
170: for I=P to D
171: A+B*V[I]-P[I]→Z
172: if I[I]=1;wrt 16.2,I,P[I],Z
173: next I
174: "o"→Q$
175: ent "regression acceptee?(o/n)",Q$
176: if Q$="o";ret
177: dsp "refaire";wait 2000
178: 0→P;ent "enlever # ?",P;if P=0;jmp 2
179: 0→I[P];jmp -1
180: 0→P;ent "ramener # ?",P;if P=0;jmp 2
181: 1→I[P];jmp -1
182: 1→P;N→D
183: enp "Premier,Dernier #?",P,D
184: ret
185:
186:
187: "donnee":
188: for I=1 to 25;-1e10→P[I]→V[I];next I
189: fmt "Donees Brutes",/," #   Vol   Press",/,"     (Cm3) (KPa)"
190: wrt 16
191: dsp "entrer vol. & press.:-1=fin";wait 3000
192: fmt f2.0,f6.1,f7.0
193: 0→I
194: "loop":
195: I+1→I
196: 1→I[I]
197: ent V[I],P[I];if V[I]<0 or P[I]<0;jmp 3
198: wrt 16,I,V[I],P[I]
199: gto "loop"
200: I-1→N
201: "y"→Q$;ent "corrections?(o/n)",Q$
202: if Q$#"n";enp "corriger #?",I;enp V[I];enp P[I];jmp -1
203: ret
204:
205:
206:
207: "moindre":
208: "regress lin. Y=A+BX":
209: "sortie: A+-I,B+-J,R":
210: 0→p3→p4→p5→p6→p7→p8→p9→p10
211: for I=p1 to p2
212: if I[I]=0;gto "next"
213: p8+1→p8
214: V[I]→p9;P[I]→p10
215: p9+p3→p3
216: p10+p4→p4
217: p9p9+p5→p5
218: p10p10+p6→p6
219: p9p10+p7→p7
220: "next":next I
221: (p8p7-p3p4)/(p8p5-p3p3)→B
222: (p4-Bp3)/p8→A
223: √((p6-Ap4-Bp7)/(p8-2))→p9
```

```
224: p9*√(p5/(p8p5-p3p3))→I
225: p9/√(p5-p3p3/p8)→J
226: (p8p7-p3p4)/√((p8p5-p3p3)(p8p6-p4p4))→R
227: R*R→R
228: ret
229:
230:
231: "graphique":
232: dsp "preparer traceuse:CONTINUE";stp
233: scl 0,X,0,Y;csiz 1.3,1,1,0
234: axe 0,0,X/5,Y/5;fxd 0
235: "lblX":
236: for I=0 to .9X by X/5
237: plt I,0;cplt -1.7,1;lbl I
238: next I
239: csiz 1.7,1.1;cplt 1,1;lbl "V(cm3)"
240: "lblY":
241: csiz 1.3,1.1,1,0
242: fxd 0
243: for I=Y/5 to 4Y/5 by Y/5
244: plt 0,I;cplt 0,-.3;lbl I
245: next I
246: csiz 1.5,1,1,90
247: plt 0,Y;cplt -6,-3;lbl "P(KPa)"
248: csiz 1,1,.7,0
249: "points":
250: fxd 0
251: for I=1 to N
252: if P[I]>0;plt V[I],P[I],1;cplt -.3,-.3;lbl "+"
253: if int(I/2)=I/2;cplt -2,1.5;lbl I
254: next I
255: ret
*2802
```

APPENDIX E

RESULTS OF THE COMPUTER SIMULATION OF THE CRITICAL DEPTH PROBLEM

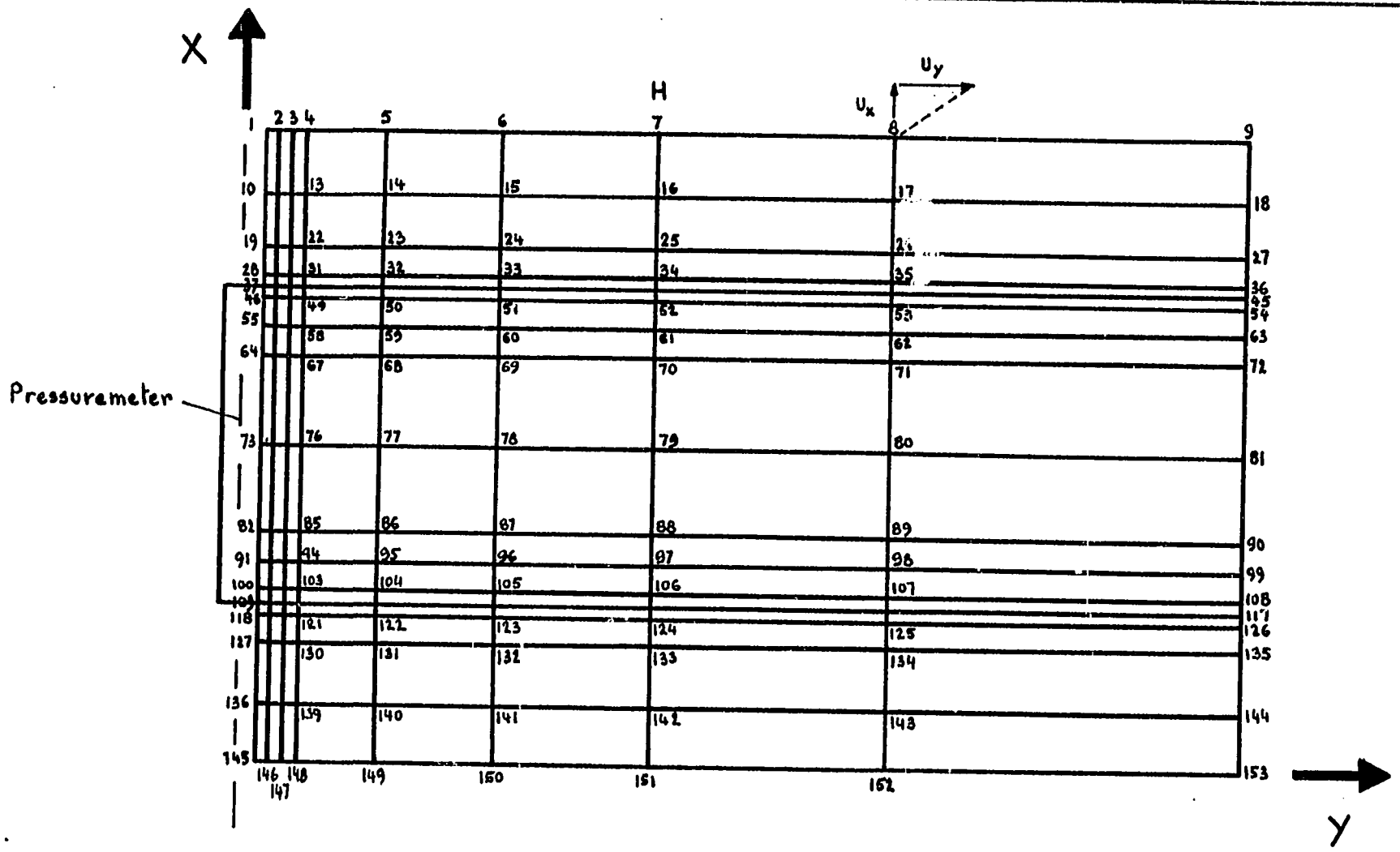

Fig. 386 - Numbering of the Nodes

Node No.	Vertical Displacement U_x (m.)	Horizontal Displacement U_y (m.)
1	-0.2577D-17	-0.2282D-06
2	-0.2681D-17	-0.1671D-05
3	-0.3044D-17	-0.2661D-05
4	-0.9358D-17	-0.3637D-05
5	-0.1947D-17	-0.4855D-06
6	0.1426D-17	0.6541D-05
7	0.9532D-18	0.7681D-05
8	0.5033D-18	0.4303D-05
9	0.4491D-18	0.5684D-18
10	-0.2120D-04	-0.1486D-06
11	-0.2020D-04	-0.1975D-05
12	-0.1820D-04	-0.3199D-05
13	-0.1287D-04	-0.3179D-05
14	0.2019D-05	0.3275D-05
15	0.2832D-05	0.8620D-05
16	0.7616D-06	0.8016D-05
17	0.6298D-07	0.4308D-05
18	-0.2151D-07	0.5658D-18
19	-0.6258D-04	0.1551D-04
20	-0.4949D-04	0.1021D-04
21	-0.3247D-04	0.1190D-04
22	-0.1671D-04	0.1555D-04
23	0.6088D-05	0.1824D-04
24	0.4608D-05	0.1374D-04
25	0.1256D-05	0.8932D-05
26	0.1066D-06	0.4320D-05
27	-0.3718D-07	0.2386D-18
28	-0.1090D-03	0.5375D-04
29	-0.4888D-04	0.5076D-04
30	-0.2431D-04	0.5204D-04
31	-0.1418D-04	0.4844D-04
32	0.7519D-05	0.2776D-04
33	0.4865D-05	0.1599D-04
34	0.1348D-05	0.9407D-05
35	0.1129D-06	0.4319D-05
36	-0.3945D-07	0.6554D-19
37	-0.1330D-03	0.2559D-03
38	-0.4053D-04	0.1593D-03
39	-0.1863D-04	0.1143D-03
40	-0.1332D-04	0.8125D-04
41	0.7746D-05	0.3388D-04
42	0.4922D-05	0.1758D-04
43	0.1366D-05	0.9732D-05
44	0.1132D-06	0.4318D-05
45	-0.3943D-07	0.4386D-19
46	-0.1072D-03	0.4570D-03
47	-0.4679D-04	0.2686D-03
48	-0.2428D-04	0.1759D-03
49	-0.1482D-04	0.1132D-03
50	0.7296D-05	0.3990D-04
51	0.4914D-05	0.1922D-04
52	0.1343D-05	0.1005D-04
53	0.1116D-06	0.4318D-05
54	-0.3877D-07	0.6548D-19
55	-0.5137D-04	0.5006D-03
56	-0.5158D-04	0.3053D-03
57	-0.3518D-04	0.2107D-03
58	-0.1824D-04	0.1410D-03
59	0.5773D-05	0.4912D-04
60	0.4710D-05	0.2164D-04
61	0.1240D-05	0.1049D-04
62	0.1049D-06	0.4321D-05
63	-0.3623D-07	0.1280D-18
64	-0.4007D-04	0.4157D-03
65	-0.3265D-04	0.2673D-03
66	-0.2645D-04	0.1980D-03
67	-0.1702D-04	0.1458D-03
68	0.3711D-05	0.5974D-04
69	0.3880D-05	0.2467D-04
70	0.1014D-05	0.1099D-04
71	0.8446D-07	0.4328D-05
72	-0.2871D-07	0.4316D-18
73	-0.1660D-18	0.5518D-03
74	-0.1084D-18	0.3404D-03
75	-0.8470D-19	0.2422D-03
76	-0.4066D-19	0.1717D-03
77	0.8894D-20	0.6969D-04
78	-0.7200D-20	0.2882D-04
79	0.6670D-20	0.1173D-04
80	0.8001D-21	0.4340D-05
81	0.4174D-21	0.1023D-17
82	0.4007D-04	0.4157D-03
83	0.3265D-04	0.2673D-03
84	0.2645D-04	0.1980D-03
85	0.1702D-04	0.1458D-03
86	-0.3711D-05	0.5974D-04
87	-0.3880D-05	0.2467D-04
88	-0.1014D-05	0.1099D-04
89	-0.8446D-07	0.4328D-05
90	0.2871D-07	0.4316D-18
91	0.5137D-04	0.5006D-03
92	0.5158D-04	0.3053D-03
93	0.3518D-04	0.2107D-03
94	0.1824D-04	0.1410D-03
95	-0.5773D-05	0.4912D-04
96	-0.4710D-05	0.2164D-04
97	-0.1240D-05	0.1049D-04
98	-0.1049D-06	0.4321D-05
99	0.3623D-07	0.1280D-18
100	0.1072D-03	0.4570D-03
101	0.4679D-04	0.2686D-03
102	0.2428D-04	0.1759D-03
103	0.1482D-04	0.1132D-03
104	-0.7296D-05	0.3990D-04
105	-0.4914D-05	0.1922D-04
106	-0.1343D-05	0.1005D-04
107	-0.1116D-06	0.4318D-05
108	0.3877D-07	0.6548D-19
109	0.1330D-03	0.2559D-03
110	0.4053D-04	0.1593D-03
111	0.1863D-04	0.1143D-03
112	0.1332D-04	0.8125D-04
113	-0.7746D-05	0.3388D-04
114	-0.4922D-05	0.1758D-04
115	-0.1366D-05	0.9732D-05
116	-0.1132D-06	0.4318D-05

Fig. 387 - Vertical and Horizontal Displacements Results for the Deep Pressuremeter Test

Node No.	Vertical Displacement U_x (m.)	Horizontal Displacement U_y (m.)
117	0.3943D-07	0.4386D-19
118	0.1090D-03	0.5375D-04
119	0.4888D-04	0.5076D-04
120	0.2431D-04	0.5204D-04
121	0.1418D-04	0.4844D-04
122	-0.7519D-05	0.2776D-04
123	-0.4865D-05	0.1599D-04
124	-0.1348D-05	0.9407D-05
125	-0.1129D-06	0.4319D-05
126	0.3945D-07	0.6554D-19
127	0.6258D-04	0.1551D-04
128	0.4949D-04	0.1021D-04
129	0.3247D-04	0.1190D-04
130	0.1671D-04	0.1555D-04
131	-0.6088D-05	0.1824D-04
132	-0.4608D-05	0.1374D-04
133	-0.1256D-05	0.8932D-05
134	-0.1066D-06	0.4320D-05
135	0.3718D-07	0.2386D-18
136	0.2120D-04	-0.1486D-06
137	0.2020D-04	-0.1975D-05
138	0.1820D-04	-0.3199D-05
139	0.1287D-04	-0.3179D-05
140	-0.2019D-05	0.3275D-05
141	-0.2832D-05	0.8620D-05
142	-0.7616D-06	0.8016D-05
143	-0.6298D-07	0.4308D-05
144	0.2151D-07	0.5658D-18
145	0.2577D-17	-0.2282D-06
146	0.2681D-17	-0.1671D-05
147	0.3044D-17	-0.2661D-05
148	0.9358D-17	-0.3637D-05
149	0.1947D-17	-0.4855D-06
150	-0.1426D-17	0.6541D-05
151	-0.9532D-18	0.7681D-05
152	-0.5033D-18	0.4303D-05
153	-0.4491D-18	0.5684D-18

Fig.387 - (cont'd) Vertical and Horizontal Displacements Results for the Deep Pressuremeter Test

Node No.	Vertical Displacement U_x (m.)	Horizontal Displacement U_y (m.)
1	-0.4572D-04	-0.7227D-05
2	-0.4402D-04	-0.6947D-05
3	-0.4187D-04	-0.7471D-05
4	-0.3909D-04	-0.8416D-05
5	-0.1382D-04	-0.4869D-05
6	0.2396D-05	0.4129D-05
7	0.4950D-05	0.7110D-05
8	0.3916D-05	0.4306D-05
9	0.3702D-05	0.4322D-18
10	-0.5465D-04	-0.1873D-07
11	-0.5259D-04	-0.8984D-06
12	-0.4927D-04	-0.1392D-05
13	-0.4141D-04	-0.5300D-06
14	-0.1055D-04	0.5972D-05
15	0.3910D-05	0.9098D-05
16	0.5099D-05	0.7652D-05
17	0.3699D-05	0.4212D-05
18	0.3360D-05	0.4355D-18
19	-0.8400D-04	0.1661D-04
20	-0.7069D-04	0.1200D-04
21	-0.5305D-04	0.1429D-04
22	-0.3622D-04	0.1856D-04
23	-0.4339D-05	0.2203D-04
24	0.4497D-05	0.1571D-04
25	0.4848D-05	0.9135D-05
26	0.3440D-05	0.4231D-05
27	0.3037D-05	0.1799D-18
28	-0.1270D-03	0.5490D-04
29	-0.6666D-04	0.5237D-04
30	-0.4173D-04	0.5412D-04
31	-0.3082D-04	0.5110D-04
32	-0.1944D-05	0.3139D-04
33	0.4426D-05	0.1821D-04
34	0.4628D-05	0.9838D-05
35	0.3313D-05	0.4261D-05
36	0.2915D-05	0.4844D-19
37	-0.1490D-03	0.2570D-03
38	-0.5643D-04	0.1608D-03
39	-0.3423D-04	0.1162D-03
40	-0.2828D-04	0.8369D-04
41	-0.1078D-05	0.3735D-04
42	0.4314D-05	0.1989D-04
43	0.4442D-05	0.1030D-04
44	0.3220D-05	0.4289D-05
45	0.2835D-05	0.3204D-19
46	-0.1215D-03	0.4580D-03
47	-0.6102D-04	0.2699D-03
48	-0.3827D-04	0.1776D-03
49	-0.2829D-04	0.1154D-03
50	-0.9078D-06	0.4317D-04
51	0.4174D-05	0.2157D-04
52	0.4220D-05	0.1074D-04
53	0.3122D-05	0.4322D-05
54	0.2756D-05	0.4740D-19
55	-0.6352D-04	0.5015D-03
56	-0.6367D-04	0.3065D-03
57	-0.4709D-04	0.2122D-03
58	-0.2976D-04	0.1429D-03
59	-0.1544D-05	0.5208D-04
60	0.3829D-05	0.2399D-04
61	0.3833D-05	0.1134D-04
62	0.2967D-05	0.4381D-05
63	0.2637D-05	0.9177D-19
64	-0.4990D-04	0.4165D-03
65	-0.4244D-04	0.2683D-03
66	-0.3611D-04	0.1992D-03
67	-0.2639D-04	0.1474D-03
68	-0.2528D-05	0.6230D-04
69	0.2903D-05	0.2695D-04
70	0.3258D-05	0.1199D-04
71	0.2741D-05	0.4469D-05
72	0.2479D-05	0.3078D-18
73	-0.5541D-05	0.5523D-03
74	-0.5539D-05	0.3411D-03
75	-0.5487D-05	0.2430D-03
76	-0.5359D-05	0.1727D-03
77	-0.3898D-05	0.7150D-04
78	-0.9325D-06	0.3076D-04
79	0.1462D-05	0.1291D-04
80	0.2073D-05	0.4686D-05
81	0.2026D-05	0.7513D-18
82	0.3699D-04	0.4161D-03
83	0.2956D-04	0.2678D-03
84	0.2338D-04	0.1985D-03
85	0.1401D-04	0.1465D-03
86	-0.6018D-05	0.6104D-04
87	-0.4570D-05	0.2626D-04
88	-0.1120D-06	0.1218D-04
89	0.1402D-05	0.4819D-05
90	0.1531D-05	0.3281D-18
91	0.4891D-04	0.5009D-03
92	0.4911D-04	0.3057D-03
93	0.3273D-04	0.2112D-03
94	0.1584D-04	0.1416D-03
95	-0.7643D-05	0.5027D-04
96	-0.5298D-05	0.2311D-04
97	-0.4983D-06	0.1167D-04
98	0.1171D-05	0.4851D-05
99	0.1340D-05	0.9957D-19
100	0.1051D-03	0.4573D-03
101	0.4472D-04	0.2689D-03
102	0.2223D-04	0.1764D-03
103	0.1281D-04	0.1138D-03
104	-0.8874D-05	0.4097D-04
105	-0.5426D-05	0.2061D-04
106	-0.7102D-06	0.1122D-04
107	0.1008D-05	0.4873D-05
108	0.1190D-05	0.5152D-19
109	0.1311D-03	0.2563D-03
110	0.3871D-04	0.1597D-03
111	0.1682D-04	0.1148D-03
112	0.1154D-04	0.8179D-04
113	-0.9146D-05	0.3490D-04
114	-0.5384D-05	0.1893D-04
115	-0.8016D-06	0.1089D-04
116	-0.9027D-06	0.4887D-05

Fig. 388 - Vertical and Horizontal Displacements Results for the Shallow Pressuremeter Test

Node No.	Vertical Displacement U_x (m.)	Horizontal Displacement U_y (m.)
117	0.1089D-05	0.3472D-19
118	0.1074D-03	0.5408D-04
119	0.4727D-04	0.5111D-04
120	0.2272D-04	0.5246D-04
121	0.1262D-04	0.4895D-04
122	-0.8750D-05	0.2873D-04
123	-0.5278D-05	0.1730D-04
124	-0.8483D-06	0.1056D-04
125	0.7999D-06	0.4900D-05
126	0.9856D-06	0.5216D-19
127	0.6129D-04	0.1583D-04
128	0.4820D-04	0.1054D-04
129	0.3119D-04	0.1229D-04
130	0.1545D-04	0.1603D-04
131	-0.7085D-05	0.1916D-04
132	-0.4947D-05	0.1500D-04
133	-0.8483D-06	0.1007D-04
134	0.6523D-06	0.4915D-05
135	0.8276D-06	0.1915D-18
136	0.2059D-04	0.1396D-06
137	0.1959D-04	-0.1670D-05
138	0.1759D-04	-0.2845D-05
139	0.1228D-04	-0.2745D-05
140	-0.2492D-05	0.4111D-05
141	-0.2998D-05	0.9794D-05
142	-0.5652D-06	0.9130D-05
143	0.3149D-06	0.4926D-05
144	0.4184D-06	0.4593D-18
145	0.2538D-17	0.5442D-07
146	0.2634D-17	-0.1375D-05
147	0.2983D-17	-0.2319D-05
148	0.9145D-17	-0.3218D-05
149	0.1756D-17	0.3235D-06
150	-0.1382D-17	0.7688D-05
151	-0.6161D-18	0.8786D-05
152	-0.1441D-20	0.4929D-05
153	0.5120D-19	0.4634D-18

Fig.388 - (cont'd) Vertical and Horizontal Displacements Restults for the Shallow Pressuremeter Test

APPENDIX F

RESULTS OF THE MULTILAYER ELASTIC ANALYSIS OF THE PLATE TESTS

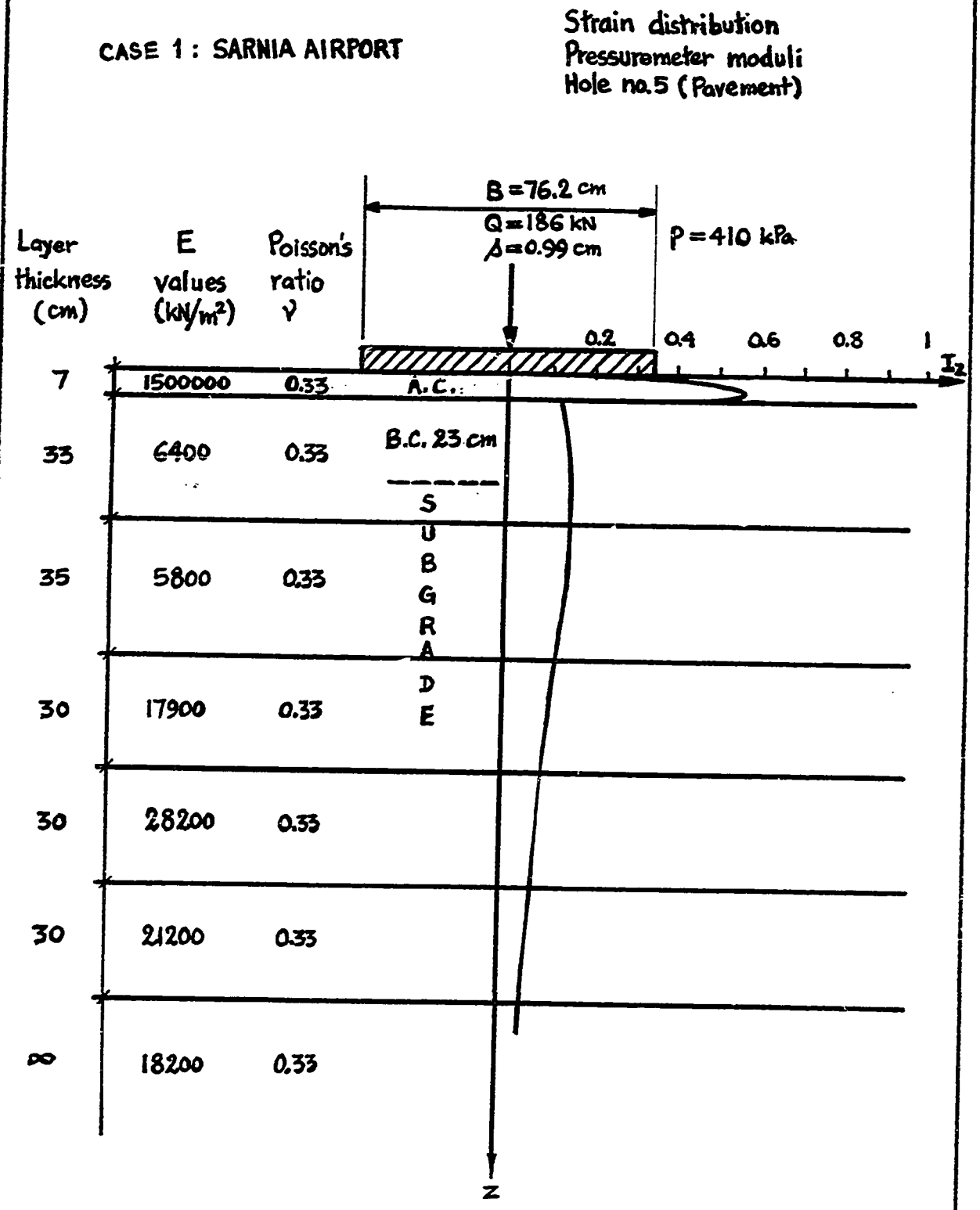

Fig. 389 - Plate test analysis. I_z curve and settlement. Sarnia. Pressuremeter moduli. Hole No. 5. Pavement test.

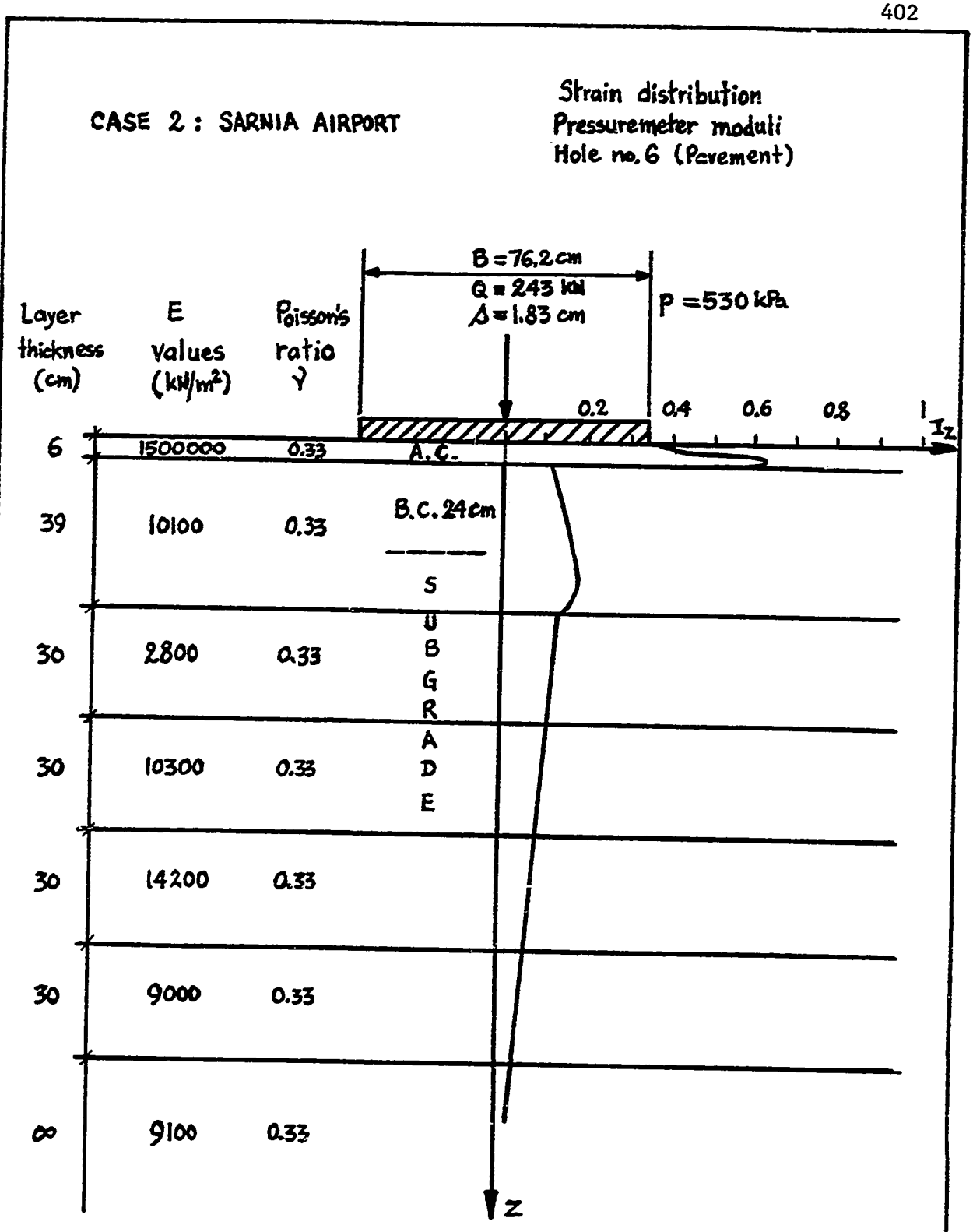

Fig.390 - Plate test analysis. I_z curve and settlement. Sarnia. Pressuremeter moduli. Hole No. 6. Pavement test.

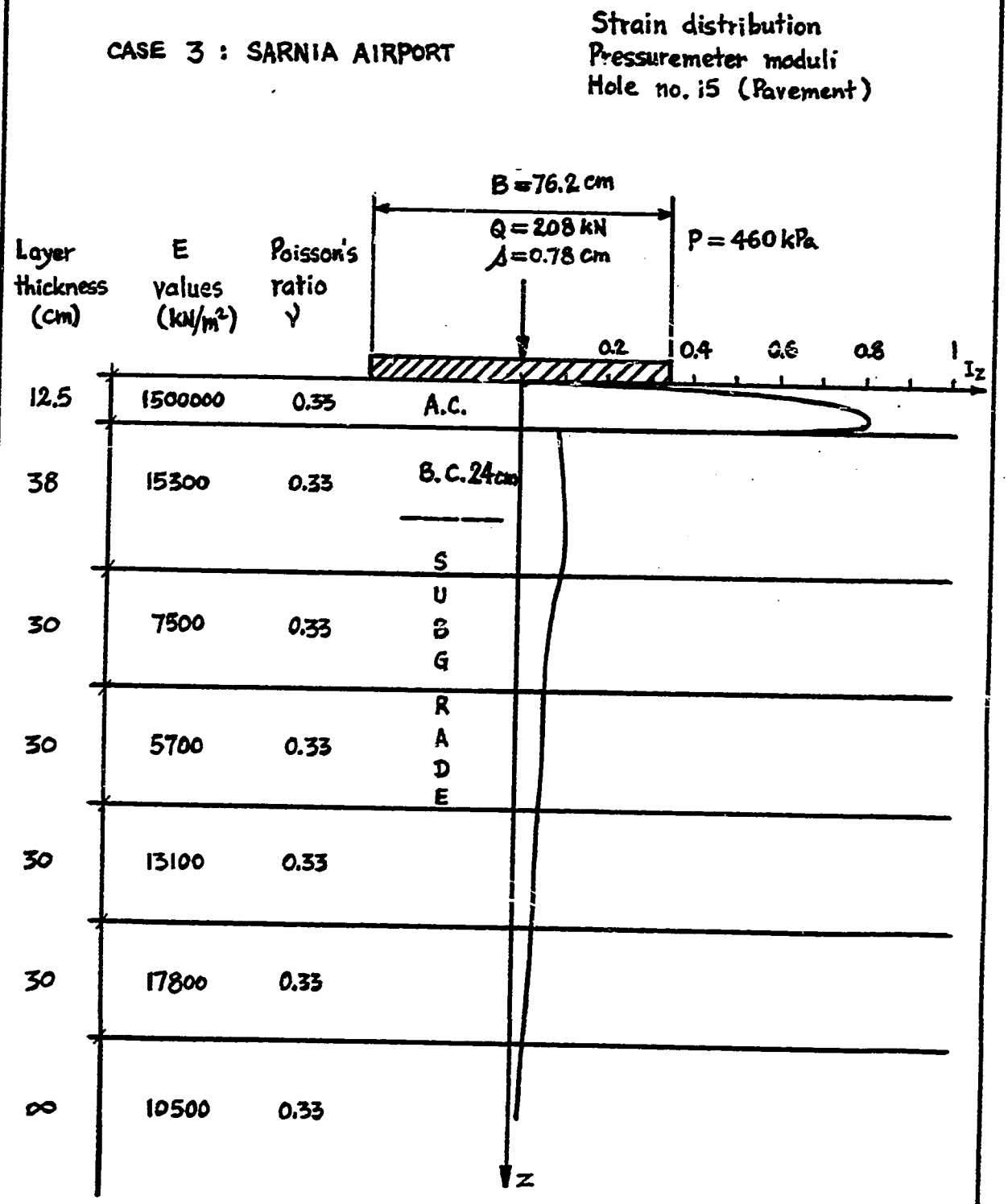

Fig. 391 - Plate test analysis. I_z curve and settlement. Sarnia. Pressuremeter moduli. Hole No. 15. Pavement test.

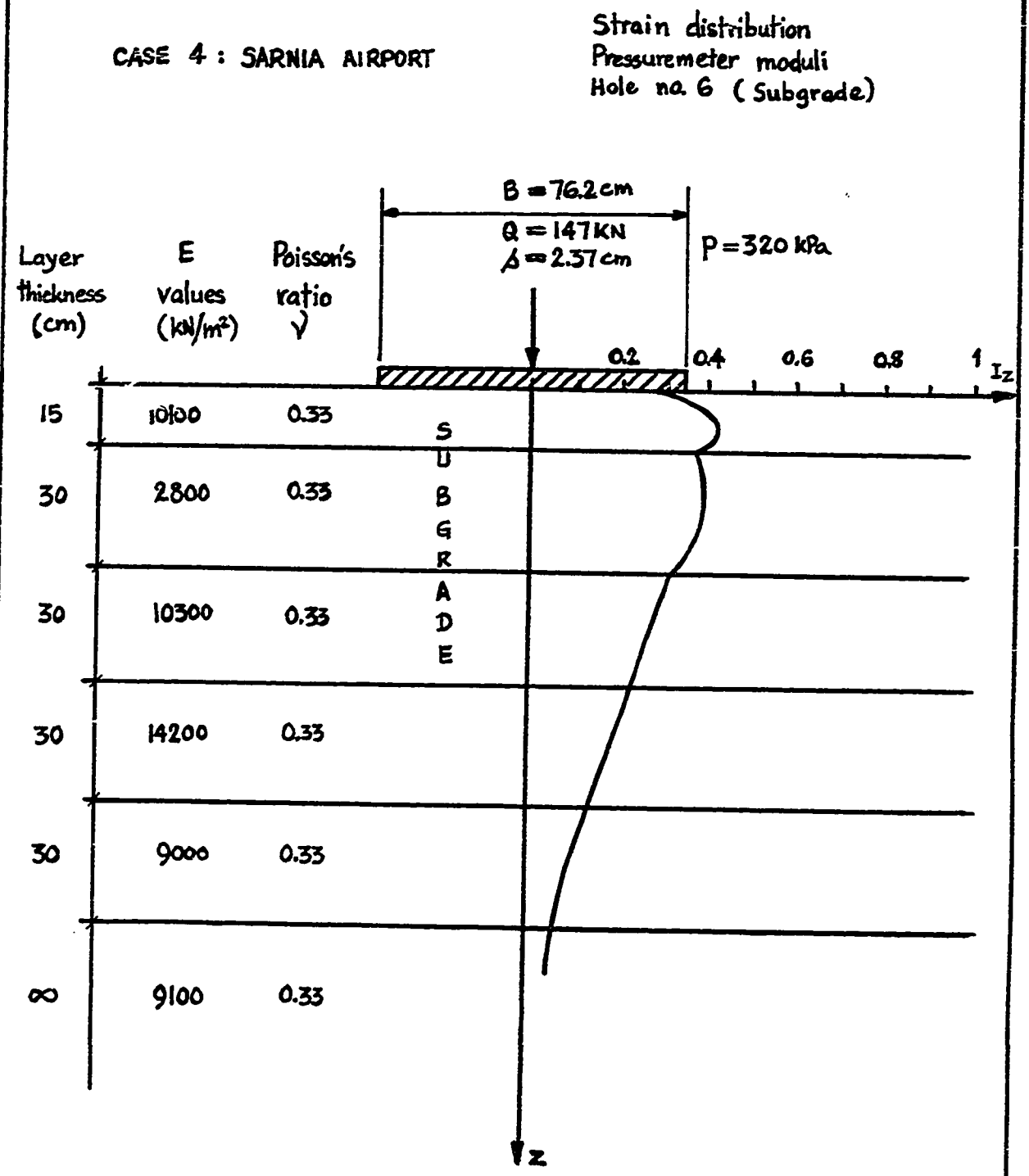

Fig. 392 - Plate test analysis. I_z curve and settlement. Sarnia. Pressuremeter moduli. Hole No. 6. Subgrade test.

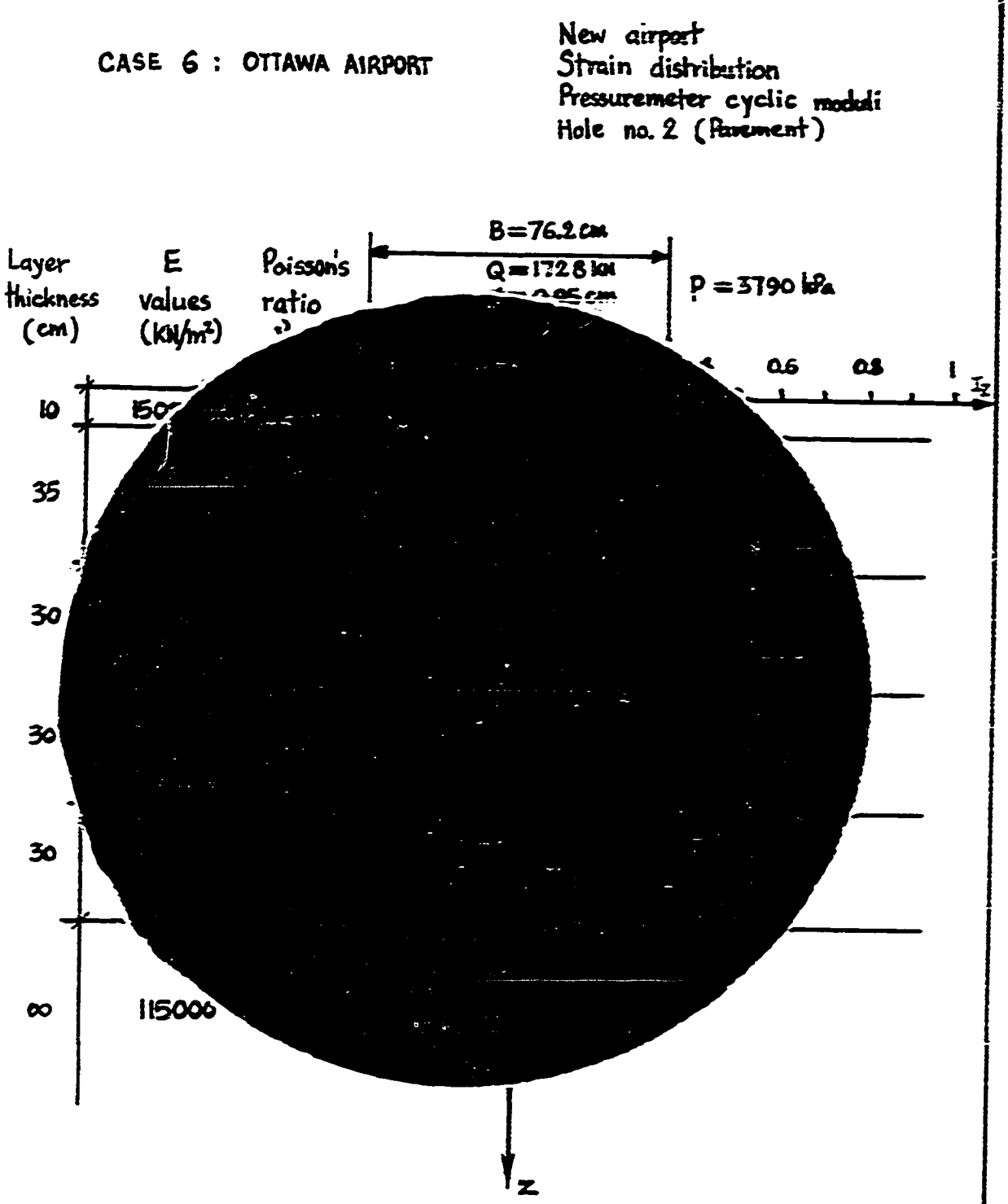

Fig. 393 - Plate test analysis. I_z curve and settlement. Ottawa: New Airport. Pressuremeter cyclic moduli. Hole No. 2. Pavement test.

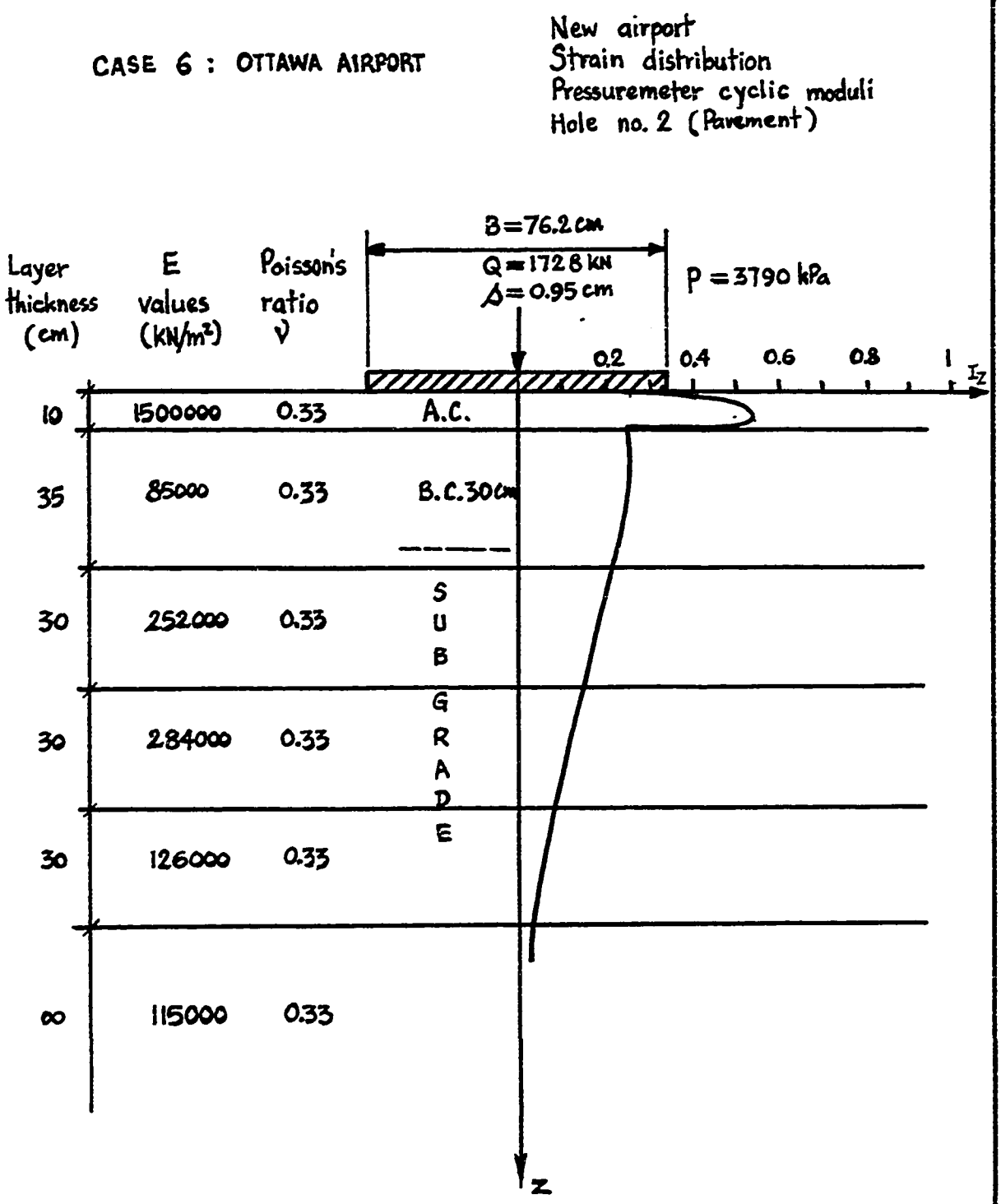

Fig. 393 - Plate test analysis. I_z curve and settlement. Ottawa: New Airport. Pressuremeter cyclic moduli. Hole No. 2. Pavement test.

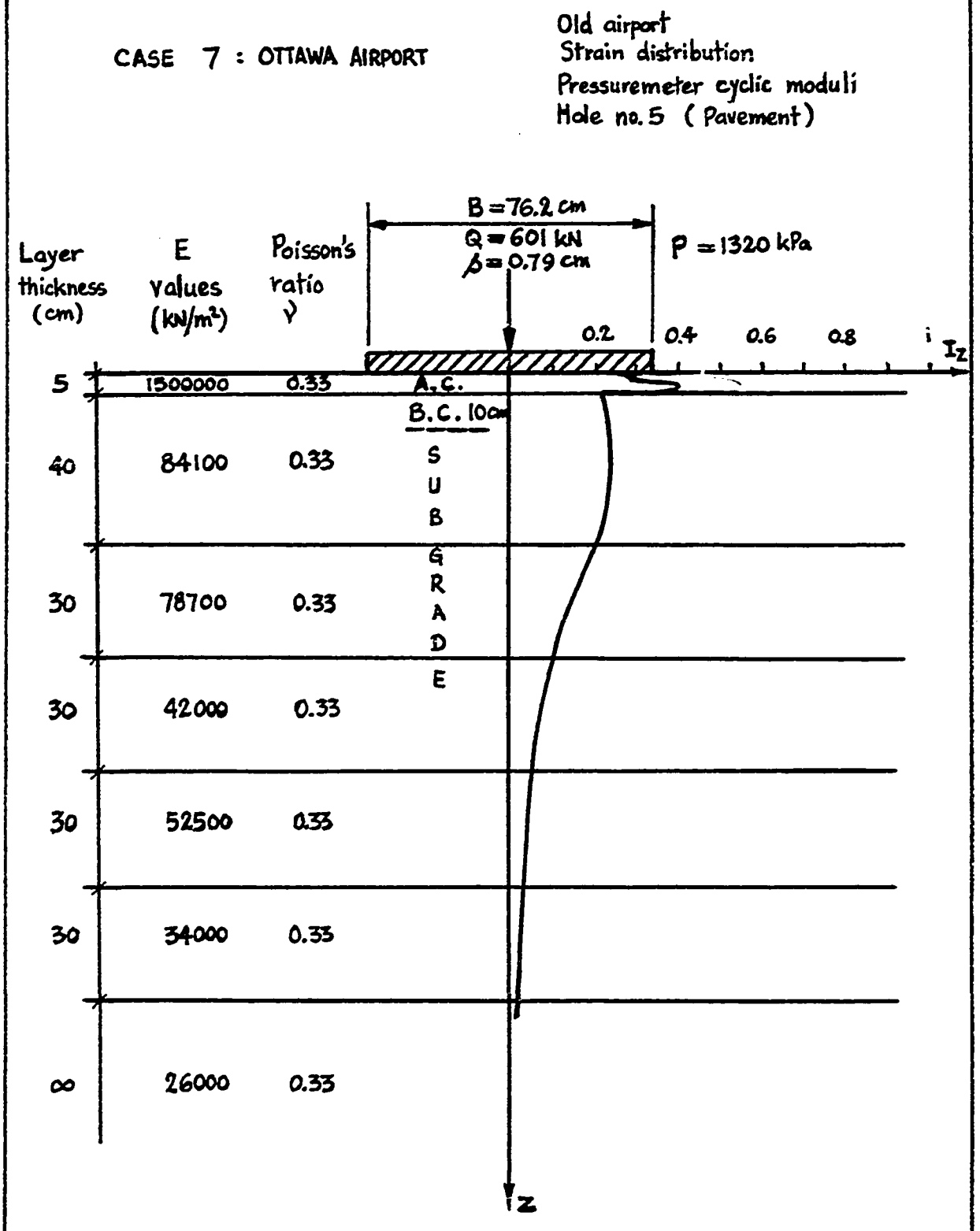

Fig.394 - Plate test analysis. I_z curve and settlement. Ottawa: Old Airport. Pressuremeter cyclic moduli. Hole No.5. Pavement test.

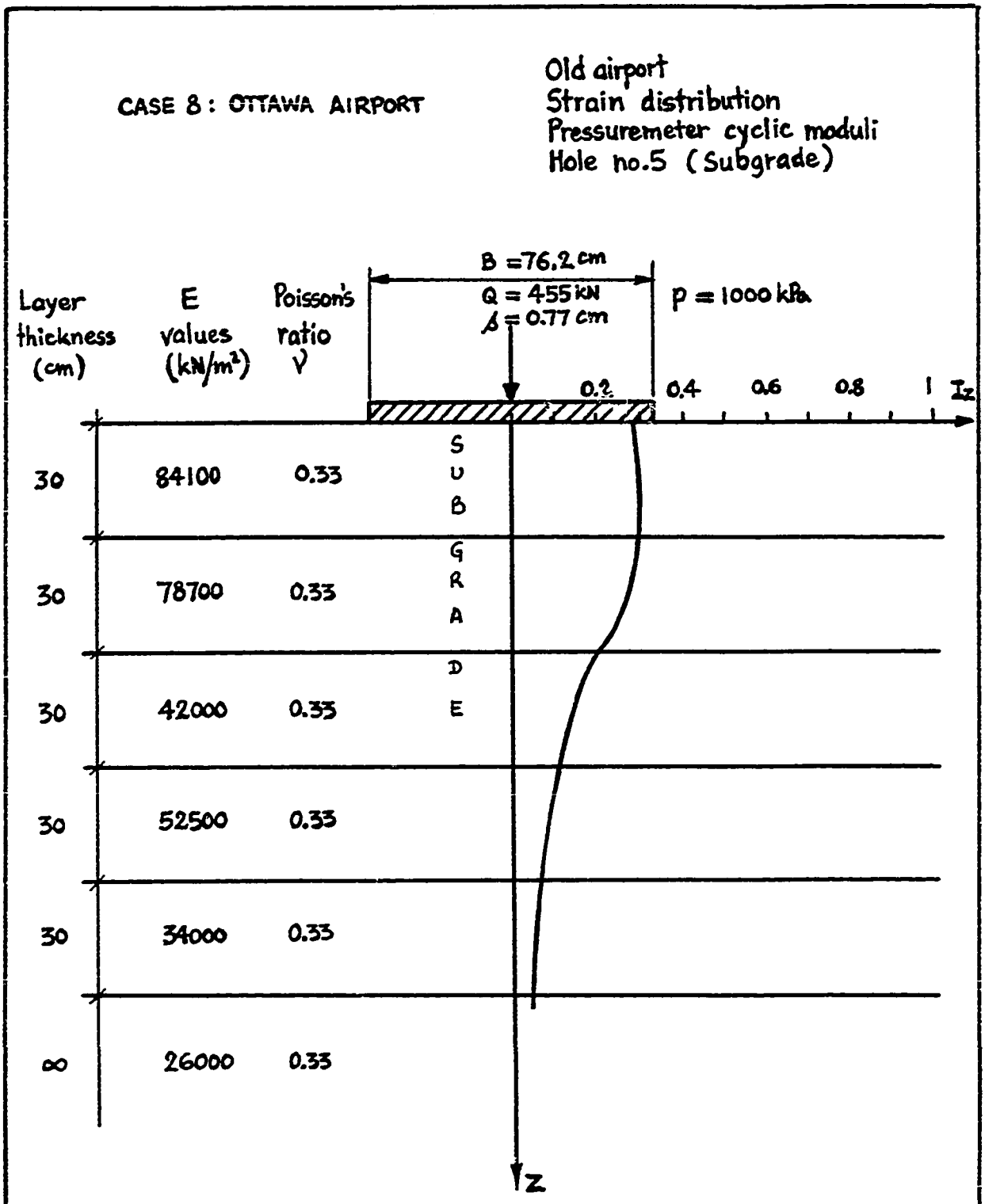

Fig. 395 - Plate test analysis. I_z curve and settlement. Ottawa: Old Airport. Pressuremeter cyclic moduli. Hole No. 5 Subgrade test.

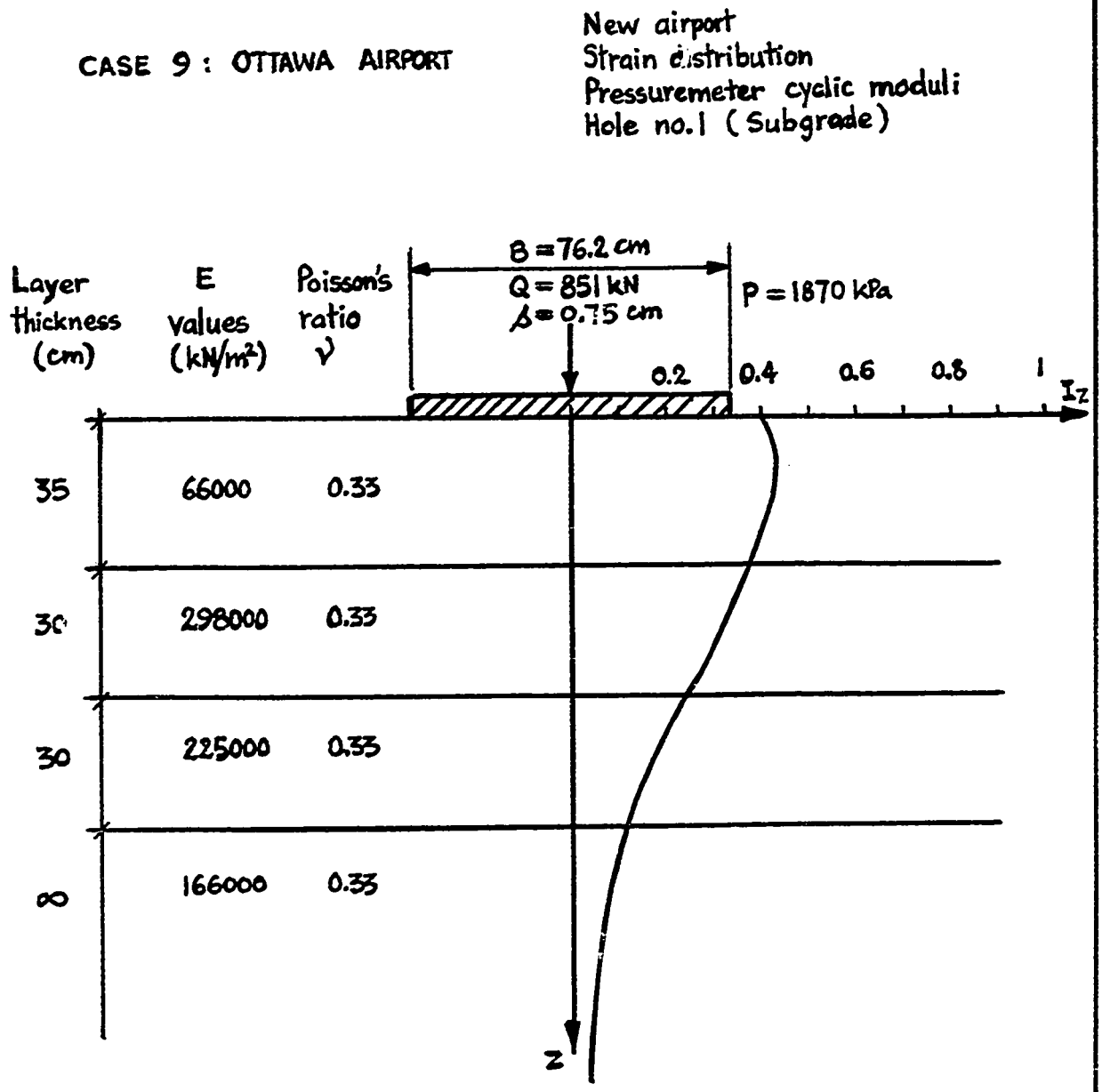

Fig. 396 - Plate test analysis. I_z curve and settlement. Ottawa: New Airport. Pressuremeter cyclic moduli. Hole No. 1. Subgrade test.

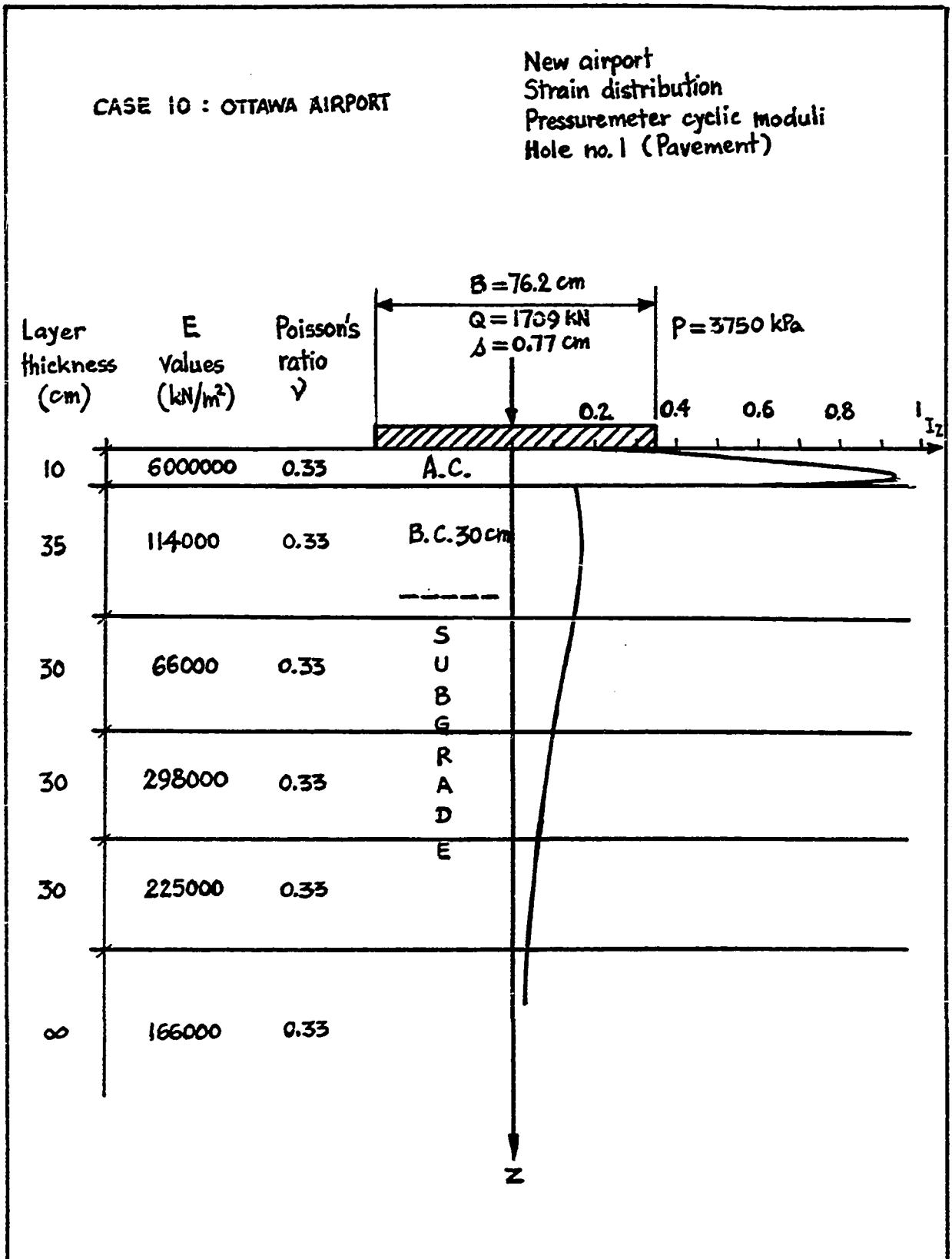

Fig. 397 - Plate test analysis. I_z curve and settlement. Ottawa: New Airport. Pressuremeter cyclic moduli. Nole No. 1. Pavement test. Asphalt modulus: 6000,000 kPa.

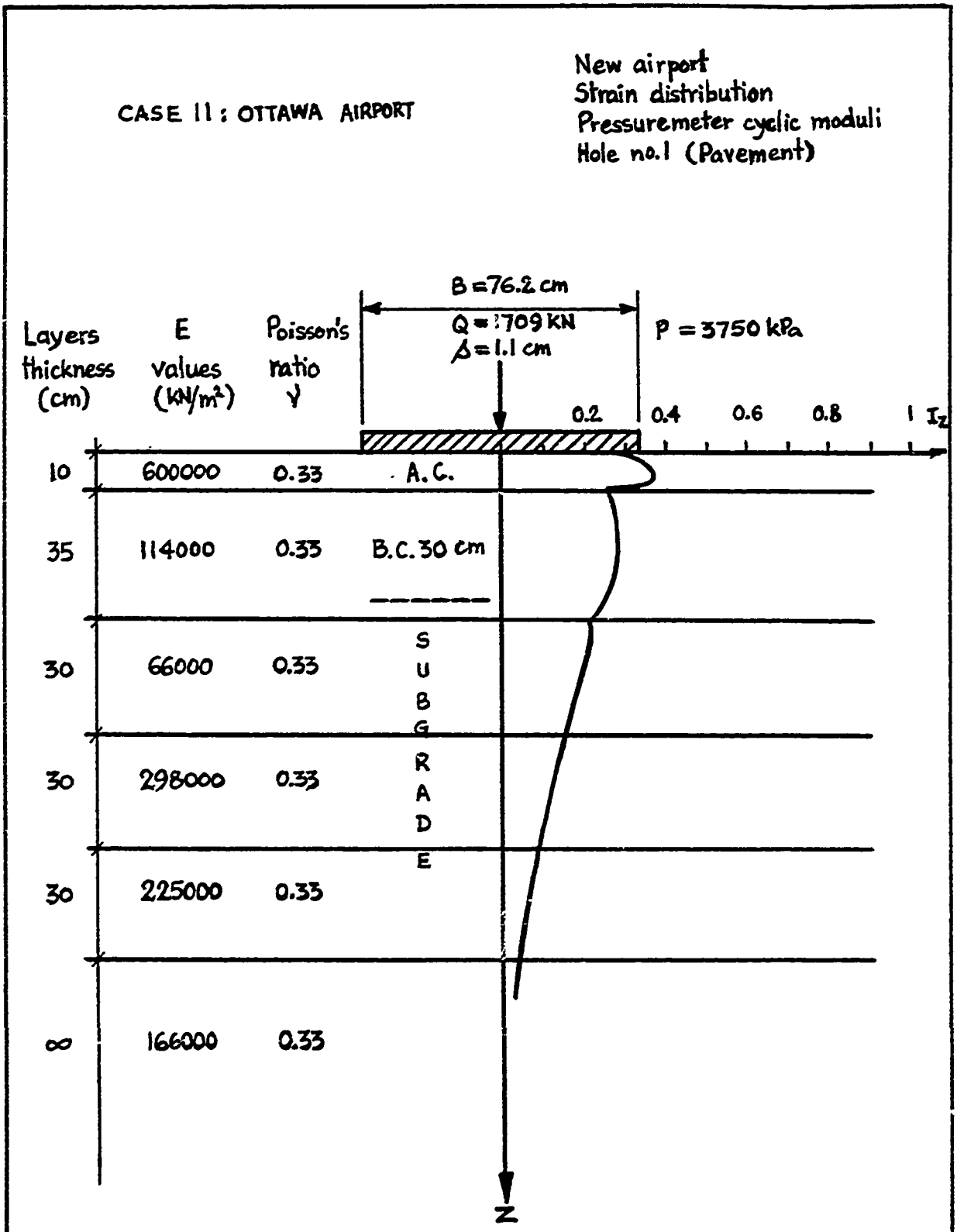

Fig. 398 - Plate test analysis. I_z curve and settlement. Ottawa: New Airport. Pressuremeter cyclic moduli. Hole No. 1. Pavement test. Asphalt modulus: 600,000 kPa.

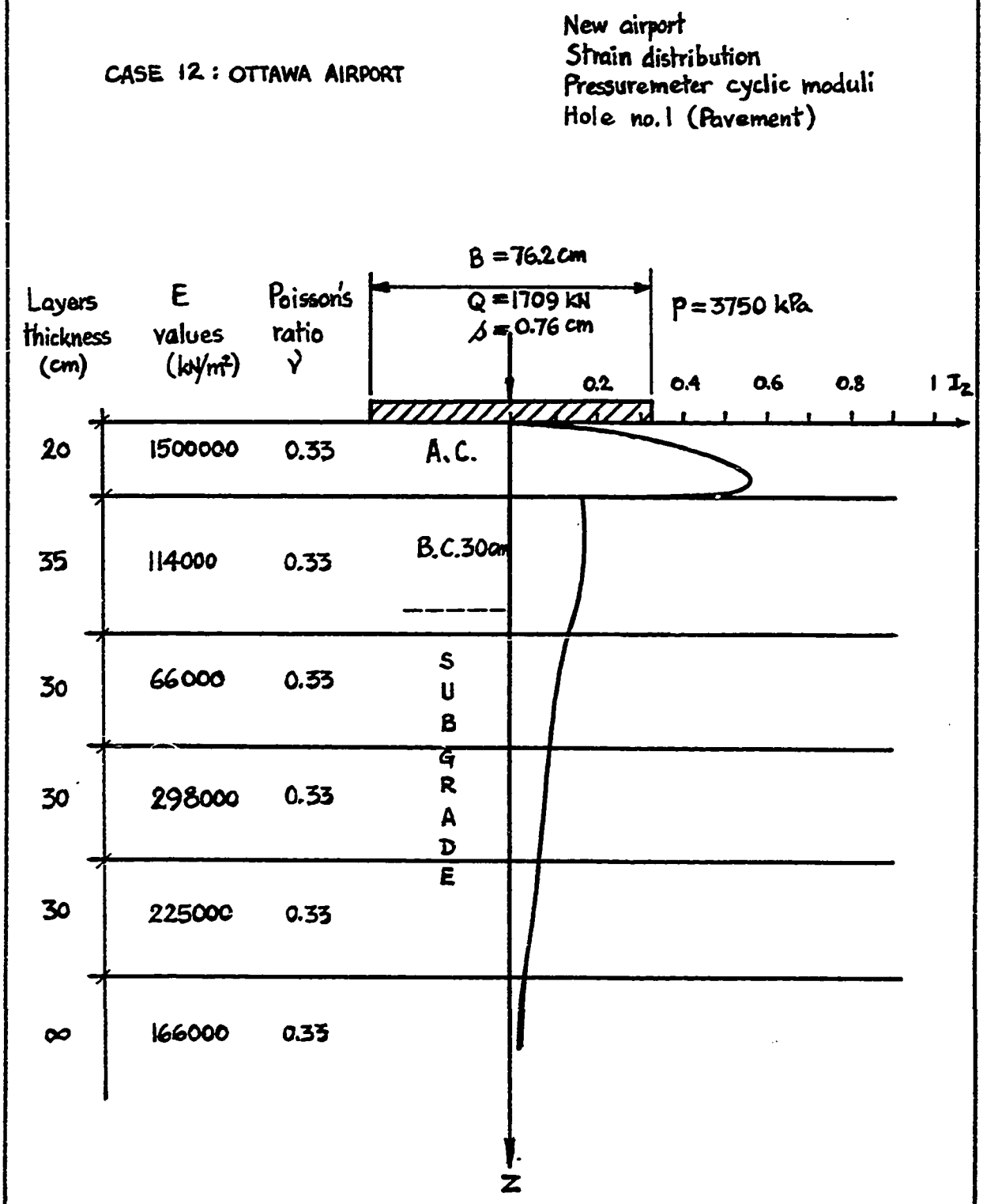

Fig. 399 - Plate test analysis. I_z curve and settlement. Ottawa: New Airport. Pressuremeter cyclic moduli. Hole No. 1. Pavement test. Asphalt thickness: 20 cm.

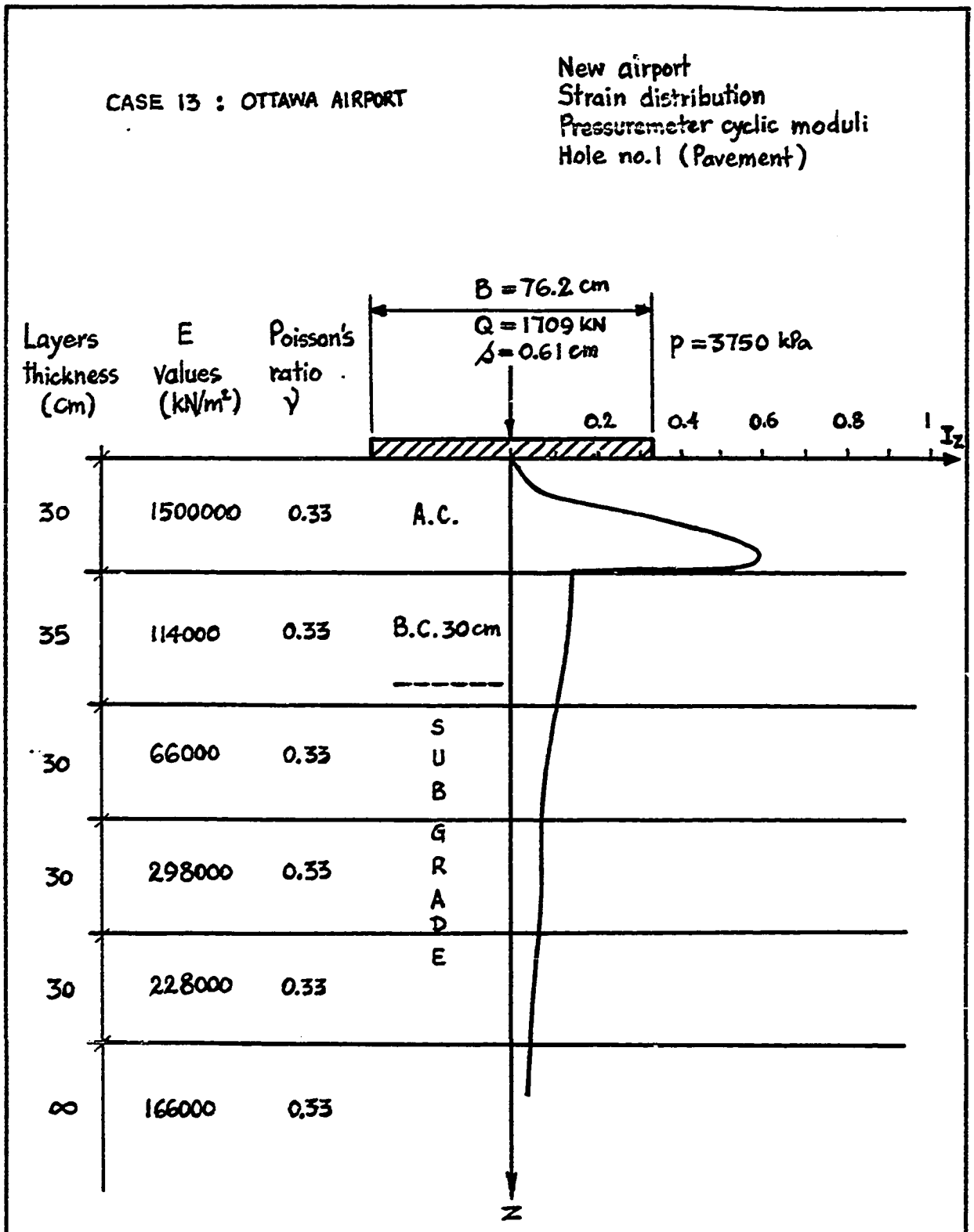

Fig. 400 - Plate test analysis. I_z curve and settlement. Ottawa: New Airport. Pressuremeter cyclic moduli. Hole No. 1. Pavement test. Asphalt thickness: 30 cm.

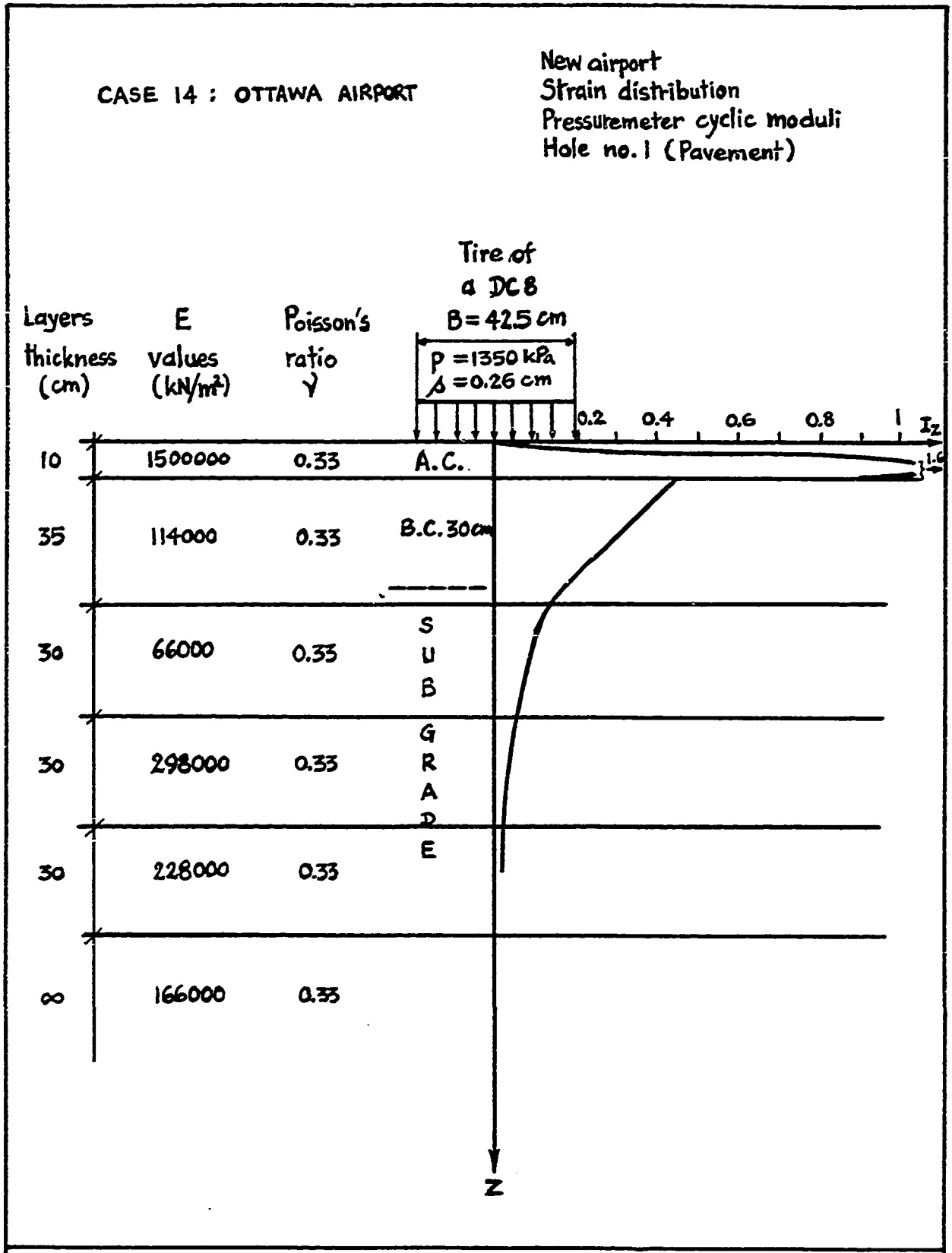

Fig. 401 - Tire load analysis. I_z curve and settlement. Ottawa: New Airport. Pressuremeter cyclic moduli. Hole No. 1. Pavement test.

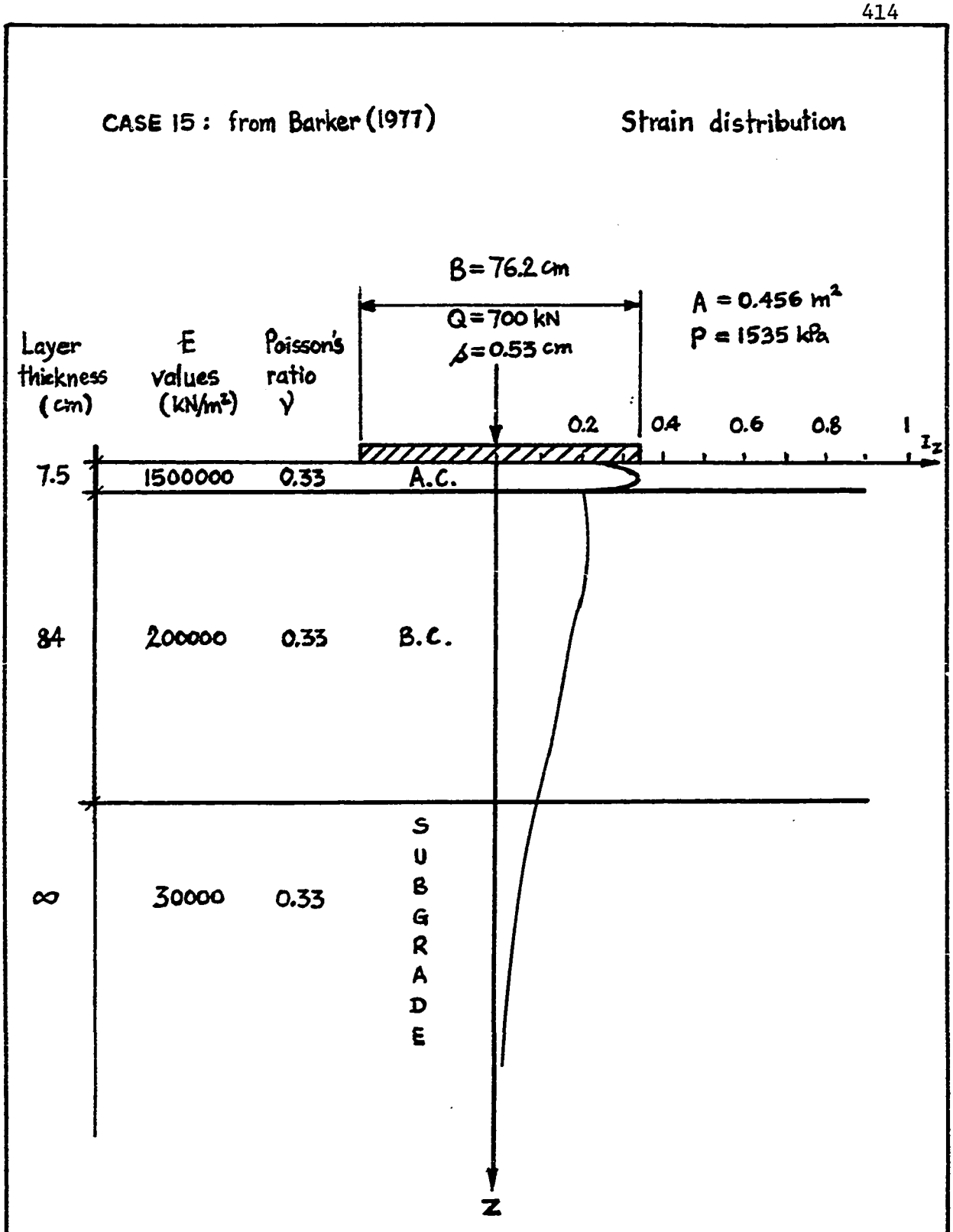

Fig. 402 - Plate test analysis. I_z curve and settlement. From Barker, 1977. Pavement test.

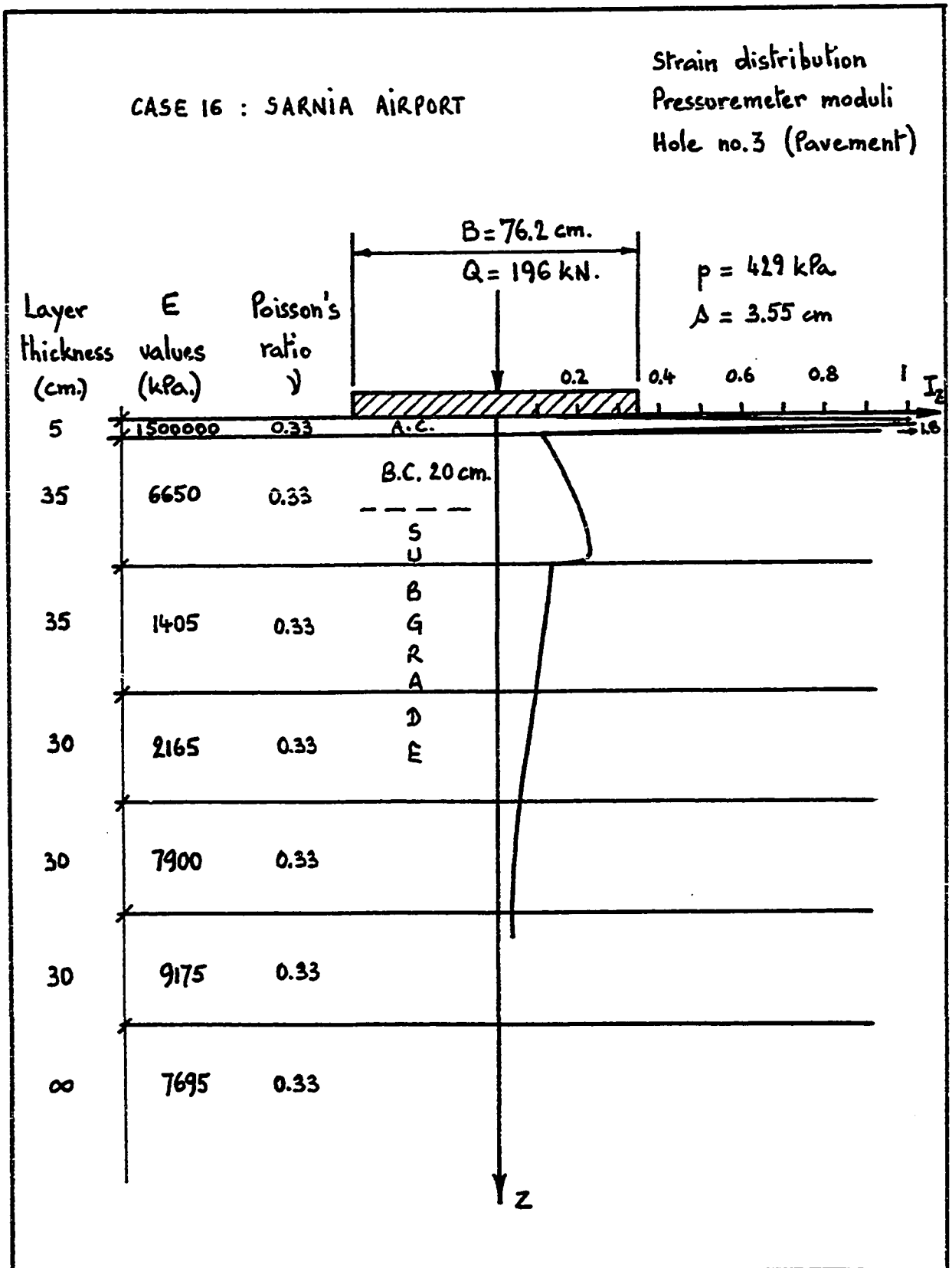

Fig. 403 - Plate test analysis. I_z curve and settlement. Sarnia. Pressuremeter moduli. Hole No. 3. Pavement test.

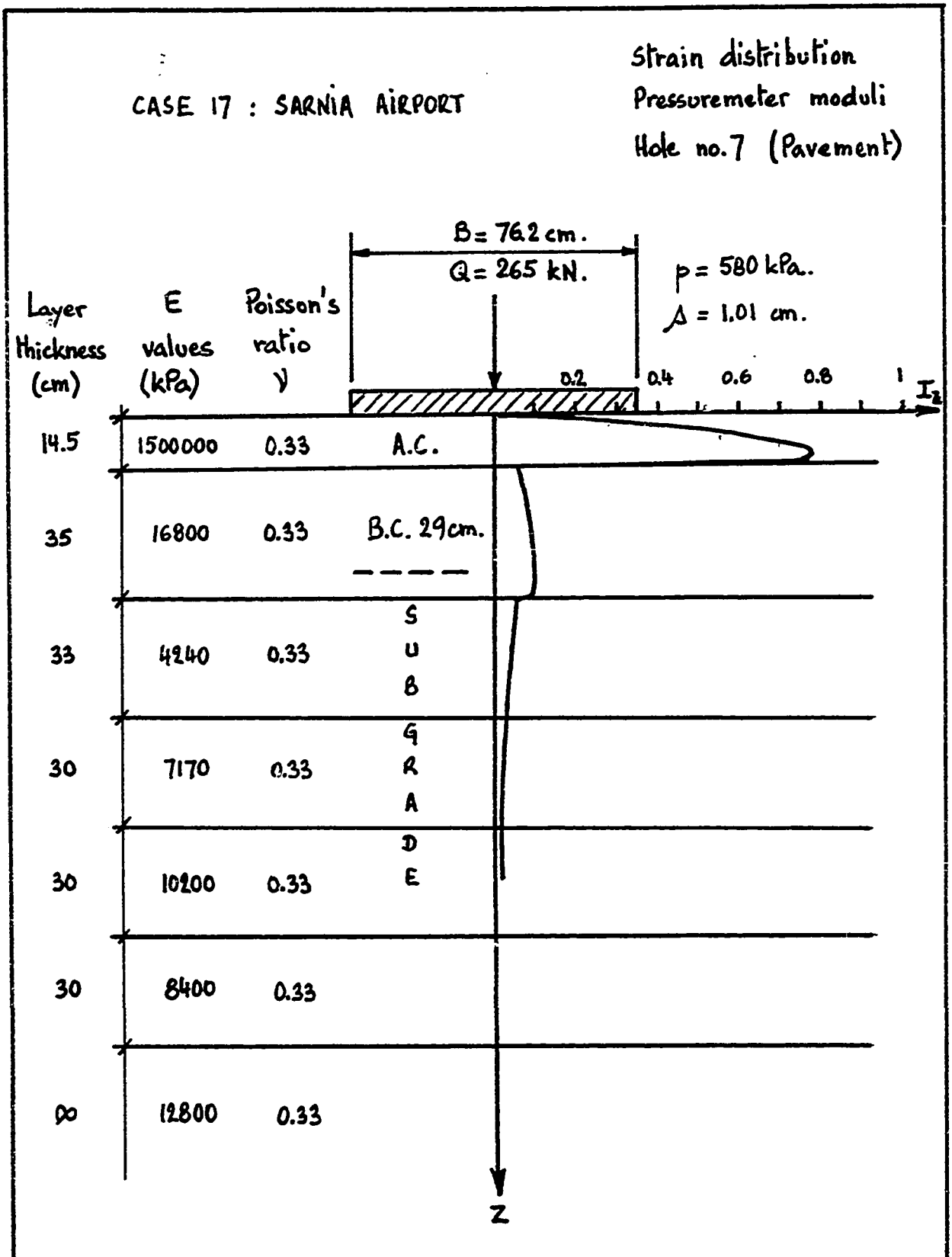

Fig. 404 - Plate test analysis. I_z curve and settlement. Sarnia. Pressuremeter moduli. Hole No. 7. Pavement test.

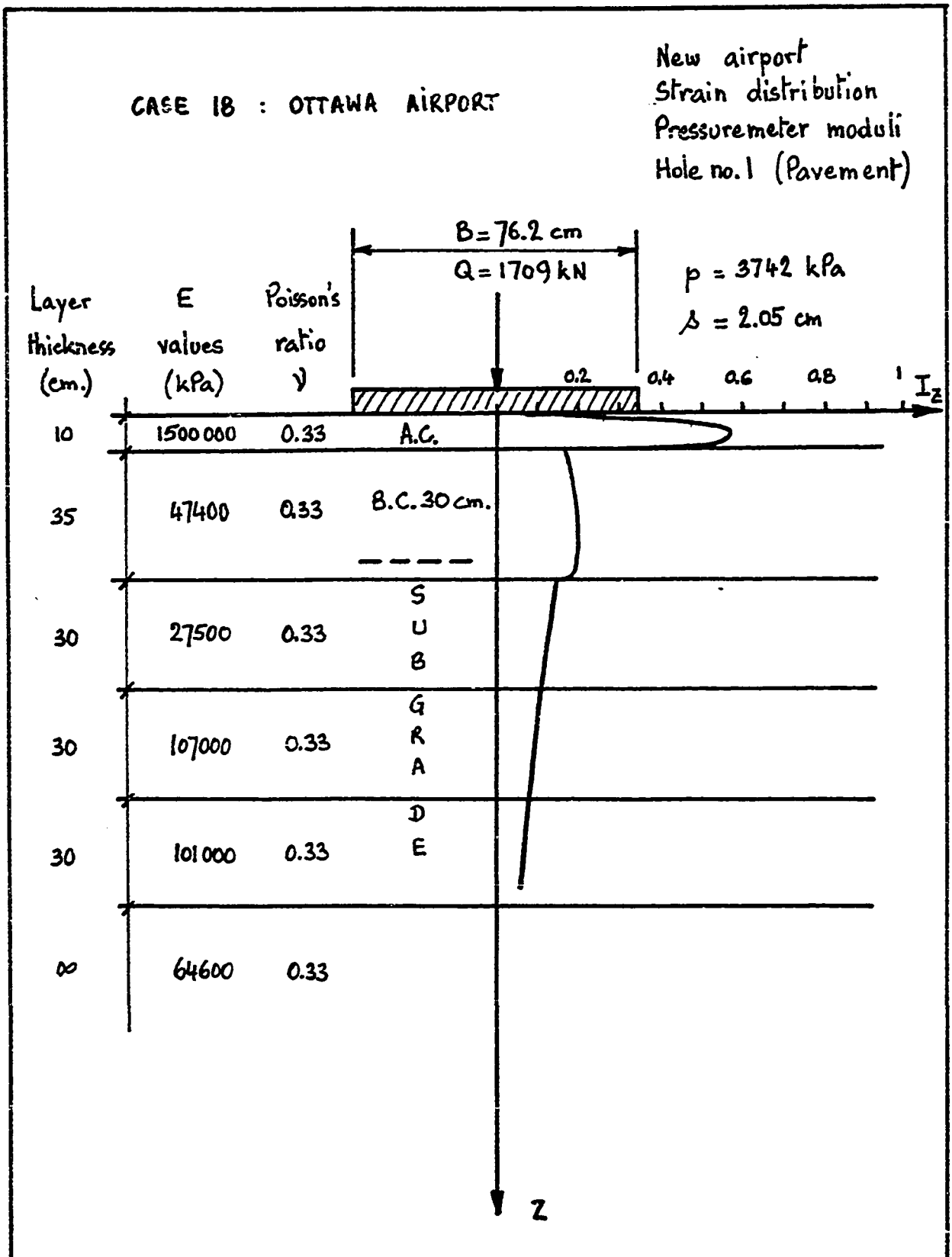

Fig. 405 - Plate test analysis. I_z curve and settlement. Ottawa: New Airport. Pressuremeter moduli. Hole No. 1. Pavement test.

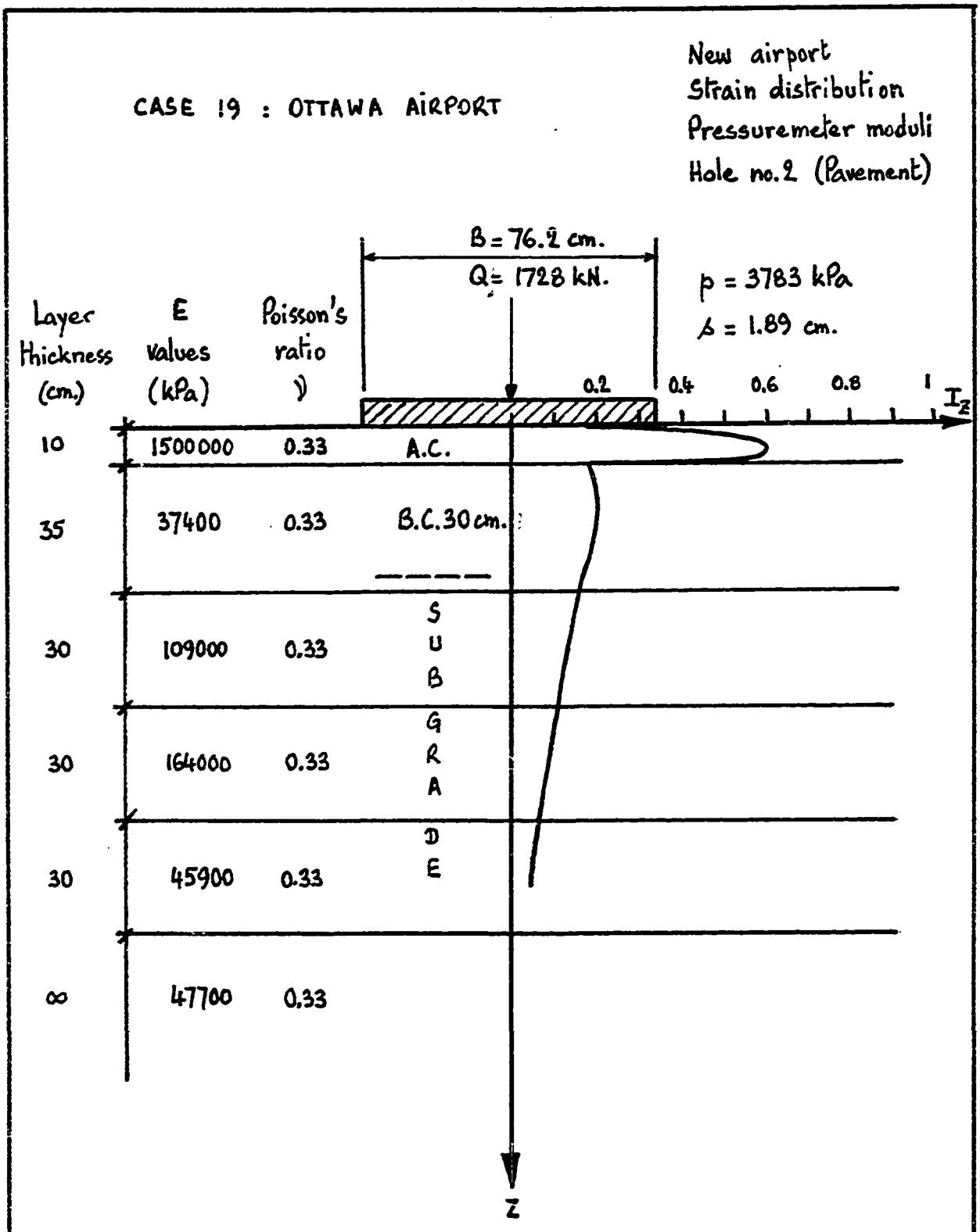

Fig. 406 - Plate test analysis. I_z curve and settlement. Ottawa: New Airport. Pressuremeter moduli. Hole No. 2. Pavement test.

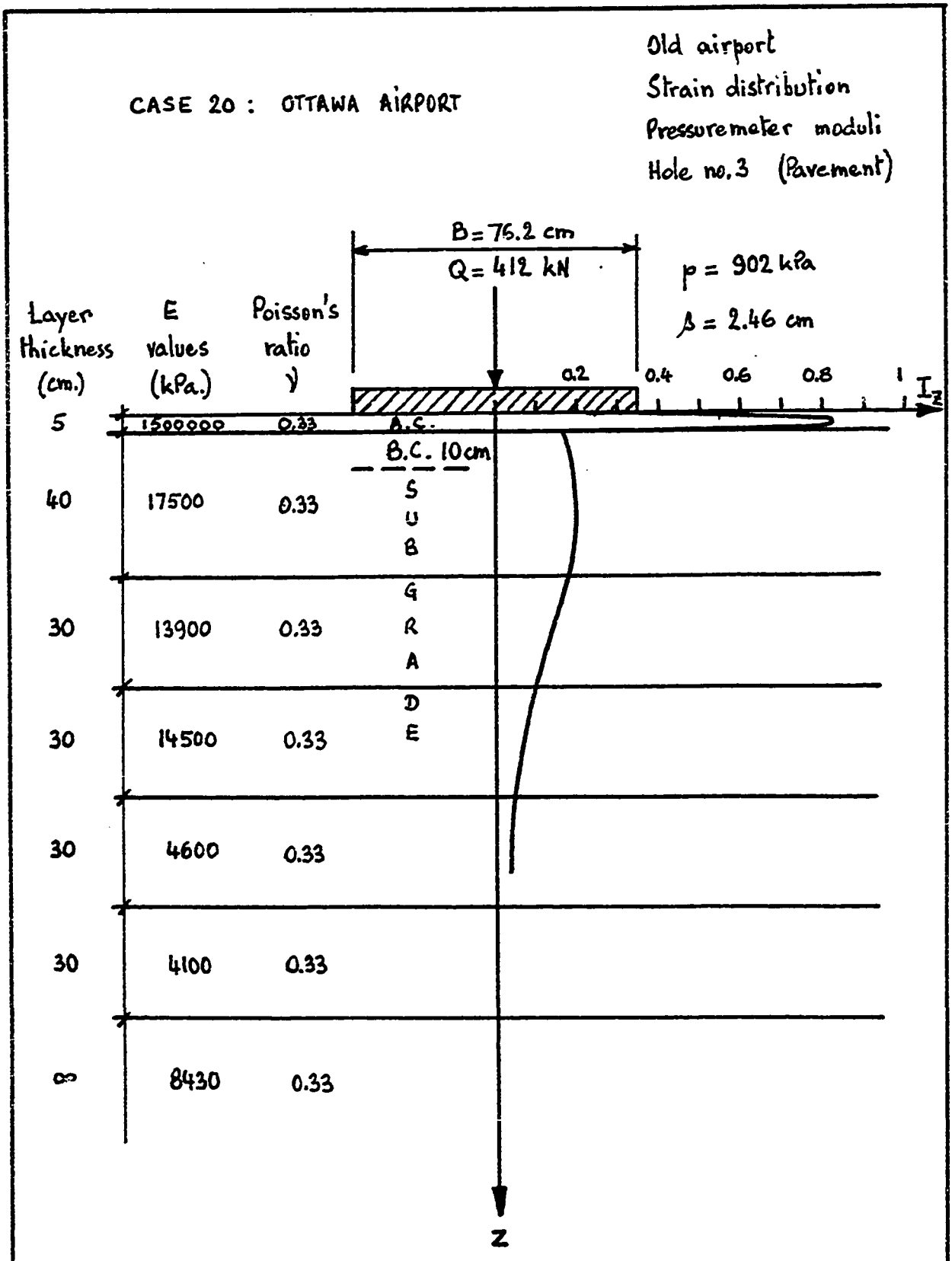

Fig. 407 - Plate test analysis. I_z curve and settlement. Ottawa: Old Airport. Pressuremeter moduli. Hole No. 3. Pavement test.

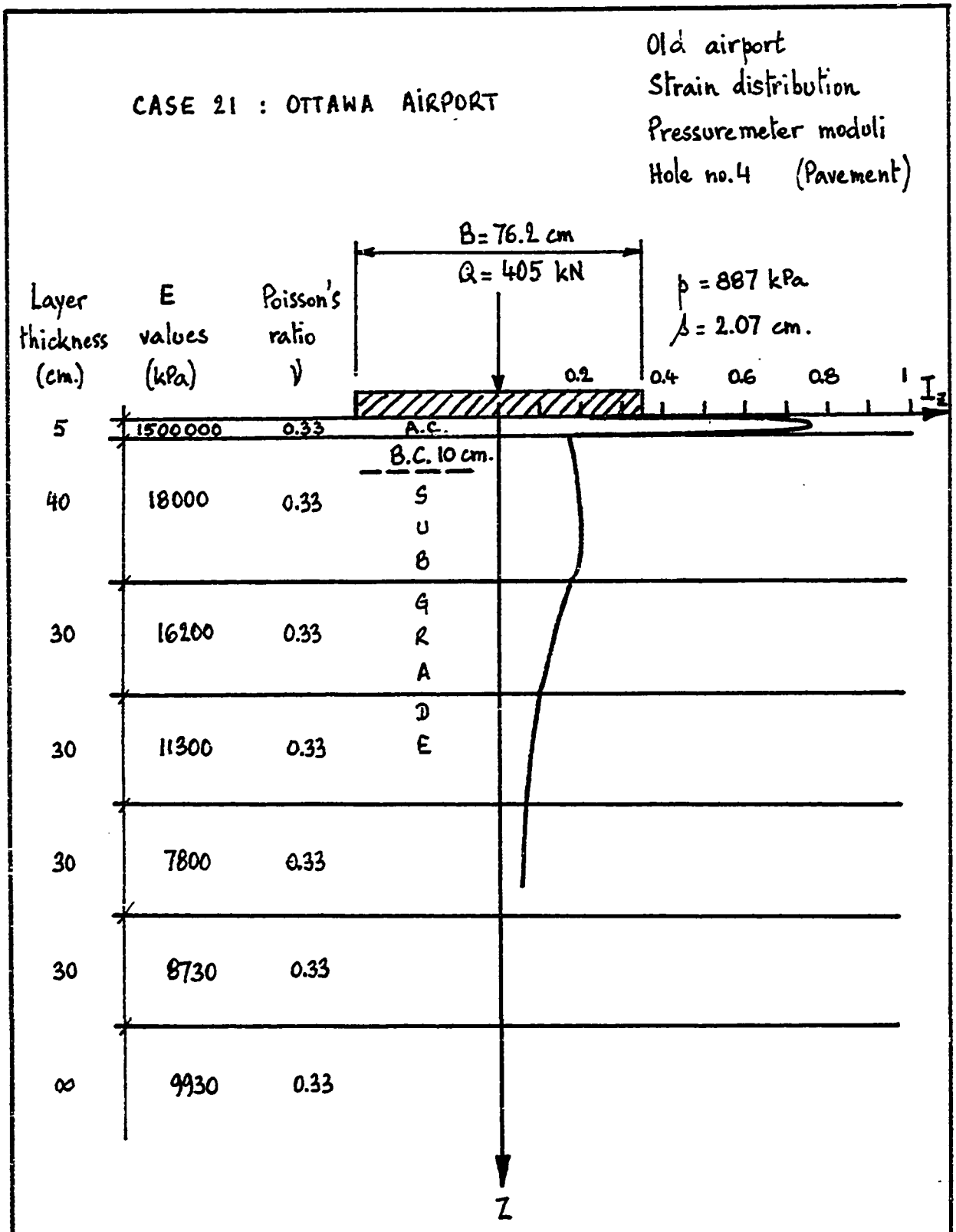

Fig.408 - Plate test analysis. I_z curve and settlement. Ottawa: Old Airport. Pressuremeter moduli. Hole No. 4. Pavement test.

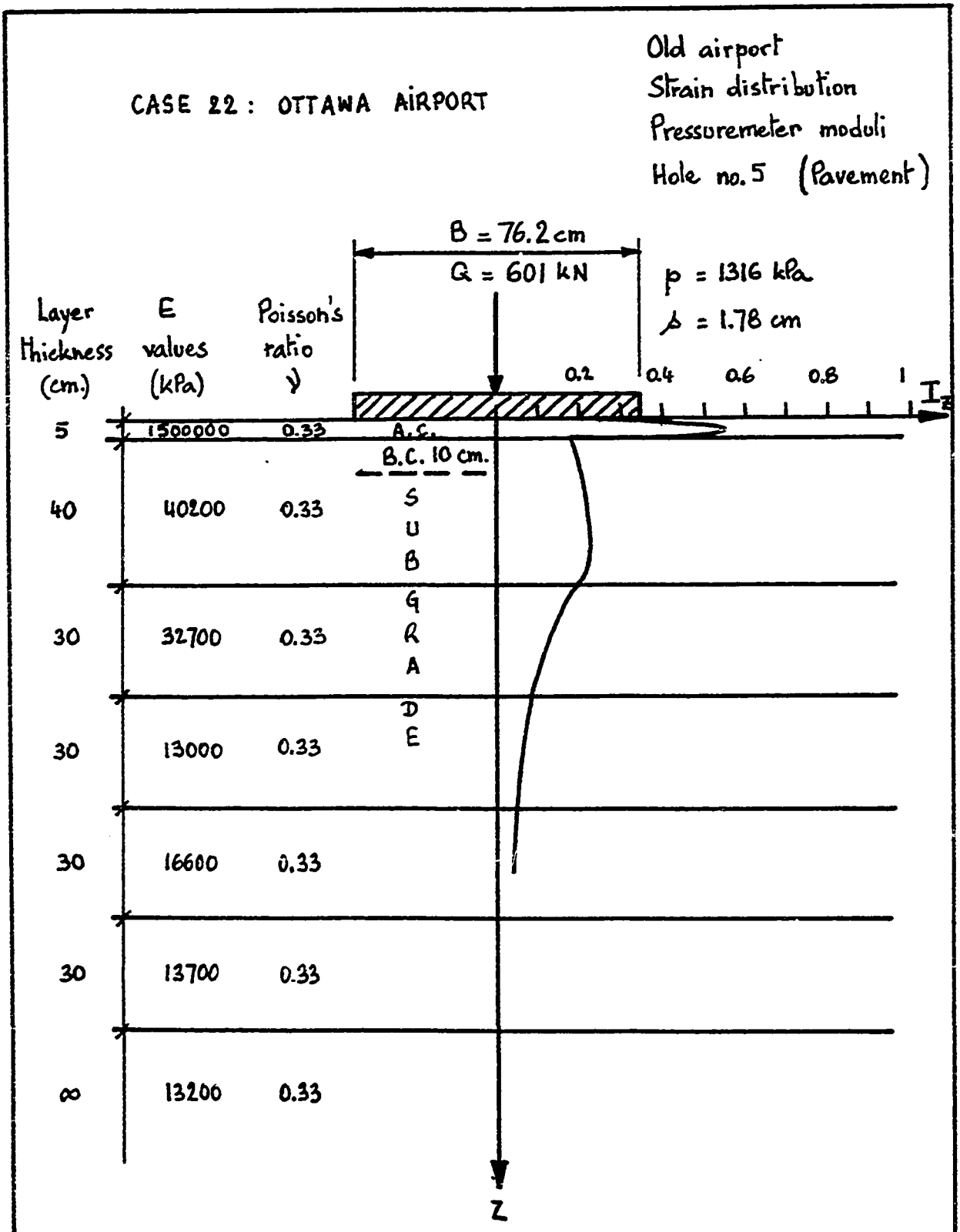

Fig. 409 - Plate test analysis. I_z curve and settlement. Ottawa: Old Airport. Pressuremeter moduli. Hole No. 5. Pavement test.

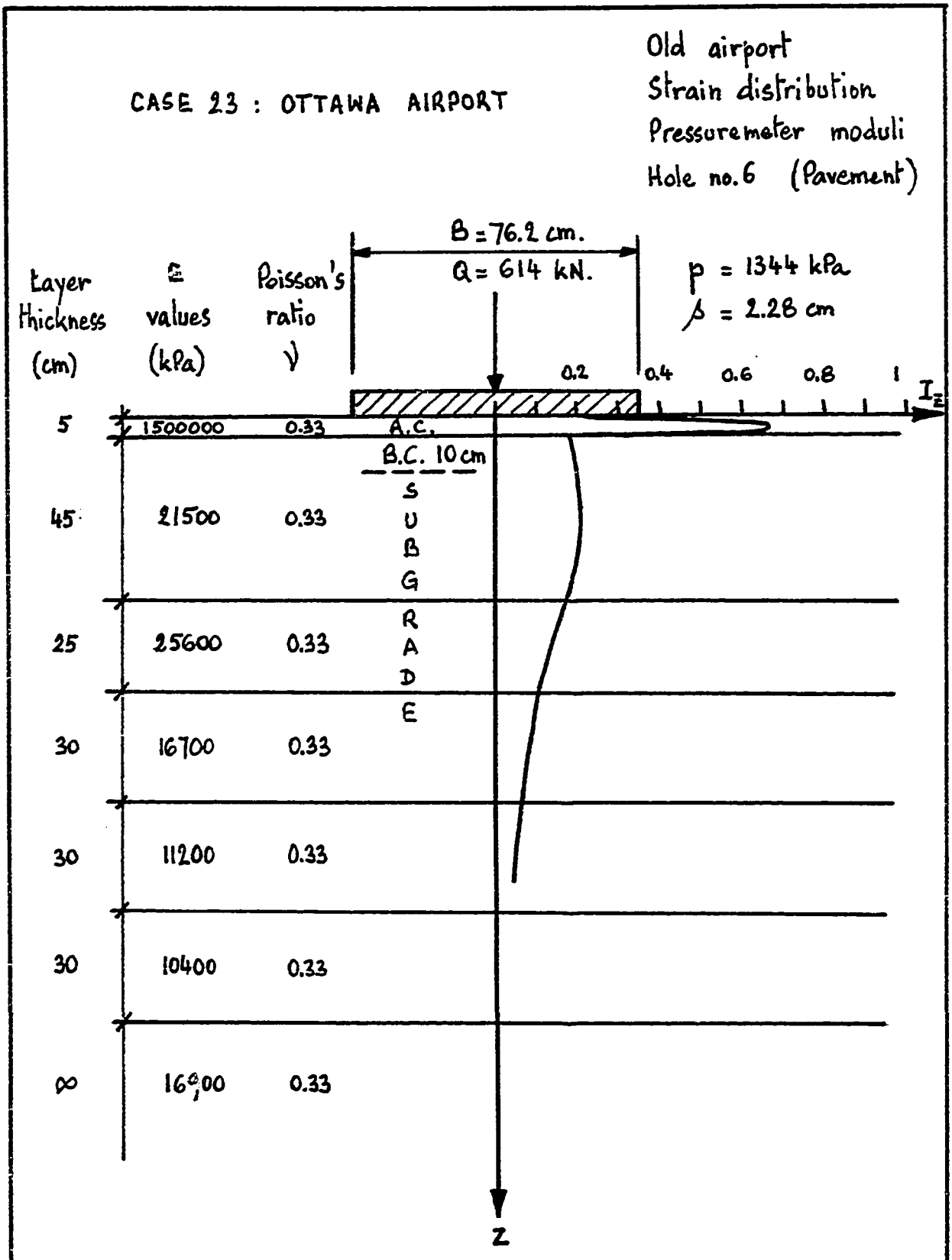

Fig. 410 - Plate test analysis. I_z curve and settlement. Ottawa: Old Airport. Pressuremeter moduli. Hole No. 6. Pavement test.

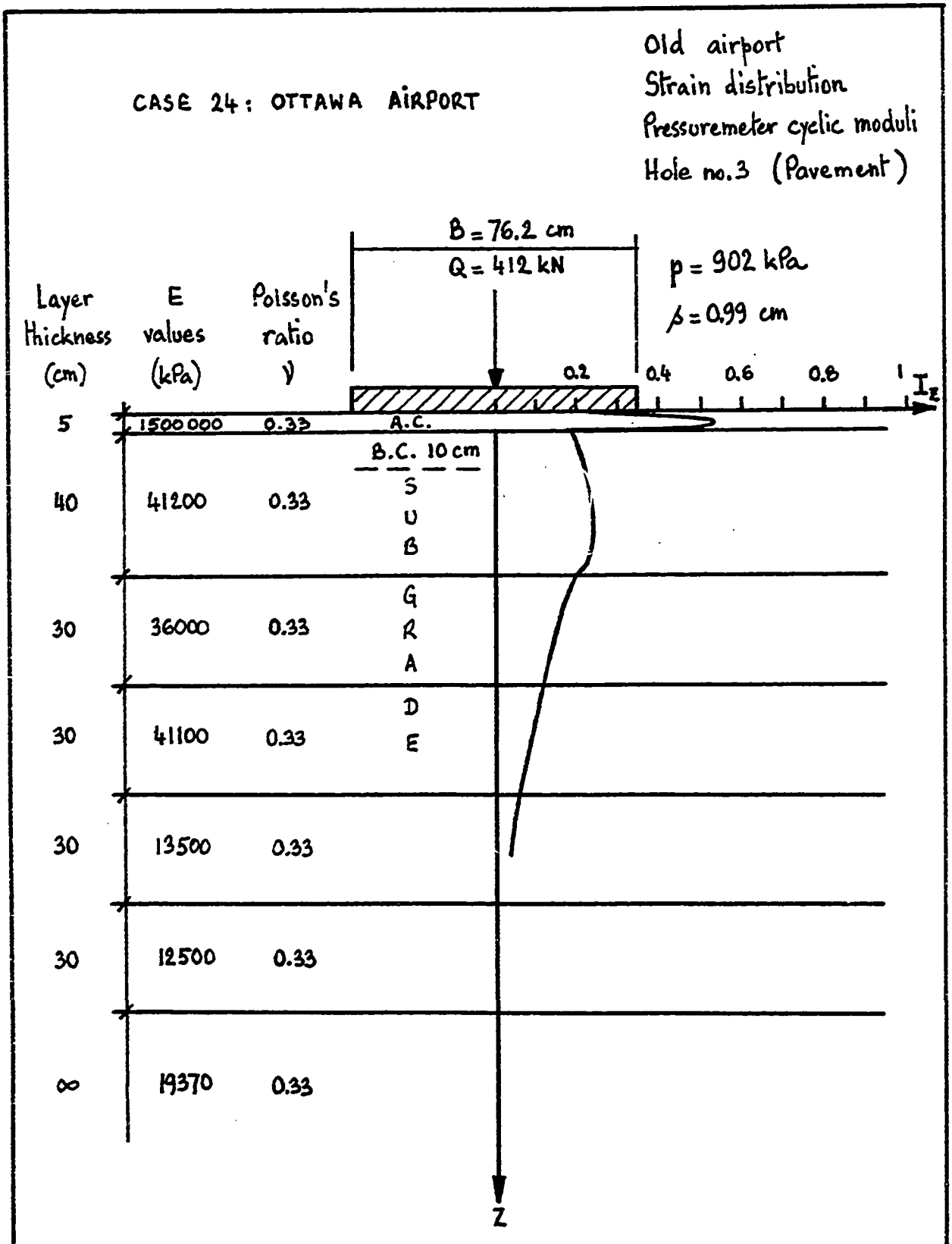

Fig. 411 – Plate test analysis. I_z curve and settlement. Ottawa: Old Airport. Pressuremeter cyclic moduli. Hole No. 3. Pavement test.

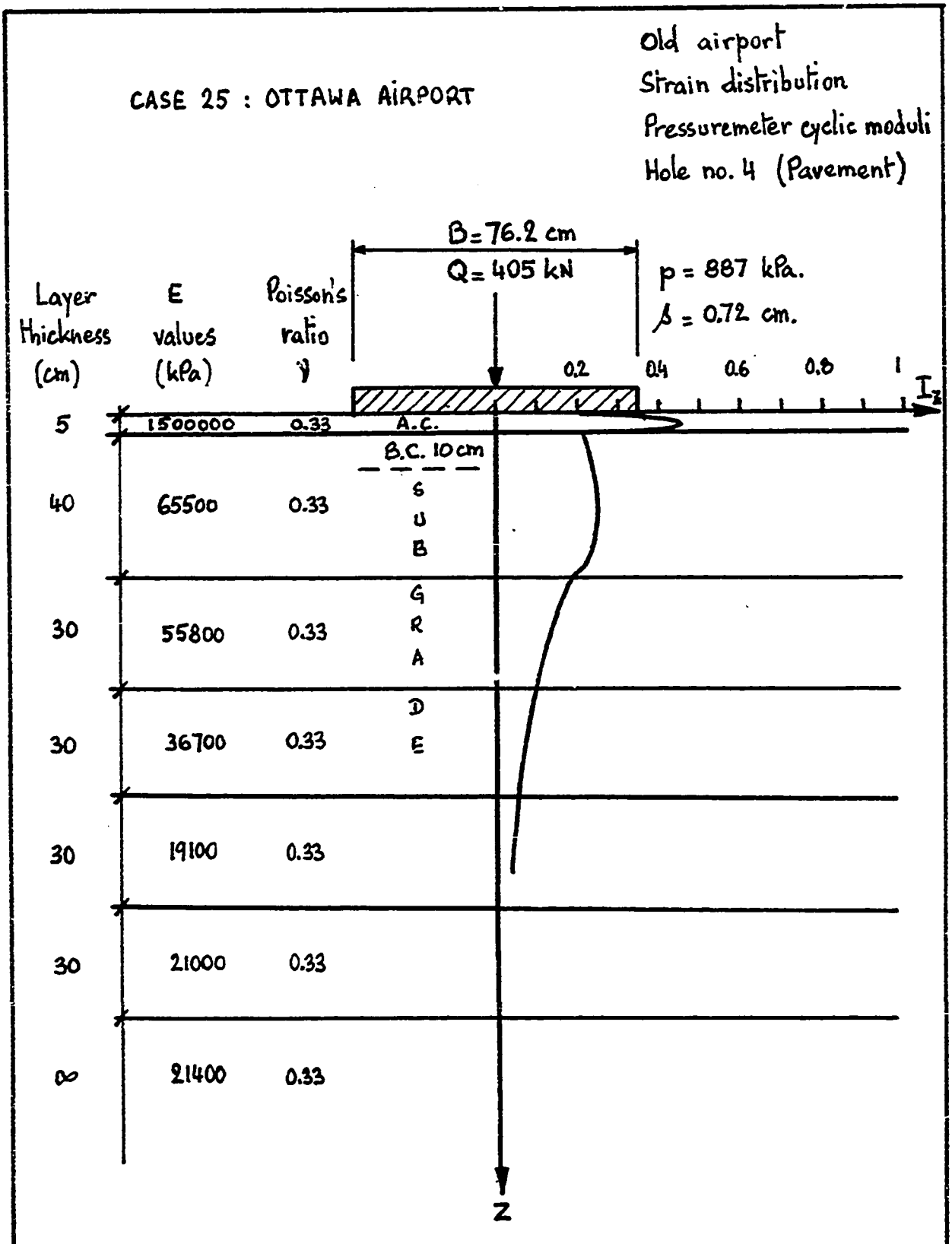

Fig.412 - Plate test analysis. I_z curve and settlement. Ottawa: Old Airport. Pressuremeter cyclic moduli. Hole No. 4. Pavement test.

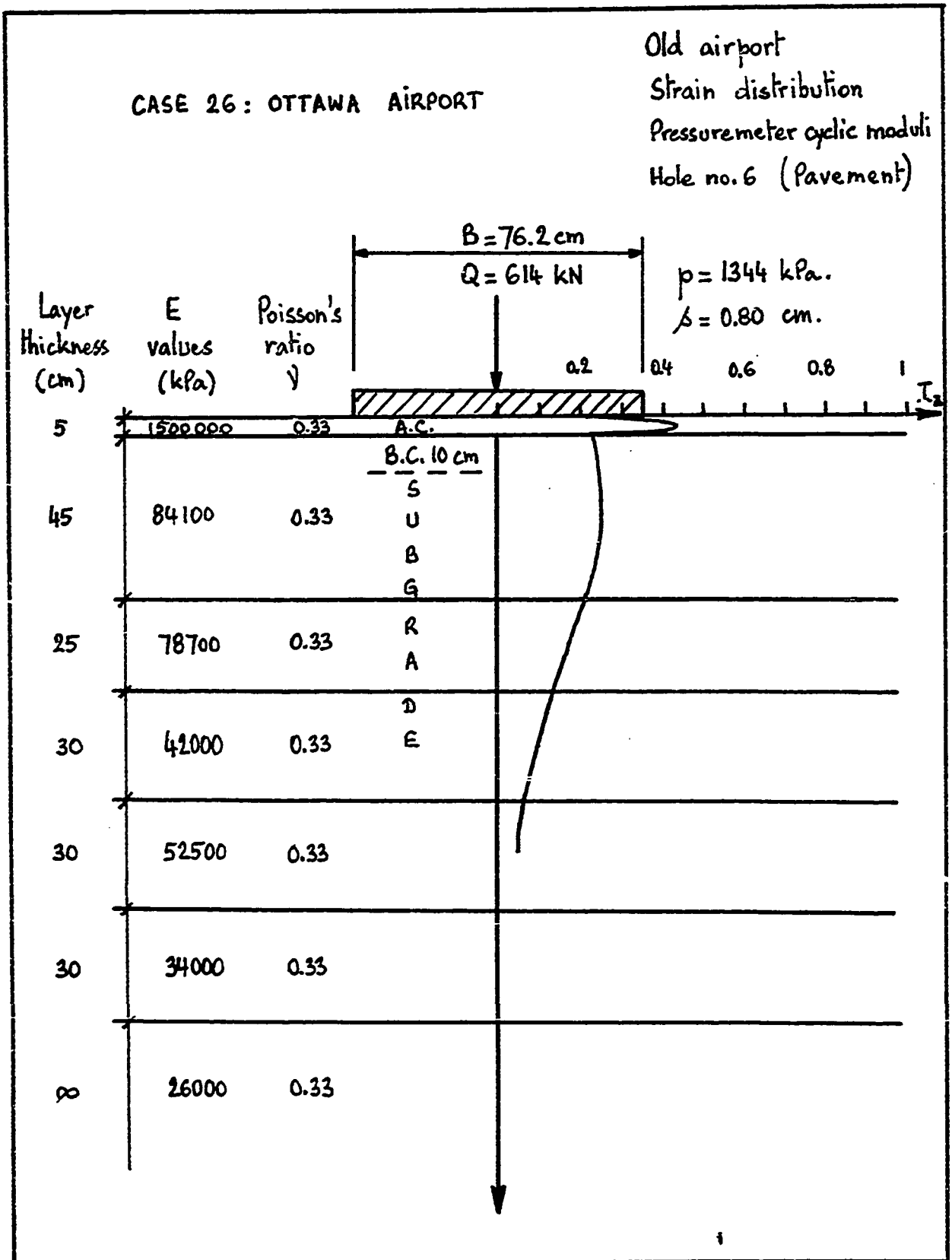

Fig. 413 - Plate test analysis. I_z curve and settlement. Ottawa: Old Airport. Pressuremeter cyclic moduli. Hole No. 6. Pavement test.

APPENDIX G

RESULTS OF THE MULTILAYER ELASTIC PAVEMENT ANALYSIS

CASE 1 : SARNIA AIRPORT

Pressuremeter moduli
No overlay
Design plane : Convair 440
$\varepsilon_H = 2.92 \times 10^{-3}$
$\varepsilon_V = 12.7 \times 10^{-3}$
$\Delta = 1.1$ cm

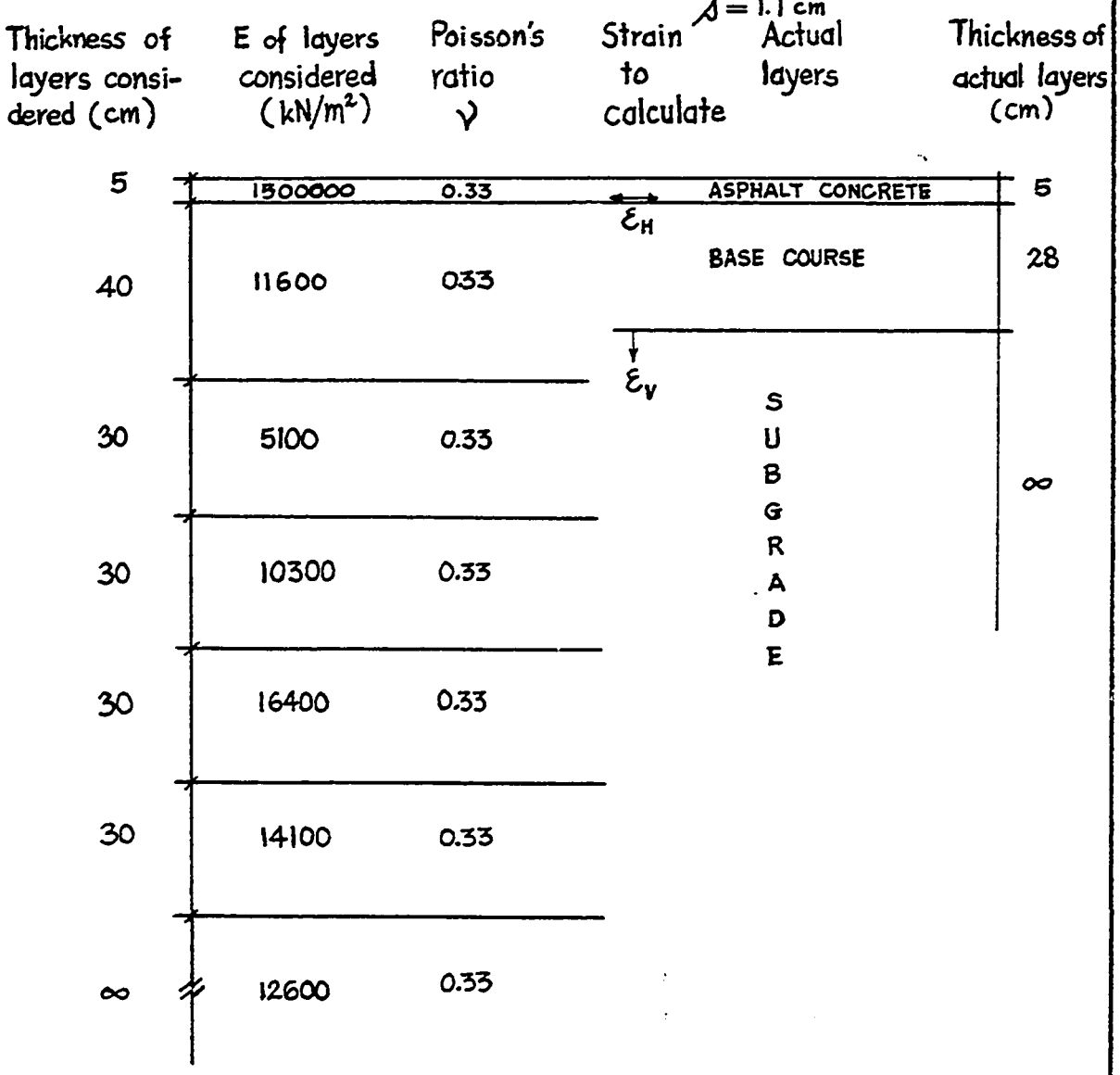

Fig. 414 - Multilayer elastic analysis - Sarnia. Pressuremeter moduli. No overlay. Asphalt modulus: 1500000 kPa.

CASE 2 : SARNIA AIRPORT

Pressuremeter moduli
Overlay
Design plane: convair 440
$\varepsilon_H = 1.01 \times 10^{-3}$
$\varepsilon_V = 4.81 \times 10^{-3}$
$\Delta = 0.52$ cm

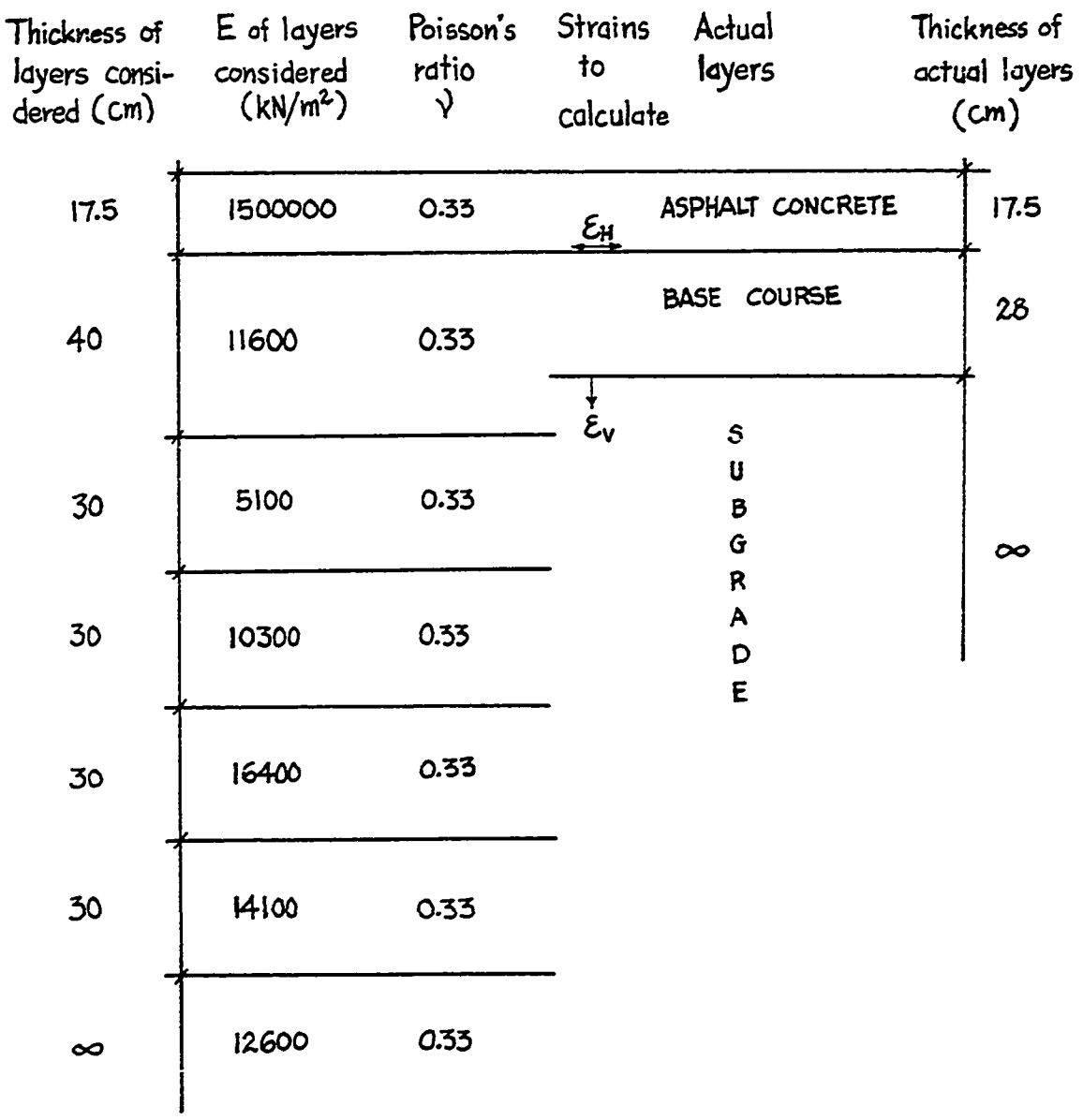

Fig. 415 - Multilayer elastic analysis - Sarnia. Pressuremeter moduli. Overlay. Asphalt modulus: 1500000 kPa.

CASE 3 : SARNIA AIRPORT

Pressuremeter cyclic moduli
No overlay
Design plane : convair 440
$\varepsilon_H = 1.91 \times 10^{-3}$
$\varepsilon_V = 6.89 \times 10^{-3}$
$\Delta = 0.61$ cm

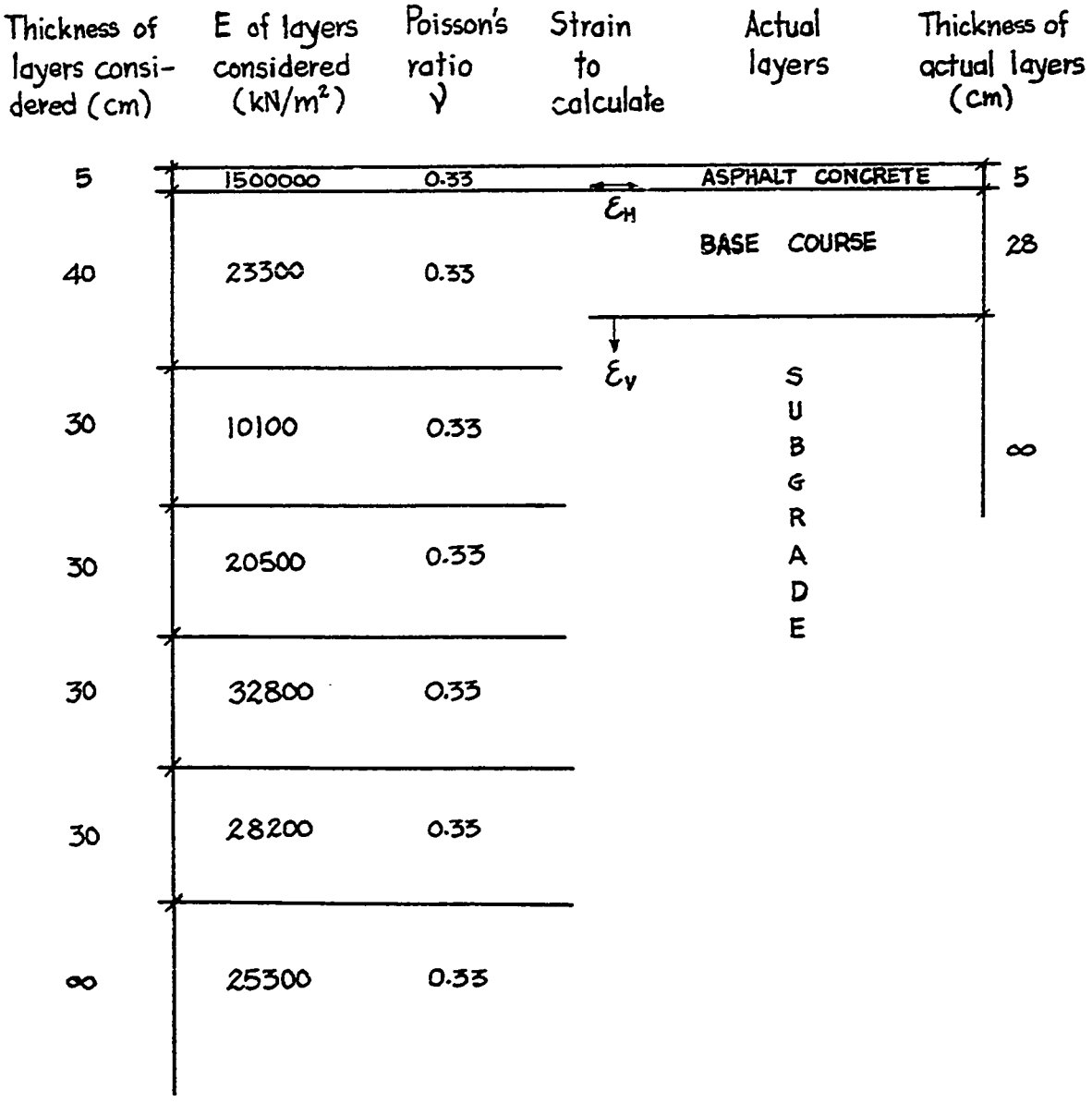

Fig. 416 - Multilayer elastic analysis - Sarnia. Pressuremeter cyclic moduli. No overlay. Asphalt modulus: 1500000 kPa.

CASE 4: SARNIA AIRPORT

Pressuremeter cyclic moduli
No overlay
Design plane: convair 440
$\varepsilon_H = 1.05 \times 10^{-3}$
$\varepsilon_V = 5.9 \times 10^{-3}$
$\Delta = 0.50$ cm

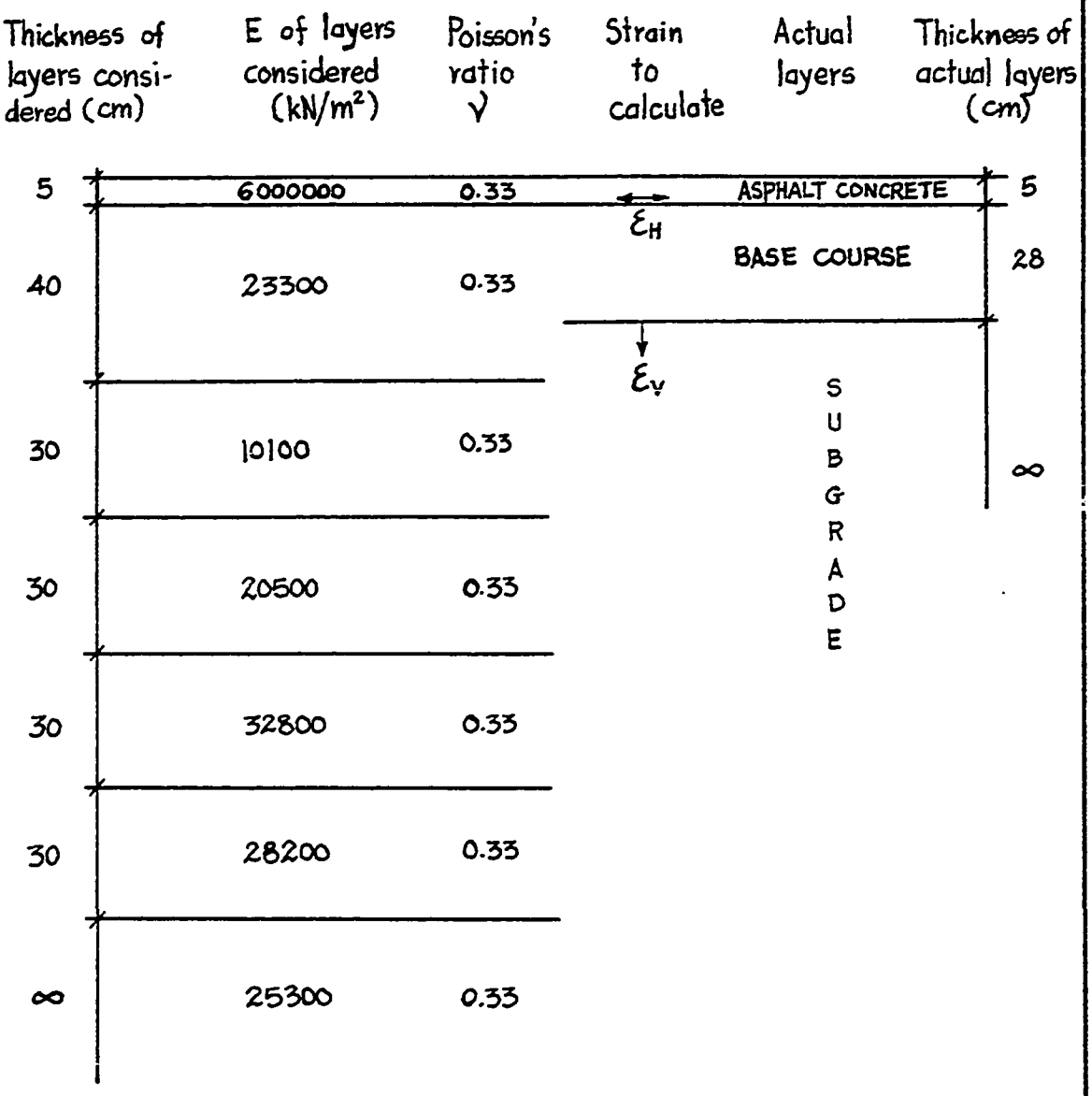

Fig. 417 - Multilayer elastic analysis - Sarnia. Pressuremeter cyclic moduli. No overlay. Asphalt modulus: 6000000 kPa.

CASE 5 : SARNIA AIRPORT

Pressuremeter cyclic moduli
Overlay
Design plane: convair 440
$\varepsilon_H = 0.81 \times 10^{-3}$
$\varepsilon_V = 3.1 \times 10^{-3}$
$\delta = 0.31$ cm

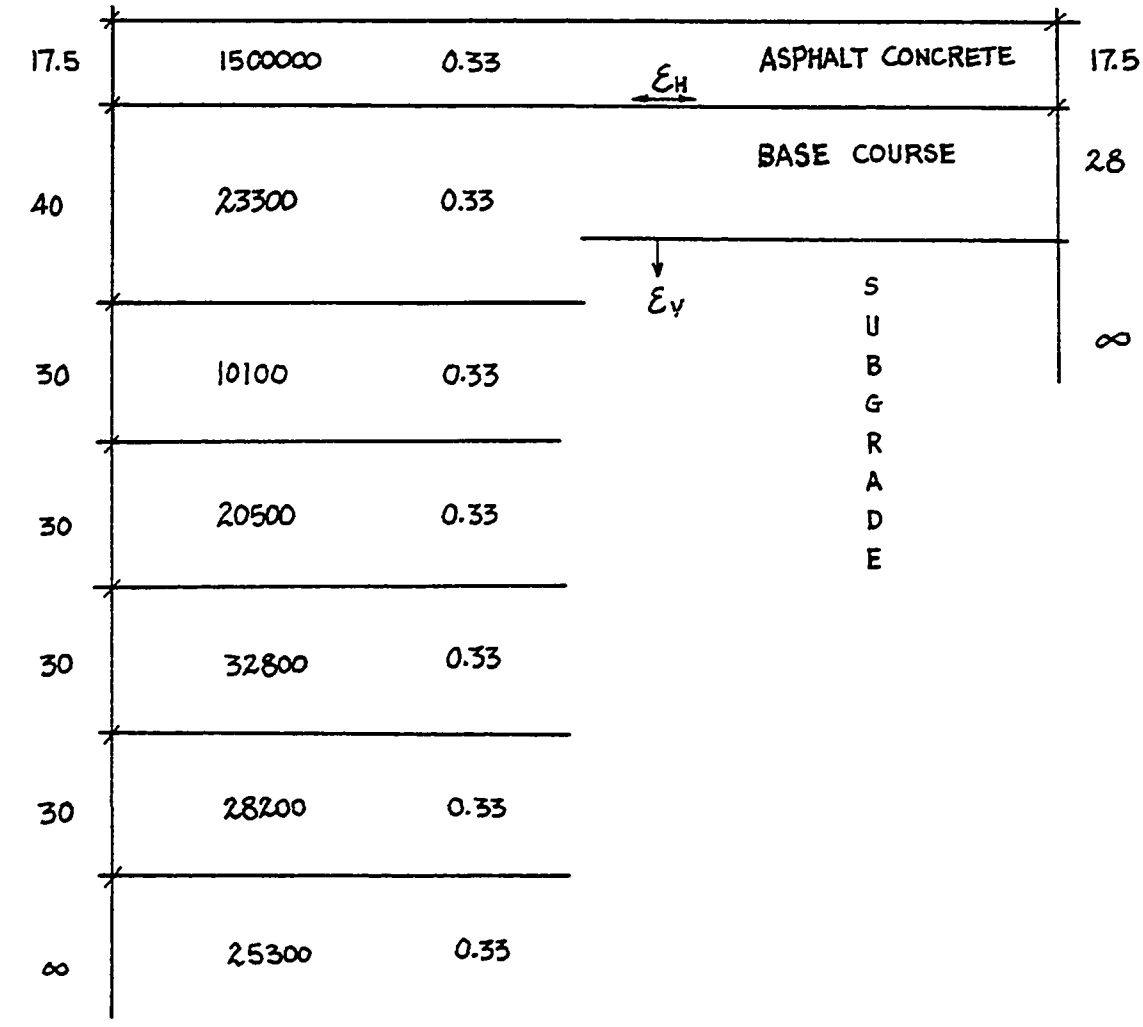

Fig. 418 - Multilayer elastic analysis - Sarnia. Pressuremeter cyclic moduli. Overlay. Asphalt modulus: 1500000 kPa.

CASE 6 : SARNIA AIRPORT

Pressuremeter cyclic moduli
Overlay
Design plane : convair 440
$\varepsilon_H = 0.3 \times 10^{-3}$
$\varepsilon_V = 1.8 \times 10^{-3}$
$\Delta = 0.21$ cm

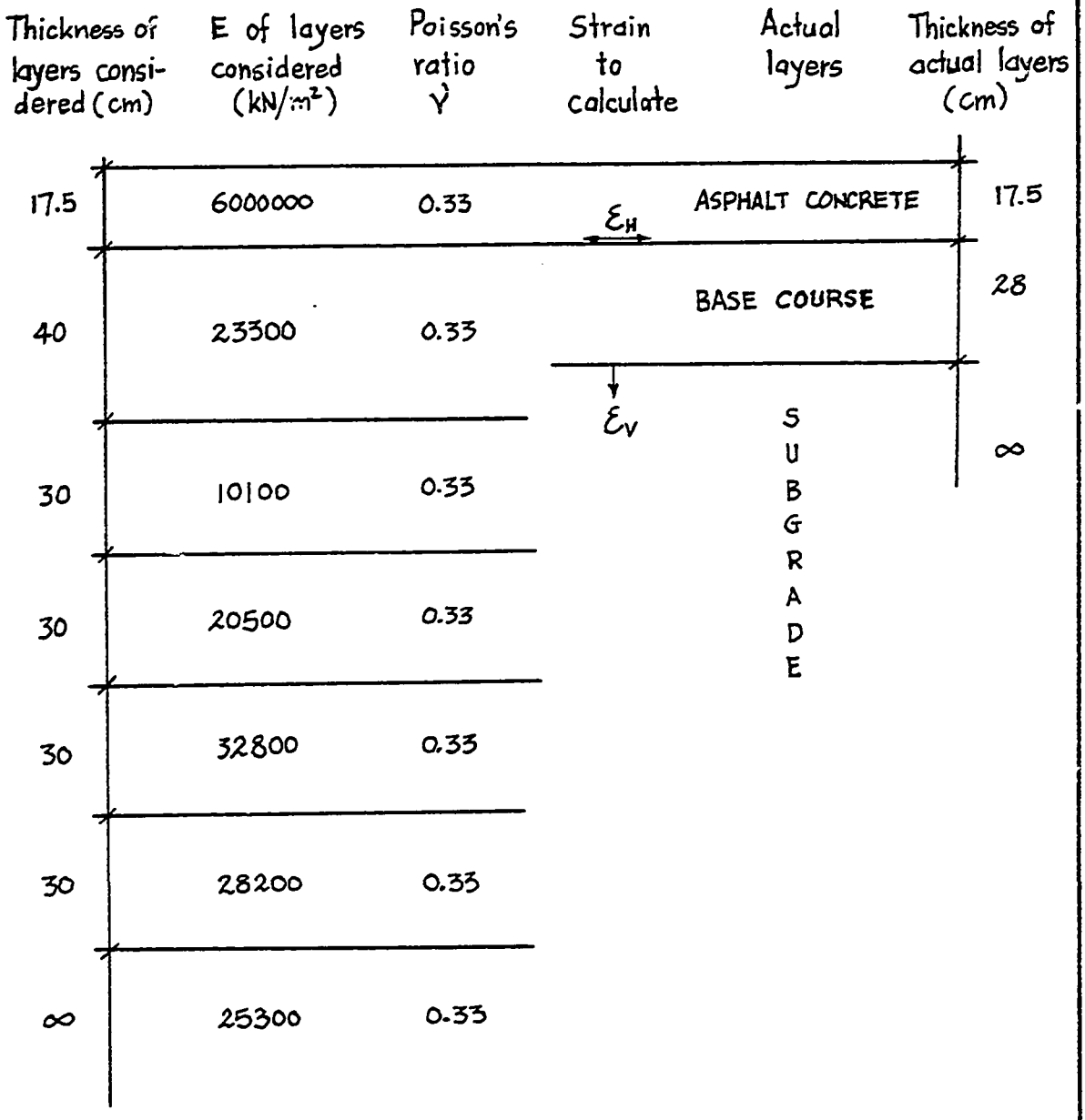

Fig. 419 - Multilayer elastic analysis - Sarnia. Pressuremeter cyclic moduli. Overlay. Asphalt modulus: 6000000 kPa.

CASE 7 : SARNIA AIRPORT

Pressuremeter cyclic moduli
Overlay
Design plane : convair 440
$\varepsilon_H = 0.28 \times 10^{-3}$
$\varepsilon_V = 1.71 \times 10^{-3}$
$\delta = 0.2$ cm

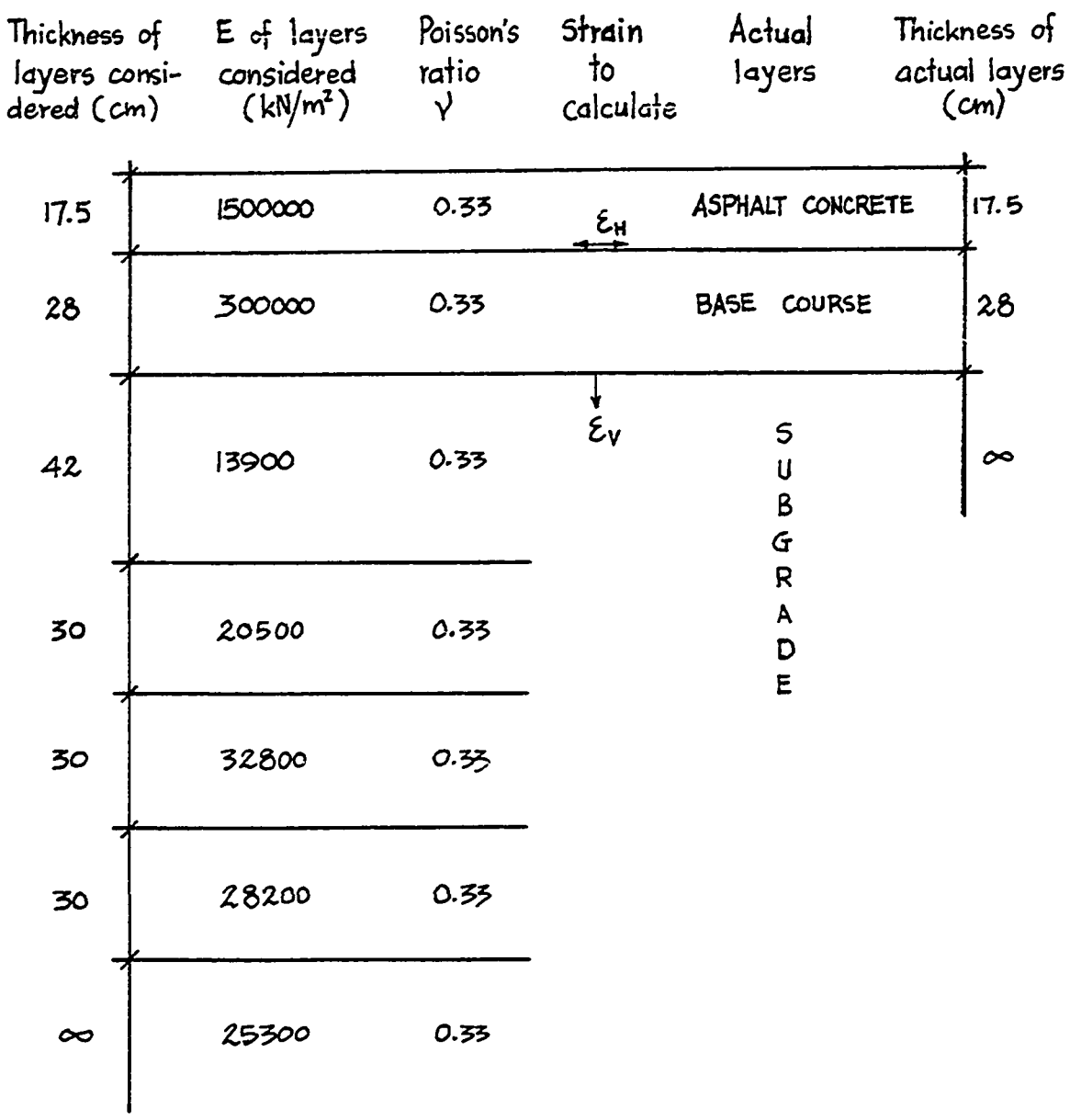

Fig. 420 - Multilayer elastic analysis - Sarnia. Pressuremeter cyclic moduli. Overlay. Asphalt modulus: 1500000 kPa. Base modulus: 300000 kPa.

CASE 9 : OTTAWA AIRPORT

New airport
Pressuremeter cyclic moduli
Design plane : DC8-63
$\varepsilon_H = 0.9 \times 10^{-3}$
$\varepsilon_V = 2.29 \times 10^{-3}$
$\Delta = 0.31$ cm

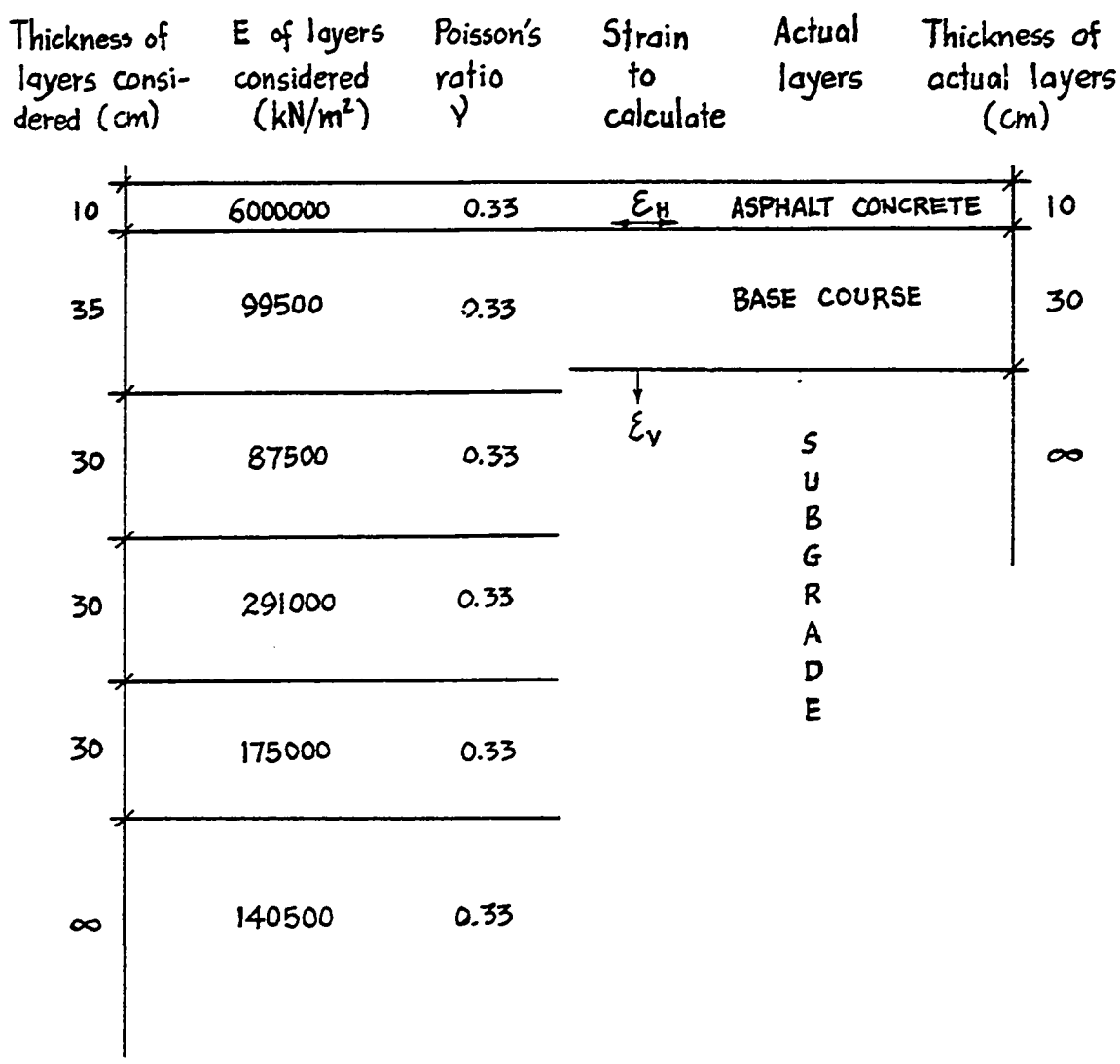

Fig. 421 - Multilayer elastic analysis - Ottawa: New airport. Pressuremeter cyclic moduli. Asphalt modulus: 1500000 kPa.

CASE 10 : OTTAWA AIRPORT

New airport
Pressuremeter cyclic moduli
Design plane : DC 8-63
$\varepsilon_H = 0.66 \times 10^{-3}$
$\varepsilon_V = 2.86 \times 10^{-3}$
$\delta = 0.28$ cm

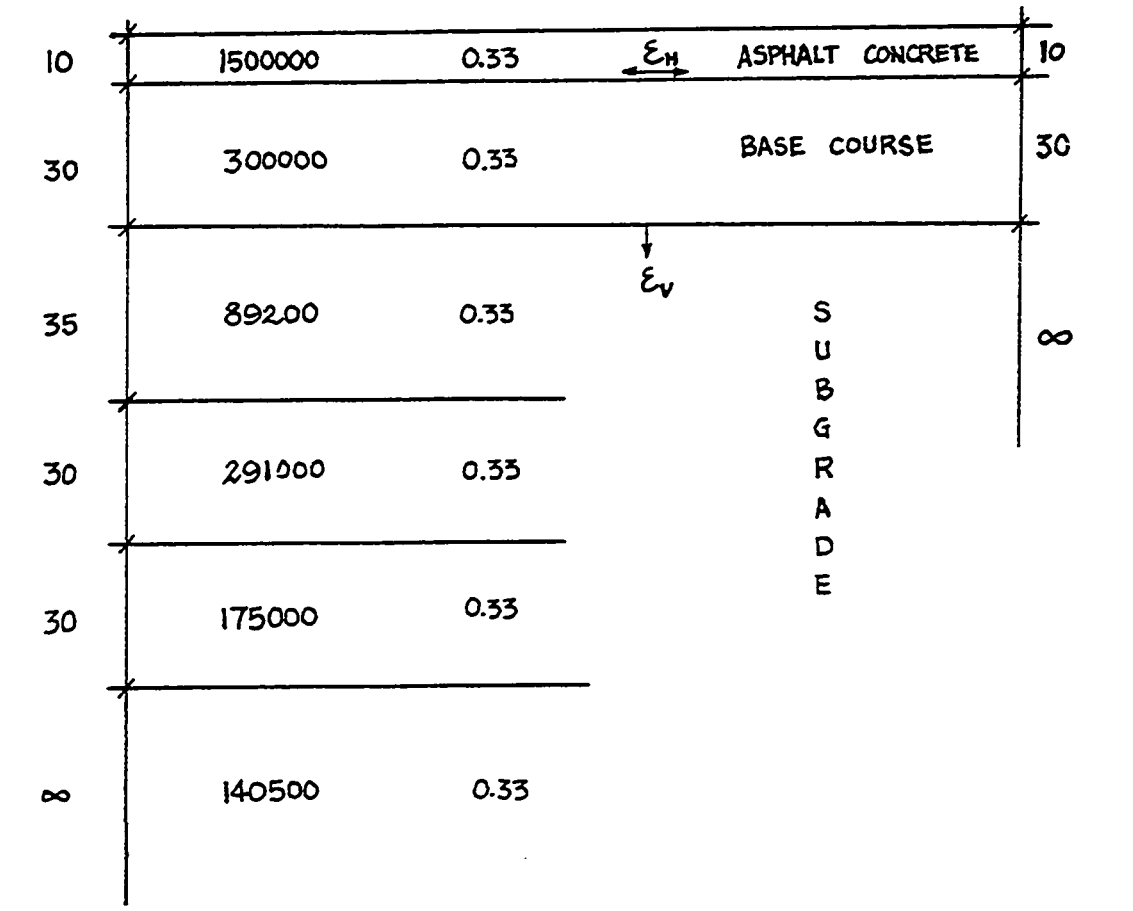

Fig. 422 - Multilayer elastic analysis. Ottawa: New airport. Pressuremeter cyclic moduli. Asphalt modulus: 1500000 kPa. Base modulus: 300000 kPa.

CASE 11 : OTTAWA AIRPORT

Old airport
Pressuremeter cyclic moduli
Design plane : DC3
$\varepsilon_H = 0.44 \times 10^{-3}$
$\varepsilon_V = 3.03 \times 10^{-3}$
$\delta = 0.22$ cm

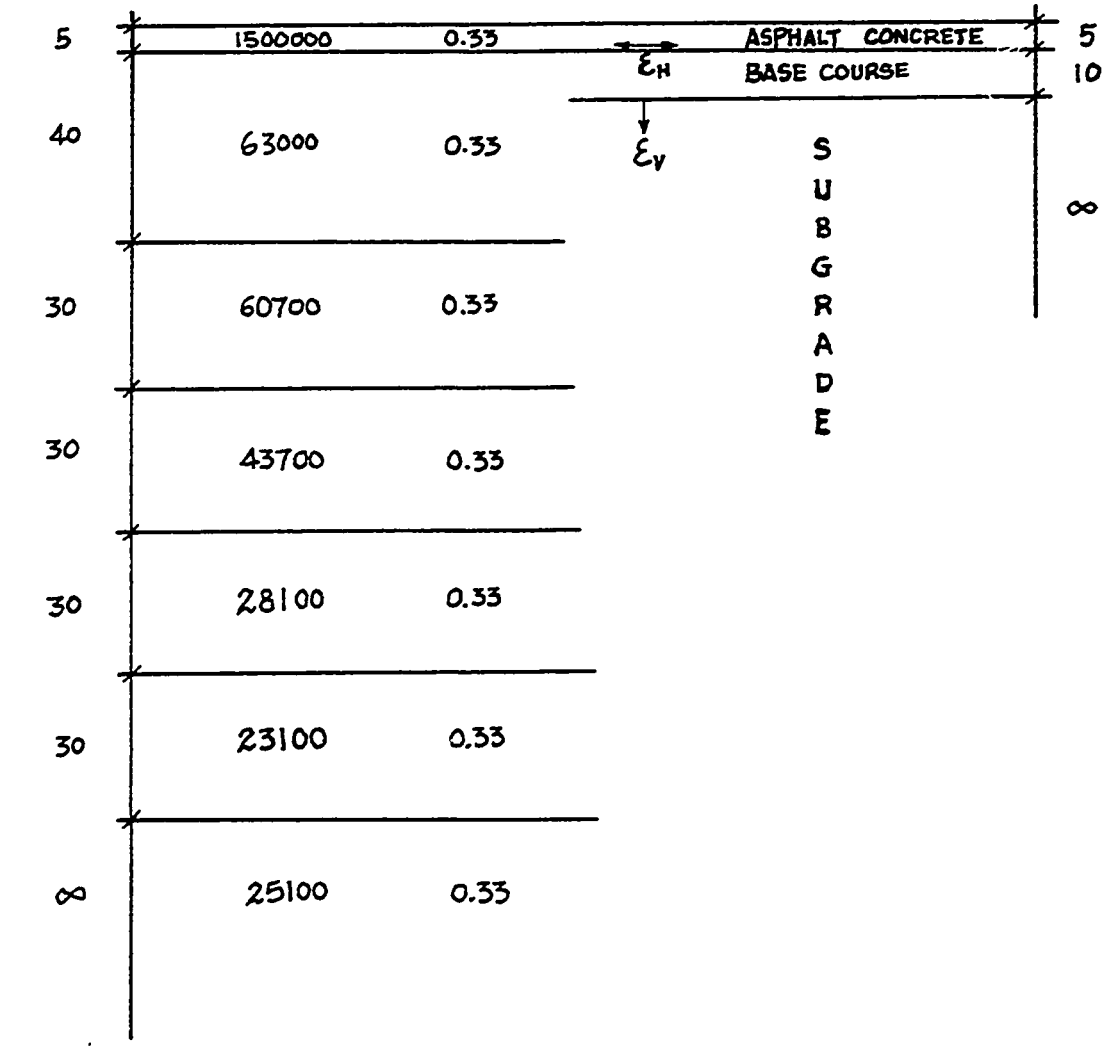

Fig. 423 - Multilayer elastic analysis. Ottawa: Old airport. Pressuremeter cyclic moduli. Asphalt modulus: 1500000 kPa.

CASE 12 : OTTAWA AIRPORT

Old airport
Pressuremeter cyclic moduli
Design plane : DC3
$\varepsilon_H = 0.39 \times 10^{-3}$
$\varepsilon_V = 2.4 \times 10^{-3}$
$\Delta = 0.19$ cm

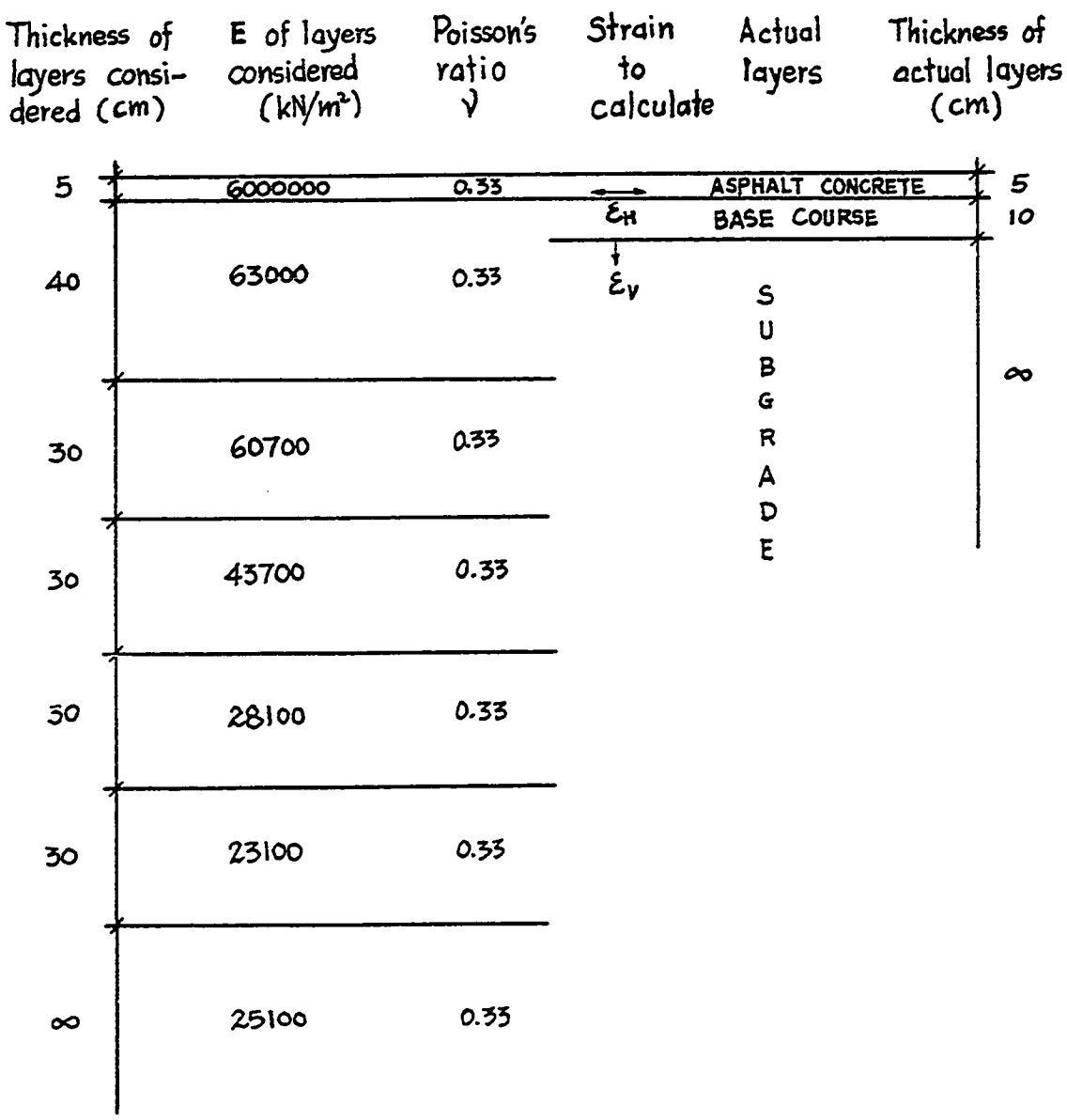

Fig.424 - Multilayer elastic analysis. Ottawa: Old airport. Pressuremeter cyclic moduli. Asphalt modulus: 6000000 kPa.

CASE 13 : OTTAWA AIRPORT

Old airport
Pressuremeter cyclic moduli
Design plane : DC 3
$\varepsilon_H = 0.07 \times 10^{-3}$
$\varepsilon_V = 2.63 \times 10^{-3}$
$\delta = 0.17$ cm

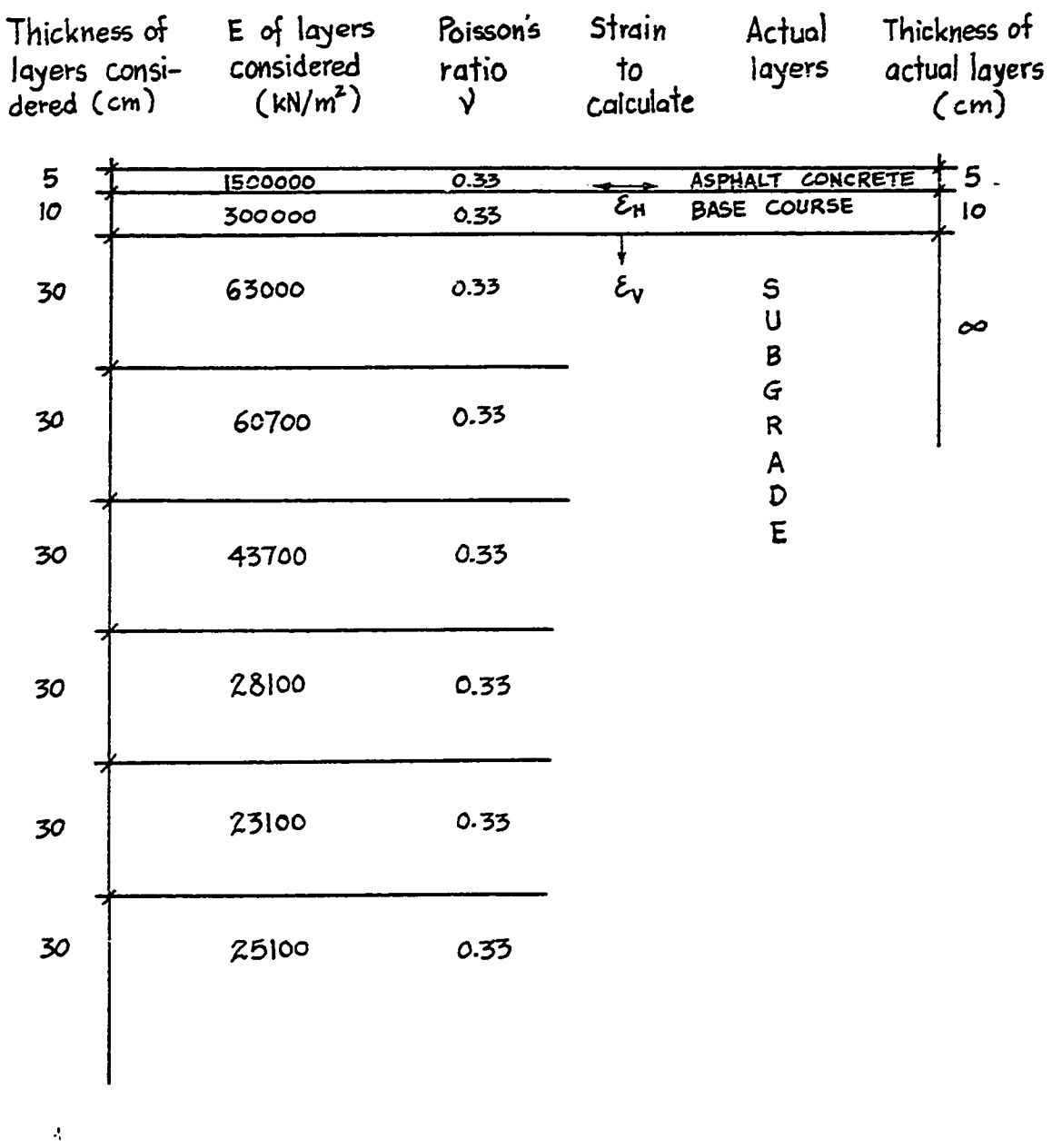

Fig. 425 - Multilayer elastic analysis. Ottawa: Old airport. Pressuremeter cyclic moduli. Asphalt modulus: 1500000 kPa. Base modulus: 300000 kPa.